ELUCIDATING THE IMMUNOMODULATORY MECHANISMS OF THE KSHV PROTEIN vOX2

By

KAREN MISSTEAR

A thesis submitted to
The University of Birmingham
for the degree of
DOCTOR OF PHILOSOPHY

The School of Cancer Sciences
College of Medical and Dental Sciences
The University of Birmingham
April 2010

Abstract

CD200 is a transmembrane protein with known immunoregulatory activities exerted via its receptor, CD200R. The Kaposi's sarcoma associated-herpesvirus (KSHV) ORF *K14* lytic cycle gene product, vOX2, shares 36% protein identity with cellular CD200. Both vOX2 and CD200 ligate CD200R with similar affinity. The main aim of this project was to determine whether vOX2 and CD200 regulate the function of human leukocytes. Thus, vOX2, CD200 and an inactive KSHV protein KCPmut were fused to the Fc region of human IgG1. vOX2:Fc and CD200:Fc exerted no effect upon isolated neutrophils, but suppressed granulocyte oxidative activity in whole blood by up to 25%. B lymphoblastoid cells were engineered to express full-length vOX2 or CD200 and utilized as antigen-presenting cells for Epstein Barr Virus-specific human T cell clones. vOX2 and CD200 suppressed IFNγ production by up to 50% in seven $CD8^+$ $CD200R^+$ T cell clones and one $CD4^+$ $CD200R^+$ clone. Mechanistically, vOX2 and CD200 suppressed the phosphorylation of ERK1/2, p38 and Akt kinases. This is the first evidence of a role for both cellular CD200 and KSHV vOX2 in negatively modulating antigen-specific T cell activity. The negative regulation of T cells by vOX2 probably contributes to KSHV evasion of antigen-specific T cell responses during lytic replication.

Acknowledgements

Firstly, and most importantly, I would express my heartfelt thanks to my supervisor, Prof. David Blackbourn, for his continual help, encouragement and guidance throughout my PhD. Secondly, many thanks go to my second supervisor, Prof. Janet Lord, for her support and advice. I am very grateful to the members of the Blackbourn research group, most notably Dr Rachel Colman, Dr Simon Chanas and Rachel Wheat, for their help and advice as well as their friendship and support. I am also thankful for the support I received from members of the Lord group, especially Hema Chahal for her neutrophil expertise and friendship. For their invaluable advice I would like to express my gratitude to Dr Alan Hislop and Prof. Martin Rowe. I am indebted to the numerous colleagues who supplied me with reagents and advice, particularly members of Prof. Alan Rickinson's group who provided me with T cell clones. Finally, I would like to thank Bruce and Gillian Misstear, David Misstear and Neil Keegan for their unwavering support and confidence in me.

Table of Contents

List of Figures

List of Tables

Acronyms, abbreviations and notations

aa	Amino acid
AIDS	Acquired immune deficiency syndrome
ANG2	Angiopoietin 2
AP-1	Activator protein-1 complex
APC	Antigen presenting cell
BAC	Bacterial artificial chromosome
BCBL-1	Body cavity-based lymphoma cell line
BEC	Blood vascular endothelial cell
BMMC	Bone marrow-derived mast cell
BSA	Bovine serum albumin
CCP	Complement control protein
CD200R	CD200 receptor
CDC	Centers for Disease Control
Cdk	Cyclin-activated kinase
cGVHD	Chronic graft-versus host disease
CHO	Chinese hamster ovary
CIA	Collagen-induced arthritis
CLL	Chronic lymphocytic leukaemia
CMV	Cytomegalovirus
CNS	Central nervous system
CPE	Cytopathic effect
CTL	Cytotoxic T lymphocyte
CTLA-4	Cytotoxic T lymphocyte antigen-4
DAF	Decay-accelerating factor
DC	Dendritic cell
DH	Dihydroxyacid dehydratase
DHR	Dihydrorhodamine
DMSO	Dimethyl sulfoxide
DMVEC	Dermal microvascular endothelial cells
DNA	Deoxyribonucleic acid
dNTP	Deoxyribonucleotide triphosphate
EAE	Experimental autoimmune encephalomyelitis
EAU	Experimental autoimmune uveoretinitis
EBV	Epstein Barr Virus
EDTA	Ethylenediaminetetraacetic acid
EGFP	Enhanced green fluorescent protein
EHV2	Equine herpesvirus 2
ELISA	Enzyme-linked immunosorbant assay
ER	Endoplasmic reticulum
ERK	Extracellular-signal related kinase
EU	Endotoxin unit
FBS	Foetal bovine serum
FcRn	Neonatal Fc receptor
fMLP	Formylmethionyl-leucyl-phenylalanine
gB	Glycoprotein B
G-CSF	Granulocyte-colony stimulating factor
GFP	Green fluorescent protein
GM-CSF	Granulocyte macrophage-colony stimulating factor
GPCR	G protein-coupled receptor
GPI	Glycosylphosphatidylinositol
GST	Glutathione S-transferase
HA	Haemagglutinin
HAART	Highly active antiretroviral therapy
HBSS	Hank's buffered saline solution

HHV-8	Human herpesvirus 8
HIV	Human immunodeficiency virus
HLA	Human leukocyte antigen
HMEC	Human microvascular endothelial cells
HOCl	Hypochlorous acid
HRP	Horseradish peroxidase
HSV	Herpes simplex virus
HVS	Herpesvirus saimiri
ICAM-1	Intercellular adhesion molecule 1
IFA	Immunofluorescence assay
Ig	Immunoglobulin
IgSF	Immunoglobulin Superfamily
IL	Interleukin
IL8RB	Interleukin 8 receptor beta
IFN	Interferon
IM	Infectious mononucleosis
iNOS	Inducible nitric oxide synthase
IP_3	Inositol 1,4,5-triphosphate
IP10	Interferon-inducible protein 10
IRF	Interferon regulatory factors
ISRE	Interferon-stimulated response element
ITAM	Immunoreceptor tyrosine-based activation motif
JNK	c-Jun amino-terminal kinase
KCP	KSHV complement control protein
KS	Kaposi's sarcoma
KSHV	Kaposi's sarcoma-associated herpesvirus
LAL	Limulus amoebocyte lysate
LANA	Latency-associated nuclear antigen
LAT	Linker for activation of T cells
LBP	Lipopolysaccharide binding protein
LCL	Lymphoblastoid cell line
LEC	Lymphatic endothelial cell
LPS	Lipopolysaccharide
mAb	Monoclonal antibody
MAPK	Mitogen activated protein kinase
MCD	Multicentric Castleman's Disease
mCD200/R	Murine CD200 / CD200 receptor
MCP-1	Monocyte chemotactic protein 1
MDM	Monocyte-derived macrophage cells
MHC	Major histocompatibility complex
MIF	Macrophage migration inhibitory factor
MIP	Macrophage inflammatory protein
MIR	Modulator of immune recognition
M-MLV RT	Moloney Murine Leukemia Virus Reverse Transcriptase
MM	Multiple myeloma
MPO	Myeloperoxidase
mRNA	Messenger ribonucleic acid
MS	Multiple sclerosis
MV	Myxoma virus
NADPH	Nicotinamide adenine dinucleotide phosphate
NFAT	Nuclear factor of activated T cells
NF-κB	Nuclear factor-κ B
NK	Natural killer cell
NO	Nitric oxide
NOD	Non-obese diabetic mice
NOS	Nitric oxide synthase
ORF	Open reading frame

PAMP	Pathogen-associated molecular patterns
PBMC	Peripheral blood mononuclear cell
PBML	Peripheral blood mononuclear leukocyte
PBS	Phosphate buffered saline
PCR	Polymerase chain reaction
PECAM	Platelet/endothelial cell adhesion molecule
PEL	Primary effusion lymphoma
PFA	Paraformaldehyde
PFU	Plaque-forming units
PHA	Phytohaemagglutinin
PHOX	Phagocyte oxidase
PI3K	Phosphatidylinositol 3-kinase
PIP_2	Phosphatidylinositol-4,5-biphosphate
PKB/C	Protein kinase B or protein kinase C
PKR	Protein kinase dsRNA-regulated
PMA	Phorbol 12-myristate 13-acetate
PVDF	Polyvinylidene fluoride
RA	Rheumatoid arthritis
rCD200/R	Rat CD200 / CD200 receptor
RDA	Representational difference analysis
(t)RBF	(Telomerised) rhesus fibroblasts
RCP	RRV complement control protein
RFP	Red fluorescent protein
RLU	Relative light units
ROS	Reactive oxygen species
RRV	Rhesus rhadinovirus
RTA	Replication and transcription activator
SCID	Severe combined immunodeficiency
SDS-PAGE	Sodium dodecyl sulphate polyacrylamide gel electrophoresis
SEM	Standard error of the mean
SHIP	Src homology 2 domain containing inositol phosphatase
siRNA	Short interfering ribonucleic acid
SLP-76	Src homology 2 domain-containing leukocyte protein of 76 kDa
SOX	Shutoff and endonuclease
SPR	Surface plasmon resonance
Stat4	Signal transducer and activator of transcription 4
STI	Sexually transmitted infection
TAP	Transporter associated with antigen processing protein
T-bet	T box transcription factor
TCR	T cell receptor
Th	T helper cell
TGFβ	Transforming growth factor-β
TLR	Toll-like receptor
TMB	3,3’5,5’-Tetramethyl-benzidine
TNF	Tumour necrosis factor
TPA	12-*O*-tetradeconoylphorbol-13-acetate
Treg	Regulatory T cell
TRIM	T cell receptor-interacting molecule
UL	Unique long region
US	Unique short region
VEGF	Vascular endothelial growth factor
VSV-G	Vesicular stomatitis virus envelope glycoprotein
WT	Wild type
Zap70	ζ-chain associated protein kinase 70

Chapter 1. Introduction

Though Kaposi's sarcoma (KS) was described in the nineteenth century, its aetiological agent, Kaposi's sarcoma-associated herpesvirus (KSHV), was not identified until 1994 (Chang *et al*., 1994). KSHV is also the aetiological agent of primary effusion lymphoma (PEL) and Multicentric Castleman's disease (MCD) (reviewed by Rezaee *et al*., 2006). Proteins encoded by the virus appear to exert immunoregulatory effects upon the infected individual, and thus may be potential therapeutic agents for the treatment of autoimmune diseases and transplant recipients.

The overall aim of this research project was to elucidate the mechanisms of action of KSHV vOX2 and its cellular counterpart, CD200, on innate and adaptive immunity *in vitro* and *ex vivo* (see Section 1.9 for specific objectives). This introduction provides a brief history of KS and the identification of KSHV as an infectious aetiological agent. The vOX2 protein expressed by a KSHV lytic gene, *ORF K14*, and its cellular counterpart, CD200, a protein with known immunoregulatory activities are then discussed, followed by an overview of innate and adaptive immune responses, focusing on neutrophils, monocytes and T cells.

Experimental methodologies are explained in detail in Chapter 2. The activities of recombinant soluble forms of vOX2 and CD200 on human granulocytes, monocytes and lymphocytes are described in Chapters 3 and 4. Data presented in Chapter 5 illustrate the roles of native vOX2 and CD200 expressed on the surface of antigen-presenting cells (APCs) in modulating the response of antigen-specific human T cell clones to stimulation. The mechanism behind the suppression of T cell activity by vOX2 and CD200 is examined in Chapter 6. Data presented in Chapter 7 relate to the expression of CD200R, the cognate receptor for CD200, by human T cells. Another viral homologue of CD200 encoded by rhesus rhadinovirus (RRV), and three human cytomegalovirus (CMV) proteins are described

in Chapter 8 with reference to their role in modulating the activity of human T cell clones. Methodologies are described in detail in Chapter 2 and will be referred to throughout, and lists of materials and raw data are included in the Appendices. Final conclusions are drawn in Chapter 9.

Names originally assigned to the proteins and viruses of interest in this thesis have altered over the years. KSHV was formally named human herpesvirus 8 (HHV-8), but will be referred to as KSHV in this thesis, out of respect for the scientists who isolated it (Chang *et al*., 1994). CD200, a human glycoprotein originally named OX-2, will be referred to by its newer title of CD200.

1.1. *Herpesviruses*

The herpesviruses share a structure distinct from any other virus, with an outer envelope enclosing a proteinaceous tegument, surrounding an icosahedral protein capsid which itself encloses a double-stranded DNA genome of 125-290 kbp (Davison *et al*., 2009). KSHV, like all herpesviruses, exists in two replicative states, latent and lytic. Latently infected cells contain an extrachromosomal circularised genome, known as an episome (reviewed by Wen and Damania, 2009). The infected cells contain very few viral transcripts and no viral particles as the virus does not replicate during latency. Therefore, latency allows the virus to remain dormant in the host due to the minimal expression of viral antigens, thus reducing the immune response. However, replication of the virus is essential for maintaining infection. The replicative phase of the viral lifecycle is known as the lytic cycle, and requires the transcription of genes that mediate the switch from latency to lytic replication (see Section 1.3.3). Genes are expressed in sequence during lytic replication, and can be subdivided into immediate-early genes that are regulators of transcription, and early or late genes, responsible for viral DNA synthesis and virion assembly (Wen & Damania, 2009).

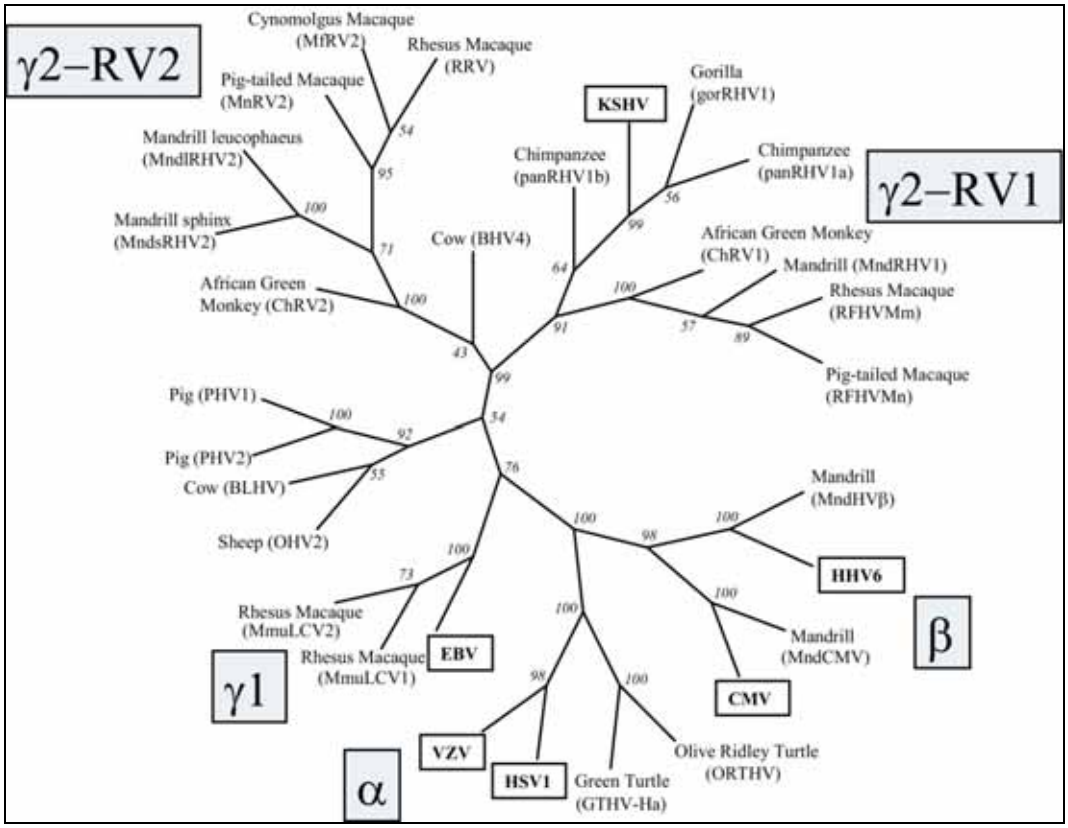

Figure 1.1 *Herpesviridae* phylogenetic tree. The distribution of herpesviruses within three subfamilies of the *Herpesviridae* family (prior to the revised taxonomic classification (Davison *et al*., 2009)). The phylogenetic relationship of 36 herpesviruses to six representative viruses (boxed) was determined. They were divided into subfamilies by PCR strategies using consensus-degenerate hybrid oligonucleotide primers (CODE-HOP) derived from a gene encoding a DNA polymerase that is highly conserved across the *Herpesviridae* family. The illustration is reproduced from Rose (Rose, 2005).

Three families of *Herpesviridae* are incorporated into the order *Herpesvirales*. The *Herpesviridae* family comprises mammalian, bird and reptile herpesviruses, the *Alloherpesviridae* comprises fish and frog herpesviruses, and a bivalve herpesvirus is the sole member of the *Malacoherpesviridae* family (Davison *et al*., 2009). The family *Herpesviridae* is further divided into three subfamilies, the *alphaherpesvirinae*, *betaherpesvirinae* and *gammaherpesvirinae* (**Figure 1.1**), of which KSHV is a member (Davison *et al*., 2009). The *gammaherpesvirinae* subfamily encompasses four genera, macaviruses, percaviruses, lymphocryptoviruses and rhadinoviruses. The

lymphocryptoviruses include Epstein Barr virus (EBV). KSHV is classed as a rhadinovirus along with herpesvirus saimiri (HVS), and RRV (Davison *et al*., 2009). Initially, the γ_1-lymphocryptoviruses were believed to infect only Old World primates, great apes and humans, and the γ_2-rhadinoviruses to infect New World primates (reviewed by Damania and Desrosiers, 2001). However, the discovery of KSHV in humans, in 1994 (Chang *et al*., 1994), closely followed by the isolation of RRV from Old World rhesus macaque (Desrosiers *et al*., 1997), disproved this hypothesis. Members of both genera naturally infect Old and New World primates.

1.2. *Kaposi's sarcoma (KS)*

First described by the Hungarian physician Moritz Kaposi (originally Kohn), in 1872, KS, a dermal pigmented sarcoma, was primarily diagnosed in elderly Mediterranean men. KS originally presented as a geographically distinct disease, occurring in equatorial Africa and the Mediterranean (reviewed by Cohen *et al*., 2005). However, a sharp increase in cases of KS in homosexual men in the 1980s correlated with human immunodeficiency virus (HIV) infection and the acquired immune deficiency syndrome (AIDS) epidemic. Subsequent epidemiological studies suggested an infectious causative agent for KS. This agent was subsequently identified in 1994 as KSHV (Chang *et al*., 1994). KS is associated with HIV infection, and is an AIDS-defining disease. However, though HIV infection increases the risk of developing KS, the main risk factor is infection with KSHV, with or without HIV infection (Beral & Newton, 1998).

KS can be subdivided into four clinical categories:

(i) Classic KS, first identified by Kaposi in elderly Mediterranean men is uncommon world-wide, but prevalent in Mediterranean populations. It is usually not the cause of death. The disease is isolated to lower limb dermis, the involvement of visceral organs is rare, and

progression slow (reviewed by Cohen *et al*., 2005). Brown *et al*. examined a cohort of HIV-negative classic KS patients in Italy to identify possible risk factors for the disease (Brown *et al*., 2006b). Both KS patients and healthy individuals were seropositive for KSHV, though a higher proportion of KS individuals had KSHV-infected peripheral blood mononuclear cells (PBMCs). EBV was identified in a higher percentage of PBMCs than KSHV in both groups, but appeared to be independent of the risk for developing classic KS. Individuals with KS exhibited lower concentrations of erythrocytes and lymphocytes (including $CD4^+$ and $CD8^+$ T cells), and increased numbers of monocytes. These factors are associated with a higher risk for developing classic KS. The individuals with the highest risk for developing KS were those below the age of 69 and with low levels of circulating lymphocytes, suggesting that pre-existing immunosuppressive factors may increase the risk of KSHV-infected individuals developing KS (Brown *et al*., 2006b).

(ii) *AIDS-associated KS* (or epidemic KS) is prevalent in HIV-positive homosexual men, but less common in HIV-negative haemophilic patients, and is an AIDS-defining condition. These observations suggested that blood is not a primary mode of virus transmission. Though the incidence of KS in HIV-positive individuals was once 30-50% (Cannon *et al*., 2003), highly active antiretroviral therapy (HAART) has reduced its incidence in HIV-infected populations. Disease onset of AIDS-associated KS is significantly more rapid, and progression is more aggressive than the classic form, affecting the visceral organs in conjunction with the skin, causing rapid morbidity (reviewed by Horenstein *et al*., 2008).

(iii) *Endemic KS*, noted in young men and children of equatorial Africa following the original descriptions of KS, is now one of the most common cancers in several African countries, presumably due to the rapid increase in HIV infection on this continent. Prior to the AIDS epidemic, KS was rare in the USA, Europe and Northern and Southern Africa

(Parkin, 2006). Since the rapid spread of HIV, KS incidences have increased across the USA and Europe and the rest of the developed world (0.1% of total cancer cases), but KS was still more prevalent in developing countries in 2002 (1.1% of all cancers). Due lack of data, the incidence of KS in developed countries was estimated based on data collected by US Surveillance Epidemiology and End Results, a component of the National Cancer Institute (Parkin, 2006). KS disease course may be slow or aggressive, depending on the HIV status of the individual or perhaps immunological suppression due to exposure to regional volcanic soils (Ziegler *et al*., 2003). The risk for developing KS in Uganda, where it is the most common cause of cancer in males, may be attributed to more than just increasing rates of HIV-infection. Ziegler and colleagues identified twelve risk factors associated with KS in Ugandan patients, including geographical location, wealth, religion, ownership of goats or pigs, and alcohol intake (Ziegler *et al*., 2003). A longitudinal study of the rates of KS in a defined region of Uganda (Kampala) between 1991 and 2006 revealed that KS is still the most prevalent cancer in males, but that the incidence of KS has declined over time (Parkin *et al*., 2010). The incidence of KS in females of that region has remained constant, but the age of onset has increased slightly, from the 20s to the late 30s. These authors suggest that the decrease in incidence and increased age of onset of KS may be due to the availability of anti-retroviral therapy for HIV infection (Parkin *et al*., 2010).

Oral transmission of KSHV between sexual partners or between mother and child seems likely (Mbulaiteye & Goedert, 2008). Quantifying KSHV load in breast milk and saliva by amplifying the KSHV *ORF26* gene by polymerase chain reaction (PCR) revealed the absence of KSHV in breast milk from all of the mothers sampled (Brayfield *et al*., 2004), though 29% of the mothers had detectable KSHV in cells isolated from their saliva. However, only 21% of infants (up to 12 months old) with anti-KSHV antibodies were born to mothers whose saliva was positive for KSHV (Brayfield *et al*., 2004). Mbulaiteye and

colleagues quantified the KSHV viral load in saliva samples from mothers (with unknown HIV status) and their children in Uganda (Mbulaiteye *et al*., 2006). Two of six mother-child pairs who were seropositive for KSHV were infected with the same strain of KSHV (genotype A5), sharing 100% homology with the *K1* gene, suggesting direct transmission of the virus. Amino acid changes in the *K1* gene between other mother-child pairs may be due to selective pressure on the virus to evolve. However, this study did not identify whether the virus was transmitted from mother to child, or vice-versa (Mbulaiteye *et al*., 2006). Please see Section 1.3.8 for further discussion of the modes of transmission of KSHV.

Whitby and colleagues agreed with the view that endemic forms of KS are attributed to environmental factors, and that such factors cause latent KSHV infections to become lytically active, thus increasing viral shedding and risk of transmission (Whitby *et al*., 2007). Extracts from plants, marine animals and fungi gathered worldwide were examined for their ability to induce lytic replication of KSHV in latently infected BCP-1 cells. 5.1% of compounds extracted from African regions were activators of KSHV replication, and were more potent activators, in comparison with 4.7% of samples taken from the rest of the world. However, the percentages of KSHV-reactivating extracts obtained from both the Caribbean and South America (5.6%) and The Philippines and Indonesia (7.2%) were higher than those taken from Africa (5.1%). Examining four extracts that appeared to induce KSHV reactivation, these authors found that the majority of KSHV messenger ribonucleic acids (mRNAs) investigated were induced by exposure to the extracts, including early lytic cycle mRNAs of *K14*, encoding vOX2. The use of many of the activating extracts in medicines, basket making and food suggests that a large proportion of the population may be exposed to them. A further consideration is the fact that many traditional medicines used in Africa are chewed before administration, thus predicting a mechanism for oral transmission of the virus (Whitby *et al*., 2007). Similarly, exposure to saliva by the sucking of insect bites on children

by their KSHV-seropositive mothers is a possible mechanism of transmission (Coluzzi *et al*., 2003).

(iv) *Iatrogenic KS*; KSHV can be transmitted by organ transplantation, primarily to recipients of donor kidneys, and involves the visceral organs in nearly 50% of cases. Therefore, transplant recipients are at 500-1000 times greater risk than the general population of developing KS (the incidence of KS is dependent on geographical location). Continued prophylactic immunosuppression subsequent to transplantation extends disease progression, which generally spontaneously regresses upon the withdrawal of suppression (Cannon *et al*., 2003).

1.3. *Kaposi's sarcoma-associated herpesvirus (KSHV)*

1.3.1. The identification and sequencing of KSHV

In 1994 Chang and colleagues discovered a unique virus in KS tissues from AIDS patients (Chang *et al*., 1994). KS had been observed to occur more frequently in homosexual AIDS patients as opposed to those with haemophilia, suggesting an infectious causative agent, transmitted by certain sexual practices rather than by blood – haemophiliacs are infected with HIV through receiving contaminated blood products – though no known virus could be identified. The representational difference analysis (RDA) technique was employed to identify DNA sequences specific and unique to KS tissue, and absent from healthy tissue. Two sequences (330bp and 631bp) showed homology to herpesviruses, principally EBV (Chang *et al*., 1994). This herpesvirus has a double-stranded deoxyribonucleic acid (DNA) genome and is associated with nasopharyngeal carcinoma and lymphoma (Young & Rickinson, 2004). EBV is also the causative agent of infectious mononucleosis (IM), more commonly known in the UK as glandular fever. EBV infects most individuals asymptomatically, and is transmitted by oropharyngeal secretions, subsequently infecting B

cells (Young & Rickinson, 2004). The unique gamma herpesvirus-related sequences were confined almost entirely to KS tissue in AIDS patients, therefore Chang and colleagues named the newly identified virus 'KSHV'.

Russo *et al*. published the genomic sequence of KSHV in 1996, following analysis of KSHV-infected PEL cell lines (Russo *et al*., 1996). They compared the KSHV genome with that of EBV and HVS and found that the majority of the KSHV genes shared protein identity and sequence similarity with those of HVS and EBV. Russo *et al*. estimated the genome of KSHV to be approximately 165kb in size, incorporating a 145kb coding region with 85 ORFs (Russo *et al*., 1996). The coding region may be subdivided into seven highly conserved regions, separated by genes unique to KSHV or its subfamily (Jarviluoma & Ojala, 2006). Concurrently, Moore and colleagues published data confirming that the KSHV sequences identified by Chang *et al*. were similar to those of other gammaherpesviruses, especially HVS, but encoded a new, distinct virus (Moore *et al*., 1996).

Renne and colleagues generated a body cavity-based lymphoma cell line (BCBL-1) for the laboratory culture and propagation of KSHV (Renne *et al*., 1996b). They analysed body cavity-based lymphomas from AIDS patients, and identified one sample infected with KSHV in the absence of EBV. Treatment of these cells with a phorbol ester induced cell proliferation and cytotoxicity, and increased KSHV DNA copy number. This indicated that the cells were latently infected with KSHV, and that lytic replication could be induced (Renne *et al*., 1996b). By analysing KSHV-infected BCBL-1 cells and KS lung lesion tissue, Renne and colleagues estimated the genome size of KSHV to be between 160 and 170kb (Renne *et al*., 1996a), thus concurring with Russo *et al*. KSHV DNA isolated from latently-infected BCBL-1 cells had a circular episomal conformation, similar in size and structure to EBV, whereas BCBL-1 cells treated with 12-*O*-tetradeconoylphorbol-13-acetate (TPA), a phorbol ester that induces lytic replication of the virus, contained linear KSHV DNA (Renne

et al., 1996a). The KSHV genome is illustrated in **Figure 1.2** (reproduced from Rezaee *et al*., 2006).

Utilising the herpesvirus-like sequences isolated from KS tissue by Chang *et al*., Ambroziak and colleagues identified a fragment of the KSHV genome in 13 KS biopsies. Control skin samples taken from each of the individuals (HIV-positive and negative homosexual men) were positive and negative for KSHV, though the positive results were later believed to be due to contamination with KS cells. PBMCs isolated from KS patients were consistently positive for KSHV, in contrast to those taken from HIV-positive and negative controls, with the virus predominantly confined to $CD19^+$ B cells. These authors attempted to define the mode of transmission of KSHV, testing semen and saliva for the virus, but could not detect the fragment in these fluids by PCR (Ambroziak *et al*., 1995). Huang *et al*. identified KSHV DNA fragments in AIDS-associated, Classic, and African endemic (HIV-infected and HIV-negative) KS lesions. KSHV DNA was absent from HIV-negative healthy skin samples. Analysis of viral DNA sequences revealed nucleic acid alterations in the majority of AIDS-associated and African KS samples, though the viral sequence in Classic KS was predominantly unchanged, indicating a divergence of viral infection in distinct populations (Huang *et al*., 1995).

Zong *et al*. examined the myriad of studies that used PCR to identify KSHV in clinical samples (Zong *et al*., 2007). In conjunction with several reports successfully identifying KSHV in KS lesions or PBMCs, such as Huang *et al*., 1995, multiple reports have been published that falsely claim to identify KSHV in other disease tissues, such as multiple myeloma (Rettig *et al*., 1997). The large number of studies reporting false-positive data for KSHV in clinical samples were primarily due to the low copy number of KSHV DNA in tissue, the generation of short and incomplete PCR sequences of KSHV genes, and contamination of the PCR reactions with KSHV DNA from PEL cell lines in the laboratory

(Zong *et al*., 2007). In fact, contamination of PCR assays was a problem throughout the identification of KSHV in clinical samples, and will be discussed further in Section 1.3.8.

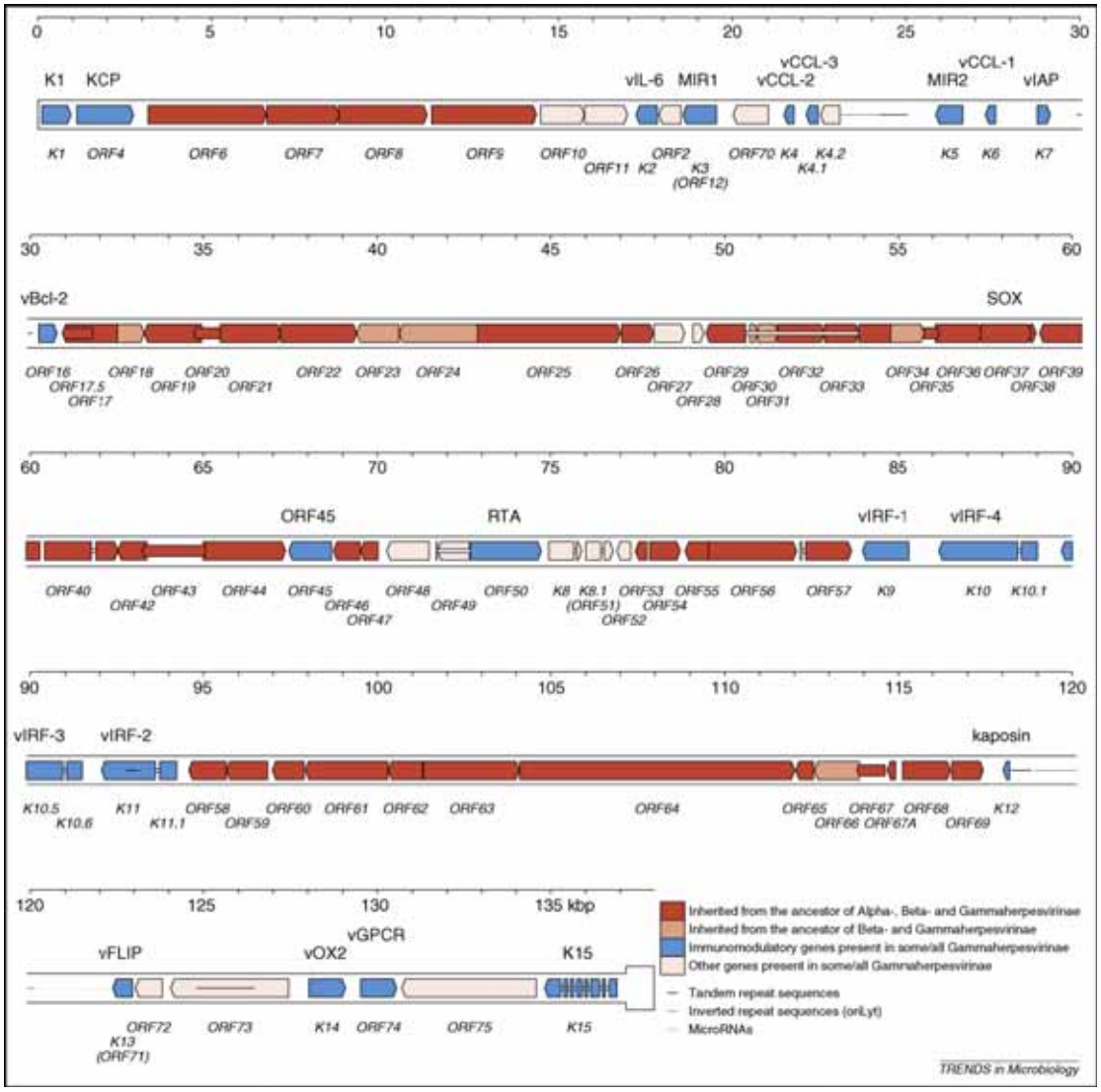

Figure 1.2 A genetic map of KSHV. The KSHV genome is approximately 170kbp in size, bordered by direct repeats at each end that ligate, resulting in circularisation of the DNA. Proteins encoded by the virus are illustrated as alternately coloured regions, depending on their origin of inheritance. vOX2 is encoded by open reading frame *K14*. This Figure is taken from Rezaee *et al*. (2006).

1.3.2. KSHV virion structure

Structurally, KSHV resembles the other members of the *Herpesviridae* family. It comprises a cell-derived lipid envelope, enclosing an icosahedral capsid, in turn encapsidating the double-stranded DNA genome (Trus *et al*., 2001).

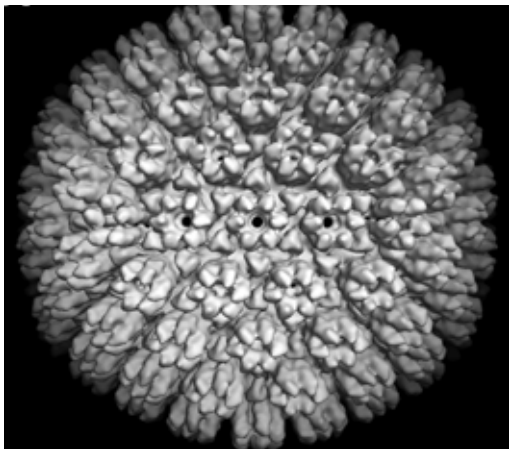

Figure 1.3 A density map of the KSHV capsid (24 Å resolution). A density map of the KSHV icosahedral capsid was generated following electron microscopy to visualise KSHV virions. The major capsid protein forms hexamers and pentamers, known as structural capsomers, and thus creating the 'floor' of the capsid. The protruding capsomers are evident on the surface of the capsid, as are the KSHV protein triplexes, the trigonal structures on the capsid floor. This Figure is taken from Trus *et al*. (2001).

The capsid and envelope are linked by a tegument composed of globular proteins, and viral glycoproteins are positioned in the envelope. The viral genome (double-stranded DNA) is encapsidated in the nucleus of infected cells. Budding through the inner nuclear membrane forms a lipid envelope, and subsequent budding from the outer nuclear membrane releases capsids into the cytoplasm (Mettenleiter *et al*., 2006). Cryo-electron microscopy analysis of the KSHV capsid by Trus *et al*. who isolated KSHV virions from BCBL-1 cells, revealed an icosahedral capsid (**Figure 1.3**) composed of a major capsid protein, two 'triplex' proteins,

and a minor capsid protein, ORF65 (Trus *et al*., 2001). Translocation of the capsids to the trans-Golgi network is the final stage of viral construction, and is assisted by viral tegument proteins. At the trans-Golgi network, viral glycoproteins and tegument proteins are assembled and the viral envelope added, creating a virion coated with a cellular vesicle. Coating of the virus with a host-derived envelope enables fusion with the host cell's plasma membrane and viral dissemination (Mettenleiter *et al*., 2006).

1.3.3. KSHV replication

Analogous to other members of the *Herpesviridae* family, the KSHV lifecycle has both latent and lytic replicative phases. A minority of its proteins are expressed during latency, in order to avoid detection by the host's immune system. Lytic replication requires the expression of many more proteins, and lytic genes are expressed in phases following reactivation of the virus. Sun *et al*. investigated the kinetics of KSHV gene expression during the viral lifecycle (Sun *et al*., 1999). Treatment of KSHV-infected BC-1 cells, a PEL cell line, with sodium butyrate induced the transcription of lytic KSHV genes, and subsequent lytic replication of the virus. Immediate-early genes (e.g. *ORF50*) were defined as those resistant to an inhibitor of protein synthesis, cycloheximide; early genes (e.g. ORF *K2*) were resistant to phosphonoacetic acid but not cycloheximide; and late lytic genes (e.g. *ORF65*) were inhibited by both (Sun *et al*., 1999).

Latently-infected endothelial 'spindle' cells dominate KS lesions (discussed further in Section 1.3.4). However, only a small proportion of KSHV-infected endothelial cells are able to maintain latent KSHV infection *in vitro*, illustrated by a loss of viral episomes (Grundhoff & Ganem, 2004). These data indicate that lytic replication (as observed in some KS tumour cells) is necessary for the maintenance of infection *in vivo* (Grundhoff & Ganem, 2004). The latency-associated nuclear antigen (LANA) encoded by *ORF73*, is one of the few

KSHV proteins expressed in cells latently infected with KSHV. LANA prevents lytic replication of KSHV by silencing the expression of genes that mediate the switch between latency and lytic replication, including the KSHV replication and transcription factor (RTA) encoded by *ORF50*. Li *et al*. generated a LANA deletion mutant of KSHV within a bacterial artificial chromosome (BAC), and infected an endothelial cell line with the recombinant virus (Li *et al*., 2008). Deleting LANA increased the number of infectious KSHV virions secreted into the culture supernatant by infected cells, indicating increased lytic replication. RTA transcripts were amplified in cells infected with LANA-negative KSHV, along with MTA transcripts (*ORF57*) and protein expression (Li *et al*., 2008). MTA is essential for KSHV lytic replication, and binds directly to RTA, forming a complex that can then bind to KSHV gene promoters, thus initiating gene transcription and thus promoting the switch to lytic replication (Palmeri *et al*., 2007). RTA induced the expression of MTA and other lytic genes *ORF59* and *ORF-K8.1* (Li *et al*., 2008). Thus, expression of LANA inhibits the concurrent expression of RTA, and the silencing of LANA increases RTA expression, in turn increasing lytic gene expression and viral replication.

So, the repression of RTA by LANA must be removed in order for KSHV to switch from latency to lytic replication. Cheng *et al*. identified two cellular kinases, Pim-1 and Pim-3 that could reactivate recombinant KSHV in epithelial (Vero) and endothelial cells (Cheng *et al*., 2009). Recombinant KSHV is a double-reporter virus that constitutively expresses green fluorescent protein (GFP). Upon lytic replication, recombinant KSHV expresses red fluorescent protein (RFP) by the activity of the RTA-responsive promoter of polyadenylated nuclear RNA (PAN), an abundant KSHV lytic transcript. Pim-1/3 interacted directly with LANA in reactivated KSHV-infected cells, but not in latently infected cells, phosphorylating the LANA protein. The Pim-LANA interaction also prevented the binding of LANA to KSHV terminal repeats, thus preventing the LANA-mediated inhibition of lytic gene

transcription (Cheng *et al*., 2009). The mitogen-activated protein (MAP) kinases, extracellular signal related kinase (ERK), c-Jun amino-terminal kinase (JNK) and p38, are also implicated in KSHV reactivation (Xie *et al*., 2008). Pharmacological inhibition of the ERK, JNK and p38 pathways subsequently suppressed the production of virions by phorbol ester-treated BCBL-1 cells, during the early stages of lytic replication. A concurrent reduction in the expression of RTA appeared to be due to the indirect inhibition of activator protein-1 complex (AP-1), a downstream target of the kinase signalling pathways, and a transcription factor that binds to and activates the RTA promoter (Xie *et al*., 2008).

Kedes and Ganem examined the abilities of several anti-viral drugs to prevent KSHV lytic replication in BCBL-1 cells. Acyclovir, ganciclovir, cidofovir and foscarnet, drugs efficacious in the treatment of other human herpesviruses, were studied, with cidofovir appearing to exert the most potent inhibition on KSHV replication, whereas a HIV protease inhibitor (A77003) had no effect. KSHV seemed to be insensitive to acyclovir. The isolation of potential anti-viral treatment for KSHV is important clinically, but also highlights the fact that the human herpesviruses are distinct in their responses to anti-viral compounds (Kedes & Ganem, 1997).

1.3.4. Transcriptional reprogramming of KSHV-infected cells

KS lesions result from proliferation and vascularisation of endothelial tissue, and may be identified by distinctive endothelial ‘spindle’ tumour cells derived from vascular or lymphatic tissue. Data presented by Wang and colleagues agree with that of others, suggesting that KSHV infects either lymphatic endothelial cells (LECs) or blood vascular endothelial cells (BECs), and then induces transcriptional reprogramming of the cells, resulting in their de-differentiation (Wang *et al*., 2004). The analysis of KS tissue biopsies by gene expression microarray isolated 1,482 genes specific to KS tissue, including cells

expressing markers of both LECs and BECs. The KS signature gene expression was associated with more LEC markers, such as CD206, than markers of BECs. The high KSHV copy number in LECs suggests that this cell population provides an optimal environment for viral replication or viral entry into the cell (Wang *et al*., 2004).

Wang and colleagues suggest a mechanism for the KSHV-induced dedifferentiation of LECs and BECs. The expression of PROX1, a homeobox transcription factor crucial to differentiation of the two cell types by upregulating LEC markers and downregulating BEC markers, is increased overall in KS tissue, but specifically downregulated in KSHV-infected LECs. This suggests that KSHV induces LECs to de-differentiate towards a BEC phenotype (Wang *et al*., 2004). The work of Hong *et al*. supports the notion of KSHV-induced reprogramming of lymphatic and vascular endothelium (Hong *et al*., 2004). These authors confirmed that the expression of PROX1 is isolated to healthy cultured human LECs, and not BECs. The infection of human dermal microvascular endothelial cells (DMVECs) with KSHV, upregulated LEC-specific genes including PROX1. These data suggest that an LEC phenotype is induced by KSHV-infection. However, only a portion of LEC-specific genes were upregulated. The infection of BECs with KSHV also induced PROX1 expression, to a level comparable with that in primary LEC. Short interfering RNA (siRNA) silenced the expression of PROX1 in KSHV-infected BECs, and downregulated the expression of LEC markers induced by KSHV, indicating a primary role for PROX1 in KSHV-mediated lymphatic reprogramming (Hong *et al*., 2004). The above data show that KSHV-infected spindle cells do not belong to any specific lineage, thus suggesting that the de-differentiation induced by KSHV results in the generation of a new lineage of cells adapted to provide optimal conditions for the virus to survive.

Spindle cells release proinflammatory cytokines, thus promoting the survival of KSHV-infected cells within the KS tumour (Grossmann *et al*., 2006). The expression of the

KSHV latent gene product, vFLIP (*ORF K13/ORF71*) by endothelial cells induces the 'spindle' phenotype and cytokine secretion, via activation of the transcription factor nuclear factor-κ B (NF-κB). NF-κB regulates genes that promote cell proliferation and anti-apoptosis, therefore indicating a means for survival of KSHV-infected spindle cells *in vivo* (Grossmann *et al*., 2006).

1.3.5. Angiogenic and oncogenic properties of KSHV

The characteristic red pigmented lesions of KS are due to tumour angiogenesis, and rupturing of the newly synthesised weak blood vessels. Pro-angiogenic factors have been identified in KS lesions, including Int-2, vascular endothelial growth factor (VEGF), and angiopoietin-1 and 2 (ANG-1/2) (Kang *et al*., 2008). KS lesions during early stages of pathogenesis are also filled with pro-inflammatory factors such as interferon-γ (IFNγ), tumour-necrosis factor-α (TNFα) and interleukin-1β (IL-1β), IL-2, IL-6 and IL-8, produced by infiltrating monocytes/macrophages and lymphocytes (Kang *et al*., 2008). KSHV infection causes endothelial cells to upregulate angiogenin, an angiogenic factor that increases endothelial cell proliferation and migration to the walls of blood vessels under construction (Sadagopan *et al*., 2009). Both latent (ORF *73*, encoding LANA) and lytic (ORF *50*, encoding RTA) KSHV genes upregulated angiogenin gene expression in endothelial cells, and secretion of the protein. Angiogenin could be detected in adjacent uninfected cells, indicating that it is endocytosed and therefore can act in a paracrine as well as autocrine fashion (Sadagopan *et al*., 2009). In addition to its role in upregulating angiogenesis, angiogenin also increased the survival of KSHV-infected, serum-starved endothelial cells, by inhibiting their apoptosis, and thus putatively contributing to KSHV oncogenesis (Sadagopan *et al*., 2009).

vIL-6 produced by KSHV infected cells may also play a role in inducing angiogenesis. Though the majority of KS lesions contain IL-6, a minority contain vIL-6 and both appear to be crucial factors in KS pathogenesis, suggesting that vIL-6 may exacerbate the effects mediated by endogenous IL-6 (Aoki *et al*., 1999). Two KSHV lytic genes encoding either glycoprotein B (gB), expressed on the viral envelope and involved in KSHV egress, or glycoprotein K8.1 (gK8.1), which facilitates KSHV virion binding to host cells and viral egress, induced the production of VEGF by KSHV-infected cells (Subramanian *et al*., 2010). Inhibiting the expression of gB and gK8.1 by transfection of KHSV-infected BCBL-1 cells with siRNA directed against the two genes, in turn suppressed the expression of *VEGF* and *IL-6*, and secretion of VEGF. Inhibiting gB and gK8.1 also reduced capillary tube formation by endothelial cells cultured in BCBL-1 conditioned medium (Subramanian *et al*., 2010). Thus, KSHV plays several roles in promoting angiogenesis; the reader can refer to Kang *et al*. for a detailed discussion (Kang *et al*., 2008).

Several KSHV proteins have been implicated in promoting tumourigenesis during KS pathogenesis. Bais *et al*. proposed that the viral G protein-coupled receptor (vGPCR) encoded by KSHV possesses tumourigenic and angiogenic properties. vGPCR induces intracellular signalling cascades subsequent to the phosphorylation of MAP kinases, JNK and p38. The KSHV vGPCR is encoded by *ORF74*, and is commonly observed in KS lesions (Bais *et al*., 1998). These authors expressed the vGPCR in fibroblasts, and injected these cells into nude mice (lacking a functional thymus and T cell population). Tumours formed in the nude mice and were associated with vGPCR expression. Putative angiogenic properties of vGPCR were illustrated by angiogenesis in KSHV-infected mice, and the proliferation of endothelial cells cultured in conditioned vGPCR-transfected cell medium (Bais *et al*., 1998). Further *in vivo* data regarding the role of vGPCR on tumourigenesis were generated by Thirunarayanan and colleagues, who demonstrated that tumour formation in nude mice by

vGPCR-expressing fibroblasts, could in turn induce tumourigenesis in immunocompetent mice (Thirunarayanan *et al*., 2007). KS occurs in immunocompromised individuals, correlating with the formation of vGPCR-expressing tumours in nude mice. However, transplantation of vGPCR-expressing tumours from nude mice to immunocompetent mice results in rapid oncogenesis and tumour formation in human leukocyte antigen (HLA)-matched recipients, indicating that vGPCR tumours may develop mechanisms to evade the host response (Thirunarayanan *et al*., 2007).

KSHV proteins contribute to tumourigenesis by altering the host cell cycle. Cell cycle proteins such as cyclin D are crucial for progress of the cell cycle, forming complexes with cyclin-activated kinases (cdks), and their interaction is prevented by specific inhibitors to prevent aberrant continuous cell cycling. KSHV v-cyclin (encoded by latent gene *ORF72*), a homologue of cyclin D, is resistant to cyclin/cdk inhibitors and thus drives the cell cycle resulting in excessive proliferation of cells latently infected with KSHV (Jarviluoma & Ojala, 2006).

LANA plays an important role in KS tumourigenesis as well as in the maintenance of KSHV latency. Both LANA expression and KSHV infection upregulate the expression of *Survivin* and the cellular protein it encodes. Survivin is involved in the inhibition of apoptosis, and upregulated in many cancers, including lung, breast and prostate (Lu *et al*., 2009). LANA upregulates the expression of survivin by forming complexes with Sp-1 and p53 transcription factors, which then bind directly to the upstream promoter of *Survivin*. *In vivo*, KS tissues highly express survivin, and blocking its expression in KSHV-infected cells by small hairpin interfering RNA (shRNA) slowed their proliferation (Lu *et al*., 2009).

c-Myc, a transcription factor that is found in a mutated form in many cancers, and facilitates cell proliferation and survival, is expressed by KSHV-infected PEL cell lines (Liu *et al*., 2007). Though the wild-type form of c-Myc is expressed by KSHV-infected cells, its

half-life is prolonged, apparently due to LANA-mediated inhibition of c-Myc phosphorylation at threonine 58. The reduced phosphorylation of threonine 58 in the presence of LANA, in turn reduces c-Myc ubiquitination, and enhances the phosphorylation of the serine 62 residue of c-Myc. The modification of c-Myc phosphorylation by LANA contributes to decreased apoptosis and increased c-Myc transcriptional activity, thus enhancing oncogenesis (Liu *et al*., 2007).

1.3.6. Genetic risk factors for KSHV infection and KS development

The genetic profiling of both classic KS patients and KSHV-seropositive individuals revealed specific cytokine haplotypes conferring a higher risk for KS development (Brown *et al*., 2006a). Two polymorphisms of *Interleukin-8 receptor beta* (*IL8RB*), a gene encoding a GPCR with high affinity for IL-8, were associated with reduced incidence of Classic KS (Brown *et al*., 2006a). IL-8 (a neutrophil chemoattractant) is highly expressed in AIDS-KS cell lines, KS tissue biopsies, and KS serum, in comparison to controls and promotes cell proliferation and angiogenesis (Masood *et al*., 2001). The KSHV vGPCR is a homologue of the human IL-8 receptors, and is constitutively active, stimulating cells to secrete IL-6 and IL-8 via the upregulation of cellular transcription factors (Montaner *et al*., 2004). The inflammatory infiltrate characteristic of KS lesions is produced by KSHV-infected spindle cells as well as infiltrating monocytes and lymphocytes; it promotes the survival of B cells and the development of spindle cells and enhances KSHV DNA load (Monini *et al*., 1999). Though the function of the specific *IL8RB* polymorphisms associated with reduced KS incidence is unknown, it is possible that these receptors have reduced affinity for their ligand, thus reducing the IL-8/vGPCR/IL-8R feedback pathway, and altering the inflammatory phenotype characteristic of KS lesions. An alteration in cytokine production may also impact the T cell response to infection.

Foster *et al*. demonstrated that the inheritance of certain polymorphisms of *IL6* increased the likelihood of HIV-positive homosexual men developing KS (Foster *et al*., 2000). Individuals who were homozygous for the *IL6*-174 GG allele, associated with increased IL-6 production, were more likely to develop KS, whereas fewer individuals with KS expressed the *IL6*-174 CC allele, associated with reduced cytokine production (Foster *et al*., 2000). These data support the notion that increased cytokine production is associated with increased KS disease pathology.

Alkharsah *et al*. reported an association between HLA alleles, responsible for presenting viral peptide antigens to T cells, and the shedding of KSHV in saliva (Alkharsah *et al*., 2007). Real-time PCR quantitation of KSHV DNA load in cells from the saliva of a large cohort of mothers and children in South Africa revealed an association between the HLA-A*68.01 and HLA-DRB1*04 alleles and increased shedding of KSHV in saliva, though the increased risk associated with these alleles was for virus shedding, and therefore transmission, rather than KSHV infection (Alkharsah *et al*., 2007). Again, these data suggest that suppression of T cell responses, possibly due to inefficient presentation of viral peptides by HLA molecules, may underlie the increased KSHV DNA load.

The statistical analysis of a closely interrelated population in French Guinea with high KSHV seroprevalence revealed that KSHV transmission is related to the inheritance of an unidentified recessive gene (with unknown function) from mother to child (Plancoulaine *et al*., 2003). The study indicated that the KSHV infection of children born to seronegative mothers may be due to genetic susceptibility of the child, who is homozygous for an uncharacterised recessive gene. Therefore, individuals who may be deemed to be at lower risk for KSHV infection because their family members are seronegative for KSHV, actually are still at risk due to increased genetic susceptibility to infection (Plancoulaine *et al*., 2003).

1.3.7. The role of KSHV in other diseases

KSHV is the aetiological agent of both KS and PEL, and is associated with MCD (Bouvard *et al.*, 2009). The identification of KSHV in other disease tissues has been controversial and unconfirmed, and will not be discussed further. Marcelin and colleagues examined the KSHV load in clinical samples from KS, PEL and MCD patients (Marcelin *et al*., 2007). Using real-time PCR to amplify LANA (*ORF73*) they detected a higher viral load of KSHV in PBMCs from patients with active KS, in comparison to those in remission from the disease. KSHV load was also positively correlated with HIV infection. Similarly, PBMCs from individuals with active MCD also carried a greater KSHV copy number, in comparison to those in remission (Marcelin *et al*., 2007). Lymphomatous effusion fluid, extracted from the pleural or peritoneal cavities of PEL patients, contained the highest KSHV DNA copy number, and MCD blood samples had a higher KSHV load than KS PBMCs. The presence of high numbers of $CD4^+$ T cells in individuals in remission from KS suggests that increased viral load in the active disease is due to immunosuppression (Marcelin *et al*., 2007).

Cesarman *et al*. confirmed that KSHV is present in PEL tissue (first described by Chang *et al*., 1994), demonstrating that lymphomatous B cell effusions in HIV-negative lymphoma patients were positive for KSHV (Cesarman *et al*., 1996). PEL is now classified as a KSHV-associated disease. It is commonly AIDS-associated and presents in immunosuppressed individuals, such as post-transplant recipients, as well as the elderly, with a median survival time of less than six months (Carbone & Gloghini, 2008). Brimo and colleagues examined effusions from four HIV-positive PEL patients, and found that two of the four samples expressed T cell markers, CD3, CD43 and CD45RO, and two expressed CD45 a marker of lymphomas. These data contrasted with current literature which predominantly report a phenotype similar to neither B nor T cells, and consistent expression of CD45 (Brimo *et al*., 2007). All samples expressed CD30, a marker of both B and T cells,

and were infected with KSHV (Brimo *et al*., 2007). The prevailing opinion is that PEL cells originate as B cells and then differentiate towards a mature plasma B cell. However, B cell maturation is interrupted and they adopt a null phenotype, downregulating B cell-specific genes (Carbone & Gloghini, 2008). Most PEL cells are latently infected with KSHV, and oncogenesis of PEL is thought to be driven by the same genes that drive KS tumourigenesis, including LANA and v-cyclin (see Section 1.3.5) (Carbone & Gloghini, 2008).

MCD is another B cell lymphoma, characterised by KSHV-infected plasmacytic cells. In contrast to PEL, MCD cells are usually not co-infected with EBV (Carbone & Gloghini, 2008). Characterising KSHV-infected cells isolated from the lymph nodes of MCD patients, Chadburn *et al*. identified the expression of PR domain containing 1 with zinc finger domain / B lymphocyte-induced maturation protein 1 (PRDM1/BLIMP1), a transcription factor that is essential for the maturation of plasma cells, and that represses genes that promote proliferation (Chadburn *et al*., 2008). The mature plasmacytic phenotype of MCD cells contrasts with their continuous proliferation, suggesting that their terminal differentiation is blocked by KSHV infection. PRDM1/BLIMP1 was also expressed by PEL cells, but CD27, a marker of memory B cells, was solely expressed by MCD cells, indicating that though MCD and PEL cells have a similar phenotype, they are derived from B cells at different stages of differentiation (Chadburn *et al*., 2008).

KSHV itself can induce a primary disease in both immunosuppressed and immunocompetent individuals, though it is rarely reported. Symptoms, including fever, arthralgia (joint pains), splenomegaly (enlargement of the spleen) and cervical lymphadenopathy (swelling of the lymph nodes), have been observed (Dukers & Rezza, 2003). Oskenhendler reported a sudden onset of symptoms in a HIV-positive homosexual male (Oksenhendler *et al*., 1998). KSHV was detected (by PCR) in a cervical lymph node subsequent to recent KSHV seroconversion (Oksenhendler *et al*., 1998). Symptoms

attributable to a systemic viral infection were also noted in an immunodeficient (HIV-negative) child (Sanchez-Velasco *et al*., 2001). Post-mortem analysis revealed KSHV infection of bone marrow, lymph node, spleen and PBMCs, as well as non-lymphoid tissues including the lung, liver and kidney. EBV could be detected in the spleen and lymph node only, and CMV was undetectable (Sanchez-Velasco *et al*., 2001).

1.3.8. Transmission of KSHV

The sudden manifestation of KS in homosexual young men in the early 1980s was a primary indicator of the AIDS epidemic, and suggested transmission of an infectious agent. Analysis of the AIDS cases reported to the Centers for Disease Control (CDC) in the USA revealed an incidence of KS of 15%, 20,000 times greater in the HIV-infected population than in the general population. The high risk groups for developing KS included homosexual and bisexual men, HIV-infected individuals of Caribbean or African descent, HIV-positive haemophiliacs and HIV-positive heterosexual women (Beral *et al*., 1990).

Early studies suggested that KSHV infected male sexual organs, and thus was transmitted by infected semen. Initially, quantifying KSHV infection by nested PCR for *ORF26* revealed KSHV infection of semen in the majority of the HIV-positive men sampled (91%), in comparison to HIV-uninfected individuals (23%) (Lin *et al*., 1995). Staskus *et al*. identified KSHV in prostatic tissue of HIV-infected and some uninfected individuals by *in situ* RNA hybridisation (Staskus *et al*., 1997). These data correlate with a possible sexual mechanism of transmission, though KSHV in the prostate appeared to be latent and may not therefore contribute to shedding of virions, but perhaps virus-infected cells into the semen (Staskus *et al*., 1997).

Quantifying KSHV infection (by PCR) of the sexual organs and semen of the healthy population revealed a low incidence of KSHV infection in the urinary tract, female genital

tract, glans and foreskin (Monini *et al*., 1996). However, KSHV was detected at high frequency in prostatic tissue (44%), sperm (91%) and semen (81%) of the healthy population (Monini *et al*., 1996). Shortly after this, Howard *et al*. reported that KSHV was more easily detected in the peripheral blood than semen, and that it was confined to HIV-positive homosexual males (Howard *et al*., 1997). They detected KSHV DNA by nested PCR in the semen of only six of 24 (25%) HIV-infected homosexual men, and found no evidence of KSHV infection in the semen of 115 healthy males. However, KSHV was detected in the blood of 12 (50%) of the HIV-positive men, both with and without KS, indicating that infection of the peripheral blood is more common than seminal infection (Howard *et al*., 1997). An overview of KSHV detection in semen and prostate highlighted discrepancies between results generated by different research groups, and questioned the use of amplifying PCR for detecting low viral copy numbers in tissue (Blackbourn & Levy, 1997).

KSHV infection of the sexual organs and fluids is now widely disputed, and current opinion is that transmission by saliva and nasal discharge are the most likely modes of infection. Evidence for KSHV infection of the saliva was published in 1997 by Vieira *et al*., who identified KSHV DNA in saliva and PBMCs of HIV-negative and HIV-positive KS patients (Vieira *et al*., 1997). KSHV DNA was present in both cells and cell-free fractions of saliva, as an encapsidated virion (it is known that EBV is shed into the saliva as an encapsidated virion). KSHV virions in saliva were able to persistently infect the 293 cell line (derived from human embryonic kidney cells) for at least eleven passages, though EBV, present in the saliva at a ten-fold greater concentration than KSHV, infected 293 cells only briefly (Vieira *et al*., 1997).

Blackbourn and colleagues detected KSHV in the majority of HIV-infected KS patient PBMCs, saliva and nasal fluid by PCR (Blackbourn *et al*., 1998). The presence of KSHV in saliva and nasal fluid was variable, with some individuals presenting with KSHV-

positive saliva but not nasal secretions, or vice-versa, and some with detectable KSHV in both fluids. KSHV could also be observed in either secretion in KSHV (and HIV) infected individuals asymptomatic for KS. KSHV was present in both cellular components and fluid components of these secretions, indicating viral shedding from infected cells. EBV, CMV and HHV-6 were also present in saliva and nasal discharge, and were most prevalent in KS patients (Blackbourn *et al*., 1998).

Pauk *et al*. examined mucosal secretions from 27 KSHV-seropositive homosexual men, of whom 11 were seropositive for HIV (Pauk *et al*., 2000). Using PCR for a fragment of *ORF26*, KSHV was detected in saliva and oral epithelial cells in 12% of the men. Both buccal (mouth) and pharyngeal (throat) epithelial cells expressed KSHV gene transcripts associated with latency, and the buccal cells also expressed transcripts associated with lytic replication, thus indicating shedding of the virus. However, KSHV DNA was also detected in 5% of semen samples. Interestingly, the consecutive testing of individuals for KHSV DNA by PCR over several weeks revealed inconsistent results, suggesting that studies collecting samples upon just one occasion may produce false-negative results (Pauk *et al*., 2000).

Contradictory data concerning the sites of KSHV infection may be due to contamination of the PCR assays used to detect KSHV DNA. A study conducted by Pellett *et al*. of the PCR techniques used in five laboratories to detect KSHV in semen, highlighted high rates of contamination during PCR experiments (Pellett *et al*., 1999). All five laboratories analysed positive and negative controls and semen samples from the same individuals in parallel. Three laboratories produced positive results for negative controls, with contamination primarily occurring in experiments that include a nested PCR step (utilising two sets of primers). Low copy numbers of KSHV DNA in positive samples may

account for inconsistent results, in addition to possible contamination during sample collection and PCR analysis (Pellett *et al*., 1999).

In addition to the method of PCR for detection of fragments of the KSHV genome, immune serological assays were developed to aid diagnosis of KSHV infection, with less risk of contamination and subsequently more reliable results. A commonly used immunofluorescence assay measures the binding of anti-KSHV antibodies from test serum to KSHV-infected reactivated BCBL-1 cells (murine antibody-enhanced IFA). Binding is detected by mouse anti-human human IgG monoclonal antibodies and fluorescently tagged secondary antibodies. Of 91 American and 28 African individuals with KS, anti-lytic antibodies to KSHV were identified in the serum of 97% of individuals by this method. However, the detection of anti-latent antibodies was inconsistent (Lennette *et al*., 1996). 93% of homosexual HIV-positive men from an American cohort tested positive for KSHV, in comparison to 23% of HIV-positive heterosexual intravenous drug users and 21% of HIV-positive women. These data correlate with current opinion that the risk of KSHV transmission is relatively low, but that it rises with HIV-infection and sexual practises. In agreement with current estimates that KSHV seroprevalence is higher in central sub-Saharan Africa than in the USA, Lennette *et al*. estimated that KSHV seroprevalence ranged from 32% in Zimbabwe, to 100% in the Ivory Coast, in comparison to only 18-28% of individuals in the USA, from a study of healthy volunteers (Lennette *et al*., 1996).

Simpson and colleagues used an enzyme-linked immunosorbent assay (ELISA)-based technique to detect KSHV seroprevalence (Simpson *et al*., 1996). A recombinant KSHV ORF65 protein was used for the detection of anti-KSHV antibodies in the sera of KS patients, identifying them in between 81 and 94% of cases. In comparison, detection of anti-KSHV antibodies by a rabbit antibody-linked IFA, similar to murine antibody-enhanced IFA, produced similar results. However, detection of KSHV DNA in peripheral blood

mononuclear cells by PCR was not as accurate, and detected only half of the ELISA and IFA-seropositive cases (Simpson *et al*., 1996). Using the assay developed by Lennette *et al*. to confirm KSHV seronegativity in a cohort of individuals, and another existing assay, LANA-IFA (detecting anti-LANA antibodies in sera by characteristic nuclear punctuate staining of sera-treated BCBL-1 cells), to confirm KSHV infection of KS patients and HIV+/- homosexual men, Martin *et al*. developed an assay with increased sensitivity for detection of KSHV (Martin *et al*., 2000). An enzyme-based immunoassay for the binding of anti-KSHV antibodies in sera to lysed KSHV virions was highly specific and sensitive for KSHV, based on correlations between samples deemed KSHV-positive and negative by the two older methods (Martin *et al*., 2000). A comprehensive analysis of common techniques for detecting KSHV, and commercial assay, demonstrated that LANA-IFA has high specificity for KSHV but low sensitivity, whereas two commercial assays showed the opposite (Nascimento *et al*., 2007). The test with the highest specificity and sensitivity for KSHV was a whole-virus ELISA (Nascimento *et al*., 2007), with similar methods to the assay developed by Martin *et al*. Taken together, these data show that no one method of KSHV detection is infallible, and in addition to controls, at least two methods of diagnosis must be used.

The KSHV genome is moderately conserved between individuals, with the exception of some nucleotide polymorphisms. However, there is high variation between the *ORF K1* and *ORF K15* genes, thought to be due to divergence between populations (Zong *et al*., 2007). Zong and colleagues examined the constant region of the KSHV genome in 150 samples from KSHV-positive individuals to determine KSHV genomic variation between populations (Zong *et al*., 2007). Excluding the hypervariable *ORF K1/K15* genes, the samples could be divided into distinct genotypes/subtypes. Six genotypes were prevalent in sub-Saharan Africa (B, N, Q, R, F and G), two in aboriginal populations from the Pacific rim

region (D and E), and three in Eurasion populations (A/C, J and K or M) (Zong *et al*., 2007). Importantly, only one KSHV genotype could be identified in any individual. Variability in the KSHV unique regions due to nucleotide polymorphisms means that there is also significant variation within each genotype. Investigating other disease tissues in which KSHV had been reported, for example multiple myeloma, revealed contamination with DNA from the BCBL-1 cell line, with the KSHV genome matching the specific BCBL-1 KSHV genotype (Zong *et al*., 2007). Thus, contamination of clinical samples with KSHV DNA from other sources, and the reliance of PCR for only a small fragment of KSHV *ORF26* contributed to false positive results.

Though KSHV may not be transmitted via genital secretions, rather by saliva, individuals infected with other sexually transmitted infections (STIs) in addition to HIV, are at higher risk of KSHV infection (Kedes *et al*., 1996). These observations indicate a sexual mode of transmission. HIV-negative syphilis patients are at higher risk (8%) of KSHV infection than the general population (1%), with a higher risk associated with homosexual individuals (27%) over heterosexual (6%) (Kedes *et al*., 1996). Blackbourn *et al*. revealed an association between KSHV seroprevalence (quantified by murine antibody-enhanced IFA) and the number of sexual partners (Blackbourn *et al*., 1999). HIV-positive and negative homosexual men had a higher risk of KSHV infection that was associated with oral and/or anal sexual intercourse, but did not correlate with HIV infection (Blackbourn *et al*., 1999). Pauk and colleagues reported similar findings (Pauk *et al*., 2000). Analysing a cohort of HIV-seronegative homosexual men, both KSHV-positive and negative, for risk factors for KSHV infection, revealed a positive correlation between KSHV infection and age, number of male sexual partners, HIV-positive sexual partners, STIs and having a partner with KS (Pauk *et al*., 2000).

1.3.9. The immunobiology of KSHV

KSHV encodes several genes that serve to regulate the host immune response upon infection. KSHV *K14* encodes the vOX2 protein with known granulocyte-regulatory capacity (Rezaee *et al.*, 2005). vOX2 will be discussed in section 1.6.1 and is the subject of this thesis.

In addition, the KSHV genome expresses two genes, *K3* and *K5* that encode modulator of immune recognition (MIR)1 and MIR2 proteins with the ability to downregulate major histocompatibility complex I (MHCI) on the surface of the infected cell. Both MIRs can downregulate the surface expression of MHCI, though only MIR2 downregulates CD86, intercellular adhesion molecule 1 (ICAM-1) (Tomescu *et al.*, 2003) and platelet/endothelial cell adhesion molecule (PECAM) (Mansouri *et al.*, 2006). MIR1 and MIR2 ubiquitylate lysine residues on the cytoplasmic tails of CD86 and MHCI, thus inducing endocytosis and targeting these proteins for degradation (Coscoy *et al.*, 2001). CD80 is not normally endocytosed by MIR1 or MIR2, but the addition of three lysine residues to the cytoplasmic tail of a mutant CD80 targets the protein for degradation by the MIRs. The MIRs express Zn fingers of the PHD family on their cytoplasmic tails, similar to the RING fingers found in cytosolic E3 ubiquitin (Ub) ligases. These Zn E3-Ub ligase-like regions direct E2 Ub-conjugating enzymes to MHCI and CD86, thus resulting in ubiquitylation, endocytosis and subsequent degradation of the proteins (Coscoy *et al.*, 2001). Targeting of the MHC-antigen presentation pathway by viruses is discussed further in section 1.8.2.

Downregulation of MHC can lead to targeting by NK cells. KSHV bypasses this by downregulating ligands of activatory receptors on NK cells (Thomas *et al.*, 2008). MIR2 targets MHC class I-related chains (MIC)A and B ligands for NKG2D, and activation-induced C-type lectin (AICL), a ligand for NKp80, for ubiquitylation, thus reducing NK-

mediated lysis of infected cells (Thomas *et al.*, 2008). The KSHV lytic cycle gene *ORF37* encodes the lytic shutoff and exonuclease (SOX) protein which shuts off host cell gene expression. So in contrast to the MIRs which target specific cell surface proteins that signal to immune mediators such as T cells, SOX causes general suppression of gene expression by enhancing the degradation of cellular mRNA (Glaunsinger & Ganem, 2004).

Another cellular pathway hijacked by KSHV is the complement cascade. The complement system is a cascade of events triggered by the binding of complement proteins to antibody-antigen complexes (classical pathway), a lectin-bound pathogen (lectin pathway), or by direct interaction of complement components with the surface of a microorganism (alternative pathway). The activation of the pathway by any of the three interactions ultimately leads to C3 convertase, bound to the pathogen, which in turn cleaves and activates the C3 component. C3 in its variable cleaved forms enhances the innate immune response by opsonising the pathogen, thus targeting it for destruction by phagocytes, and by promoting inflammation (Murphy, 2008). KSHV complement control protein (KCP), a cell-surface lytic cycle protein encoded by *ORF4*, contains four complement control protein (CCP) domains - a formation that is shared by all other known regulators of the complement pathway - and shares homology with host complement regulators such as decay-accelerating factor (DAF) (Spiller *et al.*, 2003). KCP enhances the degradation of classical C3 convertase, and mildly accelerates the decay of alternative C3 convertase, in addition to aiding the degradation of C3 convertase products C3b and C4b, thus suppressing complement regulation of KSHV infection *in vivo* (Spiller *et al.*, 2003).

Furthermore, one of the most important cellular responses to viral infection, the IFN pathway, is also targeted by KSHV. KSHV encodes four homologues of cellular interferon regulatory factors (IRFs), transcription factors involved in initiating IFN gene expression. Cellular IRFs contribute to an anti-viral state by participating in the transcription of IFN and

IFN-responsive genes (reviewed by Areste and Blackbourn, 2009). KSHV vIRF-2 directly inhibits the activity of cellular IRF-3, and enhances its degradation, thereby disrupting the IFN signalling pathway (Areste *et al*., 2009).

Other putative KSHV immunomodulatory mechanisms have been identified **(Figure 1.4)** and the reader is referred to a detailed discussion by Aresté and Blackbourn, 2009 (Areste & Blackbourn, 2009).

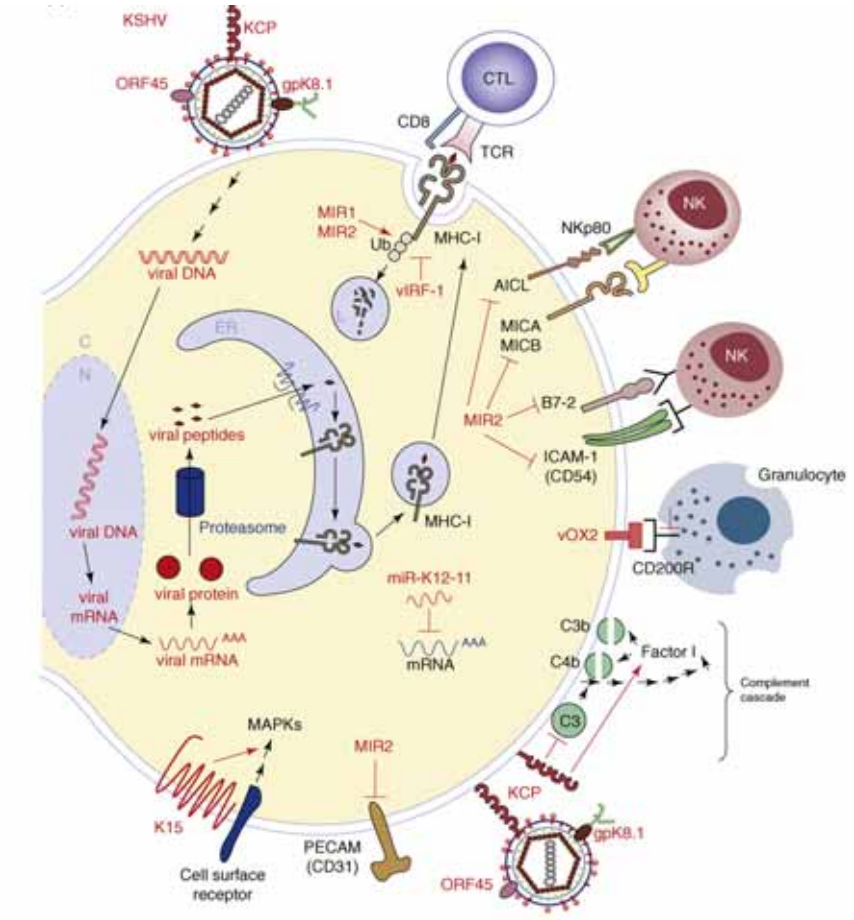

Figure 1.4. Immunobiology of KSHV. KSHV is known to infect endothelial cells, B cells, macrophages and DCs. Known immunomodulatory pathways targeted by KSHV upon infection of cells are illustrated, including downregulation of MHC by MIR1 and MIR2, concurrent downregulation of NK receptor ligands, and the suppression of granulocyte activity by KSHV vOX2. This Figure is reproduced from Aresté and Blackbourn, 2009.

1.4. *Rhesus rhadinovirus (RRV)*

Shortly after the identification of KSHV in human tissue by Chang and colleagues (Chang *et al*., 1994), a rhadinovirus (RRV) with homology to KSHV was isolated from an Asian Old World primate, the rhesus macaque (*Macaca mulatta*) (Desrosiers *et al*., 1997). Members of the macaque colony showed antibody reactivity to HVS. Fibroblasts isolated from these animals developed cytopathic effect (CPE) during culture, and the virion DNA isolated from these cells induced CPE in transfected recipient cells (Desrosiers *et al*., 1997). RRV is a member of the genus rhadinovirus of the subfamily gammaherpesvirinae (Davison *et al*., 2009). The rhadinoviruses are grouped into two distinct lineages, RV1, and RV2. KSHV (from humans), retroperitoneal fibromatosis herpesvirus strains RFHVMm and RFHV Mn (from two macaque species) and *Chlorocebus* rhadinoviruse ChRV1 (from the African green monkey) are grouped into RV1 (Rose *et al*., 1997). RRV (from macaque) and ChRV2 (from African green monkey) cluster within the RV2 group by nucleotide and amino acid identity and CG content (Greensill *et al*., 2000). The lack of a human virus in the RV2 group has led to a search for the missing member, though none has been identified so far.

The genes of one RRV isolate (H26-95) encoding DNA polymerase and glycoprotein B were sequenced and compared to homologous regions of other members of the rhadinovirus genus (Desrosiers *et al*., 1997). The glycoprotein B shared 65.5% amino acid identity with KSHV gB, and 54.4% identity with HVS gB. RRV H26-95 also appeared to encode some genes not conserved across the rhadinovirus genera, but that are present in KSHV. One example is the RRV homologue of human IL-6, sharing 18.5% amino acid identity with KSHV vIL-6 (Desrosiers *et al*., 1997).

Searles and colleagues examined another RRV isolate, 17577 (Searles *et al*., 1999). These authors described a virus with 79 ORFs, nearly all shared with KSHV, though 12 ORFs did not have homologues in the HVS genome. A comparison of the newly identified

RRV 17577 strain with RRV H26-95, revealed several base changes resulting in amino acid substitutions, though most changes appear to be silent mutations (Searles *et al*., 1999). However, some genes such as *ORF4* differ between the strains and exist as isoforms due to alternative splicing (Mark *et al*., 2007).

An important parallel between KSHV and RRV is the presence of genes encoding vIRFs. KSHV encodes four vIRFs, whereas RRV encodes eight, four of which show high sequence similarity to the other four, suggesting a gene duplication event. KSHV vIRF1, encoded by ORF *K9*, shares some homology with five of the RRV vIRFs (Searles *et al*., 1999). However, for the purposes of this project, it is the viral homologues of CD200 encoded by both KSHV (*K14*) and RRV (*R14*) that are of most significance, and will be discussed in Sections 1.6.1 and 1.6.2.

1.5. *CD200*

1.5.1. The identification of CD200 and its receptor(s) in rodents

CD200 is a type I transmembrane glycoprotein and a member of the immunoglobulin superfamily (IgSF). CD200 contains two IgSF domains, regions predicted to interact with either cell surface molecules or soluble factors, and thus initially indicating the existence of a CD200 receptor (CD200R). The short cytoplasmic tail of CD200 lacks any known signalling motifs, further supporting the concept that CD200 functions as an extracellular receptor ligand.

The extracellular domain of rat *CD200* (*rCD200)* was fused in-frame to domains 3 and 4 of rat *CD4*. The resulting soluble recombinant protein ligated a specific receptor on rat macrophages. Ligation of rCD200 with the rat CD200R (rCD200R) was inhibited by an epitope binding at the N-terminal domain of the putative receptor, thus identifying a likely site of interaction (Preston *et al*., 1997). When rat peritoneal macrophages were treated with

pervanadate (an irreversible tyrosine phosphatase inhibitor), an anti-phosphotyrosine band associated with immunoprecipitated rCD200R was isolated from the cellular lysates (Preston *et al*., 1997). Thus, macrophage tyrosine kinases phosphorylate intracellular rCD200R tyrosine residues, and subsequent dephosphorylation is inhibited by pervanadate (Wright *et al*., 2000). rCD200 is expressed in several tissues, including vascular endothelium (Ko *et al*., 2009), DCs, B cells, thymocytes, neurons, lymphocytes (Barclay, 1981) and macrophage-like cells infiltrating the central nervous system (CNS) (Matsumoto *et al*., 2007). The rCD200R is expressed on DCs, microglia (Wright *et al*., 2000) and monocytes/macrophages (Dick *et al*., 2001).

Chen and colleagues demonstrated that cells derived from mice pre-immunised with allogeneic DCs, expressed a gene showing homology to *rCD200* (Chen *et al*., 1997). The gene was believed to encode a 25kDa protein, similar to rCD200, though high glycosylation of rCD200 renders the protein approximately 47kDa in weight. The amino acid sequence of the putative murine CD200 (mCD200) protein shared 92% identity with human CD200 and 77% with rCD200. Regions with highest similarity are the transmembrane and cytoplasmic domains. Conserved residues were identified in the disulphide bonds between Ig-like domains and amongst N-glycosylation sites. Neither the human nor the rodent CD200 proteins contain known signalling sequences in their cytoplasmic domains, suggesting a requirement for interaction with a specific signalling receptor (Chen *et al*., 1997). mCD200 is expressed by neurons and endothelial tissue of the CNS (Koning *et al*., 2009), B cells, DCs, and endothelial of the spleen (Hoek *et al*., 2000).

The murine CD200R (mCD200R1) was cloned and sequenced, revealing two IgSF domains, similar to mCD200, several N-linked glycosylation sites, and a single transmembrane domain (Wright *et al*., 2000). However, the receptor has a longer cytoplasmic domain than its cognate ligand, with two conserved tyrosine residues, and a

third located within an NPXY motif. NPXY can bind adaptor molecules, thus indicating an intracellular signalling role for the mCD200R1 (Wright *et al*., 2000). mCD200R1 is expressed by macrophages, DCs, mast cells, T cells, granulocytes and monocytes (Wright *et al*., 2003) and microglia (Hoek *et al*., 2000). It is also found in bone marrow, lymph nodes, spleen and lung tissues, with a similar expression pattern to human CD200R (Wright *et al*., 2003).

Wright and colleagues identified three mCD200R-like family members in mice, sharing homology with mCD200R1 (Wright *et al*., 2003). These homologues bind DAP12, an activatory adaptor protein, probably by a positively charged lysine in their transmembrane domains, suggesting that the mCD200R family members play a contrasting role to the inhibitory mCD200R1. In mouse mast cells, the genes encoding the homologues are paired with the gene encoding DAP12 on chromosome 16. The homologues have short, apparently non-signalling cytoplasmic tails, though may bind as yet unidentified ligands (Wright *et al*., 2003).

Sequencing of mCD200R1 by Gorczynski *et al*., confirmed that there is a family of four receptors sharing considerable homology in their transmembrane regions, but expressing distinct N-terminal domains (Gorczynski *et al*., 2004b). The genes encoding mCD200R1-4 are clustered on chromosome 16, in the same region as *mCD200* (Gorczynski *et al*., 2004b). The mCD200R subtypes have an alternative nomenclature: mCD200R2 (mCD200RLc), mCD200R3 (mCD200RLb), mCD200R4 (mCD200RLa), but will be referred to by their numerical code in this thesis. Their short cytoplasmic tails suggest that mCD200R2-4 may signal in a different manner, or may be functionally inactive (Gorczynski *et al*., 2004b). The four receptor subtypes appear to be differentially distributed, with mCD200R1/4 localising predominantly to thymus and PBMCs, and CD200R2/3 expressed in bone marrow (Gorczynski *et al*., 2004a).

Voehringer *et al*. identified a fifth member of the mCD200R family by a BLAST search of the NCBI database (Voehringer *et al*., 2004). The putative mCD200R5 (mCD200RLe) sequence matched part of two sequences entered into the NCBI database by other researchers, derived from non-obese diabetic (NOD) mice. However, Voehringer could not detect the mCD200R5 in tissue extracted from C57/BL6 mice (Voehringer *et al*., 2004). Using surface plasmon resonance (SPR) to measure binding affinities of mCD200:Fc for mCD200R1-5, Hatherley *et al*. demonstrated that mCD200 is not a ligand for mCD200R2-4 (Hatherley *et al*., 2005). Akkaya *et al*. analysed the expression of the mCD200R2-5 in 22 mouse strains, and demonstrated that mCD200R3/4 were expressed in the majority of the strains (20-21 of 22), whereas mCD200R2 was expressed in less than 50% of the strains (10 of 22). Interestingly, fragments of the gene encoding mCD200R5 were detected in the strains not expressing mCD200R2. All of these mouse strains expressed mCD200R1, though two different sequences were found, differing by seven amino acids (Akkaya & Barclay, 2009). Taken together, these data suggest that mCD200 is the cognate ligand of mCD200R1, and that the putative mCD200R1 homologues are not involved in mCD200-mediated immunosuppression discussed in Section 1.5.3.

1.5.2. The identification of CD200 and its receptor in humans

By scanning the NCBI database with the sequence encoding rCD200R, Wright and colleagues identified a putative gene encoding the human CD200R (CD200R) (Wright *et al*., 2003). CD200R incorporates a single transmembrane domain and a large cytoplasmic tail containing three conserved tyrosine residues (**Figure 1.4**). It is a highly glycosylated type I cell surface glycoprotein that binds human CD200 (Wright *et al*., 2003). CD200R shares closest homology with human herpesvirus entry protein HveC, a protein that interacts with herpes simplex virus (HSV) envelope glycoprotein D, thus enabling viral entry into host

cells. Wright *et al*. also identified a homologue of the human *CD200R* gene, located on chromosome 3 and clustering with human *CD200* and *CD200R*, though the homologue appeared not to be expressed (Wright *et al*., 2003).

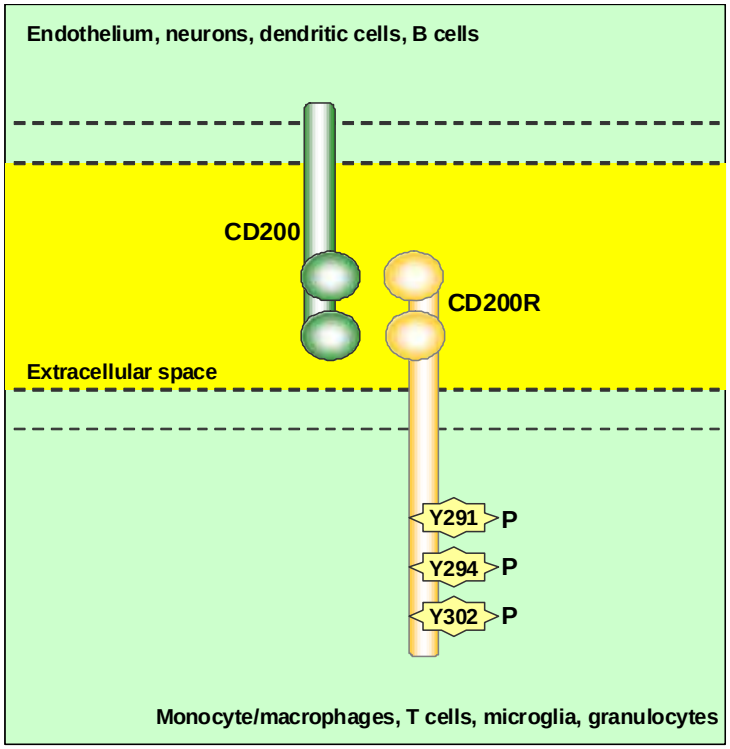

Figure 1.5 Illustration of the human CD200R and its cognate ligand, CD200. Both proteins traverse the cell membrane with a single transmembrane domain, and express two immunoglobulin superfamily-like domains extracellularly. CD200 has no known signalling domains, but the CD200R has three conserved tyrosine residues in its cytoplasmic tail through which it signals.

Vieites *et al*. also identified the *CD200R* on chromosome 3q13 by using a bioinformatics approach to compare the sequences of *rCD200R* and *mCD200R1* with the human genome (Vieites *et al*., 2003). They determined that the 52kb gene encoded a protein sharing 53% amino acid identity with rCD200R, and 52% identity with mCD200R1. Hydrophobicity studies of the putative gene product suggested that the hCD200R spans the plasma membrane, flanked by putative long N-terminal and short C-terminal tails, and comprises

nine potential N-glycosylation sites and one O-glycosylation site, in addition to the presence of a cleavable signal peptide (Vieites *et al*., 2003). Two isoforms of *CD200R* were transcribed, due to the insertion of exon 5, one encoding a cell surface receptor, and one a truncated soluble protein. Each transcript was also alternatively spliced at exon 2 resulting in the generation of four different CD200R isoforms. mRNA transcripts for the four *CD200R* isoforms were identified in the thymus, spleen, liver and placenta (Vieites *et al*., 2003).

Wright *et al*. confirmed that human CD200 bound to CD200R with a binding affinity of ~0.5μM, and its specificity was determined by blocking with an anti-CD200R antibody (Wright *et al*., 2003). CD200 appears to have a wide distribution throughout the body, and was detectable in several endothelia including kidney glomeruli and tonsil vascular endothelium, peripheral nerve bundles and central nervous tissue, particularly the cerebellum (Wright *et al*., 2001). CD200 is expressed across the brain, particularly upon neuronal cell bodies and axons, but not by astrocytes or microglia (Koning *et al*., 2009). In contrast, CD200R expression in the CNS is restricted to microglia and PBMCs (Koning *et al*., 2009). CD200R is also expressed by T cells, neutrophils, monocytes and basophils, and mRNA transcripts of *CD200R* were identified in bone marrow, lymph nodes, spleen and lung tissues (Wright *et al*., 2003).

The high number of glycosylation sites on CD200 results in an unusually large sugar content, amounting to 70% of the weight of the protein (Wright *et al*., 2000). Extensive glycosylation dictates that the production of CD200 for use in biological assays must be carried out in eukaryotic cell lines, and that the protein may be generated in different forms, dependent on the level of glycosylation and resultant protein folding (reviewed by Walsh and Jefferis, 2006).

1.5.3. Immunosuppressive activities of CD200 *in vivo*

Evidence for the *in vivo* role of CD200 was demonstrated by Hoek and colleagues, who emphasised the importance of CD200 to immune regulation by deleting *mCD200* in mice (Hoek *et al*., 2000). The expression of mCD200R1 increases in *CD200*$^{-/-}$ mice, with a simultaneous elevation in activated macrophages, and aggregates of activated microglia (the macrophages of the CNS). Facial nerve transection results in microglial activation in healthy animals but this activation is markedly accelerated in *mCD200*$^{-/-}$ mice, and is mirrored in *mCD200*$^{-/-}$ mice with experimental autoimmune encephalomyelitis (EAE) (Hoek *et al*., 2000). Increased incidence and more severe pathology of collagen-induced arthritis (CIA), a murine model of rheumatoid arthritis (RA), are also evident in *mCD200*$^{-/-}$ mice. These data indicate a hyperactivation of T lymphocytes, principal initiators of EAE and CIA, in *mCD200*$^{-/-}$ animals (Hoek *et al*., 2000). Concurring with these data, blocking the interaction between mCD200 and mCD200R1 increased EAE pathology (Wright *et al*., 2000). EAE, a murine model of multiple sclerosis, is characterised by demyelination occurring due to microglial activation and macrophage-containing infiltrates traversing the blood brain barrier. A more severe pathology developed in animals treated with an anti-mCD200R1 antibody, thus blocking mCD200-mCD200R1 interaction and inhibiting the mCD200-mediated downregulation of macrophage activity (Wright *et al*., 2000). Data published by Rijkers *et al*. differ slightly (Rijkers *et al*., 2007). These authors found no alteration in the number of myeloid cells in 14 month old *mCD200*$^{-/-}$ animals, and only 25% of knockout mice had an increased number of circulating and splenic myeloid cells at 8-12 weeks of age (Rijkers *et al*., 2007).

mCD200-mCD200R1 interaction controls macrophage activity *in vivo*, consequently preventing severe inflammatory responses to infection and thus reducing pathology. Murine alveolar macrophages exist in an antigenic environment and express higher basal levels of

mCD200R1 than myeloid cells in other anatomical sites (Snelgrove *et al*., 2008). Alveolar macrophages rapidly upregulated mCD200R1 expression in response to stimulation by IL-10 and transforming growth factor-β (TGFβ) and during influenza infection. Epithelial cells from the alveolar space expressed mCD200, and induced excessive cytokine secretion from *mCD200R1*$^{-/-}$ alveolar macrophages in comparison to those from wild-type (WT) mice. Though the expression of mCD200 by alveolar epithelial cells remained stable throughout influenza infection in WT mice, the level of mCD200 expressed by $CD4^+$/$CD8^+$ lung and lymph node T cells increased. Interestingly, T cells at the site of infection appeared to lose mCD200 expression. When *mCD200* was deleted from the animals, a greater pathology and severity of disease occurred, and was associated with greater inflammation and macrophage and T cell activity, though viral titres were similar between WT and *mCD200*$^{-/-}$ mice. Blocking mCD200-mCD200R1 interaction with an antibody provoked a similar response to infection. Conversely, administering soluble mCD200:Fc to WT animals reduced disease severity and infiltrating numbers of T cells (Snelgrove *et al*., 2008).

mCD200 is expressed by microglia, neurons, and neural and vascular endothelial cell populations inhabiting the retina. Murine experimental autoimmune uveoretinitis (EAU) is characterised by infiltrating $CD4^+$ T cells, microglial activation, and consequent damage to the retina and photoreceptors (Broderick *et al*., 2002). *mCD200*$^{-/-}$ mice developed more severe EAU than WT mice, and had enhanced numbers of infiltrating macrophages, though there was a disease incidence of 100% for both groups (Broderick *et al*., 2002). Increased macrophage infiltration into the retina of *mCD200*$^{-/-}$ mice suggested an interaction between mCD200R1-expressing macrophages and mCD200-expressing endothelial cell populations, thus preventing excessive macrophage infiltration of the retina in WT animals (Broderick *et al*., 2002). The role of CD200/CD200R interaction may be more significant in the CNS in

contrast to the rest of the body, because cell infiltration and inflammatory responses must be minimal in order to preserve the isolation of the CNS from the periphery.

1.5.4. Structure and function of soluble recombinant CD200 proteins

Much experimental data on the properties and functions of CD200 are based on observations of the activities of CD200:Fc fusion proteins (**Figure 1.5**). The fusion of proteins to the Fc domain of human immunoglobulin G1 (IgG1) molecule is used therapeutically to confer a longer half-life on the protein (Kamei *et al*., 2005). Fc-fusion proteins have a longer half-life than the native protein, but can have reduced biological activity when both are compared at the same concentration *in vivo* (Harris *et al*., 2002). The binding of Fc to the neonatal Fc receptor (FcRn) in endosomal compartments results in increased Fc recycling back to the plasma membrane and thus reduced lysosomal degradation. Fc-FcRn binding is enhanced at lower pH (5/6) in the endosome and reduced at a higher pH of 7.4 at the cell surface. Therefore, engineered Fc fusion proteins must exhibit these preferential binding properties in order to maximise the release of Fc from FcRn at the cell surface. Employment of the Fc method renders frequent drug administration unnecessary, thus reducing possible toxicity from high concentrations, and is useful for examining protein activity in biological research (Kamei *et al*., 2005).

Gorczynski and colleagues examined the role of mCD200:Fc in murine CIA. CIA was markedly inhibited by either repeated infusions of mCD200:Fc fusion protein (Gorczynski *et al*., 2001) or an anti-mCD200R1 monoclonal antibody (mAb) (Gorczynski *et al*., 2002a). mCD200:Fc reduced cytokine secretion, including TNFα and IFNγ. TNFα is the primary cytokine associated with rheumatoid arthritis in humans and is indicative of CIA (Gorczynski *et al*., 2001). mCD200:Fc-mediated inhibition of CIA pathology was associated with reduced expression of IL-1β, TNFα and IL-10 mRNA transcripts in the mCD200R1-

expressing synovium, without affecting the numbers of circulating T cells, indicating a specific role for mCD200, rather than a general suppression of inflammation (Simelyte *et al*., 2008). mCD200:Fc also reduced circulating anti-collagen antibodies in collagen-immunised mice, and increased specific antibody subtypes, eg. IgG2b (Gorczynski *et al*., 2001). Subsequent investigations by this group indicated that targeting the mCD200R1 prevented CIA-onset (Gorczynski *et al*., 2002a). They also demonstrated symptom-alleviation of arthritic mice by administration of mCD200:Fc, and by mCD200R1 ligation (Gorczynski *et al*., 2002a).

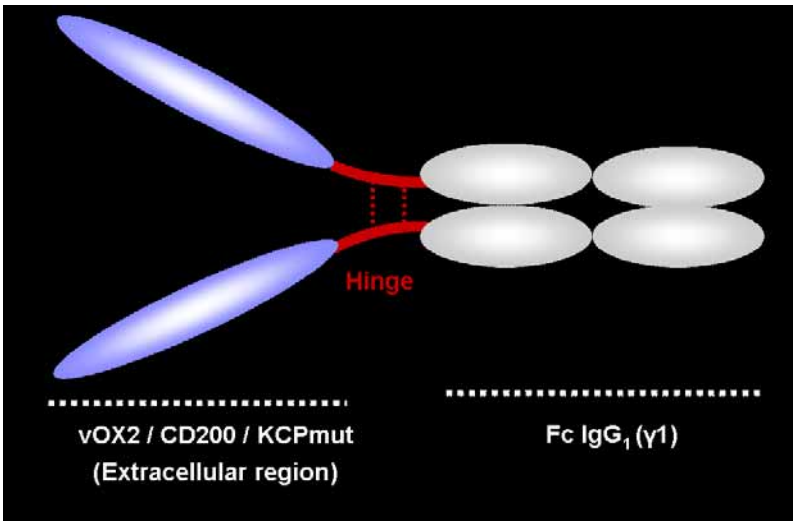

Figure 1.6 Cartoon illustrating the proposed structure of soluble Fc fusion proteins. The extracellular region of the native protein (ie. vOX2, CD200 or a control, mutant KSHV complement control protein, KCPmut) was fused in-frame with the Fc region of human IgG1 (including the IgG1 hinge region). Upon expression of the protein in a 'producer' cell, the Fc-protein is secreted from the cell and forms a dimeric structure in solution.

Cherwinski and colleagues demonstrated mCD200-mediated inhibition of an *in vivo* model of allergy (Cherwinski *et al*., 2005). The induction of passive cutaneous anaphylaxis in mice,

by injecting IgE from a sensitised mouse into another to induce type I hypersensitivity, was inhibited by ligation of the mCD200R1 with an anti-mCD200R1 antibody, in a dose dependent manner (Cherwinski *et al*., 2005).

mCD200:Fc administration also extends the survival of allografts *in vivo* (Gorczynski *et al*., 1999). Skin and renal allograft survival time was extended significantly in mice treated with mCD200:Fc, but was reduced in mice who received anti-mCD200 antibodies (Gorczynski *et al*., 1999). mCD200:Fc and an anti-mCD200R1 antibody also prolonged the survival of rat islet xenografts in mice, grafted in response to streptozocin-induced diabetes (Gorczynski *et al*., 2002b). The observed immunosuppression by mCD200:Fc was blocked by simultaneous infusion of anti-mCD200 antibodies. CTL activity decreased upon mCD200:Fc and anti-mCD200R1 administration, along with the production of IFNγ and IL-2 (Gorczynski *et al*., 2002b).

Taken together, the current literature shows that the ligation of the CD200R by its cognate ligand suppresses the immune response. When *mCD200* is deleted, inflammation and disease pathology are enhanced (Hoek *et al*., 2000; Broderick *et al*., 2002 and Snelgrove *et al*., 2008). Stimulating CD200R by ligating with its ligand has the opposite effect, reducing inflammation (Gorczynski *et al*., 2001; Gorczynski *et al*., 2002a) and suppressing the immune response to allogeneic stimulation (Gorczynski *et al*., 1999). Thus, the expression of homologous proteins by viruses would be presumed to dampen the immune response to infection, and will now be discussed.

1.6. *Viral homologues of CD200*

1.6.1. KSHV vOX2 (*ORF K14*)

KSHV vOX2, encoded by ORF *K14*, a lytic cycle gene, is expressed at the cell surface as a type I transmembrane protein. It is a glycosylated protein having five potential N-

glycosylation sites positioned in the extracellular region. N-glycosylation increases vOX2 protein size from approximately 40kDa to the 55kDa mature form (Chung *et al*., 2002). vOX2 and CD200 share approximately 36% protein identity. vOX2 is weakly expressed on the surface of JSC-1 cells (a primary effusion lymphoma cell line) latently infected with KSHV and EBV, and its expression markedly increases during lytic replication induced by TPA (Chung *et al*., 2002).

KSHV RTA appears to be crucial for the lytic replication of KSHV, and also regulates vOX2 gene expression (Zhang *et al*., 2005). Zhang *et al*. examined the possible mechanisms underlying RTA regulation of vOX2 gene expression (Zhang *et al*., 2005). The vOX2 promoter incorporates an interferon-stimulated response element (ISRE)-like domain. ISREs bind IRFs, a family of transcription factors, by a conserved N-terminal DNA-binding domain. RTA shows specificity for the vOX2 ISRE-like sequence and binds directly; this binding is inhibited by deletions in the RTA activation domain. The interaction between the vOX2 ISRE-like domain and RTA may be explained by a low sequence similarity between RTA and human IRF DNA-binding domains that bind to ISREs. These data suggest that RTA regulates the vOX2 promoter by the ISRE-like domain. Several other ISRE-containing genes in the KSHV genome may also be regulated in a similar manner by RTA, including vIL-6 (Zhang *et al*., 2005).

Though CD200 has been studied extensively, vOX2 has received less attention in the literature. However, Rezaee and colleagues described the inhibitory action of vOX2 on human neutrophils, phagocytic cells of the immune system (Rezaee *et al*., 2005). These authors created a vOX2 fusion protein by fusing extracellular *vOX2* in-frame with the Fc domain of human IgG1, and expressed the soluble protein in a Chinese Hamster Ovary (CHO) cell line for large-scale production. vOX2:Fc significantly reduced neutrophil oxidative burst induced by opsonised *Escherichia coli* (*E. coli*) in comparison to human

IgG1, though did not affect the ingestion of fluorescent *E. coli* by these cells (Rezaee *et al*., 2005).

Rezaee and colleagues defined a possible mechanism for the inhibition of neutrophil activity by vOX2:Fc (Rezaee *et al*., 2005). Upon stimulation by recombinant IFNγ, U937 monocytic cells generated the cytokine IL-8, a neutrophil chemoattractant. Incubating stimulated U937 cells with vOX2:Fc downregulated IL-8 production, thus demonstrating an indirect regulatory mechanism to control neutrophil activity. Additional inflammatory cytokines generated by stimulated macrophages, including IL-1β, IL-6, TNFα and macrophage inflammatory proteins were not affected, indicating that vOX2 specifically regulates IL-8 production (Rezaee *et al*., 2005).

The *in vivo* regulation of neutrophil activity by vOX2:Fc was demonstrated in the murine carrageenan footpad model, a model of acute inflammation. The inoculation of BALB/c mice with carrageenan, a seaweed extract, induced an acute neutrophil-driven inflammation measured as footpad thickness, that was significantly reduced by pre-treatment with vOX2:Fc, in comparison to human IgG (Rezaee *et al*., 2005).

Foster-Cuevas *et al*. examined the putative interaction between soluble vOX2 and human CD200R (Foster-Cuevas *et al*., 2004). Soluble vOX2, created by fusing the extracellular region of vOX2 to domains 3 and 4 of rat CD4, bound CD200R with an almost equal affinity to CD200. The interaction between surface vOX2 or CD200, and CD200R, reduced TNFα production by moderately activated macrophages, indicating an immunoregulatory role for vOX2 when expressed at high concentrations during lytic replication of KSHV (Foster-Cuevas *et al*., 2004).

Shiratori and colleagues provided evidence of an interaction between vOX2 and the human CD200R on other cells of the immune system (Shiratori *et al*., 2005). Human CD200R is highly expressed on basophils, a member of the granulocyte family. Ligation of

CD200R with either CD200 or vOX2 expressed on B lymphoblastoid cells inhibited basophil activation by FcεRI (Shiratori *et al*., 2005). Further evidence for vOX2- and CD200-mediated suppression of the immune response comes from studies of natural killer (NK) cells. CD200-expressing cells and reactivated KSHV-infected BC1 cells, presumed to be expressing vOX2, inhibited the lytic activity of CD200R-expressing NK cells, and their production of IFNγ (Shiratori *et al*., 2005).

Chung *et al*. examined the *in vitro* activities of soluble vOX2 on myeloid cells and concluded that vOX2:Fc exerts pro-inflammatory activities (Chung *et al*., 2002). These data contradict those of Rezaee *et al*. (2005) and Foster-Cuevas *et al*. (2004). PBMCs from healthy individuals were treated with soluble human CD200 or vOX2 proteins, created by fusing the extracellular regions of vOX2 or CD200 to Glutathione S-transferase (GST). vOX2-GST induced IL-1β and TNFα production by PBMCs, specifically monocytes/macrophages, but CD200-GST exerted no stimulatory effects. vOX2-GST-induced cytokine secretion was increased upon IFNγ-stimulation, and it induced the production of IL-6 and monocyte chemotactic protein 1 (MCP-1). Native vOX2 expressed on a B cell line also increased cytokine secretion by U937 cells stimulated with IFNγ (Chung *et al*., 2002). These data appear incongruous with the large amounts of data generated on CD200 activity and function, as a viral homologue would be expected to be adapted by a virus for the purposes of immune suppression and therefore evasion and not immune activation.

Salata *et al*. engineered CD200R-positive, primary human monocyte-derived macrophage (MDM) cells to express full-length vOX2 tagged with haemagglutinin (HA) (Salata *et al*., 2009). When vOX2 was expressed by these cells, they secreted greater concentrations of pro-inflammatory cytokines, TNFα, IL-1β, IL-6 and IFNγ. However, upon stimulation of the vOX2-expressing cells by IFNγ, cytokine secretion was reduced in

comparison to control cells. Interestingly, CD200R mRNA transcript levels inversely correlated with those of the cytokines. The CD200R-negative THP-1 human monocytic cell line was engineered to express vOX2-HA, and differentiated into a macrophage phenotype, before co-culturing with CD200R-positive MDM cells. In both the presence and absence of IFNγ, vOX2-expressing THP-1 cells induced the secretion of IL-6 and TNFα from CD200R-positive MDM cells. CD200R mRNA expression levels were also reduced in the MDM cells co-cultured with vOX2-expressing THP-1 cells (Salata *et al*., 2009). The authors suggest that vOX2 favours an inflammatory state and downregulates its receptor, CD200R. vOX2 expression also led to increased phagocytic activity by the vOX2-MDM cells, though this was reversed upon treatment with IFNγ. Along with a decrease in CD200R expression, vOX2 also reduced the percentage of MHC-I and MHC-II-expressing MDM cells, though this phenomena was reversed slightly upon IFNγ-stimulation of the cells (Salata *et al*., 2009). These data, like those of Chung *et al*. are contradictory to the multitude of studies showing an anti-inflammatory role for CD200, and indicate that the role of vOX2 must be further elucidated.

1.6.2. RRV vOX2 (*ORF R14*)

RRV vOX2 is encoded by RRV ORF *R14*. The ORF is quoted as *R14* or *R15* by different authors; for the purposes of this thesis, the gene will be referred to as *R14*. It is a late lytic protein (Pratt *et al*., 2005). Langlais *et al*. initially described the structure and certain functions of RRV vOX2 (Langlais *et al*., 2006). Two sequenced RRV strains, H26-95 and 17577 are used by researchers. The two RRV vOX2 proteins have an identical amino acid sequence and therefore the protein encoded by both strains will be referred to as RRV vOX2. RRV vOX2 shares 30% protein identity with human CD200, and 28% identity with KSHV vOX2, and like these two proteins it contains Ig-like domains (Langlais *et al*., 2006). These

authors engineered an RRV vOX2:Fc-fusion protein, and deglycosylated it with *N*-glycosidase F, revealing a core protein size of 53kDa. The glycosylated RRV vOX2 protein existed in a dimeric form, similar to human CD200. Both RRV vOX2:Fc and human CD200:Fc proteins reduced TNF transcript and protein levels in THP-1 cells in response to IFNγ treatment (Langlais *et al*., 2006). MDM cultures prepared from RRV-negative rhesus macaques were incubated with RRV vOX2:Fc and human CD200:Fc proteins. Both proteins suppressed the basal secretion of TNF, though the RRV vOX2:Fc was more effective. Cell-surface and cytoplasmic RRV vOX2 were visualised by monoclonal antibody labelling and confocal microscopy in cells 52hrs post-infection with RRV. A secreted form of the protein was also isolated from the supernatants of infected cells (Langlais *et al*., 2006).

Thus, RRV vOX2 exists in two forms, a transmembrane, cell-surface protein, similar to KSHV vOX2 and CD200, but also as a truncated and probably secreted protein. Pratt and colleagues identified two splice variants of RRV vOX2, resulting from the bicistronic transcription of *R14* and downstream *ORF74*, encoding a viral GPCR (Pratt *et al*., 2005). Splicing of the biscistronic transcript generated a 2.1kb cDNA, encoding full-length RRV vOX2, with expression localised to the cellular membrane and cytosol of cells transduced with the 2.1kb transcript tagged with HA. They also identified a 1.7kb cDNA, localising predominantly to the cytosol, and present in the supernatant of CHO cells engineered to express the HA-tagged 1.7kb construct. Both isoforms of RRV vOX2 had a similar size of 40kDa, rather than the predicted 28kDa, possibly due to glycosylation. It could be presumed that the secreted form of RRV vOX2 has the same activity as the transmembrane protein, as only the extracellular domain of the protein (fused to human IgG1 Fc) has been examined functionally. However, the function of soluble RRV vOX2 has not been investigated. The binding affinity of RRV vOX2 for human CD200R has also not been elucidated.

1.6.3. Other viral homologues of CD200

Several other viruses encode viral homologues of CD200, including HHV-6 and 7, CMV, and myxoma virus (MV). HHV-6 and 7 encode CD200 homologues with the ability to bind to human CD200R (Shiratori *et al*., 2005), but their functions have not been elucidated. MV, lethal to European rabbits but causing a mild infection in American rabbits who have adapted to the virus, encodes a viral homologue of CD200, which will be referred to as MVvOX2 for clarity. MVvOX2 is encoded by the *M141R* ORF, and comprises a 21kDa protein, expressed on the plasma membrane of infected cells. It does not appear to be crucial for either viral infection or replication in the host, though the myxomatosis pathology is reduced in mice infected with a mutant MV virus lacking MVvOX2 (MVvOX2KO) (Cameron *et al*., 2005). Macrophage activity is enhanced in the absence of MVvOX2. These data suggest that an increased immune response in the absence of MVvOX2, as evidenced by increased T cell activity thus clearing viral infection, results in the attenuated pathology noted in MVvOX2KO-infected animals. PBMCs isolated from animals infected with MVvOX2KO generate higher concentrations of inducible nitric oxide synthase (iNOS), a marker of macrophage activation, than those from animals infected with wild-type MV. These data suggest that the expression of MVvOX2 dampens the activation of macrophages (Cameron *et al*., 2005). Later work by these researchers confirmed that iNOS expression was induced in murine macrophages infected with MVvOX2KO, along with transcripts for granulocyte-colony stimulating factor (G-CSF) and TNFα (Zhang *et al*., 2009). Increased TNFα transcripts and protein secretion were due to increased activity of the NF-κB transcription factor in the absence of MVvOX2 (Zhang *et al*., 2009). Thus, MVvOX2 suppresses macrophage activity, concurring with data for KSHV vOX2 (Rezaee *et al*., 2005) and CD200 (Broderick *et al*., 2002).

The English isolate of rat CMV (CMV-E) encodes a homologue of CD200, encoded by the ORF e127, that is absent from the Maastricht rat CMV isolate (CMV-M). The CMV-E vOX2 shares 56% protein identity with rat CD200, and 46% identity with human CD200. The viral gene was most likely derived from the rat genome, as it shows greater similarity with rat and mouse CD200, than KSHV and HHV-7 vOX2s (Voigt *et al*., 2005).

No other data concerning the function of viral homologues of CD200 have been published.

1.7. *Innate immune response*

The innate immune response does not recognise or 'remember' pathogens, but rapidly responds to all foreign bodies and microorganisms that traverse the external barriers. Initially the phagocytic myeloid cells, including macrophages and neutrophils, recognise pathogens and destroy them by the secretion of toxic substances such as reactive oxygen species and anti-microbial enzymes. Cells of the innate immune system recruit mediators of the adaptive immune response, a system that expands from birth and generates memory cells that respond to every microorganism that the body encounters- a process known as immunological memory (Murphy, 2008). Two major cell populations that mediate the innate immune response are neutrophils and monocytes, and will be discussed below.

1.7.1. Neutrophil function

Neutrophils are the largest subpopulation of granulocytes. They are phagocytic cells of the immune system, either exocytosing cytotoxic proteins in response to microbial infection (Faurschou & Borregaard, 2003), or generating anti-microbial reactive oxygen species (ROS) (Dahlgren & Karlsson, 1999).

Stimulation of neutrophils induces the migration of active cytosolic nicotinamide adenine dinucleotide phosphate (NADPH)-oxidase components, $p47^{PHOX}$, $p67^{PHOX}$ and $p40^{PHOX}$ (PHOX: phagocyte oxidase), to the plasma membrane. The interaction of phosphorylated $p47^{PHOX}$ with the cytoplasmic tail of membrane-bound $p22^{PHOX}$ ($p22^{PHOX}$ forms the cytochrome b_{558} complex with $gp91^{PHOX}$ at the plasma membrane) is the last stage of NADPH oxidase assembly (Dang et al., 2006). The assembled NADPH oxidase complex catalyses an oxidation of NADPH, forming $NADP^+$ and H^+, and transferring an electron to extracellular O_2 (Dahlgren & Karlsson, 1999). The 'priming' of neutrophils by GM-CSF and TNFα involves a partial phosphorylation of $p47^{PHOX}$, possibly explaining the subsequent rapid phosphorylation and formation of NADPH oxidase upon neutrophil stimulation.

fMLP, a bacterial peptide and neutrophil chemoattractant, acts upon fMLP GPCRs located on neutrophil secretory vesicles, to induce a rapid oxidative response. fMLP stimulation is limited in healthy individuals due to inaccessibility of the intracellular fMLP receptors. Superoxide burst is dependent upon the mobilisation of secretory vesicles (and therefore fMLP receptors) to the cell surface and can only be induced in 'primed' neutrophils (Karlsson *et al*., 1995). GM-CSF was used to 'prime' isolated neutrophils before fMLP stimulation in the following experiments.

Karlsson *et al*. examined the mechanisms underlying neutrophil oxidative burst induced by *E. coli* (Karlsson *et al*., 1995). The priming of neutrophils by Gram-negative bacteria appears to be due to LPS. LPS, a component of endotoxin isolated from the walls of Gram-negative bacteria, has the ability to induce inflammatory reactions, mediated by ligating with CD14, a glycosylphosphatidylinositol (GPI)-anchored protein, and with LPS-binding protein (LBP, present in mammalian serum). This interaction results in cell activation (Nick *et al*., 1996). Inhibiting LPS activity by polymyxin B prevents an *E. coli*/fMLP-induced superoxide burst from neutrophils. However, the role of LPS is uncertain,

as LPS-coated latex beads failed to prime neutrophils for fMLP activation (Karlsson *et al*., 1995). Neutrophils react to LPS, but in a more subdued manner in comparison with their response to fMLP. fMLP stimulation results in rapid adhesion of isolated neutrophils to endothelial cells, and though LPS causes a similar degree of activation and adhesion, the time course is significantly slower, suggesting induction of distinct signalling pathways.

It is unclear which intracellular signalling cascades are induced by LPS in neutrophils. LPS-stimulation results in the phosphorylation of p38 but not ERK or JNK MAP kinases approximately 20mins following stimulation, in a dose-dependent manner. p38 activation by LPS is independent of protein kinase C (PKC) phosphorylation, unlike stimulation by PMA (Nick *et al*., 1996). Ward *et al*. demonstrated that superoxide production by neutrophils in response to *E. coli*-stimulation can be enhanced by priming the neutrophils with TNFα or LPS, and can be reduced by administering a p38 inhibitor SB203580 (Ward *et al*., 2000).

The degranulation of neutrophils is another cytotoxic facility of these cells, and involves the release of antimicrobial enzymes. During each stage of neutrophil differentiation from the myeloblast precursor, distinct secretory granules are formed. The earlier azurophilic (or primary) granules contain MPO, whereas the later granules are peroxidase-negative. Upon stimulation of neutrophils by a bacterium, the azurophilic granules exocytose and release predominantly MPO and defensins (Faurschou & Borregaard, 2003). MPO reacts with H_2O_2 generated by the NADPH oxidase complex, and then oxidises chlorine, tyrosine and nitrate to produce microbiocidal compounds, including hypochlorous acid (HOCl). Defensin proteins form pores in bacterial membranes, and can attract monocytes, $CD4^+$ and $CD8^+$ T cells to the site. Exocytosis of non-peroxidase secretory vesicles incorporates several proteins into the plasma membrane of the neutrophil, such as fMLP receptors, and the β_2-integrin CD11b, and L-selectin which both enable neutrophil-

endothelial cell adhesion. The azurophilic granules will not be exocytosed until there is a strong stimulus. The mechanism of degranulation is incompletely understood, but appears to occur in stages, linked to increasing concentrations of cytosolic Ca^{2+} (Faurschou & Borregaard, 2003).

There are few reports describing neutrophil function in KS patients. However, Ellis et al. investigated neutrophil function in AIDS patients suffering from KS (Ellis *et al.*, 1988). These individuals suffer from greater numbers of bacterial infections than the healthy population. The enhanced propensity for infection in these individuals may be due to impaired neutrophil function. Neutrophil chemotaxis appeared normal in AIDS-KS, but functionality was reduced (Ellis *et al.*, 1988).

1.7.2. Monocytes

Monocytes circulate in the blood, continuously traversing the endothelial barrier in response to infection, and differentiating into phagocytic macrophages in the tissues. Circulating monocytes are also phagocytic, though they do not often encounter infection in the bloodstream (Murphy, 2008). Macrophages secrete cytokines into the surrounding tissue, activating other macrophages. They also recruit neutrophils by producing IL-8, and monocytes by MCP-1, from the bloodstream to the tissue. IL-8 is a potent neutrophil chemokine, it exists in three forms due to post-translational processing, and binds to one of two seven-transmembrane receptors (IL-8Rα and IL-8Rβ) that are then internalised and rapidly recycled back to the cell surface. Cognate receptor binding by IL-8 induces a Ras/MAPK-mediated intracellular signalling pathway. The consequences include shedding of L-selectin from the cell surface, and enhancement of integrin expression, leading to epithelial cell adhesion and migration of neutrophils into the tissue. IL-8 also stimulates neutrophil oxidative burst and degranulation (Mukaida, 2003). The activation of monocytes

depends primarily on the cell-surface expression of TLRs that are activated by bacterial pathogen-associated molecular patterns (PAMPs), such as LPS, and are regulated by P2 receptors activated by ATP, ADP, UTP and UDP (Ben Yebdri *et al*., 2009).

1.8. *Adaptive immune response*

Following the rapid innate immune response to non-self antigens, lymphocytes differentiate and proliferate, creating long-term effector cells that mediate 'immunological memory'. These memory responses provide adaptive immunity to infection. Cells generated as part of the adaptive immune response recognise specific antigens and are recruited when the innate response is not sufficient to control the pathogen. B cells, T cells and professional APCs are crucial components of this system, and their interaction will be discussed below.

1.8.1. T cell development

T cells and B cells derive from a common lymphoid progenitor cell in the bone marrow, but T cell maturation occurs in the thymus. Miller reported in 1961 that the excision of the thymus from neonatal mice resulted in reduced numbers of lymphocytes and a tolerance of allogeneic skin grafts, indicating a suppressed immune response (Miller, 1961). Murine models of immune-suppression can be generated by preventing the development of the thymus. Deletion of the *Winged-helix nude* (*Whn*) gene in 'nude mice' leads to defects in development of the thymus and an associated T cell-deficiency. The resulting disruption in signalling between the developing ectoderm and endoderm also results in hairlessness, hence the moniker 'nude' (Reth, 1995). The importance of the thymus in human T cell development was highlighted in a study by Markert *et al*. A developmental defect leading to the lack of a functional thymus in humans, results in a condition known as DiGeorge syndrome, characterised by a profound T cell deficiency. Transplantation of allogenic thymic

tissue from HLA-matched infants to infants with DiGeorge syndrome, restored the production of T cells and their proliferative response to mitogens such as anti-CD3 and phytohaemaglutinin (PHA) (Markert *et al*., 1999).

T cells develop into distinct lineages in the thymus, defined by their surface expression of T cell receptor (TCR) subtypes and co-stimulatory proteins. The TCR gene fragments are rearranged during development in the thymus, by the excision of intervening gene fragments. For example, the δ-coding regions are deleted in α:β-destined T cells. The excised fragments exist as episomes in the T cell, and are depleted by cell division (Spits, 2002). T cells are regulated by both positive and negative selection; this ensures that the cells do not react to host antigens (resulting in autoimmune diseases). A low level interaction between newly generated α:β T cells and self-antigen presented by thymic DCs allows the T cells to survive (positive selection), whereas a high affinity for self-antigens leads to cell death (negative selection) (Spits, 2002).

Following positive selection, dual-positive $CD4^+CD8^+$ α:β T cells differentiate into exclusively $CD4^+$ or $CD8^+$ subtypes. $CD8^+$ T cells differentiate into cytotoxic T lymphocytes (CTLs) that can directly kill virus-infected cells, and $CD4^+$ cells mature into 'helper' (Th) or 'regulatory' (Treg) cells. CTLs can kill target cells by a variety of mechanisms. Upon forming a contact with a target cell, cytotoxic granules are exocytosed to the contact, or synapse, and perforin is released, forming pores in the target cell membrane. Release of other enzymes such as members of the granzyme family can induce apoptosis by cleavage of caspases, initiating an apoptotic cascade. CTLs can also kill target cells through a member of the TNF receptor death receptor family, Fas. Fas ligands expressed by the CTL ligate to the Fas receptor on target cells, inducing apoptosis via a caspase/apoptotic pathway. A common response of CTLs to stimulation is the secretion of cytokines such as IFNγ, TNF and IL-2 (Barry & Bleackley, 2002).

IFNγ has a wide range of activities, and is the sole member of the IFN type II family, structurally distinct from the type I IFNs such as IFNα. IFNγ binds to the IFNγ-R, initiating a signal cascade in the recipient cell and activating the Jak-Stat pathway, leading to transcription of IFNγ-responsive genes, often via binding of IRFs to ISRE promotor regions. IFNγ is important for amplifying the immune response to viral infection, and achieves this by several mechanisms. These include the upregulation of MHCI/II and associated proteins such as tapasin, the upregulation of anti-proliferative proteins, upregulation of proteins that impede the replication and translation of viral antigens, such as PKR (protein kinase dsRNA-regulated), and the upregulation of chemoattractants such as MCP-1 (Schroder *et al*., 2004).

IL-2 contributes to the development of Tregs, enhances the proliferation of T cells and can stimulate NK cells and B cell-Ig secretion. IL-2 binds to the IL-2R, composed of three chains which have a high affinity for IL-2 when they form a complex (Murphy, 2008). Like IFNγ, IL-2 stimulates T, B and NK cells via the Jak-Stat pathway upon IL-2R ligation. As discussed below, IL-2 is important during the T cell response to antigen peptide, and assists in the avoidance of anergy. IL-2 is also important as a survival signal for T cells, and thus must be present in the culture medium to maintain T cells and T cell clones in long-term culture. Therapeutically, IL-2 is used to amplify the number of $CD4^+$ T cells in HIV-positive individuals (Rochman *et al*., 2009).

The secretion of IFNγ by activated T cells and NK cells, as well as the presence of IL-12 produced by cells mediating the innate immune response, activates the signal transducer and activator of transcription 4 (Stat4), Stat1 and the T box transcription factor (T-bet), inducing the $CD4^+$ T cell to mature into a T_H1 cell. The activation of T-bet by IFNγ leads to the activation of Runx3, subsequent downregulation of *IL-4*, and enhanced IFNγ-responsiveness; IFNγ-responsiveness promotes T_H1-differentiation and inhibits T_H2-polarisation. T_H1 cells can also stimulate the production of antibodies by the co-stimulation

of activated antigen-specific B cells, and can stimulate an infected macrophage to digest endocytosed bacteria that have evaded its killing mechanisms (Zhou *et al*., 2009). In contrast, T_H2 cells secrete IL-4, IL-5 and IL-13, in response to IL-4-stimulation, leading to activation of the Gata3 transcription factor and subsequent T_H2-differentiation. IL-4 reduces the expression of the IL-12R β-chain, promoting T_H2-differentiation and preventing T_H1-polarisation. A third T helper cell subset, Tfh, is differentiated in response to IL-21 stimulation and controls B cell maturation, though it has not been extensively researched (Zhou *et al*., 2009).

1.8.2. Presentation of antigen to T cells

The recognition of viral antigens by T cells is dependent on the presentation of antigen peptides by MHC molecules on the surface of APCs. $CD8^+$ CTLs recognise processed peptide presented by MHC class I. Maturing MHCI proteins form a protein-complex in the endoplasmic reticulum (ER), known as the peptide-loading complex, including proteins such as transporter associated with antigen processing protein (TAP) and tapasin. Briefly, antigens are processed and degraded by the proteasomal complex; the resulting peptides are transported into the ER by TAP, loaded onto the maturing MHCI protein, and the MHCI-peptide complex transported to the cell surface via the Golgi apparatus (Hansen & Bouvier, 2009).

Viruses have evolved to target various stages of the MHC maturation and protein-loading pathway. For example, the latent EBV antigen EBNA1 expresses a repetitive Gly-Ala motif which inhibits the recognition of EBNA1-expressing cells by CTLs (Levitskaya *et al*., 1995). Levitskaya and colleagues reported that EBNA4 motifs commonly recognised by CTLs through HLA-A11, were not recognised when inserted into an intact EBNA1 sequence, and expressed in target cells (Levitskaya *et al*., 1995). In contrast, cells expressing

EBNA4 motifs within a mutant EBNA1 lacking the Gly-Ala motif were recognised and killed. It is likely that EBNA1 inhibits the degradation of viral proteins by the proteasome, therefore preventing their presentation by MHCI on the cell surface (Levitskaya *et al*., 1995).

Human CMV unique short (US) region-encoded glycoproteins can inhibit MHC-mediated peptide presentation by several mechanisms. US2 and US11 initiate the transport of MHCI heavy chains from the ER into the cytosol for degradation by the proteasome. US3, a transmembrane glycoprotein, prevents the binding of peptides to the MHCI complex, thus retaining MHCI in the ER and preventing its transport to the cell surface (Hansen & Bouvier, 2009). In contrast, hCMV US6, a transmembrane protein located in the ER, binds to the TAP/MHCI complex and prevents the TAP-mediated transport of peptides from the cytosol to the ER, possibly by preventing the ability of TAP to transfer peptides into the ER, rather than preventing peptide-TAP binding (Ahn *et al*., 1997).

KSHV also encodes proteins capable of disrupting MHC-peptide presentation to T cells, by initiating the endocytosis of mature MHC proteins from the cell surface and directing them for degradation by the endolysosomal pathway. KSHV ORFs K3 and K5 are predominantly localised to the ER; expression of these proteins does not alter the maturation of the MHC or its translocation to the cell surface, but both K3 and K5 enhance the internalisation and degradation of surface MHCI-peptide complexes (Coscoy & Ganem, 2000).

Though MHCI is expressed on the majority of cells *in vivo*, MHCII expression is generally restricted to B cells, DCs and macrophages. $CD4^+$ T cells recognise peptide presented by MHCII and in turn activate immune effector cells. For example, $CD4^+$ T cells recognising non-self antigen presented by a B cell will stimulate that B cell to produce antibodies. In contrast to MHCI molecules which bind peptides of 8-10aas, anchored by their carboxy and amino termini to the binding cleft, MHCII proteins can bind peptides of over

13aas in length that lie in the peptide-binding cleft and are stabilised by hydrogen bonds along their length. The variation in peptide-MHC linker regions amongst MHC alleles determines the peptides that each MHC complex will bind. Importantly, MHC molecules are unstable when they are not bound to peptide, and the stabilisation of the MHC complex upon peptide-binding ensures an efficient interaction with responder T cells (Murphy, 2008).

Normally, antigenic peptides presented by MHC class I or II molecules bind to the TCRs of $CD8^+$ or $CD4^+$ T cells respectively, inducing a T cell response such as proliferation and/or cytokine production. CD4 and CD8 proteins contribute to the TCR-mediated intracellular signalling pathways within the T cell, leading to downstream transcriptional activity and generation of cytokines. However, costimulatory proteins, such as CD28, must be activated concurrently with TCR-stimulation in order to induce a T cell response. In the absence of costimulation, a state known as anergy can be induced. T cell anergy is a hyporesponsive state in which a T cell cannot respond to peptide stimulation; for example, the proliferative response is curtailed (Wells, 2009). Traditionally, anergy is induced by MHC-peptide binding to the TCR in the absence of costimulation, but can also be a result of abnormal TCR stimulation. IL-2 production is dependent on CD28 costimulation. However, exogenous IL-2 enables T cells to avoid anergy in the absence of CD28 stimulation, and anergy can be induced even with CD28-costimulation if IL-2 activity is neutralised. Therefore, the anergic state is dependent on TCR/CD28 signalling in addition to IL-2 signalling through the IL-2R, and appears to be related to elevated intracellular calcium levels. Anergic T cells cannot respond effectively to stimuli, their integrin-adhesive properties are reduced, and they share a similar phenotype with $CD4^+$ $Foxp3^+$ Tregs. As a result, T cells are only fully activated in the appropriate inflammatory environment (Wells, 2009).

1.8.3. Downstream signalling cascades initiated by stimulation of the TCR

An APC presents processed peptide antigen to a T cell via its surface MHC, consequently binding the TCR αβ subunits, activating the TCR and initiating a signalling cascade (**Figure 1.6**). The ITAM motifs of the TCR ζ chain and CD3 are subsequently phosphorylated by Lck or Fyn, Src family kinases that bind to the cytoplasmic tail of CD4 and CD8. Zap70 translocates to the phosphorylated ITAM tyrosines and binds to them via its two SH2 domains. Zap70 is subsequently phosphorylated by Lck and is crucial for the development of downstream signalling cascades (Au-Yeung *et al*., 2009). Activated p-Zap70 phosphorylates LAT and SLP-76. Deletion of the gene encoding Zap70 in mice leads to severe combined immunodeficiency (SCID) due to the inability of T cells to initiate downstream signalling events upon antigen-presentation (Au-Yeung *et al*., 2009). Haas and colleagues observed that Zap70 was not phosphorylated in cells lacking functional Lck, confirming the importance of this protein in initiating the signalling cascade (Haas *et al*., 2008). The phosphorylation of LAT by Zap70 is crucial for the subsequent phosphorylation and binding of signalling proteins such as PLC-γ1 and VAV1. Zap70 directly phosphorylates five tyrosine residues on LAT, thus creating docking sites for the signalling proteins. Zap70-mediated phosphorylation of LAT is also essential for activation of the Ras pathway downstream of PLC-γ1 (Paz *et al*., 2001). SLP-76 associates with GADS, an adaptor protein that binds to phosphorylated LAT. Three tyrosine kinases on SLP-76 are phosphorylated by Zap70 and Lck, leading to PLC-γ1 activation and resultant calcium flux. All three tyrosines have similar functions. However, Y128 and Y112 are essential for SLP-76-VAV binding, and Y145 appears to play a greater role in PLC-γ1 activation, downstream calcium flux, and activation of calcium-sensitive nuclear factor of activated T cells (NFAT) (Jordan *et al*., 2006). The NFAT transcription factor family member NFATc appears to be responsible for regulating IL-4 production by T cells (Fowell *et al*., 1999).

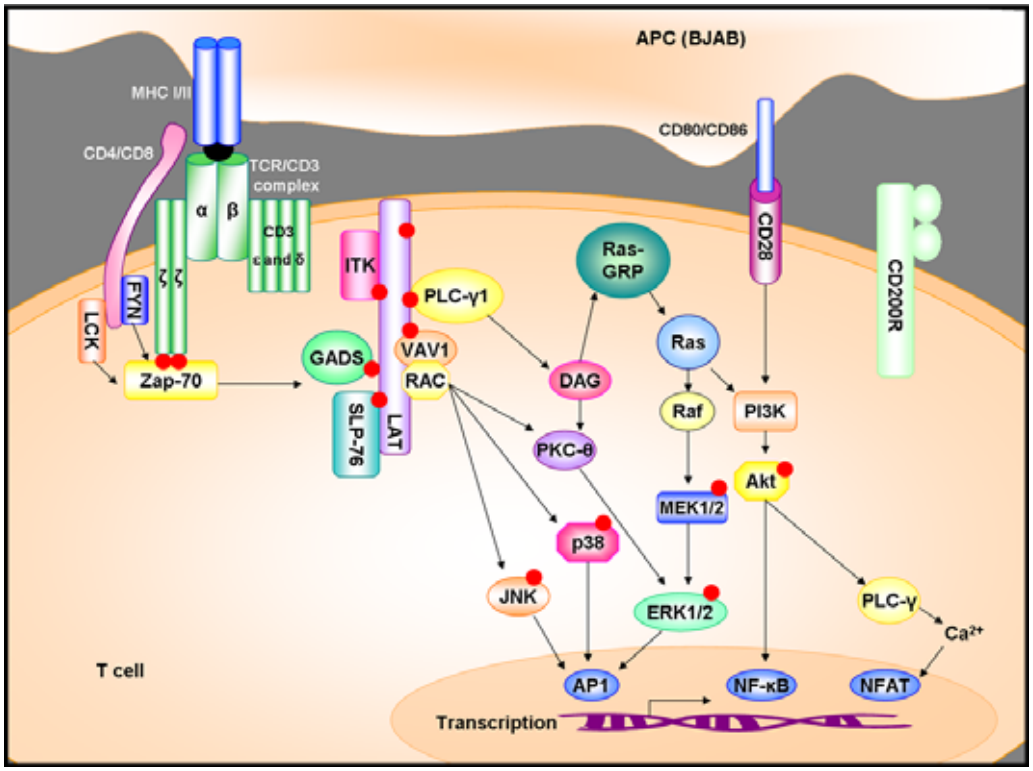

Figure 1.7 Intracellular signalling cascades initiated by TCR-mediated stimulation of a T cell. Upon TCR ligation to a MHC-peptide complex a signalling cascade is initiated, ultimately resulting in gene transcription consistent with antigen-specific T cells responses (e.g. IL-2 production). The phosphorylation of downstream signalling molecules is indicated by red dots. Zap70 is recruited to the ζ TCR subunit and subsequently phosphorylated by Fyn or Lck. p-Zap70 then phosphorylates LAT and SLP-76 adaptor proteins which recruit and phosphorylate other protein tyrosine kinases. The signalling cascade results in phosphorylation and activation of MAP kinases, and is enhanced by co-stimulation through the coreceptor CD28. This illustration is adapted from Schwartzberg *et al*. (2005), Alegre *et al*. (2001) and Abraham and Weiss (2004).

Downstream of the LAT-SLP-76 adaptor complex, several signalling molecules are activated, leading to transcription of genes that are required for antigen-specific T cell responses. The adaptor protein Ras, activated by PLC-γ1, recruits Raf-1 to the plasma membrane following TCR stimulation. Raf-1 is subsequently activated and in turn phosphorylates MEK-1 and MEK-2, the upstream initiators of ERK1/2 activation. Phosphorylated ERK (p-ERK1/2) is able to translocate to the nucleus and directly activate transcription factors such as AP-1, composed of fos and jun (Alberola-Ila & Hernandez-

Hoyos, 2003). Cleavage of phospholipid phosphatidylinositol-4,5-biphosphate (PIP_2) by PLC-γ1 generates diacylglycerol (DAG) and inositol 1,4,5-triphosphate (IP_3). IP_3 binds to IP_3 receptors on the ER, releasing Ca^{2+} ions into the cytoplasm. Calcium binds to calmodulin in the cell, which subsequently activates a phosphatase, Cn. Cn dephosphorylates the constitutively phosphorylated NFAT, thus activating it and causing dimerisation with another transcription factor, AP-1 (Baine *et al*., 2009). Both NFAT and AP-1 can bind directly to sequences of the IL-2 promoter, though the NFAT-AP-1 complex has a higher binding affinity (Chen *et al*., 1998).

Costimulation through the co-receptor CD28 augments the TCR signalling cascade. CD80 and CD86, proteins expressed by APCs, bind to CD28 on the surface of resting T cells. Activation of phosphatidylinositol 3-kinase (PI3K) by CD28 subsequently phosphorylates Akt, a protein which has been identified as the regulator of IL-2 and IFNγ-secretion in T cells (Alegre *et al*., 2001). Akt is also phosphorylated by the TCR signalling pathway downstream of Ras activation, suggesting that CD28 ligation may just enhance the TCR response rather than initiating a distinct signalling pathway.

A negative co-receptor, CTLA-4, is upregulated on activated T cells and competes with CD28 for its ligands. Ligation of CTLA-4 reduces IL-2 secretion, and suppresses intracellular ERK and JNK phosphorylation, providing a negative balance to TCR stimulation. Reduced activation of the transcription factors AP-1, NFAT and NF-κB have also been observed upon cross-linking of CTLA-4 (Alegre *et al*., 2001). NF-κB is involved in the regulation of IL-2 gene transcription, and its activity is increased in response to TCR stimulation and costimulation through CD28. NF-κB comprises dimeric complexes of p50, p52, RelA, RelB and c-Rel. The c-Rel subunit appears to be crucial for the regulation of IL-2 transcription, and is translocated to the nucleus upon degradation of inhibitory proteins that retain NF-κB in the cytosol (Kalli *et al*., 1998). The signalling pathways induced by CTLA-4

ligation have not been elucidated. However, there is some evidence that CTLA-4 can also activate PI3K and Akt, inducing an anergic state rather than stimulating cytokine secretion. This pathway also appears to rescue T cells from antigen-dependent cell death, due to the inhibition of a pro-apoptotic protein by Akt (Rudd *et al*., 2009).

1.9. *Aims and objectives of this research project*

The overall aim of this project was to elucidate the mechanisms of action of KSHV vOX2 and its cellular counterpart, CD200, on innate and adaptive immunity *in vitro* and *ex vivo*.

The specific objectives were:

- To generate a soluble recombinant CD200 Fc-fusion protein
- To investigate the activities of soluble vOX2:Fc and CD200:Fc in modulating primary human leukocyte responses to stimuli, using an inactive protein, KCPmut:Fc, as a control
- To study the activities of full-length native vOX2 and CD200 expressed by antigen-presenting cells on the response of human T cell clones to cognate peptide antigen
- To determine the mechanism of action of vOX2 and CD200 in modulating T cell responses to cognate peptide antigen
- To generate antigen-presenting cell lines expressing an RRV homologue of CD200, and three putative CMV homologues of CD200, and to investigate their role in modulating T cell clone responses to cognate antigen

Chapter 2. Materials and methods

The experimental methodologies used throughout this research project will be outlined and described in this chapter, with reference to background literature where applicable. The appendices include comprehensive lists of primers and plasmids (Appendix A), antibodies (Appendix B), and common solutions and reagents (Appendix C).

2.1. Creating a CD200:Fc fusion protein

2.1.1. Polymerase Chain Reaction (PCR)

The PCR assays referenced in this thesis were carried out in a 50µl volume with 4µg/ml sense and anti-sense primers. The thermal cycling steps were optimised for each primer pair, in particular the annealing and elongation steps. Every PCR reaction contained the following; 1.25U proof-reading DNA polymerase (Promega), 2mM deoxyribonucleotide triphosphates (dNTPs), and 1x DNA polymerase buffer (Promega). The DNA concentration was optimised for each assay.

2.1.2. Construction of the CD200:Fc expression vector

The full-length *CD200* gene had been previously inserted into the pBK-CMV vector (Rezaee, R. and Blackbourn, B., University of Birmingham). From this vector, the sequence encoding the extracellular region of human CD200 was amplified by polymerase chain reaction (PCR; see Section 2.1.1) using gene-specific primers incorporating *XbaI* and *NotI* restriction enzyme sites (primers 1F and 1R in Table I, Appendix A). The amplified *XbaI-CD200-NotI* sequence was then ligated into a blunt-end cloning vector (pCR®-Blunt II-TOPO, Invitrogen, Table II, Appendix A) and transformed chemically competent One Shot® TOP10 *E. coli* (Invitrogen). Genomic sequencing (University of Birmingham sequencing

service) of viable clones yielded several with the correct CD200 sequence, and one of these was selected for further investigation. Sequences were analysed by Sequence Scanner (version 1.0, Applied Biosystems) and Vector NTI® Advance 10 (Invitrogen) software.

Transformed bacteria were amplified by overnight incubation in LB broth (Acros Organics) containing the appropriate antibiotic for selection (kanamycin, 50μg/ml). DNA was extracted from the bacterial cultures by commercial kits (Qiagen or Promega, see Section 2.1.3). The *CD200* gene was cut from the cloning vector by digesting the adjacent restriction sites with *XbaI* (Promega) and *NotI* (Promega) and the extract was then run on a 1% agarose gel beside the digested vector. *CD200* was subsequently cut from the agarose gel and purified with a commercial kit (Qiagen) before subcloning into the expression vector (pTorsten), also digested with *XbaI* and *NotI* restriction sites, downstream of the EF1a promoter and upstream of the IgG1 Fc sequence (**Figure 2.1**). Recombinant pTorsten vector, ligated with the region of *CD200* encoding the extracellular protein domain, was transformed into competent DH5α *E. coli* and the region sequenced (University of Birmingham sequencing service) using the gene-specific primers 1F and 1R (Table I, Appendix A).

2.1.3. Extracting and purifying DNA from transformed bacteria

Commercial kits were utilised for the extraction of DNA from transformed bacterial cultures. All cultures were prepared in sterile containers by overnight incubation (37^{o}C) with constant shaking in LB broth (Table I, Appendix C) with selective antibiotics. The QIAprep® Spin Miniprep kit (Qiagen) enable isolation of DNA from small volumes (3ml), the PureYield™ Plasmid Midiprep system (Promega) was used for larger volumes (50-250ml), and the Endo-free plasmid maxi kit (Qiagen) was used to extract DNA from large volumes of bacterial culture (250ml) without endotoxin contamination. Each kit relies on a DNA-binding

membrane that enables the washing and purification of the DNA, and the extraneous material is discarded by centrifugation following lysis of the bacteria.

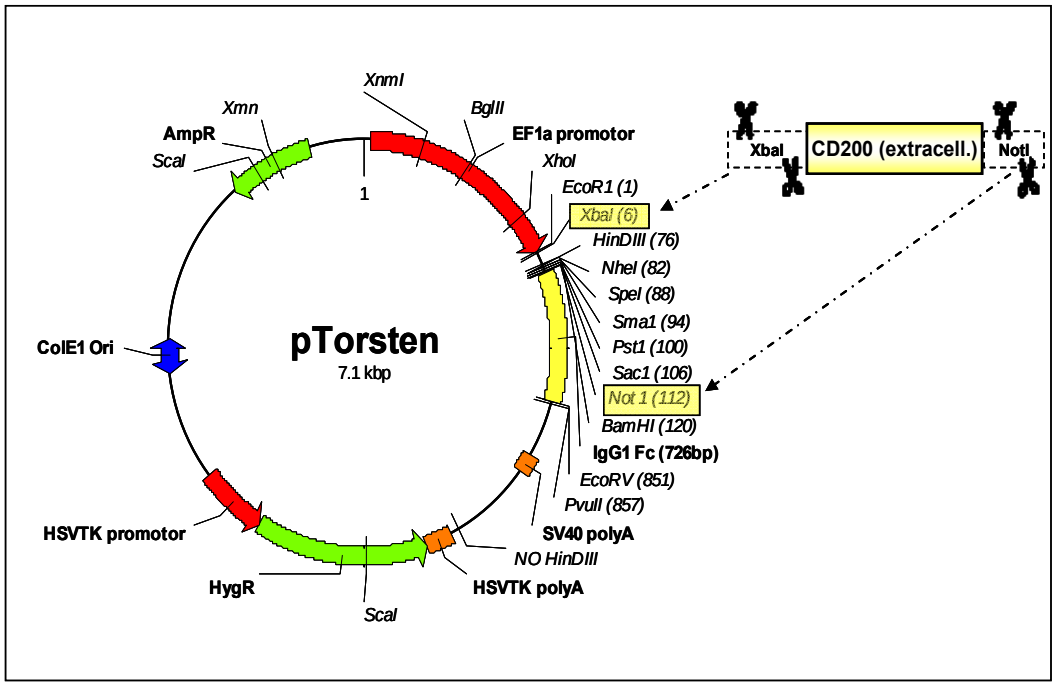

Figure 2.1 Constructing a CD200:Fc expression vector. The region of *CD200* encoding the extracellular protein domain was amplified by PCR, and two restriction sites, for enzymes NotI and XbaI, added using specific primers. *NotI-CD200-XbaI* was ligated into the pCR®4-TOPO® sequencing vector, for verification of the DNA sequence, then digested out by NotI and XbaI enzymes and ligated into the pTorsten vector, upstream of the gene encoding human IgG1 Fc (CD200-pT clone 6).

2.1.4. Transfection of CD200-pT into CHO cells, for subsequent expression of CD200:Fc

The CD200-pT plasmid (CD200-pT clone 6) was stably transfected into CHO cells by the Lipofectamine (Invitrogen) reagent method. $7x10^5$ cells were seeded into 35mm dishes and cultured overnight in pre-transfection medium (Appendix C, Table II). The following day lipofectamine reagent (5µl, Invitrogen) was diluted in RPMI 1640 (95µl, Invitrogen) and mixed with either RPMI 1640 (10µl) containing 250ng of DNA, or RPMI and water (a volume equal to that of the DNA) as a negative control. The reagents were incubated

(45mins, room temp.), then 200µl were plated onto cells cultured in RPMI 1640 (800µl) and incubated (5 hrs, 37°C, 5% CO_2) in a humidified incubator. The pre-transfection medium was then removed and replaced with 5ml post-transfection medium, and left for a further 24 hours. After this time, the medium was replaced with pre-transfection medium, and another 48 hours later it was replaced with complete medium. At this stage the selective antibiotic Hygromycin B was added to the incubating medium at the previously determined optimal concentration of 400µg/ml.

Approximately three weeks post-transfection, a limiting dilution was performed on the hygromycin-resistant CHO cells in order to select a single clone. Viable cells were resuspended at concentrations of 1 and 10 cells/ml and these cell suspensions were seeded into a 96 well plate (100µl/well). Each well was examined regularly to select those containing single colonies, which were brought to confluence, and expanded. A clone producing high amounts of CD200:Fc was selected by screening supernatants from all clones. Screening was performed by Western Blot detecting IgG1 (Fc) with an anti-human IgG (Fc-specific) horseradish peroxidise (HRP)-tagged primary antibody (see Section 2.3 for method). The clone (B7) producing the highest amount of Fc (as identified by Western blotting), was selected for CD200:Fc protein production and purification.

2.2. Recombinant Fc-protein production, purification and analysis

2.2.1. Production of recombinant Fc-fusion proteins

CHO cells stably transfected with vOX2:Fc, KCPmut:Fc or CD200:Fc, were cultured in complete CHO medium to maintain stable selection. All cells were maintained at 37°C in 5% CO_2 in a humidified incubator.

To prepare ‘producer’ cells, the stably transfected cells were passaged every four days by washing twice with phosphate buffered saline (PBS), and trypsinising with 5ml

Trypsin-EDTA (Invitrogen). Approximately $60x10^6$ cells were transferred into $1700cm^2$ expanded-surface roller bottles. These producer cells were cultured in 200ml RPMI (4% foetal bovine serum (FBS), 1% Pen-Strep, 1%L-Glu), without Hygromycin B. The concentration of FBS in the culture medium was reduced in order to minimise the number of contaminating animal proteins that may interfere with the purification process and later applications. After culturing for four days, the culture supernatant was collected and centrifuged (4225 x *g*, 15mins, 4^oC) to remove any cellular debris, and the cells discarded. The supernatant was then filtered through a 0.22μm vacuum filtration system (Millipore) to remove any residual cellular debris. At this point the supernatant was stored for up to one week at 4^oC and protected from light, to prevent degradation and/or aggregation of the protein.

2.2.2. Purification of recombinant Fc-fusion proteins

Recombinant proteins were purified by protein A affinity chromatography. Care was taken to ensure that the risk of endotoxin contamination of tubing and all other materials was minimal. Tubing was washed with 2M NaOH (60mins), and with 20% ethanol before use. All other materials were sterile, disposable consumables where possible, and solutions were prepared with endotoxin-free water (Aguettant). Supernatant was passed through the protein A column at a rate of 2ml/min (4^oC) by a peristaltic pump.

The following procedure was carried out at 4^oC. The protein A column was attached to a peristaltic pump with an incorporated spectrophotometer, and PBS passed through to stabilise the baseline reading. To elute bovine IgG, which binds with a lower affinity for protein A than the Fc-fusion proteins, 0.1M Citrate buffer (pH 5.0) was drawn through the column and the filtrate discarded. 0.1M glycine (pH 2.8-3.0) eluted the Fc-fusion proteins, and 1ml fractions were collected in sterile tubes. The pH of each protein fraction was

neutralised with 1M Tris (pH 9.0) for short-term storage, and the buffer replaced with PBS by repeated filter centrifugation through a 50kDa cut-off membrane (Millipore).

The protein concentration was determined by spectrophotometry (Nanodrop ND-1000 spectrophotometer). Protein concentration (mg/ml) was calculated as [absorbance ÷ extinction coefficient]. The extinction coefficients for 1mg/ml of each protein at 280nm are as follows: vOX2:Fc, 1.67; KCPmut:Fc, 1.14; CD200:Fc, 1.27.

2.2.3. Detection of endotoxin in purified recombinant protein stocks

Endotoxin was quantified by a commercial Limulus Amebocyte Lysate (LAL) assay, based on the observation that circulating amoebocytes in the *Limulus polyphemus* crab coagulate in response to endotoxin from gram-negative bacteria (Young *et al*., 1972). The protocol provided by the manufacturer was followed. Briefly, four standards were prepared from a stock solution of endotoxin (1.0, 0.5, 0.25, 0.1 EU/ml), and plated in duplicate (50µl) into a 96-well sterile plate warmed to 37^{o}C. Samples and blanks were also plated in duplicate. At time 0, LAL (50µl, 37^{o}C) was added to each well, and at time 10mins the synthetic substrate (100µl, 37^{o}C) was dispensed into each well in a consistent manner. The reaction was terminated at time 16mins with 25% glacial acetic acid (70µl), and the absorbance measured at 405-410nm in a multiwell plate reader (Model 680, BioRad).

A linear curve was plotted for the standards, and the mean blank value subtracted from each standard. The endotoxin concentrations (EU/ml) of each sample were calculated from the slope of the standard curve.

2.3. SDS-PAGE and Western blotting

2.3.1. SDS-PAGE

Cell lysates were diluted with an equal volume of sample buffer and 20µl was dispensed into each well, and the gel run at 100V. A ProSieve colour protein marker (Lonza) was run on each gel in order to determine the size of proteins of interest. When the tracking dye reached the bottom of the resolving gel the gel was either stained with colloidal coomassie blue or the proteins transferred to polyvinylidene fluoride (PVDF) membrane (Millipore).

2.3.2. Western Blotting

In order to detect proteins by immunoblotting, they were transferred from the SDS-PAGE gel to PVDF membrane (Millipore), a hydrophobic membrane with an approximate pore size of 0.45µm. PVDF membranes were incubated (60mins, room temp.) in 5% Marvel-TBS-0.05% Tween, or 5% bovine serum albumin (BSA)-TBS-0.05% Tween (for antibody detection of phosphorylated proteins) to block non-specific binding sites. Primary antibodies were diluted in TBS-0.05% Tween containing 3-5% Marvel milk or BSA, and incubated with the membranes (60mins, room temp., or 16hrs, 4^{o}C). After washing off excess primary antibody (10mins x3, TBS-0.05% Tween), membranes were incubated (60mins, room temp.) in an appropriate dilution of HRP-conjugated secondary antibody (in 5% Marvel-TBS-0.05% Tween or 3% BSA-TBS-0.05%). Following a further set of washing steps (10mins, x3, TBS-0.05% Tween), a enhanced chemiluminescent solution (Table II, Appendix C) was incubated (5mins, room temp.) with the membrane before exposure to photographic film. Films were developed by an automated developer.

To re-probe membranes with additional antibodies, they were incubated (5ml, 35mins, 60^{o}C) in stripping buffer (Table VII, Appendix), and washed (TBS-0.05% Tween,

5mins x1, 10mins x2). The Western Blotting procedure was then repeated from the blocking step.

2.3.3. Visualising immobilised proteins with colloidal coomassie stain

Following protein separation by SDS-PAGE, the resolving gel was transferred to a closed container and incubated in colloidal coomassie blue staining solution (Table II, Appendix C) at room temp. overnight. Gels were destained in a 1% acetic acid solution with gentle agitation until the background staining had been removed, and the stained protein bands were distinct. Gels were then vacuum-dried onto blotting paper.

2.3.4. Extracting the cellular cytosolic fraction for SDS-PAGE

Cells were collected and pelleted (5mins, 200 x *g*), cooled on ice and washed with ice-cold PBS. Pellets were then resuspended in Buffer E (Table II, Appendix C) at 10µl per $1x10^6$ cells, incubated on ice (5mins), and centrifuged (16060 x *g*, 4^oC, 5mins). Supernatants were collected and centrifuged twice (16060 x *g*, 4^oC, 5mins) and the pellets discarded. Lysates were frozen immediately at -70^oC, or analysed immediately.

2.3.5. Preparing whole cell lysates

BJAB cells were pelleted (200 x *g*, 5mins), cooled rapidly, and lysed with Nonidet-P40 (NP-40) buffer (Table II, Appendix C) by pipetting the pellet up and down. The lysate was transferred to a cold microtube and placed on a rotator (10mins, 4^oC), sonicated, and rotated again (10mins, 4^oC). The lysate was then centrifuged (16060 x *g*, 4^oC, 30mins), and the supernatant transferred to a cold microtube. Lysates were stored at -70^oC.

2.4. Immunofluorescence assays

Immunofluorescence assays (IFA) were performed on BCBL-1 cells infected with latent KSHV, or treated to induce lytic KSHV replication (by stimulation with 20ng/ml phorbol 12-myristate 13-acetate [PMA] for 4 days). Cells were washed (x3) with PBS and by centrifugation (800 x *g*) were resuspended in PBS containing 0.5% FBS, at $1x10^7$ cells/ml. Cells were spotted onto an 8-well microscope slide at 2µl/well.

Slides were fixed in either ice-cold acetone-methanol (1:1 v/v, 5mins) when probing for intracellular proteins, or in 3% methanol-free paraformaldehyde (TAAB) for the detection of cell surface proteins. Slides were air-dried after fixing. Cells for intracellular staining were incubated in 0.2% Triton x100 in PBS (30mins, room temp.) and non-specific binding sites were blocked by incubation in PBS-3% BSA (15mins).

Primary and secondary antibodies were diluted in PBS containing 3% BSA (the dilution factor was optimised for each antibody), and incubated with the cells for 60mins (37^oC) in a humidified chamber. Excess primary antibody was washed from the slides with PBS-0.1% BSA (x2), and a secondary antibody (conjugated to a fluorescent label), was incubated with the cells for one hour (37^oC in a humidified chamber). Excess secondary antibody was washed from the slides twice with PBS-0.1% BSA. Nuclear staining was performed by incubating with DAPI (10µg/ml, Sigma) for 30mins at room temp. Coverslips were mounted onto slides with ProLong® Gold (Invitrogen) and stored protected from the light. Immunofluorescence imaging was performed with a fluorescent microscope (Nikon Eclipse E600) and images collected by the Nikon ACT-1 (Nikon Corporation) software program.

2.5. Functional assays to determine leukocyte activity

2.5.1. Isolating PBMCs from peripheral blood

Peripheral blood collected from healthy donors was treated with heparan sulphate to prevent coagulation, and diluted 2:3 in RPMI 1640 (Invitrogen). Lymphoprep™ (6ml, Axis-Shield PoC) was overlaid with 15ml of the blood/RPMI mix, and the gradient centrifuged (800 x *g*, 25mins, room temp.). PBMCs were collected from the primary interface and washed in RPMI 1640 (x3, 800 x *g*, 8mins, room temp.).

2.5.2. Isolation of neutrophils and whole blood leukocytes

Whole blood was collected from healthy donors, and coagulation prevented by adding ethylenediaminetetraacetic acid disodium salt solution (EDTA, 1μM, Sigma). The leukocyte-rich plasma was separated from the erythrocytes by sedimentation with 2% dextran (Amersham, 1:6 ratio to blood). Gradient (Percoll, Sigma) centrifugation (250 x *g*, 20mins) segregated the neutrophil and whole blood leukocyte components. To isolate neutrophils from the leukocyte population, plasma was carefully dispensed onto a 79% Percoll solution (diluted in sterile saline), which rested on a 56% Percoll solution. Neutrophils were collected from the 79%:56% Percoll interface. Leukocytes were collected from the 79% Percoll:plasma interface. Both cell populations were washed in PBS and resuspended at 2 x 10^6 cells/ml (neutrophils) or 4 x 10^6 cells/ml (leukocytes) in Hank's balanced salt solution (HBSS, Invitrogen) containing calcium and magnesium, and 1% endotoxin-free bovine serum albumin (BSA, Sigma). If necessary, erythrocytes were first removed by hypotonic lysis in sterile water before the wash step.

2.5.3. Chemiluminescence assay to quantify superoxide release from isolated neutrophils or whole blood leukocytes

Due to the reductive and chemiluminescent properties of N,N'-dimethyl-9,9-biacridinium dinitrate (lucigenin, Sigma), small quantities of superoxide released by leukocytes in response to stimuli can be detected. Lucigenin is reduced by superoxide anions as follows: [$O^{2-} + Luc^{2+} \leftrightarrow O^2 + Luc^+ +$ **chemiluminescence**] (Afanas'ev *et al*., 2001).

Thus, the chemiluminescent assay was performed by plating 100µl of either neutrophils or whole blood leukocytes into wells of sterile tissue culture-treated white opaque plates (Greiner) before treatment. The cells were incubated in consistent conditions throughout the assay (37^{o}C, 5%CO_2, humidified). The cells were pretreated with recombinant Fc-fusion proteins (60mins, 37^{o}C, 5%CO_2) prior to addition of the priming agents, GM-CSF (50ng/ml, 30mins, Sigma) or human recombinant TNFα (50ng/ml, 30mins, Serotec). Lucigenin (2.5mM, diluted in HBSS-1%BSA) was added to each well and the plate protected from light. Formylmethionyl-leucyl-phenylalanine (fMLP, 10µl, 1µM, diluted in HBSS) was injected by the luminometer (Centro LB960, Berthold Technologies) at time point 0, and the relative light units (RLU) measured every 60 seconds. Data were collected by MicroWin 2000 software (version 4.3, Mikrotek Laborsysteme GmbH) and exported to Microsoft Excel for analysis.

2.5.4. Measuring myeloperoxidase (MPO) release from isolated neutrophils

The use of 3,3'5,5'-Tetramethyl-benzidine (TMB, Sigma), a substrate of peroxidase, is a popular method for measuring MPO release from degranulating cells, as it is the least toxic but sensitive colorimetric substrate available. TMB does not enter cells so its detection of MPO is restricted to the MPO released into culture supernatant (Menegazzi *et al*., 1992).

Neutrophils were isolated from the blood of a healthy donor (see Section 2.5.2) and 100µl dispensed ($2x10^6$ cells/ml in HBSS-0.5%BSA) into a sterile 96-well plate. The cells were pretreated with vOX2:Fc, KCPmut:Fc or CD200:Fc (60mins, 37°C, 5% CO_2) before stimulation with TNFα (100ng/ml, 15mins, 37°C, Serotec). MPO release from neutrophil azurophilic granules was induced by fMLP-treatment (100nM, 60mins, 37°C, 5% CO_2, Sigma). Several controls were prepared for each experiment: TNFα alone, fMLP alone, TNFα plus fMLP, or no treatment (to determine spontaneous degranulation). Positive controls were also included, using the same criteria but incubating each sample with a 1% Triton X-100 solution (5µl) for the final 10mins of the fMLP treatment period.

The 96-well plate was centrifuged (200 x *g*, 5mins, 4°C) to pellet the cells, and the supernatant transferred to another plate. An equal volume of TMB (Sigma) was added to the supernatant and a blue colour allowed to develop for 10mins. Absorbance was measured at a wavelength of 650nm by a multiwell plate reader (Emax Precision, Molecular Devices). The data were collected by the Softmax Pro (Molecular Devices) software.

2.5.5. Commercial (Phagoburst®) assay to measure superoxide release in whole blood

The Phagoburst® assay (Orpegen Pharma) relies on the properties of dihydrorhodamine (DHR) 123, a fluorogenic substrate that is oxidised to rhodamine (R) 123 by reactive oxygen species. The assay can therefore be utilised to measure superoxide production by leukocytes in response to a stimulus, opsonised *E. coli* in the present study. The quantity of R123 per cell and the percentage of cells with this oxidative activity can be determined by flow cytometric analysis.

The protocol provided by the manufacturer (Orpegen Pharma) was adhered to. Briefly, heparinised whole blood from a healthy donor was pretreated with recombinant

proteins (90mins, 37^{o}C, 5%CO_2), and aliquoted (100µl) into polystyrene tubes; the blood was then cooled in an ice bath (10mins) before proceeding with the assay. A negative control was prepared by addition of wash buffer, and a positive control by incubation of blood with PMA (1.35µM, Orpegen Pharma). Opsonised *E. coli* ($2x10^7$ bacteria, approximately 25:1 leukocyte, Orpegen Pharma) were added to each of the pretreated samples and to an untreated control (10mins, 37^{o}C). Following addition of the substrate DHR 123 (10mins, 37^{o}C), the reaction was terminated by lysis of the erythrocytes and fixation of the remaining leukocytes, and a DNA staining solution added to all samples and controls.

Oxidative activity was analysed by flow cytometry (Coulter® Epics® XL™ flow cytometer), and a total of 20,000 events collected for each sample. Using the software FlowJo7 (Tree Star Inc.) for post-collection analysis, the granulocyte population was defined by granularity and size (side scatter vs. forward scatter), and a histogram created in the FL1 (FITC) channel for the gated population (the gate excluded 95% of cells in the negative control). The difference in median fluorescence of each sample versus the *E. coli*-treated control for each individual is representative of the change in oxidative activity.

2.5.6. Determining the percentage of apoptotic neutrophils by flow cytometric analysis

The protocol for measuring neutrophil apoptosis by morphological changes was carried out as described above, but after 20 hours the cells were incubated with 3,3'-dihexyloxacarbocyanine iodide (2.3ng/ml, DiOC6, Sigma), a green fluorescent lipophilic dye (15mins, 37^{o}C, 5% CO_2). Apoptotic neutrophils lose the ability to retain DiOC6 in their mitochondria, and so have a lower fluorescence in comparison to live cells. Neutrophils were washed and resuspended in PBS before quantification by flow cytometry (Coulter® Epics® XL™, BD Bioscience). The neutrophil population was gated on by granularity (side scatter)

and size (forward scatter) as the determining characteristics, and a histogram created in the FL1 (FITC) channel. The histograms contain two peaks, one representing the viable cells that express a high level of fluorescence, and a peak that has shifted to the left due to the loss of DiOC6 from apoptotic cells. Neutrophil apoptosis may also be analysed by setting the level of fluorescence (FL1) against size, this creates a scatter plot with two neutrophil populations, viable and apoptotic.

2.5.7. Evaluating IL-8 production by monocytes adhered to plastic

PBMCs were isolated from human blood (see Section 2.5.1) and resuspended at $4x10^6$/ml in complete neutrophil medium (Table II, Appendix C). The cell suspension was aliquoted into a 48-well plate (200µl/well) and the monocytes left to adhere (60mins, 37°C, 5%CO_2). Non-adherent cells were then removed by washing four times with PBS, and once with RPMI 1640 (Invitrogen). The experiments were carried out in 200µl complete neutrophil medium. Monocytes were pretreated (60mins, 37°C, 5%CO_2) with vOX2:Fc, CD200:Fc or KCPmut:Fc (8µg/ml), or with engineered Empty-BJAB, vOX2-EGFP-BJAB or CD200-EGFP-BJAB cells (see Section 2.8.7/2.8.8), at $4.4x10^5$ BJAB cells/well. All BJAB cells were irradiated with 4000rads by a caesium source prior to use. The monocytes were then stimulated with lipopolysaccharide (1µg/ml or 50ng/ml, Sigma), or IFNγ (10ng/ml, R&D Systems). After 24 hours of incubation, the medium from each well was centrifuged (200 x *g*, 5mins) to remove any debris, and the supernatant snap frozen at -80°C.

The concentration of IL-8 in cell culture supernatants was quantified by Enzyme-linked ImmunoSorbent assay technique (ELISA, R&D Systems). The ELISA method was used to quantify both IL-8 and IFNγ later in this study. Briefly, immunosorp ELISA plates (Nunc) were coated overnight (4°C) with a capture antibody (2µg/ml anti-IFNγ, Thermo Scientific), or were purchased pre-coated with an anti-IL-8 antibody (R&D Systems). Non-

specific binding to the plate was prevented with ELISA blocking buffer (Table II, Appendix C, 2hrs, room temp.), and the plates washed three times with ELISA wash buffer (Table II, Appendix C). Culture supernatants were added to the plate (2hrs, room temp.), removed with ELISA wash buffer, and an anti-IL-8 (R&D Systems) or anti-IFNγ (Thermo Scientific) biotinylated antibody added to each well (1hr, room temp.). After washing three times, ExtrAvidin Peroxidase (2μg/ml, Sigma) was added to each well (30mins, room temp., the avidin binds with high affinity to the biotinylated antibody), and excess protein carefully removed by washing (x4). TMB substrate (Rockland) reacted with the biotin-bound peroxidise, resulting in a colorimetric change. The reaction was quenched with 1M HCl and the absorbance was measured at 450nm (subtracting 655nm) by a multiwell plate reader.

2.5.8. IFNγ-stimulation of monocytic cell lines

Human monocytic/macrophage cell lines U937 and THP-1 were maintained in complete medium (Table II, Appendix C) under normal cell culture conditions, and resuspended at $6x10^5$ cells/ml for the purposes of this experiment. Empty-BJAB, vOX2-EGFP-BJAB and CD200-EGFP-BJAB cells were irradiated (4000rads) by a caesium-137 chloride radiation source, washed four times in RPMI 1640 (Invitrogen), and resuspended ($6x10^5$ cells/ml) in complete medium. Equal volumes of the irradiated BJAB cells and U937/THP-1 cells were dispensed into a 24-well plate and stimulated with IFNγ (8ng/ml, Sigma). The supernatant was collected after 48 hours, debris pelleted (200 x *g*, 5mins), and the concentration of IL-8 quantified by ELISA (R&D Systems, see Section 2.5.8).

2.5.9. Culturing immobilised vOX2:Fc and CD200:Fc with human PBMCs

Biotinylated antibodies anti-CD3 (Miltenyi), anti-CD28 (Miltenyi), and anti-human IgG antibody (Calbiochem) were bound to commercial microbeads (0.1pg/bead, 1ml, 4^oC, 2hrs)

conjugated with an anti-biotin antibody (T cell expansion kit, Miltenyi). Recombinant Fc fusion proteins vOX2:Fc, commercial vOX2:Fc, CD200:Fc or KCPmut:Fc were then bound to the anti-IgG antibody present on the surface of the microbeads (0.2μM, 2ml, 4°C, 2hrs). Protein-binding to the microbeads was confirmed by SDS-PAGE and immunoblotting (see Sections 2.2.1 and 2.2.2) with an anti-human IgG (Fc)-HRP antibody (Sigma).

PBMCs isolated (see Section 2.5.1) from healthy donors were revived from frozen stocks, and plated at $1.5x10^6$ cells/well in pre-transfection medium. Protein-antibody-bead complexes were pelleted (2400 x *g*, 5mins) and resuspended in medium (RPMI, 10% FBS). Microbeads and PBMCs were cultured at a ratio of one bead per two cells (48h, 37°C, 5% CO_2). The concentration of IFNγ in the cell culture supernatant was quantified by ELISA (see Section 2.5.8, Thermo Scientific).

2.6. Quantifying CD200R expression by flow cytometry

2.6.1. Determining CD200R expression on human leukocytes

Please see Appendix B for a complete list of all antibodies used. Isolated human leukocytes (see Section 2.5.2) were resuspended in PBS-2% BSA (10^7 cells/ml) and incubated on ice. The cell suspension was aliquoted (100μl) into sterile tubes for flow cytometry, and incubated with mouse anti-human CD200R (60mins, 4°C, Abcam). Excess primary antibody was washed off with PBS (158 x *g*, 5mins). Fluorophore-conjugated secondary antibodies were incubated with the cells (60mins, 4°C) and the washing step carried out as before. Non-specific binding sites were blocked with mouse serum (30mins, 4°C, Sigma), and the cells washed (PBS, 158 x *g*, 5mins). Antibody-labelled cells were fixed with 2% paraformaldehyde (PFA) and stored at room temp., protected from light before analysis.

At least $1x10^5$ events were collected for each sample by flow cytometry (Beckman Coulter® Epics® XL™), and the cell populations gated according to size (forward scatter)

and granularity (side scatter) using the software program FlowJo7 (TreeStar Inc.). Histograms were created for each gated population and the CD200R expression determined by an upwards shift in fluorescence in comparison to the negative control (secondary antibody alone or isotype control).

2.6.2. Cell-surface expression of CD200R by viral peptide-specific T cells

To estimate the percentage of antigen-specific circulating $CD8^+$ T cells in an individual, MHC-peptide-fluorophore complexes bound to the T cell receptor (TCR) on these cells can be visualised by flow cytometry. The conserved β_2-microglobulin (β_2-M) light chain of the HLA molecule is mutated to create an easily accessible sulfhydryl group on the protein surface, to which biotin can bind. Heavy chain MHC subunits (α_1, α_2 and α_3) are then generated and non-covalently bound to β_2-M, and folded with a synthetic peptide. The biotin, complexed with the HLA-peptide molecule, subsequently binds to one of four sites on an avidin-fluorophore molecule, thus creating a fluorescent tetrameric unit that can ligate with peptide-specific TCRs on T cells (**Figure 2.2**; (Walter *et al*., 1998)).

PBMCs were isolated from healthy or IM patient donors (see Section 2.5.1) and stored frozen in the gaseous phase of liquid N_2. On the day of use, the PBMCs were thawed rapidly to 37°C, washed (RPMI, 770 x *g*, 8mins), and dispensed into polystyrene tubes (with a minimum of $2x10^5$ cells/tube). The cells were pelleted (770 x *g*, 8mins) and resuspended in 50µl PBS-2% FBS, with a 1:50 dilution of fluorophore-conjugated tetramer, The PBMCs were incubated (37°C) for between 12-15mins, rapidly cooled to 4°C, and washed in ice-cold PBS-2% FBS (770 x *g*, 8mins, 4°C). The cells were resuspended in an anti-CD200R antibody (Abcam, diluted in PBS-2% BSA, 60mins, 4°C), or an IgG1 isotype control (Sigma), washed again and then labelled with an anti-mouse-FITC secondary antibody (Sigma, diluted in PBS-2% BSA, 60mins, 4°C).

(a)

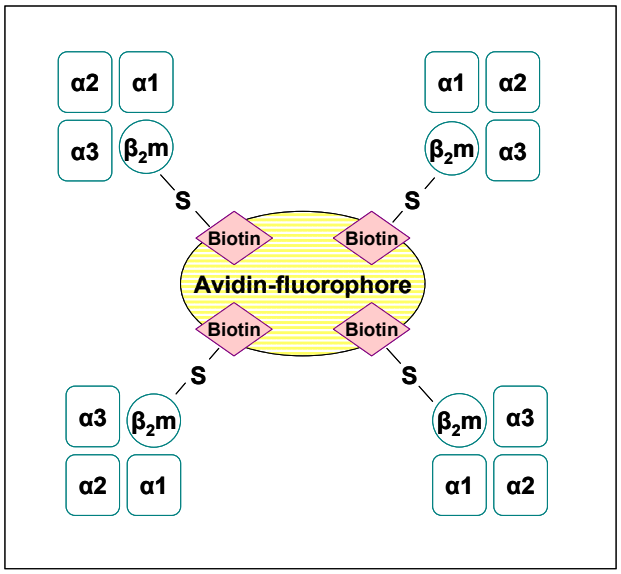

(b)

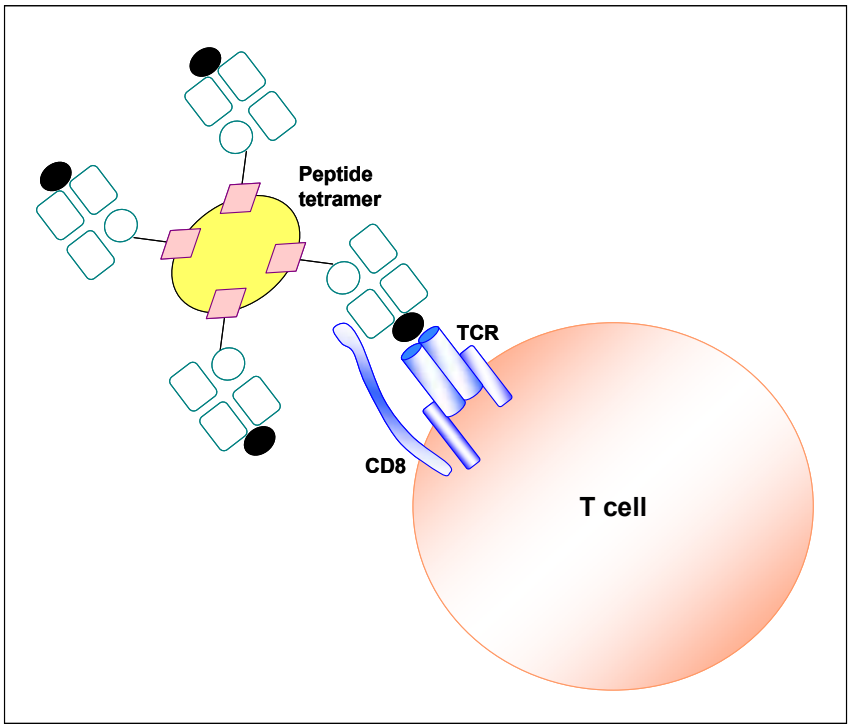

Figure 2.2 Generation of MHC-peptide-fluorophore complexes for the identification of peptide-specific T cells. (a) Light (β_2-M) and heavy chain (α_1, α_2 and α_3) MHC subunits are non-covalently bound to each other, and complexed with synthetic viral peptide antigen (not shown). Biotin is then covalently bound to the β_2-M subunit, and ligated to one of four binding sites on an avidin-fluorophore complex. **(b)** The viral peptide (back circles) complexed with MHC subunits (green), ligates to TCRs on peptide-specific T cells and can be visualised by flow cytometry. This illustration is adapted from Walter *et al*. (1998).

The cells were then washed (PBS, 770 x *g*, 8mins, 4°C) and resuspended in normal mouse serum (Sigma, 1:20 dilution in PBS, 30mins, 4°C). They were then labelled with an anti-CD4 or anti-CD8-VioBlue antibody (Miltenyi) diluted in PBS-2% BSA (60mins, room temp.). After washing (PBS, 770 x *g*, 8mins, 4°C), the cells were analysed by flow cytometry (LSRII, BD Biosciences). FlowJo7 software (TreeStar Inc.) was utilised for post-collection analysis of the data. Single staining with anti-CD8-PE (Miltenyi), anti-CD8-VioBlue (Miltenyi) or anti-CD200R (Abcam) plus anti-mouse-FITC (Sigma) were used to compensate for overlapping fluorescent signals in each sample.

2.6.3. Measuring CD200R expression on the surface of peptide-pulsed T cell clones

T cells (the human $CD8^+$ IM140.1 Y15 T cell clone or the murine B3z T cell hybridoma) were cultured overnight ($5x10^4$ cells/well, 37°C, 5% CO_2) in a round-bottomed 96-well plate. Each treatment was carried out in duplicate (to enable labelling with an isotype control antibody as well as anti-CD200R). Cells were left untreated or treated with cognate peptide antigen (IM140.1: YVLDHLIVV; B3z: SIINFEKL). The human $CD8^+$ T cell clone was also treated with phytohaemagglutinin (PHA, 3µg/ml, positive control), and an irrelevant EBV peptide (FLRGRAYGL, 5000ng/ml, negative control). Murine B3z cells were also treated with murine IFNγ (200U/ml, positive control), an irrelevant EBV peptide (YVLDHLIVV, 5000ng/ml, negative control), and PHA (3µg/ml, positive control).

The following day, the cells were harvested with a non-enzymatic cell dissociation buffer (Sigma), and dispensed into polystyrene tubes. After washing with PBS (770 x *g*, 8mins, 4°C), the cells were labelled with anti-CD200R (Abcam) or an isotype control (mouse IgG1, Sigma), (60mins, 4°C) at equal concentrations. All antibodies were diluted in PBS-2% BSA. The cells were washed in PBS (770 x *g*, 8mins, 4°C), labelled with an anti-mouse-FITC secondary antibody (Sigma, 60mins, 4°C), washed again, and analysed by flow

cytometry (Beckman Coulter® Epics® XL™). Post-collection analysis of data was carried out with FlowJo7 (TreeStar Inc.) software.

2.6.4. Quantifying the expression of CD200R by T cell clones stimulated by peptide-pulsed BJAB cells

Engineered BJAB cells were washed (PBS, 200 x *g*, 5mins), and dispensed into polystyrene tubes ($2x10^5$ cells/tube). The BJAB cells were then left untreated, or incubated with the EBV peptides PRSTVFYNIPPMPLPPSQL (500ng/ml, derived from EBNA2 protein), or YVLDHLIVV (50ng/ml, a peptide of the BRLF1 antigen), (60mins, 37°C, 5% CO_2). The cells were washed twice (PBS, 200 x *g*, 5mins), resuspended in complete medium (Table II, Appendix C) and dispensed into a 96-well flat-bottomed plate. The $CD8^+$ IM140.1 Y15 (YVL-specific) and $CD4^+$ SL c93 (PRS-specific) T cell clones were washed (RPMI, 770 x *g*, 8mins), added to the BJAB cells ($4x10^4$/well) and incubated overnight (37°C, 5% CO_2).

The next day the cells were harvested with a non-enzymatic cell dissociation buffer (Sigma) and dispensed into polystyrene tubes. After washing (PBS, 770 x *g*, 8mins, 4°C), the cells were incubated with an anti-CD200R antibody (Abcam, 60mins, 4°C), or mouse IgG1 (Sigma), washed again and then labelled with an anti-mouse-FITC secondary antibody (Sigma, 60mins, 4°C). All antibodies were diluted in PBS-2% BSA. The cells were washed (PBS, 770 x *g*, 8mins, 4°C) and resuspended in normal mouse serum (Sigma, 30mins, 4°C). The cells were then labelled (60mins, room temp.) with an anti-CD4 or anti-CD8-VioBlue antibody (Miltenyi), plus anti-CTLA-4-PE (BD Bioscience), and anti-CD28-APC (BD Bioscience), or the matching isotype controls (see Table III, Appendix B). After washing (PBS, 770 x *g*, 8mins, 4°C), the cells were analysed by flow cytometry (LSRII, BD Biosciences). FlowJo7 software (TreeStar Inc.) was utilised for post-collection analysis of the data. Anti-CD4/CD8-VioBlue (Miltenyi), anti- cytotoxic T lymphocyte antigen-4

(CTLA-4)-PE (BD Bioscience) and anti-CD28-APC (BD Bioscience) were used singly to compensate for any overlapping fluorescent signal in each sample. To determine the basal expression levels of CD200R, the above staining protocol was carried out on T cell clones cultured in the absence of BJAB cells.

2.7. Using human T cell clones as a model system to determine vOX2 and CD200 activity

2.7.1. Cloning antigen-specific T cells from infectious mononucleosis patient PBMCs

PBMCs were isolated from four buffy coats provided by National Blood Service, Birmingham, UK (see Section 2.5.1), mixed together and cultured overnight in complete T cell cloning medium (Table II, Appendix C) with PHA (10µg/ml, Sigma, 37^{o}C). The following day, the PBMCs were washed five times (RPMI, 770 x *g*, 8mins) and irradiated (4000rads, caesium-137 chloride source). PBMCs, previously isolated from an IM patient (IM235) and stored in the gaseous phase of liquid N2, were thawed, washed once in T cell cloning medium (770 x *g*, 8mins), and resuspended in T cell cloning medium at 3 cells/ml, 30 cells/ml and 300 cells/ml. The PHA-stimulated PBMCs were added to each solution at a final density of 1x10^{6} cells/ml. Cells from an autologous lymphoblastoid cell line (LCLs, prepared by long-term culture of IM235 mononuclear cells) were also irradiated (4000rads, caesium-137 chloride source), washed in RPMI 1640 (Invitrogen, 770 x *g*, 8mins), and resuspended in the PHA-treated PBMC/IM235 PBMC suspensions, at a final density of 1x10^{5} cells/ml. Each cell suspension was dispensed into wells of a round-bottomed 96-well plate (100µl/well). After one week a further 100µl of T cell cloning medium was dispensed into each well. One week later, any easily identifiable colonies of cells that had expanded in culture, were transferred to a 24-well plate, and cultured for a further two weeks in the presence of PHA-treated and irradiated PBMCs (1x10^{6} cells/well), and LCLs (1x10^{5}

cells/well). The cells were then tested for antigen-specificity by the chromium-release killing assay (see Section 2.7.2).

Other T cell clones used in this project were isolated by other investigators. They were maintained in cloning medium and restimulated with PHA-treated PBMCs and autologous LCLs, as outlined above.

2.7.2. Testing for T cell antigen specificity by chromium-release assay

^{51}Cr-labelled autologous LCLs acted as target cells in this experiment. The LCLs were engineered to express two EBV antigens endogenously, by infection with recombinant vaccinia virus; the antigens were processed and presented by MHC molecules to the putative T cells. Any peptide antigen-specific T cells that had been cloned (Section 2.7.1) would lyse only the target LCL expressing its specific antigen, releasing ^{51}Cr into the supernatant.

LCLs ($1x10^6$ cells) were infected with two vaccinia viruses, each engineered to express one EBV antigen (16hrs, 37^{o}C, 5% CO_2), at a multiplicity of infection (MOI) of 10. The EBV antigens were paired as follows: BRLF1+BMRF1, BALF5+BALF2, BMLF1+BGLF4, BHLF1+BHRF1, BARF1+BNLF2b, BLLF2+BCRF1, BILF1+BDLF3, BLLF1+BALF4, BXLF2+BNRF1, BILF2+BBRF1, BZLF1+BVRF2, LMP1+LMP2, EBNA1+EBNA2, EBNA3a+EBNA3b, EBNA3c+LP.

The next day, the LCLs were washed (RPMI, 770 x *g*, 8mins), and labelled with 50-100μCi (1.85-3.7MBq) of ^{51}Cr (Perkin Elmer, 2hrs, 37^{o}C) in sterile tubes. Excess ^{51}Cr was removed by washing (x2, RPMI, 770 x *g*, 8mins) and the LCLs resuspended in complete medium (Table II, Appendix C), before dispensing into a v-bottomed 96-well plate ($2.5x10^3$ cells/well). T cells were added to the LCLs at a ratio of 1:1 or 2:1 and incubated for 4-6hrs (37^{o}C, 5% CO_2). Untreated but radiolabelled LCLs served as a negative control (spontaneous release), and a 1% SDS solution induced 100% cell lysis, to serve as a positive control (total

release). 100µl of the culture supernatant was aspirated from each well and transferred to clean tubes. The live vaccinia virus was killed by overnight incubation in formaldehyde vapour.

^{51}Cr released into the culture supernatant by lysis of the target cells was quantified by a Cobra gamma counter (Packard). The % lysis of target cells was calculated as follows: (Test cpm - Spontaneous cpm) ÷ (Total release cpm – Spontaneous cpm). The T cells that had lysed 24%, or more, of only one vaccinia-target (expressing two antigens), were analysed a second time by examining their IFNγ-release in response to known peptides for the corresponding antigens (see Section 2.7.3).

2.7.3. Quantifying antigen-specific T cell clone activity by interferon-γ secretion

A B-lymphoblastoid cell line (BJAB) transduced with a retroviral expression vector containing *vOX2* or *CD200* (see Section 2.8.6) were HLA-matched to several human T cell clones and acted as APCs in these experiments. BJAB cells transduced with an empty vector were used as a control. Engineered BJAB cells were washed once with PBS (200 x *g*, 5mins), counted and dispensed into polystyrene tubes (for a final density of $6x10^4$ cells/well). EBV peptide antigens (corresponding to each peptide-specific T cell clone) were diluted in serum-free RPMI, and added to the BJABs (60mins, 37^{o}C). Molecular-grade dimethyl sulfoxide (DMSO) served as a vehicle control. The cells were washed twice in PBS (200 x *g*, 5mins) to remove any peptide left in solution, and resuspended in complete medium (Table II, Appendix C). 100µl of the BJAB suspension was dispensed into each well of a v-bottomed 96-well plate (Nunc). The T cell clones were counted, washed once in complete medium (770 x *g*, 8mins), resuspended in complete medium and dispensed onto the BJAB cells (100µl, $1x10^3$ cells/well). Following 16 hours of co-culture (37^{o}C, 5% CO_2), the supernatants were aspirated, and IFNγ concentrations determined by ELISA (Section 2.5.8).

2.7.4. Measuring the accumulation of intracellular IFNγ and IL-2 in human T cell clones

Engineered BJAB cells were washed in PBS (200 x *g*, 5mins) and dispensed into polystyrene tubes (2.5 x 10^5 cells). They were then incubated with EBV peptide antigens (60mins, 37°C, 5% CO_2), washed twice (PBS, 200 x *g*, 5mins), and resuspended in complete medium (Table II, Appendix C). Antigen-specific T cell clones were washed in complete medium (770 x *g*, 8mins) and dispensed into the tubes containing peptide-pulsed BJAB cells ($3x10^4$ T cells/tube in 80µl). The cells were centrifuged gently (100 x *g*, 3mins) and incubated for 60mins (37°C, 5% CO_2) before the addition of 20µl brefeldin A (to make a final conc. of 7.5µg/ml). Brefeldin A disrupts the structure and function of the Golgi apparatus, thereby inhibiting protein transport and resulting in an accumulation of cytokines in the Golgi. The cells were then incubated for a further 1, 2 or 4hrs (as indicated in the results section of Chapter 5) before fixation with 1.5% formaldehyde (10mins, room temp.). After washing in PBS (770 x *g*, 8mins, 4°C), the fixed cells were resuspended in PBS and stored overnight (4°C).

The next day, the cells were washed with PBS (770 x *g*, 8mins, 4°C), and incubated with anti-CD4 or anti-CD8 fluorophore-conjugated antibodies (Miltenyi, 60mins, 4°C), to label the T cell clones. All antibodies were diluted in PBS-2% BSA. After washing with PBS (770 x *g*, 8mins, 4°C), the cells were permeabilised with ice-cold methanol (30mins, 4°C) and then washed once with ice-cold PBS, and twice with PBS-2% BSA (770 x *g*, 8mins, 4°C). Fluorophore-conjugated antibodies reactive with IFNγ and IL-2 were incubated with the cells (BD Biosciences, 60mins, room temp.) and residual antibody washed away with PBS (770 x *g*, 8mins, 4°C). Antibody-labelling of the T cell clones was quantified by flow cytometric analysis (LSRII, BD Biosciences), and post-collection analysis of the data carried

out with FlowJo7 software (TreeStar Inc.). The cells were labelled with each antibody alone to compensate for any overlapping fluorescent signal in each sample.

2.7.5. Investigating intracellular signalling pathways downstream of T cell receptor ligation

Engineered BJAB cells ($2.5x10^5$) were incubated in 100µl complete medium (Table II, Appendix C), with the relevant EBV peptide (60mins, 37°C). T cell clones (final density of $3x10^4$ cells/well) were added to the BJAB cells and centrifuged (3mins, 150 x *g*) to place the cells in contact with each other. The cells were incubated at 37°C for the appropriate time period, and cell activity immediately quenched by addition of 16% formaldehyde (TAAB) to produce a final concentration of 1.5% (10mins, room temp.).

The cells were vortexed lightly between each wash and incubation period to prevent clumping. After fixation, the cells were washed twice in ice-cold PBS (770 x *g*, 8mins, 4°C), and incubated with anti-CD4 or anti-CD8-VioBlue antibodies (Miltenyi, 60mins, 4°C). All antibodies were diluted in PBS-2% BSA. Residual antibody was removed by washing with ice-cold PBS (770 x *g*, 8mins, 4°C), and the cells permeabilised with 100% methanol (30mins, 4°C) to enable labelling of intracellular antigens. Methanol was removed by washing once with ice-cold PBS, and twice with PBS-2% BSA (770 x *g*, 8mins, 4°C), before labelling with antibodies directed against the phosphorylated forms of several intracellular signalling molecules: anti-phospho-ERK1/2-PE, anti-phospho-p38-Alexa Fluor 647, anti-phospho-ζ-chain associated protein kinase 70 (Zap70)-Alexa Fluor 647, anti-phospho-Src homology 2 domain containing leukocyte protein of 76 kDa (SLP-76)-PE, anti-phospho-linker for activation of T cells (LAT)-PE, and anti-phospho-Akt-Alexa Fluor 647 (BD Biosciences, see Appendix B, 60mins, room temp.). Residual antibody was removed by washing with PBS-2% BSA (770 x *g*, 8mins, 4°C), the cells resuspended in PBS, and

analysed by flow cytometry (LSRII, BD Biosciences). FlowJo7 software (TreeStar Inc.) was utilised for post-collection analysis of the data.

2.7.6. Phenotyping the engineered BJAB cells

Engineered BJAB cells were washed with PBS (200 x *g*, 5mins) and dispensed into polystyrene tubes ($2x10^5$ cells/tube). The cells were incubated with anti-CD80 (Invitrogen), anti-CD86 (Invitrogen) or anti-HLA-DR (R&D Systems) antibodies, all diluted in PBS-2% BSA (60mins, 4^oC), or an isotype control (mouse IgG1, Sigma) before labelling with an anti-mouse-PE secondary antibody (Invitrogen). Cells were also labelled with anti-HLA-ABC directly conjugated with PE (Serotec) or Alexa Fluor 647 (Biolegend); see Table III, Appendix B, for matching isotype controls.

The expression of vOX2 and CD200 on the surface of engineered BJAB cells was carried out regularly. BJAB cells were washed with once with PBS (200 x *g*, 4^oC, 5mins), labelled with either anti-vOX2 (not commercial) or anti-CD200 (BD Pharmingen), washed once with PBS (200 x *g*, 4^oC, 5mins) and labelled with anti-mouse or anti-rabbit fluorophore-conjugated secondary antibodies (see Table II, Appendix B). Residual antibody was removed by washing with PBS (200 x *g*, 4^oC, 5mins), and protein expression quantified by flow cytometry (LSRII, BD Biosciences, or Coulter® Epics® XL™, BD Bioscience).

2.7.7. Quantifying the extent of HLA-ABC internalisation by BJAB cells

Engineered BJAB cells were washed (PBS, 200 x *g*, 5mins), dispensed into polystyrene tubes ($2.5x10^6$ cells/tube) and pelleted (200 x *g*, 5mins). The cells were resuspended in anti-HLA antibody (W6/32, in-house) diluted in RPMI (10% FBS, 1% Pen-Strep), and incubated (60mins, 4^oC) with frequent mixing. This step labelled all extracellular HLA-ABC. The cells were washed (x3, PBS, 200 x *g*, 5mins, 4^oC), dispensed into x9 polystyrene tubes (for each

cell type), and resuspended in warm 500µl of RPMI (10% FBS, 1% Pen-Strep, 37°C). The cells were incubated (37°C) for 0, 20, 40 or 60mins, then rapidly cooled and washed (PBS, 200 x *g*, 5mins, 4°C). The cells were then incubated with an anti-mouse-FITC secondary antibody (Sigma, 60mins, 4°C) to label any HLA remaining on the cell surface. The BJAB cells were washed (PBS, 200 x *g*, 5mins, 4°C), resuspended in PBS, and analysed on a Beckman Coulter® Epics® XL™ flow cytometer. Post-collection analysis of data was carried out with FlowJo7 (TreeStar Inc.). Each time-point was carried out in duplicate, and an isotype control (mouse IgG2a-FITC, BD Biosciences) acted as a control. Cells were labelled with each antibody separately in order to compensate for any overlapping fluorescent signal in each sample.

2.8. Constructing an RRV vOX2-expressing cell line

2.8.1. Infecting rhesus fibroblasts with RRV

Primary and telomerised rhesus macaque fibroblasts (RFB/tRFB) were maintained in complete RFB medium (Table II, Appendix C) in a humidified incubator. One hour prior to infection with either H26-95 or 17577 RRV strains, confluent cells were treated with hexadimethrine bromide (polybrene, 2µg/ml, Sigma) to enhance viral infection. The polybrene was removed and replaced with one part infectious virus, and two parts medium. At 3 days post-infection the cells were passaged (1 in 3 split), and the virus-containing medium divided between each new flask of cells. CPE was visible at 2-5 days post-passage, and images captured by a Zeiss Axiovert 40CFL microscope, with Axiovision 4.6 software. Virus-containing medium was snap-frozen at -70°C for later infections.

2.8.2. Determining the infectivity of RRV

Primary RFB cells were dispensed into a 6-well plate and allowed to become confluent.

Serial dilutions of RRV-containing medium (see Section 2.8.1) were made (ten-fold dilutions from 10^{-1} to 10^{-7}), and 100µl of each dilution added to 3 wells containing confluent RFB cells. The cells were incubated with virus for 24hrs (37°C, 5% CO_2). 1.4% Nobles agar was melted and cooled to 45°C before mixing with 2x medium (see Table II, Appendix C), and 4ml added to each well after aspirating the virus-containing medium. Once CPE was evident, the viral plaques in each well were counted and the number of plaque-forming units (PFU) calculated as follows: number of plaques x 10 x dilution factor = PFU/ml.

2.8.3. Extracting RNA from infected telomerised rhesus fibroblasts

Following the appearance of CPE in infected tRFB cells, they were trypsinised and pelleted. RNA was extracted from the cell pellet using a commercially-available kit (Qiagen); briefly, the cells were homogenised in lysis buffer, and passed 5-10 times through a 20-gauge needle. 1 volume of 70% ethanol was added to the homogenised cells, and the solution passed through a spin column (≥8000 *g*, 15sec). The column was then washed several times, and the RNA eluted in RNase-free H_20.

2.8.4. Northern Blotting

RNA samples (both total RNA and mRNA) were separated on a MOPS/formaldehyde gel (see Table II, Appendix C). RNA samples were deproteinised and denatured in the following solution: 2.2M formaldehyde, 15% formamide, 0.5x MOPS buffer (Table II, Appendix C, 15mins, 55°C). Ethidium bromide (2µg, Sigma) was included in the total RNA samples for visualisation by UV radiation. Following separation of the RNA, the gel was washed in dH_20 and 10x SSC (Table II, Appendix C), and the RNA transferred to Hybond-N nylon membrane (Amersham Biosciences) by capillary blotting in 10x SSC for 48 hours.

To create a radiolabelled probe, the translated region of the RRV vOX2 gene (*R14*)

was amplified by PCR (primers 2F and 2R, Table I, Appendix A), extracted from an agarose gel and purified using a commercially available kit (Qiagen). To radioactively label the probe, 25ng of DNA was denatured and then amplified by random priming, incorporating deoxycytidine 5'-triphosphate [α-^{32}P] (dCTP, Perkin Elmer), by means of a kit (Invitrogen). To remove traces of unincorporated nucleotides, primers, enzymes and salts from the labelled probe solution, a series of wash steps was carried out in a filter column (Qiagen). Briefly, large DNA fragments (>10kb) and oligonucleotides ($\geq$17 bases) were bound to the silica membrane within the column, and all unbound impurities washed through and discarded. The probe was eluted with 100µl H_20, denatured (95^oC, 5 mins), and hybridised with the blot.

The nylon membrane was rinsed in H_20, then pre-hybridised in hybridisation buffer (30mins, 60^oC, Table II, Appendix C). The buffer was discarded and replaced with 30ml fresh hybridisation buffer, and 50µl of the radiolabelled probe. The blot was hybridised overnight at 60^oC, and then washed to remove background signal as follows: rinsed in 2x SSC (Table II, Appendix C, 0.1% SDS; washed twice (5mins) in 2x SSC-0.1% SDS, washed twice (10mins) in 1x SSC-0.1% SDS; and washed four times (5mins) in 0.1x SSC-0.1% SDS, taking care to wash both sides of the membrane. While still damp, the membrane was wrapped in plastic, and exposed to hyperfilm (Amersham Biosciences).

2.8.5. Constructing an RRV vOX2-EGFP fusion protein

In order to examine the activities of native vOX2 and CD200, the B lymphoblastoid cell line BJAB had been engineered to express by retroviral transduction, transmembrane vOX2 and CD200, or an empty vector as control (Colman, C, unpublished). These cells were HLA-matched to human T cell clones (see Chapters 5, 6 and 7 for detailed descriptions) and therefore could be used in a model system of T cell function. In order to determine the

function of RRV vOX2 in this system, the same method must be followed in order to express the protein in the same cell type and by the same method. However, as there is no antibody directed against RRV vOX2, an enhanced green fluorescent protein (EGFP) was used as a tag for visualisation.

cDNA was prepared from RNA extracted from H26-95 RRV-infected tRFB (see Section 2.8.3), using 200U of Moloney Murine Leukemia Virus Reverse Transcriptase (M-MLV RT, Invitrogen), and random primers (Promega), following the manufacturer's instructions (Invirogen). A recombinant ribonuclease inhibitor (40U, RNAseOUT, Invitrogen) was included to minimise degradation of the RNA, and all steps carried out rapidly on ice.

The full sequence of RRV vOX2 *R14* was amplified by PCR (see Section 2.1 for method) incorporating a long 'buffer' sequence at either end beyond the coding regions (see primers 4F and 4R, Table I, Appendix A). This PCR product was ligated into a commercial sequencing plasmid (pCR®-Blunt II-TOPO, Invitrogen, Table II, Appendix A), and amplified by transformation of chemically competent One Shot® TOP10 *E. coli* (Invitrogen), and overnight shaking culture in LB broth (Acros Organics) with kanamycin selection (50µg/ml). One clone was selected for future investigation following sequencing.

(a)

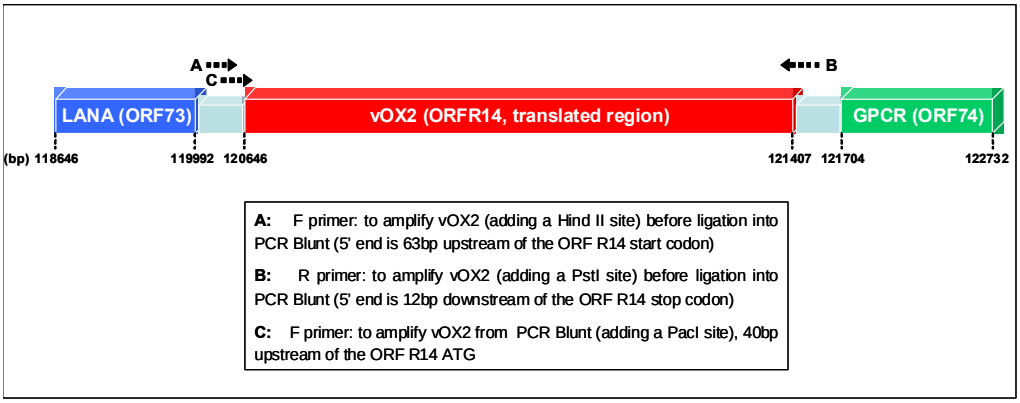

(b)

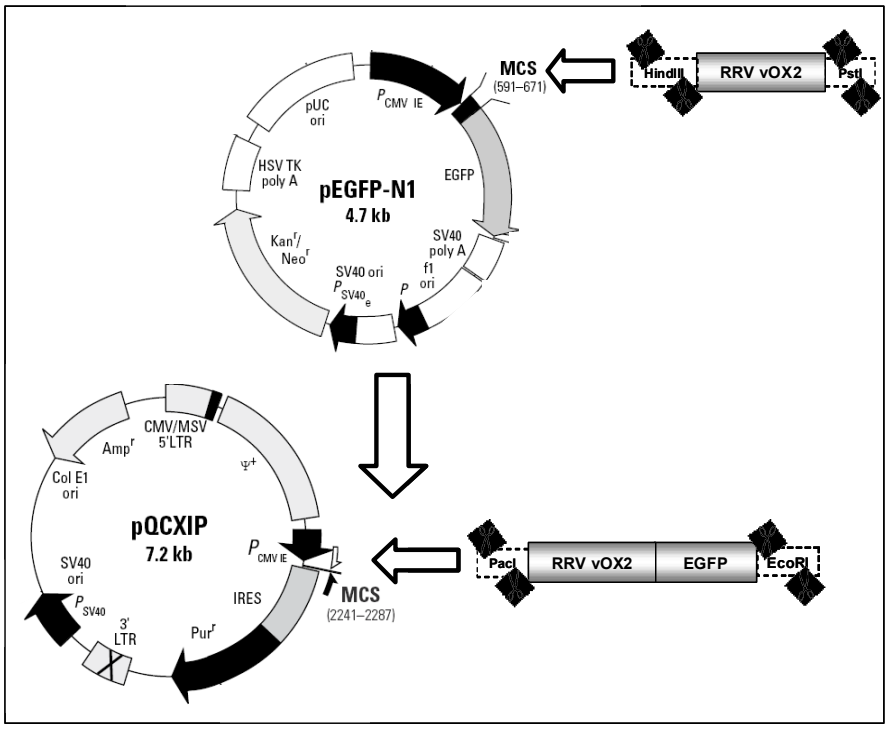

Figure 2.3 Cloning strategy to construct an RRV vOX2-EGFP fusion protein. (a) The *vOX2* gene (ORF R14) lies between the genes encoding LANA and the RRV GPCR. The entire ORF was amplified from cDNA derived from RRV-infected cells and ligated into a subcloning vector (pCR®-Blunt II-TOPO, Table II, Appendix A). **(b)** The translated region of *vOX2* was amplified from pCR®-Blunt II-TOPO by PCR with the addition of *HindIII* and *PstI* restriction sites, and ligated into the pEGFP-N1 vector, upstream of *EGFP*. Both *vOX2* and *EGFP* were amplified by PCR (as one sequence) with the addition of *PacI* and *EcoRI* sites, ligated into pCR®-Blunt II-TOPO and then extracted from the subcloning vector by restriction enzymes *PacI* and *EcoRI*. The retroviral vector pQCXIP was also digested with *PacI* and *EcoRI* before ligation with the *PacI-vOX2-EGFP-EcoRI* insert.

Primers incorporating restriction sites for HindIII and PstI enzymes (primers 5F and 5R, Table I, Appendix A; and primers A and B, **Figure 2.3**, **a**) amplified full-length RRV vOX2 *R14* (including the ATG start codon, and excluding the stop codon) from pCR®-Blunt II-TOPO by PCR, before ligation into the pEGFP-N1 plasmid (digested with *HindII* and *PstI*), upstream of the *EGFP* gene to create a vOX2-EGFP chimaera. The *vOX2-EGFP* sequence was then amplified by primers encoding *PacI* (primer C, **Figure 2.3**, **a**) and *EcoRI* (primers 6F and 6R, Table I, Appendix A) and again inserted into (pCR®-Blunt II-TOPO, Invitrogen, Table II, Appendix A) for sequencing. Once the sequence was determined to be correct and in-frame, *vOX2-EGFP* was digested by *PacI* and *EcoRI* restriction enzymes, and inserted into the pQCXIP retroviral vector (Table II, Appendix A), that had been digested with *PacI* and *EcoRI*. See **Figure 2.3 (b)** for an overview of the cloning strategy. Digestion of the modified plasmid with *PacI* and *EcoRI* released a fragment of the correct size. An endotoxin-free maxiprep (Qiagen, manufacturers instructions followed) enabled the isolation of pure, endotoxin-free copies of the pQCXIP plasmid containing RRV *vOX2-EGFP*.

2.8.6. Retroviral transduction of BJAB cells

Retroviral transduction was selected to introduce the RRV *vOX2-EGFP* gene into BJAB cells. Once the *vOX2-EGFP* chimaeric gene had been inserted into the pQCXIP plasmid (Table II, Appendix A), it was transfected into a packaging cell line (ie. GP2-293, Clontech), stably expressing the viral *gag* and *pol* genes, essential for viral particle formation. The pQCXIP plasmid confers puromycin resistance and expresses genes necessary for viral transcription, packaging and processing. The partition of genes necessary for viral production prevents the production of replication-competent virus upon recombination events, and means that virus cannot replicate in the target cells as the plasmid lacks the genes encoding structural proteins.

The packaging cell line, GP2-293 was plated in 60mm culture dishes at $1x10^6$ cell/plate in complete GP2-293 medium lacking antibiotic (Table II, Appendix C) and incubated overnight (37°C, 5% CO_2). The following day the medium was replaced, with the addition of chloroquine (25μM, Sigma), and cells were co-transfected with 5μg of both pQCXIP and the VSV-G plasmid, diluted in RPMI 1640 (1ml, Invitrogen) and lipofectamine (20μl, Invitrogen). The vesicular stomatitis virus envelope glycoprotein (VSV-G) facilitates virus entry through binding to the lipid bilayer and plasma membrane of the recipient cell, and cannot be stably expressed in the packaging cell line due to its toxicity. After 18hrs, the medium was aspirated and replaced with complete GP2-293 medium (Table II, Appendix C). Following a further 48-72hrs, the virus-containing medium was filtered through a 0.45μm filter, aliquoted, and stored at -80°C. Two controls were also prepared: lipofectamine-only and pQCXIP-negative.

The BJAB cells to be transduced were plated out at 2×10^5 cells per well in a 12 well plate, in pre-transfection medium (2mls, Table II, Appendix C), containing polybrene 4μg/ml, Sigma). The retroviral stocks were thawed and 500μl dispensed onto each well. The cells were placed under puromycin (1μg/ml, Sigma) selection after 24hrs. Stable selection of transduced cells could be visualised via the EGFP fluorescence of those transduced with pQCXIP-vOX2-EGFP and both from the killing of the lipfectamine-only control cells, and the absence of EGFP in the pQCXIP-negative control. Stably transduced cells were maintained in complete medium, and cultured long-term under puromycin selection.

2.9. Statistics

Statistical analysis of the data was carried out using SPSS 16.0 software (IBM Inc.) and is referred to throughout the thesis. Statistical significance is presented as (*$p<0.05$), (**$p<0.01$) or (***$p<0.001$).

Chapter 3. Production and analysis of Fc-fusion proteins

The generation of soluble forms of CD200 and KSHV vOX2 proteins for functional studies in *in vitro* models will be described in this chapter, with reference to the relevant methods outlined in Chapter 2. Comparative studies were performed on the engineered soluble CD200 and vOX2 proteins, and another engineered KSHV protein, KCPmut:Fc, served as a negative control.

3.1 Producing and analysing CD200:Fc

As discussed in Chapter 1, Fc-fusion proteins have a longer half-life *in vivo* and are therefore often used therapeutically because a low concentration is efficacious (Kamei *et al*., 2005). Fc-fusion proteins are also useful for conducting research into the function of transmembrane proteins, negating the need to introduce engineered cells into functional experiments. Fusing human IgG1-Fc to the extracellular region of a protein of interest enables the large-scale production of the protein by secretion from engineered cells, and its subsequent purification and analysis. However, the disadvantage of Fc proteins is their limited stability in storage. Oxidation of the methionine residues on the two Fc domains, C_H2 and C_H3, leads to aggregation of the protein, though the high glycosylation of proteins produced by CHO cells reduces this risk slightly (Liu *et al*., 2008).

Cells had been engineered previously in our laboratory (Rezaee *et al*., 2005) to produce vOX2:Fc, so a similar strategy was adopted to generate CD200:Fc. The *CD200* sequence encoding the extracellular domain of the CD200 protein was fused in-frame with the gene encoding the Fc region of human IgG1, in the pTorsten expression vector (see Chapter 2.1; CD200-pT clone 6). This insertion results in the expression of a soluble protein that will be secreted into the culture medium by cells transfected with the expression vector.

CHO cells were transfected with the CD200-pT plasmid, and stable transfectants selected with hygromycin B. Limiting dilution of the transfectants (Chapter 2.1.4) isolated a clone secreting high levels of the recombinant protein. To test for protein secretion, culture supernatants were sampled from several clones, and relative protein concentration was determined by SDS-PAGE and immunoblotting (Chapter 2.3) with an anti-human IgG1(Fc)-specific antibody (Table I, Appendix B). Each clone secreted different quantities of the recombinant protein (**Figure 3.1**). The Fc fragment is the strong lower band, approximately 26kDa in size. Clone B7 was selected for good protein expression and expanded. The CD200:Fc protein is the larger band, of approximately 70kDa.

The concentration of CD200:Fc protein secreted into the culture supernatant by clone B7 cells was enhanced by growing the cells in a small volume of medium in expanded-surface area roller bottles (Chapter 2.2.1). Due to previous endotoxin-contamination of vOX2:Fc generated in this laboratory (data not shown), care was taken to ensure that all equipment was disposable and certified endotoxin-free, or was thoroughly sterilised. CD200:Fc protein was purified from the culture fluid of clone B7 by protein A affinity chromatography (Chapter 2.2.2). Protein A is a component of *Staphylococcus aureus* bacterial cell walls and has high affinity for human IgG1. Contaminating bovine IgG from the FBS present in CHO cell culture medium was eluted selectively by lowering the pH within the protein A column (**Figure 3.2**; first peak of the chromatogram), and the CD200:Fc-protein was then eluted with a more acidic pH (**Figure 3.2**; second peak). In this manner, pure CD200:Fc was collected for analysis.

Every batch of CD200:Fc protein was analysed by coomassie blue staining, and purified protein resolved by SDS-PAGE and immunoblotting with anti-CD200 and anti-human IgG(Fc) antibodies. Staining the reduced gel with colloidal blue (Chapter 2.3.3) revealed a distinct band of protein that reduced in intensity with reduced protein

concentration (**Figure 3.3**, **a**). To confirm that the purified protein was CD200:Fc, an SDS-PAGE gel loaded with proteins from the same batch as that depicted in **Figure 3.3 (a)**, was transferred to PVDF membrane and immunoblotted with an anti-CD200:Fc antibody (see Table I, Appendix B). The lower protein band (**Figure 3.3**, **b**) corresponds to the expected 48kDa size of monomeric CD200 (Clark *et al*., 2008), indicating that the larger protein of approximately 70kDa (**Figure 3.3, a**, **b**) represents dimeric protein resistant to denaturation, as described for vOX2:Fc (see Section 3.2).

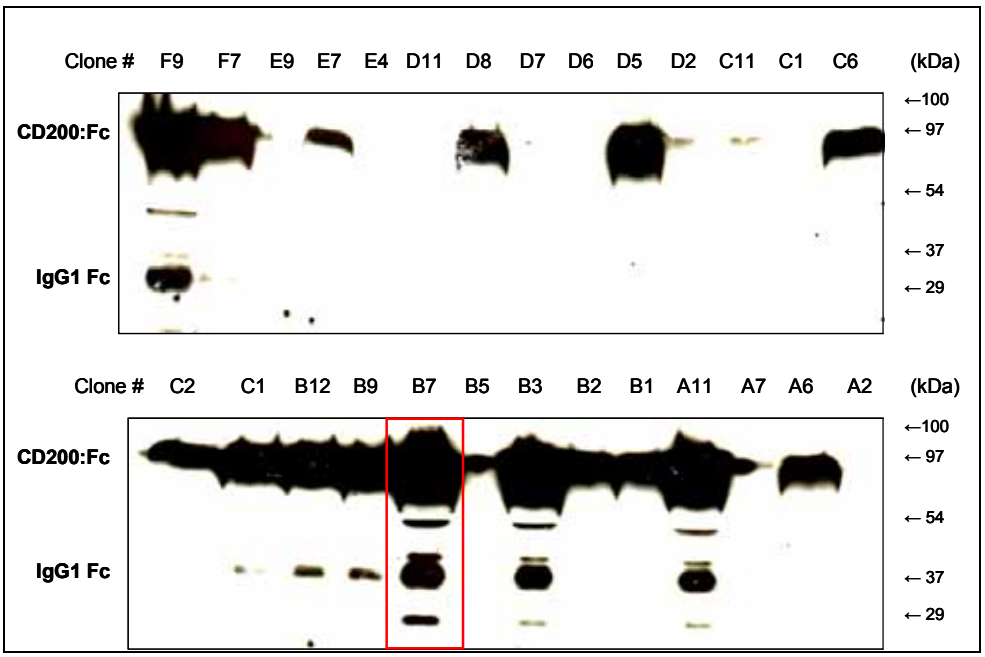

Figure 3.1 Screening CD200-pT-transfected CHO cell clones for optimal CD200:Fc protein production. CHO cells, stably transfected with CD200-pT and cloned by limiting dilution, were evaluated for their CD200:Fc production. 10µl of culture supernatant from a confluent 24-well plate was subjected to SDS-PAGE, followed by immunoblotting with a commercial anti-human IgG1 (Fc) antibody. Four clones (F9, B7, B3 and A11) secreting CD200:Fc into the culture supernatant were identified. Clone B7 was selected for further analysis and subsequent protein production.

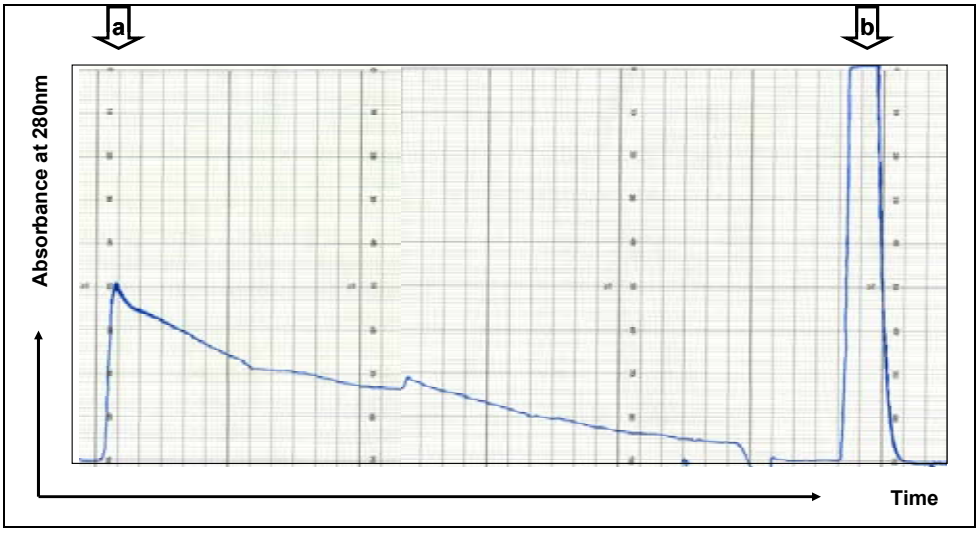

Figure 3.2 Purification of CD200:Fc by protein A affinity chromatography. Cell supernatant was passed through a protein A column. 0.1M Citrate buffer (pH 5.0) eluted bovine IgG (peak **a**), which binds with a lower affinity to protein A than the Fc-fusion proteins. 0.1M glycine (pH 2.8-3.0) eluted CD200:Fc, seen as the second and higher peak **(b)** in the chromatogram. The identity of the eluted CD200:Fc was confirmed by immunoblotting. This figure is also representative of the data obtained in the present thesis during purification of vOX2:Fc and KCPmut:Fc recombinant proteins.

(a) Coomassie blue stain **(b) Immunoblotting for CD200**

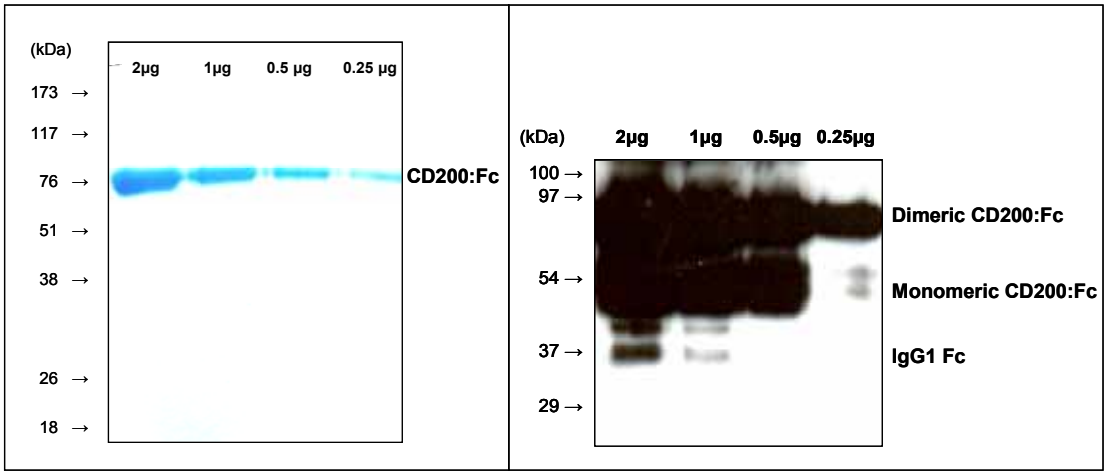

Figure 3.3 Visualising purified CD200:Fc proteins by staining with colloidal coomassie blue and immunoblotting. Recombinant CD200:Fc was purified by affinity chromatography and separated by SDS-PAGE. **(a)** Colloidal coomassie staining visualised the protein. **(b)** CD200:Fc was detected by immunoblotting with an anti-CD200 commercial antibody. The amount (µg) of protein loaded in each well is indicated.

3.2 Producing and analysing KCPmut:Fc and vOX2:Fc

Stable cell lines expressing engineered soluble forms of KSHV complement control protein (KCP), KCPmut:Fc (Mark *et al*., 2004) and vOX2, called vOX2:Fc (Rezaee *et al*., 2005) had been generated previously. KCPmut:Fc is a soluble and functionally incompetent form of KCP, discussed in Chapter 1.3.9.

KCPmut:Fc was generated in collaboration with our laboratory by Mark *et al*. by site-directed mutagenesis of three positively charged lysines (Lys-64, Lys-65, Lys-88) between CCP domains 1 and 2, to glutamines, lacking a charge. The KCP-mediated decay of classical C3 convertase is almost completely abolished in the mutant protein, along with its ability to act as a cofactor in the degradation of C3b and C4b (Mark *et al*., 2004).

vOX2:Fc and KCPmut:Fc proteins were produced and purified in parallel with CD200:Fc for the experiments outlined in this thesis, and were analysed by SDS-PAGE. Both monomeric and dimeric forms of vOX2:Fc were evident when the purified protein was analysed by SDS-PAGE and subsequent immunoblotting with anti-vOX2:Fc or anti-human IgG1(Fc)-specific antibodies (**Figure 3.4**, **a**). Previous analysis of vOX2:Fc by mass spectrometry had confirmed the presence of dimeric and monomeric protein even under reducing conditions (Rezaee, S.A.R., University of Birmingham PhD thesis, 2006). Rezaee reported a dominant protein band of approximately 65-70kDa in size. Further stocks of the vOX2:Fc protein were produced at the National Biomanufacturing facility under the auspices of Eden Bioscience.

The immunoblotting pattern for KCPmut:Fc under reducing conditions corresponded to that reported previously in the literature (Mark *et al*., 2004). Two clear bands (of 95kDa and 50kDa) correspond to dimeric and monomeric KCPmut:Fc respectively (**Figure 3.4**, **b**).

The concentration of vOX2:Fc protein supplied by Eden Bioscience was quantified by analysing vOX2:Fc by SDS-PAGE in concert with serial dilutions of known concentrations of BSA (**Figure 3.5, a**) and mouse IgG2a (**Figure 3.5, b**).

The extent of endotoxin contamination of vOX2:Fc, CD200:Fc and KCPmut:Fc was quantified by the LAL assay (see Chapter 2.2.3). High levels of endotoxin of initial batches of purified vOX2:Fc had been identified and would confound downstream functional analysis. The method of purification was therefore altered and all equipment was sterile and certified endotoxin-free where possible. Every batch of purified protein was analysed for endotoxin, and all protein with endotoxin contamination >1EU/ml (the limit of resolution of the LAL assay) was discarded (**Figure 3.6**). Protein fractions with low endotoxin contamination and high protein concentration were pooled and used in all experiments to minimise heterogeneous results from batch to batch variation.

(a) Immunoblotting for vOX2:Fc **(b) Immunoblotting for KCPmut:Fc**

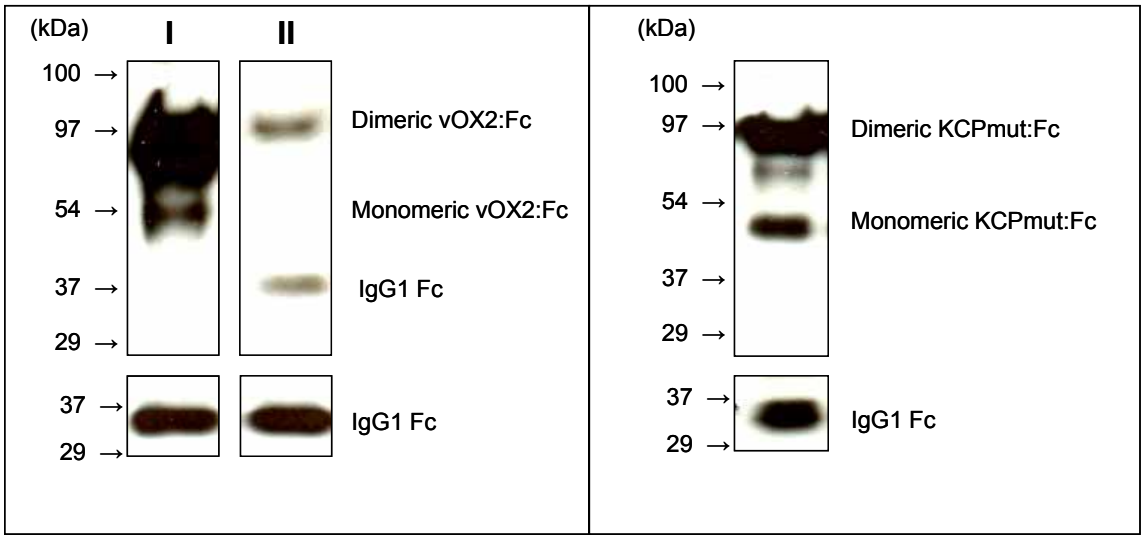

Figure 3.4 Analysis of affinity-purified vOX2:Fc and KCPmut:Fc recombinant proteins by Western Blot. The proteins were separated by SDS-PAGE. **(a)** Immunoblotting with first anti-vOX2 monoclonal antibody (**I**), and then anti-vOX2 polyclonal antibody (**II**) revealed both dimeric and monomeric forms of vOX2:Fc (in the sample protein sample). **(b)** Anti-KCP antibody reacted with dimeric and monomeric forms of recombinant KCPmut:Fc. A commercial anti-human IgG1 (Fc-specific) antibody identified the Fc region of the recombinant proteins, **(a)** and **(b)** bottom panels. The identities of dimeric and monomeric forms of vOX2:Fc had been previously confirmed by mass spectrometry (see Rezaee, S.A.R., PhD thesis, 2006).

(a)

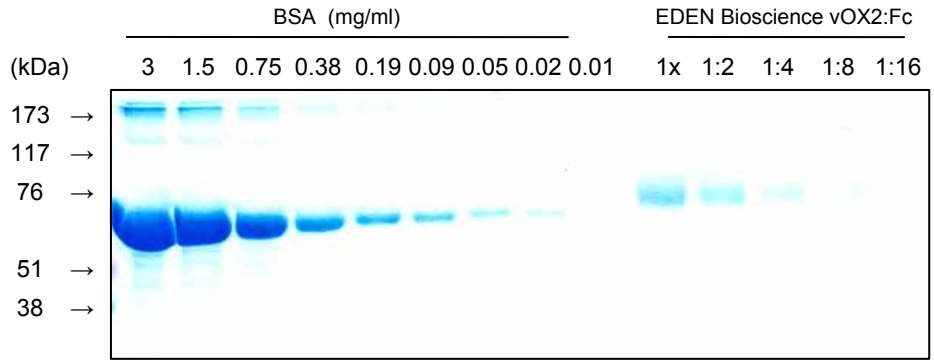

(b)

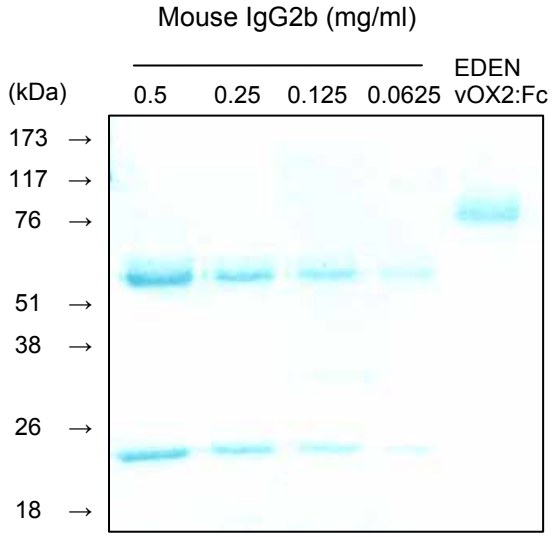

Figure 3.5 Determining the concentration of commercially prepared vOX2:Fc. To determine the concentration of vOX2:Fc prepared by Eden Bioscience, the proteins were denatured and separated by SDS-PAGE, and compared with known amounts of either bovine serum albumin (BSA) **(a)**, or a murine antibody IgG2a **(b)**. The gels were stained with colloidal coomassie blue to visualise the proteins. In panel **(a)**, the concentration of vOX2:Fc was deduced to be between 0.19 and 0.09mg/ml, and in panel **(b)**, the protein concentration was estimated to be between 0.25 and 0.125mg/ml. The protein was thereafter assumed to be 0.15mg/ml.

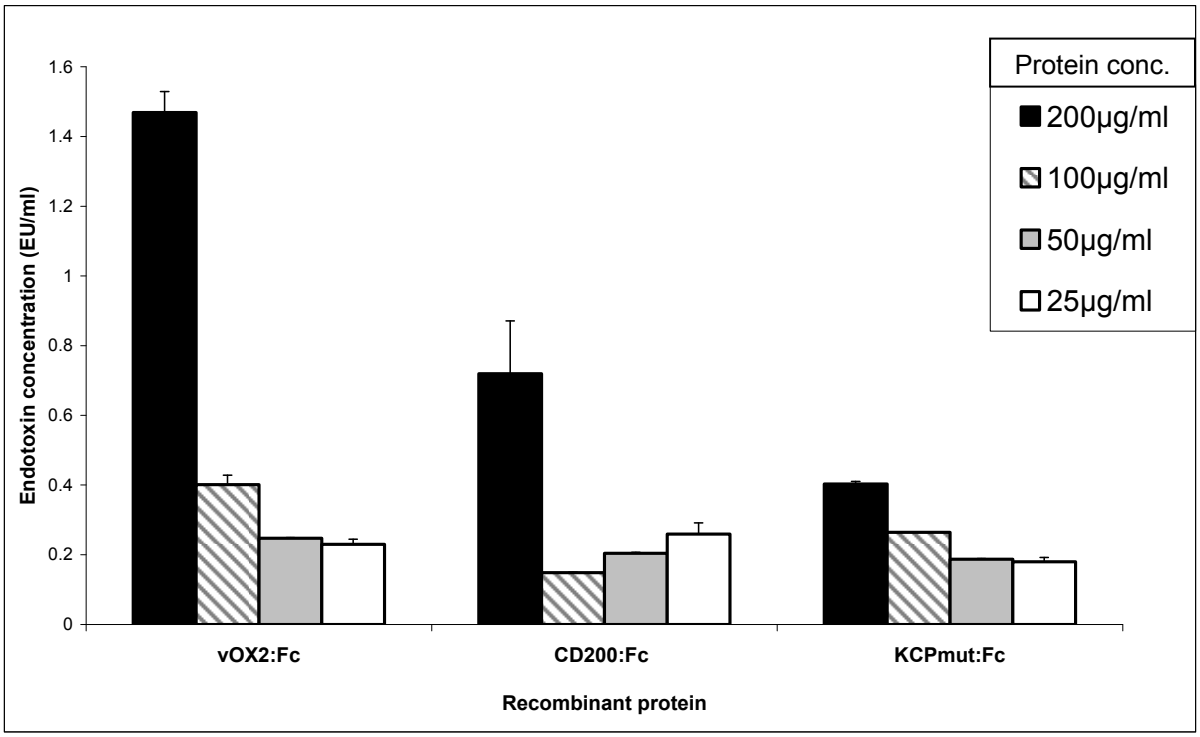

Figure 3.6 Quantification of endotoxin levels in purified recombinant protein stock solutions. The endotoxin levels of purified recombinant protein stocks were quantified by the Limulus amoebocyte lysate (LAL) assay. Endotoxin units (EU) are a measure of the level of endotoxin as determined by LAL, and do not directly correlate with lipopolysaccharide concentration. Each sample was analysed in duplicate, and the data presented as means ± SEM.

3.3 Discussion

CHO cell clones stably transfected with CD200-pT were analysed for their production of CD200:Fc, and clone B7 was subsequently selected as the highest producer for further study. CD200:Fc was purified from this clone for use in *in vitro* functional assays of neutrophil and leukocyte activity (Chapter 4). vOX2:Fc and KCPmut:Fc were also purified from previously engineered cell lines, and the immunoblotting profiles (**Figure 3.4**) were confirmed as consistent with previous reports (Rezaee, S.A.R., 2006, PhD thesis) and (Mark *et al*., 2004). Although analysis by SDS-PAGE allows for comparison with the literature and between batches of protein, it does not determine functional activity.

KCPmut:Fc was selected as a negative control for functional experiments. It is imperative that the presence of the human IgG1 Fc region is controlled for in these experiments, as the Fc domain can bind to specific receptors (FcγRs) expressed on human leukocytes, thus initiating either stimulatory or inhibitory responses. *In vivo*, IgG1 binds to pathogens and then to FcγRs expressed on the surface of phagocytic cells, initiating an innate immune response. Because aggregates of IgG1 bound to a pathogen can be distinguished from soluble antibodies by the phagocyte, monomeric IgG1 binding and dissociating rapidly does not initiate a response. IgG1 can stimulate neutrophils to generate reactive oxygen species and anti-microbial enzymes, as well as directly inducing killing by NK cells and macrophages (Murphy, 2008). Ligation of FcγRs can also suppress the immune response. For example, IgG1-FcγRIIB binding inhibits the B cell receptor (BCR)-mediated proliferation and maturation of B cells into plasma (antibody-secreting) cells, and negatively regulates the activatory FcγRs on macrophages, neutrophils and mast cells (reviewed in Nimmerjahn and Ravetch, 2006).

Therefore, any alteration in leukocyte function that occurs as a result of KCPmut:Fc treatment can be discounted and assumed to be a result of the Fc domain ligating to its receptor on the surface of phagocytic cells. Results obtained with the negative control protein may also be a consequence of factors such as endotoxin contamination. As discussed in Chapter 1, endotoxin, or lipopolysaccharide (LPS), a component of gram-negative bacterial cell walls, is a potent stimulator or 'primer' of neutrophils (Nick *et al*., 1996). The ligation of Toll-like receptors (TLRs) on the surface of immune effector cells by endotoxin leads to the expression of pro-inflammatory cytokines, thus amplifying the immune response. *In vivo*, administering a low dose of LPS to a healthy human results in a rapid increase in circulating TNFα and IL-1β (pro-inflammatory cytokines), closely followed by anti-inflammatory cytokines such as IL-10 (Andreasen *et al*., 2008). Proliferation of neutrophils, monocytes and lymphocytes occurs within 90mins of LPS treatment, thus inducing systemic inflammation (reviewed in Andreasen *et al*., 2008). Therefore, the endotoxin content of vOX2:Fc, CD200:Fc and KCPmut:Fc is extremely important, and is difficult to control for as many components of cell culture medium, such as FBS, are contaminated. In addition to sterilizing all equipment, the endotoxin levels within each batch of protein were determined (**Figure 3.6**) and any protein with >1EU/ml was discarded. The U.S. Food and Drug Administration (FDA, www.fda.gov), uses the LAL assay to quantify endotoxin contamination of drugs and medical devices. They recommend an upper limit of 0.5EU/ml for endotoxin contamination of drugs, and that no more than 5EU/kg body mass should be administered to humans. For our purposes, the protein stocks were diluted substantially and so a concentration of 1EU/ml of the stock was chosen as the maximum endotoxin level for these experiments.

Chapter 4. The roles of soluble CD200:Fc and vOX2:Fc in modulating leukocyte activity

Due to extensive research on the roles of both native CD200 and CD200:Fc in modulating the immune response, and data demonstrating a neutrophil-suppressive role for KSHV vOX2:Fc (Rezaee *et al*., 2005), the initial experiments outlined in this chapter investigated the influences of vOX2:Fc and CD200:Fc soluble proteins on the function of human leukocytes.

4.1. CD200R is expressed on human leukocytes

Before examining whether vOX2:Fc or CD200:Fc soluble proteins could alter the function of primary leukocytes, the expression of human CD200R on granulocytes, monocytes and lymphocytes was confirmed by flow cytometry (see **Figure 4.1**). Both vOX2 and CD200 bind to human CD200R with similar affinity (Foster-Cuevas *et al*., 2004). Primary leukocytes were isolated from the blood of healthy human donors (Chapter 2.5.2), and stained with an anti-CD200R monoclonal antibody and a matched fluorophore-conjugated secondary antibody (Chapter 2.6.1). The cell populations were identified and gated in the FSC vs. SSC plot (**Figure 4.1**, **a**), ie. lymphocytes, monocytes and granulocytes. Within each population, the fluorescence value for the isotype control antibody stained cells was compared with that for the cells labelled with anti-CD200R (**Figure 4.1**, **b**). A clear shift in fluorescence for anti-CD200R stained cells confirmed the expression of cell-surface CD200R on all three cell types. Following confirmation of CD200R expression by leukocytes, aspects of the function of these cells were analysed in the presence and absence of CD200:Fc and vOX2:Fc, as described below.

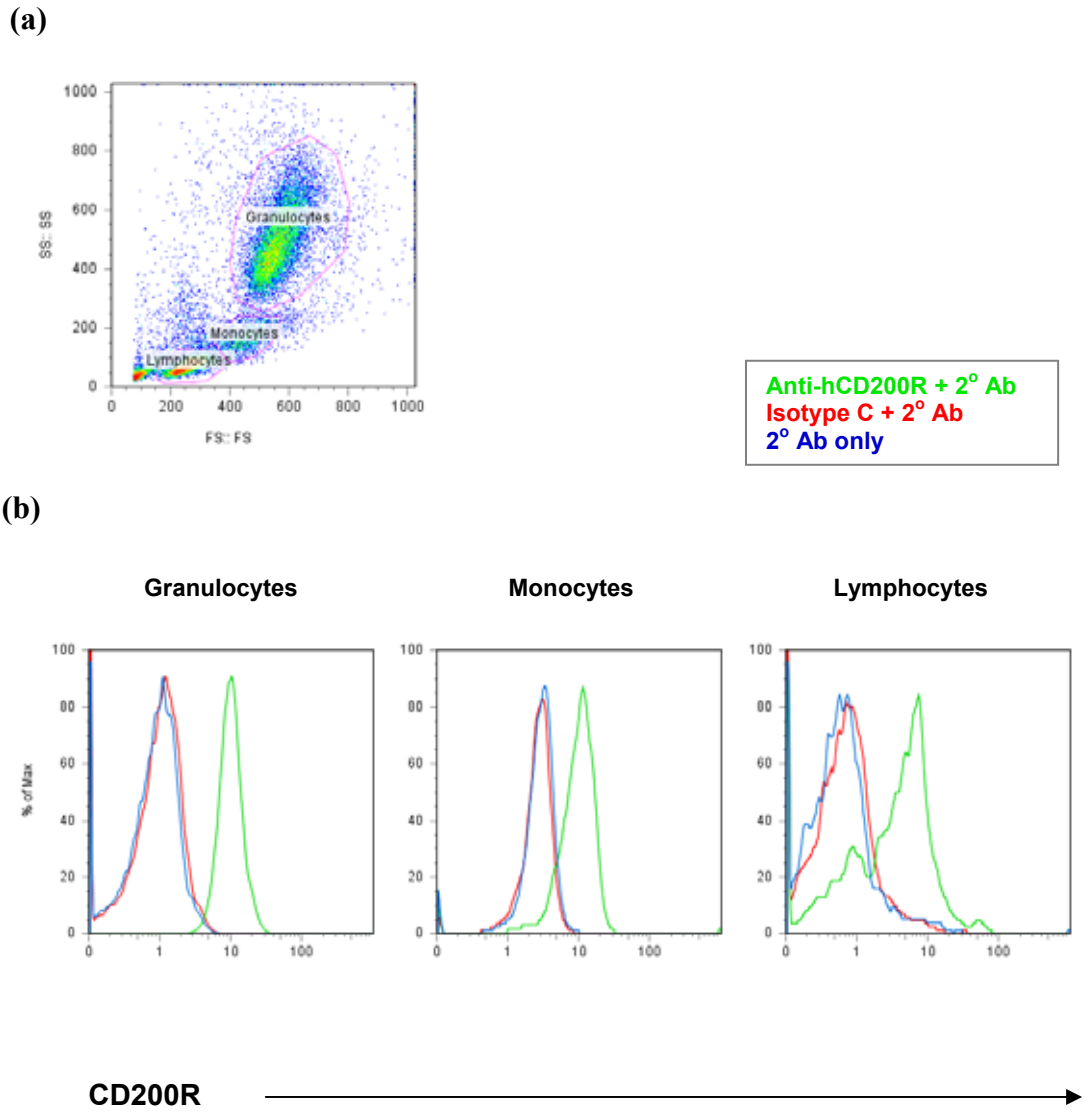

Figure 4.1 CD200R expression on primary human leukocytes. Leukocytes were isolated from healthy human donors by gradient centrifugation, and labelled with an anti-CD200R antibody for flow cytometric analysis. The three major leukocyte populations were isolated by size and granularity **(a)**, and CD200R expression quantified (green), in comparison to the secondary antibody only (blue line), and an isotype control antibody (red) **(b)**. These data are representative of two independent experiments carried out with leukocytes isolated from two healthy donors.

4.2. vOX2:Fc and neutrophil function

Since neutrophils express CD200R (**Figure 4.1**), for which vOX2 and CD200 are ligands, vOX2 and CD200 might regulate neutrophil activity. There are three methods by which the function of primary human neutrophils may be measured. The release of superoxide anions into the surrounding environment, via the assembly of the NADPH oxidase complex, can be measured by reactivity of chemiluminescent substrates with the extracellular superoxide anions (**Figure 4.2**, **1**), the oxidative activity of the NADPH oxidase complex can be measured by oxidation of a fluorescent compound (**Figure 4.2**, **2**), and the release of antimicrobial enzymes from intracellular secretory granules can be measured (**Figure 4.2**, **3**). These methods are detailed in Chapter 2.5.3-5.

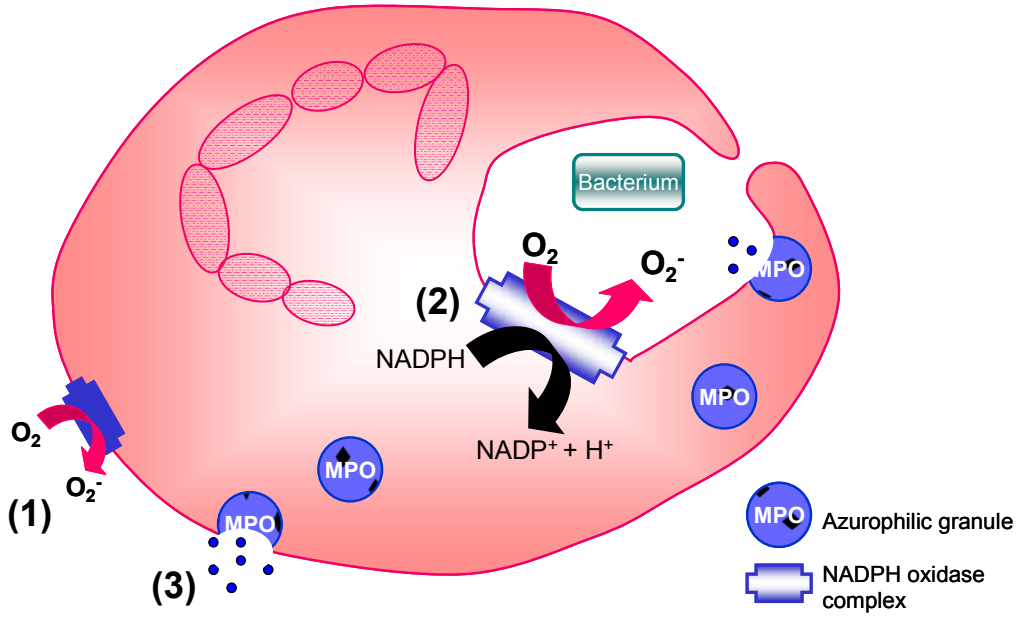

Figure 4.2 Measuring primary human neutrophil activity. Biological activities of human neutrophils isolated from whole blood were analysed by three methods. **(1)** The release of superoxide anions (O_2^-) into the extracellular milieu was quantified by the subsequent reduction of lucigenin, resulting in chemiluminescence. **(2)** Flow cytometric quantification of the reduction of a fluorogenic substrate within granulocytes gauged the intracellular superoxide generation by the NADPH oxidase complex. **(3)** Neutrophil degranulation, specifically the release of myeloperoxidase from neutrophil azurophilic granules, was measured by the activity of the enzyme on a peroxidase substrate.

4.2.1. Optimisation of the neutrophil superoxide burst chemiluminescence assay

The neutrophil superoxide release assay relies on the reductive and luminescent properties of lucigenin (N,N'-dimethyl-9,9-biacridinium dinitrate). Lucigenin is reduced by superoxide ions, resulting in chemiluminescence, and therefore can sensitively quantify superoxide production by leukocytes (Afanas'ev *et al*., 2001).

Although lucigenin reduction is a recognised method for detecting superoxide release, initial experiments during the present study revealed high variability in the magnitude of the detectable superoxide released by isolated neutrophils. Therefore several experiments were undertaken to optimise this assay. Initially, the detectable superoxide discharged by neutrophils was suboptimal, with the luminometer detecting less than 500 RLU for peak superoxide release. To determine whether the cell isolation protocols for both neutrophils and whole blood leukocytes were rendering the neutrophils non-functional, a maximal release of superoxide was induced by treatment with PMA (2nM). A slow, extended increase in superoxide production, reaching approximately $3x10^4$ RLU, in response to PMA treatment, was observed in both isolated neutrophils and whole blood leukocytes (data not shown), indicating that the cells were functional.

Next, the neutrophils were incubated in an opaque white high-binding plate instead of a black 96-well plate, because the reflective white lining results in an amplification of the chemiluminescent signal. Comparison of two priming agents, TNFα and GM-CSF, identified GM-CSF as the optimal priming agent (data not shown). Although the magnitude of superoxide release was enhanced with GM-CSF treatment, the neutrophils also responded to treatment with fMLP alone, indicating that a factor unrelated to the protocol was causing non-specific activation of the cells.

To determine whether either a component of the luminometer plates or the presence of a contaminant was activating the neutrophils during treatment, a comparison was made of

two methods. Cells were either treated in a luminometer plate, or were incubated in a cell culture-treated plate before transfer to a luminometer plate prior to reading. The transfer of cells following their treatment results in a low detectable superoxide burst, in comparison with those that were not transferred (**Figure 4.3**, **a**). These results suggest that only a small number of activated neutrophils are transferred due to their adherence to the plastic tissue culture plate. Neutrophils remaining in suspension do not produce superoxide anions in response to GM-CSF treatment (Johnson & Gomez-Cambronero, 1995), and are more likely to be transferred to the luminometer plate than activated adherent cells. However, though the superoxide burst produced by the non-transferred cells was substantial, they were still activated in the presence of fMLP, but the absence of GM-CSF priming (**Figure 4.3**, **a**). These data suggest that they may have been reacting to a component of the plate they were incubated in, or a reagent contaminant. As a result of these experiments, the neutrophils were not transferred from the plate in which they were cultured for superoxide release assays.

Next, to examine whether an intrinsic component of the luminometer plates being used was activating the cells, four 96-well white opaque plates with different properties, supplied by three biotechnology companies were compared in parallel with neutrophils isolated from one donor. Thus, both high-binding and tissue-culture treated sterile plates were sourced for comparison. The neutrophils were non-specifically activated in each plate (**Figure 4.3**, **b**), regardless of its sterility or binding properties, indicating that either reagent contamination or investigator experience was the cause of spontaneous neutrophil priming.

To determine whether either reagent contamination or investigator experience was the cause of neutrophil activation, another researcher (Investigator two, **Figure 4.3**, **c**) who is highly experienced in neutrophil analyses, performed the experiment in parallel with myself (Investigator 1). Investigators 1 and 2 isolated neutrophils in parallel, with separate reagents and in separate locations, but from blood taken from the same healthy donor at the same

time. The cells isolated by Investigator 2 responded well to GM-CSF, and the magnitude of superoxide release from cells treated with fMLP alone was only approximately 25% of that detected in neutrophils stimulated with both GM-CSF and fMLP. In contrast, the superoxide release from neutrophils isolated by Investigator 1 was of a much lower magnitude, and the detectable superoxide released from cells stimulated with fMLP alone was approximately 50% of the release induced by both GM-CSF and fMLP. These results suggested that reagent contamination was the source of variability in the magnitude and duration of superoxide release.

Substituting certified endotoxin-free BSA into the HBSS-1% BSA solution abolished all non-specific activation of the neutrophils (**Figure 4.3**, **d**). A comparison of the four luminometer plates from three sources in parallel with the use of sterile BSA showed no substantial differences between the detectable superoxide produced in each plate. Superoxide induced by fMLP alone was approximately only 15% of the superoxide release by cells treated with GM-CSF and fMLP. The replacement of sterile-filtered BSA with certified endotoxin-free BSA eliminated the spontaneous neutrophil activation and facilitated a short, defined release of superoxide, visualised as a peak in relative light units 1 minute after addition of fMLP. Certified endotoxin-free BSA was used in all subsequent assays, in conjunction with sterile, tissue culture-treated white opaque 96-well plates from Greiner; the cells were treated and the output read in the luminometer plates without cell transfer.

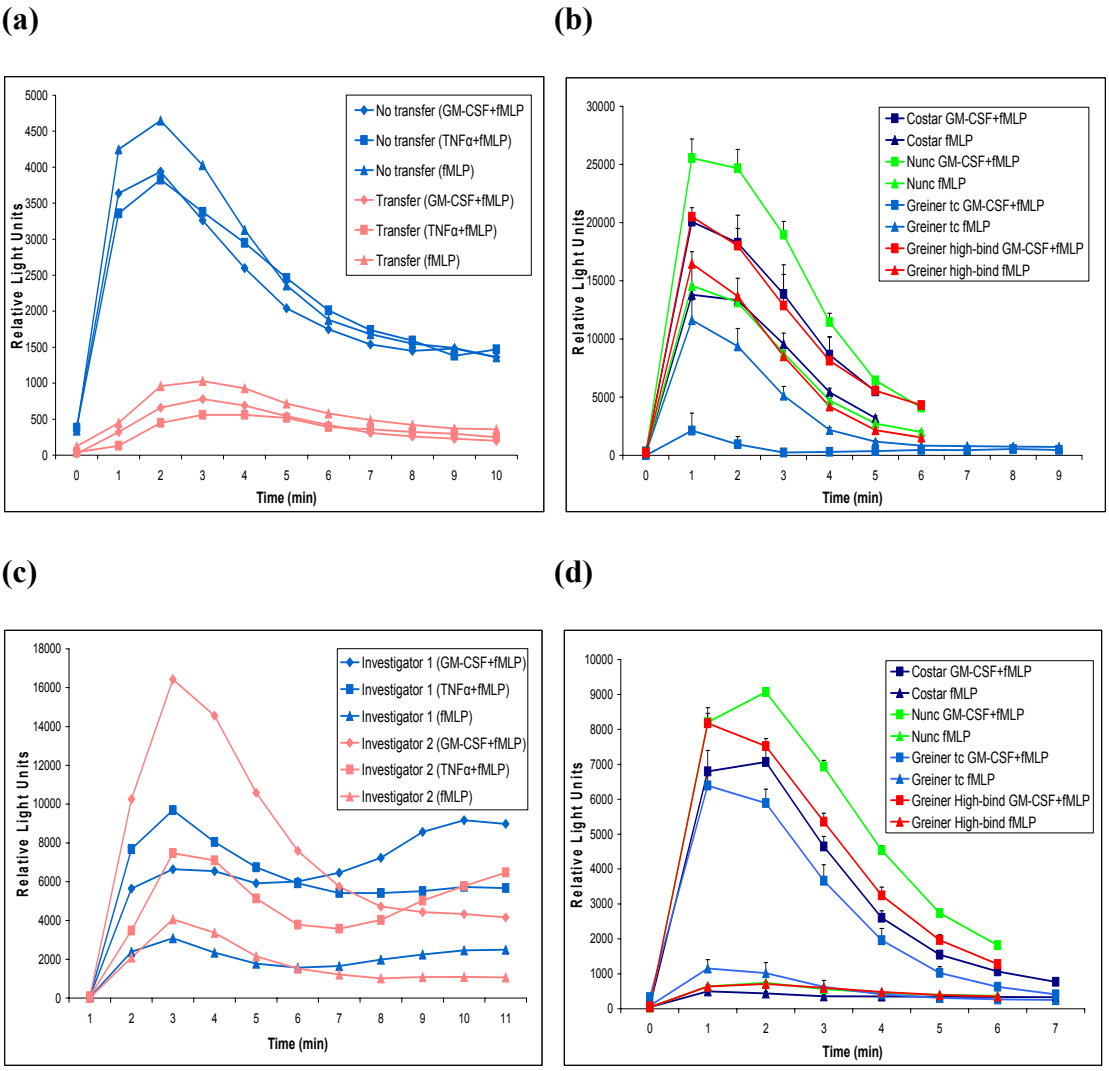

Figure 4.3 Optimisation of a chemiluminescent assay for quantifying neutrophil superoxide release. Neutrophils were isolated from the blood of a healthy donor by density gradient centrifugation, and primed for superoxide release with either GM-CSF or TNFα (both at 50ng/ml, 30mins, 37°C). Release of superoxide from the cells was induced by treatment with fMLP (1μM) and detected by reaction with lucigenin. **(a)** Neutrophils were treated, and either incubated and the output read in a 96-well opaque white microplate, or transferred from a cell culture-treated 96-well plate to an opaque plate. **(b)** Evaluating the impact of microplates from different sources on neutrophil superoxide release. Neutrophils were primed and incubated in a range of four luminometer plates from three sources to examine whether the sterility or binding properties of each plate affect superoxide release. **(c)** Neutrophils were isolated from the blood of one healthy donor by two investigators in parallel using separate reagents, and the superoxide assay then carried out in parallel. **(d)** The BSA used in previous experiments **(a**, **b**, **c)** was suspected to contain contaminants, resulting in the activation of neutrophils regardless of any subsequent treatments. To test this suspicion, isolated neutrophils were resuspended in buffer containing BSA that was certified as endotoxin-free. The neutrophils were also incubated in four test plates to evaluate any differences between the plates (as in **b**) in addition to replacing the BSA. All spontaneous bursting in response to fMLP treatment alone was reduced, compared with **(c)**, suggesting that the original BSA was the source of a contaminant activating the neutrophils.

4.2.2. Leukocyte and neutrophil superoxide burst in the presence of vOX2:Fc and CD200:Fc

Neutrophils and leukocytes were isolated from healthy donor blood. They were primed with GM-CSF and stimulated with fMLP to induce a rapid secretion of superoxide anions that were quantified by a chemiluminescent assay (Chapter 2.5.3). The typical kinetics of superoxide generation by neutrophil and leukocytes are presented in (**Figure 4.4**, **a**) and (**Figure 4.4**, **b**) respectively. Oxidative burst is characterised by a short, sharp increase in chemiluminescence, corresponding to superoxide release that gradually exhausts. Incubation of either the neutrophils or leukocytes with vOX2:Fc before stimulation did not alter the kinetics of oxidative burst, nor the relative amounts of superoxide released at the peak time of production, in comparison to either untreated cells, or cells treated with KCPmut:Fc (**Figure 4.4**, **c** and **d**). In the leukocyte population, neutrophils are the primary secretors of superoxide; however, small subpopulations of basophils and eosinophils can contribute to the superoxide production. Monocytes may also directly impact neutrophil activity by the production of cytokines such as the potent chemoattractant IL-8.

To determine the dose-dependent response of neutrophils and leukocytes to the recombinant proteins, the oxidative burst of these cells was quantified in the presence of increasing concentrations of vOX2:Fc, CD200:Fc or KCPmut:Fc (**Figure 4.5**). As before, the cells were pre-incubated with the recombinant proteins before stimulation, at concentrations of 0.8, 4, 8, 16 and 40μg/ml. The superoxide levels at the peak time of release (measured as RLU), were calculated as a percentage of the luminescence (RLU) generated by stimulated cells without protein treatment. With increasing concentrations of recombinant proteins, there was a slight increase in the peak level of superoxide generation. However, this increase with vOX2:Fc and CD200:Fc is indistinguishable from cells treated with the control

protein KCPmut:Fc. Therefore, the effect is likely to be non-specific and unrelated to protein activity.

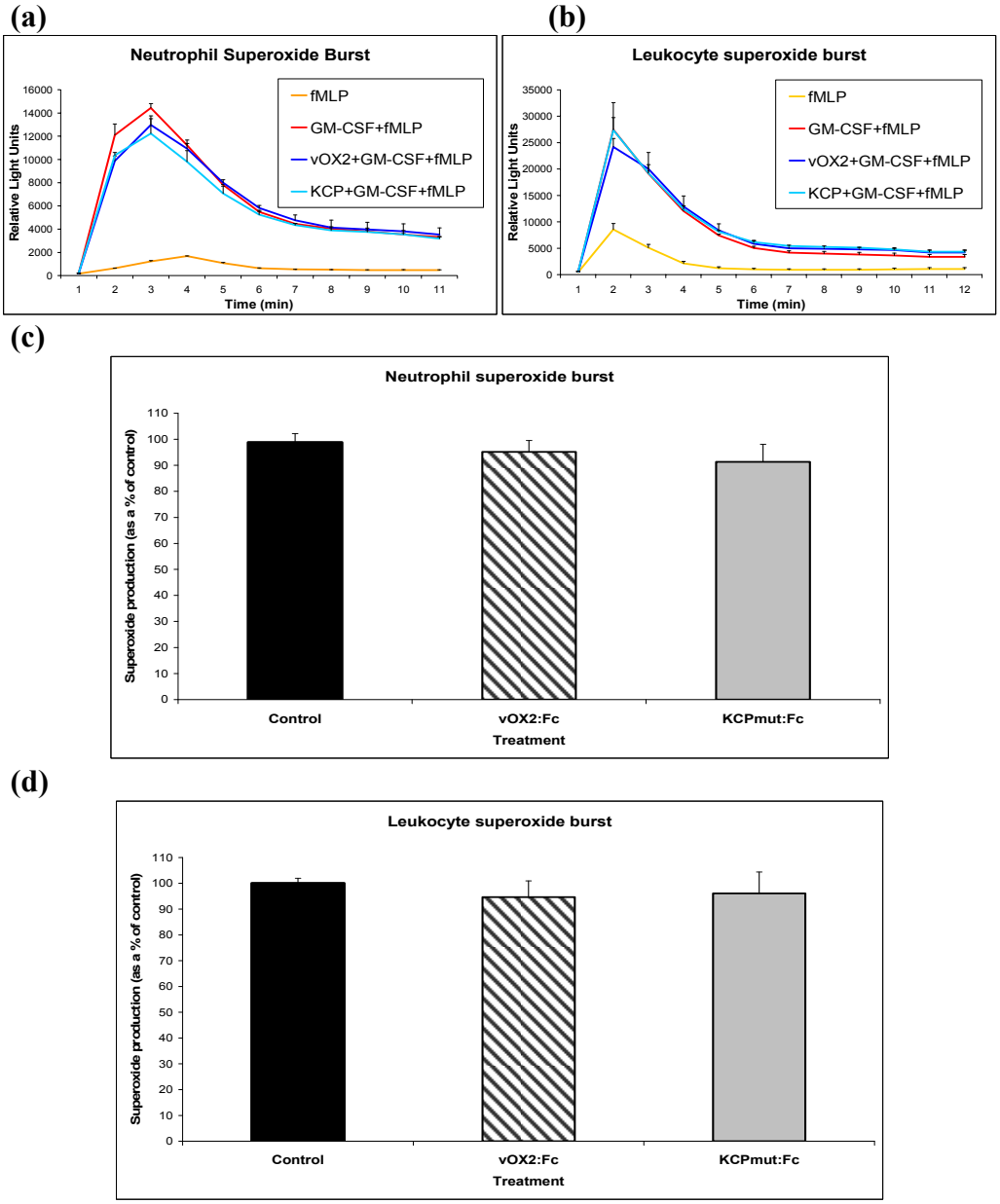

Figure 4.4 Neutrophil superoxide release is not altered by pre-treatment with vOX2:Fc (8µg/ml). Neutrophils or leukocytes were isolated from the blood of a healthy donor by density gradient centrifugation, and either pretreated with vOX2:Fc or KCPmut:Fc (8µg/ml, 60mins, 37^{o}C), or left untreated. They were then 'primed' by treatment with GM-CSF (50ng/ml, 37^{o}C, 30 mins). Superoxide burst was induced by treatment with fMLP (1µM) and detected by reaction with lucigenin. Two independent experiments were carried out for each cell type, and each treatment was carried out in duplicate. Data were calculated as a percentage of the peak superoxide burst from cells treated with GM-CSF and fMLP alone. Examples of the rapid superoxide burst in response to fMLP treatment at time 0 are shown in **(a)** and **(b)**; peak superoxide production was quantified, and data pooled, **(c)** and **(d)**.

(a)

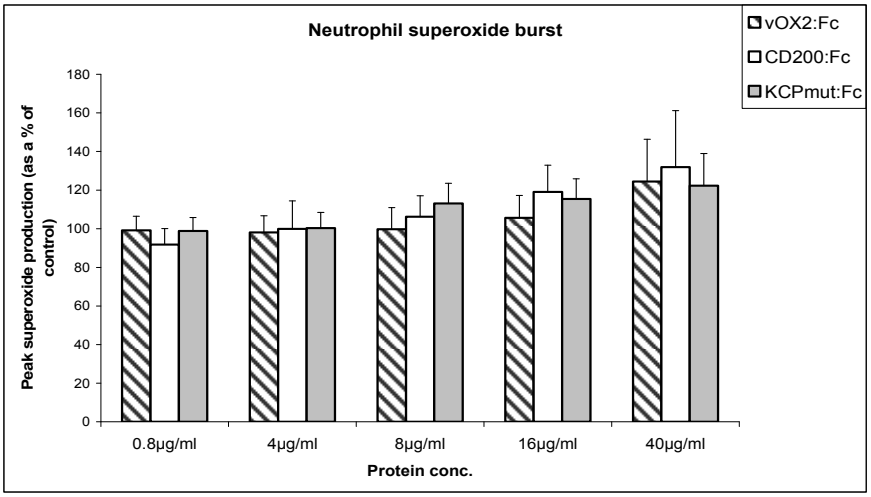

(b)

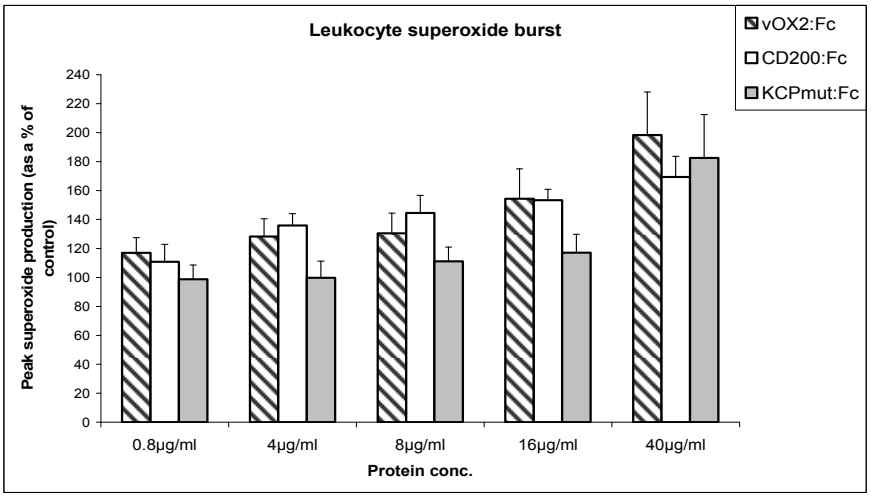

Figure 4.5 Peak superoxide burst from isolated neutrophils and leukocytes is not altered by vOX2:Fc or CD200:Fc. Neutrophils and leukocytes were isolated from the blood of a healthy donor and 'primed' with GM-CSF (50ng/ml, 30mins). Oxidative burst was induced by treatment with fMLP (1µM) and detected by reaction with lucigenin. Pretreatment with vOX2:Fc, CD200:Fc or KCPmut:Fc (60mins, 37^{o}C, 5% CO_2) of **(a)** isolated neutrophils or **(b)** leukocytes, generated no significant change, though the trend was for peak superoxide production to increase slightly with increasing protein concentrations. Data were pooled from four **(a)** or three **(b)** independent experiments, each performed on cells from separate donors; all treatments were carried out in duplicate. Data were calculated as a % of the peak superoxide burst from control cells treated with GM-CSF and fMLP alone, and represented as means ± SEM.

4.2.3. The oxidative activity of granulocytes in whole blood is moderately suppressed by vOX2:Fc and CD200:Fc

Rather than measuring the generation of superoxide anions by isolated cell populations, a more physiologically relevant measure of neutrophil activity is to measure the oxidative capacity of the NADPH oxidase complex within granulocytes *in situ* in whole blood. Briefly, whole blood from a healthy donor was incubated with vOX2:Fc, CD200:Fc or KCPmut:Fc and then treated with opsonised *E. coli* (Chapter 2.5.5). Subsequent analysis of the *E coli*.-stimulated granulocyte population by flow cytometry enabled us to quantify oxidative activity by a shift in fluorescence due to the oxidation of a fluorogenic substrate. Increased fluorescence represents increased oxidative activity. Oxidative activity was evident in cells stimulated with *E. coli*, or PMA, in comparison to untreated cells (**Figure 4.6**, **a**).

Both vOX2:Fc and CD200:Fc moderately suppressed the oxidative activity in granulocytes (**Figure 4.6**, **b**). Treatment with vOX2:Fc (8μg/ml) significantly suppressed oxidative activity by 17.12% ± 8.04 SEM (*$p<0.05$, univariate ANOVA) in comparison to the untreated control, and was reduced by 22.3% ± 5.09 SEM ($p=0.09$, univariate ANOVA), when the concentration was increased to 24μg/ml. CD200:Fc was slightly more efficacious, with 8μg/ml significantly reducing oxidative activity by 19.13% ± 6.92 SEM (*$p<0.05$, univariate ANOVA) in comparison to control, and 24μg/ml CD200:Fc reducing it by 24.34% ± 6.07 SEM (*$p<0.05$, univariate ANOVA). The negative control, KCPmut:Fc, showed a mild suppressive effect at 24μg/ml, reducing oxidative burst by 12.17% ± 8.49 SEM (not statistically significant), but did not alter oxidation when administered at 8μg/ml (4.26% ± 4.5 SEM). Oxidative activity was quantified as the median fluorescence for each sample, normalised to control (treatment with *E. coli* alone).

(a)

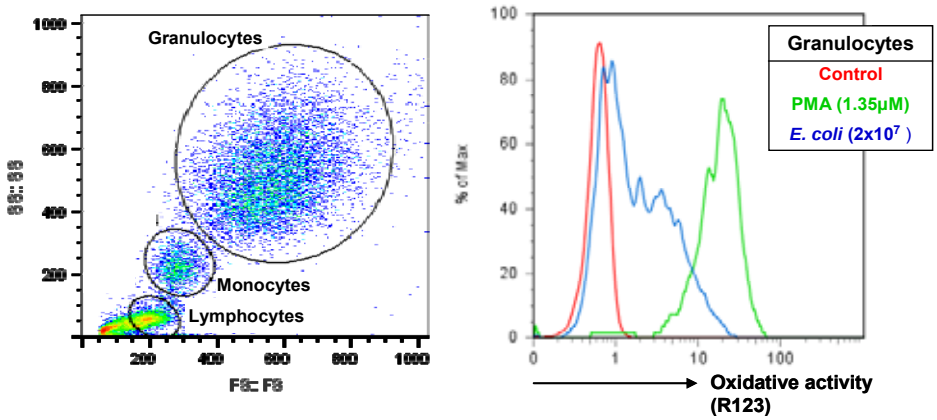
Granulocytes
Monocytes
Lymphocytes
SS: SS
FS: FS
% of Max
Granulocytes
Control
PMA (1.35µM)
E. coli (2x10^7)
Oxidative activity
(R123)

(b)

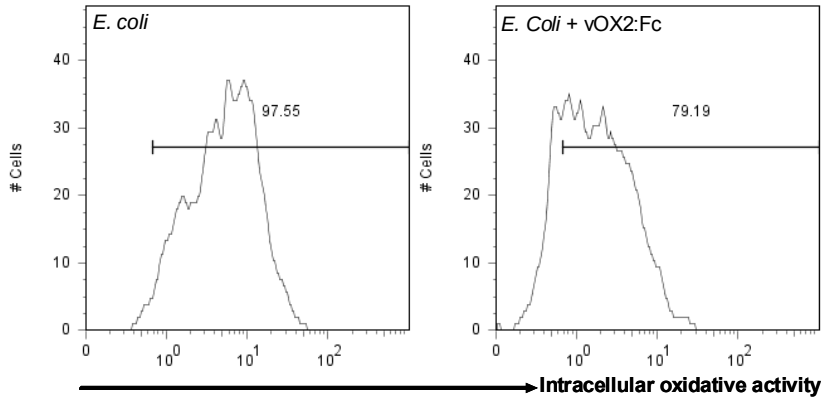
E. coli
97.55
E. Coli + vOX2:Fc
79.19
Cells
Intracellular oxidative activity

(c)

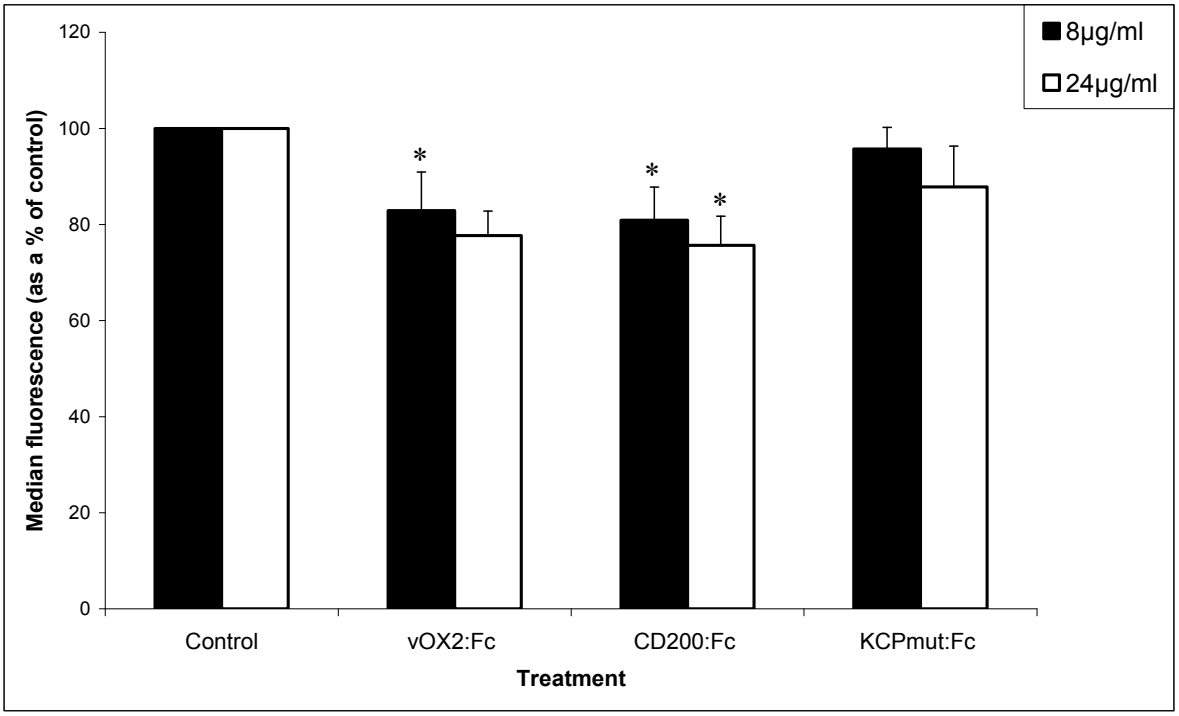
8µg/ml
24µg/ml
Median fluorescence (as a % of control)
Control
vOX2:Fc
CD200:Fc
KCPmut:Fc
Treatment

Figure 4.6 Treatment with either vOX2:Fc or CD200:Fc reduces granulocyte oxidative activity in whole blood. Pre-treatment of heparinised whole blood with vOX2:Fc or CD200:Fc (8 or 24μg/ml, 60mins, 37^{o}C) from healthy donors reduces oxidative activity in response to opsonised *E. coli* and in comparison with blood treated with either KCPmut:Fc or *E. coli* (control) alone. The granulocyte population was gated by size and granularity (**a**, left panel), and the extent of oxidative activity in each sample was determined by flow cytometric quantification of the intracellular fluorogenic substrate dihydrorhodamine 123 (**a**, right panel). **(c)** Representative histograms depicting the percentage shift of granulocytes upon pretreatment with vOX2:Fc (8μg/ml), illustrating reduced R-123 fluorescence, and therefore suppressed oxidative activity. **(b)** The median fluorescence for each sample was normalised to control (treatment with *E. coli* alone), and data pooled from four independent experiments (see Appendix D for raw data). 8μg/ml vOX2:Fc significantly reduced granulocyte oxidative activity ($F(3, 25) = 3.31$; $^{*}p<0.05$) but the difference was not significant at 24μg/ml vOX2:Fc ($F(3, 7) = 2.31$; $p = 0.09$). CD200:Fc significantly reduced granulocyte oxidative activity when administered at 8μg/ml ($F(3, 25) = 3.31$; $^{*}p<0.05$) or 24μg/ml ($F(3, 7) = 2.31$; $^{*}p<0.05$). KCPmut:Fc did not alter oxidative activity at either 8μg/ml ($F(3, 25) = 3.31$; $p = 0.49$) or 24μg/ml ($F(3, 7) = 2.31$; $p = 0.27$) when analysed by a univariate ANOVA test (SPSS software).

4.2.4. vOX2:Fc and neutrophil degranulation

Primary human neutrophils were treated with vOX2:Fc, CD200:Fc or KCPmut:Fc before stimulation with TNFα and fMLP (see Chapter 2.4.4 for method). The absorbance values are a relative measure of MPO release, and were normalised for each Fc-protein treatment to the absorbance value for cells treated with TNFα and fMLP alone (**Figure 4.7**). There was a trend towards a reduction in MPO release with increasing protein concentration. However, treatment with the negative control protein, KCPmut:Fc, also reduced MPO release so no specific effect of either vOX2:Fc or CD200:Fc can be inferred.

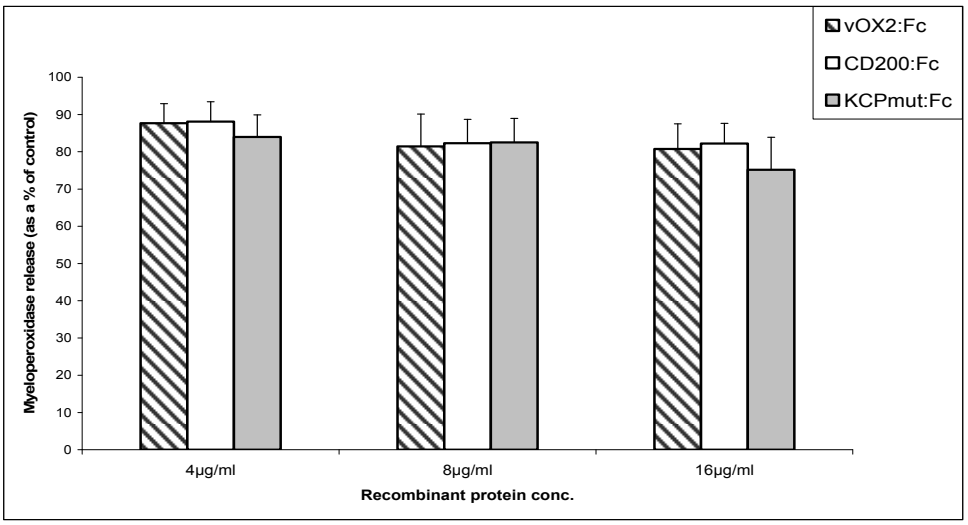

Figure 4.7 Neutrophil degranulation was not altered by pre-treatment with either vOX2:Fc or CD200:Fc. Neutrophils were isolated from the blood of a healthy donor by density gradient centrifugation, and pretreated with recombinant proteins (60mins, 37°C). Myeloperoxidase (MPO) release from azurophilic granules was stimulated by TNFα (100ng/ml) and fMLP (100nM), and detected by colorimetric reaction with TMB, a substrate of peroxidase. Data from three independent experiments, carried out on blood from separate donors, were pooled and are presented as means ± SEM; all treatments were carried out in duplicate.

4.2.5. vOX2:Fc does not alter neutrophil viability

Once isolated from blood, primary neutrophils have a short lifespan in culture, and approximately 50% of the cells will spontaneously apoptose after about 20hrs. The rate of apoptosis in the presence of a compound of interest can therefore be determined in comparison to untreated control cells. Thus, to determine whether the treatment of neutrophils with either vOX2:Fc or CD200:Fc would alter the rate of their spontaneous apoptosis, neutrophils from a healthy donor were pretreated in parallel with vOX2:Fc, CD200:Fc or KCPmut:Fc. Apoptosis was quantified by flow cytometry (Chapter 2.5.6), by determining the percentage of cells that retained the fluorescent dye DiOC6 in their mitochondria. Neither vOX2:Fc nor CD200:Fc induced cell death or rescued the isolated neutrophils from apoptosis (**Figure 4.8**), in comparison to control KCPmut:Fc-treated cells. A decrease in neutrophil viability after 9 hours, following pre-treatment with vOX2:Fc or

CD200:Fc (24μg/ml), also occurred in the cells pretreated with the negative control protein KCPmut:Fc (24μg/ml), and so cannot be considered a direct result of either vOX2 or CD200 activity. GM-CSF and TNFα were included as controls, as the two agents rescue neutrophils from and induce apoptosis, respectively. Morphological analysis of neutrophil apoptosis also indicated no effect of vOX2:Fc or CD200:Fc (data not shown).

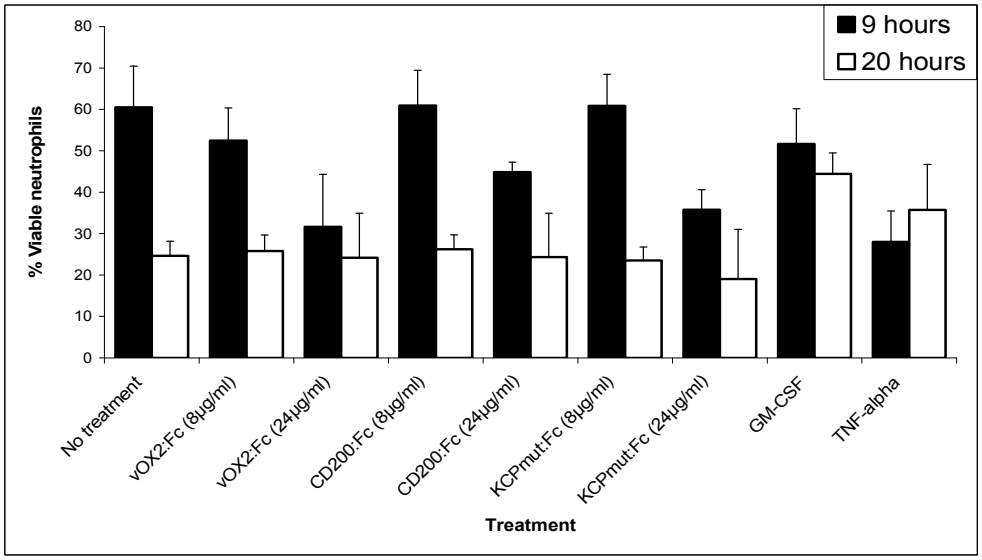

Figure 4.8 Neutrophil viability is unaffected by vOX2:Fc. Neither vOX2:Fc or CD200:Fc induced cell death, nor rescued neutrophils from apoptosis when co-cultured with primary neutrophils for up to 20 hours. Cell viability was determined by flow cytometric quantification of the retention of the fluorescent mitochondrial dye (DiOC6). Data were pooled from six independent experiments, carried out with blood from separate donors.

4.3. The neutrophil chemoattractant, IL-8

Although neither soluble vOX2 (vOX2:Fc) nor CD200 (CD200:Fc) influenced neutrophil function directly nor substantially in our assays, the hypothesis was that they may regulate monocyte function via surface CD200R, which in turn may deregulate neutrophil function indirectly. Thus, the ability of monocytes to secrete IL-8, a potent neutrophil chemoattractant, was examined in the context of putative vOX2/CD200-monocyte interaction.

To determine whether native vOX2 or CD200 could alter the production of IL-8 by stimulated monocytes, *vOX2* and *CD200* were inserted into retroviral vectors, and BJAB cells (a B-lymphoblastoid cell line) were transduced to stably express the proteins (Chapter 2.8.6). Initially, two human monocytic cell lines, U937 and THP-1, were stimulated with IFNγ for 48hrs in the presence of BJAB cells (1:1) expressing native vOX2 (vOX2-BJAB), CD200 (CD200-BJAB) or transduced with an empty vector (Empty-BJAB) (**Figure 4.9**, **a**). IL-8 secretion by U937 cells was unchanged in the presence of vOX2 or CD200. However, the secretion of IL-8 by THP-1 cells was moderately suppressed by vOX2-BJAB cells, by 18.55% ± 8.94 SEM in comparison to the Empty-BJAB control and by 23.43% ± 7.94 SEM in the presence of CD200-BJAB cells. The difference did not reach significance when the data were analysed by one-way ANOVA (SPSS software). To determine the expression of CD200R by the two cell lines, unstimulated U937 and THP-1 cells were labelled with anti-CD200R antibody and co-stained with a fluorophore-conjugated secondary antibody. CD200R expression was determined by comparison with control cells stained with both isotype control antibody and secondary antibody, or secondary antibody alone (**Figure 4.9**, **b**). The histograms clearly demonstrate cell surface expression of CD00R on U937 cells, but not THP-1 cells.

(a)

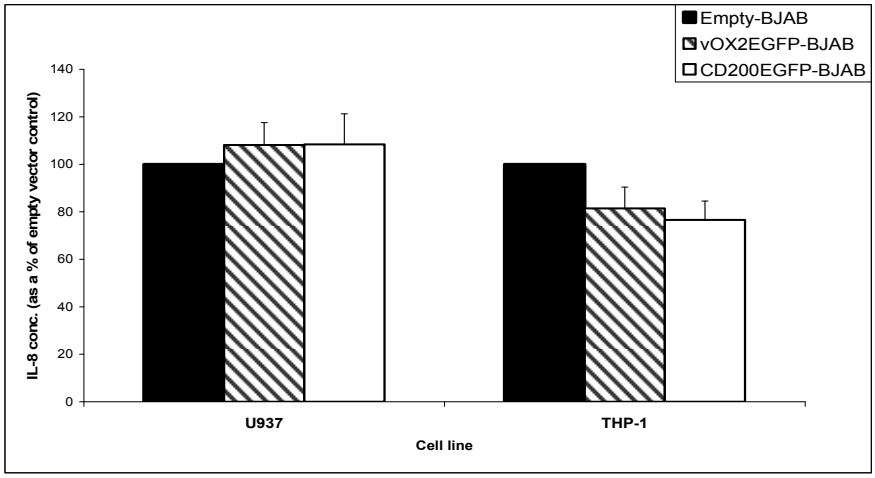

(b)

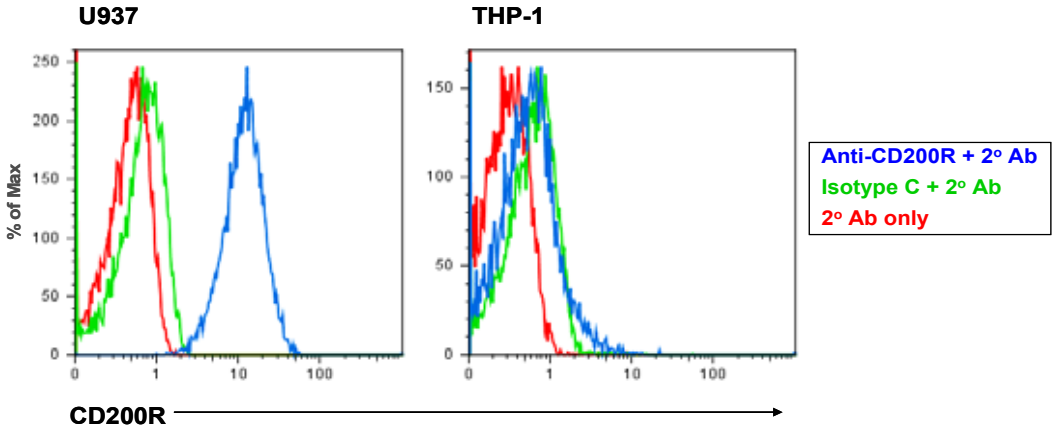

Figure 4.9 vOX2 and CD200 modestly reduce IL-8 production by co-cultured monocytic CD200R$^-$ THP-1 cells, but not CD200R$^+$ U937 cells. (a) BJAB cells expressing native vOX2 or native CD200 (fused in-frame with EGFP), were irradiated and co-cultured with two human monocytic cell lines (U937 and THP-1) for 48 hours. THP-1 and U937 cells were stimulated with IFNγ (8ng/ml) during co-culture with the engineered BJAB cells. IL-8 secretion by U937 cells was not altered, but IL-8 secretion by THP-1 cells, co-cultured with vOX2EGFP-BJAB or CD200EGFP-BJAB cells, was reduced to 81.45% ± 8.94 SEM and 76.57% ± 7.94 SEM of the control respectively. Empty-BJAB cells were used as a control. IL-8 concentration in supernatants was determined by commercial ELISA. Data from five (U937) and four (THP-1) independent experiments were pooled and are presented as means ± SEM. **(b)** The expression of CD200R on the surface of U937 and THP-1 cells was quantified by flow cytometry. Staining with anti-CD200R and a fluorophore-conjugated secondary antibody (blue) revealed CD200R expressed on the surface of U937 cells, but not THP-1 cells, in comparison to the isotype control-stained cells (green), or cells stained with the secondary antibody only (red).

Next, the effects of both soluble and native vOX2 and CD200 on primary human monocytes were determined. PBMCs were isolated from the blood of healthy donors, and the monocytes isolated by allowing them to adhere to plastic. The adherent monocytes were incubated with vOX2:Fc, CD200:Fc or KCPmut:Fc (8μg/ml, 60mins, 37^{o}C) and the basal secretion of IL-8 determined by commercial ELISA. The data were pooled and presented as mean ± SEM (**Figure 4.10**, **a**). There was no demonstrable change in the generation of IL-8 by monocytes in the presence or absence of vOX2:Fc or CD200:Fc, in comparison to untreated cells, or those treated with KCPmut:Fc. Plastic-adherent primary monocytes were incubated with vOX2 or CD200-expressing BJAB cells and then stimulated with LPS (**Figure 4.10**, **bi**). Alternatively, they were incubated with LPS-treated engineered BJAB cells (**Figure 4.10**, **bii**). In both cases the presence of vOX2 or CD200 on the BJAB cell did not alter the IL-8 secretion by monocytes, or in some cases increased it slightly, in comparison to empty vector control cells; however the error bars negate any differences between the means.

To investigate the activity of native vOX2 and CD200 on IL-8 producing endothelial cells, human microvascular endothelial cells (HMEC), an immortalised cell line, were incubated with vOX2/CD200/empty vector BJAB cells for 60mins, stimulated with TNFα, and the IL-8 concentration of the supernatant quantified by commercial ELISA after 4hrs. vOX2 and CD200 did not alter the production of IL-8 by HMEC cells (**Figure 4.11**).

(a)

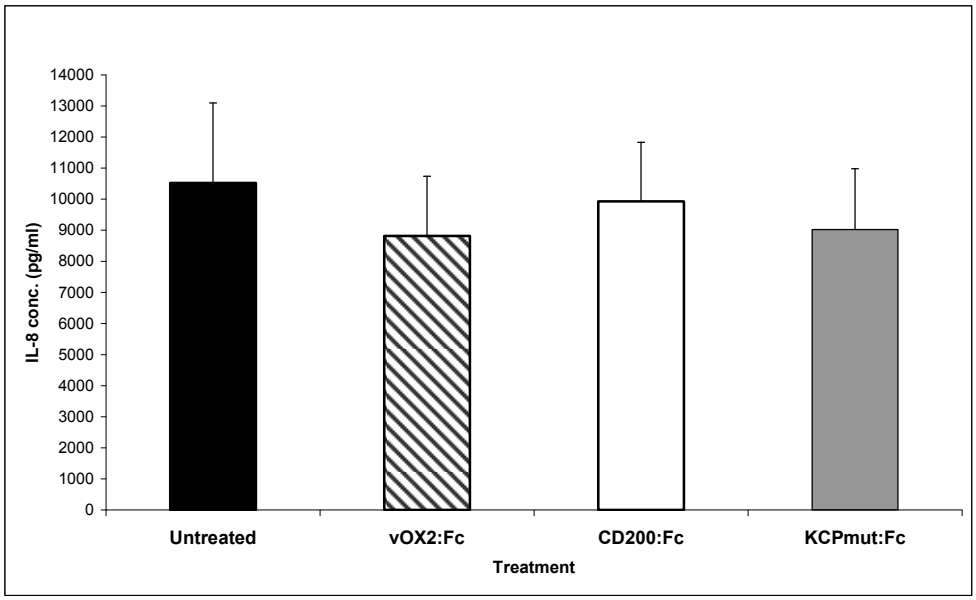

(b)

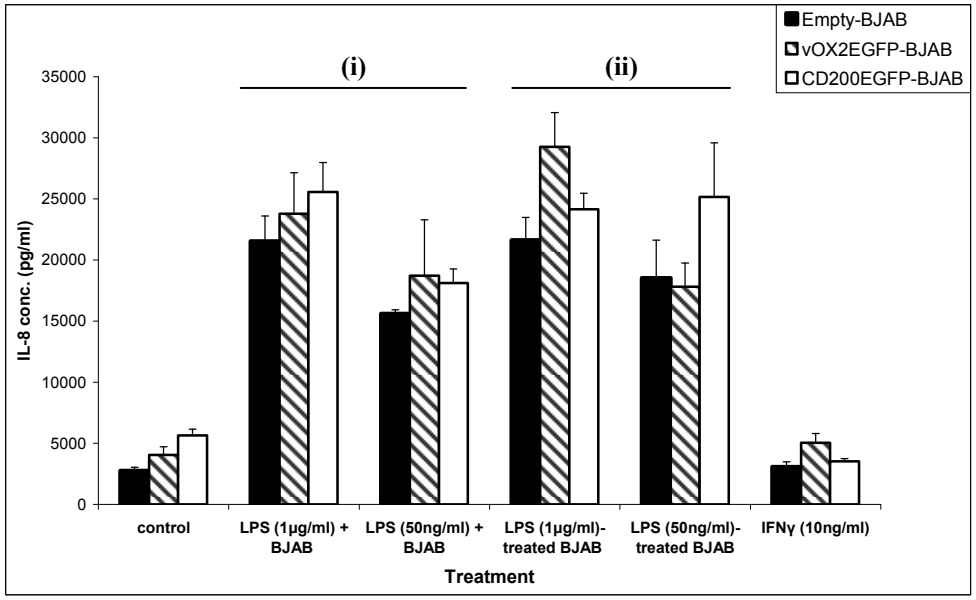

Figure 4.10 Neither soluble nor native membrane-bound vOX2 or CD200 alter IL-8 secretion by primary monocytes. Plastic-adherent monocytes derived from PBMCs were treated with **(a)** vOX2:Fc, CD200:Fc or KCPmut:Fc (8µg/ml, 37^{o}C, 16 hours), or **(b)** were co-cultured with BJAB cells engineered to express either native vOX2 or CD200 fused in-frame with EGFP, or an empty vector. **(bi)** Monocytes were cocultured with untreated engineered BJAB cells and then stimulated with LPS, or **(bii)** were co-cultured with LPS-treated BJAB cells. Supernatants were collected after overnight incubation for IL-8 quantification by ELISA. All BJAB cells were irradiated before use (4000rads, caesium-137 chloride source). Data were pooled from three independent experiments, and expressed as means ± SEM.

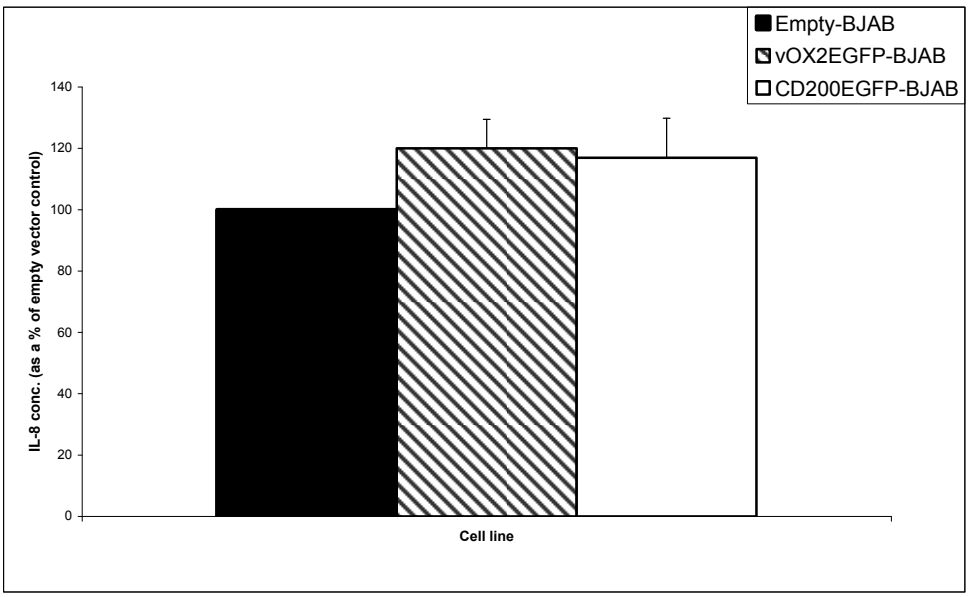

Figure 4.11 vOX2 and CD200 do not alter IL-8 production by co-cultured HMEC endothelial cells. BJAB cells expressing native vOX2 or native CD200 (fused in-frame with EGFP), were irradiated and co-cultured with TNFα-stimulated human microvascular endothelial cells (HMEC) for 4 hours. After 60mins of co-culture with the engineered BJAB cells, HMEC were stimulated with TNFα (10U/ml). Empty-BJAB cells were used as a control. IL-8 concentration in supernatants was determined by commercial ELISA. Data from three independent experiments were pooled and are presented as means ± SEM.

4.4. Do soluble vOX2:Fc and CD200:Fc influence T cell activity?

In order to determine whether the soluble vOX2 and CD200 proteins interact with other leukocytes- such as T cells- and whether immobilising the proteins would increase their efficacy, another system was developed. The hypothesis was that if the negative stimulus (ie. vOX2 or CD200) was presented to the T cell in concert with the positive stimulus (ie. anti-CD3 and anti-CD28), the negative signal may override the positive. Physiologically, the T cell might be expected to recognise vOX2 expressed on the surface of an APC (for example, on the surface of KSHV-infected B cells), coincident with cognate antigen (ie. KSHV antigens), which is when vOX2 might be expected to offer some protection to the infected cell.

(a)

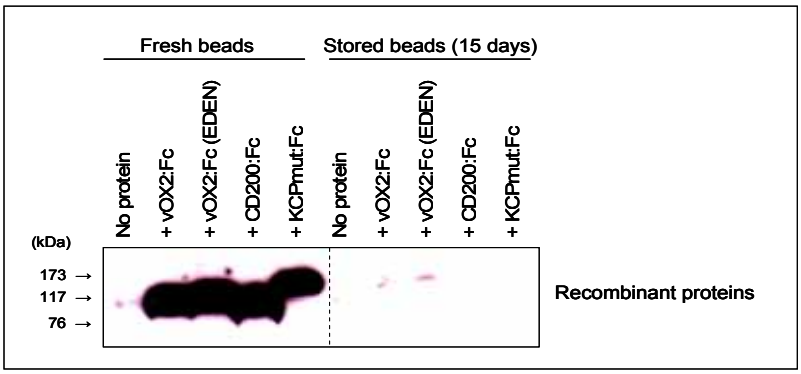

(b)

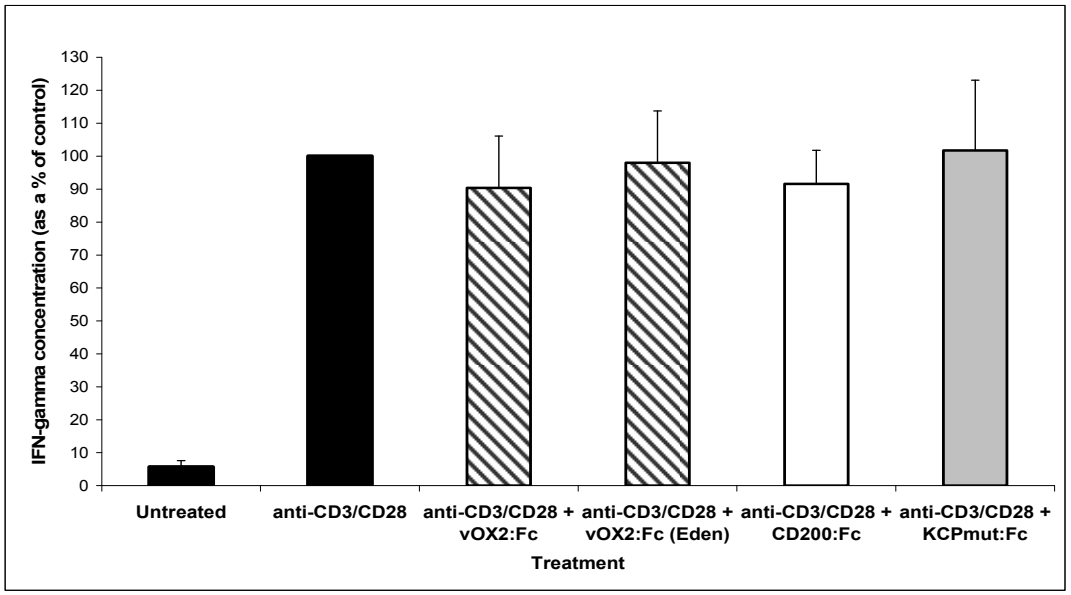

Figure 4.12 Neither immobilised vOX2:Fc nor CD200:Fc alter the response of PBMCs to stimulating anti-CD3 and anti-CD28 antibodies. Commercial microbeads conjugated to an anti-biotin antibody were labelled with anti-CD3, anti-CD28 and anti-IgG biotinylated antibodies (0.1pg protein/bead, 4^{o}C, 2hrs). vOX2:Fc, commercial vOX2:Fc (EDEN), CD200:Fc or KCPmut:Fc were then bound to the anti-IgG antibody (0.2μM, 4^{o}C, 2hrs). **(a)** Bead-protein complexes were separated by SDS-PAGE and immunoblotted with an anti-human IgG1 (Fc) antibody to detect the bead-bound protein (left panel). Fc-proteins dissociated from the beads after 15 days (4^{o}C) and was undetectable by immunoblotting (right panel) so only freshly prepared beads were used. **(b)** PBMCs isolated from the blood of healthy donors were stimulated with vOX2:Fc and CD200:Fc-loaded micro-beads. After 48hrs of culture, IFNγ release was quantified by ELISA as a measure of T cell activation. Two independent experiments were carried out, with PBMCs from six healthy donors, and data are represented as means ± SEM.

To verify the effects of vOX2 and CD200 on primary T cells, PBMCs were isolated from the blood of healthy donors and incubated with microbeads. These beads were engineered to present anti-CD3 and anti-CD28 antibodies, and a recombinant protein. The proteins were vOX2:Fc, commercially prepared vOX2:Fc (Eden Bioscience), CD200:Fc or KCPmut:Fc. The presence of recombinant proteins on the microbeads was confirmed by SDS-PAGE and immunoblotting (**Figure 4.12**, **a**, left-hand panel). Recombinant proteins were found to dissociate from the beads rapidly (**Figure 4.12**, **a**, right-hand panel), and were therefore produced and used immediately. T cell function was judged by quantifying IFNγ secretion, and Fc-protein-negative microbeads acted as a control to gauge the stimulating effects of anti-CD3 and anti-CD28. The quantification of IFNγ in culture supernatants by ELISA revealed no specific difference in IFNγ secretion by vOX2 or CD200-treated cultures, in comparison to KCPmut:Fc (**Figure 4.12**, **b**).

4.5. Discussion

Neither vOX2:Fc nor CD200:Fc directly altered the function of primary neutrophils when three parameters were measured: oxidative burst (**Figure 4.4** and **Figure 4.5**), degranulation (**Figure 4.7**), and apoptosis (**Figure 4.8**). In contrast, treatment of whole blood with either vOX2:Fc or CD200:Fc modestly suppressed the oxidative activity of granulocytes (**Figure 4.6**), with the data reaching statistical significance. These data agree partially with those of Rezaee *et al*. who demonstrated suppression of neutrophil oxidative burst by vOX2:Fc, though CD200:Fc was not analysed (Rezaee *et al*., 2005). The moderate suppression observed in the present study may be due to direct but weak interaction of the recombinant proteins with CD200R on neutrophils or with other granulocytic cells, eosinophils and basophils. Alternatively, it may be a result of indirect modulation of granulocytic activity via another leukocyte subpopulation, such as monocytes. No evidence exists in the literature

demonstrating an interaction between vOX2 or CD200 and eosinophils. However, basophils have been studied in this context (Shiratori *et al*., 2005).

As discussed in Chapter 1, both soluble and native forms of vOX2 and CD200 suppressed the FcεRI-mediated degranulation of human primary CD200R-expressing basophils (Shiratori *et al*., 2005). In contrast, two research groups have studied mCD200R-like proteins that are expressed on basophils and appear to act as stimulants. Voehringer and colleagues examined the mCD200R1-like proteins, and described the expression of an isoform of mCD200R3 with the ability to recruit the adaptor protein DAP12 (Voehringer *et al*., 2004). Stimulation of mCD200R3 on murine basophils with an agonist antibody induced degranulation and anaphylaxis *in vivo* (Kojima *et al*., 2007). However, these authors demonstrated that mCD200 is not a ligand of this receptor (Kojima *et al*., 2007). Data demonstrating a stimulatory property of the mCD200R1-like proteins were gathered in mice (Kojima *et al*., 2007) and not in humans. Human CD200R shares 52% sequence identity with mCD200R1 (Vieites *et al*., 2003), and appears to share its inhibitory properties (Foster-Cuevas *et al*., 2004) and (Snelgrove *et al*., 2008). Thus the evidence gathered by Kojima *et al*. does not disprove our hypothesis that CD200 and vOX2 negatively regulate human granulocytes. Basophils comprise less than 1% of circulating leukocytes, which would explain the very moderate suppression of granulocyte oxidative activity, if they are the primary cell type negatively modulated by vOX2 and CD200.

It is possible that granulocytes are not directly negatively modulated by vOX2:Fc or CD200:Fc, but that an interaction between CD200R on monocytes and the recombinant proteins leads to an alteration in cytokine production, such as the neutrophil chemoattractant IL-8, thus indirectly influencing granulocyte activity. In the present study, no inhibition of IL-8 production by U937 cells could be detected (**Figure 4.9**, **a**). Previous data generated in our laboratory did demonstrate a suppression of IL-8 secretion by U937 cells (Rezaee *et al*.,

2005). However, IL-8 production by stimulated THP-1 cells was modestly inhibited (**Figure 4.9**, **a**), though the inhibition was not statistically significant. Evidence for the suppression of IL-8 production by CD200:Fc treatment of U937 cells was published by Jenmalm and colleagues (Jenmalm *et al*., 2006). These authors demonstrated that soluble human CD200 or an anti-CD200R antibody suppressed the IFNγ-mediated IL-8 secretion from U937 cells, and that the level of inhibition increased with CD200R expression (Jenmalm *et al*., 2006). However, our data are undermined by the absence of CD200R on the suppressible THP-1 cells, and its presence on the uninhibited U937 cells (**Figure 4.9**, **b**). The lack of a negative effect on human primary monocytes by CD200 or vOX2 (**Figure 4.10**) renders these data questionable.

The secretion of IL-8 from the vascular endothelial cell line, HMEC (**Figure 4.11**) was not influenced by native vOX2 or CD200. There is no evidence in the literature pertaining to the role of vOX2 or CD200 in modulating endothelial cell IL-8 production. However, evidence in the literature indicates that CD200 modifies the interaction of endothelial cells with monocytes (Ko *et al*., 2009). mCD200R1$^+$ monocytes bound to mCD200$^+$ vascular endothelial cells and the interaction between mCD200R1 and its cognate ligand prevented cell adhesion, thus reducing monocyte influx into the tissues. Ko *et al*. incubated a murine macrophage cell line with a peptide corresponding to the extracellular domain of mCD200. The number of macrophages that subsequently adhered to a murine brain endothelial line was reduced, possibly due to a concurrent downregulation in integrin β2 and ICAM-1 on the macrophage. Adhesion of CD200R$^+$ Jurkat T cells to CD200$^+$ HMECs could also be suppressed when the HMEC cells were pre-incubated with an anti-CD200 antibody (Ko *et al*., 2009). Therefore, in the present study perhaps the putative interaction between HMEC cells and CD200R$^+$ cells should have been analysed, whereas the interaction between HMEC and CD200-expressing cells was investigated.

Though a vOX2- and CD200-mediated suppression of IL-8 secretion by a monocytic cell line, THP-1, was observed, no inhibition of primary monocyte IL-8 secretion occurred (**Figure 4.11**). Primary cells are obviously more physiologically relevant than cell lines and our data suggest no effect of either vOX2 or CD200 on primary cells. Very little evidence for the interaction between CD200 or vOX2 and monocytes has been published. However, soluble CD200:Fc reduced the secretion of IFNγ, TNF, IL-5 and IL-13 from *Clostridium tetani*-stimulated PBMCs, an effect which was isolated to $CD200R^+$ monocytes (Jenmalm *et al*., 2006). Other studies have been carried out on monocyte-related myeloid cells, such as microglia, the macrophages of the CNS. Meuth *et al*. confirmed previous evidence (Wright *et al*., 2000) that blocking CD200-CD200R interaction in the CNS exacerbated disease pathology in a murine model of MS (EAE) (Meuth *et al*., 2008). Inhibiting mCD200R1 ligation with a blocking antibody enhanced the infiltration of activated macrophages into spinal cord lesions of EAE animals. These macrophages were more sensitive to IFNγ and exacerbated neuronal cell death (Meuth *et al*., 2008). These data indicate that CD200-CD200R interactions are necessary *in vivo* to prevent excessive myeloid cell response to tissue damage. If CD200R ligation to its cognate ligand is prevented, thus exacerbating monocyte activity, then CD200-CD200R ligation must exert a suppressive effect. Following this premise, CD200 (and hypothetically vOX2) should be able to suppress the activity of $CD200R^+$ cells in the present study, again indicating a problem with the recombinant proteins.

Due to an observation in our laboratory that native, membrane-bound vOX2 and CD200 could suppress IFNγ secretion by human T cell clones (Colman and Blackbourn, unpublished observations), the activity of unpurified T cells within a PBMC context were evaluated following treatment with immobilised vOX2:Fc and CD200:Fc. Neither protein influenced T cell IFNγ secretion induced by treatment with anti-CD3 and anti-CD28

antibodies (**Figure 4.12**). The putative negative (vOX2/CD200) and positive (anti-CD3/CD28) signals were presented to the cells simultaneously, though the stimulus may have been too great for the immobilised proteins to surmount.

The absence of an effect on monocytes, neutrophils or T cells in this study may be due to the use of excessive stimuli that vOX2 or CD200 cannot overcome, or may indicate that the soluble Fc-fusion proteins are not physiologically active. Therefore, for the remainder of this study, the roles of vOX2 and CD200 were determined by the activities of full-length vOX2 and CD200 proteins expressed on the surface of B lymphoblastoid cells.

Chapter 5. Using antigen-specific T cell clones to investigate the activity of native vOX2 and CD200

The impact of vOX2 and CD200 on T cell function was investigated due to evidence in the literature that CD200 suppresses the CTL response, and initial experiments in our laboratory that supported this hypothesis (Colman, R. and Blackbourn, D. unpublished observations). All subsequent assays were carried out with native vOX2 and CD200 expressed on the surface of BJAB cells, in order to reproduce physiological conditions as closely as possible.

5.1. Evidence for an effect of CD200 on T cell function

The relationship between CD200 and T cells has been examined extensively by one research group. Gorczynski *et al*. observed that the stimulation of mCD200R2 expressed by subsets of bone marrow-derived cells, by anti-mCD200R antibodies, led to the maturation of DCs unable to effectively induce a CTL response in a mixed lymphocyte culture. The failure of these DCs to induce a CTL response appeared to be a result of increased numbers of $CD4^+CD25^+$ T cells in the mixed lymphocyte culture. So, stimulating mCD200R2 led to the development of antigen-presenting DCs that in turn induced the expansion of Tregs, and stimulation of mCD200R1 on DCs *in vitro* reduced CTL activity and IFNγ secretion. *In vivo*, the administration of mCD200R2-derived DCs to mice prior to allografting reduced the CTL response to the skin allograft, and concurrently increased the number of $CD4^+CD25^+$ T cells (Gorczynski *et al*., 2004b).

Later work by these researchers indicated that the treatment of anti-CD3/CD28-stimulated, CD8-depleted thymocytes with a stimulating anti-mCD200R1 antibody reduced the number of $CD4^+CD25^+$ Treg cells, and their suppressive activity (Gorczynski *et al*., 2005). The activity of the T cells was determined by the lysis of ^{51}Cr-containing target cells, releasing ^{51}Cr into the supernatant, and by the secretion of IFNγ. The reduced number of

Tregs in anti-mCD200R1-treated cultures resulted in increased lysis of target cells and IFNγ production. However, the isolation of DCs from a bone marrow culture incubated with anti-mCD200R2/3 antibodies, and subsequent culture of these DCs with a mixed population of cells derived from murine lymph nodes, enhanced the number of $CD4^+CD25^+$ Tregs in that culture (Gorczynski *et al*., 2005). Concurring data were published in 2008 by the same group, demonstrating that in the absence of mCD200R1 (*mCD200R1*$^{-/-}$ mice), DCs cultured in the presence of mCD200:Fc could induce a Treg subpopulation in a mixed lymphocyte culture, in comparison to DCs from WT mice. The transfer of these DCs, developed during mCD200:Fc-treatment, to mice undergoing allogeneic skin grafting, promoted graft survival. Interestingly, these tolerogenic DCs had an unusual toll-like receptor profile, expressing TLR2 and TLR3 and thus presenting with an immature DC phenotype. Stimulating the CD200:Fc-treated DCs with TLR ligands such as LPS reduced their tolerogenic potential, indicated by an increase in CTL activity, enhanced graft rejection *in vivo*, and reduced numbers of Tregs in the culture (Gorczynski *et al*., 2008). These data indicate that mCD200R subsets have opposite activities, both upregulating and downregulating the maturation of suppressive Tregs, via the differential maturation of immature DCs that ultimately induce either a tolerogenic response, or activate cytotoxic T cells upon maturation.

5.2. Optimising a model system to investigate the activity of vOX2 and CD200 on T cell function

Initial observations made in our laboratory suggested that full-length vOX2 and CD200, expressed on the surface of APCs, could suppress the secretion of IFNγ by human T cell clones (Colman, R., unpublished). Therefore, a model system was established to examine the putative inhibition of antigen-specific human T cell clones by vOX2 and CD200 expressed by APCs. As mentioned in Chapter 4, vOX2 and CD200 were expressed on the surface of a B lymphoblastoid cell line (BJAB) by retroviral transduction (Chapter 2.8.6) to provide the

APC, and cells transduced with an empty vector acted as a control. The BJAB cells were HLA-matched to human EBV antigen peptide-specific T cell clones isolated from the blood of IM patients, and a healthy EBV-seropositive donor (see Chapter 2.7.1-2). The BJAB cells were therefore able to present exogenous cognate peptide to the T cell clones, eliciting a response (see **Figure 5.1**). Measurable responses to T cell stimulation include the generation of cytokines such as IFNγ and IL-2. For the purposes of this study, cytokines were measured exogenously by ELISA, and endogenously by flow cytometry. The signalling cascades initiated in T cells by peptide-stimulation were later examined by flow cytometry (Chapter 6).

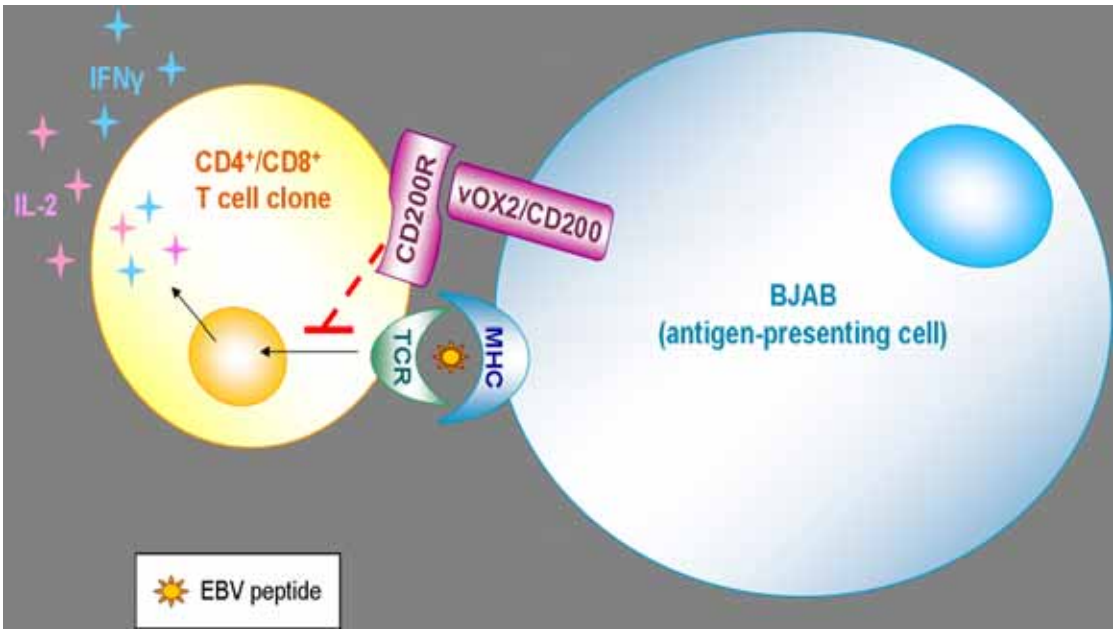

Figure 5.1 Antigen-specific human T cell clones: a model system for examining the activities of native vOX2 and CD200 expressed on antigen-presenting cells (APCs). In order to determine whether the presence of vOX2 or CD200 on APCs alters the response of T cells to cognate peptide, either native vOX2 or native human CD200 were expressed on the surface of cells of the BJAB line by retroviral transduction. BJAB cells were loaded with exogenous Epstein Barr virus (EBV) antigen peptides, and co-cultured with HLA-matched antigen-specific human T cell clones. After 16hrs of co-culture, IFNγ release was quantified by ELISA, providing a measure of T cell activation. Phosphorylation of intracellular signalling molecules within the T cell clones was analysed by flow cytometry (Chapter 6), in addition to the intracellular retention of IFNγ and IL-2 cytokines.

Initial data presented in this chapter concern the generation of six T cell clones from an IM donor. The vOX2 and CD200-mediated suppression of T cell clone activity (measured by the production of IFNγ and IL-2) is then discussed, with reference to eight clones isolated from three donors. Relevant methodologies are outlined in Chapter 2 and will be referred to throughout this chapter.

5.3. Antigen-specific T cell clones

With thanks to A.R. Rickinson, in the School of Cancer Sciences in Birmingham we are fortunate to have access to reagents and expertise regarding the generation of viral antigen-specific T cell clones. Wallace and colleagues initially reported the cloning of HLA-peptide-specific T cells directed against EBV antigens, confirmed by the effective killing of HLA-typed EBV-positive cells. These cytotoxic clones were maintained in long-term culture, and retained their antigen specificity (Wallace *et al*., 1982). Phenotyping cloned antigen-specific T cells is now more efficient since the development of fluorophore-conjugated MHC-peptide complex tetramers (see Chapter 2.6.2 and Chapter 7). Tetramers specifically label T cells directed against an MHC-restricted antigen peptide and therefore can recognise memory T cells present at a very low frequency *in vivo*. Tetramer-labelling of antigen-specific cells in the blood enables a simultaneous analysis of surface proteins by flow cytometry, and also provides a method for isolating these T cells from a PBMC population. Dunbar and colleagues reported that the peptide-specific tetramers did not activate the T cells, and confirmed their specificity by culturing cloned T cells (isolated by tetramer-labelling) with peptide-loaded HLA-matched target cells (Dunbar *et al*., 1998).

The T cell clones analysed in this thesis were primarily isolated from IM patients, a disease initiated by primary EBV infection. EBV-specific T cells account for between 1-40% of the amplified $CD8^+$ T cell population during IM, and are primarily directed against immediate early and early lytic cycle antigens (Hislop *et al*., 2007). Analysis of T cells from

IM donors indicated that the T cells were in an activated state, expressing CD38, but that upon regression of disease, the number of T cells directed against lytic antigens diminished. The remaining memory T cells directed against latent and lytic antigens were in a resting state, regardless of the low level of antigen still present in the infected individual (Hislop *et al*., 2007). The frequency of $CD8^+$ T cells directed against lytic and latent EBV antigens varies between individuals, and is described in Chapter 7. A small population of $CD4^+$ memory T cells are generated in response to EBV, though they have not been studied extensively. $CD4^+$ T cells are directed against latent and lytic EBV proteins and some secrete IFNγ in response to peptide stimulation (Hislop *et al*., 2007).

In the present chapter, the effect of KSHV vOX2 on antigen-specific T cell responses was determined. In parallel, the cellular orthologue CD200 was compared. Thus, T cell clones were derived, their peptide-specificity mapped and their reactivity to HLA-matched APCs, engineered to express either vOX2 or CD200, determined.

5.4. Generating T cell clones from the blood of an IM patient

IM patients have a larger $CD8^+$ T cell population than healthy EBV seropositive individuals, and therefore the isolation of $CD8^+$ EBV antigen-specific T cells from IM blood is facilitated. Briefly, PBMCs from an IM patient (IM235) were diluted to approximately 1 cell per well, and incubated with irradiated mixed PMA-stimulated PBMCs and autologous lymphoblastoid cell lines (LCLs), which are EBV-transformed mononuclear cells. The allogeneic response stimulates the T cells, and the presentation of EBV antigens by the LCLs stimulates peptide-specific T cells to proliferate (Chapter 2.7.1). Identifiable clones (visible expansion of cells in one well by the naked eye) were expanded by the same method and tested for peptide specificity by a ^{51}Cr-release cytotoxicity assay.

Clone number x	EBV antigens expressed by autologous LCLs (target cells)														
	BRLF1 and BMRF1	BALF5 and BALF2	BMLF1 and BGLF4	BHLF1 and BHRF1	BARF1 and BNLF2b	BLLF2 and BCRF1	BILF1 and BDLF3	BLLF1 and BALF4	BXLF2 and BNRF1	BILF2 and BBRF1	BZLF1 and BVRF2	LMP1 and LMP2	EBNA1 and EBNA2	EBNA3z and EBNA3b	EBNA3c and LP
1	0	0	0	0	0	2	0	0	0	0	0	7	0	4	0
2	0	0	2	0	2	0	0	0	2	2	0	8	0	4	2
3	0	0	4	0	0	0	0	0	0	0	0	6	0	4	0
4	0	0	4	0	0	0	0	0	0	0	0	4	0	0	0
5	0	0	5	0	4	0	1	0	3	0	0	7	0	4	1
6	0	0	4	0	0	0	2	0	1	0	0	9	0	1	1
7	14	0	0	0	0	0	0	2	7	0	0	8	0	5	0
8	0	0	0	0	2	0	0	0	1	0	0	7	0	0	0
9	0	0	6	0	0	0	0	0	0	0	0	6	0	5	0
10	0	0	0	0	0	0	0	0	1	0	0	5	0	0	0
11	0	0	8	0	0	0	0	0	3	0	1	3	0	4	0
12	0	0	1	0	0	0	0	0	0	0	0	3	0	1	0
13	0	0	8	0	0	2	0	0	5	0	0	7	0	4	0
14	0	0	0	0	0	0	0	0	4	0	0	8	1	4	0
15	0	0	12	0	0	0	1	0	7	0	2	8	0	4	0
16	0	0	0	0	3	0	1	0	2	0	0	5	0	0	0
17	0	1	36	0	0	0	2	1	3	3	0	9	3	11	2
18	16	0	5	0	4	0	1	0	6	4	0	8	0	4	1
19	0	0	6	0	0	0	0	0	3	0	3	8	0	1	0
20	0	0	0	0	0	0	0	0	0	0	1	10	0	1	0
21	8	0	4	3	0	0	15	9	26	11	14	24	11	19	14
22	0	0	0	0	15	0	0	0	0	1	0	7	0	0	0
23	0	0	3	0	0	0	2	0	3	0	0	6	0	3	0
24	0	0	5	0	0	0	0	0	4	1	0	10	0	4	0
25	0	0	3	0	0	0	5	0	10	1	5	11	0	7	0
26	0	0	2	0	2	0	0	0	3	0	0	9	0	3	4
27	15	8	0	7	4	2	3	12	18	10	11	11	9	13	5
28	2	1	6	0	0	0	0	0	0	1	0	7	0	2	0
29	25	17	1	13	0	22	24	0	30	19	17	23	19	31	0
30	0	1	0	0	0	0	0	0	0	0	0	10	1	4	0
31	0	0	0	0	0	0	2	0	2	0	0	5	0	0	0
32	0	0	0	0	0	0	3	0	3	0	0	5	0	0	20
33	23	21	25	24	0	4	15	16	34	17	22	28	25	25	0
34	12	8	7	0	2	0	0	2	9	0	5	10	1	8	3
35	1	0	4	0	3	0	1	2	11	0	0	11	0	6	2
36	11	3	0	0	5	0	2	4	7	2	4	14	2	8	0
37	2	0	0	0	0	0	0	0	2	0	3	7	0	2	0
38	0	0	0	0	2	0	0	0	2	0	0	7	0	0	0
39	43	1	23	0	0	0	0	0	8	0	0	5	0	6	0
40	51	2	3	0	2	0	0	0	4	0	2	7	0	6	0
41	26	0	9	0	0	0	0	0	2	0	0	7	0	0	0
42	38	0	11	0	0	0	0	0	5	0	0	12	0	7	5
43	27	12	53	25	0	8	32	28	39	30	24	37	20	30	0
44	0	8	7	6	0	0	4	3	4	2	2	14	2	5	0
45	43	34	47	35	0	13	28	30	46	21	36	42	39	44	0
46	1	1	0	0	3	0	0	0	0	0	0	8	1	0	0
47	34	0	6	1	0	0	1	0	6	0	2	7	0	3	0
48	43	0	4	0	4	0	1	0	6	0	3	10	0	4	1
49	0	0	5	0	0	0	6	0	4	2	2	0	4	6	0
50	36	14	45	40	0	43	36	40	58	25	40	32	42	46	0
51	4	0	13	5	2	7	9	6	13	2	4	11	6	8	3
52	0	3	3	0	1	3	4	1	3	2	2	7	6	0	1
53	0	22	3	0	6	0	3	0	6	0	0	9	0	4	0
54	8	2	5	0	4	7	5	6	14	0	6	11	10	7	2
55	4	0	6	0	2	3	7	0	8	3	1	11	5	6	1
56	2	0	9	0	9	3	8	3	8	2	0	7	2	5	8
57	0	5	0	0	0	14	18	16	29	17	13	27	15	23	9
58	0	4	22	0	0	0	2	1	1	0	1	8	0	0	0
59	0	1	0	51	0	1	1	1	6	0	0	7	1	4	0
60	39	27	0	0	0	0	37	45	55	1	34	39	40	41	0
61	3	0	37	0	1	0	5	0	1	0	0	7	0	0	0
62	4	0	3	0	2	0	2	0	1	3	4	8	3	4	0
63	24	0	2	0	8	0	0	0	4	0	0	8	2	3	0
64	7	16	0	0	12	1	17	19	27	5	16	20	24	9	15
65	7	12	14	0	8	0	10	14	21	5	8	22	11	13	11
66	9	7	19	3	8	7	9	7	16	0	6	25	7	10	1
67	1	0	4	0	0	5	0	0	9	6	2	8	3	2	6
68	17	8	5	0	12	17	13	12	21	13	13	17	15	19	12
69	0	0	15	6	1	4	2	2	8	4	3	6	1	6	6
70	0	5	8	0	4	0	3	1	3	0	4	9	7	2	1
71	43	5	0	0	1	0	0	0	5	0	0	7	1	7	0
72	4	1	2	0	1	0	0	0	4	0	1	7	2	5	0
73	0	2	0	0	0	32	5	0	5	0	0	7	0	4	28
74	23	0	3	0	0	0	36	45	47	34	27	36	37	40	0
75	3	27	26	0	0	2	3	0	1	1	0	7	3	5	0
76	4	0	0	0	0	2	5	0	5	0	0	9	3	3	0
77	33	0	6	4	0	13	4	0	2	0	0	4	1	0	0
78	47	0	2	0	0	5	4	0	6	0	0	6	3	6	0
79	26	0	3	0	6	0	5	2	5	0	0	8	1	3	8
80	11	6	0	0	8	4	12	15	2	6	9	16	10	14	3
81	17	13	3	0	3	0	5	4	14	5	3	10	7	6	0
82	51	0	5	0	2	0	3	0	5	0	1	9	1	3	3
83	5	3	5	7	0	0	8	0	3	3	0	9	6	6	22
84	30	30	33	0	19	10	31	37	26	27	26	28	31	31	9
85	6	5	11	0	7	11	11	8	12	0	6	17	10	13	1
86	30	13	0	0	12	0	5	2	9	0	2	10	2	6	12
87	28	3	23	0	9	15	16	20	32	11	15	32	19	23	7
88	11	0	14	0	1	4	7	6	12	4	5	17	5	11	0
89	20	0	0	0	2	3	4	0	2	0	0	6	1	4	1
90	19	5	6	0	13	4	4	2	10	0	0	5	2	4	19
91	13	19	33	0	0	16	27	29	36	13	22	31	21	25	0
92	0	3	0	0	2	0	0	1	3	0	0	7	1	5	0
93	0	0	0	3	4	1	2	0	1	0	1	6	4	5	0
94	47	0	4	0	4	1	1	1	6	0	0	9	1	4	2
95	5	0	9	0	8	7	5	0	11	1	0	6	6	7	0
96	0	1	3	0	2	3	0	1	4	1	0	4	0	4	2
97	40	0	0	0	0	0	0	0	3	3	1	0	0	0	0
98	0	0	0	0	0	0	0	0	0	0	0	7	1	0	2
99	0	0	5	0	0	0	0	1	3	0	0	6	2	0	2
100	3	0	1	0	0	0	0	0	0	0	3	6	0	2	0
101	0	0	0	0	2	0	0	0	0	0	2	1	2	0	8
102	9	2	12	0	3	0	0	8	11	5	8	6	10	3	0
103	44	0	2	0	0	0	0	0	0	0	1	4	0	0	8
104	0	0	0	0	0	0	1	0	0	0	1	4	1	5	6
105	2	0	10	0	3	1	4	4	0	6	6	6	7	3	0
106	1	0	1	0	4	0	2	0	0	0	0	4	4	1	0
107	0	0	0	0	3	0	0	0	2	0	3	5	1	1	0
108	30	0	2	0	2	0	0	0	0	0	0	5	0	0	1
109	1	0	3	0	0	0	1	0	5	1	0	7	0	0	1
110	2	0	4	0	0	0	0	0	1	0	0	4	1	1	0
111	1	0	5	0	0	0	0	1	0	0	2	6	0	0	10
112	13	0	11	0	1	0	0	0	0	4	9	11	10	0	0
113	0	0	0	0	0	0	0	0	0	0	5	0	0	0	0
114	0	0	3	0	0	0	1	0	0	0	1	4	0	7	1
115	2	0	3	0	0	0	0	0	8	2	3	4	0	3	0
116	0	0	4	0	0	0	1	0	7	0	4	4	2	0	1
117	1	1	5	0	0	1	0	0	2	0	6	5	0	3	24
118	30	2	24	0	0	4	0	7	9	19	19	21	21	2	1
119	0	0	0	0	1	0	0	0	0	0	0	3	0	0	5
120	2	0	7	0	0	0	9	3	1	0	4	3	2	19	0
121	0	0	3	0	0	0	0	0	8	0	1	3	0	2	3
122	4	0	5	0	1	2	2	1	6	0	4	4	5	4	0
123	1	1	0	0	0	0	0	0	0	0	0	4	0	3	2
124	0	2	0	0	1	0	0	1	37	0	2	5	0	5	0
125	2	3	6	0	7	0	0	0	6	0	3	3	4	6	19
126	17	13	13	0	5	10	0	18	27	11	13	18	27	0	1
127	3	0	7	3	1	0	0	3	10	0	3	6	1	0	0
128	1	0	3	0	3	0	7	2	4	0	1	4	3	18	6
129	6	0	8	0	0	4	1	8	11	0	1	9	9	6	3
130	5	2	6	0	0	0	1	0	2	0	2	4	0	4	0
131	2	2	2	0	2	4	5	0	0	0	3	0	0	7	1
132	30	1	7	0	3	2	4	2	4	0	3	5	1	4	0
133	0	0	0	0	5	1	0	0	0	0	0	4	0	3	0
134	11	0	3	0	0	1	0	0	0	0	1	6	0	3	0

Table 5.1 Screening newly isolated IM235 T cell clones for EBV antigen specificity by quantifying ^{51}Cr release from autologous target LCL cells. Each T cell clone was co-cultured with ^{51}Cr-loaded autologous LCLs expressing two EBV antigen peptides via infection with vaccinia vectors. Those that responded to one target only are highlighted in yellow, and the values represent the % lysis of target cells, calculated from basal lysis (LCLs alone) and maximal lysis (SDS-treatment) controls.

(a)

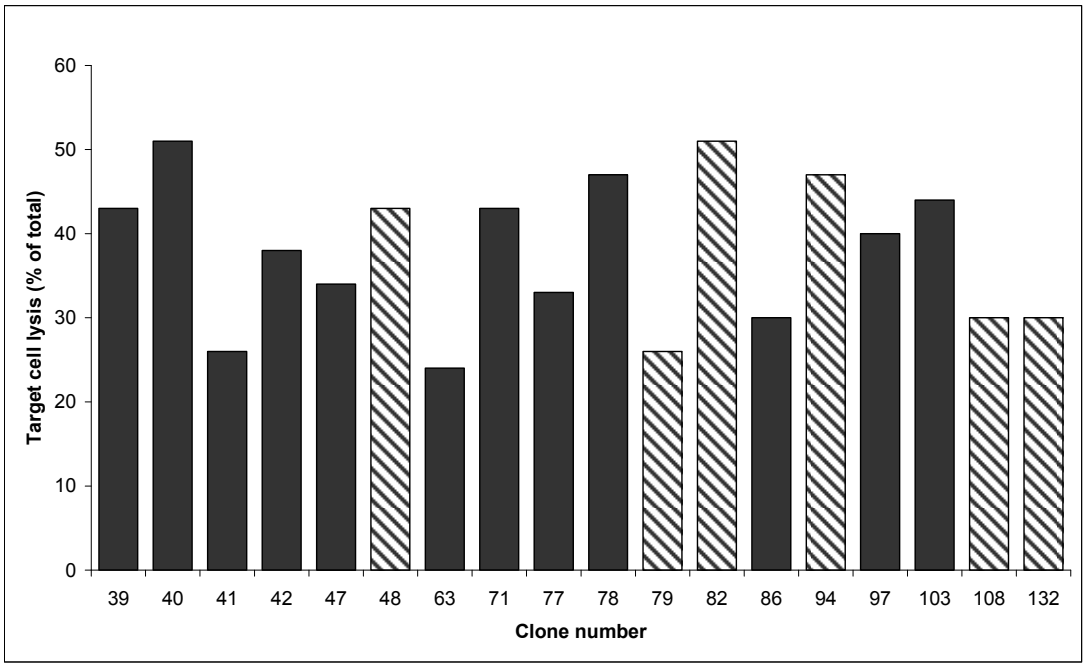

(b)

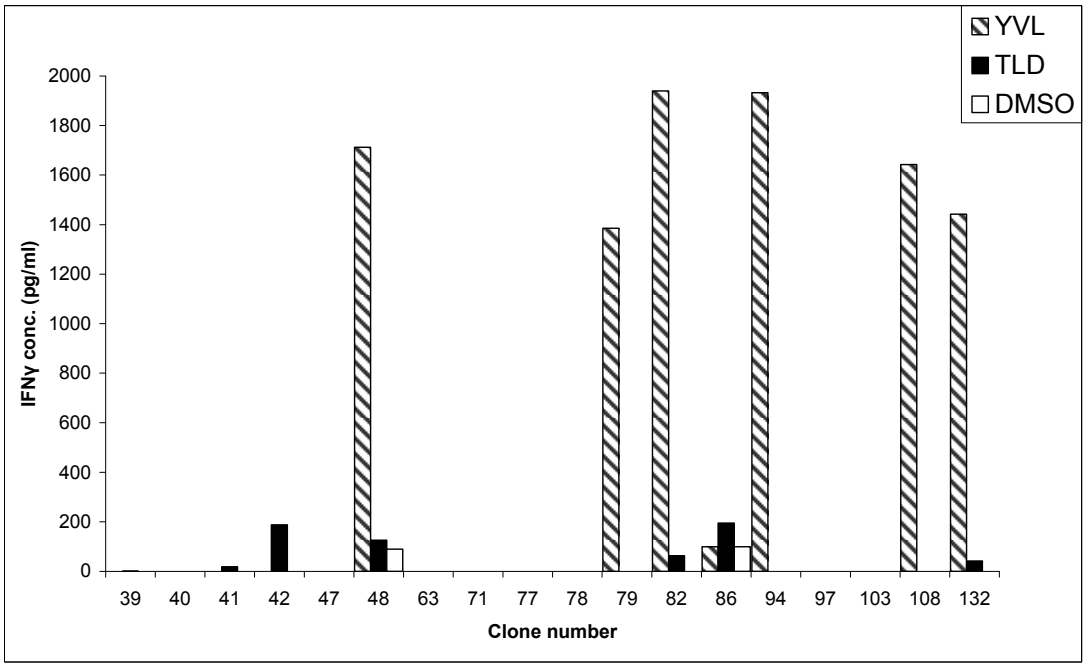

Figure 5.2 Epitope mapping of newly isolated IM235 T cell clones. (a) A highlight of the ^{51}Cr release assay data from 18 cells that responded to co-expressed antigens BRLF1 and BMRF1 (highlighted in yellow in **Table 5.1**). Response to antigen is measured as a % of target cells lysed by the T cell clone. **(b)** The response of these 18 clones to antigen peptides was determined by IFNγ-release. Putative peptide-specific T cell clones (those represented in **(a)**) were incubated with BJAB cells pulsed with either a common HLA-A2.01-restricted BRLF1 peptide (striped columns) YVLDHLIVV, or a BMRF1 peptide TLDYKPLSV (black columns) also restricted to HLA-A2.01, presented by autologous LCLs. IFNγ production was quantified by ELISA. There was no response to a DMSO control (white columns). Responses to antigens other than BRLF1 and BMRF1 were discounted because peptides were not available for these antigens.

^{51}Cr-loaded autologous LCLs were engineered to express two EBV antigens, and incubated with each putative T cell clone (Chapter 2.7.2). The release of ^{51}Cr into the supernatant indicated killing of the target cells (LCLs) by antigen-specific T cells (**Table 5.1**). Subsequent analysis of responder clones by measuring IFNγ production in response to peptide presentation by HLA-matched BJAB cells, revealed six T cell clones, IM235 c48, c79, c82, c94, c108 and c132, all with specificity for an HLA-A2.01-restricted BRLF1 peptide YVLDHLIVV (YVL, **Figure 5.2**, **b**). No clones reacted substantially to the TLDYKPLSV peptide of BMRF1, also restricted through HLA-A2.01. There was only a minimal response to a vehicle control.

All subsequent experiments on the impact of vOX2 and CD200 on human T cell clones were carried out with eight clones (**Table 5.2**). These included the six CD8$^+$ IM235 clones (c48, c79, c82, c94, c108 and c132) (**Figure 5.2**, **b**). Two previously isolated T cell clones were also studied. **(i)** The CD8$^+$ IM140.1 Y15 clone, also directed against the YVL peptide, was derived from an IM patient by another researcher. **(ii)** The CD4$^+$ SL c93 clone, specific for PRSTVFYNIPPMPLPPSQL (PRS) peptide of an HLA-DR-restricted EBNA2 protein, was isolated from a healthy donor by another researcher.

	Clone name	Donor	Peptide specificity	EBV antigen	HLA restriction	
CD8$^+$	IM140.1 Y15	IM140 (IM patient)	**YVL**DHLIVV	BRLF1 (lytic)	HLA-A2.01	} 'workhorse' clones
CD4$^+$	SL c93	ICS3804 (EBV-seropositive donor)	**PRS**TVFYNIPPMPLPPSQL	EBNA2 (latent)	HLA-DR7, 52a, 52b, 52c	
CD8$^+$	IM235 c48	IM235 (IM patient)	**YVL**DHLIVV	BRLF1 (lytic)	HLA-A2.01	
CD8$^+$	IM235 c79	IM235 (IM patient)	**YVL**DHLIVV	BRLF1 (lytic)	HLA-A2.01	
CD8$^+$	IM235 c82	IM235 (IM patient)	**YVL**DHLIVV	BRLF1 (lytic)	HLA-A2.01	
CD8$^+$	IM235 c94	IM235 (IM patient)	**YVL**DHLIVV	BRLF1 (lytic)	HLA-A2.01	
CD8$^+$	IM235 c108	IM235 (IM patient)	**YVL**DHLIVV	BRLF1 (lytic)	HLA-A2.01	
CD8$^+$	IM235 c132	IM235 (IM patient)	**YVL**DHLIVV	BRLF1 (lytic)	HLA-A2.01	

Table 5.2 Summary of the T cells clones utilised in this research project. Donor ID numbers, peptide specificities and HLA restrictions are tabulated. Two of the clones acted as 'workhorse' clones, and were used for extensive investigation into the mechanism of action of vOX2 and CD200.

5.5. Expressing vOX2 and CD200 in a B lymphoblastoid cell line

vOX2 is a KSHV lytic cycle protein (Zhang *et al*., 2005) expressed on the surface of KSHV-infected cells. To confirm the expression of vOX2, BCBL-1 cells, latently infected with KSHV, were first labelled with an anti-LANA antibody to verify KSHV infection (Chapter 2.4). LANA was identifiable by its characteristic nuclear punctuate staining (Kedes *et al*., 1997) in cells latently infected with KSHV (**Figure 5.3**, **a**, right panel). Cell surface vOX2 on BCBL-1 cells latently infected with KSHV was stained with a polyclonal anti-vOX2 antibody. vOX2 was only detectable on the surface of a small percentage of BCBL-1 cells, presumably the small percentage of cells that spontaneously undergo lytic replication of the virus (**Figure 5.3**, **b**, right panel). However, treating the cells with PMA to induce lytic replication of KSHV, enhanced the expression of vOX2 by these cells, indicating that it is expressed on KSHV-infected cells *in vivo* during replication of the virus (**Figure 5.3**, **c**, right panel). The nuclei of all cells were labelled with DAPI (**Figure 5.3**, **a**, **b**, **c**, left panels).

In order to replicate the *in vivo* expression of vOX2 on KSHV-infected cells, BJAB cells were engineered to express full-length vOX2 and CD200 by retroviral transduction (see Chapter 2.8.6 for methodology). Either *vOX2* or *CD200* were inserted into a bicistronic expression vector, enabling the co-transcription and translation of the inserted gene and a gene conferring puromycin-resistance on the cell. The expression of vOX2 on the surface of engineered BJAB cells was determined by labelling cells with a polyclonal anti-vOX2 antibody and quantifying its fluorescence by flow cytometry (**Figure 5.4**, **a**). CD200 expression was detected with a commercial anti-CD200 monoclonal antibody (**Figure 5.4**, **b**). vOX2-BJAB, and Empty-BJAB cells stained with anti-CD200 antibody served as negative controls, and vice-versa for CD200-BJAB stained with anti-vOX2. Protein expression was determined by this method before each functional assay was carried out. Full-length vOX2 and CD200 were also generated as EGFP fusion proteins (**Figure 5.4**, **c**),

by in-frame fusion of the gene encoding the protein of interest and *EGFP* before insertion into the expression vector.

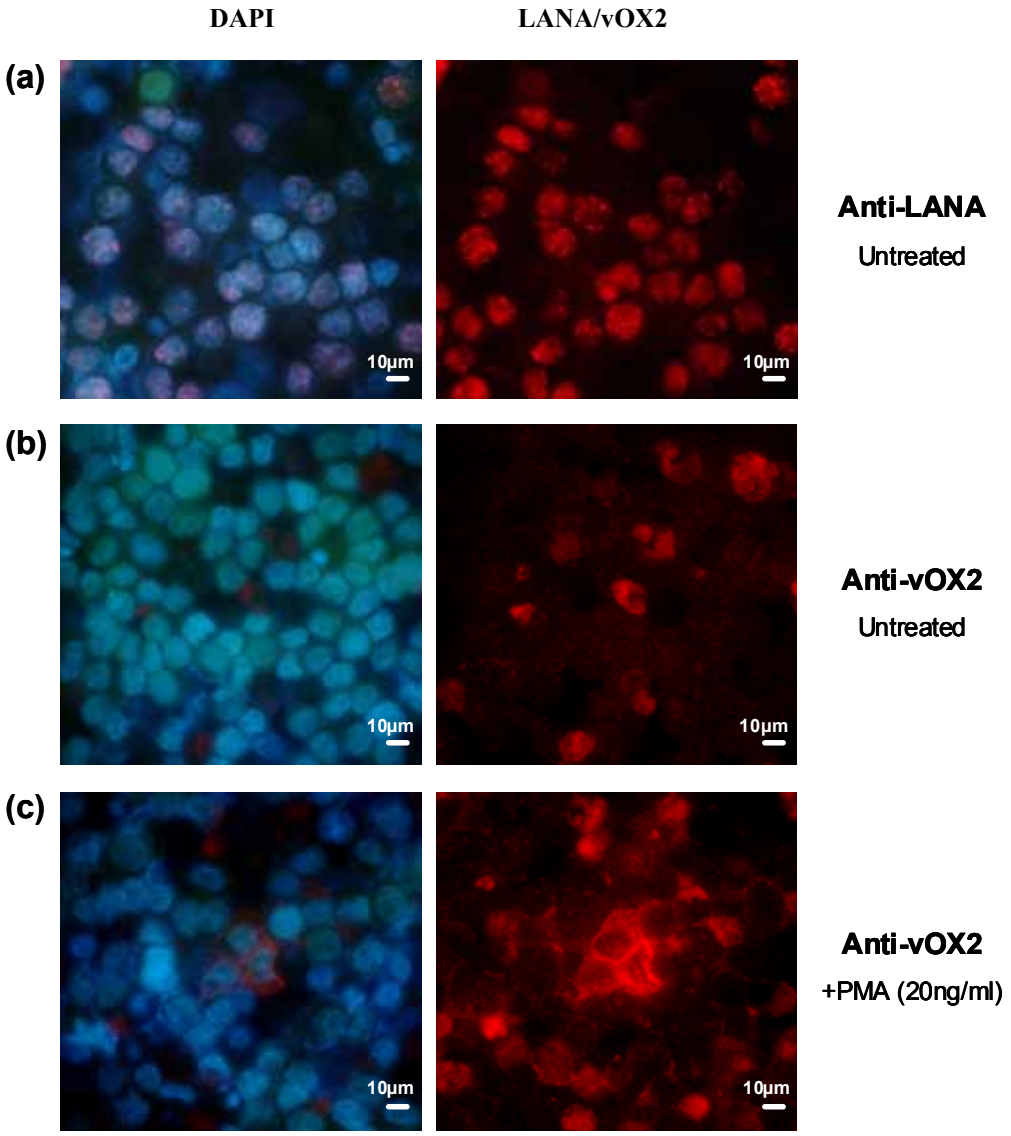

Figure 5.3 Immunofluorescence imaging of cell-surface vOX2 on KSHV-infected BCBL-1 cells. BCBL-1 cells, latently infected with KSHV, were cultured either without PMA, or with PMA (20ng/ml) for four days, to induce lytic replication. The cells were then fixed and permeabilised. Intracellular latent nuclear antigen (LANA) was detected in both unstimulated (data not shown) and PMA-treated BCBL-1 cells. vOX2 was detected (by a polyclonal antibody) on the cell surface of the majority of PMA-treated cells, but very few unstimulated cells, as expected. The images on the left depict DAPI staining of the nuclei, and the images on the right show antigen-specific fluorescent antibody labelling of LANA or vOX2. Minimal PE-staining evident in the DAPI images are a result of spectral bleed-through (cross-over of fluorescence emissions). These images are representative of those collected in four independent experiments.

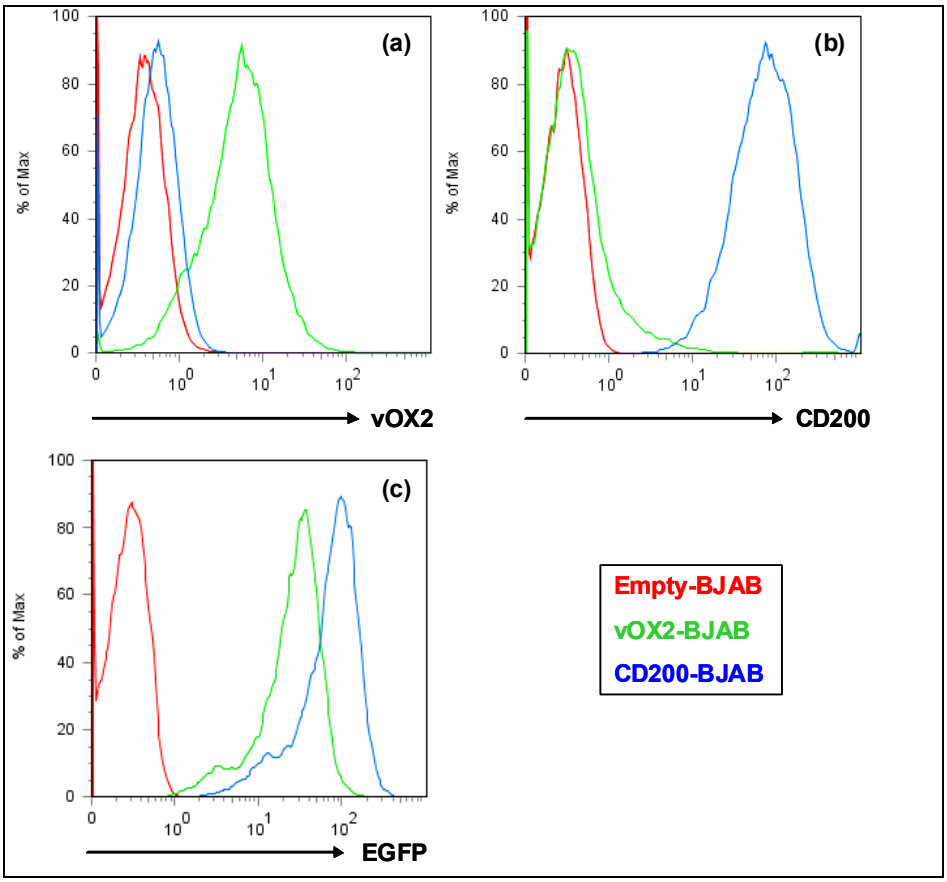

Figure 5.4 Expression of vOX2 and CD200 on the surface of engineered B-lymphoblastoid BJAB cells. Expression levels of **(a)** native vOX2 and **(b)** native CD200 on engineered BJAB cells were determined by flow cytometry following incubation of the cells with specific primary antibodies and phycoerythrin-conjugated secondary antibodies. **(c)** BJAB cells engineered to express native forms of vOX2 or CD200 fused in-frame with EGFP; protein expression was quantified by flow cytometry (fluorescence in the FL1 channel).

5.6. Suppression of T cell clone activity by vOX2 and CD200 determined by extracellular IFNγ secretion

The secretion of IFNγ into the culture supernatant by peptide-stimulated T cells serves as a measure of T cell responses. Empty-BJAB, vOX2-BJAB and CD200-BJAB cells were pulsed with peptide and incubated with HLA-matched peptide-specific human T cell clones

(Chapter 2.7.3). Our method to grow T cell clones is to culture them with mixed PMA-stimulated PBMCs to induce an allogeneic response, along with autologous or HLA-matched LCLs expressing EBV antigens. Therefore, the T cells are hyper-activated state following restimulation. To determine temporal effects, the newly isolated YVL-specific T cells from an IM donor (IM235) were analysed over time post-restimulation of the cells. vOX2-BJAB cells were not included in every experiment due to their low rate of proliferation and the frequently observed loss of vOX2 protein from the cell surface during long-term culture (data not shown). All extracellular IFNγ data in this chapter are presented as line graphs, with a data point for each peptide concentration and each BJAB cell type. The use of line graphs aids the comparison between the three BJAB cell types. The error bars indicate the standard error of the mean between triplicate samples within each experiment. Each experiment is represented by a separate graph because the IFNγ concentration varied between experiments, and normalising the data to that obtained for the Empty-BJAB control within each experiment would obscure the pattern of stimulation in relation to peptide concentration.

$CD8^+$ IM235 clone 48 was tested weekly from 21 days to 41 days post-restimulation (**Figure 5.5**). A trend towards suppression of IFNγ-secretion by T cells incubated with vOX2-BJAB or CD200-BJAB cells, in comparison with those stimulated by Empty-BJAB cells, was observed 21, 35 and 41 days post-restimulation. However, the generation of IFNγ by T cells 28 days post-restimulation was not suppressed in the presence of vOX2 or CD200. Similarly, the secretion of IFNγ by clone IM235 c79 was reduced by vOX2 and CD200 on days 21, 35 and 41 post-restimulation, in comparison to Empty-BJAB-treated controls, but was not altered on day 28 (**Figure 5.6**). Likewise, the response of IM235 c82 was suppressed at all time points (14, 21, 28, 35 and 41 days post-restimulation) by vOX2-BJAB and CD200-BJAB cells (**Figure 5.7**). Similarly, the secretion of IFNγ by IM235 c94 T cell clone

was also suppressed on days 15, 21, 28, 35 and 41 days post-restimulation (**Figure 5.8**). IM235 c108 T cell IFNγ-secretion was suppressed by CD200-BJAB 15, 21, 35 and 41 days post-restimulation (**Figure 5.9**). 21 days post-restimulation, vOX2-BJAB did not alter the concentration of IFNγ deposited by the IM235 c108 T cells, though CD200 suppressed T cell activity in this experiment. However, after 35 days, vOX2-BJAB showed a similar suppressive activity to CD200-BJAB cells. No suppression of IM235 c108 T cell activity by either vOX2 or CD200 was observed on day 21 post-restimulation (**Figure 5.9**). vOX2 and CD200-BJAB cells modestly showed a trend towards inhibiting IFNγ-secretion by IM235 c132 cells at all time points, with the exception of day 28 post-restimulation (**Figure 5.10**).

Two other T cell clones were examined periodically for their suppression by vOX2 and CD200. These clones were used extensively in later experiments (see Chapters 6 and 7) and the ability of vOX2 and CD200 to reduce their IFNγ production was initially determined by this method before other experiments were carried out. These two clones were isolated by other scientists in the Institute, and their passage numbers are unknown. However, they could be successfully restimulated, and proliferated rapidly upon restimulation (data not shown), indicating that they have not yet reached senescence. The majority of the experiments carried out on these cells are presented in this chapter and are representative of the variation in data collected; all experiments were carried out between 14 days and 64 days post-restimulation. IFNγ-secretion by the $CD4^+$ SL c93 clone was attenuated in the presence of CD200-BJAB cells in nearly every experiment, though the level of suppression varied between experiments and with peptide concentration (**Figure 5.11**). The effect of vOX2-BJAB cells on the $CD4^+$ SL c93 was not examined as extensively as CD200-BJAB due to the lack of availability of the cells, as explained above. Its inhibitory activity also appears more variable than CD200-BJAB cells (**Figure 5.12**). CD200-BJAB cells consistently inhibited IFNγ-secretion by the $CD8^+$ IM140.1 Y15 T cell clone, though the level of suppression fluctuated between and

within experiments as before (**Figure 5.13**). Consistent with findings for the $CD4^+$ clone, the activity of vOX2 on $CD8^+$ IM140.1 Y15 responses was variable but overall tended towards suppression (**Figure 5.14**).

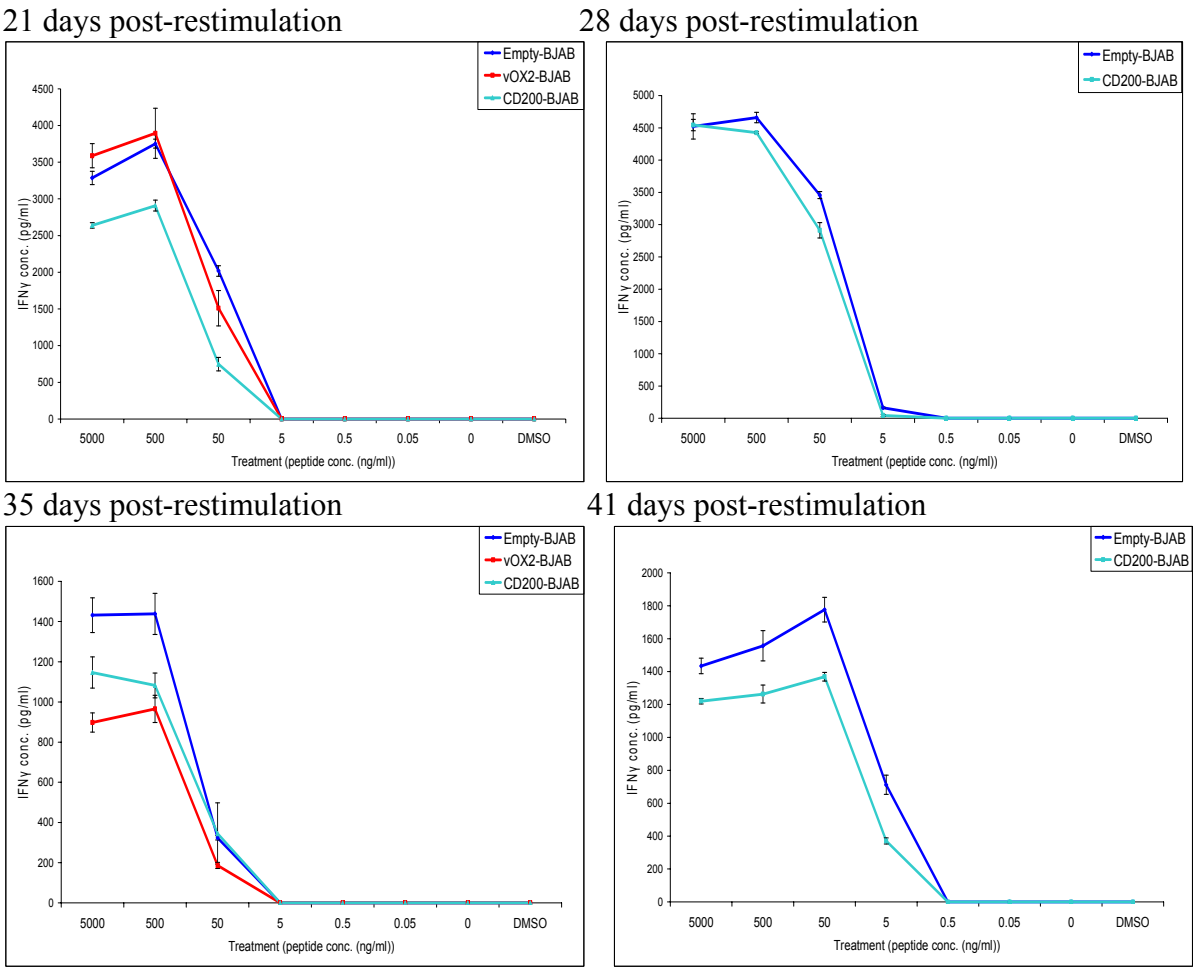

Figure 5.5 vOX2 and CD200-mediated suppression of $CD8^+$ T cell clone IM235 c48 in relation to time post-restimulation. IFNγ-secretion by the YVL-specific T cell clone IM235 c48 was tested weekly, post-restimulation, to determine the extent of vOX2 or CD200-mediated suppression. BJAB cells engineered to express either native vOX2 or CD200, or transduced with an empty vector, served as antigen-presenting cells. These BJAB cells were pulsed with BRLF1 peptide YVLDHLIVV for one hour, washed, and then co-cultured with the T cell clone for 16 hours (each treatment was carried out in triplicate). IFNγ-release was quantified by ELISA. All values represented as 0pg/ml IFNγ were beyond the limit of detection of this ELISA (<31.25pg/ml).

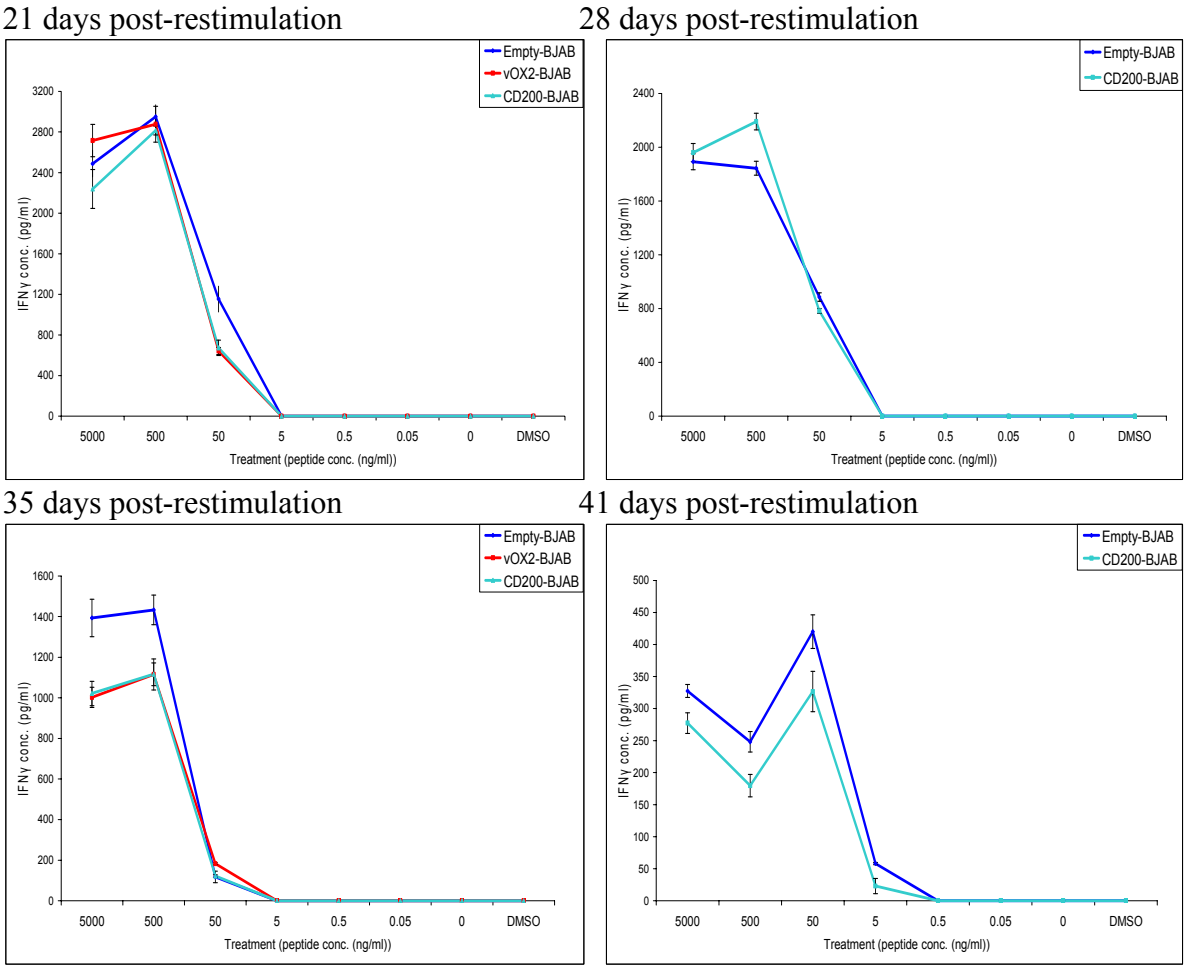

Figure 5.6 vOX2 and CD200-mediated suppression of CD8$^+$ T cell clone IM235 c79 in relation to time post-restimulation. IFNγ-secretion by the YVL-specific T cell clone IM235 c79 was tested weekly, post-restimulation, to determine the extent of vOX2 or CD200-mediated suppression. BJAB cells engineered to express either native vOX2 or CD200, or transduced with an empty vector, served as antigen-presenting cells. These BJAB cells were pulsed with BRLF1 peptide YVLDHLIVV for one hour, washed, and then co-cultured with the T cell clone for 16 hours (each treatment was carried out in triplicate). IFNγ-release was quantified by ELISA. All values represented as 0pg/ml IFNγ were beyond the limit of detection of this ELISA (<31.25pg/ml).

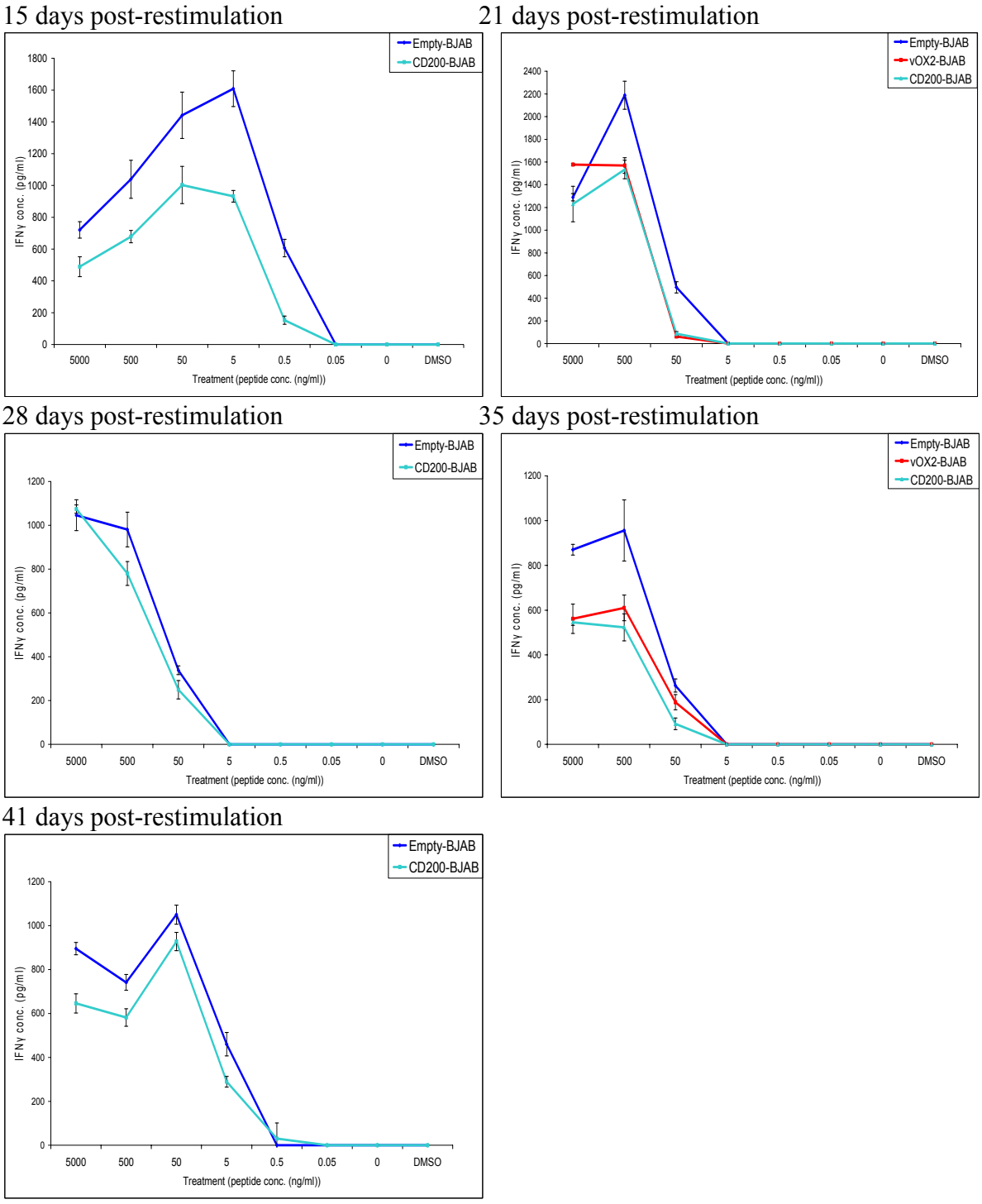

Figure 5.7 vOX2 and CD200-mediated suppression of CD8$^+$ T cell clone IM235 c82 in relation to time post-restimulation. IFNγ-secretion by the YVL-specific T cell clone IM235 c82 was tested weekly, post-restimulation, to determine the extent of vOX2 or CD200-mediated suppression. BJAB cells engineered to express either native vOX2 or CD200, or transduced with an empty vector, served as antigen-presenting cells. These BJAB cells were pulsed with BRLF1 peptide YVLDHLIVV for one hour, washed, and then co-cultured with the T cell clone for 16 hours (each treatment was carried out in triplicate). IFNγ-release was quantified by ELISA. All values represented as 0pg/ml IFNγ were beyond the limit of detection of this ELISA (<31.25pg/ml).

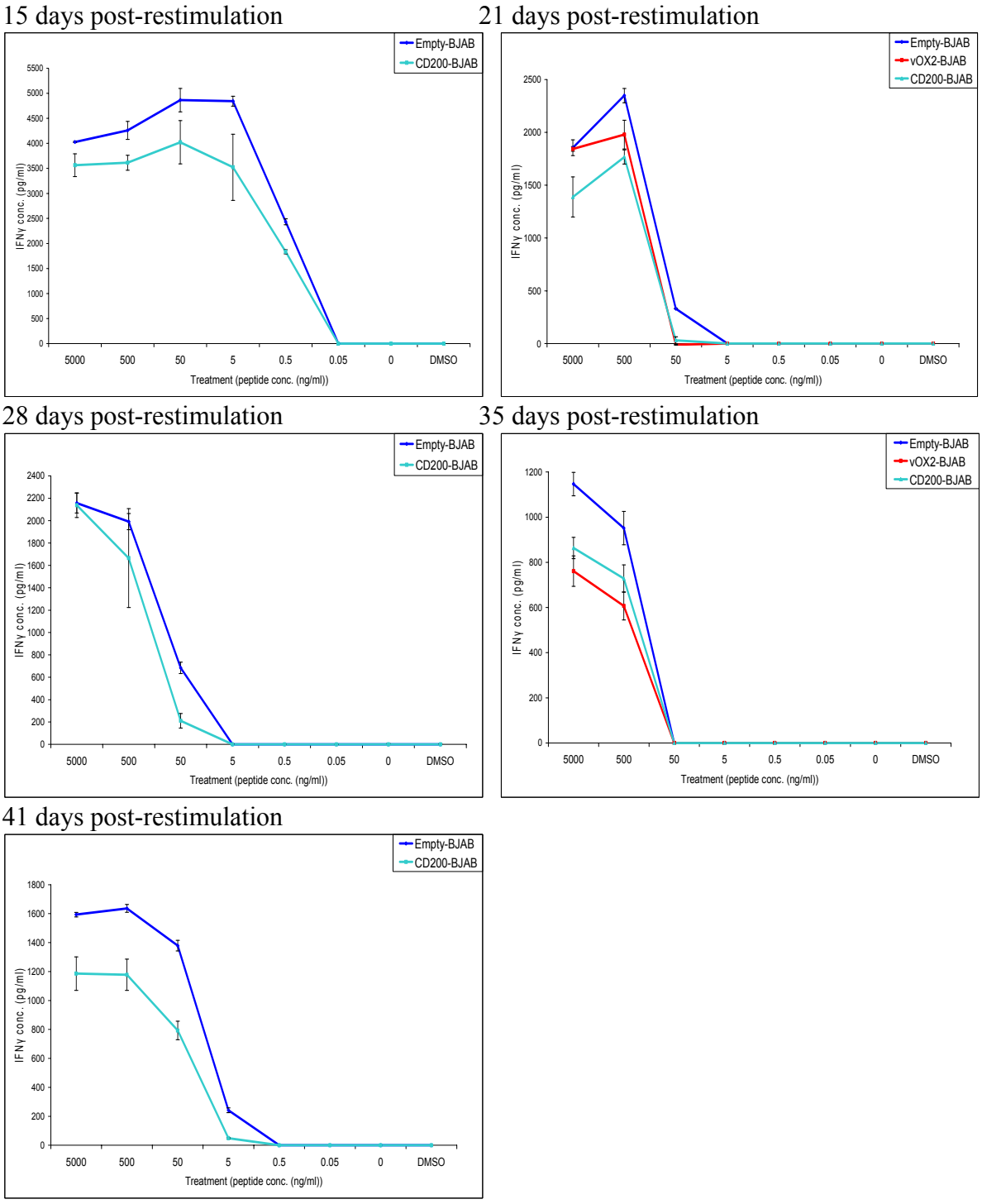

Figure 5.8 vOX2 and CD200-mediated suppression of CD8$^+$ T cell clone IM235 c94 in relation to time post-restimulation. IFNγ-secretion by the YVL-specific T cell clone IM235 c94 was tested weekly, post-restimulation, to determine the extent of vOX2 or CD200-mediated suppression. BJAB cells engineered to express either native vOX2 or CD200, or transduced with an empty vector, served as antigen-presenting cells. These BJAB cells were pulsed with BRLF1 peptide YVLDHLIVV for one hour, washed, and then co-cultured with the T cell clone for 16 hours (each treatment was carried out in triplicate). IFNγ-release was quantified by ELISA. All values represented as 0pg/ml IFNγ were beyond the limit of detection of this ELISA (<31.25pg/ml).

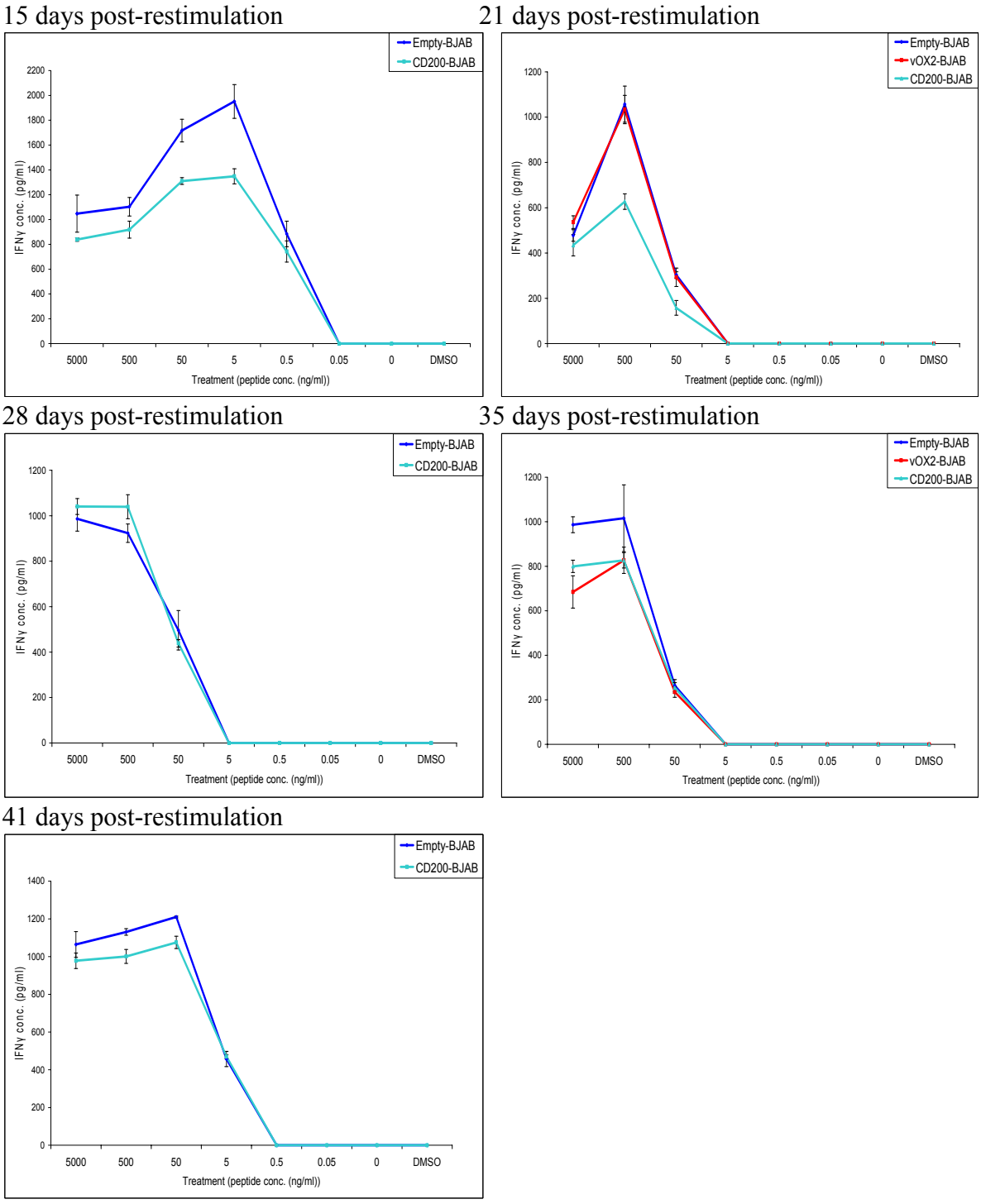

Figure 5.9 vOX2 and CD200-mediated suppression of CD8$^+$ T cell clone IM235 c108 in relation to time post-restimulation. IFNγ-secretion by the YVL-specific T cell clone IM235 c108 was tested weekly, post-restimulation, to determine the extent of vOX2 or CD200-mediated suppression. BJAB cells engineered to express either native vOX2 or CD200, or transduced with an empty vector, served as antigen-presenting cells. These BJAB cells were pulsed with BRLF1 peptide YVLDHLIVV for one hour, washed, and then co-cultured with the T cell clone for 16 hours (each treatment was carried out in triplicate). IFNγ-release was quantified by ELISA. All values represented as 0pg/ml IFNγ were beyond the limit of detection of this ELISA (<31.25pg/ml).

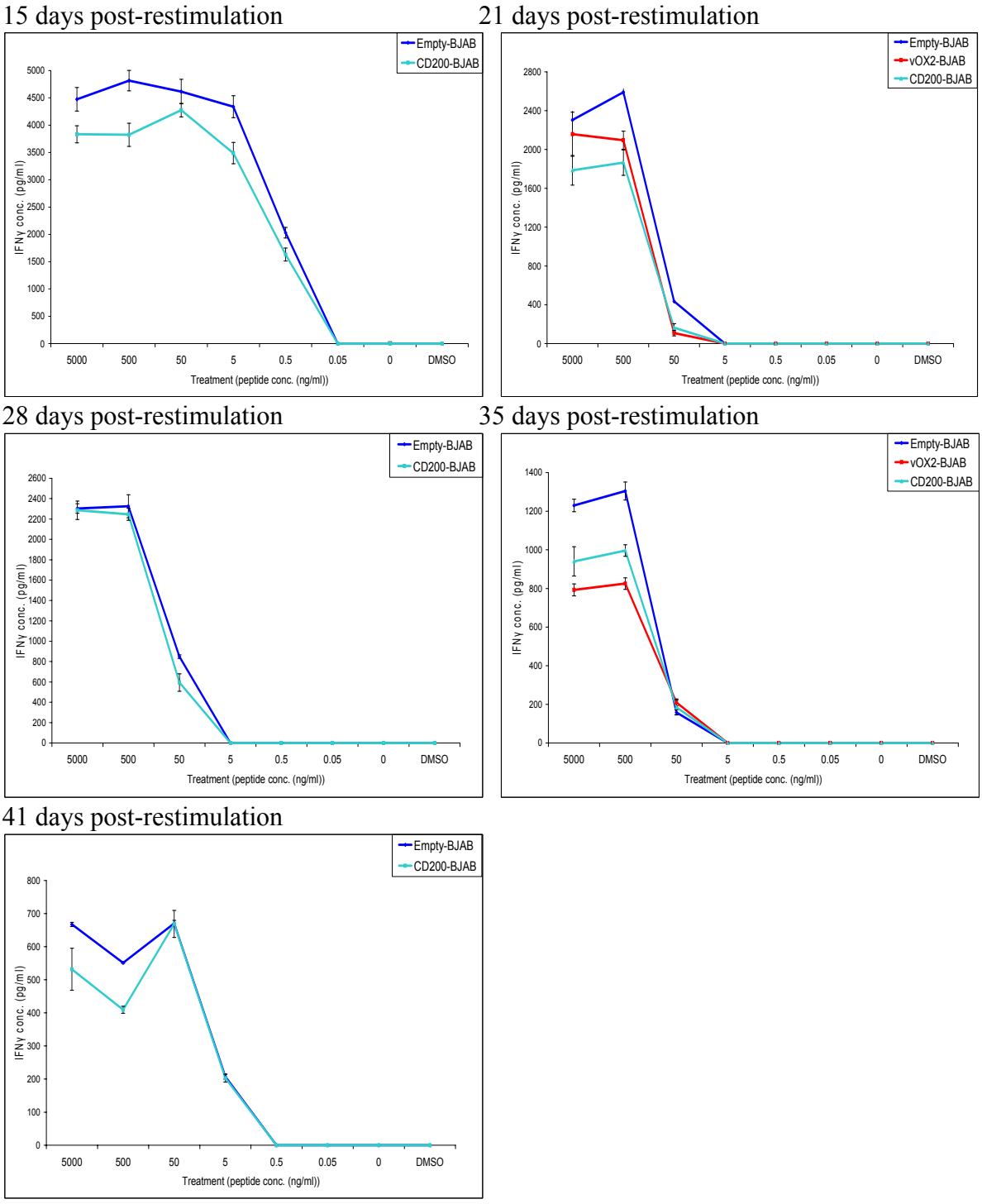

Figure 5.10 vOX2 and CD200-mediated suppression of $CD8^+$T cell clone IM235 c132 in relation to time post-restimulation. IFNγ-secretion by the YVL-specific T cell clone IM235 c132 was tested weekly, post-restimulation, to determine the extent of vOX2 or CD200-mediated suppression. BJAB cells engineered to express either native vOX2 or CD200, or transduced with an empty vector, served as antigen-presenting cells. These BJAB cells were pulsed with BRLF1 peptide YVLDHLIVV for one hour, washed, and then co-cultured with the T cell clone for 16 hours (each treatment was carried out in triplicate). IFNγ-release was quantified by ELISA. All values represented as 0pg/ml IFNγ were beyond the limit of detection of this ELISA (<31.25pg/ml).

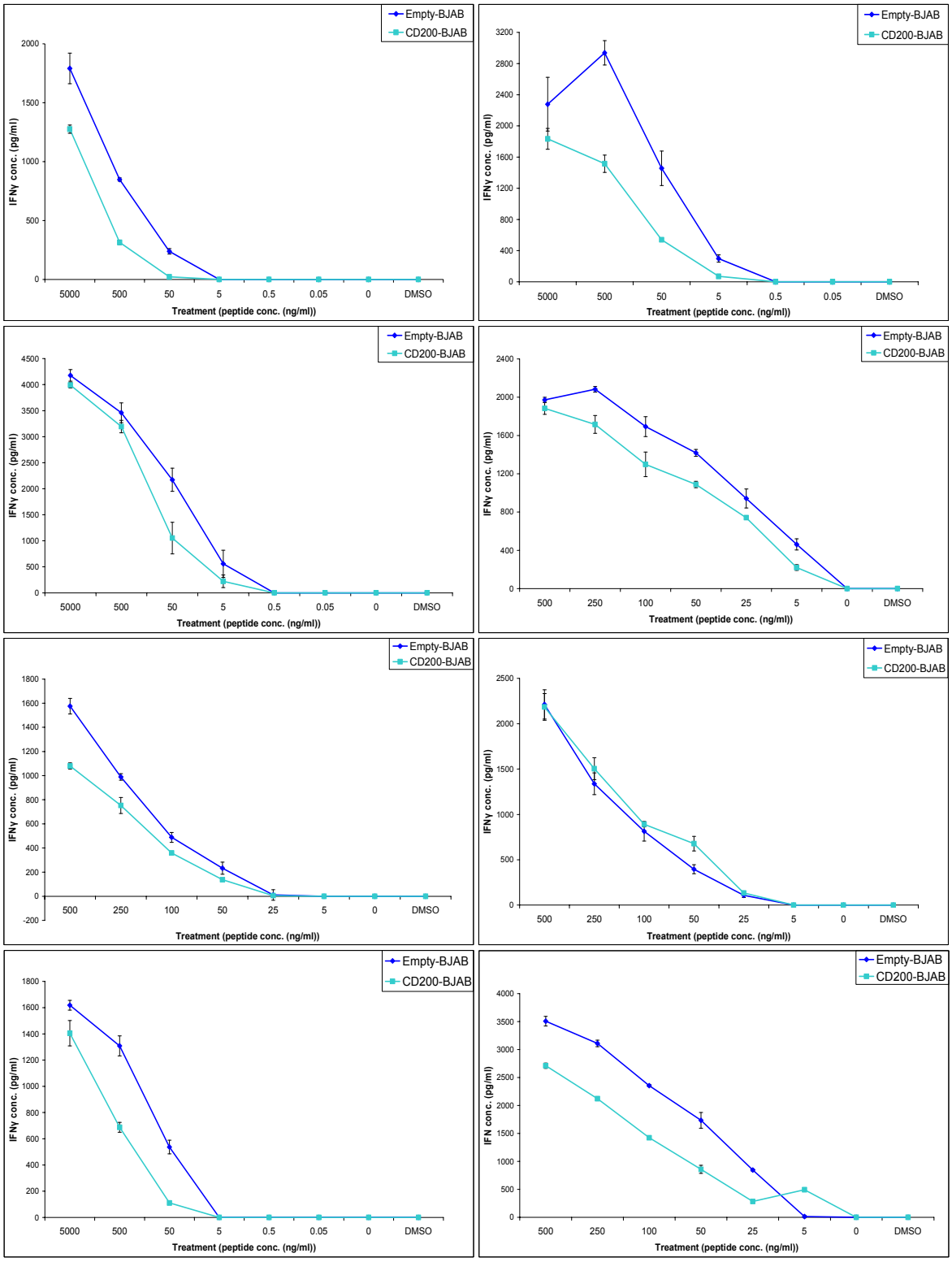

Figure 5.11 CD200-mediated suppression of the CD4$^+$ T cell clone SL c93. BJAB cells engineered to express native CD200, or transduced with an empty vector, served as antigen-presenting cells. BJAB cells were pulsed with PRSTVFYNIPPMPLPPSQL, a peptide derived from EBV EBNA2, for one hour, washed, and then co-cultured with the T cell clone for 16 hours (each treatment was carried out in triplicate). IFNγ-release was quantified by ELISA. All values represented as 0pg/ml IFNγ were beyond the limit of detection of this ELISA (<31.25pg/ml).

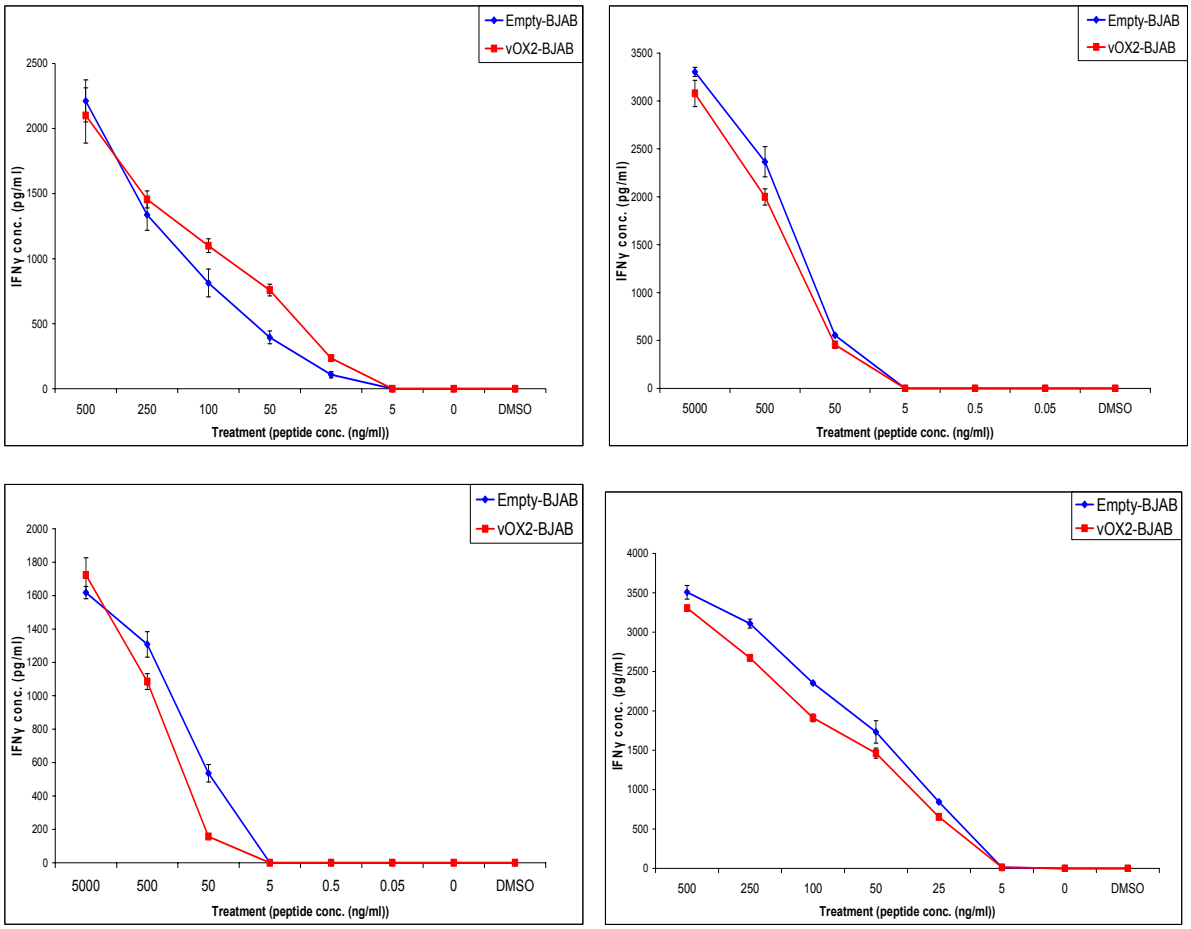

Figure 5.12 vOX2-mediated suppression of the CD4$^+$ T cell clone SL c93. BJAB cells engineered to express native vOX2, or transduced with an empty vector, served as antigen-presenting cells. BJAB cells were pulsed with PRSTVFYNIPPMPLPPSQL, an peptide derived from EBV EBNA2, for one hour, washed, and then co-cultured with the T cell clone for 16 hours (each treatment was carried out in triplicate). IFNγ-release was quantified by ELISA. All values represented as 0pg/ml IFNγ were beyond the limit of detection of this ELISA (<31.25pg/ml).

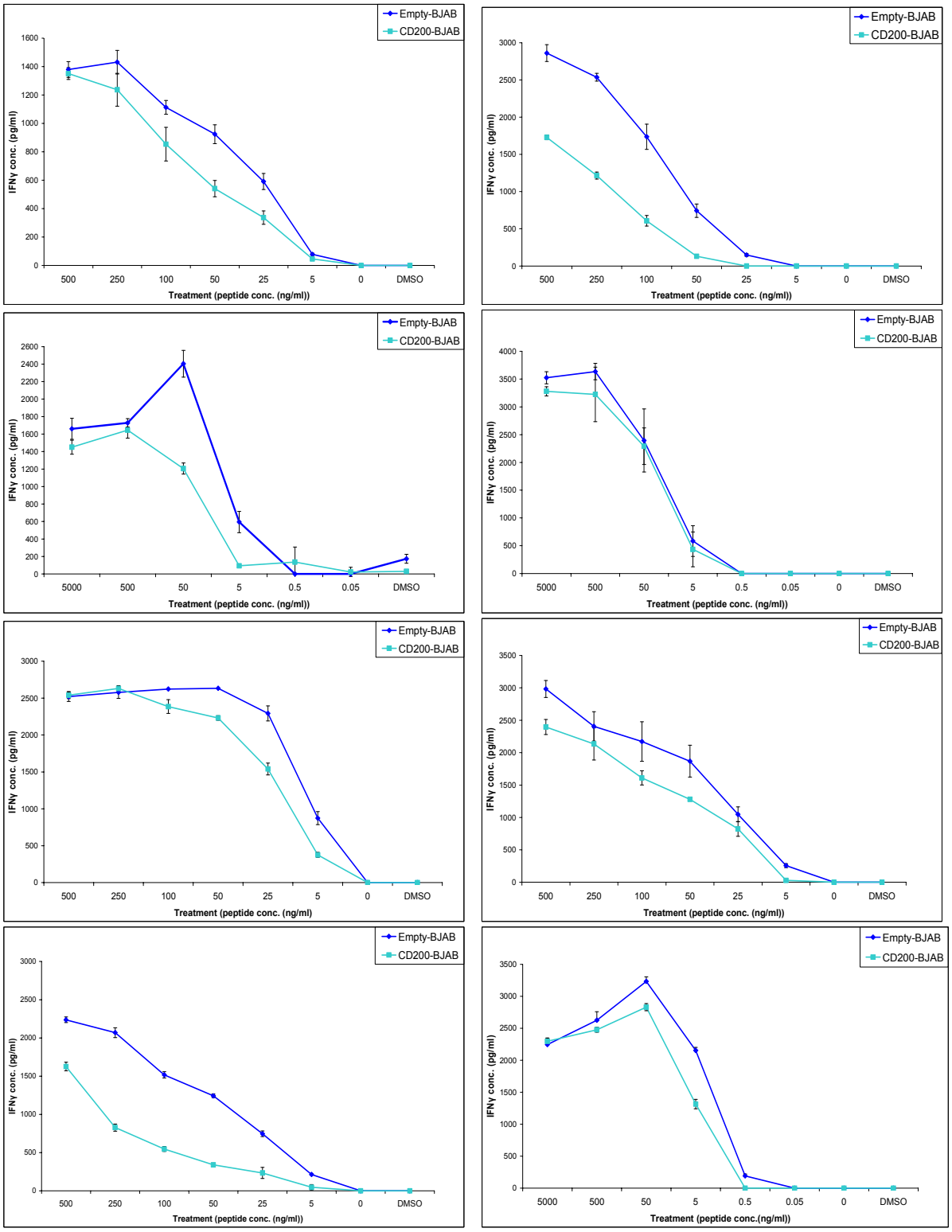

Figure 5.13 CD200-mediated suppression of the CD8$^+$ T cell clone IM140.1 Y15. BJAB cells engineered to express native CD200, or transduced with an empty vector, served as antigen-presenting cells. BJAB cells were pulsed with the peptide YVLDHLIVV, derived from EBV BRLF1, for one hour, washed, and then co-cultured with the T cell clone for 16 hours (each treatment was carried out in triplicate). IFNγ-release was quantified by ELISA. All values represented as 0pg/ml IFNγ were beyond the limit of detection of this ELISA (<31.25pg/ml).

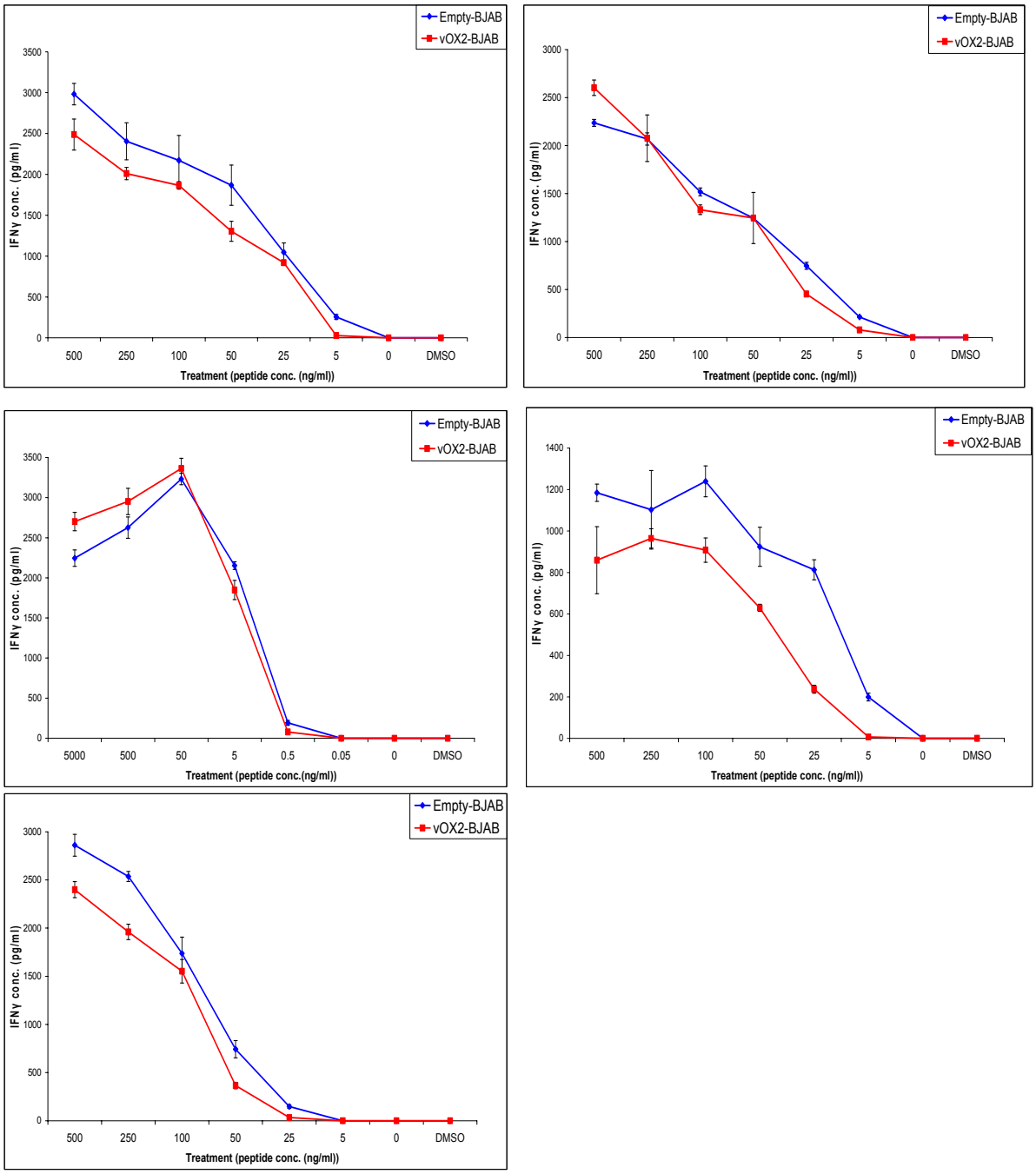

Figure 5.14 vOX2-mediated suppression of the CD8$^+$ T cell clone IM140.1 Y15. BJAB cells engineered to express native vOX2, or transduced with an empty vector, served as antigen-presenting cells. BJAB cells were pulsed with the peptide YVLDHLIVV, derived from EBV BRLF1, for one hour, washed, and then co-cultured with the T cell clone for 16 hours (each treatment was carried out in triplicate). IFNγ-release was quantified by ELISA. All values represented as 0pg/ml IFNγ were beyond the limit of detection of this ELISA (<31.25pg/ml).

5.7. Suppression of T cell clone activity by vOX2 and CD200, determined by intracellular IFNγ and IL-2

Quantifying secreted IFNγ by ELISA relies on a high concentration of the cytokine in the supernatant that is accumulated over several hours. Therefore, the T cells are exposed to both the putative inhibitory factor (vOX2 or CD200) and the stimulus (peptide) for an extended period. If the accumulation of IFNγ within the T cell is measured by a sensitive flow cytometric technique, a shorter incubation period is required. This assay was therefore established. Empty-BJAB, vOX2-BJAB and CD200-BJAB cells were pulsed with exogenous peptide and incubated with HLA-matched, peptide-specific T cell clones for 60mins. Brefeldin A was then added to the culture to inhibit cytokine secretion, and the cells incubated for a further 1, 2 or 4hrs before fixation (Chapter 2.7.4). Accumulated intracellular cytokines were then quantified by anti-IL-2 or anti-IFNγ antibodies following permeabilisation. Anti-CD4 or anti-CD8 antibodies distinguished the T cells from the BJAB cells. To obtain a % change from control, in the presence of vOX2 or CD200-BJAB cells, in the presence or absence of peptide, the data were normalised to those for peptide-loaded Empty-BJAB controls at each time point,. Please see Appendix D, Tables II and III for the raw data.

IL-2 accumulating within the stimulated $CD4^+$ SL c93 clone was reduced modestly by vOX2-BJAB and CD200-BJAB cells at all time points in four independent experiments (**Figure 5.15**, **a**). In the absence of stimulation, neither vOX2 nor CD200 altered the generation of IL-2 by the T cells. The suppressive effect of vOX2-BJAB cells appeared to be marginally reduced with time after Brefeldin A treatment. At 1hr post-Brefeldin A treatment, T cells incubated with peptide-pulsed vOX2-BJAB contained only 80.62% ± 4.94 SEM of the IL-2 present in T cells cultured with Empty-BJAB cells (*$p<0.05$, by univariate ANOVA). In comparison, by 2hrs, levels of IL-2 were increased slightly to 87.59% ± 4.04

SEM of control, and by 4hrs were 84.18% ± 17.28 SEM of control, upon stimulation by vOX2-BJAB cells. CD200 was slightly more effective at suppressing IL-2 production. At 1hr post-Brefeldin A treatment, the concentration of IL-2 in cells stimulated by CD200-BJAB cells was only 70.36% ± 2.19 SEM of control (**p<0.01, by univariate ANOVA). The suppression of IL-2 was maintained over time, and at 2hrs-post-Brefeldin A, IL-2 levels were 74.4% ± 1.9 SEM of control (**p<0.01, by univariate ANOVA), and were 69.24% ± 7.46 SEM of control at 4hrs post-Brefeldin A treatment.

The generation of IFNγ in the $CD4^+$ clone was reduced to a greater degree by vOX2 and CD200 than IL-2 (**Figure 5.15**, **b**). There was a slight reduction in the inhibitory effect with time. Peptide-pulsed vOX2-BJAB cells inhibited the accumulation of IFNγ in co-cultured T cells at 1hr post-Brefeldin A to 63.23% ± 9.3 SEM of control (*p<0.05, univariate ANOVA), and IFNγ levels were similar after 2hrs, at 66.65% ± 14.12 SEM of control (***p<0.001, univariate ANOVA), but increased after 4hrs, to 67.94% ± 31.33 SEM, in comparison to peptide-pulsed Empty-BJAB cells. CD200-BJAB cells also suppressed the generation of IFNγ, and were more effective than vOX2. T cells incubated with CD200-BJAB cells contained only 47.35% ± 5.12 SEM of the IFNγ present in cells stimulated by Empty-BJAB for 1hr post-Brefeldin A treatment (**p<0.01, univariate ANOVA). By 2hrs post-Brefeldin A, IFN levels had dropped further, to 37.71% ± 5.11 SEM of control (***p<0.001, univariate ANOVA), but rose again slightly by 4hrs, to 53.92% ± 10.66 SEM. Due to the pronounced CD200-mediated suppression of IFNγ at 2hrs post-Brefeldin A treatment, this time point was chosen for all subsequent assays.

The accumulation of IL-2 in the $CD8^+$ IM140.1 Y15 T cell clone was modestly suppressed by vOX2, to 74.07% ± 10.71 SEM of control in three independent experiments. T cells co-cultured with peptide-pulsed CD200-BJAB cells also accumulated less IL-2, and levels were reduced to 79.63% ± 11.61 SEM of control (**Figure 5.16**, **a**), though data did not

reach statistical significance. In comparison, the IFNγ generated by these cells was almost halved in the presence of vOX2 and CD200, in three independent experiments. T cells stimulated by peptide-pulsed vOX2-BJAB cells produced only 62.68% ± 14.39 SEM of the IFNγ generated by Empty-BJAB-stimulated cells, and CD200-BJAB were even more efficacious, reducing IFNγ to 40.42% ± 13.55 SEM of control (*$p<0.05$, by univariate ANOVA) (**Figure 5.16**, **b**).

IL-2 production by the $CD8^+$ IM235 c48 clone was not altered by vOX2 or CD200 in two independent experiments (**Figure 5.17**, **a**). Nevertheless, the accumulation of IFNγ in $CD8^+$ IM235 c48 cells was dramatically reduced in two independent experiments (**Figure 5.17**, **b**). T cells cultured with peptide-pulsed vOX2-BJAB produced much lower amounts of IFNγ (35.72% ± 22.94 SEM) than those cultured with peptide-pulsed Empty-BJAB cells (100%). CD200-BJAB cells also suppressed IFNγ production, to 27.51% ± 22.59 SEM of the IFNγ generated by cells stimulated by Empty BJAB (**Figure 5.17**, **b**).

IM235 c79 cell activity, measurable by intracellular IL-2 (**Figure 5.18**, **a**) and IFNγ (**Figure 5.18**, **b**) was not altered by vOX2 in three independent experiments. However, cells cultured with peptide-pulsed CD200-BJAB cells accumulated only 60.27% ± 17.15 SEM of the IFNγ present in Empty-BJAB-stimulated cells (**Figure 5.18**, **b**).

The production of IL-2 by peptide-stimulated $CD8^+$ IM235 c94 T cells was not altered by either vOX2 or CD200 in two independent experiments (**Figure 5.19**, **a**). However, both vOX2 and CD200 were capable of modestly suppressing to varying extents the accumulation of IFNγ in this clone. T cells stimulated by vOX2-BJAB contained 80.6% ± 8.8 SEM of IFNγ present in T cells stimulated by Empty-BJAB, and CD200 reduced IFNγ to 66.09% ± 11.5 SEM of control (**Figure 5.19**, **b**).

(a)

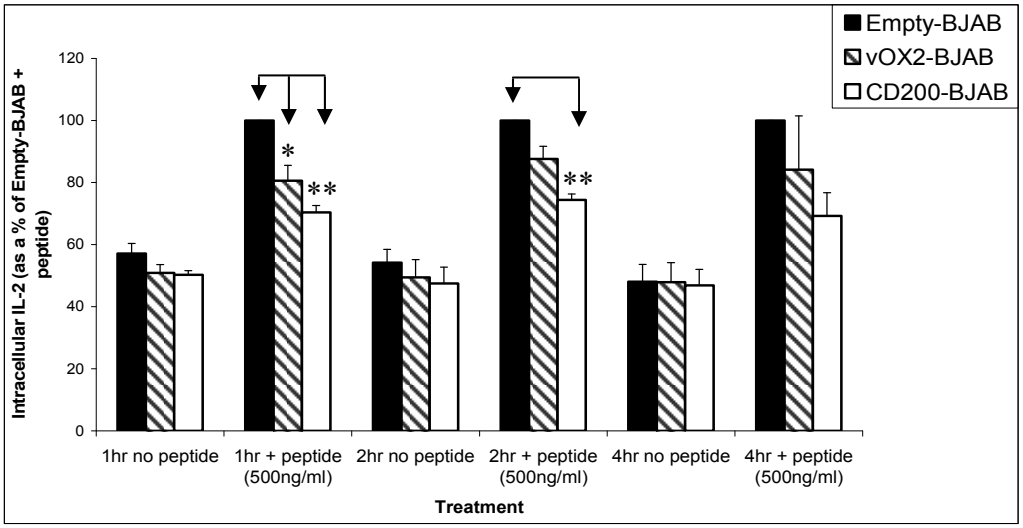

(b)

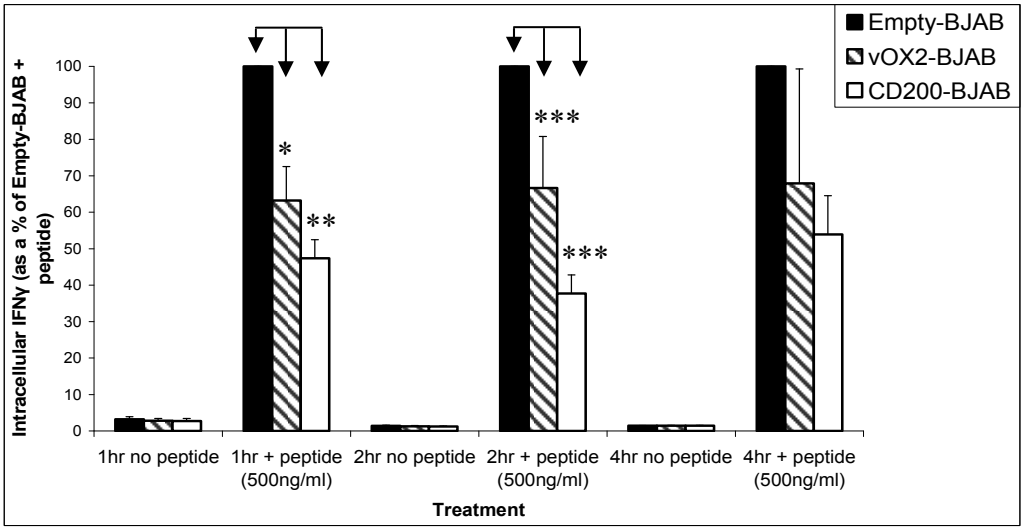

Figure 5.15 Expression of vOX2 and CD200 on antigen-presenting cells, reduces the accumulation of intracellular IL-2 and IFNγ over time in the CD4$^+$ SL c93 T cell clone. EBV antigen-specific T cell clones were incubated for 60mins with cognate antigen peptide-pulsed BJAB cells transduced with an empty vector, or engineered to express native vOX2 or CD200. Brefeldin A (7.5µg/ml) was added to the BJAB cell and T cell co-culture, and the cells incubated for a further 1, 2 or 4hrs. Intracellular **(a)** IL-2 and **(b)** IFNγ were detected by fluorophore-conjugated monoclonal antibodies, and quantified by flow cytometry. Data from four independent experiments were pooled, normalised to Empty-BJAB + peptide controls at each time point (1hr, n=2; 2hr, n=4; 4hr n=2), and presented as mean ± SEM. IL-2 production was not altered by vOX2 or CD200 in the absence of peptide, nor after 4hrs of peptide treatment, but was significantly reduced after 1hr ($F(2, 3) = 23.27$; *$p<0.05$ for vOX2-BJAB and **$p<0.01$ for CD200-BJAB) and 2hrs ($F(2, 9) = 5.59$; **$p<0.01$ for CD200-BJAB, $p = 0.14$ for vOX2-BJAB) when analysed by univariate ANOVA (SPSS software). IFNγ production was not altered by vOX2 or CD200 in the absence of peptide, nor after 4hrs of peptide treatment, but was significantly reduced after 1hr ($F(2, 3) = 19.43$; *$p<0.05$ for vOX2-BJAB and **$p<0.01$ for CD200-BJAB), and 2hrs ($F(2, 9) = 65.68$; ***$p<0.001$ for both vOX2- and CD200-BJAB) when analysed by univariate ANOVA (SPSS software).

(a)

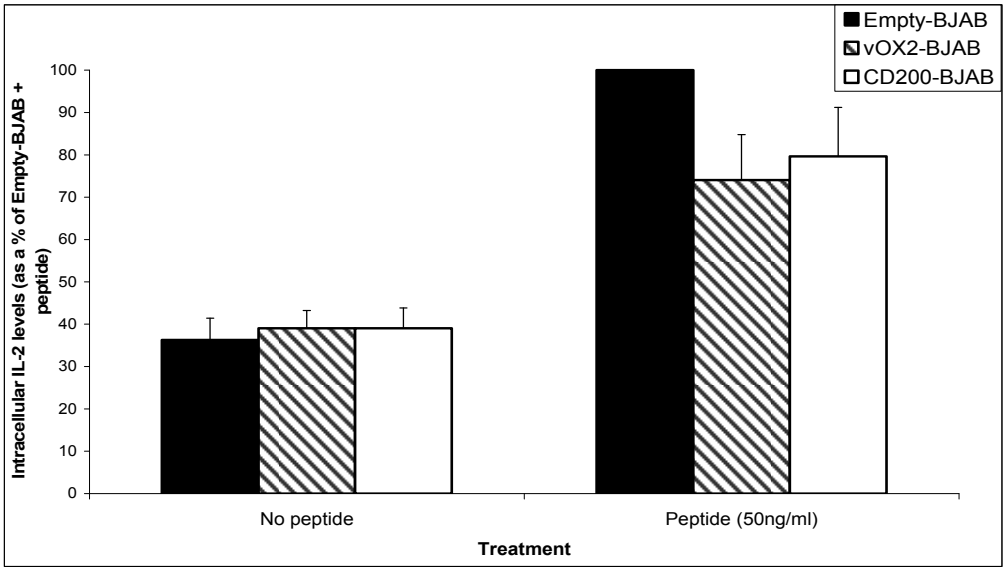

(b)

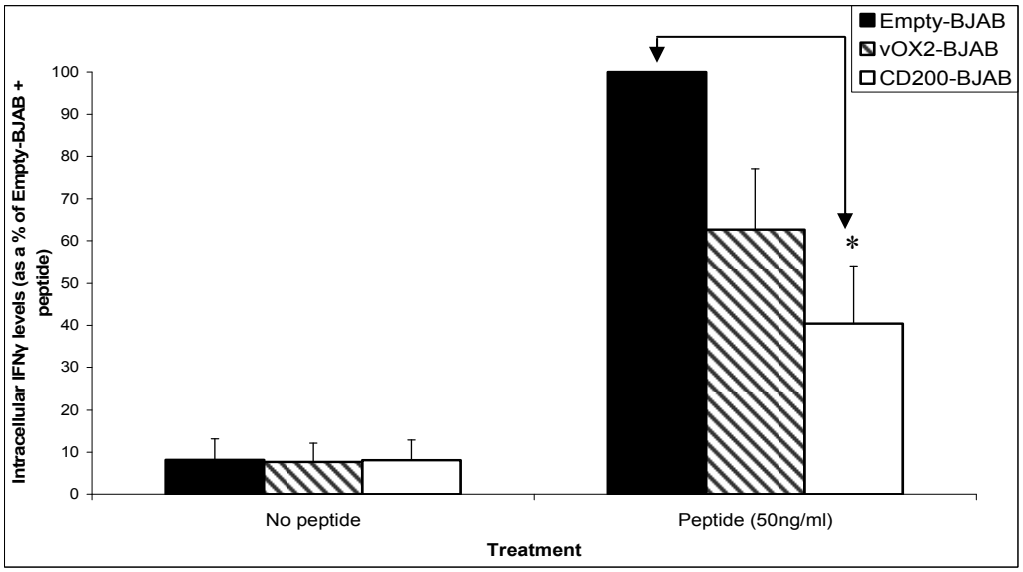

Figure 5.16 Expression of vOX2 and CD200 on antigen-presenting cells, reduces the accumulation of intracellular IL-2 and IFNγ in the CD8$^+$ IM140.1 Y15 T cell clone. EBV antigen-specific T cell clones were incubated for 60mins with cognate antigen peptide-pulsed BJAB cells transduced with an empty vector, or engineered to express native vOX2 or CD200. Brefeldin A (7.5μg/ml) was added to the BJAB cell and T cell co-culture, and the cells incubated for a further 2hrs. Intracellular **(a)** IL-2 and **(b)** IFNγ were detected by fluorophore-conjugated monoclonal antibodies, and quantified by flow cytometry. Data from three independent experiments were pooled, normalised to the Empty-BJAB + peptide control, and presented as mean ± SEM. IL-2 production was not significantly altered by vOX2 or CD200 in the absence of peptide, nor after 2hrs of peptide treatment when analysed by univariate ANOVA (SPSS software). IFNγ production was not altered by vOX2 or CD200 in the absence of peptide, but was significantly reduced by CD200 after 2hrs of peptide treatment ($F(2, 6) = 6.96$; $p = 0.06$ for vOX2-BJAB and $*p<0.05$ for CD200-BJAB), when analysed by univariate ANOVA (SPSS software).

(a)

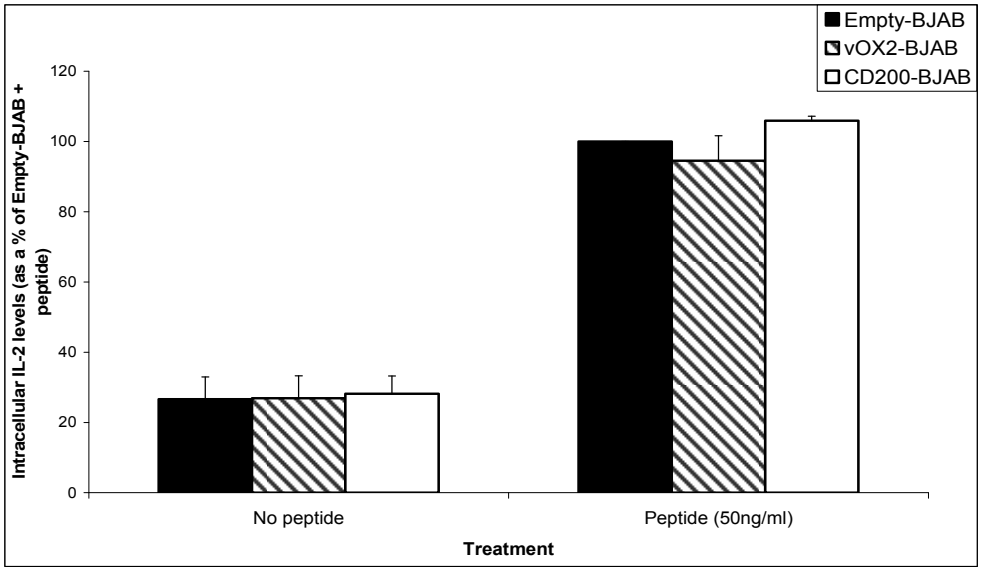

(b)

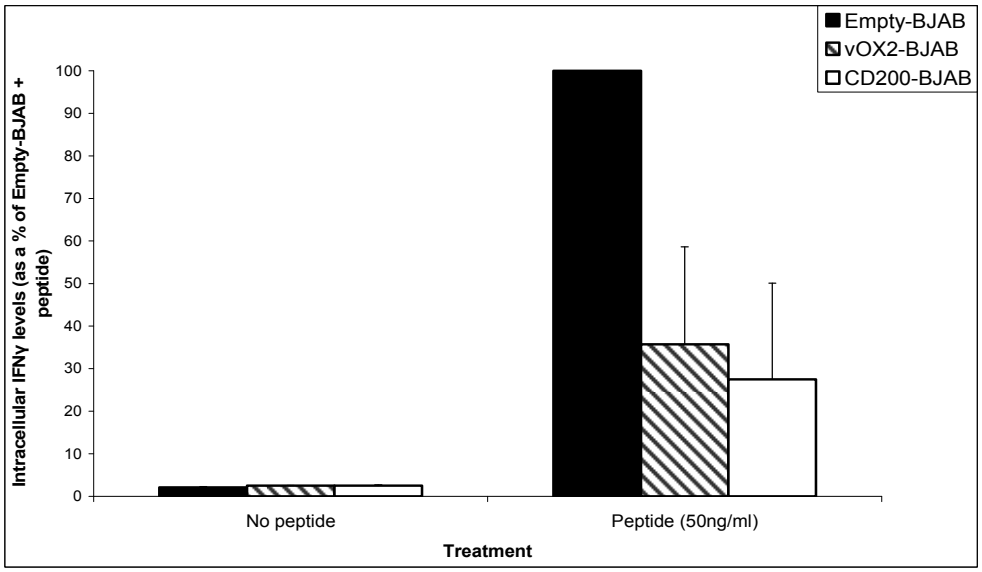

Figure 5.17 Expression of vOX2 and CD200 on antigen-presenting cells, reduces the accumulation of intracellular IFNγ but not IL-2 in the CD8$^+$ IM235 c48 T cell clone. EBV antigen-specific T cell clones were incubated for 60mins with cognate antigen peptide-pulsed BJAB cells transduced with an empty vector, or engineered to express native vOX2 or CD200. Brefeldin A (7.5μg/ml) was added to the BJAB cell and T cell co-culture, and the cells incubated for a further 2hrs. Intracellular **(a)** IL-2 and **(b)** IFNγ were detected by fluorophore-conjugated monoclonal antibodies, and quantified by flow cytometry. Data from two independent experiments were pooled, normalised to the Empty-BJAB + peptide control, and presented as mean ± SEM. IL-2 production was not significantly altered by vOX2 or CD200 in the absence of peptide, nor after 2hrs of peptide treatment when analysed by univariate ANOVA (SPSS software). IFNγ production was not altered by vOX2 or CD200 in the absence of peptide, and the observed reduction in IFNγ with peptide treatment in the presence of vOX2 and CD200, does not reach statistical significance ($F(2, 3) = 4.56$; $p = 0.09$ for vOX2-BJAB and $p = 0.07$ for CD200-BJAB), when analysed by univariate ANOVA (SPSS software).

(a)

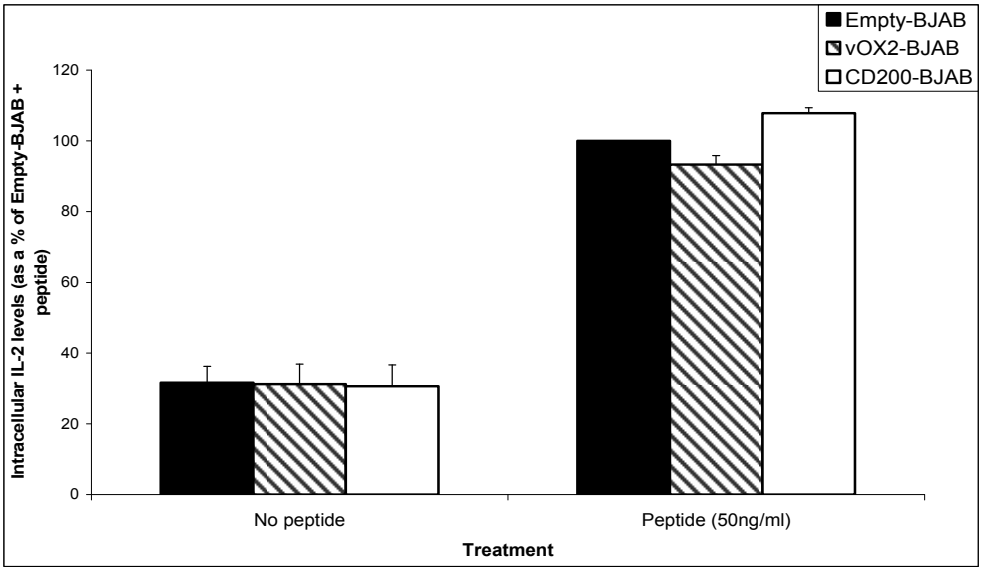

(b)

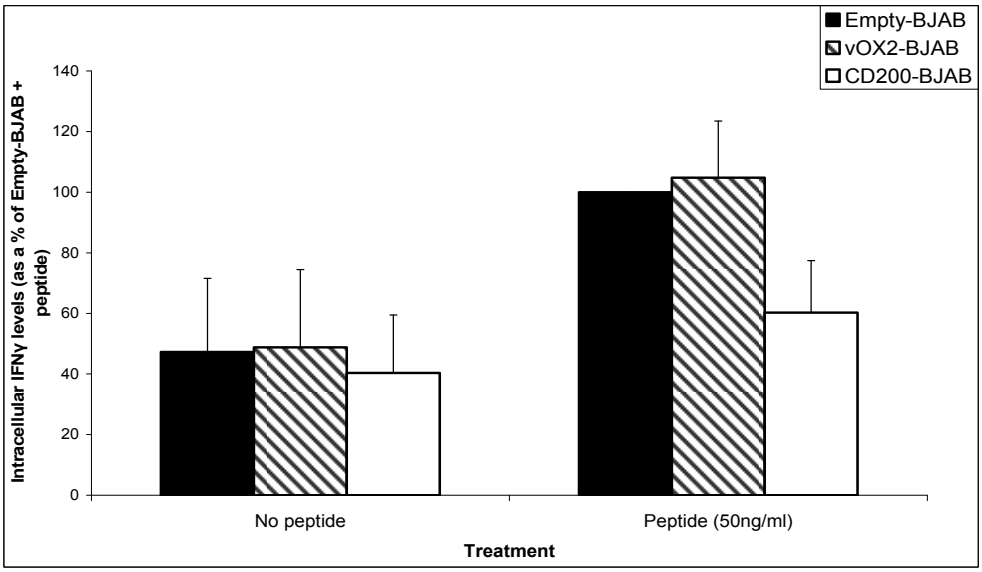

Figure 5.18 Expression of CD200 on antigen-presenting cells, reduces the accumulation of intracellular IFNγ but not IL-2 in the CD8$^+$ IM235 c79 T cell clone. EBV antigen-specific T cell clones were incubated for 60mins with cognate antigen peptide-pulsed BJAB cells transduced with an express empty vector, or engineered to express native vOX2 or CD200. Brefeldin A (7.5μg/ml) was added to the BJAB cell and T cell co-culture, and the cells incubated for a further 2hrs. Intracellular **(a)** IL-2 and **(b)** IFNγ were detected by fluorophore-conjugated monoclonal antibodies, and quantified by flow cytometry. Data from three independent experiments were pooled, normalised to the Empty-BJAB + peptide control, and presented as mean ± SEM. IL-2 production was not significantly altered by vOX2 or CD200 in the absence of peptide, nor after 2hrs of peptide treatment when analysed by univariate ANOVA (SPSS software). IFNγ production was not altered by vOX2 or CD200 in the absence or presence of peptide when analysed by univariate ANOVA (SPSS software).

(a)

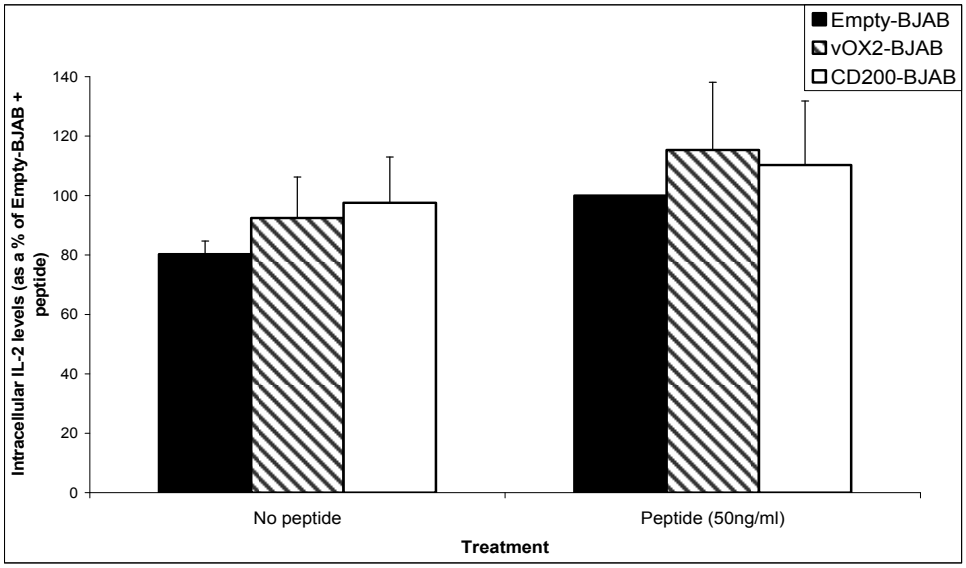

(b)

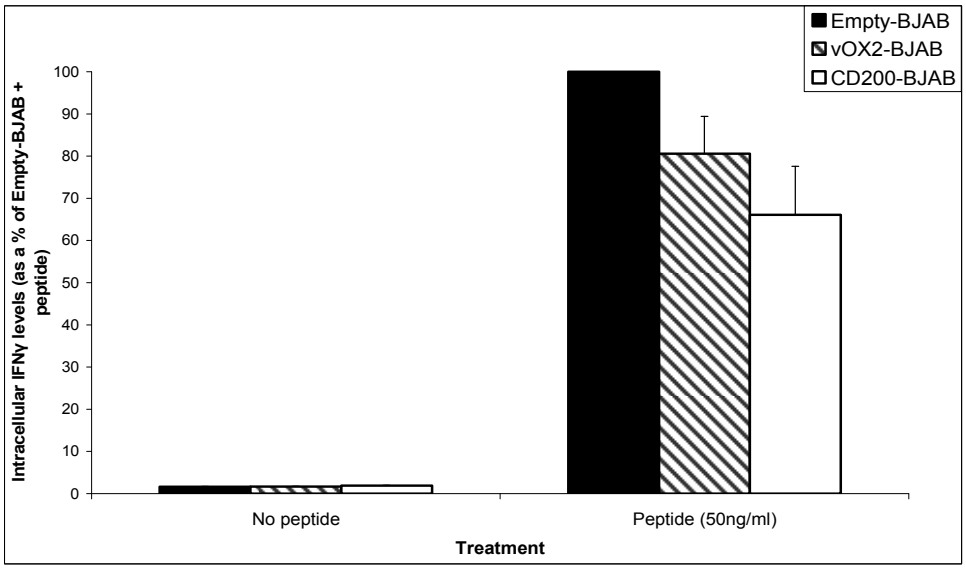

Figure 5.19 Expression of vOX2 and CD200 on antigen-presenting cells, reduces the accumulation of intracellular IFNγ but not IL-2 in the CD8$^+$ IM235 c94 T cell clone. EBV antigen-specific T cell clones were incubated for 60mins with cognate antigen peptide-pulsed BJAB cells engineered to express empty vector, native vOX2 or CD200. Brefeldin A (7.5μg/ml) was added to the BJAB cell and T cell co-culture, and the cells incubated for a further 2hrs. Intracellular **(a)** IL-2 and **(b)** IFNγ were detected by fluorophore-conjugated monoclonal antibodies, and quantified by flow cytometry. Data from two independent experiments were pooled, normalised to the Empty-BJAB + peptide control, and presented as mean ± SEM. IL-2 production was not significantly altered by vOX2 or CD200 in the absence of peptide, nor after 2hrs of peptide treatment when analysed by univariate ANOVA (SPSS software). IFNγ production was not altered by vOX2 or CD200 in the absence of peptide, and the observed reduction in IFNγ with peptide treatment in the presence of vOX2 and CD200, does not reach statistical significance ($F(2, 3) = 4.14$; $p = 0.2$ for vOX2-BJAB and $p = 0.06$ for CD200-BJAB), when analysed by univariate ANOVA (SPSS software).

$CD8^+$ IM140.1 Y15			
	16hr incubation	2hr post-Brefeldin A	
vOX2	**Extracellular IFNγ**	**Intracellular IFNγ**	**Intracellular IL-2**
500ng/ml cognate peptide	93.71% ± 8.7		
50ng/ml cognate peptide	78.27% ± 10.4	62.68% ± 14.39	74.07% ± 10.71
	16hr incubation	2hr post-Brefeldin A	
CD200	**Extracellular IFNγ**	**Intracellular IFNγ**	**Intracellular IL-2**
500ng/ml cognate peptide	* 86.29% ± 4.97		
50ng/ml cognate peptide	** 61.26 % ± 10.06	* 40.42% ± 13.55	79.63% ± 11.61

$CD4^+$ SL c93			
	16hr incubation	2hr post-Brefeldin A	
vOX2	**Extracellular IFNγ**	**Intracellular IFNγ**	**Intracellular IL-2**
500ng/ml cognate peptide	89.18% ± 3.15	*** 66.65% ± 14.12	87.59% ± 4.04
50ng/ml cognate peptide	96.91% ± 34.13		
	16hr incubation	2hr post-Brefeldin A	
CD200	**Extracellular IFNγ**	**Intracellular IFNγ**	**Intracellular IL-2**
500ng/ml cognate peptide	** 71.69% ± 8.17	*** 37.71% ± 5.11	** 74.4% ± 1.9
50ng/ml cognate peptide	58.98% ± 17.74		

Table 5.3 Cumulative data for the production of IFNγ and IL-2 by the $CD8^+$ IM140.1 and $CD4^+$ SL c93 antigen-specific T cell clones. The secretion of IFNγ into the culture supernatant by T cell clones cocultured with either peptide-pulsed vOX2-BJAB or CD200-BJAB cells for 16hrs was quantified by ELISA. The data for two peptide concentrations were calculated as a percentage of the data for Empty-BJAB cocultures. The accumulation of IFNγ or IL-2 in the T cell clones was quantified by flow cytometry, and the data calculated as a percentage of the data for peptide-pulsed Empty-BJAB cocultures. Any statistical significance attributable to the vOX2 or CD200-mediated suppression of IFNγ or IL-2 production is indicated by *($p<0.05$), **($p<0.01$) or ***($p<0001$), as determined by univariate ANOVA (SPSS software).

$CD8^+$ IM235 c48			
	16hr incubation	2hr post-Brefeldin A	
vOX2	**Extracellular IFNγ**	**Intracellular IFNγ**	**Intracellular IL-2**
500ng/ml cognate peptide	89.84% ± 11.47		
50ng/ml cognate peptide	* 66.44% ± 5.01	35.72% ± 22.94	94.52% ± 7.13
	16hr incubation	2hr post-Brefeldin A	
CD200	**Extracellular IFNγ**	**Intracellular IFNγ**	**Intracellular IL-2**
500ng/ml cognate peptide	* 78.06% ± 5.39		
50ng/ml cognate peptide	* 68.04% ± 13.91	27.51% ± 22.59	105.88% ± 1.31

$CD8^+$ IM235 c79			
	16hr incubation	2hr post-Brefeldin A	
vOX2	**Extracellular IFNγ**	**Intracellular IFNγ**	**Intracellular IL-2**
500ng/ml cognate peptide	99.5% ± 13.14		
50ng/ml cognate peptide	109.9% ± 29.2	104.76% ± 18.71	93.31% ± 2.51
	16hr incubation	2hr post-Brefeldin A	
CD200	**Extracellular IFNγ**	**Intracellular IFNγ**	**Intracellular IL-2**
500ng/ml cognate peptide	90.49% ± 8.12		
50ng/ml cognate peptide	74.77% ± 10.41	60.27% ± 17.15	107.86% ± 1.53

$CD8^+$ IM235 c94			
	16hr incubation	2hr post-Brefeldin A	
vOX2	**Extracellular IFNγ**	**Intracellular IFNγ**	**Intracellular IL-2**
500ng/ml cognate peptide	99.03% ± 0		
50ng/ml cognate peptide	* 66.67% ± 9.43	80.6% ± 8.8	115.31% ± 22.78
	16hr incubation	2hr post-Brefeldin A	
CD200	**Extracellular IFNγ**	**Intracellular IFNγ**	**Intracellular IL-2**
500ng/ml cognate peptide	*** 79.52% ± 2.51		
50ng/ml cognate peptide	** 41.34% ± 12.91	66.09% ± 11.5	110.31% ± 21.56

	IM235 c82	IM235 c108	IM235 c132
vOX2	**Extracellular IFNγ**		
500ng/ml cognate peptide	*** 67.76% ± 3.95	92.34% ± 5.44	** 72.09% ± 8.81
50ng/ml cognate peptide	* 42.1% ± 29.6	97.53% ± 5.32	78.9% ± 53.89
	IM235 c82	**IM235 c108**	**IM235 c132**
CD200	**Extracellular IFNγ**		
500ng/ml cognate peptide	*** 69.63% ± 4.57	85.37% ± 6.96	** 79.74% ± 4.39
50ng/ml cognate peptide	* 56.81% ± 13.16	* 80.69% ± 6.37	83.45% ± 13.71

Table 5.4 Cumulative data for the production of IFNγ and IL-2 by the $CD8^+$ IM235 antigen-specific T cell clones. The secretion of IFNγ into the culture supernatant by T cell clones cocultured with either peptide-pulsed vOX2-BJAB or CD200-BJAB cells for 16hrs was quantified by ELISA. The data for two peptide concentrations were calculated as a percentage of the data for Empty-BJAB cocultures. The accumulation of IFNγ or IL-2 in the T cell clones was quantified by flow cytometry, and the data calculated as a percentage of the data for peptide-pulsed Empty-BJAB cocultures. Any statistical significance attributable to the vOX2 or CD200-mediated suppression of IFNγ or IL-2 production is indicated by *($p<0.05$), **($p<0.01$) or ***($p<0001$), as determined by univariate ANOVA (SPSS software).

5.8. Discussion

The data presented in this chapter demonstrate a consistent trend towards attenuation by full-length vOX2 and CD200 proteins of T cell function, measured by cytokine production (**Tables 5.3-5.4**). The suppressive trend is consistent for all eight clones tested, from three donors, with two peptide specificities. Both vOX2 and CD200 were able to reduce the secretion of IFNγ by eight human antigen peptide-specific T cell clones, when they were expressed on the surface of the stimulating APCs. The effect was subtle but consistent, despite inherent variability, and more pronounced with higher peptide concentrations. CD200 was consistently more effective. Both vOX2 and CD200 also reduced the intracellular accumulation of IL-2 and IFNγ in six T cell clones, though to varying degrees for each clone. The suppressive activities of CD200, and more particularly, vOX2, were variable between experiments and clones, regardless of their passage number or length of time post-restimulation. CD200R expression by the T cell clones was investigated (Chapter 7) though no relationship between CD200R expression and degree of suppression of the clones could be determined. It is possible that the levels of expression of vOX2 and CD200 by the engineered BJAB cells could impact their ability to suppress T cell activity. It was observed throughout this study that vOX2 expression levels were lower than those of CD200 (or at least lower levels of fluorescence were seen during flow cytometric analysis of vOX2/CD200 expression; **Figure 5.4**). It would be interesting in the future to determine whether vOX2 is expressed at higher or lower levels by engineered BJAB cells than KSHV-infected cells induced into lytic replication.

Indirect evidence for the modulation of cytokines by CD200 *in vivo* demonstrates that CD200 reduces cytokine production (Broderick *et al*., 2002; Gorczynski *et al*., 2001; Gorczynski *et al*., 1999). *mCD200*$^{-/-}$ mice presented with increased IFNγ and IL-10 during the development of EAU (Broderick *et al*., 2002), and the administration of mCD200:Fc to

mice exhibiting CIA pathology (Gorczynski *et al*., 2001), or those that had received allografts (Gorczynski *et al*., 1999), reduced the secretion of inflammatory cytokines, including IFNγ, IL-2 and TNFα. Though these authors could not provide a mechanism for the CD200-mediated suppression of cytokine production. The modification of cytokine profiles may be due to the altered development of T cells in the presence of CD200-treated DCs. Gorczynski *et al*. demonstrated that stimulation of mCD200R2, but not mCD200R1, induced a regulatory subset of DCs, which in turn appear to enhance the development of $Foxp3^+$ Tregs that have a suppressive function (prolonging the survival of allografts) *in vivo* (Gorczynski *et al*., 2004b; Gorczynski *et al*., 2005; Gorczynski *et al*., 2008). Sato and colleagues reported that a subset of bone marrow-derived DCs expressed mCD200R3, and that the administration of $mCD200R^+$ DCs to mice presenting with chronic graft-versus host disease (cGVHD) reduced its severity and incidence. The reduced cGVHD pathology corresponded to reduced TNFα, IL-12 and IFNγ levels in the serum, and with increased numbers of $CD4^+CD25^+Foxp3^+$ Tregs (Sato *et al*., 2009). The induction of Tregs by CD200 may partly explain the reduced inflammatory cytokine profiles reported previously, but the direct effect of vOX2 or CD200 on antigen-specific cytotoxic T cells has never been reported. These two T cell subtypes act in opposition, indicating that if Tregs are upregulated, then CTLs must be suppressed.

Evidence for an indirect suppressive effect of soluble CD200 on CTLs was published by Gorzcynski *et al*., who observed that the addition of mCD200:Fc to a mixed lymphocyte cell culture reduced cell-stimulation (by allogeneic stimulator spleen cells) and a subsequent CTL response (Gorczynski *et al*., 1999). Suppression of IFNγ-production (Gorczynski *et al*., 2005) and IL-2-secretion (Gorczynski *et al*., 2004a) by mixed leukocyte cultures was also observed upon stimulation of the mCD200R1-4 on the surface of stimulator cells by monoclonal antibodies. These observations concur with the data presented in this chapter

(**Figures 5.5-5.19**), that CD200 and vOX2 when expressed on the surface of APCs suppress the responses of antigen-specific CTL. The mechanism may depend on vOX2 or CD200 ligating with the CD200R on the T cell clones. However, this interaction was not examined. Thus, an additional explanation for the immunosuppressive activities of CD200 observed by Gorczynski and Broderick *et al*. in their murine studies is that CD200 directly suppresses CTL responses, including IFNγ production.

Interestingly, IFNγ itself can alter the expression of CD200. Transcription of the *CD200* gene and cell surface expression of CD200 were enhanced by treatment of T lymphoid cell lines with IFNγ and/or TNFα (Chen *et al*., 2009). Intracellular signalling pathways initiated by the ligation of IFNγ and TNFα with their respective receptors, activates the transcription factors STAT1, IRF-1, and NF-κB. Gorzcysnki and colleagues demonstrated that these three factors bound to cis-elements upstream of the *CD200* transcriptional start site, thus enhancing *CD200* gene transcription in response to IFNγ or TNFα (Chen *et al*., 2009). The expression of vOX2 is also associated with IFNγ due to the presence of an ISRE-like domain within the *vOX2* promoter (Zhang *et al*., 2005). However, Zhang *et al*. did not demonstrate binding of IRFs to the ISRE-like sequence within the *vOX2* promoter, though they did show binding of RTA and subsequent upregulation of *vOX2* transcription (Zhang *et al*., 2005). Given the negative regulation of IFNγ production by CD200 and vOX2 demonstrated in the present chapter, and the proposed positive regulation of CD200 by IFNγ (Chen *et al*., 2009), the results together indicate an autoregulatory feedback loop between IFNγ and CD200 to maintain homeostasis.

It would be interesting to discover whether the upregulation of vOX2 (*K14*) or *CD200* occurs in our T cell clone model system. Retroviral constructs would have to be generated containing the upstream enhancer/promoter regions, before expressing in BJAB cells. If the two proteins were upregulated in the presence of IFNγ, this would provide a

regulatory feedback mechanism to control the level of suppression exerted by the proteins. Their resultant suppression of IFNγ secretion, as observed in our model system, would in turn reduce vOX2 and CD200 expression, and failure to effectively reduce IFNγ levels would theoretically further induce expression of the suppressive proteins.

In this study, T cell responses were quantified by cytokine production. However, T cell responses to stimulation include $CD8^+$ cytotoxicity, and proliferation. CD200 expressed by an APC can alter the proliferative properties of T cells, in addition to their secretion of cytokines (Pallasch *et al*., 2009). The proliferation of, and IFNγ production by, $CD200R^+$ autologous T cells in response to CD40L-stimulated $CD200^+$ chronic lymphocytic leukaemia cells (CLLs) was increased when ligation of CD200R to its cognate ligand was prevented by an anti-CD200 antibody. In a mixed lymphocyte reaction, the percentage of cytotoxic $CD8^+$ T cells increased when CD200 was blocked, and the number of Tregs were reduced (Pallasch *et al*., 2009). These data concur with those published by Gorczynski *et al*. who demonstrated that mCD200 can amplify the number of Treg cells in a mixed culture (Gorczynski *et al*., 2005). The effect of vOX2 and CD200 on T cell proliferation was not analysed in this study. The human T cell clones used for these experiments do proliferate in response to stimuli, but they are constitutively active as they are cultured in medium containing IL-2, and they require a strong stimulus (allogeneic PBMCs and LCLs) in order to proliferate. The proliferative response of primary T cells in the presence of vOX2 or CD200-expressing stimulator cells would be interesting to investigate in the future.

Rygiel and colleagues also demonstrated that CD200 regulates the proliferation of T cells in response to infection (Rygiel *et al*., 2009). The lack of mCD200 in *mCD200*$^{-/-}$ mice exacerbated the immune-mediated pathology associated with influenza infection, by increasing T cell activation and load. Increased weight loss and lung damage in *mCD200*$^{-/-}$ mice coincided with amplified numbers of lymphocytes, including $CD8^+$mCD200R1$^+$ T cells

in the airways. Depleting $CD4^+$ and $CD8^+$ T cells in these mice attenuated disease pathology (Rygiel *et al*., 2009). The suppressive activity of CD200 may under some circumstances have a detrimental effect *in vivo*. CD200 reduces the T cell response to CLL tumour cells, thus preventing effective clearing (Pallasch *et al*., 2009). CD200 is also expressed by several tumour cell lines, including neuroblastoma (Siva *et al*., 2008). CD200 was highly expressed in solid human tumours, in comparison to weak staining of the skin and moderate expression in normal ovaries. Ovarian cancer and melanoma cell lines expressing CD200 significantly reduced the secretion of IFNγ and IL-2 by allogeneic mixed lymphocyte cultures, whereas cells lacking CD200 were unable to alter the cytokine profile (Siva *et al*., 2008). Data published by Stumpfova and colleagues further confirm the ability of CD200 to maintain tumours *in vivo* (Stumpfova *et al.*, 2010). CD200 is expressed by metastatic squamous cell carcinoma (SCC) in mice and humans, and deleting mCD200 reduces the metastatic potential of these cells (Stumpfova *et al.*, 2010).

The expression of vOX2 on the surface of KSHV lytically-infected cells (**Figure 5.3**) would presumably reduce the CTL response to infection, thus allowing KSHV to replicate to higher titres and facilitate the establishment of persistent infection. Research has been continuing to establish whether CD200 may be an effective target for therapy, and the development of anti-CD200 monoclonal antibodies for therapeutic treatment of CLL and MM is in progress (www.alexionpharm.com).

Evidence is presented in this chapter that full-length vOX2 and CD200, expressed on the surface of non-professional APCs, such as B cells, can directly interact with cytotoxic $CD8^+$ and $CD4^+$ T cells and inhibit their responses. The method of this direct interaction is not known, though the obvious hypothesis is that both vOX2 and CD200 are ligating CD200R expressed on the T cell, as reported previously (Foster-Cuevas *et al*., 2004). This receptor ligation may then initiate an inhibitory signalling cascade, as described by Zhang *et*

al. in murine mast cells (Zhang *et al*., 2004). Therefore, the rational next step would be to examine whether signalling pathways initiated in the T cells clones upon peptide-stimulation are altered in the presence of vOX2 or CD200. A modification of intracellular signalling cascades would also confirm authenticity of the observed vOX2 and CD200-mediated suppression of T cells. These experiments were performed, the putative modification of TCR-signalling was examined and the data are presented in Chapter 6.

Chapter 6. vOX2 and CD200-mediated suppression of human T cell clones: mechanism of action

The observed attenuation of T cell clone responses by vOX2 and CD200 (Chapter 5) is mediated via an unknown mechanism. One likely route is by ligation of the CD200R on the surface of T cell clones by vOX2 and CD200. Both molecules bind this receptor with similar affinity (Foster-Cuevas *et al*., 2004). Zhang and colleagues observed a modification of signalling pathways within engineered murine mast cells upon ligation of the mCD200R1 by mCD200:Fc (Zhang *et al*., 2004), correlating with decreased cell activity (Cherwinski *et al*., 2005). Therefore, the aim of the experiments outlined in this chapter was to identify vOX2 and CD200-mediated alterations in T cell signalling cascades.

6.1. Initiation of downstream signalling cascades by ligation of CD200R

As mentioned above, the group of Phillips examined the signalling pathways underlying the inhibition of mast cell degranulation by CD200-CD200R ligation that they had reported previously (Cherwinski *et al*., 2005). Initially they engineered primary mouse mast cells to over-express mCD200R1. The CD200R1-expressing mast cells were then incubated with mCD200:Fc, prior to stimulation by antigen cross-linking of FcεRI. mCD200:Fc-treatment suppressed the degranulation of mouse mast cells in comparison to treatment with a control Fc-fusion protein (Cherwinski *et al*., 2005). They then identified the intracellular signalling events altered following mCD200R1 ligation by either soluble mCD200:Fc or mCD200 expressed on NIH3T3 (mouse embryonic fibroblast) cells (Zhang *et al*., 2004). They detected rapid phosphorylation of intracellular mCD200R1 tyrosine residues following ligation of the receptor. 'Downstream of kinase' (Dok) 1 and 2 adaptor proteins were activated by phosphorylation upon stimulation of the mCD200R1. Activated Dok proteins

subsequently engaged RasGAP and Src homology 2 domain containing inositol phosphatase (SHIP), inhibitory effector molecules involved in the inhibition of MAP kinase signalling cascades (**Figure 6.1**). The recruitment of inhibitory RasGAP and SHIP by the CD200R signalling cascade was further substantiated by reduced phosphorylation of Ras (an upstream activator of the MAP kinases), and consequently of the MAP kinases ERK, p38 and JNK themselves (Zhang *et al*., 2004).

Later work by these researchers identified the intracellular mCD200R1 tyrosine residues responsible for initiating downstream signalling cascades. Stimulating murine bone marrow-derived mast cells (BMMCs) by ligating the mCD200R4 activatory receptor resulted in rapid cell degranulation and downstream phosphorylation of p38, JNK and ERK MAP kinases (Zhang *et al*., 2004). This stimulation could be inhibited by treatment with an anti-mCD200 antibody (Zhang and Phillips, 2006). However, cells expressing a mutant mCD200R1 lacking either the Y286 or Y297 tyrosine residues were not inhibited by receptor ligation. Both of these residues were required for the phosphorylation of mCD200R1 upon ligand binding, as well as Dok1, Dok2 and SHIP phosphorylation. The mutant mCD200R1 lacking Y286 and Y297 was also unable to associate with Dok and RasGAP. The Src family of kinases may be responsible for the initial phosphorylation of mCD200R1 tyrosines, as evidenced by the treatment of BMMCs with a Src family kinase inhibitor, completely abolishing the phosphorylation of mCD200R1 and Dok1, and the association of RasGAP with Dok1 (Zhang and Phillips, 2006).

Initially, all CD200R-ligation studies were carried out in mouse cells, until Mihrshahi and colleagues investigated the human CD200R intracellular tyrosine residues (Mihrshahi *et al*., 2009). These authors engineered U937 cells to express full-length CD200R, or CD200R with a truncated cytoplasmic tail, or with each of its three tyrosine residues converted to a phenylalanine. IL-8-secretion was reduced in IFNγ-stimulated U937 cells expressing the

native receptor, but not those expressing the truncated form of the CD200R. This inhibitory effect was induced by free, immobilised and antibody cross-linked anti-CD200 mAb, as well as CD200-expressing cells, and a soluble CD200 protein (Mihrshahi *et al*., 2009). The inhibitory activities of immobilised anti-CD200 mAb on LPS-stimulated CD200R-expressing U937 cells, were abrogated upon deletion of the third intracellular tyrosine residue (Y302), and slightly reduced in the absence of the first tyrosine (Y291), though the Y294 appeared to be unnecessary for inhibitory signalling (Mihrshahi *et al*., 2009).

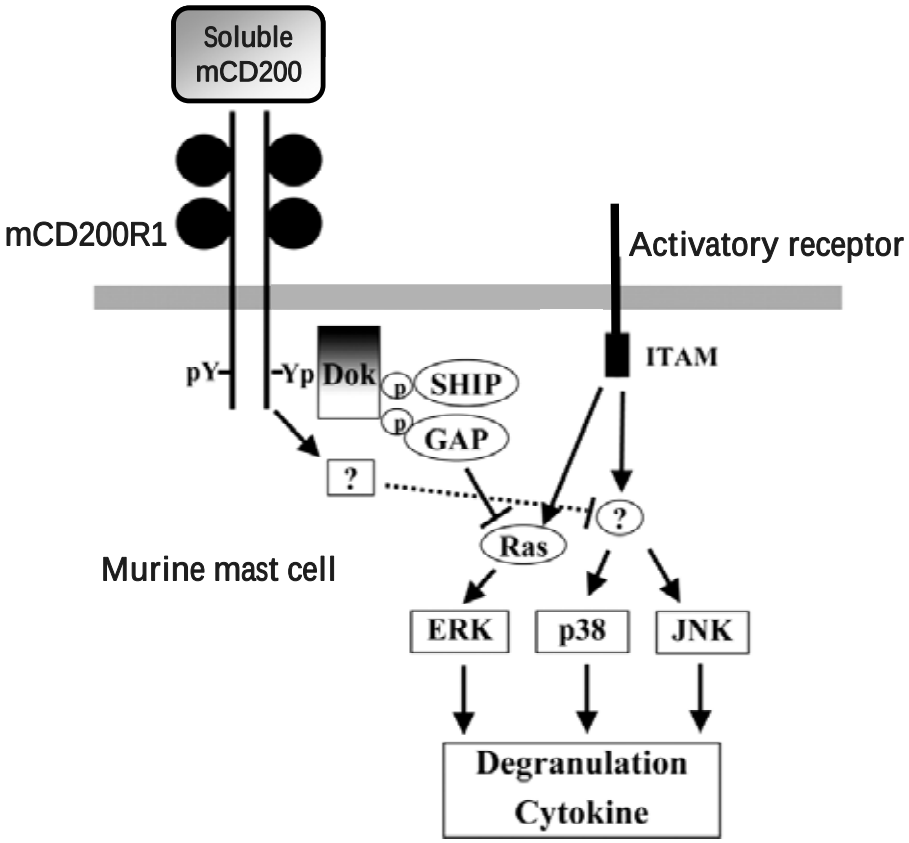

Figure 6.1 Putative intracellular signalling cascades underlying the mCD200-mediated inhibition of murine mast cells. The phosphorylation of mitogen-activated protein (MAP) kinases by immunoreceptor tyrosine-based activation motif (ITAM)-containing receptors was inhibited by mCD200-mCD200R1 ligation. The recruitment of Dok adaptor proteins by the mCD200R1, in turn employed inhibitory effector molecules that prevented MAP kinase phosphorylation and subsequent mast cell degranulation and cytokine release (adapted from Zhang *et al*., 2004).

Phosphorylated mCD200R1 recruits Dok1 and 2 adaptor proteins (Zhang *et al*., 2004). Using SPR to measure binding affinities, Mihrshahi *et al.* identified a strong interaction between Dok2 and phosphorylated residues Y302 and Y291 of the human CD200R. Though Dok1 also bound to these residues, the affinity was ten-fold less than that of Dok2. However, the authors demonstrated that Dok1 bound to a phospho-tyrosine residue of Dok2, and therefore may be indirectly recruited to the site (Mihrshahi *et al*., 2009). Following stimulation of the mCD200R1 the inhibitory effector protein SHIP is recruited (Zhang *et al*., 2004). Mihrshahi and colleagues confirmed that SHIP has a weak association with Dok1, but also demonstrated that SHIP was recruited by truncated human CD200R, lacking the signalling region of its intracellular domain, verifying that it does not directly interact with CD200R (Mihrshahi *et al*., 2009). In comparison, both Dok2 and RasGAP were phosphorylated upon the ligation of native CD200R by anti-CD200, and were not activated in cells expressing the truncated receptor. Inhibiting Dok2 and RasGAP expression by interfering RNA abolished the CD200R-mediated inhibition of LPS-stimulated U937 cells. Taken together, these data indicate that Dok2 and RasGAP are essential for effective CD200R-signalling, being recruited by the CD200R. However, Dok1 and SHIP appear to be bystanders since knockdown of these proteins had no effect on CD200R-mediated inhibition (Mihrshahi *et al*., 2009).

The Dok adaptor proteins have been examined in T cells without reference to CD200R ligation. The Dok2 adaptor protein is constitutively weakly phosphorylated in $CD4^+$ and $CD8^+$ T cells. However, upon stimulation of the TCR by CD3, Dok phosphorylation is markedly increased (Dong *et al*., 2006). Downstream of TCR signalling, Dok2 associates with SHIP1, forming a complex with activated LAT and subsequently becoming phosphorylated. When Dok1 and Dok2 were knocked down by siRNA, Zap70, LAT, SLP-76, PLC-γ1 and downstream Akt kinase all exhibited greater phosphorylation

(Dong *et al*., 2006). These data indicate that Dok proteins act as negative regulators in response to T cell stimulation by ligation of the TCR. Moreover, in concert with the data described above, it suggests that ligation of the CD200R may increase Dok activity, thus further enhancing inhibitory regulation of T cell function.

The majority of data regarding CD200R signalling have been collected in mast cells or monocytic cell lines. Due to the observed inhibition of human T cell clone activity (Chapter 5), the next step was to determine whether vOX2 or CD200 altered signalling cascades induced by peptide-stimulation of the TCR.

6.2. Quantifying phosphorylated signalling molecules in human T cell clones by flow cytometry

The identification of phosphorylated proteins exclusively in T cells while they are in co-culture with antigen-presenting cells is rendered difficult due to the dual cell population. Conventional methods such as separating proteins by SDS-PAGE and identifying them by western blotting rely on a single cell type. Therefore, flow cytometry was the only viable option as the cell populations can be separated on the basis of their phenotype. The advent of sensitive flow cytometric techniques for measuring the phosphorylation status of proteins has allowed accurate analysis of intracellular signalling cascades. Haas and colleagues compared western blotting and flow cytometric techniques and revealed some discrepancies between the two in quantifying phospho-protein kinetics (Haas *et al*., 2008). However, the flow cytometric technique involves less manipulation of the cells – they are left intact rather than being lysed for SDS-PAGE – and it also enables the quantitative analysis of a larger number of samples with greater ease and speed.

A protocol was optimised (Chapter 2.7.5) to quantify several intracellular signalling molecules within T cells, distinguished from BJAB cells by labelling with anti-CD4 or anti-

CD8 antibodies. The molecules examined were limited by the availability of phospho-specific antibodies suitable for flow cytometry (Appendix B, Table I). p-LAT, p-Zap70, p-SLP-76, p-Akt, p-ERK1/2 and p-p38 levels were examined in T cells stimulated with HLA-matched Empty-BJAB, vOX2-BJAB or CD200-BJAB cells and cognate antigen. As discussed in Chapter 1, Zap70 is recruited by the phosphorylation of CD3 and rapidly phosphorylates LAT and SLP-76, forming a complex that in turn recruits and phosphorylates other signalling proteins. Downstream of this complex, MAP kinases are phosphorylated and initiate transcription (reviewed in Schwartzberg *et al*., 2005). Akt, a protein kinase is also phosphorylated downstream of TCR ligation and following stimulation of the co-receptor CD28 (reviewed by Alegre *et al*., 2001).

This chapter details the optimisation of the assay and provides the data obtained from the T cell-BJAB co-cultures. Two representative clones were selected for these signalling assays from the studies revealing vOX2 and CD200 inhibition of T cell function (Chapter 5). These T cells were the $CD8^+$ IM140.1 Y15 YVL(BRLF1)-specific and $CD4^+$ SL c93 PRS(EBNA2)-specific clones.

6.2.1. Optimising the signalling assay

T cell clones were chemically stimulated to induce the phosphorylation of intracellular signalling proteins, and thus determine the specificity of phospho-specific antibodies (**Figure 6.2**). 5mM H_2O_2 induced the phosphorylation of Akt, SLP-76, LAT and Zap70, and treatment with 20ng/ml PMA resulted in ERK1/2 and p38 phosphorylation. Phosphorylation of each of these molecules was readily detected (**Figure 6.2**, **a**).

Once the efficacy of the phospho-protein-specific antibodies had been confirmed, a technique for distinguishing T cell clones from the BJAB cells was optimised. T cell clones were labelled with anti-CD4 or anti-CD8 antibodies as appropriate, and dead cells and debris

discounted by gating on all live cells in the FSC vs SSC scatter plot. The live cells were then analysed by granularity and CD4/CD8 expression (SSC vs. Pacific Blue), revealing a distinct T cell population with low granularity and high fluorescence (**Figure 6.2**, **b**). Only cells within this population were analysed for phospho-protein expression.

Next, a time-course of T cell-stimulation was carried out to determine what length of stimulation resulted in peak phosphorylation of signalling proteins. The $CD4^+$ SL c93 T cell clone was incubated with cognate peptide antigen-pulsed Empty-BJAB cells for 2, 5 or 10mins, the reaction quenched with formaldehyde, and intracellular signalling molecules labelled with phospho-specific antibodies (Chapter 2.7.5). The phospho-protein expression at each time point was calculated as a % of the median fluorescence for untreated cells. ERK1/2, p38, Akt and SLP-76 were noticeably phosphorylated upon peptide stimulation (up to 285% of control levels), in comparison to p-LAT and p-Zap70 which were minimally increased by peptide-stimulation (**Figure 6.3**). Optimal protein phosphorylation generally occurred at 2 or 5mins post-stimulation. 5mins of stimulation was chosen as the time point for all signalling assays, since logistically this treatment time was the most reproducible. A peptide concentration of 500ng/ml was chosen for all $CD4^+$ SL c93 signalling assays. This concentration was the lowest to induce the phosphorylation of signalling proteins, and higher concentrations did not significantly increase protein phosphorylation (data not shown).

(a)

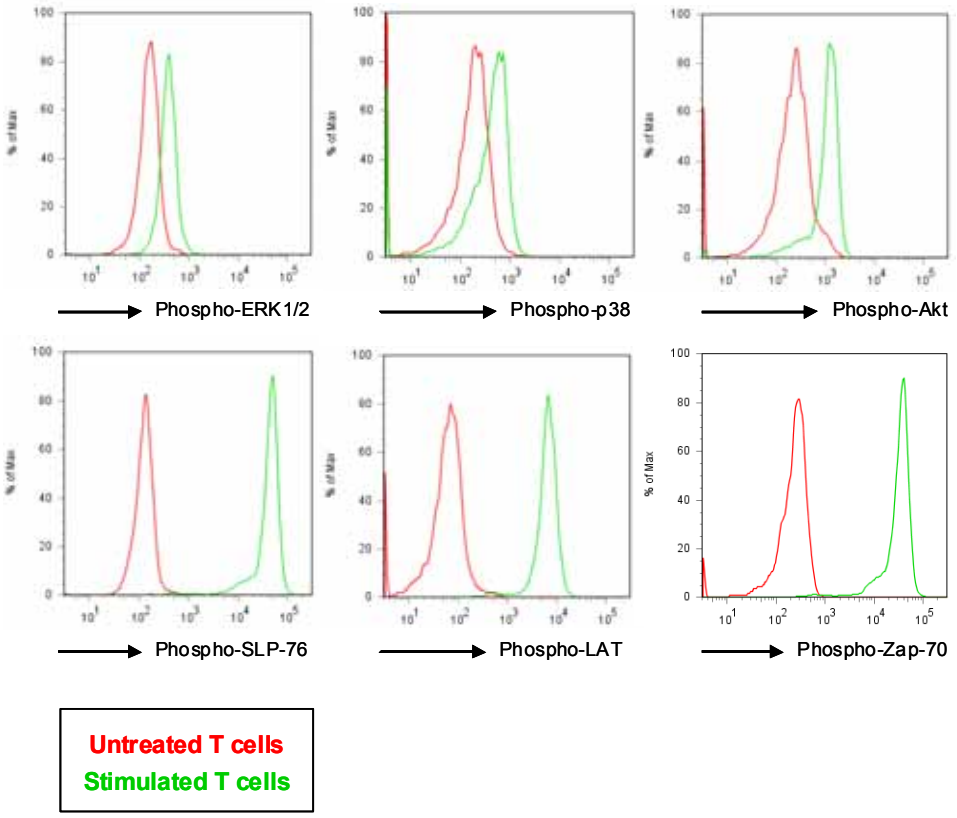

(b)

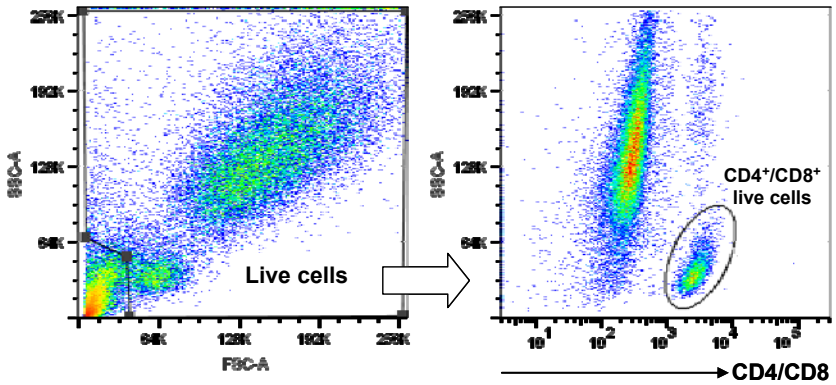

Figure 6.2 Optimising an intracellular signalling assay for the T cell clones. (a) Testing the efficacy of phospho-specific antibodies. The T cells ($CD4^+$ SL c93 or $CD8^+$ IM140.1 Y15 clones) were chemically stimulated for 10mins to induce the phosphorylation of intracellular signalling molecules. The stimulating agents used were 5mM H_2O_2 (Akt, SLP-76, LAT and Zap70), or 20ng/ml PMA (ERK1/2 and p38). **(b)** In order to distinguish the T cells from the antigen-presenting cells (BJAB), T cells were labelled with an anti-CD4 or anti-CD8 fluorophore-conjugated monoclonal antibody, and characterised within the live cell population by their side-scatter value.

(a)

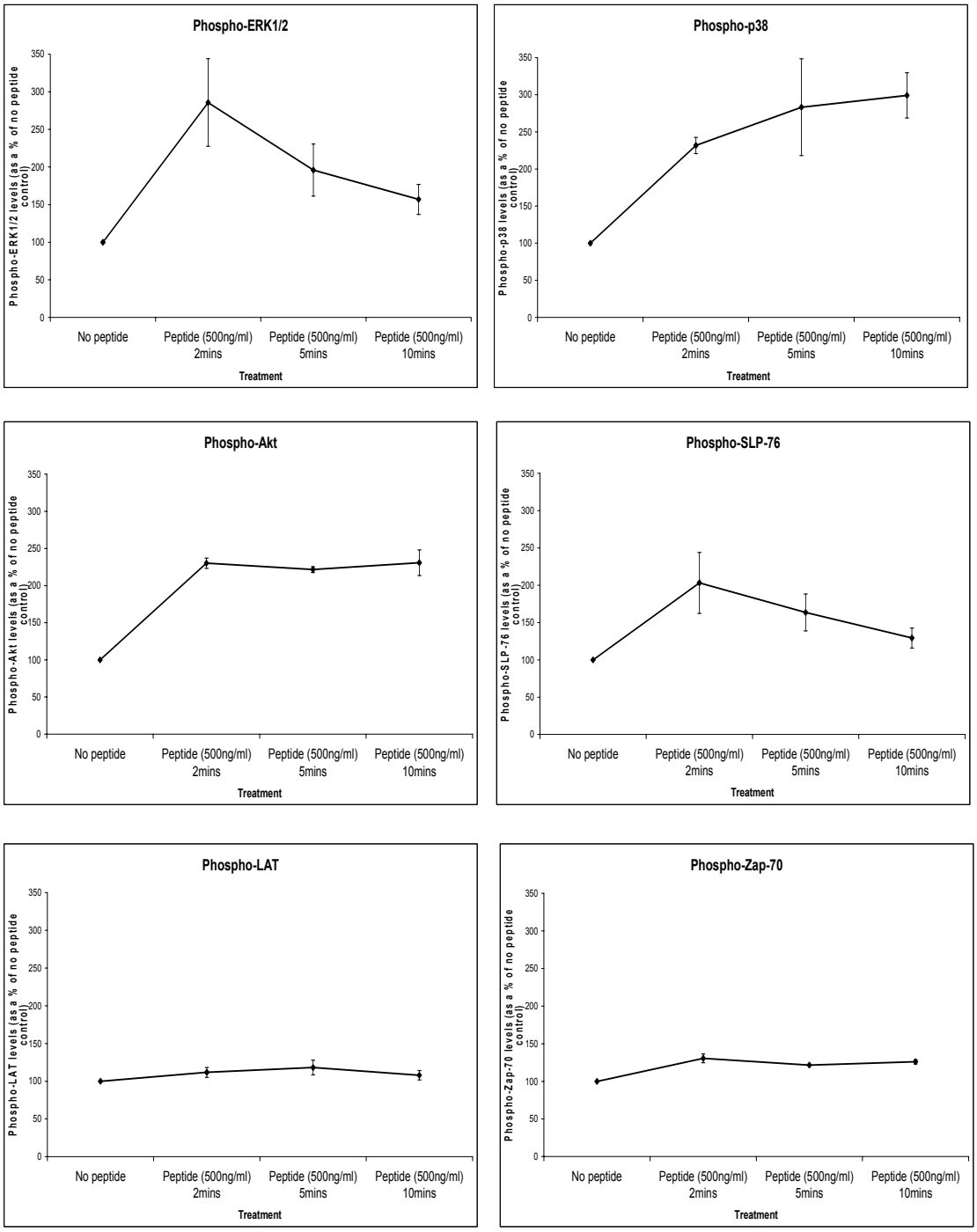

Figure 6.3 (a) Determining the optimal time after T cell stimulation to measure the phosphorylation of signalling molecules ($CD4^+$ SL c93 clone). T cell clones were incubated with antigen peptide-pulsed Empty-BJAB cells for 2, 5 or 10mins, the reaction quenched with formaldehyde, and the phosphorylation levels of seven molecules measured by flow cytometry. The data for three independent experiments were pooled and are displayed as a % of no peptide control.

(b)

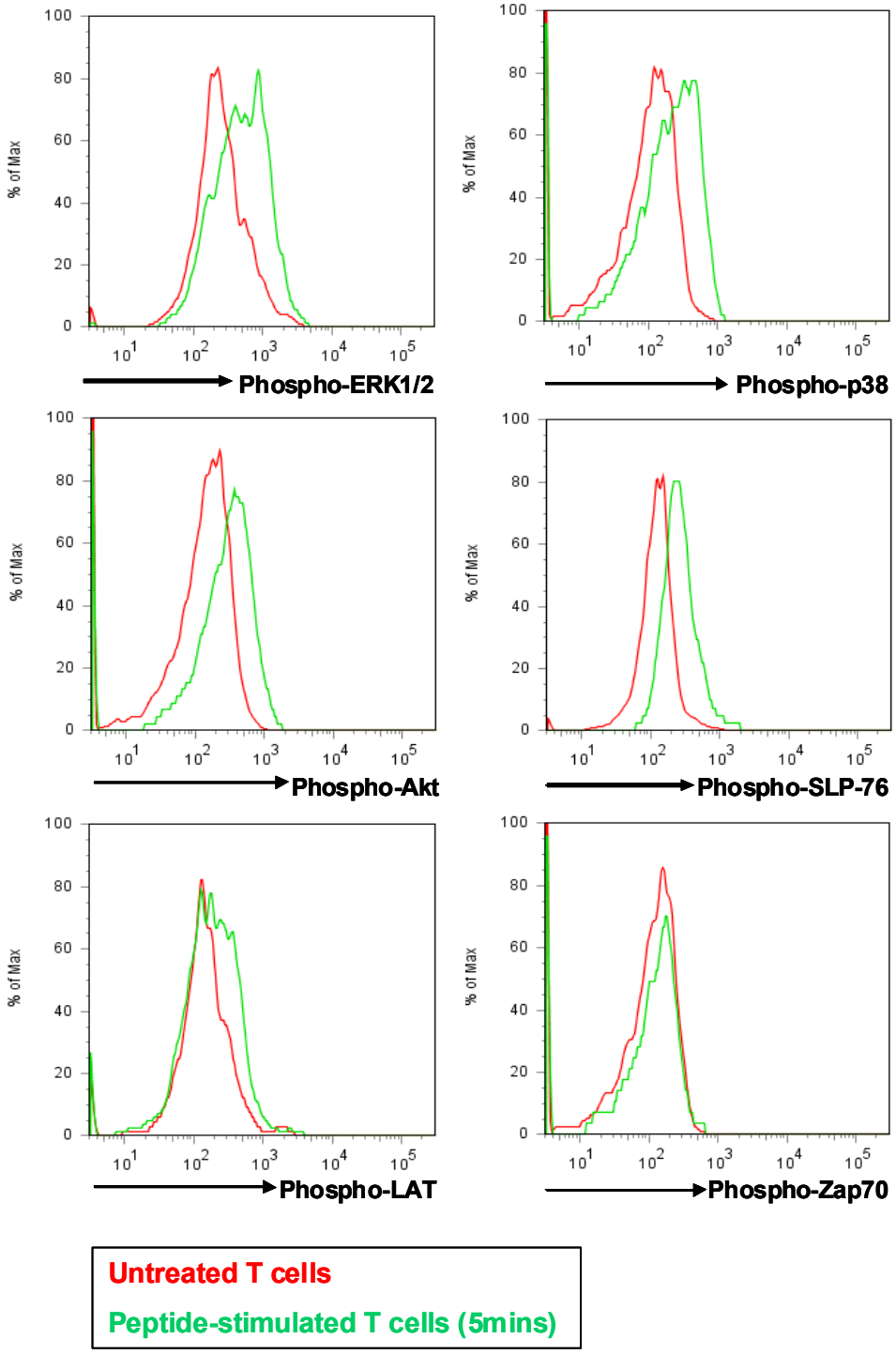

Figure 6.3 (b) Determining the optimal time after T cell stimulation to measure the phosphorylation of signalling molecules ($CD4^+$ SL c93 clone). Histograms displaying the median fluorescence of cells labelled with anti-phospho-protein antibodies following 5mins stimulation with antigen peptide. This time point was used for all subsequent assays. These data are from one experiment and are representative of those data collected from three experiments, pooled and plotted in **(a)**.

6.2.2. Modification of signalling proteins by vOX2 and CD200 in the $CD4^+$ SL c93 T cell clone

Phosphorylation of signalling proteins in the presence or absence of vOX2 and CD200 was first examined in the $CD4^+$ SL c93 T cell clone. IFNγ-secretion and the intracellular accumulation of IFNγ and IL-2 were reduced in this clone by vOX2 and CD200 expressed on the APC (Chapter 5). The MAP kinases, activated downstream of TCR-stimulation, were studied initially. ERK1/2 phosphorylation in this T cell clone was significantly reduced by vOX2 and CD200 (**Figure 6.4**) across seven independent experiments. p-ERK1/2 was not modified by vOX2 or CD200 in the absence of peptide stimulation.

The data presented in **Figures 6.4** to **6.16** were calculated as the % of Empty-BJAB + peptide, using the median fluorescence for each sample. This approach does not take into account the shift from basal levels upon stimulation (ie. the shift in fluorescence from 'no peptide' to '+ peptide' = 100% of the phospho-protein induced by control cells). To demonstrate the reduction in the *shift* from basal to stimulated levels, by vOX2 and CD200, the following calculation was carried out. The median fluorescence value for each 'no peptide' sample was subtracted from the value for its matching '+ peptide' sample in each experiment, and then taken as a % of Empty-BJAB-cultures. For example, [(vOX2-BJAB + peptide) – (vOX2-BJAB no peptide)] ÷ [(Empty-BJAB + peptide) – (Empty-BJAB no peptide)] x 100. The means for each experiment were then calculated. By this method, p-ERK1/2 in the $CD4^+$ T cell clone SL c93 was reduced to 50.73% ± 11.27 SEM of the maximal shift in ERK1/2 phosphorylation when stimulated by vOX2-BJAB. Interestingly, CD200 was slightly less effective at suppressing ERK1/2 phosphorylation, and reduced p-ERK1/2 to 59.73% ± 11.34 SEM of control. The suppression of p-ERK1/2 is statistically significant for both vOX2 and CD200; $p < 0.001$ (indicated by *** in the Figures) when

analysed by a univariate ANOVA (SPSS 16.0 software, SPSS Inc.). Statistical significance of $p<0.01$ is signified by **, and $p<0.05$ by *.

There was also a trend towards suppression of p38 phosphorylation by vOX2 and CD200 (**Figure 6.5**) in eight independent experiments. p-p38 was reduced in $CD4^+$ T cells to 74.71% ± 6.68 SEM of the maximum induced by Empty-BJAB, upon stimulation by vOX2-expressing BJAB cells, and again was reduced by a slightly lesser degree by CD200-BJAB, to 80.4% ± 7.02 SEM of control. However, due to high variation between experiments, the result was not statistically significant by univariate ANOVA.

Both peptide-pulsed vOX2 and CD200-BJAB cells significantly suppressed the phosphorylation of Akt kinase in the $CD4^+$ T cell clone (**Figure 6.6**). Again, vOX2 was a more potent suppressor of p-Akt, and reduced p-Akt to 65.29% ± 7.26 SEM of control. Peptide-pulsed CD200-BJAB cells also suppressed the phosphorylation of Akt, to 77.98% ± 1.46 SEM of control. Both vOX2 and CD200 significantly suppressed p-Akt (***$p<0.001$) in five independent experiments when analysed by univariate ANOVA.

Upstream of the MAP kinases, LAT acts as a docking protein for signalling molecules, and is directly phosphorylated by Zap70 upon TCR stimulation. In the $CD4^+$ SL c93 clone, detection of LAT phosphorylation by peptide stimulation was minimal (as noted in **Figure 6.3**) in four independent experiments, and no modification by vOX2 or CD200 could therefore be observed in the presence or absence of peptide (**Figure 6.7**). Detection of p-LAT in T cells stimulated by vOX2-BJAB was similar to that in Empty-BJAB-stimulated cells (101.72% ± 2.31 SEM of control). Similarly, CD200-BJAB did not alter detectable p-LAT expression in T cells, which was present at 98.32% ± 3.14 SEM of control levels. SLP-76 is associated with the LAT complex of adaptor proteins, and is also directly activated by Zap70. SLP-76 phosphorylation was detectable upon peptide-stimulation, but neither vOX2 nor CD200 suppressed its activation (**Figure 6.8**). The initial protein phosphorylated by TCR

stimulation, Zap70, is responsible for activating a cascade of signalling proteins. Zap70 phosphorylation was readily detectable; p-Zap70 was not suppressed by vOX2 or CD200 (**Figure 6.9**).

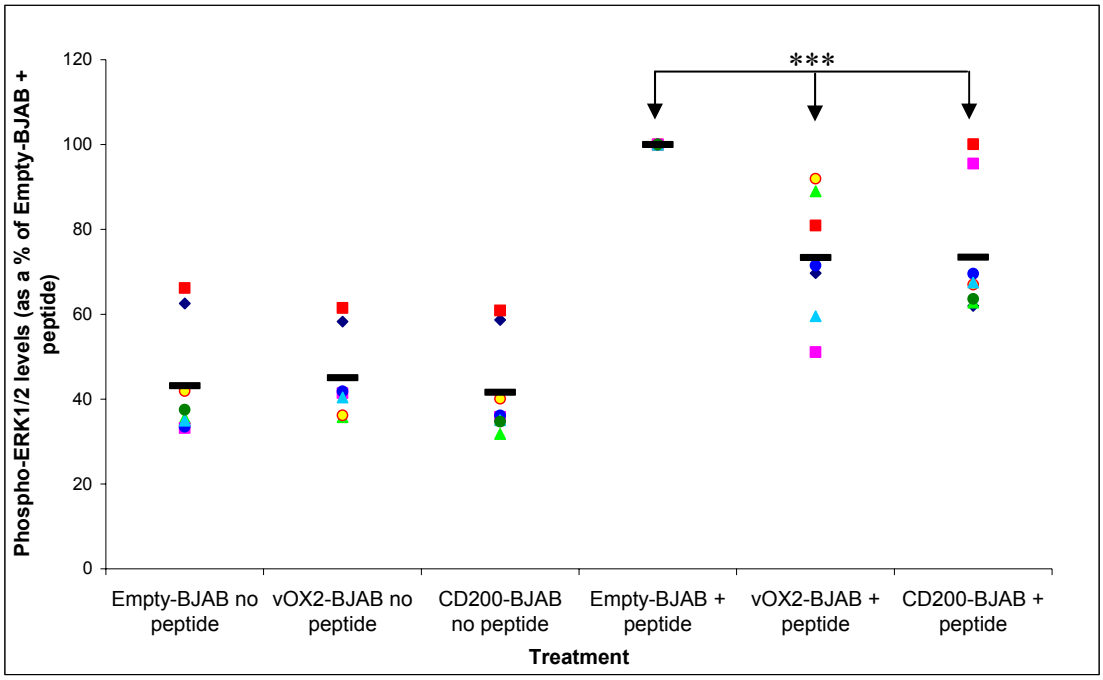

Figure 6.4 vOX2 and CD200-mediated suppression of ERK1/2 MAP kinase phosphorylation in the CD4$^+$ SL c93 T cell clone. The CD4$^+$ EBV antigen-specific T cell clone SL c93 was incubated for 5mins with cognate antigen peptide-pulsed BJAB cells engineered to express empty vector, native vOX2 or native CD200. Intracellular phospho-ERK1/2 was detected by a fluorophore-conjugated monoclonal antibody, and quantified by flow cytometry. Phospho-ERK1/2 levels for each sample are normalised to the Empty-BJAB + peptide control within each experiment. Each coloured icon indicates an independent experiment. Seven independent experiments are plotted on this graph. The mean of each sample group is represented by a black bar. There was no significant difference between Empty, vOX2 and CD200-BJAB cells without peptide ($F(2, 20) = 0.15$; $p = 0.86$ across the three groups), when analysed by a univariate ANOVA test (SPSS software). However, vOX2 and CD200-BJAB significantly suppressed p-ERK1/2 in comparison to Empty-BJAB ($F(2, 20) = 12.34$; ***$p < 0.001$ for both).

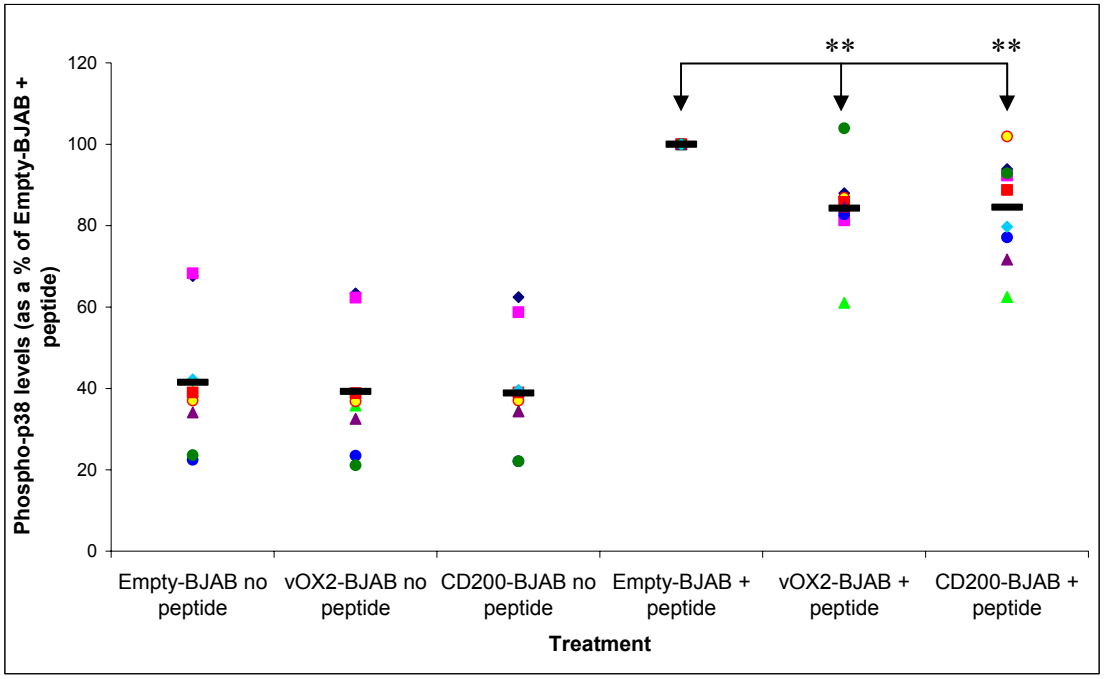

Figure 6.5 vOX2 and CD200-mediated suppression of p38 MAP kinase phosphorylation in the CD4$^+$ SL c93 T cell clone. The CD4$^+$ EBV antigen-specific T cell clone SL c93 was incubated for 5mins with cognate antigen peptide-pulsed BJAB cells engineered to express empty vector, native vOX2 or native CD200. Intracellular phospho-p38 was detected by a fluorophore-conjugated monoclonal antibody, and quantified by flow cytometry. Phospho-p38 levels for each sample are normalised to the Empty-BJAB + peptide control within each experiment. Each coloured icon indicates an independent experiment. Eight independent experiments are plotted on this graph. The mean of each sample group is represented by a black bar. There was no significant difference between Empty, vOX2 and CD200-BJAB cells without peptide ($F(2, 23) = 0.08$; $p = 0.93$ across the three groups), when analysed by a univariate ANOVA test (SPSS software). However, vOX2 and CD200-BJAB significantly suppressed p-p38 in comparison to Empty-BJAB ($F(2, 23) = 7.34$; $^{**}p < 0.01$ for both).

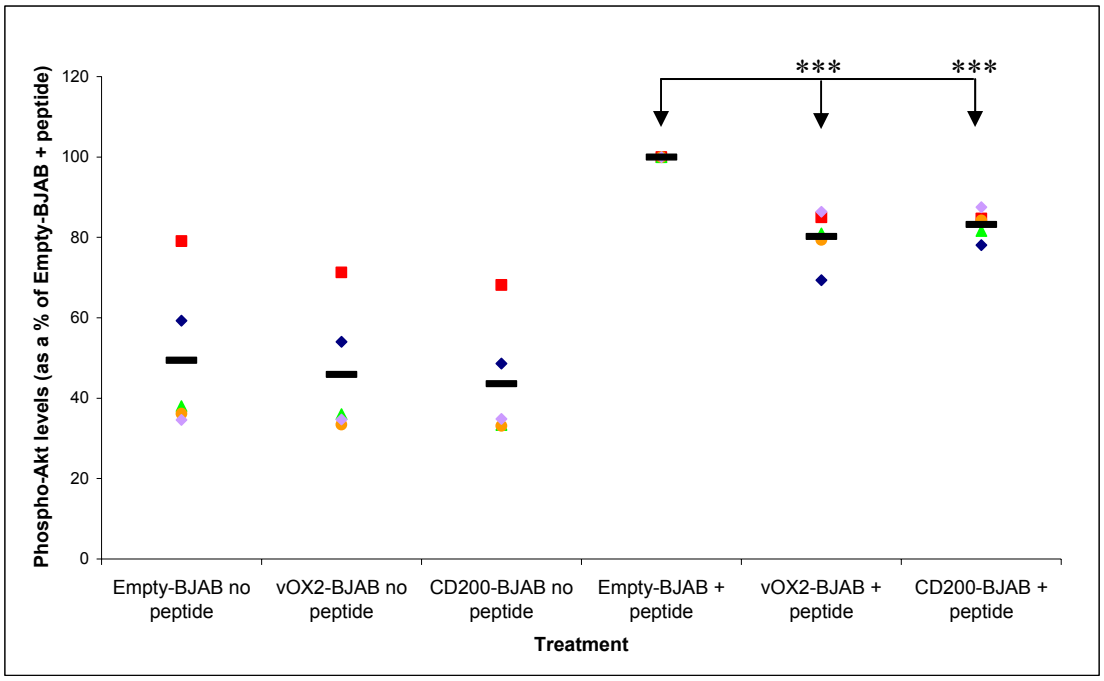

Figure 6.6 vOX2 and CD200-mediated suppression of Akt kinase phosphorylation in the CD4$^+$ SL c93 T cell clone. The CD4$^+$ EBV antigen-specific T cell clone SL c93 was incubated for 5mins with cognate antigen peptide-pulsed BJAB cells engineered to express empty vector, native vOX2 or native CD200. Intracellular phospho-Akt was detected by a fluorophore-conjugated monoclonal antibody, and quantified by flow cytometry. Phospho-Akt levels for each sample are normalised to the Empty-BJAB + peptide control within each experiment. Each coloured icon indicates an independent experiment. Five independent experiments are plotted on this graph. The mean of each sample group is represented by a black bar. There was no significant difference between Empty, vOX2 and CD200-BJAB cells without peptide ($F(2, 12) = 0.15$; $p = 0.87$ across the three groups), when analysed by a univariate ANOVA test (SPSS software). However, vOX2 and CD200-BJAB significantly suppressed p-Akt in comparison to Empty-BJAB ($F(2, 12) = 29.48$; ***$p < 0.001$ for both).

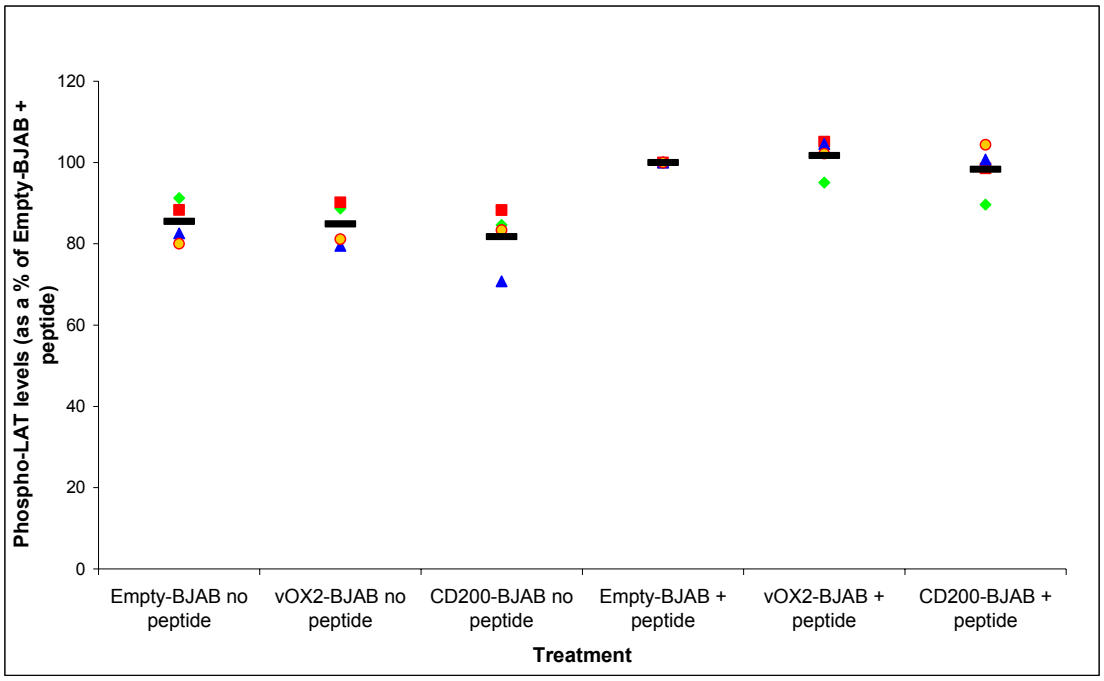

Figure 6.7 LAT phosphorylation in the CD4$^+$ SL c93 clone was not altered by vOX2 or CD200 expressed by BJAB cells. The CD4$^+$ EBV antigen-specific T cell clone SL c93 was incubated for 5mins with cognate antigen peptide-pulsed BJAB cells engineered to express empty vector, native vOX2 or native CD200. Intracellular phospho-LAT was detected by a fluorophore-conjugated monoclonal antibody, and quantified by flow cytometry. Phospho-LAT levels for each sample are normalised to the Empty-BJAB + peptide control within each experiment. Each coloured icon indicates an independent experiment. Four independent experiments are plotted on this graph. The mean of each sample group is represented by a black bar. There was no significant difference between Empty, vOX2 and CD200-BJAB cells without peptide ($F(2, 9) = 0.43$; $p = 0.66$ across the three groups), when analysed by a univariate ANOVA test (SPSS software). In the peptide-treated samples, vOX2 and CD200-BJAB did not induce a significant suppression of p-LAT in comparison to Empty-BJAB ($F(2, 9) = 0.57$; $p = 0.59$ across the three groups).

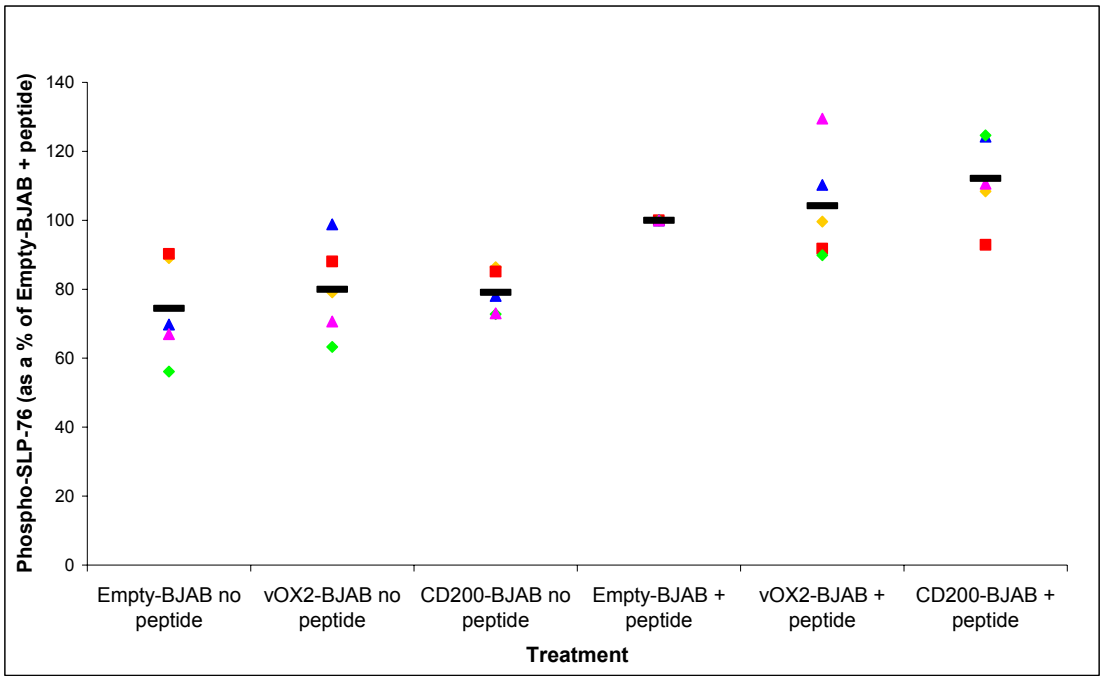

Figure 6.8 SLP-76 phosphorylation in the CD4$^+$ SL c93 clone was not altered by vOX2 or CD200 expressed by BJAB cells. The CD4$^+$ EBV antigen-specific T cell clone SL c93 was incubated for 5mins with cognate antigen peptide-pulsed BJAB cells engineered to express empty vector, native vOX2 or native CD200. Intracellular phospho-SLP-76 was detected by a fluorophore-conjugated monoclonal antibody, and quantified by flow cytometry. Phospho-SLP-76 levels for each sample are normalised to the Empty-BJAB + peptide control within each experiment. Each coloured icon indicates an independent experiment. Five independent experiments are plotted on this graph. The mean of each sample group is represented by a black bar. There was no significant difference between Empty, vOX2 and CD200-BJAB cells without peptide ($F(2, 12) = 0.29$; $p = 0.75$ across the three groups), when analysed by a univariate ANOVA test (SPSS software). In the peptide-treated samples, vOX2 and CD200-BJAB did not induce a significant suppression of SLP-76 in comparison to Empty-BJAB ($F(2, 12) = 0.31$; $p = 0.3$ across the three groups).

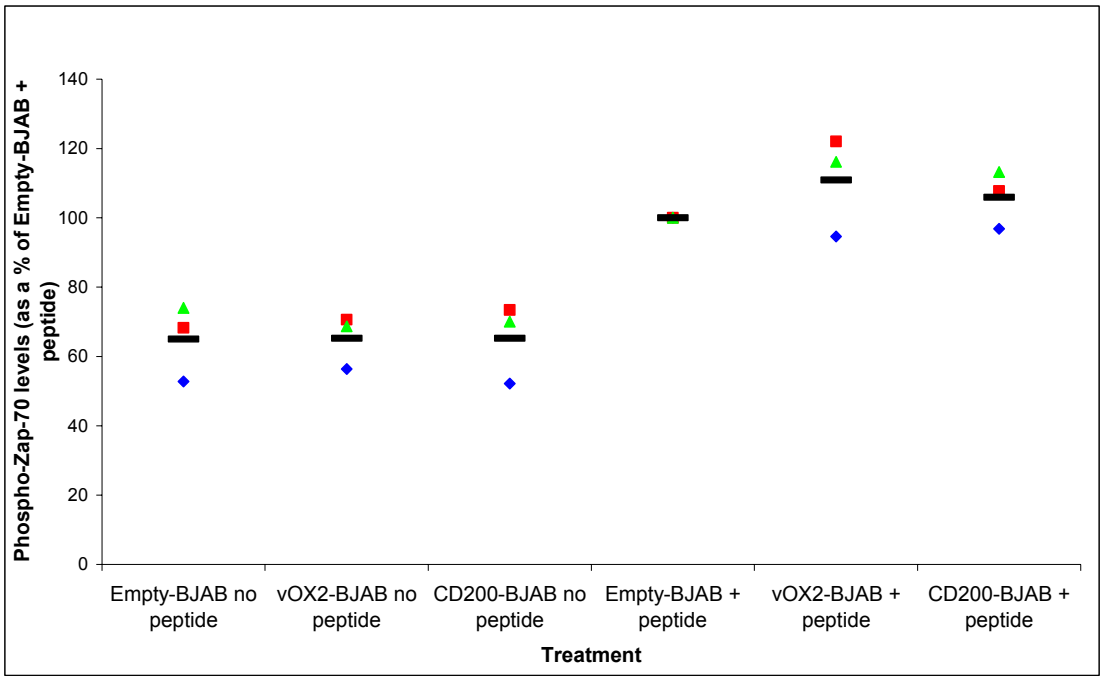

Figure 6.9 Zap70 phosphorylation in the CD4$^+$ SL c93 clone was not altered by vOX2 or CD200 expressed by BJAB cells. The CD4$^+$ EBV antigen-specific T cell clone SL c93 was incubated for 5mins with cognate antigen peptide-pulsed BJAB cells engineered to express empty vector, native vOX2 or native CD200. Intracellular phospho-Zap70 was detected by a fluorophore-conjugated monoclonal antibody, and quantified by flow cytometry. Phospho-Zap70 levels for each sample are normalised to the Empty-BJAB + peptide control within each experiment. Each coloured icon indicates an independent experiment. Three independent experiments are plotted on this graph. The mean of each sample group is represented by a black bar. There was no significant difference between Empty, vOX2 and CD200-BJAB cells without peptide ($F(2, 6) = 0$; $p = 1$ across the three groups), when analysed by a univariate ANOVA test (SPSS software). In the peptide-treated samples, vOX2 and CD200-BJAB did not induce a significant suppression of Zap70 in comparison to Empty-BJAB ($F(2, 6) = 0.97$; $p = 0.24$ across the three groups).

6.2.3. Modification of signalling proteins by vOX2 and CD200 in the $CD8^+$ IM140.1 Y15 T cell clone

Activation of downstream signalling kinases ERK1/2, p38 and Akt was suppressed by vOX2 and CD200 in the $CD4^+$ SL c93 T cell clone, though the phosphorylation of upstream adaptor molecules were not altered. In order to determine whether this selective inhibitory activity was cell-type specific, the same experiments were carried out on the $CD8^+$ IM140.1 Y15 clone, having a different peptide specificity (and HLA restriction). A YVL peptide concentration of 50ng/ml was chosen for all $CD8^+$ IM140.1 Y15 signalling assays. This concentration was the lowest to induce phosphorylation of signalling proteins and higher concentrations did not substantially increase protein phosphorylation (data not shown). The phosphorylation of ERK1/2 in the $CD8^+$ T cell clone IM140.1 was dramatically reduced to almost basal levels by vOX2 and CD200-expressing BJAB cells (**Figure 6.10**) in four independent experiments. p-ERK1/2 was reduced to only 23.14% ± 10.45 SEM of control levels in the presence of vOX2, and was present at only 29.82% ± 12.37 SEM of control levels when incubated with peptide-pulsed CD200-BJAB cells. This substantial suppression of ERK1/2 phosphorylation was statistically significant when analysed by univariate ANOVA (**$p<0.001$). Likewise, the phosphorylation of Akt kinase was significantly reduced by vOX2, to only 62.99% ± 15.85 SEM of control, and was also suppressed by CD200-BJAB, to 62.01% ± 6.58 SEM of Empty-BJAB-treated control cells (**Figure 6.12**). This reduction was statistically significant when analysed by univariate ANOVA (**$p<0.05$) in five independent experiments. Similarly to results obtained for the $CD4^+$ clone, a trend towards suppression of p38 phosphorylation was observed for the $CD8^+$ clone when incubated with peptide-pulsed vOX2 or CD200-BJAB cells (**Figure 6.11**) in five independent experiments. p-p38 was reduced to 77.27% ± 19.12 SEM of control by vOX2,

and to 82.05% ± 16.58 SEM by CD200-BJAB. However the trend was not statistically significant by univariate ANOVA.

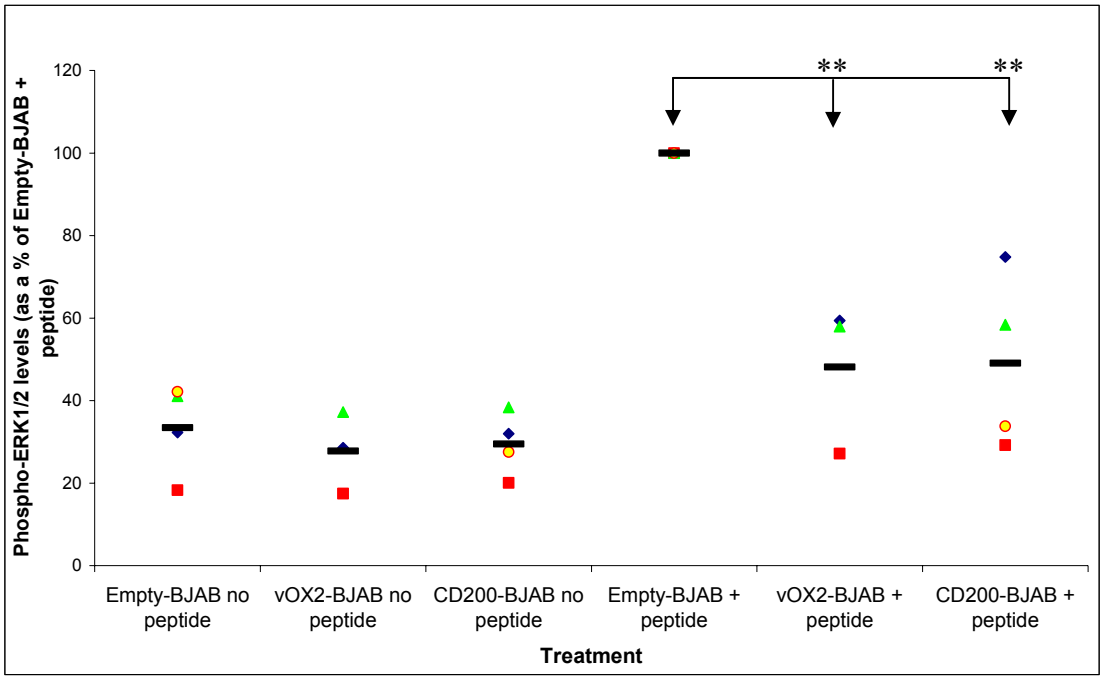

Figure 6.10 vOX2 and CD200-mediated suppression of ERK1/2 MAP kinase phosphorylation in the CD8$^+$ IM140.1 Y15 T cell clone. The CD8$^+$ EBV antigen-specific T cell clone IM140.1 Y15 was incubated for 5mins with cognate antigen peptide-pulsed BJAB cells engineered to express empty vector, native vOX2 or native CD200. Intracellular phospho-ERK1/2 was detected by a fluorophore-conjugated monoclonal antibody, and quantified by flow cytometry. Phospho-ERK1/2 levels for each sample are normalised to the Empty-BJAB + peptide control within each experiment. Each coloured icon indicates an independent experiment. Four independent experiments are plotted on this graph. The mean of each sample group is represented by a black bar. There was no significant difference between Empty, vOX2 and CD200-BJAB cells without peptide ($F(2, 8) = 0.34$; $p = 0.73$ across the three groups), when analysed by a univariate ANOVA test (SPSS software). However, vOX2 and CD200-BJAB significantly suppressed p-ERK1/2 in comparison to Empty-BJAB ($F(2, 8) = 13.16$; $^{**}p < 0.01$ for both).

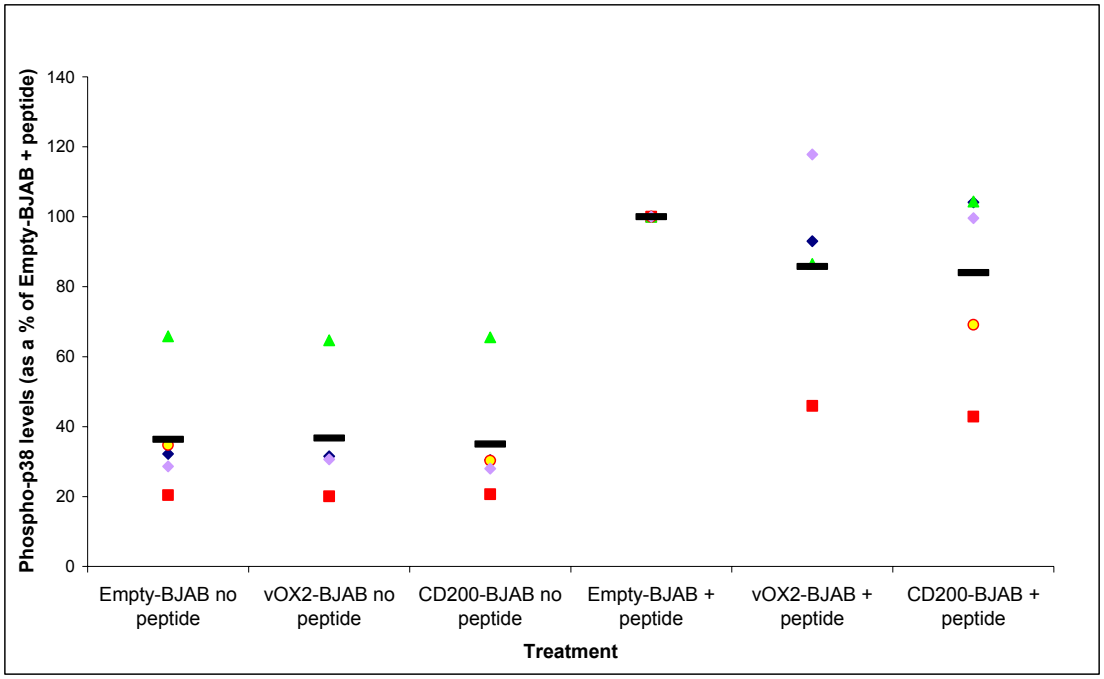

Figure 6.11 A trend towards vOX2 and CD200-mediated suppression of p38 MAP kinase phosphorylation in the CD8$^+$ IM140.1 Y15 T cell clone. The CD8$^+$ EBV antigen-specific T cell clone IM140.1 Y15 was incubated for 5mins with cognate antigen peptide-pulsed BJAB cells engineered to express empty vector, native vOX2 or native CD200. Intracellular phospho-p38 was detected by a fluorophore-conjugated monoclonal antibody, and quantified by flow cytometry. Phospho-p38 levels for each sample are normalised to the Empty-BJAB + peptide control within each experiment. Each coloured icon indicates an independent experiment. Five independent experiments are plotted on this graph. The mean of each sample group is represented by a black bar. There was no significant difference between Empty, vOX2 and CD200-BJAB cells without peptide ($F(2, 11) = 0.01$; $p = 0.99$ across the three groups), when analysed by a univariate ANOVA test (SPSS software). In the peptide-treated samples, vOX2 and CD200-BJAB did not induce a significant suppression of p-p38 in comparison to Empty-BJAB ($F(2, 11) = 0.73$; $p = 0.5$ for both).

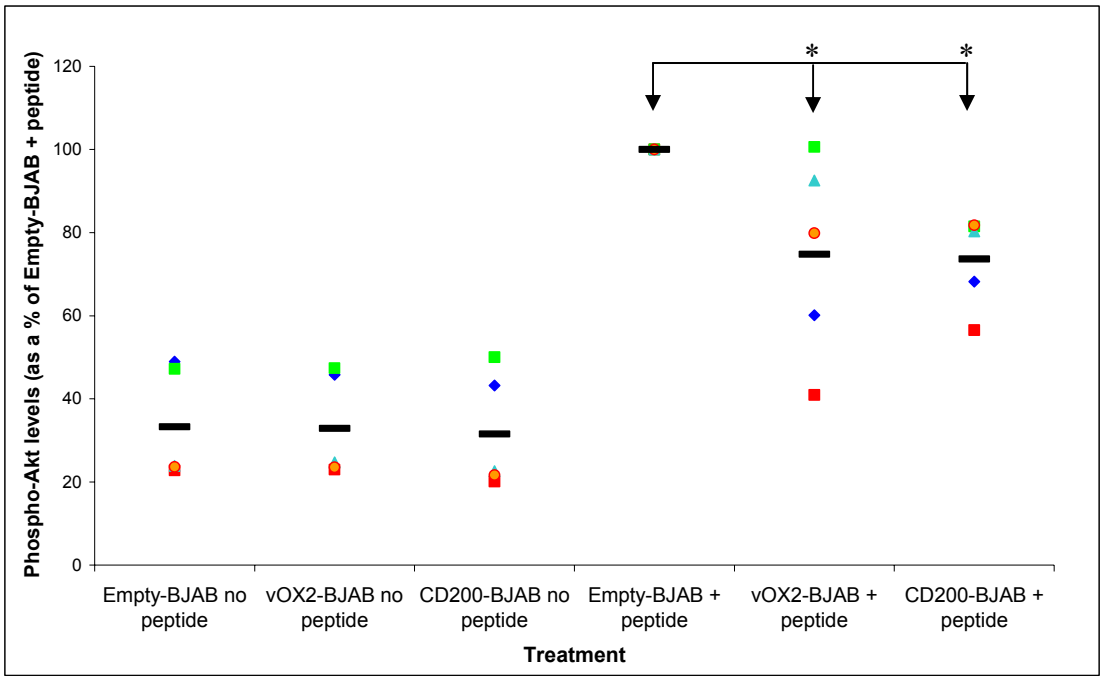

Figure 6.12 vOX2 and CD200-mediated suppression of Akt kinase phosphorylation in the CD8$^+$ IM140.1 Y15 T cell clone. The CD8$^+$ EBV antigen-specific T cell clone IM140.1 Y15 was incubated for 5mins with cognate antigen peptide-pulsed BJAB cells engineered to express empty vector, native vOX2 or native CD200. Intracellular phospho-Akt was detected by a fluorophore-conjugated monoclonal antibody, and quantified by flow cytometry. Phospho-Akt levels for each sample are normalised to the Empty-BJAB + peptide control within each experiment. Each coloured icon indicates an independent experiment. Five independent experiments are plotted on this graph. The mean of each sample group is represented by a black bar. There was no significant difference between Empty, vOX2 and CD200-BJAB cells without peptide ($F(2, 12) = 0.02$; $p = 0.98$ across the three groups), when analysed by a univariate ANOVA test (SPSS software). However, vOX2 and CD200-BJAB significantly suppressed p-Akt in comparison to Empty-BJAB ($F(2, 12) = 4.65$; $^*p < 0.05$ for both).

In this $CD8^+$ T cell clone, the signalling proteins upstream of the MAP kinases in the TCR cascade, SLP-76 and Zap70, were also not affected by vOX2 or CD200. LAT phosphorylation was not detectable in these cells upon peptide-stimulation (see Appendix D). SLP-76 was noticeably phosphorylated by peptide-pulsed BJAB cells, but was not modified by expression of vOX2 or CD200 on the surface of the APC (**Figure 6.13**) in four independent experiments.

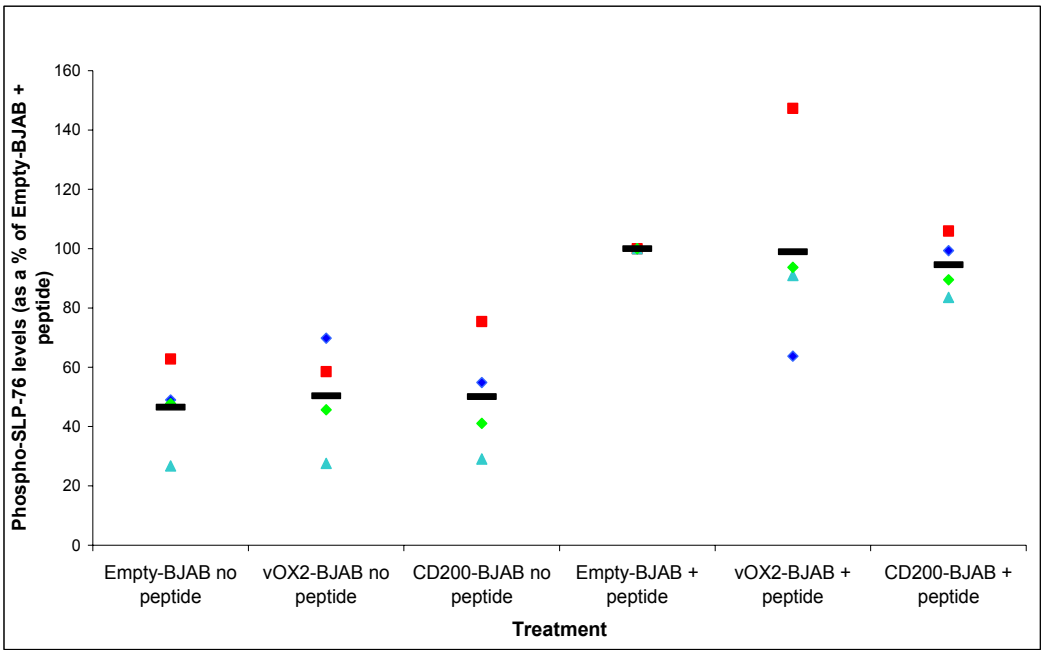

Figure 6.13 SLP-76 phosphorylation in the $CD8^+$ IM140.1 Y15 clone was not altered by vOX2 or CD200 expressed by BJAB cells. The $CD8^+$ EBV antigen-specific T cell clone IM140.1 Y15 was incubated for 5mins with cognate antigen peptide-pulsed BJAB cells engineered to express empty vector, native vOX2 or native CD200. Intracellular phospho-SLP-76 was detected by a fluorophore-conjugated monoclonal antibody, and quantified by flow cytometry. Phospho-SLP-76 levels for each sample are normalised to the Empty-BJAB + peptide control within each experiment. Each coloured icon indicates an independent experiment. Four independent experiments are plotted on this graph. The mean of each sample group is represented by a black bar. There was no significant difference between Empty, vOX2 and CD200-BJAB cells without peptide ($F(2, 9) = 0.06$; $p = 0.94$ across the three groups), when analysed by a univariate ANOVA test (SPSS software). In the peptide-treated samples, vOX2 and CD200-BJAB did not induce a significant suppression of p-SLP-76 in comparison to Empty-BJAB ($F(2, 9) = 0.08$; $p = 0.93$ across the three groups).

The phosphorylation of Zap70, upstream of LAT and SLP-76, was also not altered by vOX2 or CD200 in four independent experiments. Zap70 was noticeably phosphorylated in response to peptide (**Figure 6.14**), but p-Zap70 levels in vOX2-BJAB-treated $CD8^+$ cells were similar (94.34% ± 8.34 SEM) to those in Empty-BJAB-treated cells (100%). CD200-BJAB cells also did not affect p-Zap70, with levels in CD200-BJAB-treated $CD8^+$ cells at 96.12% ± 6.14 SEM of those treated with Empty-BJAB cells.

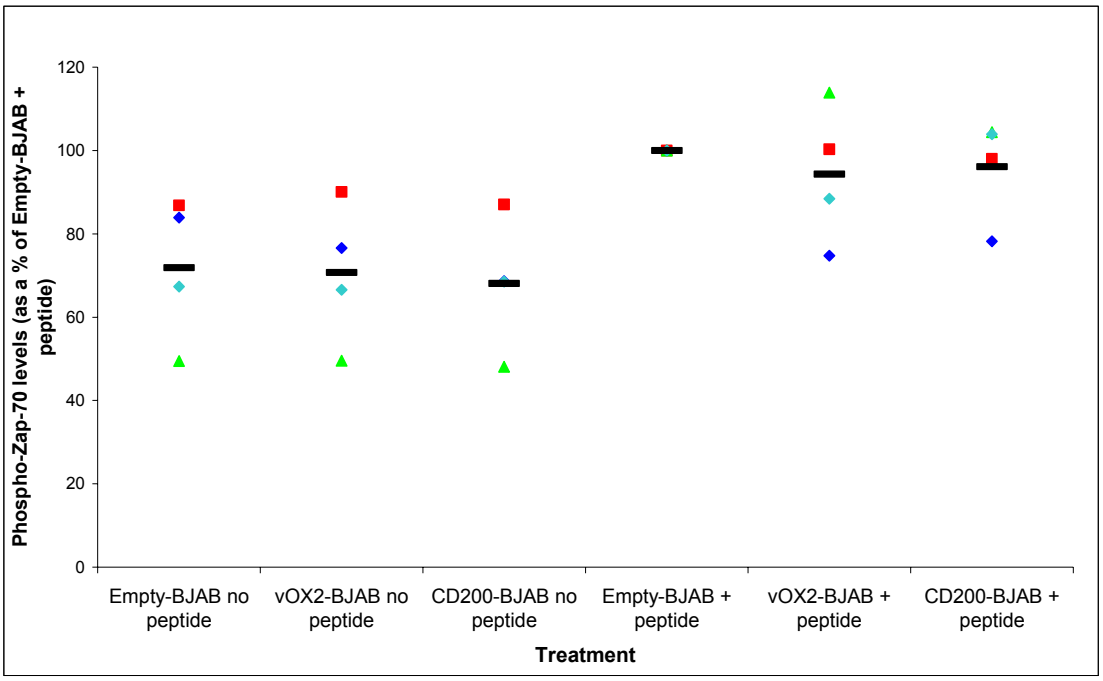

Figure 6.14 Zap70 phosphorylation in the $CD8^+$ IM140.1 Y15 clone was not altered by vOX2 or CD200 expressed by BJAB cells. The $CD8^+$ EBV antigen-specific T cell clone IM140.1 Y15 was incubated for 5mins with cognate antigen peptide-pulsed BJAB cells engineered to express empty vector, native vOX2 or native CD200. Intracellular phospho-Zap70 was detected by a fluorophore-conjugated monoclonal antibody, and quantified by flow cytometry. Phospho-Zap70 levels for each sample are normalised to the Empty-BJAB + peptide control within each experiment. Each coloured icon indicates an independent experiment. Four independent experiments are plotted on this graph. The mean of each sample group is represented by a black bar. There was no significant difference between Empty, vOX2 and CD200-BJAB cells without peptide ($F(2, 9) = 0.05$; $p = 0.95$ across the three groups), when analysed by a univariate ANOVA test (SPSS software). In the peptide-treated samples, vOX2 and CD200-BJAB did not induce a significant suppression of p-Zap70 in comparison to Empty-BJAB ($F(2, 9) = 0.23$; $p = 0.8$ across the three groups).

6.2.4. Modification of ERK1/2 and p38 by vOX2 and CD200 in the $CD8^+$ IM235 c48 T cell clone

Due to the observed vOX2 and CD200-mediated suppression of ERK1/2 phosphorylation, and the trend towards reduced p-p38 in both the $CD4^+$ SL c93 and the $CD8^+$ IM140.1 Y15 T cell clones, another $CD8^+$ clone was examined. The isolation and clonal selection of IM235 c48 was described in Chapter 5. IFNγ-secretion by this clone was suppressed by vOX2 and CD200, both of which were also able to inhibit the intracellular accumulation of IL-2 and IFNγ. The phosphorylation of ERK1/2 was suppressed by vOX2 and CD200 in the $CD8^+$ IM235 c48 clone (**Figure 6.15**) in four independent experiments. p-ERK1/2 levels in T cells cultured with peptide-pulsed vOX2-BJAB were reduced to 69.62% ± 16.25 SEM of the maximal stimulation by Empty-BJAB, and were reduced to 60.63% ± 8.72 SEM by CD200-BJAB. The CD200-mediated suppression is statistically significant by univariate ANOVA (*$p<0.05$) but vOX2-mediated suppression of p-ERK1/2 did not reach significance, due to the high deviation between experiments. Neither vOX2 nor CD200 altered the phosphorylation of p38 in four independent experiments (**Figure 6.16**).

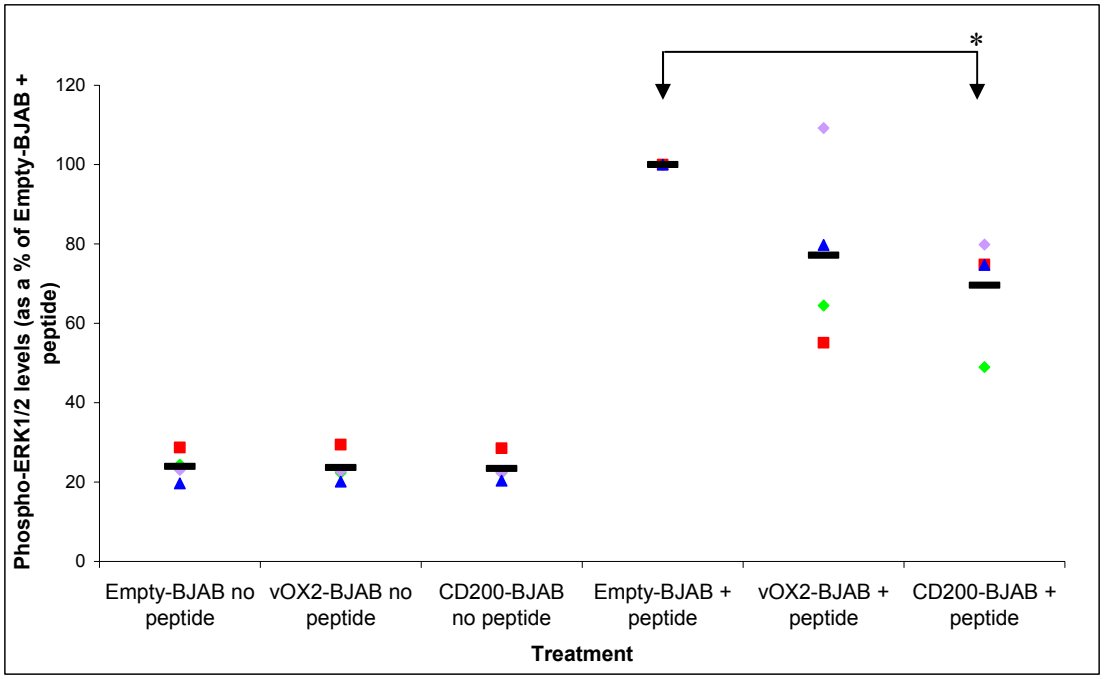

Figure 6.15 vOX2 and CD200-mediated suppression of ERK1/2 MAP kinase phosphorylation in the CD8$^+$ IM235 c48 T cell clone. The CD8$^+$ EBV antigen-specific T cell clone IM235 c48 was incubated for 5mins with cognate antigen peptide-pulsed BJAB cells engineered to express empty vector, native vOX2 or native CD200. Intracellular phospho-ERK1/2 was detected by a fluorophore-conjugated monoclonal antibody, and quantified by flow cytometry. Phospho-ERK1/2 levels for each sample are normalised to the Empty-BJAB + peptide control within each experiment. Each coloured icon indicates an independent experiment. Four independent experiments are plotted on this graph. The mean of each sample group is represented by a black bar. There is no significant difference between Empty, vOX2 and CD200-BJAB cells without peptide ($F(2, 9) = 0.02$; $p = 0.98$ across the three groups), when analysed by a univariate ANOVA test (SPSS software). However, CD200-BJAB induces a significant suppression of p-ERK1/2 in comparison to Empty-BJAB ($F(2, 9) = 3.98$; $^*p < 0.05$), though vOX2 does not ($p = 0.072$).

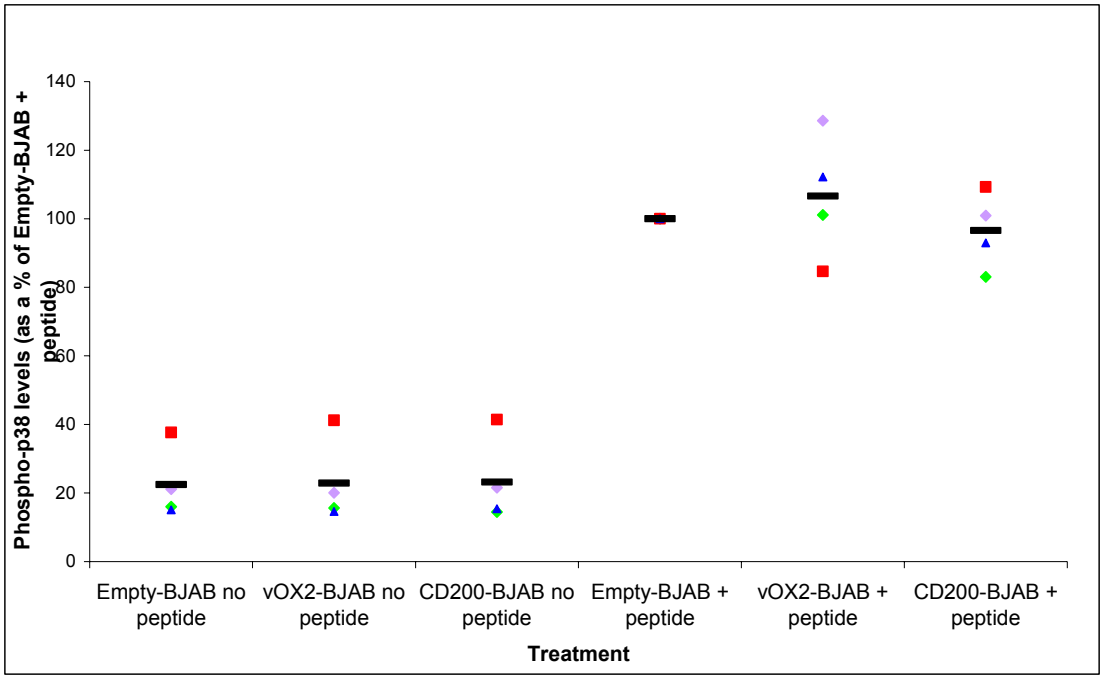

Figure 6.16 p38 phosphorylation in the CD8$^+$ IM235 c48 clone was not altered by vOX2 or CD200 expressed by BJAB cells. The CD8$^+$ EBV antigen-specific T cell clone IM235 c48 was incubated for 5mins with cognate antigen peptide-pulsed BJAB cells engineered to express empty vector, native vOX2 or native CD200. Intracellular phospho-p38 was detected by a fluorophore-conjugated monoclonal antibody, and quantified by flow cytometry. Phospho-p38 levels for each sample are normalised to the Empty-BJAB + peptide control within each experiment. Each coloured icon indicates an independent experiment. Four independent experiments are plotted on this graph. The mean of each sample group is represented by a black bar. There is no significant difference between Empty, vOX2 and CD200-BJAB cells without peptide ($F(2, 9) = 0.004$; $p = 1$ across the three groups), when analysed by a univariate ANOVA test (SPSS software). In the peptide-treated samples, vOX2 and CD200-BJAB do not induce a significant suppression of p-p38 in comparison to Empty-BJAB ($F(2, 9) = 0.68$; $p = 0.5$ for both).

Mean (normalised to Empty-BJAB data) ± SEM

p-ERK1/2 levels

	Empty-BJAB + peptide	vOX2-BJAB + peptide	CD200-BJAB + peptide
CD4+ (SL c93)	100	*** **50.73**% ± 11.27	*** **59.73**% ± 11.34
CD8+ (IM140.1 Y15)	100	** **23.14**% ± 10.45	** **29.82**% ± 12.37
CD8+ (IM235 c48)	100	* **69.62**% ± 16.25	* **60.63**% ± 8.72

p-p38 levels

	Empty-BJAB + peptide	vOX2-BJAB + peptide	CD200-BJAB + peptide
CD4+ (SL c93)	100	** **74.71**% ± 6.68	** **80.4**% ± 7.02
CD8+ (IM140.1 Y15)	100	77.27% ± 19.12	82.05% ± 16.58
CD8+ (IM235 c48)	100	106.02% ± 14.18	95.61% ± 5.86

p-Akt levels

	Empty-BJAB + peptide	vOX2-BJAB + peptide	CD200-BJAB + peptide
CD4+ (SL c93)	100	*** **65.29**% ± 7.26	*** **77.98**% ± 1.46
CD8+ (IM140.1 Y15)	100	* **62.99**% ± 15.85	* **62.01**% ± 6.58

Table 6.1 A summary of the suppression of intracellular signalling molecules by vOX2 and CD200. The 'no peptide' value for each sample was subtracted from the '+ peptide' value to account for baseline levels of phosphorylation. The data for vOX2 and CD200-BJAB were then normalised by calculating the % of the Empty-BJAB value within each experiment. The * indicate the degree of statistical significance (* $p<0.05$; **$p<0.01$; ***$p<0.001$) as determined by univariate ANOVA (SPSS software).

6.3. Mimicking vOX2 and CD200-mediated suppression of p-ERK1/2 with a pharmacological inhibitor

In order to determine whether the observed suppression of ERK1/2 phosphorylation by vOX2 and CD200 (**Figure 6.4/10/15** and **Table 6.2**), alters the production of IFNγ (as seen in Chapter 5) by T cells, pharmacological inhibition of p-ERK1/2 was performed. PD98059 specifically inhibits MAP kinase kinase (MEK1/ MAPKK1), upstream of ERK1/2, thus preventing the phosphorylation of ERK1/2 (Alessi *et al*., 1995). The effect of PD98059 on cell viability was determined by incubating $CD4^+$ SL c93 and $CD8^+$ IM140.1 Y15 T cell clones overnight with increasing concentrations of the inhibitor (**Figure 6.17**). Cell viability was quantified by the trypan blue exclusion assay. PD98059 did not alter cell viability in comparison to a vehicle-treated control in two independent experiments. The same concentrations of PD98059 were administered to BJAB/T cell co-cultures to examine whether the inhibitor could suppress IFNγ-secretion. PD98059 mildly suppressed IFNγ-secretion by $CD4^+$ cells (to 79.1% ± 9.49 SEM of control, 50μM) (**Figure 6.17**, **c**), but was more efficacious at inhibiting $CD8^+$ cell IFNγ-production (53.16% ± 9.8 SEM of control, 50μM) (**Figure 6.17**, **d**), in three independent experiments. Next, the PD98059 inhibitor was introduced to the intracellular signalling assay in an attempt to imitate the inhibition of p-ERK1/2 by vOX2 and CD200 (**Figure 6.18**). The T cells were incubated with 1, 5, 10 or 50μM PD98059, during their stimulation by peptide-pulsed Empty-BJAB cells, or were preincubated with PD98059 prior to stimulation. Both treatment and pretreatment with PD98059 induced similar results.

p-ERK1/2 levels were calculated as before (Section 6.4.2) with data from three independent experiments. PD98059 (10μM) induced a similar level of suppression of p-ERK1/2 in the $CD4^+$ SL c93 clone as either vOX2 or CD200. Thus, PD98059 (10μM) reduced p-ERK1/2 phosphorylation to 71.01% ± 12.14 SEM of the control value (**Figure**

6.18, **a**), compared to suppression by vOX2 (73.38% ± 5.3 SEM) and CD200 (73.44% ± 5.39 SEM) (**Figure 6.4**). PD98059 (10μM) was also the optimal concentration for suppressing ERK1/2 phosphorylation in the $CD8^+$ IM140.1 Y15 clone. p-ERK1/2 was reduced to 46.36% ± 3.81 SEM of the Empty-BJAB (no inhibitor) control (**Figure 6.18**, **b**), similar to the p-ERK1/2 levels detected in the presence of vOX2 (48.16% ± 10.52 SEM) and CD200 (49.05% ± 10.7 SEM) of control (**Figure 6.10**).

Having established the concentration of the ERK1/2 pharmacological inhibitor required to suppress p-ERK1/2 to a similar extent found with either vOX2 or CD200 (**Figure 6.18**), the effects on IFNγ production were determined. T cells were incubated overnight with peptide-pulsed Empty-BJAB cells in the presence or absence of 10μM PD98059. Across all peptide concentrations in two independent experiments, IFNγ-secretion by $CD4^+$ SL c93 cells was reduced in the presence of PD98059 (**Figure 6.19**), in a similar pattern to that observed with the expression of vOX2 or CD200 on the surface of the APC (Chapter 5.12/5.13). Similarly, IFNγ secretion by incubating $CD8^+$ T cells (IM140.1 Y15) with PD98059 reduced extracellular IFNγ at all peptide concentrations (**Figure 6.20**). PD98059 treatment also reduced the accumulation of IFNγ within the $CD8^+$ IM140.1 Y15 and $CD4^+$ SL c93 T cell clones, to 27.87% ± 1.8 SEM (*$p<0.05$, t-test), and 67.78% ± 7.27 SEM (*$p<0.05$, t-test) respectively (**Figure 6.21**). Cumulative data to compare the level of suppression of IFNγ production by PD98059, with the extent of suppression by vOX2-BJAB and CD200-BJAB (**Table 6.3**) demonstrate that PD98059 inhibits IFNγ to a greater degree than either vOX2 or CD200.

(a) $CD4^+$ SL c93 cell viability

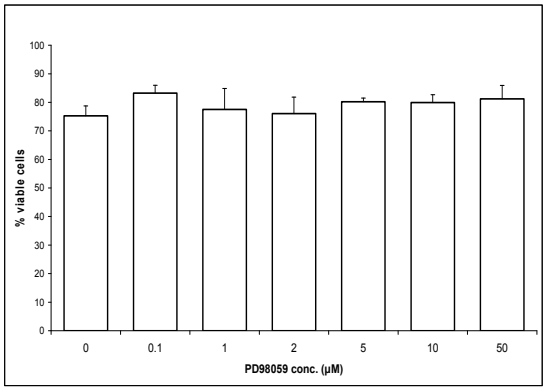

(b) $CD8^+$ IM140.1 Y15 cell viability

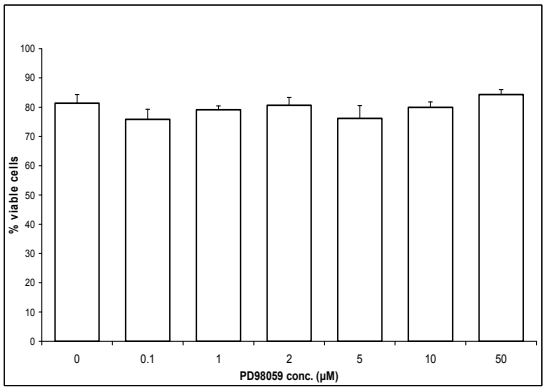

(c) $CD4^+$ SL c93 IFNγ release

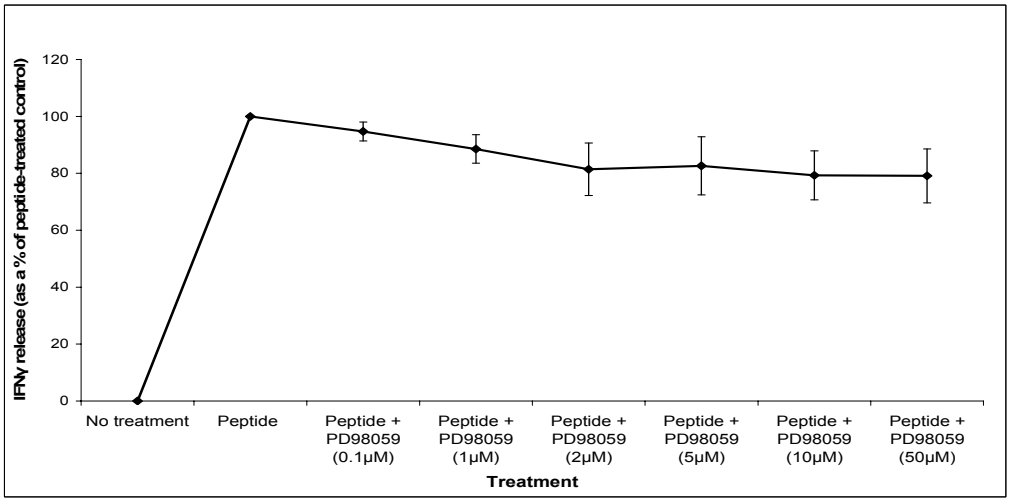

(d) $CD8^+$ IM140.1 Y15 IFNγ release

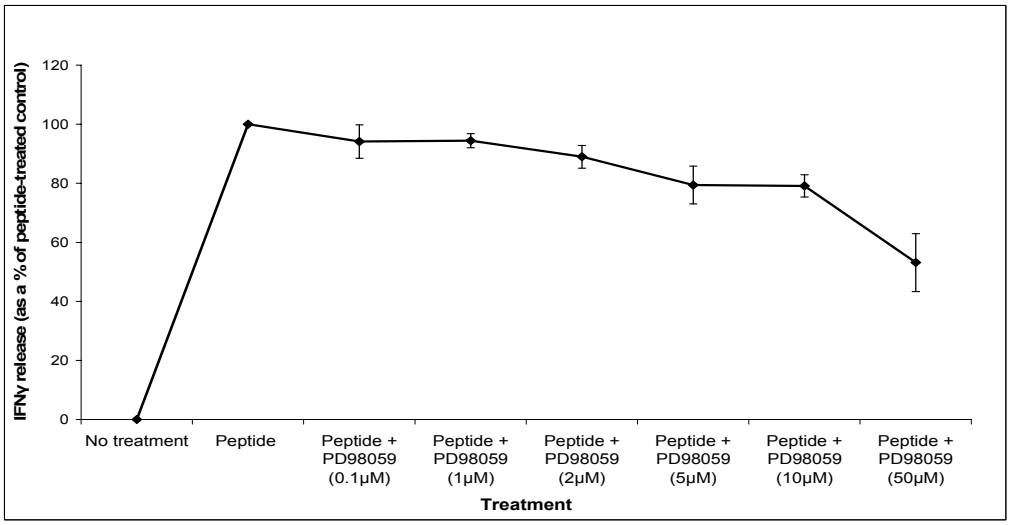

Figure 6.17 Testing an ERK inhibitor, PD98059 against T cell viability and activity. (a) $CD4^+$ SL c93 and **(b)** $CD8^+$ IM140.1 Y15 T cell clones were incubated (16h, 37^{o}C) with PD98059, and cell viability determined by a trypan blue exclusion assay (% viability = the % of cells that do not absorb trypan blue). Data from two independent experiments were pooled. **(c)** The $CD4^+$ SL c93 and **(d)** $CD8^+$ IM140.1 Y15 T cell clones were incubated with cognate peptide antigen-loaded BJAB cells (500ng/ml PRS peptide or 50ng/ml YVL peptide respectively) in the presence of a range of concentrations of PD98059, a pharmacological inhibitor of ERK phosphorylation. IFNγ-release was quantified by ELISA and the results normalised to peptide-treated control; data were pooled from three independent experiments.

(a) $CD4^+$ SL c93 T cell clone

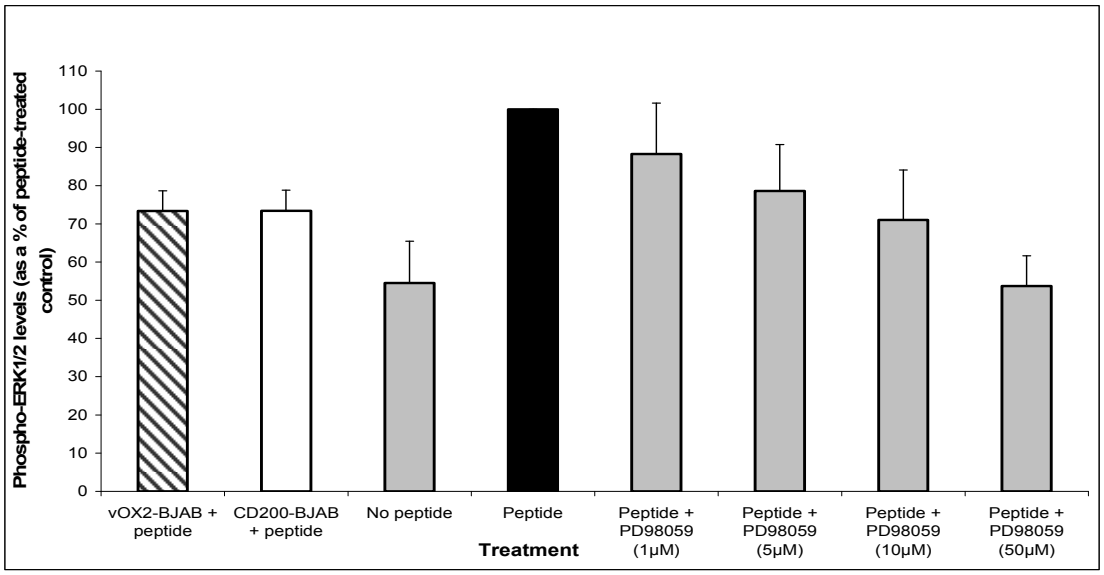

(b) CD8+ IM140.1 Y15 T cell clone

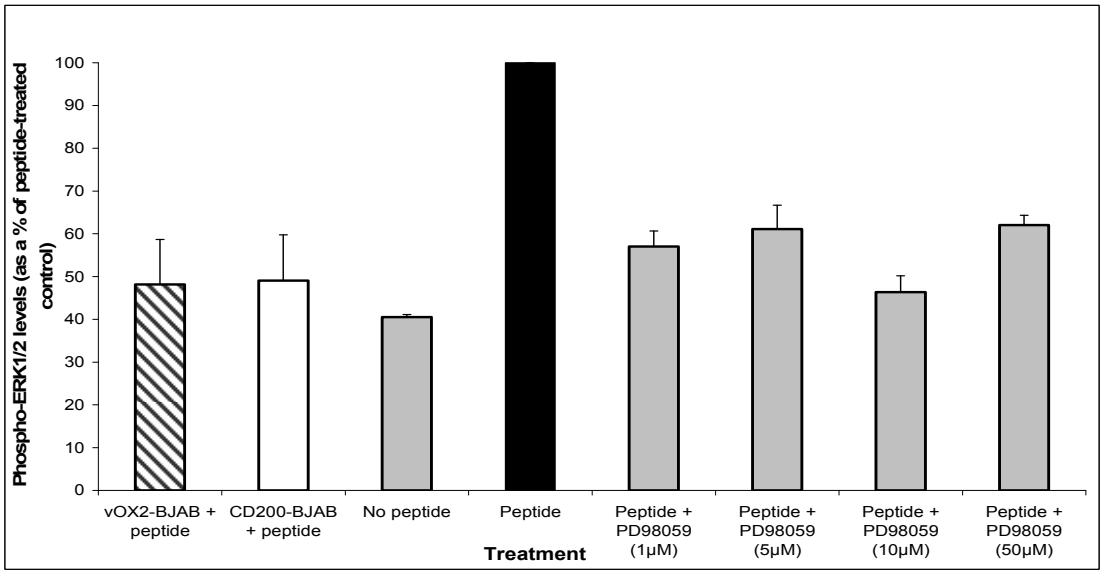

Figure 6.18 Using a pharmacological inhibitor of ERK phosphorylation to mirror the suppression of ERK1/2 phosphorylation by vOX2 and CD200. (a) The $CD4^+$ SL c93 and **(b)** $CD8^+$ IM140.1 Y15 T cell clones were treated with an ERK inhibitor (PD98059) while being stimulated with antigen peptide-pulsed BJAB cells. The reaction was quenched after 5mins with 1.5% formaldehyde, and the level of ERK1/2 phosphorylation quantified by flow cytometric analysis. The level of p-ERK1/2 suppression by vOX2 or CD200-BJAB cells found in previous experiments is included in the above graphs, in order to identify the concentration of PD98059 that results in an equivalent inhibition of ERK1/2 phosphorylation. Data from **(a)** three or **(b)** two independent experiments were pooled and presented as a % of p-ERK1/2 levels resulting from stimulation by peptide-pulsed BJAB cells.

(a) CD4$^+$ SL c93 T cell clone

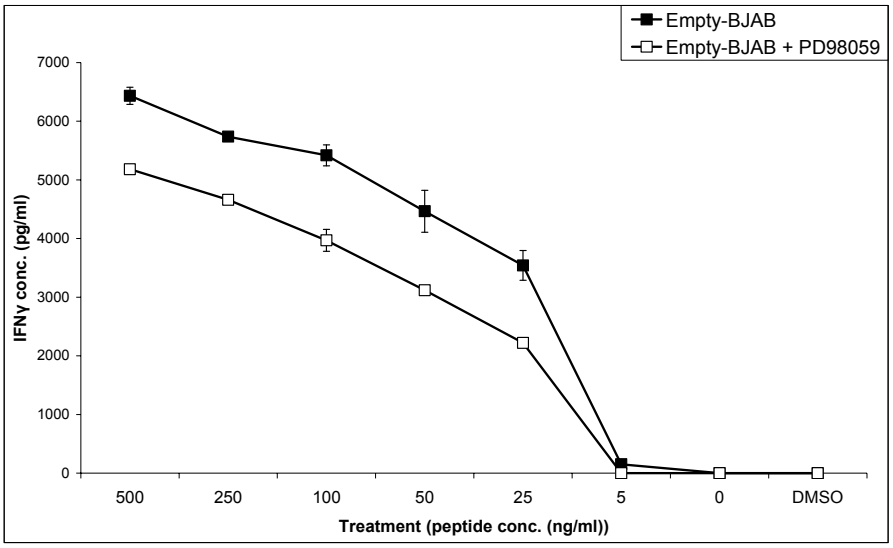

(b) CD4$^+$ SL c93 T cell clone replicate experiment

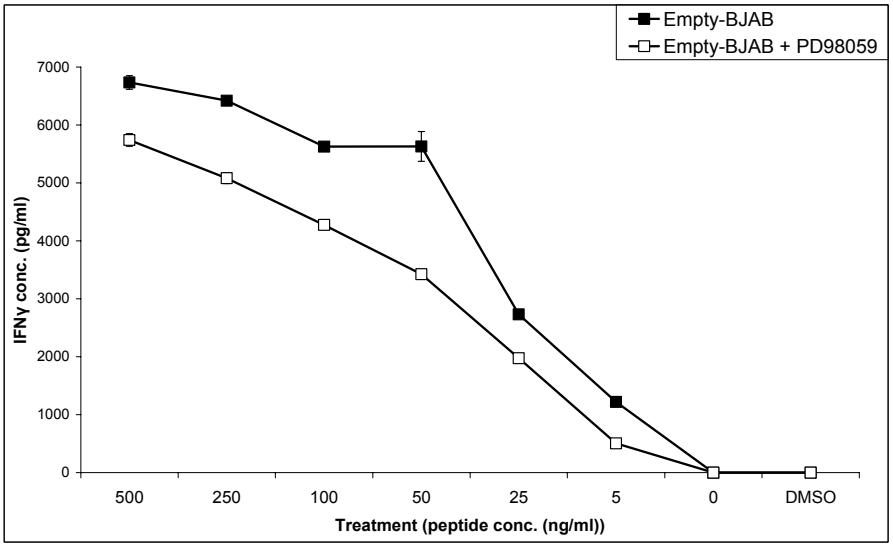

Figure 6.19 Mimicking the activities of vOX2 and CD200 by inhibiting the phosphorylation of ERK1/2 with a pharmacological inhibitor, PD98059, suppresses the secretion of IFNγ by the CD4$^+$ SL c93 T cell clone. BJAB cells transduced with an empty vector were peptide-pulsed and incubated with the T cell clone cells for 16hrs. The cells were incubated in the presence or absence of PD98059 (10μM) to suppress phospho-ERK1/2 levels to the same degree as achieved by expression of either vOX2 or CD200 (see **Figure 6.4**). IFNγ secretion was quantified by ELISA, and the data from triplicate wells pooled and presented as mean ± SEM; data from separate independent experiments are presented in each graph.

(a) CD8$^+$ IM140.1 Y15 T cell clone

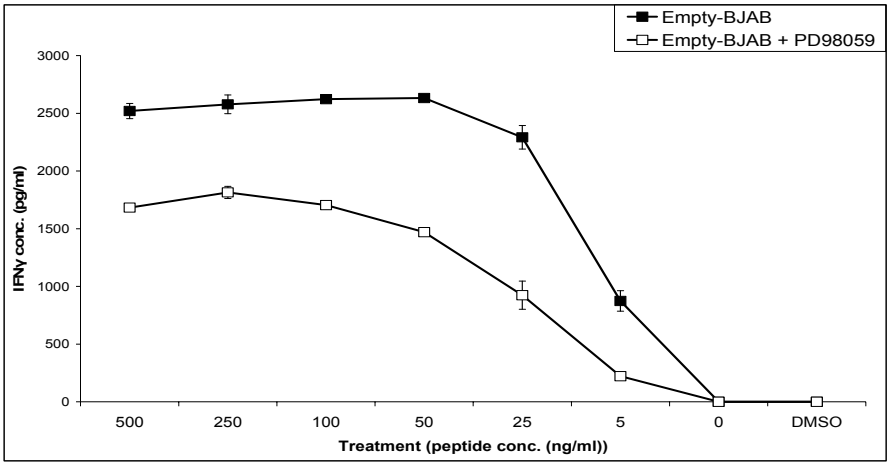

(b) CD8$^+$ IM140.1 Y15 T cell clone replicate experiment

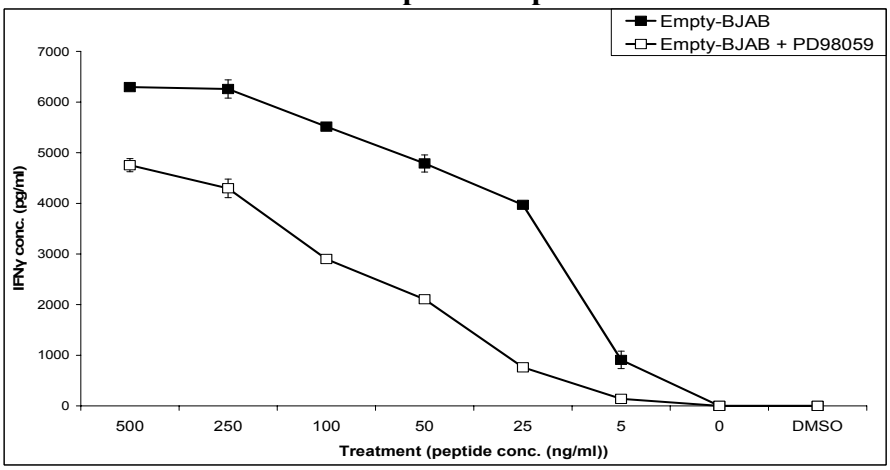

(c) CD8$^+$ IM140.1 Y15 T cell clone replicate experiment

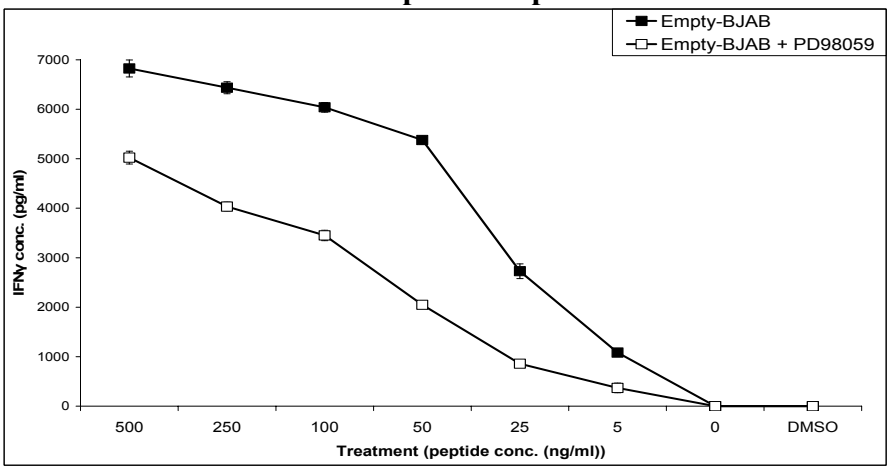

Figure 6.20 Mimicking the activities of vOX2 and CD200 by inhibiting the phosphorylation of ERK1/2 with a pharmacological inhibitor, PD98059, suppresses the secretion of IFNγ by the CD8$^+$ IM140.1 Y15 T cell clone. BJAB cells transduced with an empty vector were peptide-pulsed and incubated with the T cell clone cells for 16hrs. The cells were incubated in the presence or absence of PD98059 (10μM) to suppress phospho-ERK1/2 levels to the same degree as achieved by expression of either vOX2 or CD200 (see **Figure 6.10**). IFNγ secretion was quantified by ELISA, and the data from triplicate wells pooled and presented as mean ± SEM; data from separate independent experiments are presented in each graph.

(a) $CD4^+$ SL c93 T cell clone

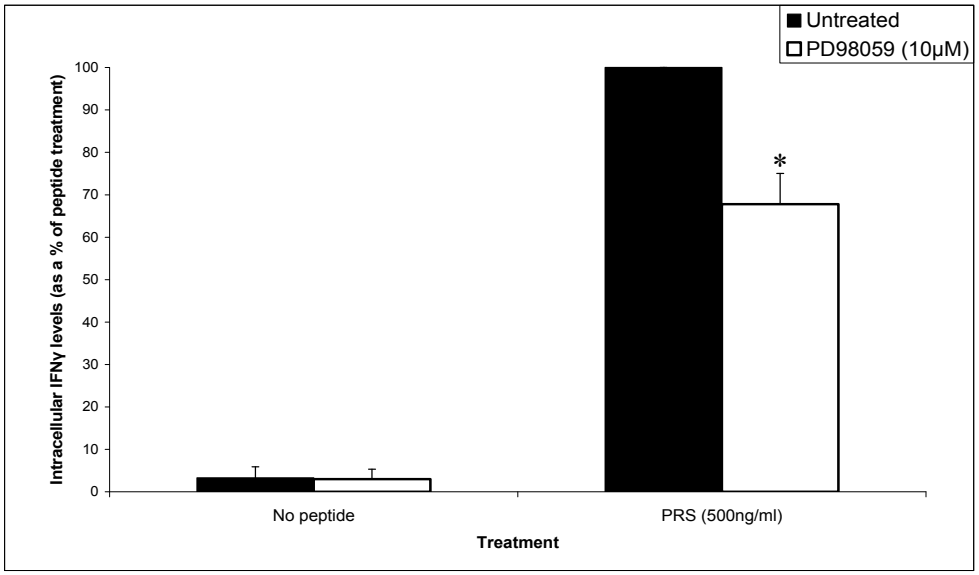

(b) $CD8^+$ IM140.1 Y15 T cell clone

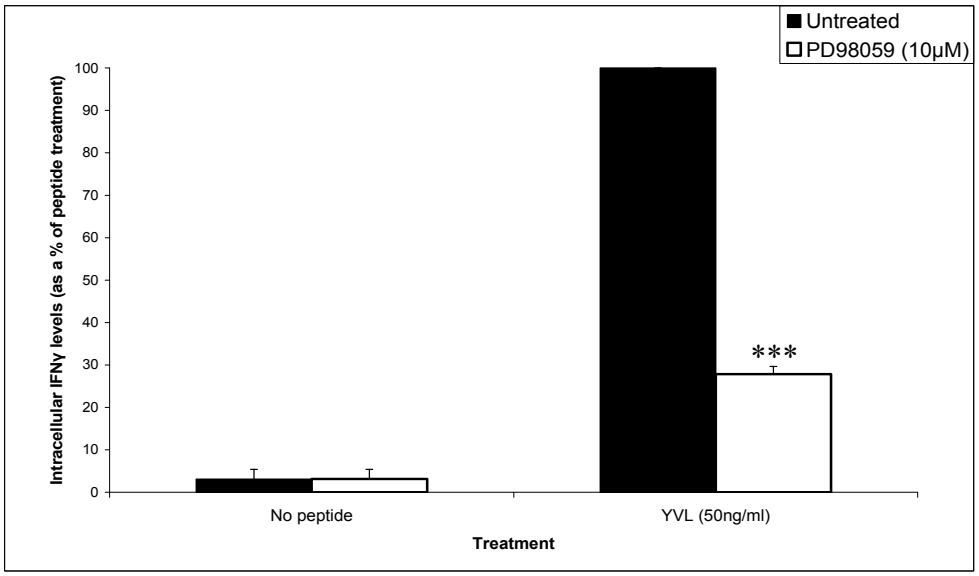

Figure 6.21 Mimicking the activities of vOX2 and CD200 by inhibiting the phosphorylation of ERK1/2 with a pharmacological inhibitor, PD98059, suppresses the accumulation of IFNγ in the $CD8^+$ IM140.1 Y15 and $CD4^+$ SL c93 T cell clones. (a) The $CD8^+$ IM140.1 Y15 and **(b)** CD4+ SL c93 T cell clones were incubated for 60mins with cognate antigen peptide-pulsed BJAB cells transduced with an empty vector, or engineered to express vOX2 or CD200. Brefeldin A (7.5μg/ml) was added to the BJAB and T cell co-culture, and the cells incubated for a further 2hrs. Intracellular IFNγ was detected with fluorophore-conjugated monoclonal antibodies, and quantified by flow cytometry. Data from three independent experiments were pooled, normalised to the Empty-BJAB + peptide control, and presented as mean ± SEM. PD98059 treatment did not alter IFNγ production in the absence of peptide, but significantly suppressed the production of IFNγ by peptide-stimulated $CD4^+$ SL c93 ($F(4, 2) = 5.16$; *$p<0.05$) and $CD8^+$ IM140.1 Y15 ($F(4, 2) = 13.71$; ***$p<0.001$) T cell clones when the data were analysed by an independent two-tailed t-test (SPSS software).

$CD8^+$ IM140.1 Y15							
	Extracellular IFNγ				Intracellular IFNγ		
	vOX2	CD200	PD98059		vOX2	CD200	PD98059
500ng/ml peptide	93.71% ± 8.7	* 86.29% ± 4.97	71.95% ± 2.65	500ng/ml peptide			
50ng/ml peptide	78.27% ± 10.4	** 61.26 % ± 10.06	45.98% ± 5.21	50ng/ml peptide	62.68% ± 14.39	* 40.42% ± 13.55	*** 27.87% ± 1.80

$CD4^+$ SL c93							
	Extracellular IFNγ				Intracellular IFNγ		
	vOX2	CD200	PD98059		vOX2	CD200	PD98059
500ng/ml peptide	89.18% ± 3.15	** 71.69% ± 8.17	82.9% ± 2.35	500ng/ml peptide	*** 66.65% ± 14.12	*** 87.59% ± 4.04	* 67.78% ± 7.27
50ng/ml peptide	96.91% ± 34.13	58.98% ± 17.74	65.34% ± 4.49	50ng/ml peptide			

Table 6.2 Comparative data illustrating the roles of vOX2, CD200 and the pharmacological ERK1/2 inhibitor PD98059 in suppressing IFNγ production by the $CD8^+$ IM140.1 Y15 and $CD4^+$ SL c93 T cell clones. The presence of either vOX2 or CD200 on the surface of peptide-pulsed BJAB cells suppressed the secretion of IFNγ, as well as the accumulation of IFNγ within T cell clones. Treating the T cell clones with PD98059 (10μM), to mimic the extent of vOX2 and CD200-mediated suppression of ERK1/2 phosphorylation, suppressed the secretion of IFNγ in response to cognate peptide antigen, and the accumulation of IFNγ intracellularly. The data are presented as a percentage of the data for the Empty-BJAB coculture (mean ± SEM). The * indicate the degree of statistical significance (* $p<0.05$; ** $p<0.01$; *** $p<0.001$) as determined by univariate ANOVA or independent two-tailed t-tests (SPSS software).

6.4. Phenotyping the engineered BJAB cells

The observed vOX2 and CD200-mediated suppression of T cell cytokine production, and the modification of downstream signalling molecules by vOX2 and CD200, may be due to a direct interaction between either vOX2 or CD200 and molecules on the surface of the T cell. Both vOX2 and CD200 are capable of ligating CD200R with similar affinity (Foster-Cuevas *et al*., 2004) and T cells express CD200R (Chapter 7). However, there is a possibility that engineering BJAB cells to express either vOX2 or CD200 alters the expression of other cell-surface proteins. HLA molecules are crucial for the stimulation of T cells by presenting processed antigen peptides to the TCR. Co-stimulatory molecules CD80 and CD86 (B7.1

and B7.2) are also crucial for T cell stimulation, and TCR stimulation in the absence of co-stimulation can result in anergy. CD80 and CD86 bind to CD28 on resting cells, amplifying the TCR-mediated stimulation, and bind with higher affinity to CTLA-4, an inhibitory receptor that is upregulated on activated cells providing a negative feedback loop to regulate T cell activity (Murphy, 2008). Therefore, the expression of HLA-ABC (components of the MHC-I complex), HLA-DR (a component of MHC-II), and CD80 and CD86 were quantified on the surface of vOX2- and CD200-expressing BJAB cells in comparison to BJABs transduced with the empty vector (Empty-BJAB).

Cell surface proteins were labelled with antigen-specific monoclonal antibodies (see Chapter 2.7.6 and Appendix B, Table I), or an isotype control, and levels quantified by flow cytometry. The median fluorescence value for each isotype control was subtracted from the value for the antibody-labelled sample, and vOX2-BJAB and CD200-BJAB levels expressed as a % of Empty-BJAB control. HLA-DR expression was slightly reduced on vOX2-BJAB cells, to 78% ± 12.04 SEM of control, but was not altered on CD200-BJAB (93.79% ± 9.86 SEM of control) cells in four independent experiments (**Figure 6.22**, **a**). The expression of CD80 was also reduced slightly on both vOX2-BJAB, to 78.82% ± 4.0 SEM of control, and CD200-BJAB, to 81.77% ± 5.32 SEM of Empty-BJAB control levels, in five independent experiments (**Figure 6.22**, **b**), and this difference was statistically significant according to one-way ANOVA (**$p<0.01$). In contrast, CD86 levels were modestly amplified on vOX2 and CD200-expressing cells in five independent experiments, though the results were not statistically significant. CD86 expression on vOX2-BJAB was increased to 120.7% ± 16.54 SEM of control, and to 118.71% ± 6.04 SEM of control, on CD200-BJAB cells (**Figure 6.22**, **c**).

The reduction of cell-surface HLA-ABC (MHC-I) on vOX2-BJAB and CD200-BJAB cells was more pronounced, and was significant according to one-way ANOVA

analysis of the data (***p<0.001). HLA-ABC levels were reduced to 67.42% ± 2.47 SEM of control on vOX2-BJAB cells, and to 71.12% ± 2.12 SEM on CD200-BJAB cells (**Figure 6.23**, **a**). Though surprisingly HLA-ABC expression on BJAB cells expressing vOX2 or CD200 fused to EGFP was similar to HLA-ABC on Empty-BJAB cells. HLA-ABC expression on vOX2-EGFP-BJAB cells was 86.4% ± 7.85 SEM of the Empty-BJAB control, and 89.74% ± 6.1 SEM of control on CD200-EGFP-BJAB cells (**Figure 6.23**, **b**).

To determine whether the observed suppression of cell-surface HLA-ABC on vOX2-BJAB and CD200-BJAB was due to increased internalisation of the protein, the following assay was carried out (Chapter 2.7.7). Briefly, engineered BJAB cells were placed on ice and saturated with an anti-HLA-ABC antibody. The cells were then warmed to 37^{o}C and incubated for the times indicated (**Figure 6.24**). HLA-ABC internalisation was quenched by placing the cells on ice, and the remaining HLA-ABC antibody-labelled proteins were labelled with a fluorophore-conjugated secondary antibody before analysis by flow cytometry. Therefore, the more HLA-ABC that can be detected in this assay, as determined by higher fluorescence, the less protein has been internalised. The expression of HLA-ABC on the surface of vOX2-BJAB and CD200-BJAB was consistently lower than the levels on Empty-BJAB cells, but this disparity did not increase with increased incubation times. Therefore the rate of internalisation of HLA-ABC was unaffected by vOX2 or CD200.

Thus, surface HLA-ABC expression is reduced on vOX2-BJAB and CD200-BJAB cells, but the rate of internalisation does not change in the presence of either vOX2 or CD200. The total amount of HLA-ABC protein in these cells is lower than in Empty-BJAB cells, quantification by Western Blot and densitometry was performed (see Chapter 2.3 for method). Each densitometric value for HLA-ABC was normalised to the calregulin content of that sample. Firstly, the cytosolic fraction was isolated (Chapter 2.3.4) and analysed for HLA-ABC content. HLA-ABC expression by vOX2-BJAB was lower than the empty vector

control in both experiments (reduced to 30.92% and 62.98% of Empty-BJAB control), but HLA-ABC was not reduced to the same extent in CD200-BJAB (78.74% and 87.64% of control) (**Figure 6.25**, **a**, **b**). Interestingly, and consistent with flow cytometric data (**Figure 6.23**, **b**), HLA-ABC levels were not reduced overall in BJAB cells expressing vOX2 (68.09% and 123.59%) or CD200 (91.07% and 96.6%) fused in-frame with EGFP (**Figure 6.25**, **a**, **b**). Secondly, whole cell lysates were prepared (Chapter 2.3.5). There was a slight decrease in HLA-ABC levels in vOX2-BJAB cells (87.41% of control) but a slight increase in HLA-ABC in CD200-BJAB cells, to 114.4% of control (**Figure 6.25**, **c**). Overall from three independent experiments, two analysing cytosol and one cell lysate, HLA-ABC protein was reduced to 60.3% ± 16.34 SEM of control in vOX2-BJAB, but was only reduced marginally in CD200-BJAB cells, to 93.6% ± 10.71 SEM of the Empty-BJAB control, and neither difference reached statistical significance. There was no modification of HLA-ABC protein expression in vOX2-EGFP-BJAB cells, which contained 104.85% ± 18.38 SEM of control, or in CD200-EGFP-BJAB cells that expressed 103.09% ± 9.39 SEM of Empty-BJAB control HLA-ABC levels (**Figure 6.25**, **d**).

(a)

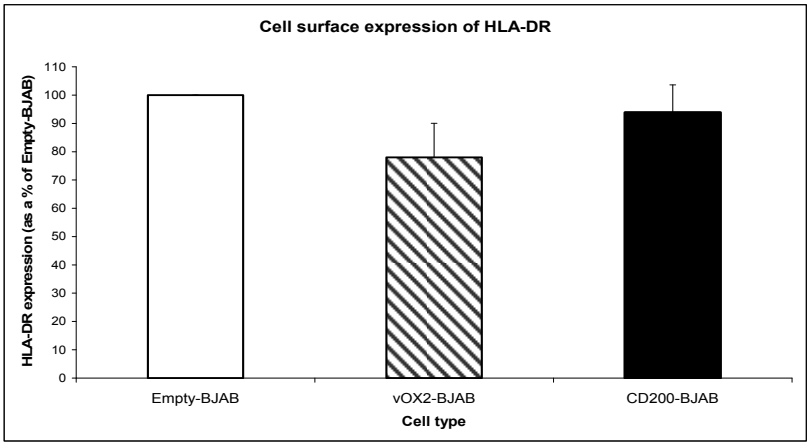

(b)

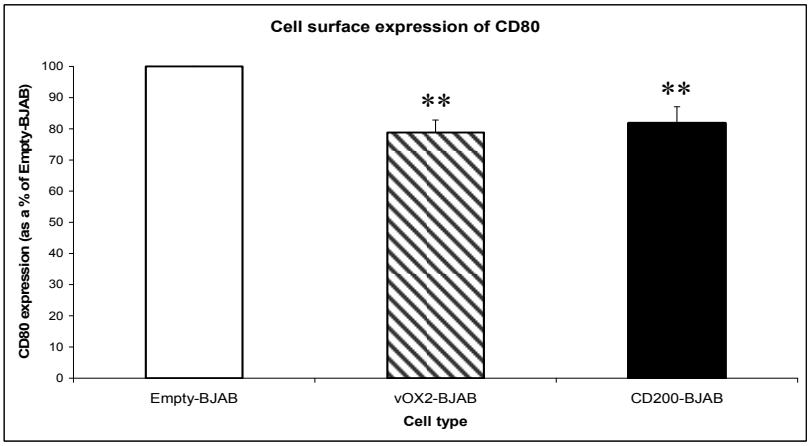

(c)

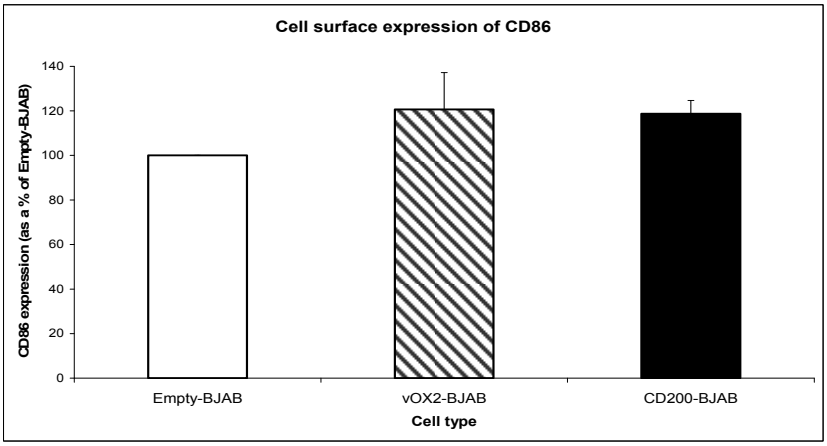

Figure 6.22 Cell-surface expression levels of HLA-DR, CD80 and CD86 are not altered by the presence of native vOX2 or CD200 on the cell. BJAB cells were engineered to express native vOX2, CD200 or an empty vector. Extracellular **(a)** HLA-DR, **(b)** CD80 and **(c)** CD86 levels on the engineered BJAB cells were quantified by flow cytometry, using specific monoclonal antibodies conjugated to fluorophores. The data were pooled from four **(a)** or five **(b)**, **(c)** independent experiments. Neither HLA-DR nor CD86 expression was altered on the surface of vOX2- or CD200-BJAB cells in comparison to Empty-BJAB, but CD80 expression was significantly reduced on the surface of both vOX2- and CD200-BJAB ($F(2, 12) = 8.80$; $^{**}p<0.01$ for both) when analysed by one-way ANOVA (SPSS software).

(a)

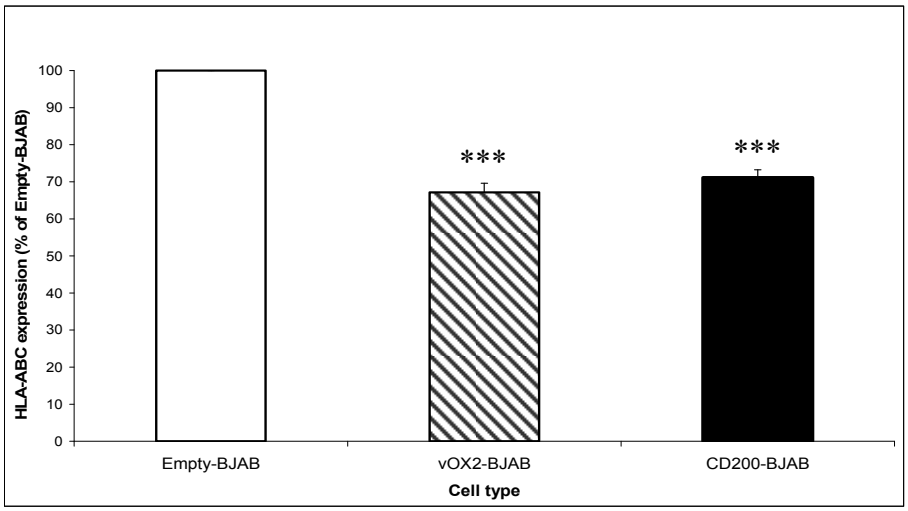

(b)

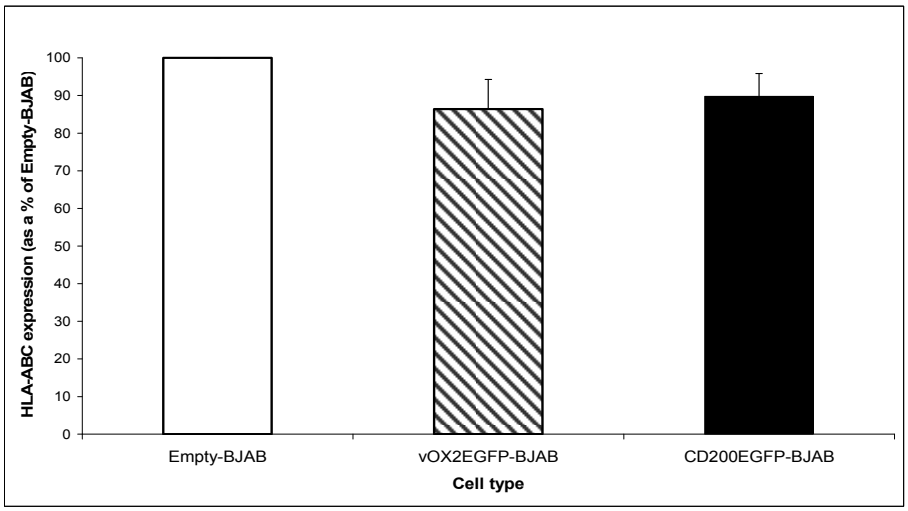

Figure 6.23 Cell-surface expression levels of HLA-ABC are reduced on the surface of both vOX2 and CD200-expressing cells. BJAB cells were engineered to express native vOX2, CD200 or an empty vector. Extracellular HLA-ABC was quantified by flow cytometry, using specific monoclonal antibodies conjugated to a fluorophore. **(a)** BJAB cells expressing native vOX2 or CD200, **(b)** or those expressing vOX2 or CD200 fused in-frame with EGFP. Three independent experiments were carried out for each cell type, and the value of the isotype control median fluorescence subtracted from the sample before normalising to normalising to the fluorescence value obtained for the Empty-BJAB control. HLA-ABC expression was significantly reduced on the surface of vOX2-BJAB and CD200-BJAB ($F(2, 12) = 96.35$; ***$p<0.001$ for both), but was not altered on cells expressing EGFP-tagged vOX2 or CD200, when the data were analysed by univariate one-way ANOVA (SPSS software).

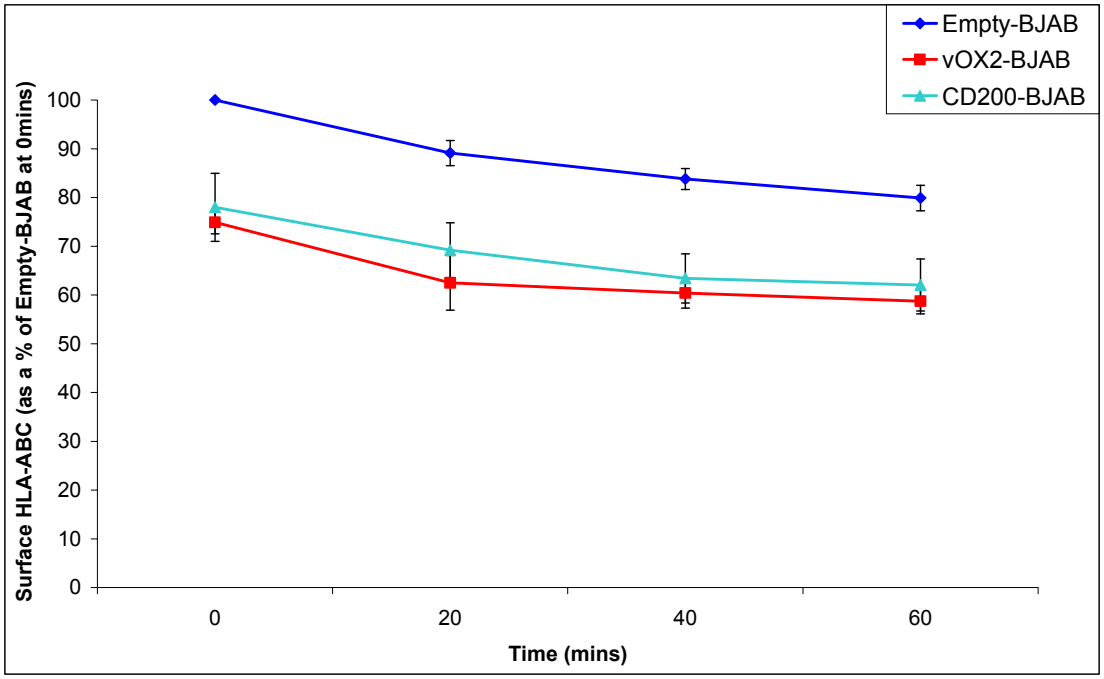

Figure 6.24 The rate of HLA-ABC internalisation from the cell-surface is not altered when vOX2 or CD200 are expressed on the cell. BJAB cells engineered to express either vOX2 or CD200 were labelled with an anti-HLA-ABC antibody (unconjugated) on ice for one hour. The cells were then warmed to 37^{o}C and incubated for the time indicated on the graph. After rapid cooling on ice the anti-HLA-ABC antibody remaining on the cell-surface was labelled with a fluorophore-conjugated secondary antibody and the cells analysed by flow cytometry (Beckman Coulter EPICs XL). The data from two independent experiments were pooled, and represented as a % (± SEM) of the HLA-ABC remaining on the surface of Empty-BJABs at 0mins.

(a) Cytosol fraction replicate 1 (densitometric data) (immunoblot)

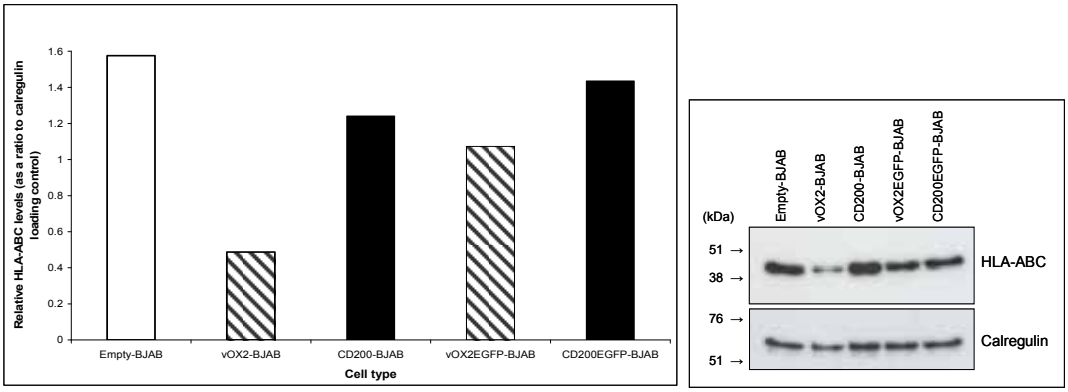

(b) Cytosol fraction replicate 2 (densitometric data) (immunoblot)

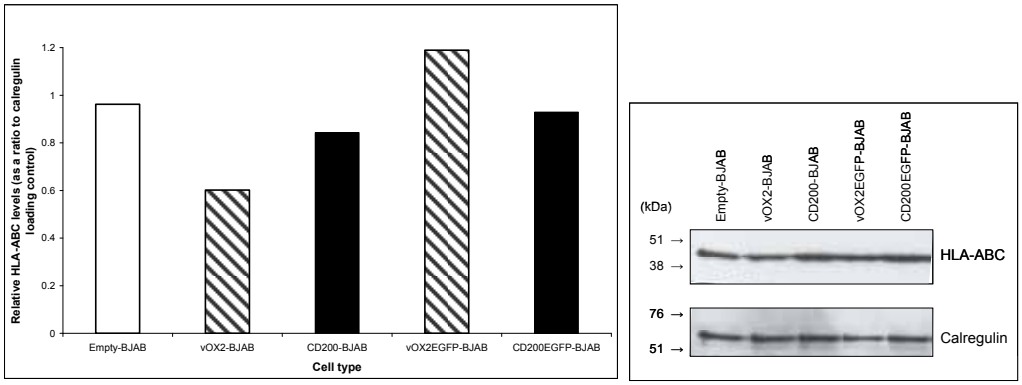

(c) Whole cell lysate (densitometric data) (immunoblot)

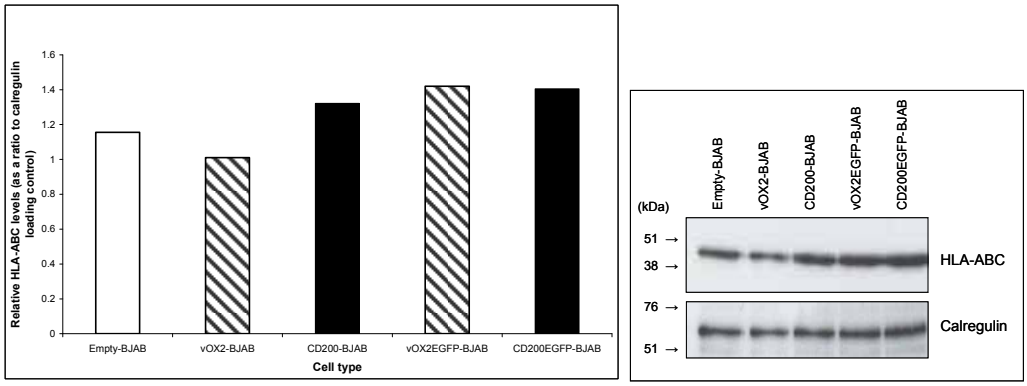

(d) Cumulative data

	Empty-BJAB	vOX2-BJAB	CD200-BJAB	vOX2EGFP-BJAB	CD200EGFP-BJAB
Mean	100	60.30	93.60	104.85	103.09
SEM		± 16.34	± 10.71	± 18.38	± 9.39

Figure 6.25 Quantifying HLA-ABC by immunoblotting of engineered BJAB cell lysates reveals a downregulation of HLA-ABC in vOX2-expressing cells. Lysates were prepared for BJAB cells engineered to express vOX2, CD200, vOX2 or CD200 fused in-frame with EGFP. **(a)**, **(b)** Cytosolic fractions or **(c)** whole cell lysates were prepared, proteins separated by SDS-PAGE and HLA-ABC quantified by immunoblotting

with a specific antibody. Densitometry was carried out on each immunoblot and the data normalised by calculating the ratio of HLA-ABC to a calregulin loading control for each sample. **(d)** The densitometric data were then pooled and presented as a % of the Empty-BJAB control. The reduced HLA-ABC expression by vOX2-BJAB cells does not reach statistical significance when the cumulative data are analysed by one-way ANOVA (SPSS software).

6.5. Discussion

vOX2 and CD200 significantly inhibited the activation of ERK1/2 (**Figures 6.4/10/15**) and Akt kinases (**Figures 6.6/12**), and moderately suppressed p38 phosphorylation (**Figures 6.5/11/16**). Flow cytometric analysis of phospho-proteins enables the analysis of a single cell population in a mixed culture. The observed phosphorylation of intracellular signalling molecules confirmed that as expected, the T cell clones were activated by peptide-pulsed BJAB cells. Inhibition of ERK1/2 activation appears to be directly linked to attenuated T cell activity. Thus, pharmacological inhibition of ERK1/2 phosphorylation to the level observed by vOX2 or CD200 expression on APCs (**Figures 6.4/10/15**) reduced IFNγ secretion (**Figures 6.19/20**) and intracellular accumulation of IFNγ (**Figure 6.21**). The level of pharmacological inhibition of secretion was similar to that obtained by ectopic expression of vOX2 and CD200 on APCs, though slightly greater.

As mentioned earlier, Zhang and colleagues reported a mCD200R1-mediated suppression of ERK1/2, p38 and JNK in murine mast cells, corresponding to decreased degranulation and cytokine secretion (Zhang *et al*., 2004). These authors compared the activities of kinase inhibitors and found that inhibiting all three kinases potently reduced mast cell degranulation and secretion of TNF and IL-13, whereas inhibiting only p-p38 and p-JNK suppressed cell activation to a lesser degree (Zhang *et al*., 2004). Taken together, the

work of Zhang *et al*. (Zhang *et al*., 2004) and the present study demonstrate that CD200- and vOX2-mediated suppression of ERK1/2 phosphorylation alters cell activity.

Decreased ERK1/2 phosphorylation has previously been associated with altered T cell activity, and has been correlated with UV-mediated immunosuppression. Mice grafted with UV-irradiated tissue, or exposed to UV light, developed many more tumours when their lymphocytes were replaced with cells from UV-irradiated animals (Fisher & Kripke, 1982). Li-Weber and colleagues demonstrated that UV-mediated immunosuppression is linked to the inhibition of T cell activity and to ERK1/2 phosphorylation (Li-Weber *et al*., 2005). Primary human T cells, isolated from peripheral blood, were stimulated by anti-CD3/CD28 antibodies, or by PMA and ionomycin treatment, and subsequently produced IFNγ, IL-2, IL-4 and TNFα cytokines. Both the secretion of these proteins and transcription of their coding genes were inhibited by UV irradiation, correlating with reduced expression and translocation of transcription factors AP-1 and NF-κB. In Jurkat T cells, UV irradiation blocked the phosphorylation of ERK1/2 in response to PMA/ionomycin-treatment, but surprisingly it enhanced p-JNK and p-p38 levels. The same effects were recapitulated in anti-CD3/CD28-stimulated human peripheral blood T cells. When p38 was chemically inhibited, translocation of NF-κB to the nucleus was restored, and inhibition of JNK prevented the UV-mediated suppression of ERK1/2 phosphorylation. Inhibiting both p38 and JNK in UV-irradiated T cells restored IL-2 and IFNγ-secretion in response to stimulation (Li-Weber *et al*., 2005). These published data indicate that ERK1/2 is directly suppressed by JNK and p38; however, in the present study p-p38 was not increased above control levels. p-JNK was not analysed because there were no suitable phospho-specific antibodies available. It would be interesting to determine whether inhibiting p38 and JNK phosphorylation could abrogate the vOX2 and CD200-mediated suppression of IFNγ-production.

Further evidence for attenuated T cell responses to peptide resulting from reduced p-ERK1/2 expression was published by Santos and colleagues. Macrophage migration inhibitory factor (MIF), a cytokine expressed by resting and activated T cells, enhances ERK1/2 phosphorylation and is associated with rheumatoid arthritis. Deleting the gene coding for MIF reduced RA disease severity in mice, apparently due to reduced T cell activity in response to antigen stimulation (determined by reduced IFNγ secretion). Reduced antigen-stimulation of $CD4^+$ splenocytes isolated from *MIF*$^{-/-}$ mice correlated with suppressed ERK1/2 phosphorylation, and chemically inhibiting p-ERK1/2 also reduced T cell proliferation in response to antigen. However, in their model, ERK1/2 phosphorylation was suppressed leading to attenuated T cell activity, but p-Akt was not altered (Santos *et al*., 2008). These data contrast with those of this study, in which both p-ERK1/2 and p-Akt were suppressed.

Akt kinase is activated by the TCR signalling cascade, but its activity is amplified by costimulation through the CD28 receptor following ligation with CD80 or CD86. Akt enhances transcription of the *IL-2* gene, and augments the production of both IL-2 and IFNγ (Kane *et al*., 2001). Conversely, the suppression of Akt phosphorylation in the present study may just enhance the inhibition of T cell activity resulting from the suppression of ERK1/2 phosphorylation. The pharmacological inhibition of ERK1/2 (**Figure 6.18**) mimicked the degree of inhibition induced by vOX2 and CD200 (**Figures 6.4/10/15**) and appeared to account for the vOX2 and CD200-mediated suppression of IFNγ-secretion (**Figures 6.19-21**). In fact, PD98059 was more efficacious at suppressing IFNγ production in response to both high (500ng/ml) and moderate (50ng/ml) concentrations of cognate peptide antigen (**Table 6.2**), in comparison to vOX2 and CD200 expressed on the surface of the APC. Therefore, the observed suppression of p38 and Akt may have an additive effect upon the vOX2- and CD200-mediated inhibition of T cell activity.

Although all phospho-proteins analysed in this study were amplified by chemical stimulation (**Figure 6.2**), not all of them were measurable following peptide stimulation. p-Zap70, LAT and SLP-76 are activated immediately post-TCR stimulation, and initiate the signalling cascade leading to the phosphorylation of ERK1/2, p38 and Akt (Au-Yeung *et al*., 2009). All three molecules were phosphorylated by chemical stimulation (**Figure 6.2**), but were not activated to the same extent by peptide stimulation. The amplification of Zap70 phosphorylation following H_2O_2 treatment (**Figure 6.2**) mirrors published data. Haas and colleagues analysed the kinetics of Zap70 phosphorylation by flow cytometry, in response to CD3 stimulation or H_2O_2 treatment (Haas *et al*., 2008). Flow cytometric analysis revealed a marked difference between the two stimulating agents. H_2O_2 treatment increased the phosphorylation of Zap70 by tenfold in comparison to anti-CD3 stimulation. H_2O_2 also prolonged the life of the phospho-protein which was still detectable 30mins post-stimulation, in contrast to anti-CD3 stimulation which induced peak p-Zap70 levels 1-3mins post-CD3 stimulation (Haas *et al*., 2008). These data correlate with the visible increase in p-Zap70 in response to H_2O_2 (**Figure 6.2**), which contrasts with a greatly attenuated phosphorylation of Zap70 in peptide-stimulated T cells 5mins after exposure to peptide-pulsed APCs (**Figures 6.9/14**).

Haas *et al*. observed similar phosphorylation kinetics for LAT. LAT was rapidly phosphorylated and de-phosphorylated in response to CD3 stimulation, but the life of the phospho-protein was prolonged by H_2O_2-treatment (Haas *et al*., 2008). Rapid dephosphorylation may explain the minimal levels of p-LAT observed upon peptide-stimulation of the $CD4^+$ SL c93 T cell clone (**Figure 6.7**), and the negligible levels in the $CD8^+$ IM140.1 Y15 clone (see Appendix D for raw data). In contrast, LAT was obviously phosphorylated upon stimulation of the T cell clones by H_2O_2 (**Figure 6.2**). Phosphorylation of SLP-76 upon TCR-stimulation ultimately enhances IL-2 production by the stimulated T

cell. Overexpression of SLP-76 amplified *IL-2* transcription, whereas mutating its signalling tyrosine residues abrogated the transcription of the gene coding for IL-2 (Bubeck Wardenburg *et al*., 1996). Thus, SLP-76 phosphorylation is vital for effective T cell stimulation via its TCR. SLP-76 was phosphorylated in response to chemical (**Figure 6.2**) and antigen-stimulation (**Figures 6.8/13**), but inhibition by either vOX2 or CD200 could not be detected. The phosphorylation of Zap70, LAT and SLP-76 occurs rapidly upon TCR ligation, and therefore the extent of phosphorylation is linked to the number of TCRs stimulated on the T cell. In comparison, the signalling cascade amplifies as each subsequent protein is activated, which explains the relative ease of detection of p-ERK1/2, p-p38 and p-Akt, downstream of the LAT-SLP-76 adaptor complex. Thus at this stage inhibition of upstream signals cannot be ruled out, but can only be inferred from the reduction in ERK1/2 phosphorylation.

It would be reasonable to assume that a ~30% reduction in HLA-ABC expression on the surface of APCs engineered to express either vOX2 or CD200 (**Figure 6.23**), would reduce the T cell-stimulating potential of these APCs. However, HLA-DR expression was not reduced. The $CD4^+$ SL c93 clone specificity is restricted to HLA-DR subsets 7, 52a, 52b or 52c, and ERK1/2, p38 and Akt phosphorylation were reduced in this clone (**Figures 6.4/6**), in addition to attenuated IFNγ and IL-2 production (Chapter 5). Overall, p-ERK1/2, p38 and p-Akt were not suppressed to a greater degree in HLA-A2.01-restricted $CD8^+$ clones IM140.1 and IM235 c48 (see **Table 6.1** for a synopsis of the data), indicating that reduced HLA expression was unlikely to be a factor in the attenuation of the signalling cascades. Expression of CD80 and CD86 were also quantified on engineered BJAB cells. Both CD80 and CD86 ligate the stimulatory coreceptor CD28, and the inhibitory CTLA4 with a slightly higher affinity. The expression of CD80 on vOX2 and CD200-expressing BJAB cells was reduced, whereas CD86 expression was modestly increased.

The data presented in this chapter indicate that vOX2 and CD200 alter the activation of signalling proteins downstream in the TCR signalling cascade. This modification does not appear to be due to altered co-stimulatory protein expression on the cells engineered to express either vOX2 or CD200, and therefore must be due to direct interaction between these two proteins and proteins expressed by the T cell, such as CD200R. Ligation and subsequent phosphorylation of the CD200R by vOX2 and CD200 could not be determined in this study due to the lack of specific antibodies suitable for flow cytometric analysis of our mixed cell populations. The identification of signalling proteins such as Dok and RasGAP, associating with mCD200R1 (Zhang *et al*., 2004) and human CD200R (Mihrshahi *et al*., 2009), also could not be repeated in this study, again due to a dearth of appropriate antibodies. Therefore, the modification of proteins downstream of the TCR signalling cascade cannot be proved to be due to CD200R-ligation by vOX2 and CD200. But the effect of vOX2 and CD200 on CD200R expressed by the T cells can be determined, and those data are presented in the next chapter.

Chapter 7. Modulation of CD200R on T cells by vOX2 and CD200

So far, a suppression of human T cell clone activity by vOX2 and CD200 has been observed (Chapter 5), and is hypothesised to be due to ligation of these proteins with the CD200R, thus leading to downregulation of the TCR signalling cascade (Chapter 6). If CD200R ligation negatively regulates the activity of the T cells, then a modification of CD200R expression by either stimulatory factors (ie, cognate peptide antigen), or putative negative factors (ie. vOX2 and CD200), would alter the ability of vOX2 and CD200 to suppress cell activity. The rationale for these studies was that if downstream signalling events initiated by CD200R ligation underlie the suppression of T cell clone activity, then the possible modulation of CD200R expression should be considered. The regulation of CD200R expression on T cells by native vOX2 or CD200 expressed on the surface of an APC was investigated in both anergising and stimulating systems.

7.1 Determining the percentage of CD200R$^+$ antigen-specific T cells

Initially, the basal expression of CD200R was measured by flow cytometry on *ex vivo* antigen-specific T cells. In order to detect viral antigen-specific $CD8^+$ T cells in EBV- and CMV-infected individuals, PBMCs were isolated from the blood and incubated with MHC-peptide-fluorophore tetramers (Chapter 2.6.2). Briefly, the tetrameric complexes consist of MHC subunits folded with viral antigen peptide, and conjugated to a fluorophore. The cells were then stained with anti-CD8 and anti-CD200R antibodies (Table I, Appendix B). The $CD8^+$ cells were gated upon within the live population. The $CD8^+$ cells were then distributed across a scatter plot by their CD200R or matching isotype control antibody fluorescence, and

antigen tetramer fluorescence. The percentage of $CD200R^+peptide^+$ cells was calculated for each peptide antigen, and the results tabulated (**Table 7.1**).

Approximately 65% of $CD8^+$ T cells from a healthy EBV-seropositive donor (A) express CD200R (**Figure 7.1**, panels **b** and **d**, upper quadrants). Of Donor A's $CD8^+CD200R^+$ T cells, 0.68% were directed against the FLR peptide (**Figure 7.1**, **b**, upper-right quadrant) derived from the EBV latent protein EBNA3A (in comparison to a total 1.04% FLR^+ cells), and 0.42% were specific for the RAK peptide (**Figure 7.1**, **d**, upper-right quadrant) of the lytic protein BZLF1 (0.68% RAK^+ cells in total). Both of these viral peptides are restricted through the same MHC subtype, HLA-B8. Please see Hislop *et al*. (2007) supplemental material for a comprehensive list of EBV antigen peptides and their HLA restriction. Examining the $CD8^+$ T cells isolated from an IM patient (IM135) that are reactive against the same viral antigen peptides, RAK and FLR, revealed a similar pattern (**Figure 7.2**). 89.17% of IM135's $CD8^+$ T cells were CD200R positive (**Figure 7.2**, **b** and **d**, upper quadrants) and the majority of tetramer-positive cells also expressed CD200R. The percentages of peptide-specific $CD8^+CD200R^+$ T cells differed quite markedly between Donor A and IM135. 0.97% of IM135's $CD8^+CD200R^+$ T cells were positive for FLR, of 1.12% FLR^+ cells in total (**Figure 7.2**, **b**, upper-right quadrant), and 15.4% were reactive against RAK, of a total 17.45% RAK^+ cells (**Figure 7.2**, **d**, upper-right quadrant). Donor B exhibited a comparable RAK and FLR staining pattern of their $CD8^+CD200R^+$ cells to Donor A (1.39% FLR^+, 1.07% RAK^+, **Figure 7.3**, b and **d**), as did Donor E (0.92% FLR^+, 2.44% RAK^+, **Figure 7.4**, **b** and **d**).

Donor C also possesses $CD8^+$ $CD200R^+$ RAK and FLR-specific T cells. In addition, this donor's $CD8^+$ T cells were reactive against two CMV proteins; IE1, an immediate early protein (ELK peptide), and the early protein pp50 (VTE peptide) (**Figure 7.5**). See Khan (2007) for a comprehensive list of CMV antigen peptides and their HLA restrictions.

Interestingly, though the ELK peptide is restricted through HLA-B8, similarly to RAK and FLR, VTE is restricted through HLA-A1, and yet there was no alteration in the pattern of CD200R expression. A greater percentage of this donor's $CD8^+CD200R^+$ T cells were reactive to the CMV proteins pp50 (VTE peptide, 4.9%, from a total 7.1%, **Figure 7.5**, **f**) and IE1 (ELK peptide, 7.19% from a total 11.65%, **Figure 7.5**, **h**) than the EBV antigens EBNA3A (FLR peptide, 0.48% from a total 1.01%, **Figure 7.5**, **b**) and BZLF1 (RAK peptide, 1.37% from a total 2.01%, **Figure 7.5**, **d**). Donor D was also seropositive for both CMV and EBV. But this donor's peptide-specific T cells are restricted through alternative HLA epitopes. A high percentage of this individual's T cells were specific for EBV antigen peptides restricted through HLA-B35.01. 1.66% of the $CD8^+CD200R^+$ T cells were specific for the latent antigen EBNA1 (HPV peptide) from a total of 3.1% HPV^+ cells (**Figure 7.6**, **a** and **b**), and another 4.85% (from a total 12.37%) were directed against the EPL peptide derived from the EBV lytic cycle protein BZLF1, rather than RAK (**Figure 7.6**, **c** and **d**). 1.53% of Donor D's $CD8^+CD200R^+$ T cells were directed against a CMV antigen pp65 (NLV peptide), of a total 3.02% NLV^+ cells, restricted through HLA-A2 (**Figure 7.6**, **e** and **f**). $CD8^+CD200R^+$ T cells isolated from Donor F (**Figure 7.7, b** and **d**, upper quadrants) were reactive with CMV antigen peptides YSE (1.3% of a total 2.33% YSE^+ cells, **Figure 7.7**, **b**), derived from the phospho-protein pp65, and VTE (2.53% of a total 4.69%, **Figure 7.7**, **d**), derived from the early protein pp50. Both peptides are restricted through HLA-A1. For all donors examined in this study, between 56.26% and 89.4% of their $CD8^+$ T cells expressed CD200R, and a similar percentage of those T cells directed against viral antigen peptides were positive for the CD200R.

	EBV peptides								CMV peptides							
	FLRGRAYGL		RAKFKQLL		HPVGEADYFEY		EPLPQGQLTAY		VTEHDTLLY		ELKRKMIYM		NLVPMVATV		YSEHPTFTSQY	
	FLR^+	$FLR^+CD200R^+$	RAK^+	$RAK^+CD200R^+$	HPV^+	$HPV^+CD200R^+$	EPL^+	$EPL^+CD200R^+$	VTE^+	$VTE^+CD200R^+$	ELK^+	$ELK^+CD200R^+$	NLV^+	$NLV^+CD200R^+$	YSE^+	$YSE^+CD200R^+$
Donor A	1.04%	72.11%	0.58%	77.59%												
Donor B	1.85%	82.16%	1.31%	90.84%												
Donor C	1.01%	81.19%	2.01%	85.57%					7.10%	81.13%	11.65%	71.16%				
Donor D					3.10%	90.32%	12.37%	95.31%					3.02%	87.42%		
Donor E	1.65%	93.94%	4.40%	84.09%												
Donor F									4.69%	68.02%					2.33%	80.69%
IM135	1.12%	96.43%	17.45%	95.70%												

Table 7.1 Cumulative data illustrating the percentage of primary $CD8^+CD200R^+$ T cells that are directed against EBV or CMV peptide antigens. PBMCs, isolated from six healthy CMV-, EBV-, or dual EBV/CMV-seropositive donors, and an IM patient were stained with both anti-CD8 and anti-CD200R antibodies. To test for antigen specificity the T cells were incubated with EBV/CMV peptide-MHC tetrameric complexes for 15mins at 37°C. The percentage of antigen-specific $CD8^+CD200R^+$ cells was determined by flow cytometry.

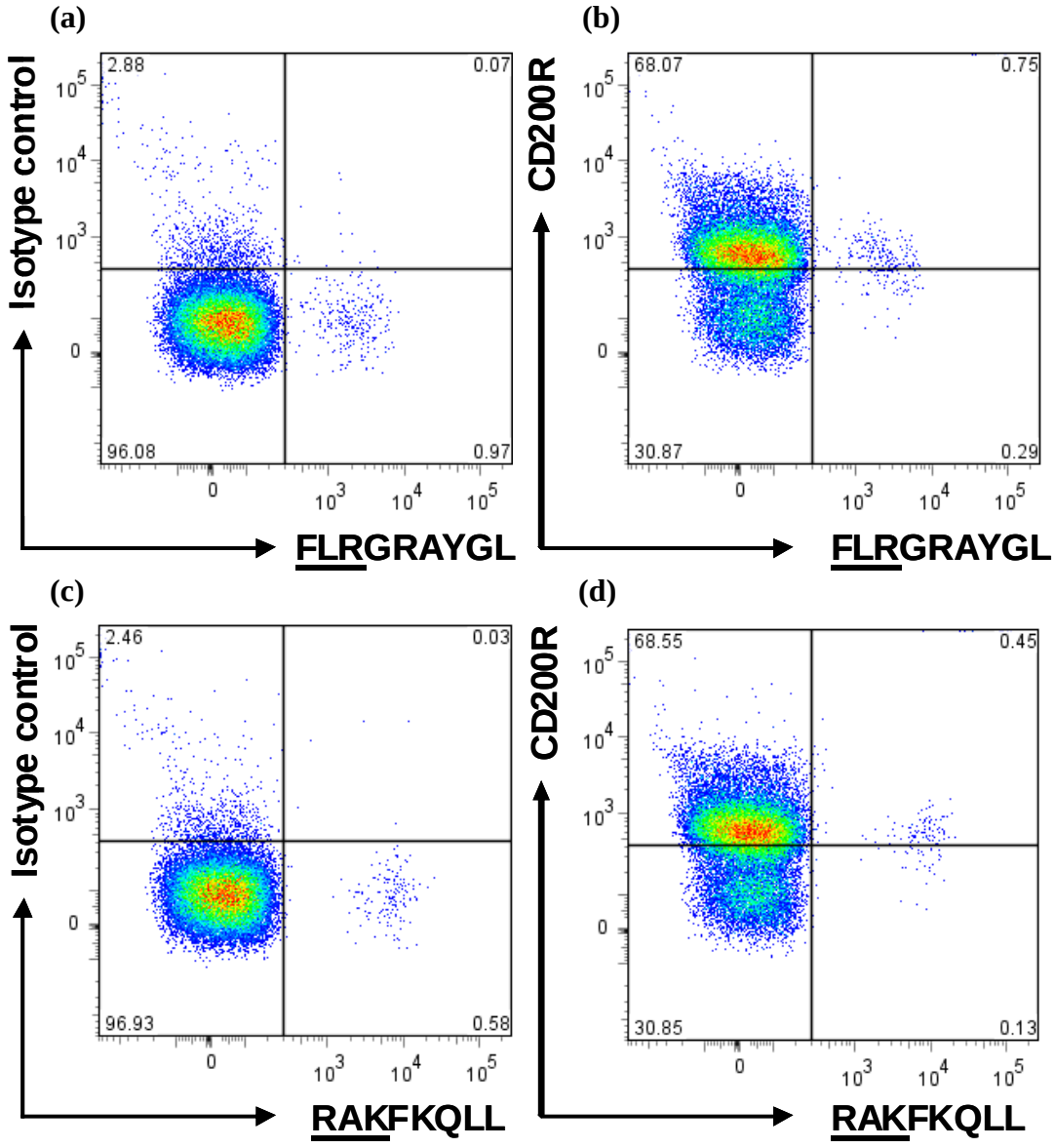

Figure 7.1 EBV peptide antigen-specific CD8$^+$ T cells from a healthy EBV-seropositive donor express CD200R. PBMCs isolated from a healthy EBV-seropositive donor (Donor A), were labelled with an anti-CD8 fluorophore-conjugated antibody, and co-stained with an anti-CD200R antibody (or an isotype control). To test for antigen peptide specificity, the T cells were incubated with EBV peptide-MHC tetrameric complexes for 15mins at 37^{o}C. CD8$^+$ T cells that are dual-positive for both tetramer and CD200R are shown in the upper-right quadrant of each scatter plot. The FLR peptide is derived from the EBV latent protein EBNA3A. In contrast, RAK is derived from a lytic cycle protein, BZLF1. Both peptides are restricted through HLA-B8.

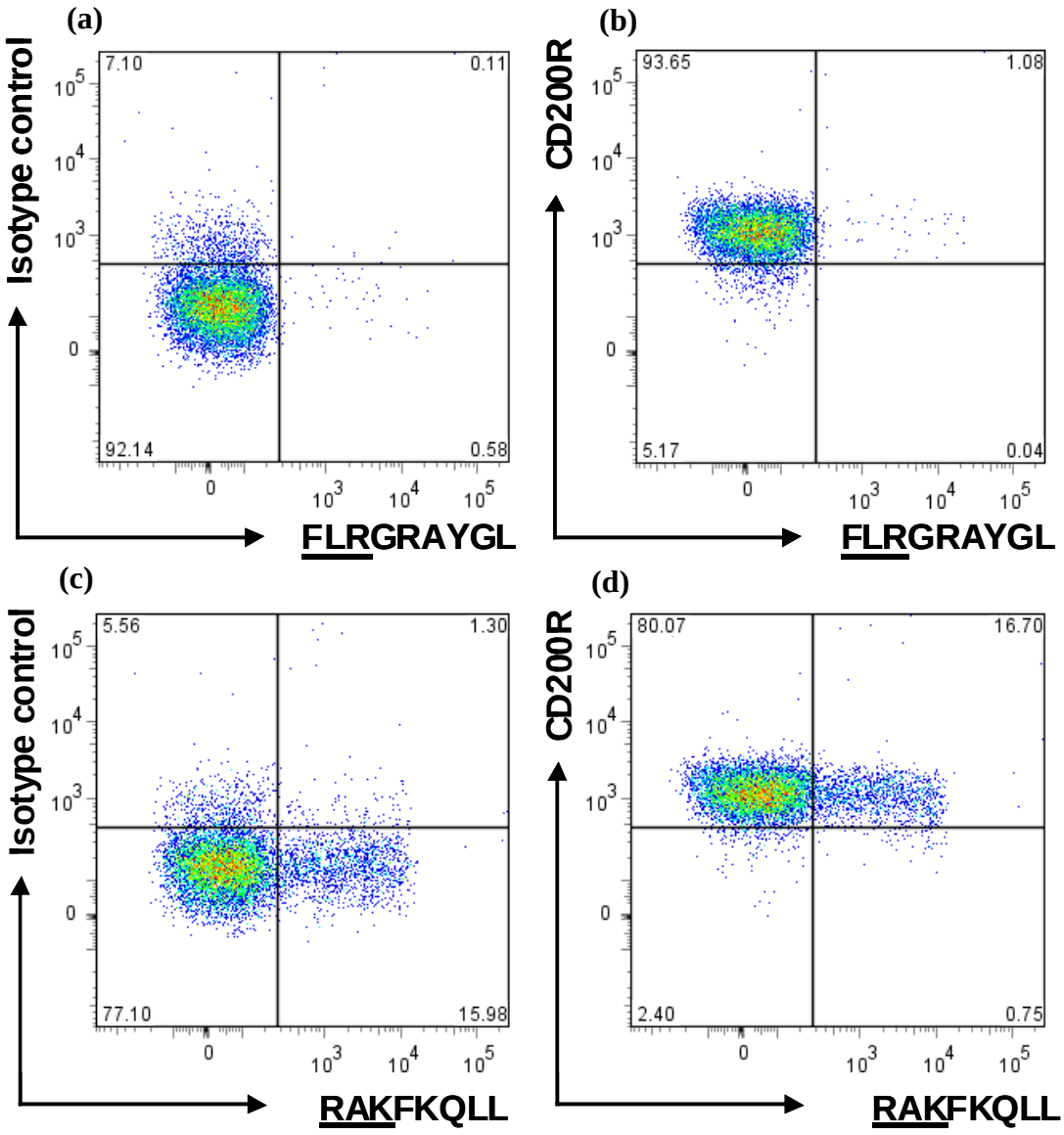

Figure 7.2 EBV peptide antigen-specific CD8$^+$ T cells from an IM patient express CD200R. PBMCs isolated from an IM patient (IM135), were labelled with an anti-CD8 fluorophore-conjugated antibody, and co-stained with an anti-CD200R antibody (or an isotype control). To test for antigen peptide specificity, the T cells were incubated with EBV peptide-MHC tetrameric complexes for 15mins at 37^{o}C. CD8$^+$ T cells that are dual-positive for both tetramer and CD200R are shown in the upper-right quadrant of each scatter plot. The FLR peptide is derived from the EBV latent protein EBNA3A. In contrast, RAK is derived from a lytic cycle protein, BZLF1. Both peptides are restricted through HLA-B8.

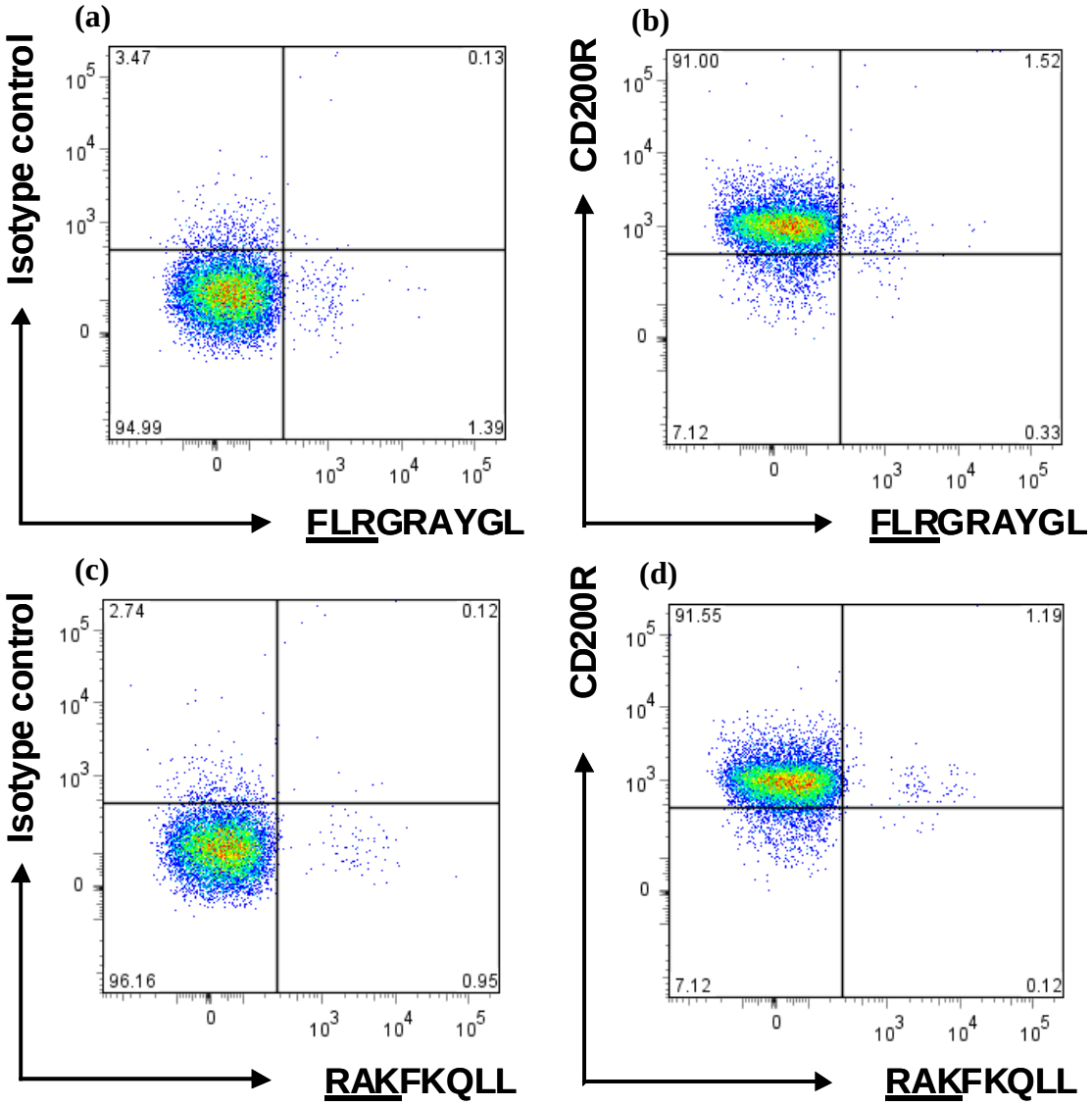

Figure 7.3 EBV peptide antigen-specific CD8$^+$ T cells from a healthy EBV-seropositive donor express CD200R. PBMCs isolated from a healthy EBV-seropositive donor (Donor B), were labelled with an anti-CD8 fluorophore-conjugated antibody, and co-stained with an anti-CD200R antibody (or an isotype control). To test for antigen peptide specificity, the T cells were incubated with EBV peptide-MHC tetrameric complexes for 15mins at 37^{o}C. CD8$^+$ T cells that are dual-positive for both tetramer and CD200R are shown in the upper-right quadrant of each scatter plot. The FLR peptide is derived from the EBV latent protein EBNA3A. In contrast, RAK is derived from a lytic cycle protein, BZLF1. Both peptides are restricted through HLA-B8.

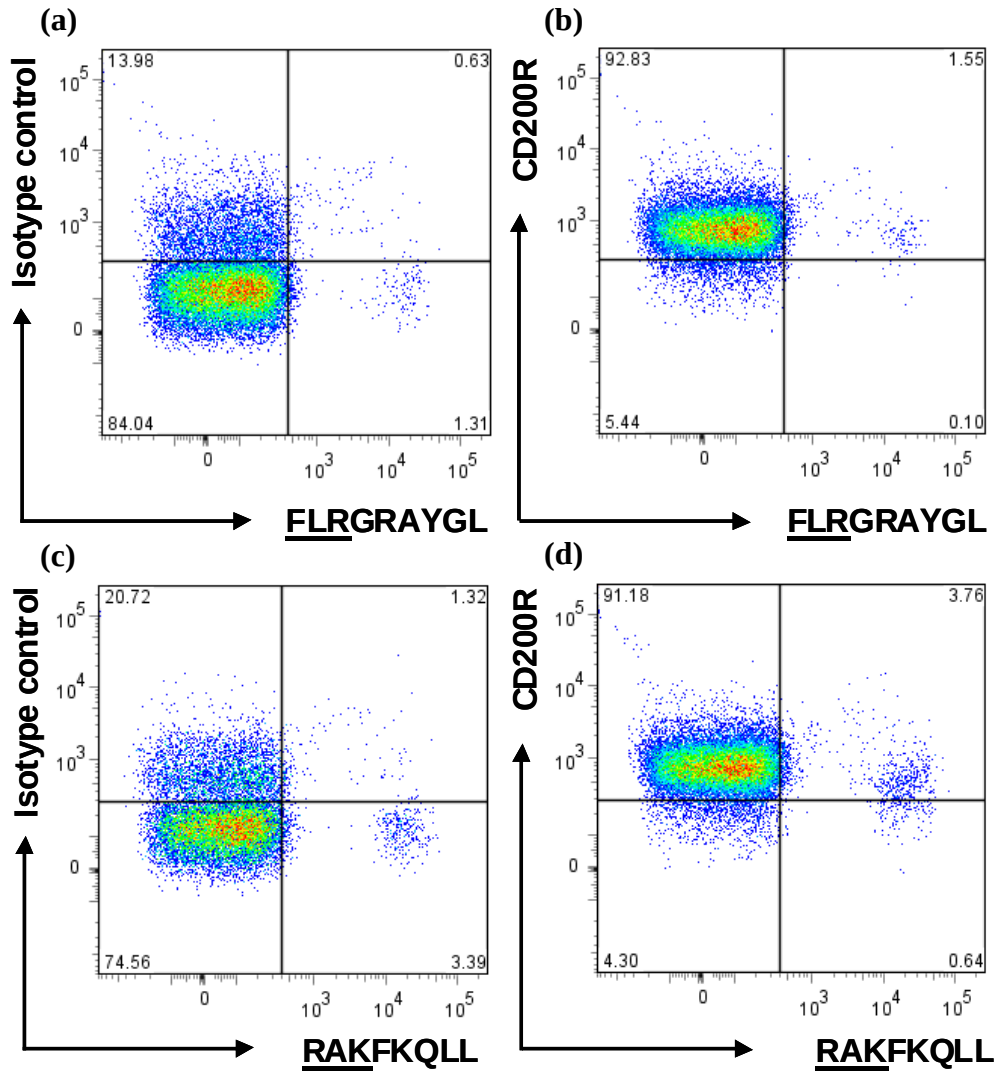

Figure 7.4 EBV peptide antigen-specific CD8$^+$ T cells from a healthy EBV-seropositive donor express CD200R. PBMCs isolated from a healthy EBV-seropositive donor (Donor E), were labelled with an anti-CD8 fluorophore-conjugated antibody, and co-stained with an anti-CD200R antibody (or an isotype control). To test for antigen peptide specificity, the T cells were incubated with EBV peptide-MHC tetrameric complexes for 15mins at 37^{o}C. CD8$^+$ T cells that are dual-positive for both tetramer and CD200R are shown in the upper-right quadrant of each scatter plot. The FLR peptide is derived from the EBV latent protein EBNA3A. In contrast, RAK is derived from a lytic cycle protein, BZLF1. Both peptides are restricted through HLA-B8.

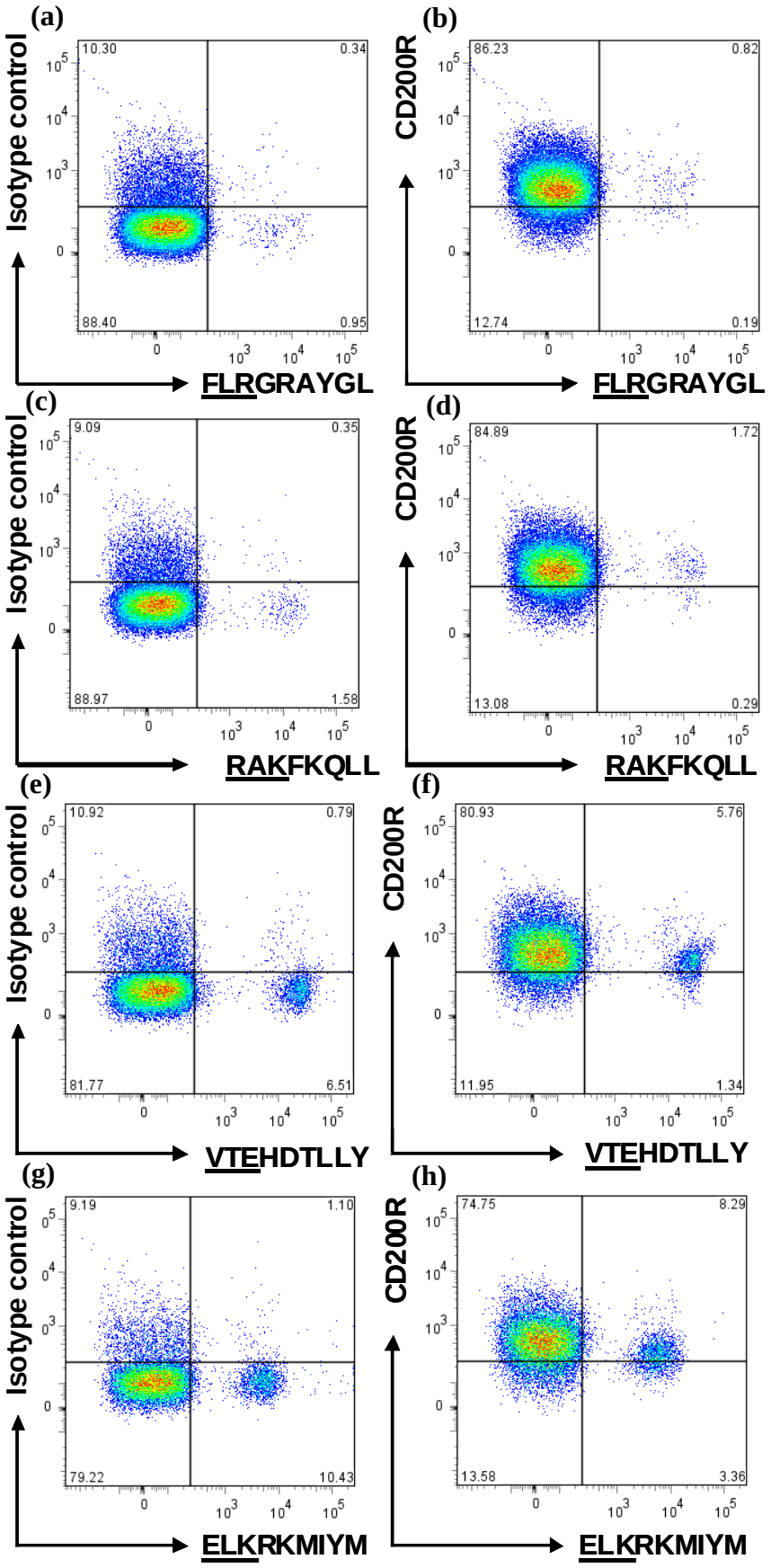
(a)
Isotype control
10.30
0.34
88.40
0.95
FLRGRAYGL
(b)
CD200R
86.23
0.82
12.74
0.19
FLRGRAYGL
(c)
Isotype control
9.09
0.35
88.97
1.58
RAKFKQLL
(d)
CD200R
84.89
1.72
13.08
0.29
RAKFKQLL
(e)
Isotype control
10.92
0.79
81.77
6.51
VTEHDTLLY
(f)
CD200R
80.93
5.76
11.95
1.34
VTEHDTLLY
(g)
Isotype control
9.19
1.10
79.22
10.43
ELKRKMIYM
(h)
CD200R
74.75
8.29
13.58
3.36
ELKRKMIYM

Figure 7.5 EBV and CMV peptide antigen-specific $CD8^+$ T cells from a healthy EBV- and CMV-seropositive donor express CD200R. PBMCs, isolated from a healthy EBV and CMV-seropositive donor (Donor C), were labelled with an anti-CD8 fluorophore-conjugated antibody, and co-stained with an anti-CD200R antibody (or an isotype control). To test for antigen peptide specificity, the T cells were incubated with EBV peptide-MHC tetrameric complexes for 15mins at 37^{o}C. $CD8^+$ T cells that are dual-positive for both tetramer and CD200R are shown in the upper-right quadrant of each scatter plot. The FLR peptide is derived from the EBV latent protein EBNA3A. In contrast, RAK is derived from a lytic cycle protein, BZLF1. Both peptides are restricted through HLA-B8. The ELK peptide is also restricted through HLA-B8 and is encoded as part of the CMV protein IE1, an immediate early protein. VTE peptide is restricted through HLA-A1 and is the product of an early CMV protein, pp50.

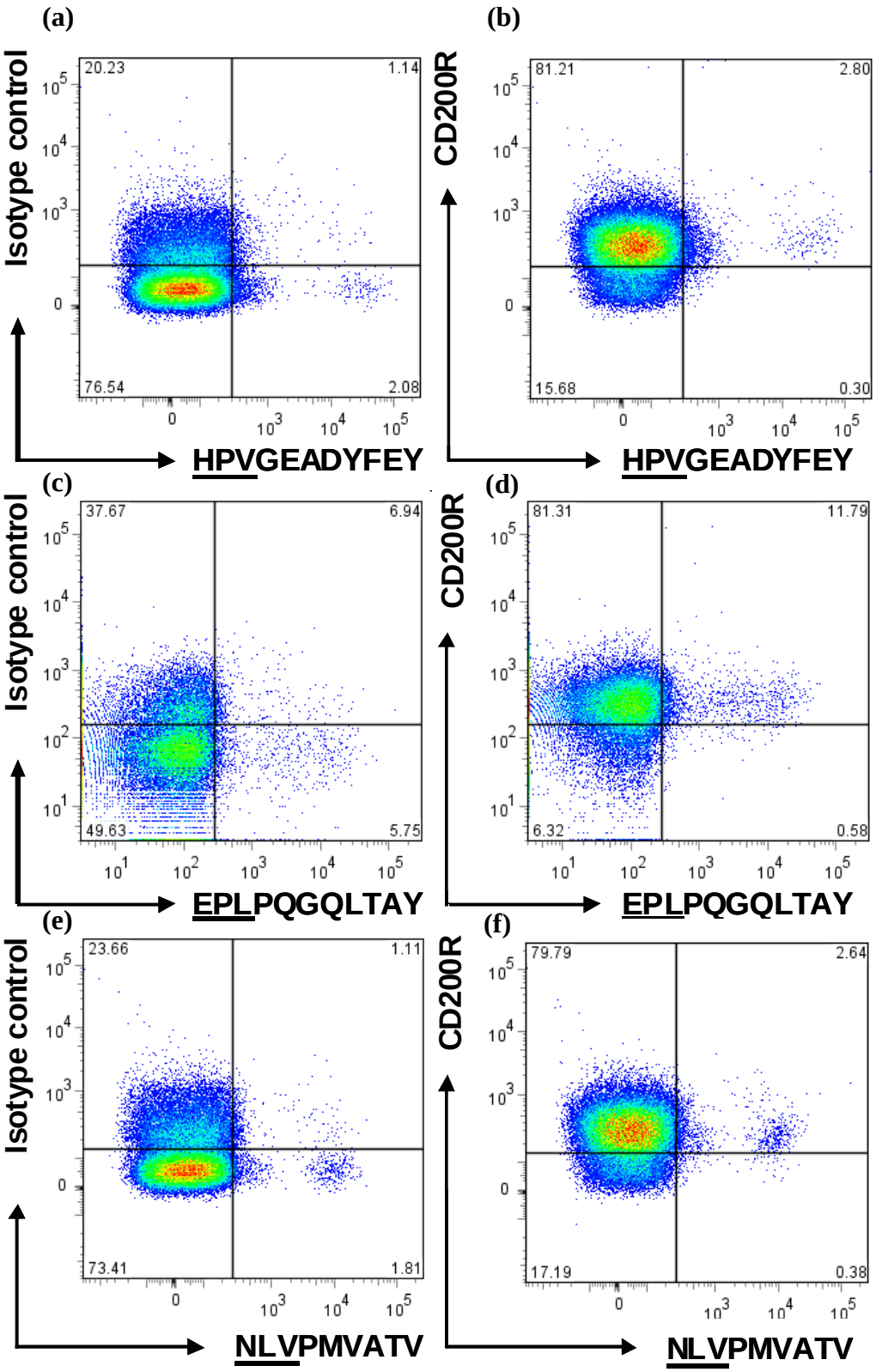

Figure 7.6 EBV and CMV peptide antigen-specific CD8$^+$ T cells from a healthy EBV- and CMV-seropositive donor express CD200R. PBMCs, isolated from a healthy EBV- and CMV-seropositive donor (Donor D), were labelled with an anti-CD8 fluorophore-conjugated antibody, and co-stained with an anti-CD200R antibody (or an isotype control). To test for antigen peptide specificity, the T cells were incubated with EBV peptide-MHC tetrameric complexes for 15mins at 37°C. CD8$^+$ T cells that are dual-positive for both

tetramer and CD200R are shown in the upper-right quadrant of each scatter plot. The NLV peptide is derived from a CMV phospho-protein pp65, and is restricted through HLA-A2. HPV peptide is derived from the EBV latent antigen EBNA1. In contrast, EPL is derived from the lytic protein BZLF1 (coordinates 54-63). Both HPV and NLV are restricted through HLA-B35.01.

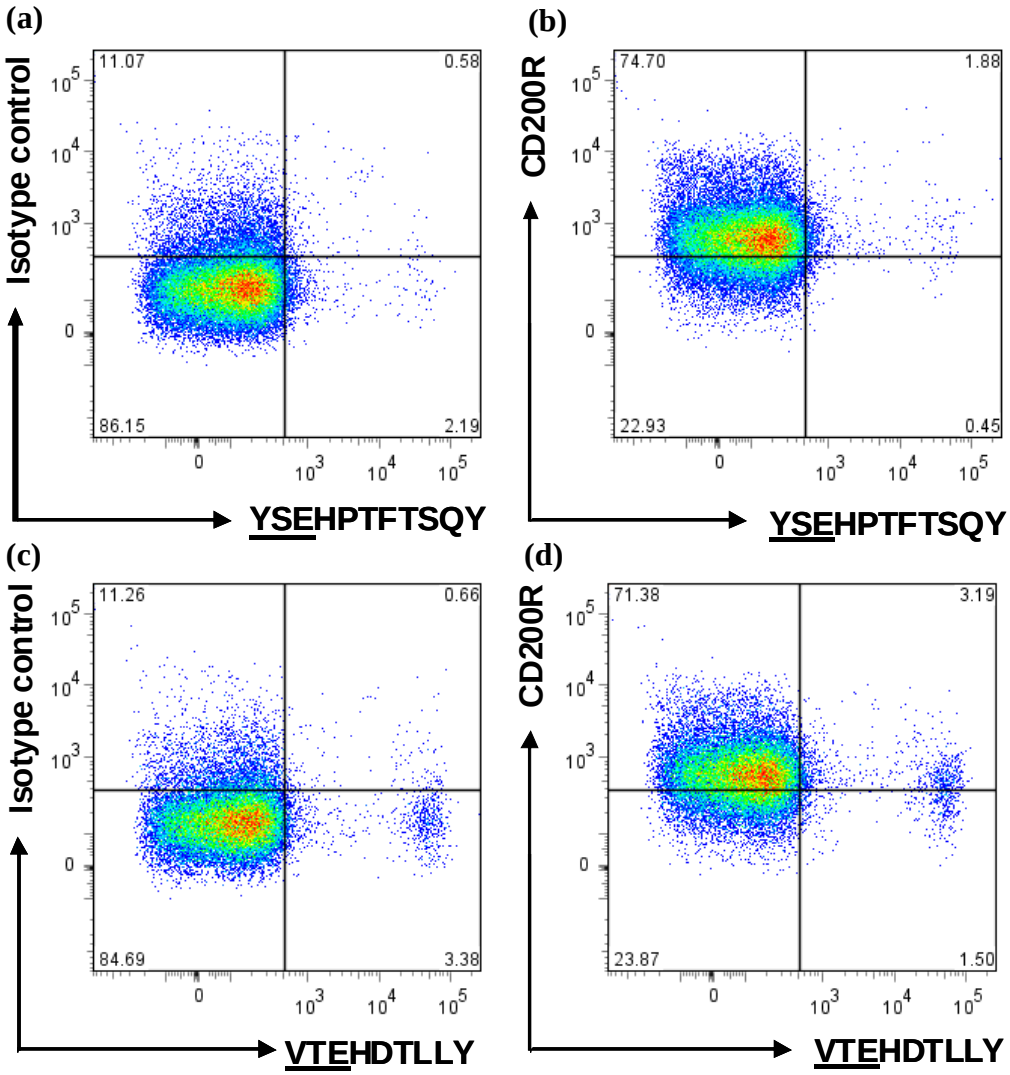

Figure 7.7 CMV peptide antigen-specific CD8$^+$ T cells from a healthy CMV-seropositive donor express CD200R. PBMCs, isolated from a healthy CMV-seropositive donor (Donor F), were labelled with an anti-CD8 fluorophore-conjugated antibody, and co-stained with an anti-CD200R antibody (or an isotype control). To test for antigen peptide specificity, the T cells were incubated with EBV peptide-MHC tetrameric complexes for 15mins at 37^{o}C. CD8$^+$ T cells that are dual-positive for both tetramer and CD200R are shown in the upper-right quadrant of each scatter plot. The VTE peptide is the product of an early CMV protein, pp50. YSE is derived from pp65, a viral phospho-protein. Both peptides are restricted through HLA-A1.

7.2 Basal expression of CD200R, CTLA-4 and CD28 on human antigen-specific T cell clones

In addition to CD200R, T cells express two proteins, CD28 and CTLA-4 that act in opposition to each other, either amplifying the TCR signalling cascade (CD28) and thus enhancing T cell activity, or suppressing TCR-mediated cell activation (CTLA-4). CTLA-4 and CD28 are expressed on the surface of T cells, and compete for the ligands CD80 (B7.1) and CD86 (B7.2) expressed upon the surface of APCs such as dendritic cells, but also on endothelia, macrophages, B and T cells. CD28 is expressed on naïve T cells and is activated by CD80/86 in conjunction with TCR-ligation, enhancing cell metabolism and proliferation (Murphy, 2008). Phosphorylation of the cytoplasmic tail of CD28 following ligation with its cognate ligands enables the recruitment and binding of intracellular signalling molecules such as PI3K. PI3K activation leads to the activation of the protein kinase B (PKB)/Akt pathway, subsequently increasing T cell metabolism by altering several signalling pathways (Rudd *et al*., 2009). In contrast, CTLA-4 is normally absent or at very low levels on the T cell surface (though is constitutively expressed on Tregs), but is upregulated by stimulated T cells. CTLA-4 has a much higher affinity than CD28 for CD80 and CD86. One method by which CLTA-4 inhibits T cell activity is by binding to the TCRζ chain and recruiting negative regulatory phosphatases such as SHP, thus dephosphorylating the initial proteins involved in the TCR signalling cascade including LAT (Lee *et al*., 1998). Both CD28 and CTLA-4 interact with CD80 and CD86 via a conserved amino acid motif, and although CD80 has a higher affinity than CD86 for both receptors, CD86 is more widely expressed (reviewed in Sansom and Walker, 2006). CTLA-4 has traditionally been difficult to detect on the cell surface by flow cytometry. Alegre and colleagues reported that the majority of murine CTLA-4 was localised within the cell, and when expressed on the cell surface, was rapidly endocytosed (Alegre *et al*., 1996).

Borriello and colleagues reported that rCD200 shares some amino acid identity with murine CD80 and CD86, and that all three proteins express extracellular domains composed of IgV- and IgC-like regions (Borriello *et al*., 1997). *rCD200* shared a moderate sequence identity of between 24% and 35% with *CD80* and *CD86*, when the extracellular IgV-like and IgC-like domains were analysed. However, rCD200 did not bind to murine CD28 or CTLA4. Though rCD200 was not a ligand for mCD28, it did induce the proliferation of primary $CD4^+$ murine T cells, similar to CD80-CD28 ligation, though without the concurrent cytokine production that is evident when CD28 is activated. rCD200-mediated T cell proliferation could be inhibited with an anti-rCD200 antibody. Proliferation induced by CD80 was not affected by anti-rCD200, thus confirming that rCD200 did not ligate CD28 (Borriello *et al*., 1997). A putative similarity between CD200 and ligands for CD28 and CTLA-4, further underlines the need to analyse the expression of these receptors on the vOX2 and CD200-suppressible T cell clones.

Initially, the basal levels of CD200R, CD28 and CTLA-4, on $CD8^+$ human T cell clones IM235 c48, c79 and c94, and IM140.1 Y15, in addition to the $CD4^+$ T cell clone SL c93, were quantified by flow cytometry (Chapter 2.6.4).

Though CD200R expression was variable between the $CD8^+$ and $CD4^+$ human T cell clones (**Figure 7.8**), its expression was not found to alter over time post-restimulation (data not shown), or to be related to proliferative potential in culture (data not shown). Basal CD200R expression was quantified for these T cell clones in four independent experiments, at 15, 34 and 45 (carried out twice) days post-restimulation. The data were consistent between each assay; therefore, one representative data set is presented. Both CD200R and CD28 were expressed at variable levels by each clone, but in accordance with the literature, CTLA-4 expression was low or undetectable (**Figure 7.8**).

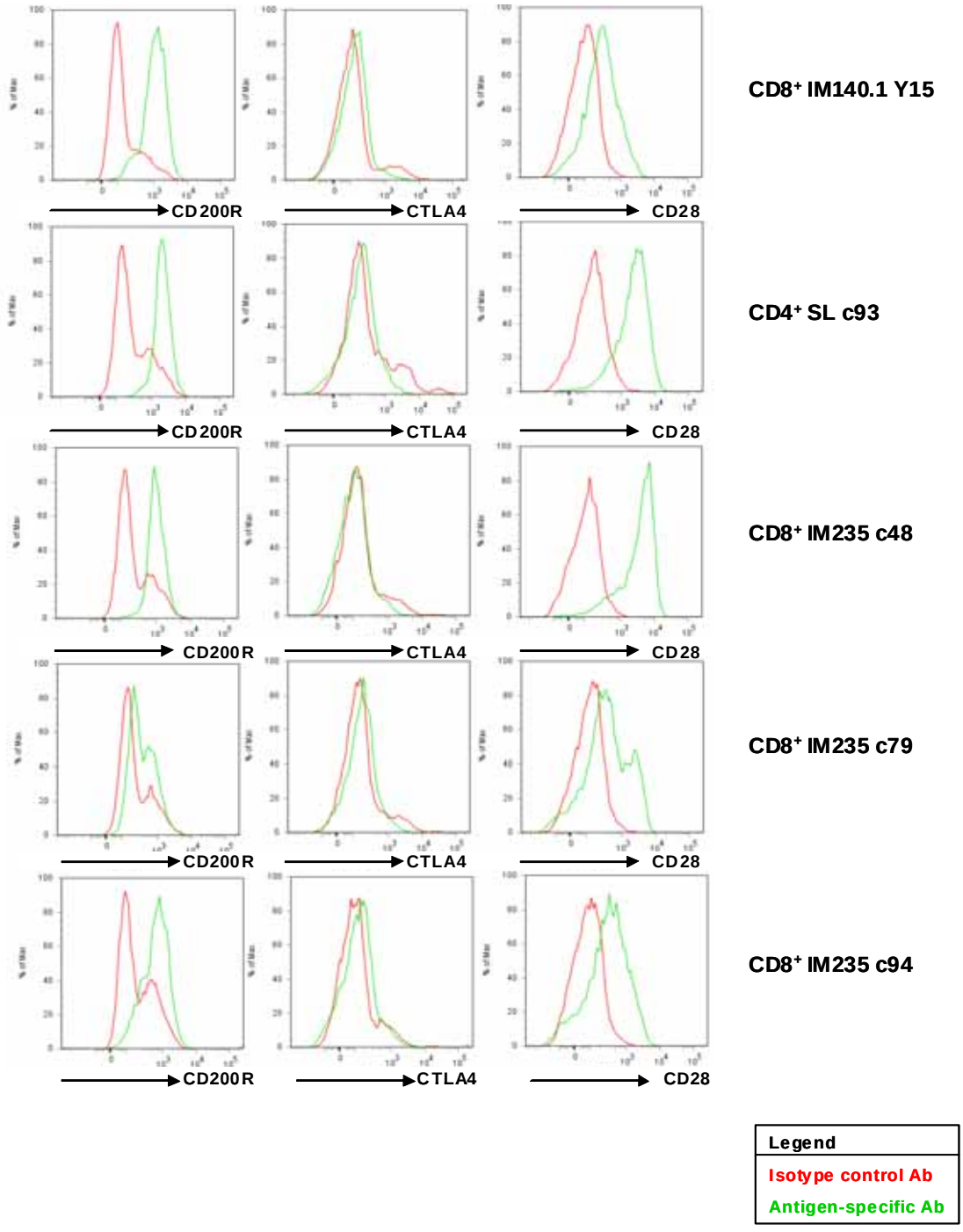

Figure 7.8 Basal expression of CD200R, CTLA-4 and CD28 on human T cell clones. Expression of CD200R, CTLA-4 and CD28 were quantified by flow cytometry for five human T cell clones (34 days after restimulation). These data are representative of four independent experiments analysing CD200R expression, and two independent experiments quantifying CD28 and CTLA-4 expression.

7.3 The regulation of CD200R expression on T cell clones by cognate peptide antigen-stimulation

Having established that CD200R is expressed on antigen-specific $CD8^+$ T cells *ex vivo*, and on human T cell clones, CD200R levels were measured on T cells cocultured with antigen. Initially an antigen-specific murine T cell hybridoma line, B3z, was utilised to optimise the expression assay, and then the human T cell clones were evaluated. Briefly, B3z cells were cultured overnight with either their cognate antigen peptide SIINFEKL, derived from ovalbumin, in the absence of an APC, or with stimulating agents PHA (3μg/ml) or murine IFNγ (200U/ml). An EBV antigen peptide YVLDHLIVV derived from the lytic protein BRLF1 (henceforth referred to as YVL), served as a negative control (Chapter 2.6.3). Flow cytometric analysis of mCD200R1 expression the following day demonstrated that mCD200R1 levels on the cell surface increased in a peptide dose-dependent manner upon stimulation with cognate antigen peptide, by up to 345% ± 86.2 SEM of the untreated control (**Figure 7.9**). The other stimulating agents failed to alter mCD200R1 expression.

A similar experiment was carried out with a YVL-specific human T cell clone (IM140.1 Y15), without APCs. The T cell clones presented peptide to each other in the absence of APCs. Cell death was observed, presumably due to cytotoxic activity of the T cells in culture (data not shown). Surprisingly, with increasing concentrations of cognate peptide, the CD200R surface expression decreased, by up to 47.67% ± 4.18 SEM of the untreated control (**Figure 7.10**). However, CD200R expression also decreased upon stimulation with PHA, to 64.63% ± 1.63 SEM with PHA. Thus, suppression of CD200R expression appeared to correlate with stimulation and not with particular stimuli. However, the suppression of CD200R expression in the presence of an irrelevant EBV antigen peptide (to 73.18% ± 2.96 SEM) is surprising and may be an artefact.

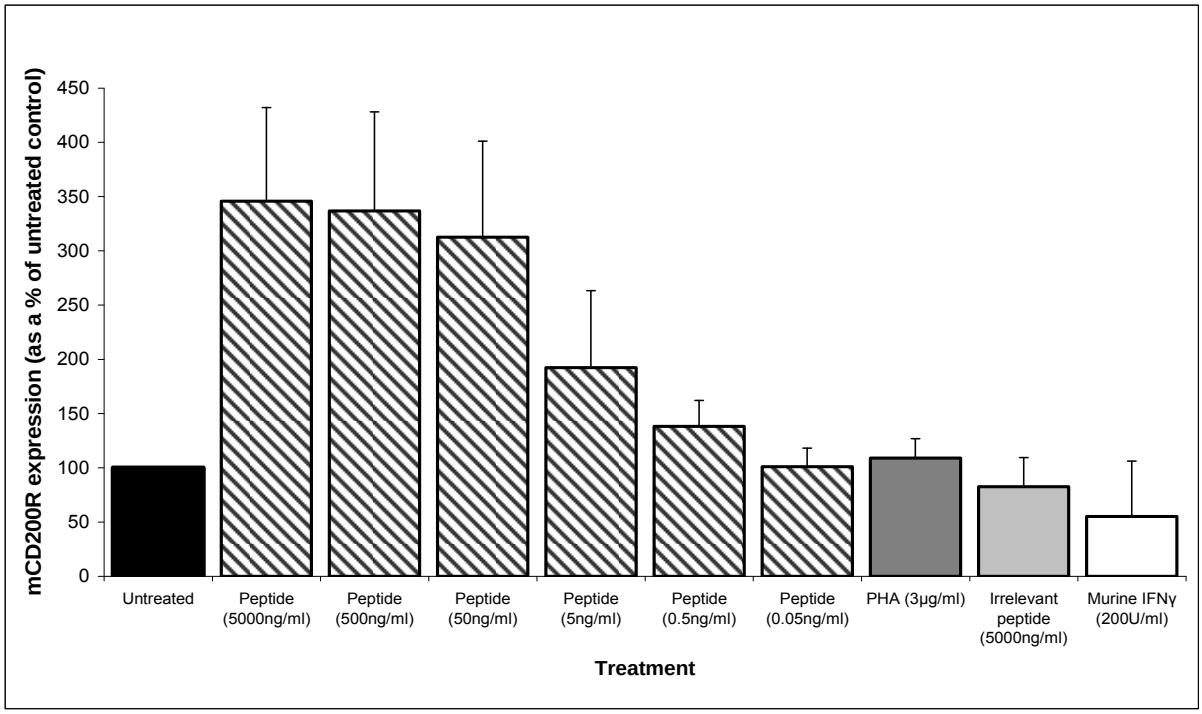

Figure 7.9 Dose-dependent elevated mCD200R expression on antigen-specific murine B3z cells with increased cognate antigen peptide stimulation. Murine B3z (T cell hybridoma) cells were incubated with the cognate peptide antigen SIINFEKL (from chicken egg ovalbumin) at a range of concentrations (16hrs, 37^{o}C). The cells were also stimulated with PHA (3µg/ml) or murine recombinant IFNγ (200U/ml), and an irrelevant EBV peptide (YVLDHLIVV, 5µg/ml), derived from BRLF1, served as a negative control. Cell surface CD200R expression was quantified by flow cytometry, and the data presented as a % of the CD200R expression on untreated cells (median fluorescence minus the fluorescence value of an isotype control for each sample). Data from four independent experiments were pooled and plotted as the mean ± SEM.

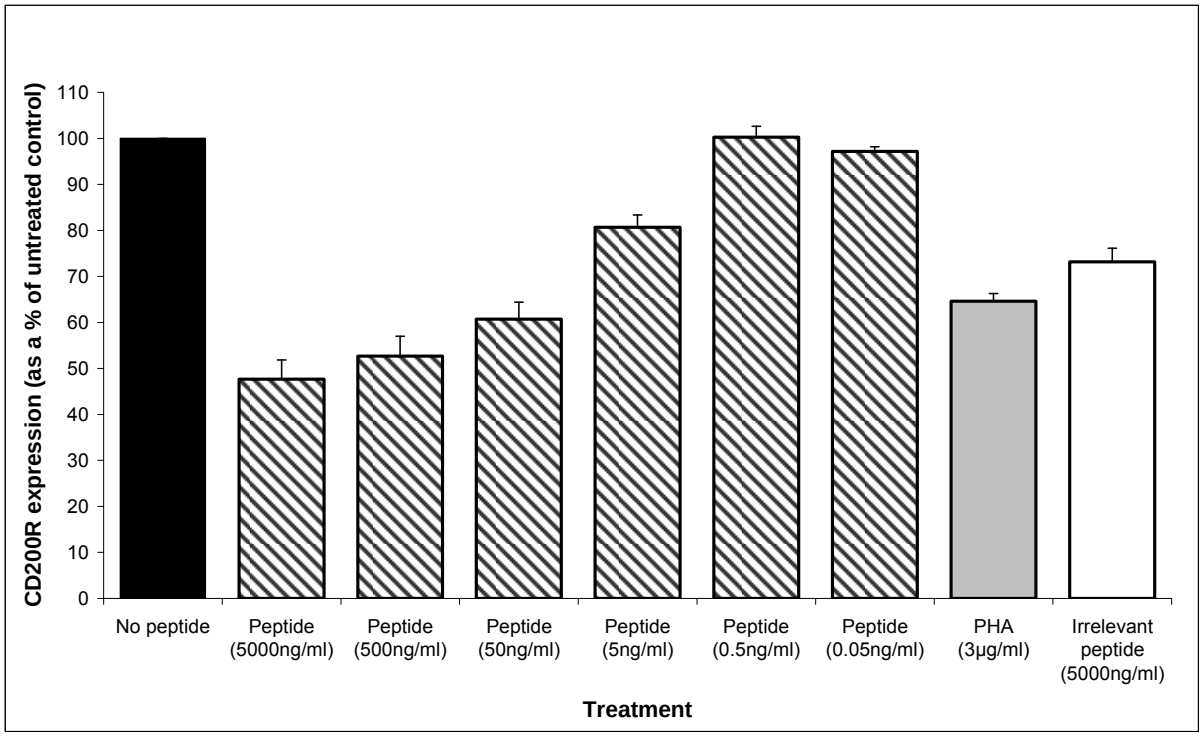

Figure 7.10 CD200R expression on an antigen-specific human T cell clone decreases with increased cognate antigen peptide stimulation. A human T cell clone (IM140.1 Y15) was incubated with its cognate antigen peptide YVLDHLIVV (derived from the EBV lytic cycle protein BRLF1) at a range of concentrations, in the absence of an antigen-presenting cell (16hrs, 37^{o}C). Cell surface CD200R expression was quantified by flow cytometry, and the data presented as a % of the CD200R expression on untreated cells (median fluorescence minus the fluorescence value of an isotype control for each sample). Data from three independent experiments were pooled and plotted as the mean ± SEM.

7.4 vOX2 and CD200-mediated inhibition of CD200R expression

Since human antigen-specific T cell clones were demonstrated to express CD200R, in concert with primary human T cells analysed *ex vivo*, the investigation focused on whether the levels were modulated following the presentation of cognate antigen by HLA-matched APCs. The two T cell clones selected for these assays ($CD8^+$ IM140.1 Y15 and $CD4^+$ SL c93) had been studied exhaustively to determine the modulation of IFNγ and IL-2 secretion (Chapter 5) and downstream signalling events (Chapter 6) by vOX2 and CD200. Briefly,

either BJAB cells expressing vOX2 or CD200, or those transduced with an empty vector, were pulsed with antigen peptide (at the concentration utilised for all signalling assays), washed, and incubated overnight with either of the HLA-matched peptide-specific T cell clones. The following day, surface expression of CD200R, CTLA-4 and CD28 on the T cell clones was determined by flow cytometry, and the T cells identified by labelling with either an anti-CD8 or anti-CD4 antibody. The data were calculated as a percentage of the Empty-BJAB untreated cocultures, data from five independent experiments were pooled, and statistical significance was determined by univariate ANOVA (SPSS software). See Appendix D for the raw data.

CD200R expression on the $CD8^+$ IM140.1 Y15 T cell clone was reduced when the T cells were incubated with either vOX2-BJAB cells (to 46.72% ± 0.82 SEM; ***p<0.001) or CD200-BJAB (to 45.35% ± 2.67 SEM; ***p<0.001), in comparison to untreated Empty-BJAB cocultures (**Figure 7.11**, **a**). This effect was enhanced upon peptide stimulation, and CD200R levels were slightly increased in the Empty-BJAB control culture (to 112.21% ± 7.18 SEM of untreated control). CD200R levels on T cells incubated with peptide-pulsed vOX2-BJAB cells were reduced to only 29.03% 0.54 ± SEM (***p<0.001) of the peptide-pulsed Empty-BJAB control, and were reduced even further in CD200-BJAB cultures, to 27.81% 1.06 ± SEM (***p<0.001) of the control (**Figure 7.11**, **a**). Cell-surface CTLA-4 expression was also reduced in the presence of vOX2 and CD200, to 62.37% ± 0.01 SEM (***p<0.001), and 63% ± 4.13 SEM (***p<0.001) of the Empty-BJAB cocultures, respectively (**Figure 7.11**, **b**). When the APCs were loaded with cognate antigen peptide, CTLA-4 expression was increased in the Empty-BJAB culture (to 138.66% ± 6.16 SEM), but was still considerably reduced in the presence of vOX2 and CD200, to 51.61% ± 6.5 SEM (**p<0.01) and 59.13% ± 3.64 SEM (**p<0.01) of the peptide-stimulated control respectively. In contrast, CD28 expression was unchanged when the $CD8^+$ T cells were

incubated with vOX2-BJAB or CD200-BJAB, in the absence of stimulation (**Figure 7.11**, **c**). CD28 levels rose when the T cells were stimulated with Empty-BJAB pulsed with cognate antigen peptide (130.59% ± 7.47 SEM), were marginally reduced in the presence of vOX2 (83.94% ± 12.98 SEM) but were unchanged in response to CD200 (96.95% ± 8.82 SEM), in comparison to the peptide-treated Empty-BJAB control.

A similar pattern was observed in the $CD4^+$ T cell clone, SL c93 (**Figure 7.12**), although CD200R expression was not enhanced in the peptide-pulsed control culture (89.9% ± 4.76 SEM of untreated control). Again, CD200R on the surface of T cells was reduced in the presence of vOX2-BJAB (**Figure 7.12**, **a**) in the absence of peptide (to 48.25% ± 2.45 SEM of control; ***$p<0.001$) and with peptide stimulation (33.9% ± 1.4 SEM; ***$p<0.001$). CD200-expressed by BJAB cells also downregulated CD200R expression (**Figure 7.12**, **a**), to 44.78% ± 2.2 SEM of control (***$p<0.001$) in the absence of peptide, and to 30.08% ± 2.55 SEM of control (***$p<0.001$) following stimulation with cognate antigen. CTLA-4 expression on the T cells was increased by stimulation with peptide-loaded Empty-BJAB, to 122.27% ± 6.19 SEM of the untreated control, and again, was downregulated in the presence of vOX2-BJAB (to 64.03% ± 1.8 SEM untreated, ***$p<0.001$ and 66.91% ± 3.26 SEM, stimulated, *$p<0.05$) or CD200-BJAB (to 61.41% ± 2.15 SEM untreated, ***$p<0.001$ and 66.87% ± 6.84 SEM stimulated, *$p<0.05$), with or without cognate antigen peptide (**Figure 7.12**, **b**). CD28 expression was unaltered, or slightly reduced on vOX2 or CD200-treated $CD4^+$ T cells (**Figure 7.12**, **c**). CD28 levels were reduced upon peptide stimulation (to 87.75% ± 5.72 SEM of the untreated Empty-BJAB control), but were not reduced further in the presence of peptide-loaded vOX2-BJAB (94.42% ± 0.64 SEM of peptide-treated control) or CD200-BJAB (108.42% ± 4.03 SEM of control) cells.

(a) CD200R

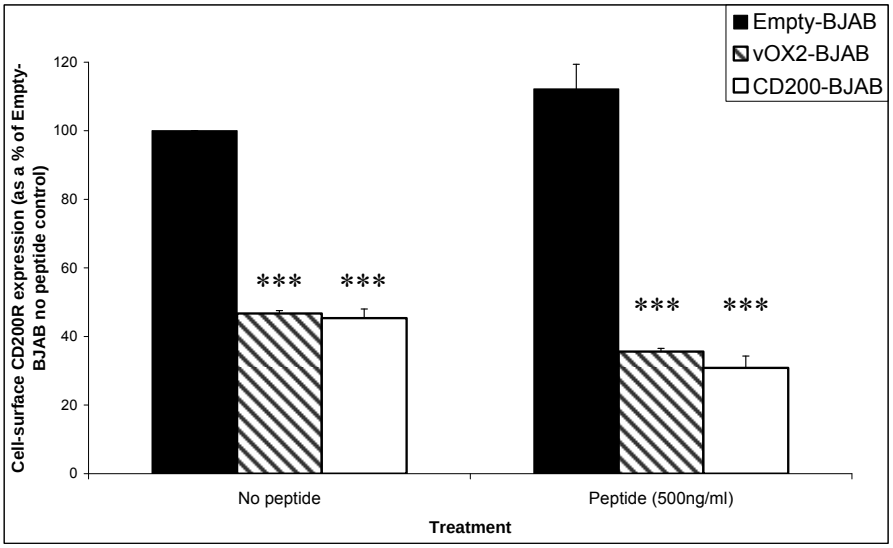

(b) CTLA-4

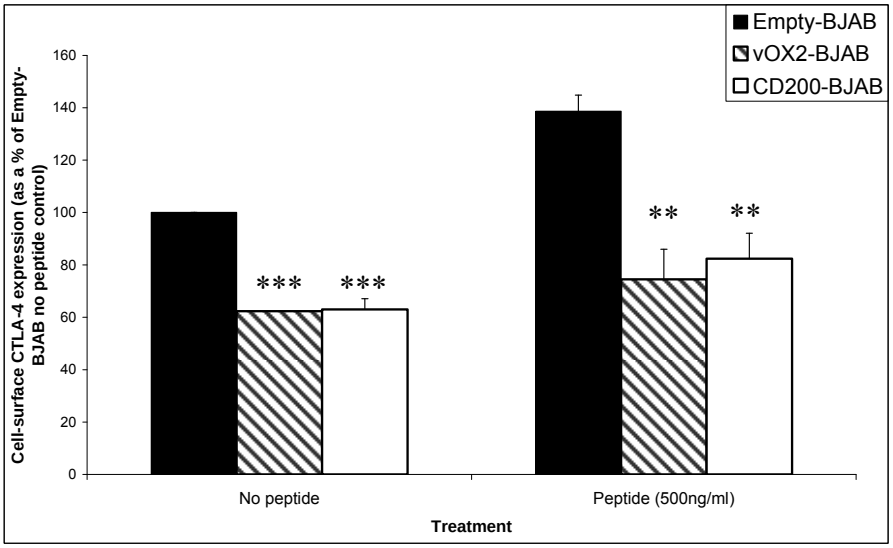

(c) CD28

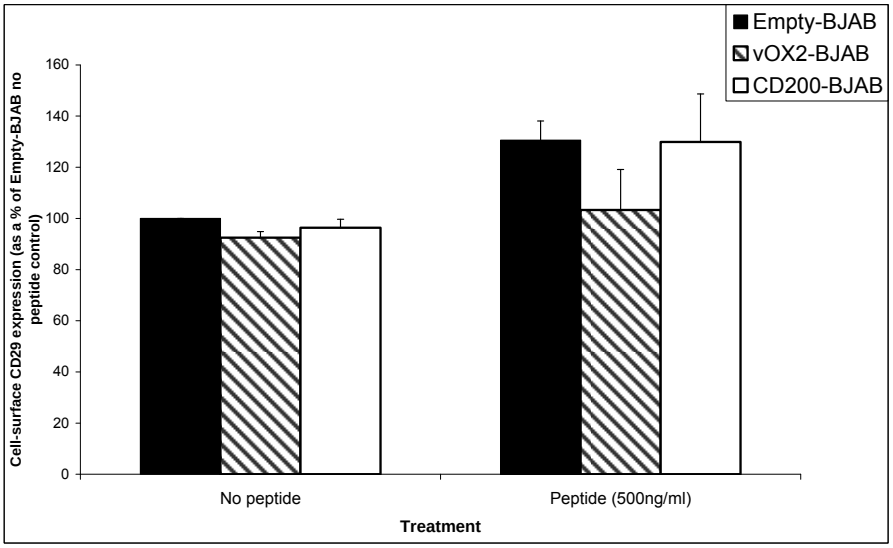

Figure 7.11 CD200R and CTLA-4 expression on the $CD8^+$ IM140.1 Y15 T cell clone are reduced when vOX2 or CD200 are expressed on the co-cultured antigen-presenting cell. Empty-BJAB, vOX2-BJAB and CD200-BJAB cells were left untreated, or pulsed with YVLDHLIVV peptide (derived from the EBV antigen BRLF1). Excess peptide was then washed off and the BJAB cells cultured overnight with the $CD8^+$ IM140.1 Y15 T cell clone specific for the YVL peptide. **(a)** CD200R, **(b)** CTLA-4 and **(c)** CD28 expression levels were quantified the next day for the $CD8^+$ population by flow cytometry and the data pooled and expressed as a % of the expression on untreated $CD8^+$ T cells cocultured with Empty-BJAB cells. Four independent experiments were carried out. CD200-BJAB co-cultures were analysed in three of those experiments, and vOX2-BJAB in two. Both vOX2 and CD200-BJAB significantly suppressed CD200R expression in comparison to Empty-BJAB, both in the absence ($F(2, 8) = 443.85$; $^{***}p < 0.001$ for both) and presence ($F(2, 8) = 60.78$; $^{***}p < 0.001$ for both) of peptide, when analysed by a univariate ANOVA test (SPSS software). Both vOX2 and CD200-BJAB significantly suppressed CTLA-4 expression in comparison to Empty-BJAB, both in the absence ($F(2, 8) = 90.54$; $^{***}p < 0.001$ for both) and presence ($F(2, 8) = 18.51$; $^{**}p < 0.01$ for both) of peptide, when analysed by a univariate ANOVA test (SPSS software). Neither vOX2 nor CD200 significantly altered the expression of CD28 ($p=0.12$ in the absence of peptide and $p=0.41$ with peptide treatment).

(a) CD200R

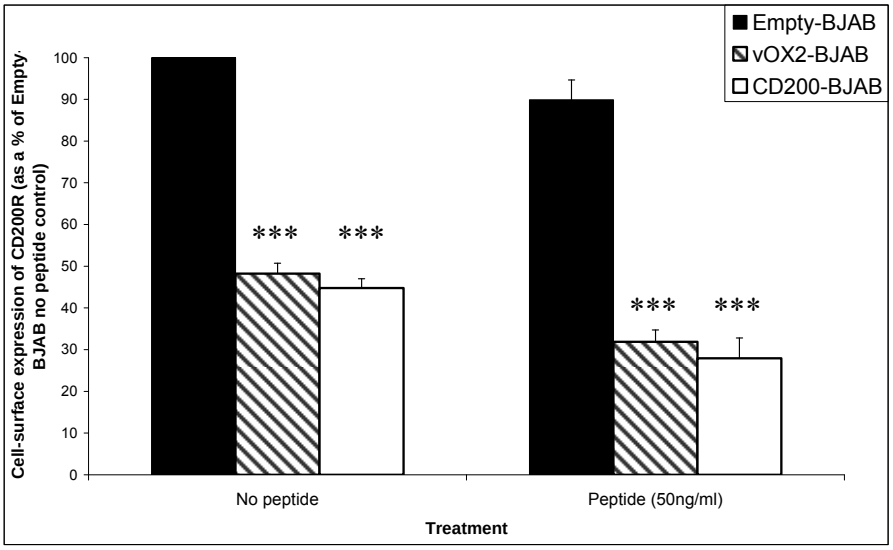

(b) CTLA-4

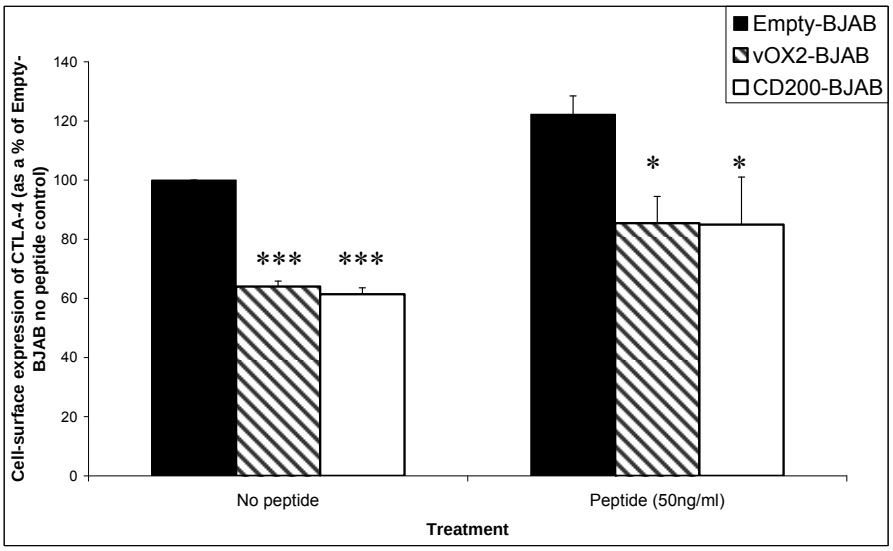

(c) CD28

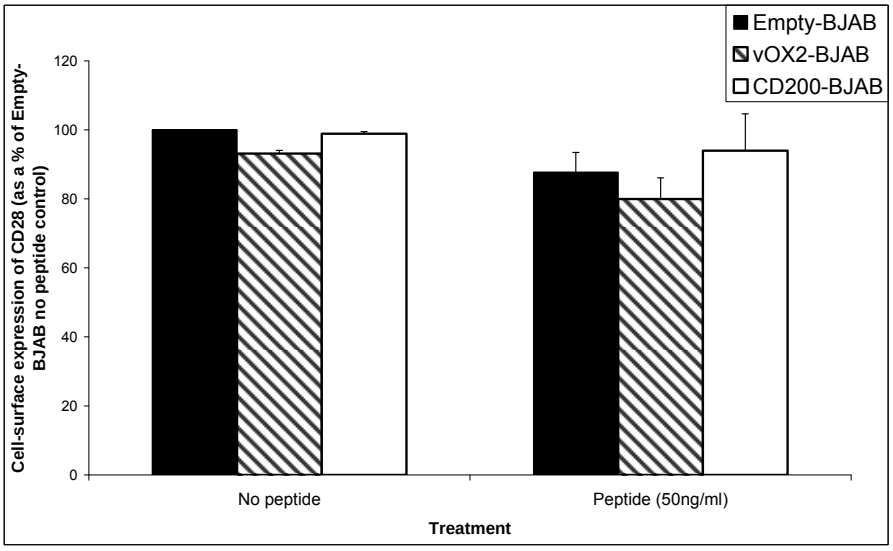

Figure 7.12 CD200R and CTLA-4 expression on the $CD4^+$ SL c93 T cell clone are reduced when vOX2 or CD200 are expressed on the co-cultured antigen-presenting cell. Empty-BJAB, vOX2-BJAB and CD200-BJAB cells were left untreated or pulsed with PRSTVFYNIPPMPLPPSQL peptide (derived from the EBV antigen EBNA2). Excess peptide was then washed off and the BJAB cells cultured overnight with the $CD4^+$ SL c93 T cell clone specific for the PRS peptide. **(a)** CD200R, **(b)** CTLA-4 and **(b)** CD28 expression levels were quantified the next day for the $CD4^+$ population by flow cytometry and the data pooled and expressed as a % of the expression on untreated cells co-cultured with Empty-BJAB cells. Five independent experiments were carried out; both vOX2 and CD200-BJAB co-cultures were analysed in three experiments. Both vOX2 and CD200-BJAB significantly suppressed CD200R expression in comparison to Empty-BJAB, both in the absence ($F(2, 8) = 481.20$; ***$p < 0.001$ for both) and presence ($F(2, 8) = 61.01$; ***$p < 0.001$ for both) of peptide, when analysed by a univariate ANOVA test (SPSS software). Both vOX2 and CD200-BJAB significantly suppressed CTLA-4 expression in comparison to Empty-BJAB, both in the absence ($F(2, 8) = 319.46$; ***$p < 0.001$ for both) and presence ($F(2, 8) = 5.34$; *$p < 0.05$ for both) of peptide, when analysed by a univariate ANOVA test (SPSS software). Neither vOX2 nor CD200 altered the expression of CD28 ($p=0.12$ in the absence of peptide, and $p=0.28$ with peptide treatment).

7.5 Discussion

The data presented in this chapter confirm that the majority of primary human $CD8^+$ T cells express the CD200R on their surface. Moreover, most $CD8^+$ T cells specific for a particular viral antigen were also $CD200R^+$. The percentage of T cells reactive against each viral peptide differed between donors. Taking the BZLF1 RAK peptide as an example, approximately 0.6% of Donor A's $CD8^+$ T cells were specific for this peptide (**Figure 7.1**), in comparison to ~1.3% of Donor B's cells (**Figure 7.4**), and 17% of the IM patient $CD8^+$ T cells (**Figure 7.2**). In contrast, only approximately 1% of IM135 $CD8^+$ T cells were directed against the latent antigen EBNA3A FLR peptide, with a similar frequency to Donor A (~1%) and Donor B (~2%%). The high percentage of IM T cells directed against an EBV immediate-early lytic protein, BZLF1 (RAK) corresponds with a previous report (Steven *et al*., 1997). Presumably it represents a response to the lytically replicating virus during IM pathogenesis.

Responses to EBV latent proteins are usually smaller than the more dominant lytic response (Hislop *et al*., 2007), and the number of $CD8^+$ T cells directed against CMV antigens is generally higher than those specific for EBV (Khan, 2007). In fact, CMV infection alters the total lymphoid population, increasing the number of circulating $CD8^+$ and $CD4^+$ memory T cells, NK cells, and B cells with age (Chidrawar *et al*., 2009). The data of the present study are consistent with these reports (**Table 7.1**), and demonstrate that most viral antigen-specific T cells express CD200R. The lack of readily available KSHV tetramers precluded determining the pattern of CD200R expression on T cells directed against this virus.

Cultured murine T cell hybridoma cells express mCD200R1. The observed upregulation of mCD200R1 on the surface of stimulated murine T hybridoma cells (**Figure**

7.9) is consistent with reports in the literature. Torrero and colleagues demonstrated that stimulating murine basophils in whole blood by both IgE-independent and IgE-dependent means resulted in an upregulation of cell surface mCD200R1, and an increase in the percentage of mCD200R1^{+} cells (Torrero *et al*., 2009). mCD200R1 was also upregulated on basophils *in vivo*, in response to infection with a parasitic nematode, and in an allergic model (sensitisation to ovalbumin). mCD200R1 expression peaked after 1-2hrs of stimulation, and was undetectable after 4hrs, indicating rapid cycling of the receptor to and from the plasma membrane (Torrero *et al*., 2009). The data of the present study are inconsistent with these of Torrero *et al*., since mCD200R1 expression increased over 16hrs post-stimulation.

The opposite result was obtained when human T cell clones were stimulated. Self-presentation of cognate antigen peptide caused a dramatic reduction in CD200R levels (**Figures 7.10/11/12**). In contrast to the study of Torrero (Torrero *et al*., 2009), Masocha observed that the *in vivo* LPS-mediated stimulation of murine microglia in the CNS reduced mCD200R1 mRNA levels (Masocha, 2009). mCD200R1 mRNA levels were significantly diminished 4hrs post-LPS treatment, and were still lower than control levels when the animals were sacrificed one year later. These findings are more consistent with those of the present study. In humans, CD200R expression in the CNS is dysregulated in the brains of Alzheimer's Disease (AD) patients (Walker *et al*., 2009). The chronic inflammation in AD brains, concomitant with reactive microglia and astrocytes, is associated with reduced neuronal CD200 and reduced neuronal, macrophage and microglial CD200R expression. Anti-inflammatory cytokines IL-4 and IL-13 amplify macrophage and microglial CD200R levels. The near absence of IL-4 in AD and elderly brains may therefore account at least in part for attenuated CD200R expression, and an inflammatory phenotype (Walker *et al*., 2009). In fact, LPS-induced microglial IL-1β secretion is attenuated by co-culture with wild-type neurons, but not with neurons isolated from IL-4$^{-/-}$ mice, expressing lower levels of

mCD200 (Lyons *et al*., 2009). To corroborate this finding, the inhibitory effect of wild-type neurons on activated microglia can be blocked with an anti-mCD200 antibody (Lyons *et al*., 2009). Furthermore, inflammation in the murine CNS induced by proinflammatory cytokines in response to a mechanical stress (foot shock) also attenuated mCD200R1 expression by hypothalamic microglia (Blandino *et al*., 2009).

So, in humans and mice inflammation in the CNS appears to correlate with reduced CD200R expression. In the present study, CD200R expressed by the $CD8^+$ IM140.1 Y15 T cell clone decreased upon self-presentation of cognate antigen (**Figure 7.10**), but it did not reduce when cognate antigen was presented to the $CD8^+$ IM140.1 Y15 and $CD4^+$ SL c93 T cell clones by HLA-matched APCs (**Figure 7.11**, **a**, and **Figure 7.12**, **a**). This result is surprising, because stimulated T cells secrete cytokines such as IFNγ, thus creating an inflammatory environment. However, surface CD200R expression was significantly reduced in the presence of either vOX2 or CD200, with and without peptide stimulation (**Figure 7.11**, **a**, and **Figure 7.12**, **a**). This correlates somewhat with data published by Rygiel, who demonstrated that CD200R expression increases on T cells in the absence of CD200 (Rygiel *et al*., 2009). The number of $mCD200R1^+$ T cells were amplified in *mCD200*$^{-/-}$ mice exhibiting a severe pathology in response to influenza infection (Rygiel *et al*., 2009). These data would suggest that the presence of CD200 negatively regulates CD200R expression, and data from the present study indicate that vOX2 acts in a similar fashion.

Consistent with the literature, CTLA-4 expression was barely detectable (Alegre *et al*., 1996), on human T cell clones. However, CTLA-4-expression was detectable on T cell clones cultured with BJAB cells, and its expression was significantly downregulated on the surface of T cells incubated with vOX2 or CD200-expressing APCs (**Figure 7.11, b**, and **Figure 7.12**, **b**), similar to the downregulation of CD200R. Downregulation of CTLA-4 expression has been observed *in vivo*. Flores-Borja and colleagues reported reduced CTLA-4

expression on regulatory T cells isolated from RA patients, though CD28 expression was unaltered (Flores-Borja *et al*., 2008). Similarly, CD28 expression was not altered by peptide stimulation in the present study, nor by either vOX2 or CD200 (**Figure 7.11, c**, and **Figure 7.12**, **c**), concurring with current opinion that CD28 is expressed on T cells regardless of their activation state (Rudd *et al*., 2009). The downregulation of CTLA-4 on RA Tregs was due to rapid internalisation, but it was restored to the surface of the cell by PMA treatment (Flores-Borja *et al*., 2008). Reduced CTLA-4 expression was also observed on umbilical cord blood T cells, but was reduced further upon stimulation of these cells (Miller *et al*., 2002).

Jago and colleagues examined basal levels of CTLA-4 on several T cell subsets (Jago *et al*., 2004). T cell clones and memory T cells have large reservoirs of intracellular CTLA-4, which is mobilised to the cell surface upon PMA stimulation (Jago *et al*., 2004). Cycling of CTLA-4 to the cell surface appears to be regulated by a transmembrane protein, the T cell receptor-interacting molecule (TRIM), which binds to CTLA-4 by a mechanism independent of its binding to the TCR/CD3 complex (Valk *et al*., 2006). CTLA-4 is removed from the plasma membrane via binding of the clathrin adaptor protein AP-2 to an intracellular motif; phosphorylation of this motif prevents AP-2 binding and thus leads to retention of CTLA-4 on the cell surface (Valk *et al*., 2008). Therefore, the downregulation of CTLA-4 on the surface of the $CD8^+$ IM140.1 Y15 and $CD4^+$ SL c93 T cell clones incubated with vOX2-BJAB and CD200-BJAB cells may be due to increased internalisation, presumably in response to a negative stimulus being provided by CD200R ligation. CTLA-4 internalisation appears to be due to its dephosphorylation, subsequently enabling binding to AP-2 and cycling back to the endosomes (Rudd *et al*., 2009). Activated mCD200R1 recruits phosphatases such as SHIP (Zhang *et al*., 2004) and human CD200R ligation reduces the phosphorylation of kinases ERK1/2 and Akt (Chapter 6). Therefore, a potential mechanism

for the downregulation of CTLA-4 expression is its dephosphorylation as a result of the CD200R signalling pathway. The consistent expression of CD28 on the T cells (**Figure 7.11**, **c**, and **Figure 7.12**, **c**) is consistent with the literature (Rudd *et al*., 2009). Because CTLA-4 has a much higher affinity for CD80 and CD86, ligands that CD28 and CLTA-4 compete for (Bhatia *et al*., 2006), surface CTLA-4 must be downregulated in order for CD28 to function.

CTLA-4 is expressed on activated T cells and is barely present on the surface of unstimulated cells (apart from Tregs). Antigen-specific T cell clones are maintained in an activated state due to regular restimulation, and the presence of cytokines such as IL-2 in the culture medium. Therefore the downregulation of CTLA-4 on T cell clones in the presence of vOX2 and CD200 may be a restoration of basal levels. However, as observed in the present studies, CTLA-4 expression was barely detectable on the surface of the T cell clones (**Figure 7.8**) indicating that its expression may not be much higher than on resting T cells. The downregulation of two inhibitory molecules, CD200R and CTLA-4 (and no alteration in the expression of CD28, an activatory coreceptor), on the surface of T cell clones in the presence of vOX2 and CD200, with and without antigen, suggests that vOX2 and CD200 inhibit the activity of the T cells. Subsequent downregulation of the inhibitory receptors would prevent aberrant inhibition of cell activity. CTLA-4 is naturally downregulated on resting T cells, and upregulated on activated cells, concurring with our hypothesis that in the presence of putative inhibitory factors, vOX2 and CD200, CTLA-4 expression is reduced. Thus CD200R may be regulated in a similar fashion to CTLA-4, ie. it is downregulated following binding to its ligands, to prevent over-inhibition of T cell activity.

Chapter 8. RRV and CMV homologues of CD200

So far a role for KSHV vOX2 and its cellular counterpart CD200 in the suppression of human T cell clone activity has been identified. Homologues of human CD200 have been identified in other viruses though their mechanisms of action have not been exhaustively researched (some of these are mentioned in Chapter 1). Thus, the little-researched RRV CD200-like protein, and three putative human CMV CD200-like proteins were analysed with respect to their ability to modulate T cell clone activity. All four proteins were expressed on the surface of BJAB cells and then introduced into our model system to determine T cell activity by the secretion of IFNγ. Relevant methodologies are described in Chapter 2 and will be referred to throughout this chapter.

8.1. Rhesus rhadinovirus (RRV)

The reader was introduced to RRV in Chapter 1.4. RRV and KSHV are members of the same genera of the *gammaherpesvirinae* subfamily, γ2-rhadinoviruses, though KSHV infects humans and the natural host of RRV is the Old World primate, rhesus macaque (Desrosiers *et al*., 1997). RRV enables the investigation of KSHV-like infection in a primate host, and induces similar pathology to KSHV (Wong *et al*., 1999). Wong *et al*. isolated RRV strain 17577 from a macaque with a multicentric lymphoproliferative disease and infected RRV-seronegative macaques with this virus (Wong *et al*., 1999). These immunosuppressed macaques, co-infected with simian immunodeficiency virus (SIV) developed pathology with similarity to MCD, though SIV-negative RRV-positive animals rarely develop lymphoproliferative disease (Wong *et al*., 1999). The putative RRV homologue of KSHV vOX2, encoded by the RRV ORF *R14* (Pratt *et al*., 2005), was expressed in BJAB cells and its biological activity investigated in our human T cell clone model system. As mentioned

previously two strains of RRV have been isolated and sequenced, RRV 17577 (Searles *et al*., 1999) and RRV H26-95 (Desrosiers *et al*., 1997). The strains differ by several base changes, but the RRV vOX2 proteins share 100% protein identity with each other (**Figure 8.1**). RRV vOX2 shares 30% protein identity with human CD200, and 28% identity with KSHV vOX2, and like these two proteins it contains Ig-like domains (Langlais *et al*., 2006). Initially, telomerised rhesus fibroblast cells (tRFB) were infected with both strains of the virus, and infectivity determined by plaque assay. The RRV vOX2 transcripts were then analysed by Northern Blotting. Due to their identical protein sequences, only the RRV H26-95 strain was selected for the generation of full-length EGFP-tagged RRV vOX2.

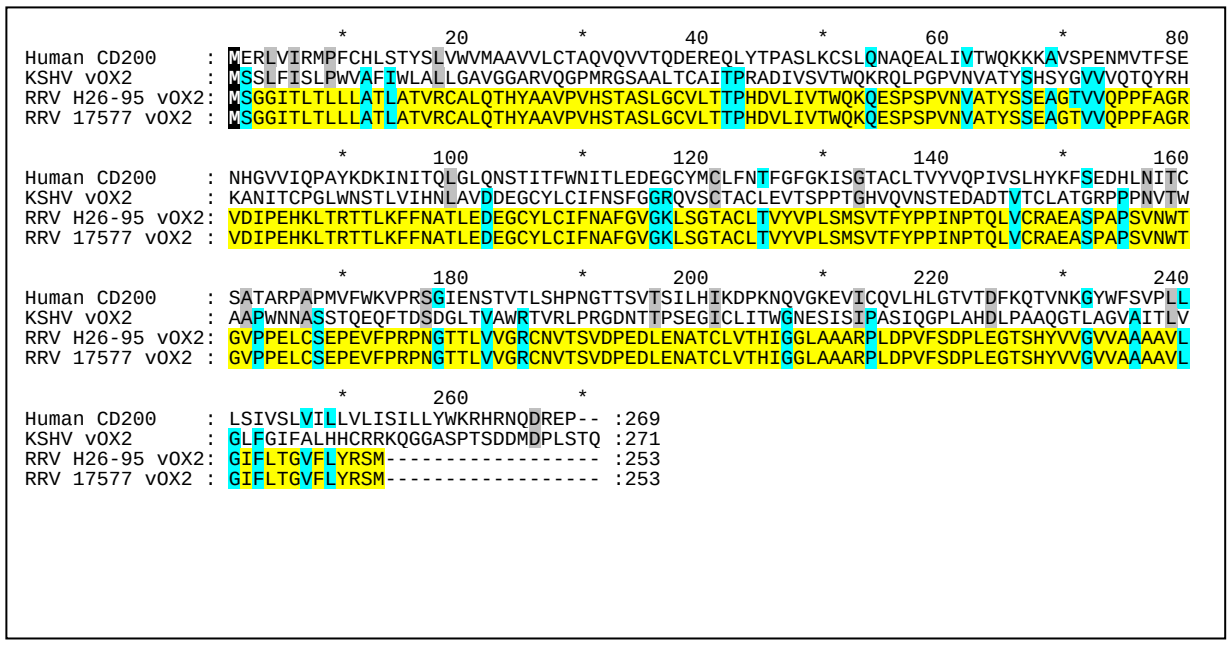

Figure 8.1 Conserved protein identities between human CD200, KSHV vOX2 and RRV vOX2 proteins. The translated regions of Human *CD200*, KSHV *K14* (vOX2) and RRV *R14* (vOX2) were aligned (GeneDoc Version 2.7) to identify conserved residues. Amino acid residues conserved between the RRV vOX2 proteins of RRV strains H26-95 and 17577 are highlighted in yellow. Residues conserved between RRV vOX2 and KSHV vOX2 or CD200 are highlighted in blue, and those conserved between KSHV vOX2 and CD200 are highlighted in grey. Residues conserved across the four proteins are shaded in black.

8.1.1. Initial analyses of RRV and RRV vOX2

In order to construct an RRV vOX2 *R14*-expression vector for the transduction of BJAB cells, we must have access to the RRV genome to enable PCR amplification of *R14*. Therefore, susceptible cells were infected with RRV, viral RNA isolated from the cells, and cDNA generated via RT-PCR. Initially, macaque cells were inoculated with RRV strains 17577 and H26-95, and the presence of the virus determined by immunoblotting for the RRV complement control protein, RCP (*ORF4*). Due to the lack of an antibody directed against RRV vOX2, RRV infection and replication were detected with anti-RCP antibody, and RRV vOX2 (*R14*) was detected by PCR for *R14*.

RRV naturally infects rhesus macaques; therefore, cells derived from macaques are utilised for the culture and propagation of RRV. Primary rhesus fibroblasts (RFB) were cultured to confluence before infection with either of the two strains of RRV, H26-95 and 17577 (**Figure 8.2**, **a** and **b** respectively). Productive infection can be determined visually by the appearance of viral 'plaques', a phenomenon known as cytopathic effect (CPE). CPE is characterised as an area of cell clearance resulting from lytic replication of the virus and subsequent cell death. The number of plaques, or regions of CPE in a known area, indicates the number of plaque forming units (PFU) present in the viral culture. The PFU titre of the virus is determined by serially diluting the virus, inoculating susceptible cells and counting the number of plaques. In order to prevent the spread of the virus from infected cells to other areas of the culture dish, the cells are enveloped in a soft agar (Chapter 2.8.2). The titre of each viral stock was determined before subsequent infections of cells.

tRFB are also susceptible to RRV infection and rapidly proliferate in culture, whereas RFB grow more slowly. Thus tRFB were used for the production of RRV stocks and for the isolation of RRV RNA. Early CPE was absent in uninfected cells (**Figure 8.3**, **a**), but was

clearly evident in tRFB infected with RRV 17577 (**Figure 8.3**, **b**) and RRV H26-95 (**Figure 8.3**, **c**). Clumped and dying cells were visible in a concentrated area, these will die leaving an area of clearing in the cell monolayer.

(a) RRV H26-95

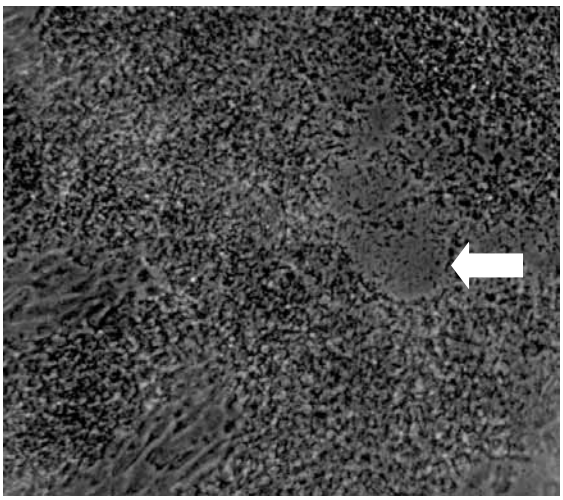

(b) RRV 17577

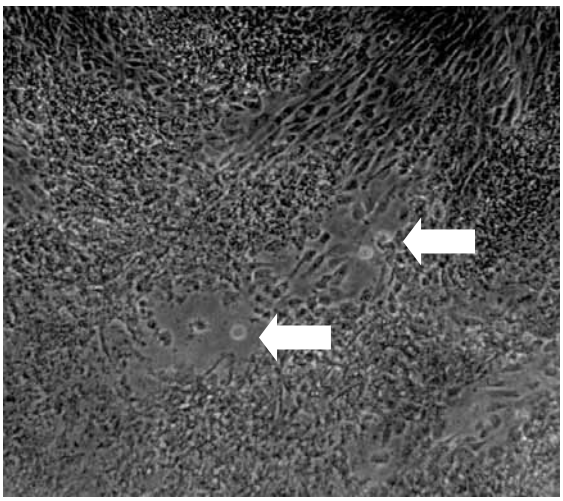

Figure 8.2 Determining the titre of rhesus rhadinovirus (RRV). Primary rhesus fibroblasts (RFB) were infected with serial dilutions of RRV strain H26-95 **(a)**, or 17577 **(b)**, then overlayed with complete medium/1.4% Nobles agar. Following the appearance of distinct zones of clearance ('plaques'), indicated by arrows, these areas were counted for each virus concentration in order to determine the number of plaque-forming units (PFU) in the viral stock solution. Each dilution was carried out in triplicate; plates that were not 100% confluent with RFB were discounted to avoid the inclusion of areas of low cell density as viral plaques.

(a) Uninfected

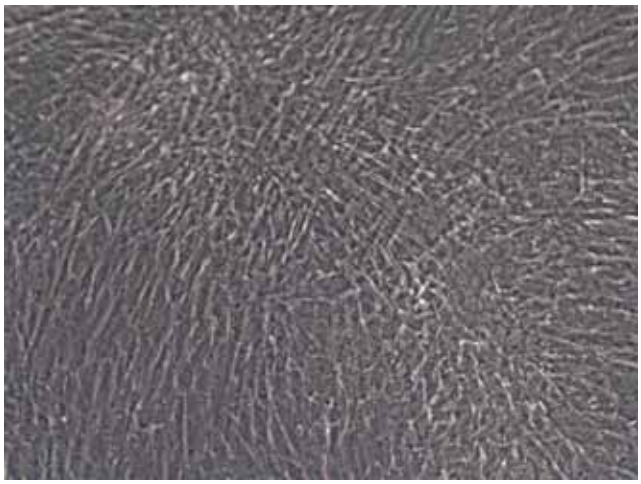

(b) RRV 17577

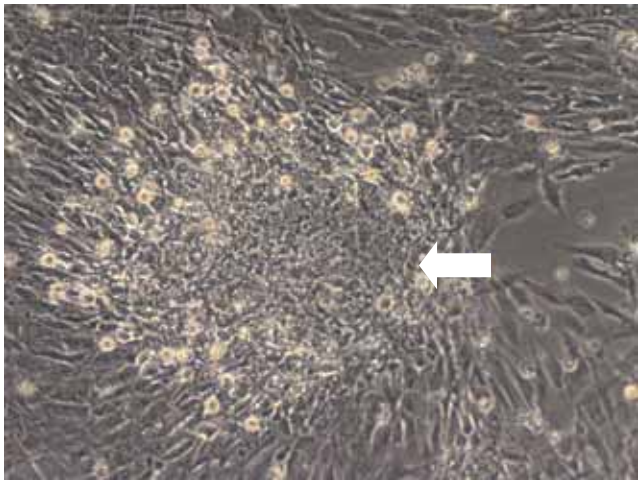

(c) RRV H26-95

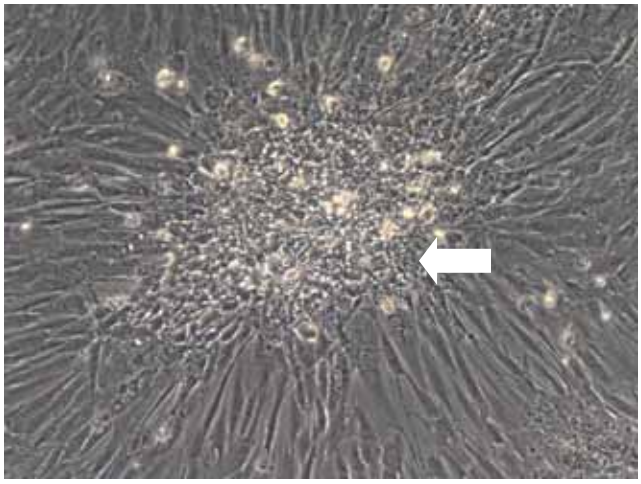

Figure 8.3 Cytopathic effect of rhesus rhadinovirus (RRV) on telomerised rhesus macaque fibroblasts (tRFB). Confluent tRFB were treated with polybrene (2μg/ml, 60mins, 37^{o}C) and **(a)** untreated, or infected with RRV strains **(b)** 17577 and **(c)** H26-95; the cells were passaged three days later. Approximately 6 days after infection, the cytopathic effect of the virus (indicated by arrows) was observed in **(b)** and **(c)** in comparison to **(a)** healthy uninfected tRFB.

RRV-infected cells were lysed and the presence of the virus confirmed by immunoblotting for RCP (**Figure 8.4**). The RCP protein differs between the H26-95 and 17577 strains of RRV. RRV H26-95 RCP contains four CCP domains, whereas RRV 17577 RCP contains eight CCP domains, though both proteins are alternatively spliced and so exist as several isoforms (Mark *et al*., 2007). A marked difference between the immunoblotting profiles of H26-95 RCP and 17577 RCP (**Figure 8.4**), is explained by the expression of alternate isoforms and subsequent glycosylation. RCP was clearly present in 17577 and H26-95-infected cells, and not in uninfected tRFB cells when analysed by immunoblotting (**Figure 8.4**, **a**). Next, the expression of RRV vOX2 (*R14*) was determined by RT-PCR. RNA was extracted from infected and uninfected tRFB cells. cDNA was generated from RNA by random priming (see Chapter 2.8.3/7), and the translated region of the vOX2 *R14* gene amplified by PCR, using primers 2F and 2R (see Appendix, Table I). RRV vOX2 *R14* was absent from uninfected cells but clearly identifiable in infected cells, and the primers amplified PCR products with an identical size in cells infected with either RRV 17577 or RRV H26-95 (**Figure 8.4**, **b**).

Northern blotting analysis enables the detection of gene transcripts and gene expression in cells by the isolation of RNA, and subsequent probing with a radiolabelled cDNA sequence matching the gene of interest. Performing northern blotting with RNA isolated from RRV-infected cells allowed us to determine whether RRV vOX2 *R14* is expressed in infected cells and to ascertain whether RRV vOX2 *R14* is spliced, resulting in protein isoforms. Northern Blotting (Chapter 2.8.4) revealed a full-length transcript of *R14*, of 5.84Kb in length, and a splice variant of 3.74Kb (**Figure 8.5**, **a**), consistent with a previous report in the literature (Pratt *et al*., 2005). The transcript sizes were extrapolated from the known sizes of a DNA ladder separated on the formaldehyde gel (not shown). The presence of RNA in the uninfected control was confirmed by labelling ribosomal RNA with

ethidium bromide and viewing under UV light (**Figure 8.5**, **b**). Pratt and colleagues infected primary rhesus fibroblasts with RRV 17577 and detected two *R14* transcripts 72hrs after infection by Northern Blotting, suggesting that *R14* is a late-lytic gene (Pratt *et al*., 2005). Our data (**Figure 8.5**) confirm that *R14* is expressed as two transcripts, and that they are almost certainly present in cells undergoing lytic replication of RRV (the cells were harvested for RNA extraction once CPE was evident). Pratt *et al*. identified a larger RRV vOX2 transmembrane protein, localised to the plasma membrane and cytosol of cells engineered to express the larger transcript, and an alternate soluble protein present in the cytosol and secreted into the supernatant by cells transduced with the smaller transcript (Pratt *et al*., 2005). BJAB cells were engineered to express the larger transmembrane isoform of vOX2.

(a) Immunoblotting for RCP **(b) RT-PCR to detect RRV vOX2 (*R14*)**

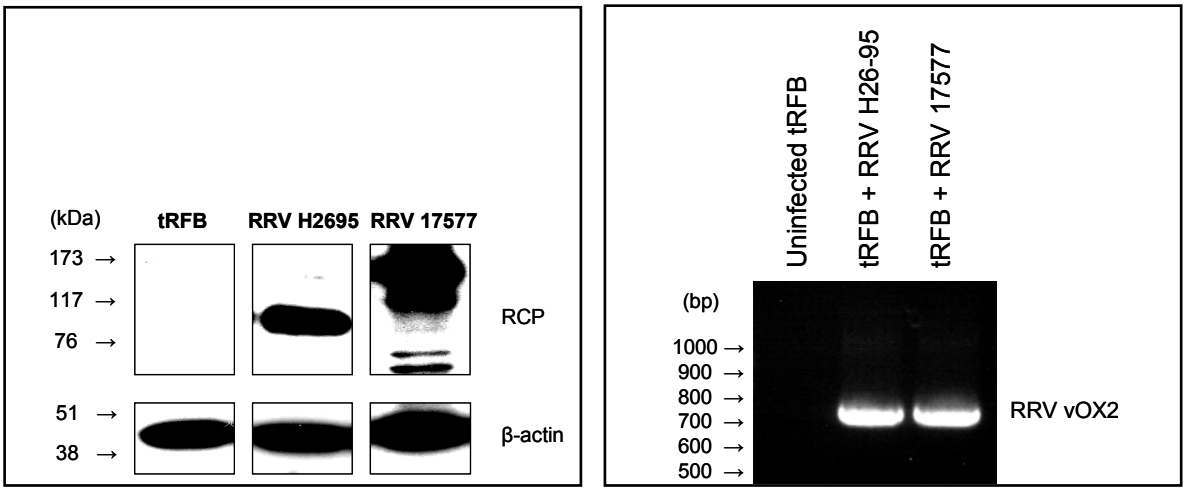

Figure 8.4 Confirming the infection of telomerised rhesus fibroblasts (tRFB) with rhesus rhadinovirus (RRV). (a) To ensure that tRFB cells harvested for viral RNA analyses were infected with RRV, cell lysates were analysed for expression of the lytic RRV protein RCP. Proteins were separated by SDS-PAGE and RCP detected with specific antibodies raised against each RRV strain. Alternative splicing of the RCP gene results in different blotting patterns for RCP between RRV strains. Immunoblotting for each strain of RCP was carried out on separate immunoblots, and an uninfected control was included for each. Irrelevant lanes were excluded, and a representative uninfected control is displayed. **(b)** RRV vOX2 *R14* was amplified from cDNA prepared from RRV-infected tRFB, and was absent in uninfected cells (left lane).

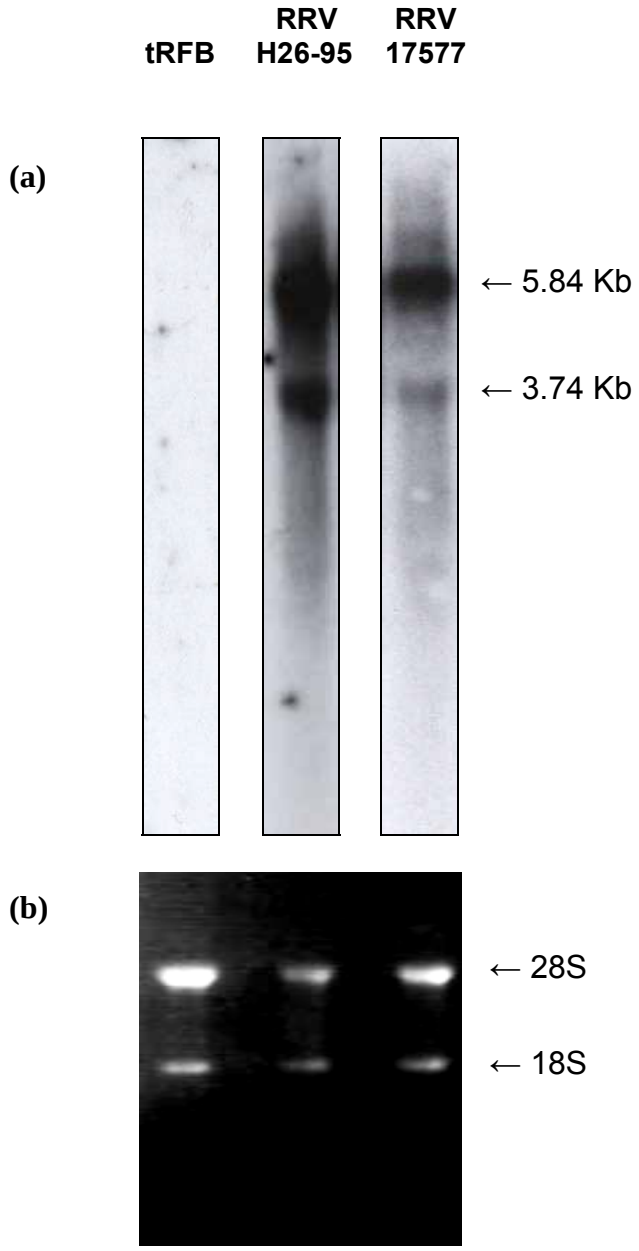

Figure 8.5 Northern blotting analysis of the rhesus rhadinovirus vOX2 gene (*R14*). RNA was extracted from uninfected or RRV-infected telomerised rhesus fibroblasts (tRFB). **(a)** RRV vOX2 *R14* was detected by probing the Northern Blot with a radiolabelled probe, generated from the translated region of the RRV vOX2 gene by RT-PCR, and labelled by the incorporation of dCTP [α-32P] by random priming. Two transcripts of RRV vOX2 *R14* were identified. **(b)** The quality of the ribosomal RNA was visualised by inclusion of ethidium bromide, confirming the presence of RNA in the uninfected control lane. All lanes presented here were taken from the same exposure of the membrane to hyperfilm, but irrelevant lanes were excluded.

8.1.2. Generating RRV vOX2-EGFP, and determining its physiological activity

Once the expression of RRV vOX2 *R14* in RRV-infected cells had been determined, and the existence of two alternative transcripts, as reported in the literature, had been confirmed, a strategy to generate full-length RRV vOX2 was developed (Chapter 2.8.6). In order to examine the activity of RRV vOX2 in our T cell clone model system, it must be expressed by our HLA-matched BJAB cells. The expression of RRV vOX2 must also be quantifiable. To achieve this, the sequence encoding full-length RRV vOX2 (from RRV strain H26-95) was fused in-frame with EGFP to enable the detection of RRV vOX2 by flow cytometry and microscopy. Briefly, the translated region of *R14* was cloned into a vector containing EGFP (pEGFP-N1). The two genes were then digested from the vector and inserted into a bicistronic retroviral expression vector (pQCXIP), to enable the co-transcription of a puromycin-resistance gene. BJAB cells were transduced with infectious retrovirus containing the *R14-EGFP* plasmid.

Transduced BJAB cells were maintained on puromycin selection and RRV vOX2 protein expression was quantified by the flow cytometric analysis of EGFP fluorescence (**Figure 8.6**). Two populations of RRV vOX2-expressing cells are evident in the histogram; both populations are fluorescing more than the Empty-BJAB control cells, indicating that all RRV vOX2-EGFP BJAB cells express the protein, but differ in their expression levels. RRV vOX2-positive cells were initially isolated by cell-sorting (BD Biosciences, data not shown) for cells highly fluorescent in the FL1 channel (EGFP), and then cultured. It was not possible to maintain a single highly-expressing population in culture. However, the RRV-EGFP expression levels were quantified before each experiment to ensure that the fluorescent profile mirrored this histogram (**Figure 8.6**).

Due to the observed downregulation of HLA-ABC on the surfaces of BJAB cells engineered to express vOX2 or CD200 (Chapter 6.4), HLA-ABC expression on RRV vOX2-

EGFP-BJAB was quantified by flow cytometric analysis, utilising fluorophore-conjugated antibodies. Surprisingly, HLA-ABC expression was slightly increased on the surface of RRV vOX2-EGFP-BJAB cells, to 125.24% ± 9.14 SEM of the HLA-ABC on present on the surface of Empty-BJAB control cells in two independent experiments (**Figure 8.7**).

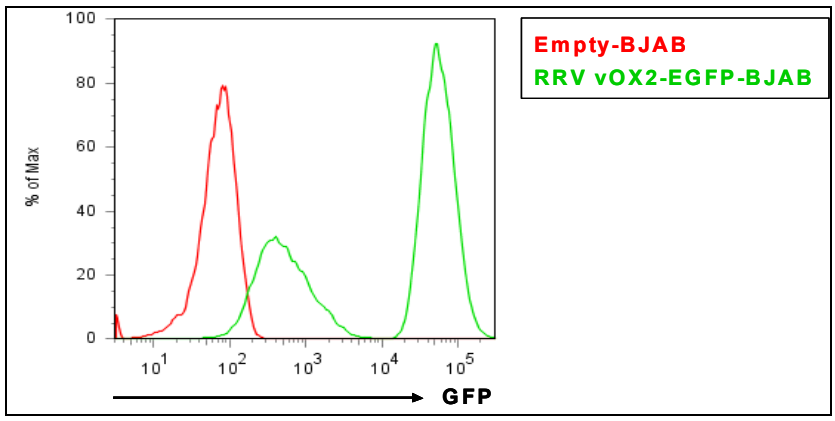

Figure 8.6 Expression of RRV vOX2 fused with EGFP on engineered BJAB cells. BJAB cells were transduced with either an empty retroviral vector, or were engineered to express RRV vOX2 tagged with EGFP by retroviral transduction. The expression of RRV vOX2-EGFP was determined by flow cytometric analysis of EGFP fluorescence (green), in comparison to Empty-BJAB control cells (red). This histogram contains the raw data from one experiment, but is representative of three independent experiments.

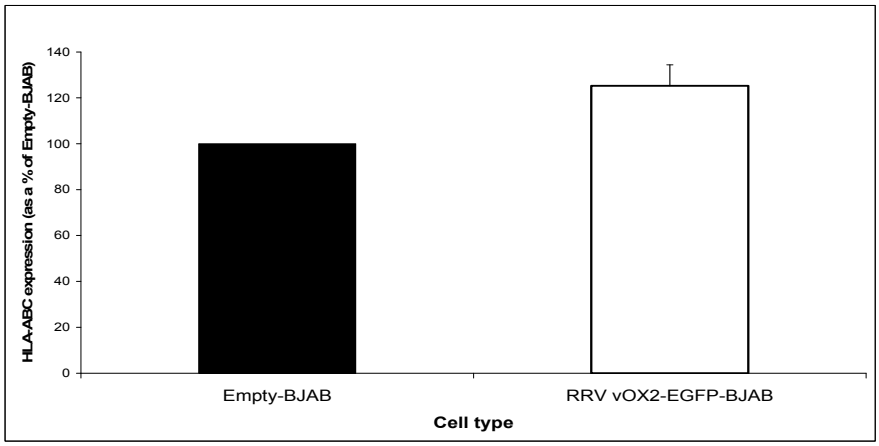

Figure 8.7 HLA-ABC expression on RRV vOX2-expressing BJAB cells is increased. BJAB cells were engineered to express RRV-vOX2-EGFP or an empty vector. Extracellular HLA-ABC was quantified by flow cytometry, using fluorophore-conjugated monoclonal antibodies. Two independent experiments were carried out with each cell type, and the value of the isotype control median fluorescence subtracted from the sample before normalising to the fluorescence value obtained for the Empty-BJAB control. The difference in HLA-ABC expression was not significant when analysed by one-way ANOVA (SPSS software).

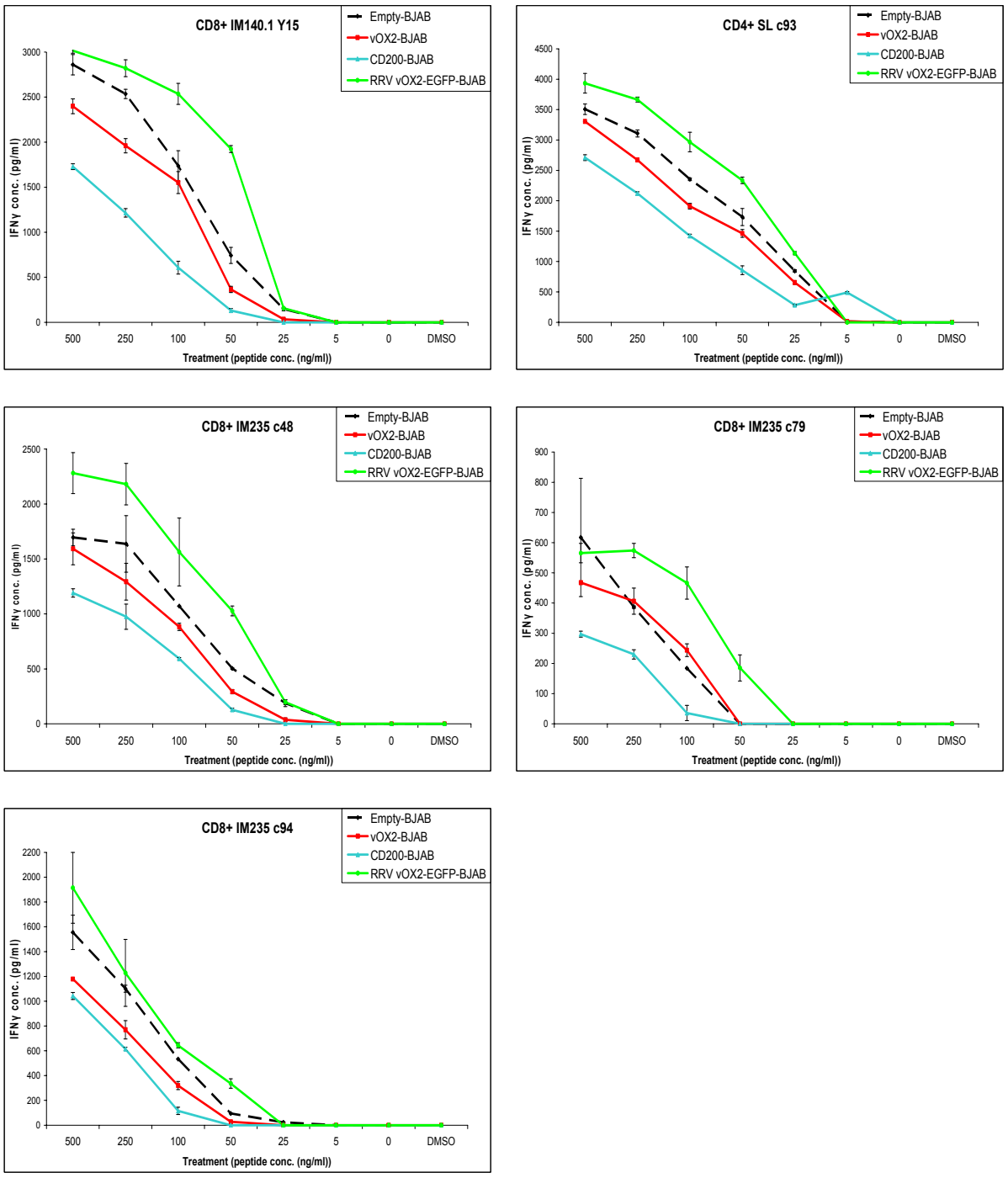

Figure 8.8 RRV vOX2 does not suppress the activity of human T cell clones. Empty-BJAB, vOX2-BJAB, CD200-BJAB or RRV vOX2-EGFP-BJAB cells, were pulsed with either YVLDHLIVV (BRLF1 peptide, IM235 and IM140.1 clones) or PRSTVFYNIPPMPLPPSQL (EBNA2 peptide, SL c93 clone) for one hour, washed, and then co-cultured with each T cell clone for 16 hours (all treatments were carried out in duplicate). IFNγ-release was quantified by ELISA. All values represented as 0pg/ml IFNγ were beyond the limit of detection of this ELISA (<31.25pg/ml). These data were gathered from one experiment, but are representative of two independent experiments.

Interestingly, the slight upregulation of HLA-ABC on the surface of RRV vOX2-EGFP-BJAB cells, in contrast to the downregulation of HLA-ABC on vOX2-BJAB and CD200-BJAB cells, mirrors the opposing functional data obtained for the three proteins. As discussed in Chapter 5, both vOX2 and CD200-expressing BJAB cells suppress the activity of human T cell clones, as measured by the secretion of IFNγ. In contrast, RRV vOX2-EGFP did not suppress IFNγ-secretion by the T cell clones, but in fact appeared to slightly increase production of the cytokine (**Figure 8.8**). The suppressive effect of CD200 (turquoise), and to a lesser extent, of vOX2 (red), was evident in comparison to the Empty-BJAB (dashed black line) control. However, RRV vOX2-EGFP BJAB cells (green) consistently induced a higher secretion of IFNγ than the Empty-BJAB control cells, in all five T cell clones. Data from one experiment (error bars denote SEM between duplicates) are presented (**Figure 8.8**) and are representative of two independent experiments. Consistent results were obtained between experiments, therefore further analysis was deemed unnecessary.

8.2. Determining the physiological activities of three putative CMV homologues of CD200

Human CMV (HHV-5) can be detected in 40 to 70% of individuals across the World's populations. CMV is usually acquired early in life, without serious pathology in immunocompetent individuals (Freeman, 2009). However, the infection of neonates by virus dissemination through the placenta can result in organ failure, damage to the CNS, and eventual death (Demmler-Harrison, 2009). Similarly, the transmission of CMV to immunocompromised hosts causes organ and tissue damage, and can increase the probability of graft rejection in CMV-negative individuals. The pathogenesis of CMV in immunocompromised individuals is incompletely understood, but immunosuppressive properties of the virus may increase the likelihood of infection with other pathogens (Freeman, 2009).

Sester *et al*. isolated $CD4^+$ CMV-specific T cells from renal dialysis recipients with an anergic phenotype. These $CD4^+$ cells expressed higher levels of programmed death-1 (PD-1) molecule, a member of the CD28 family and a negative regulator of T cell activity, than those isolated from CMV-seropositive immunocompetent or CMV-seronegative individuals. The $PD\text{-}1^{high}CD4^+$ CMV-specific T cells had a reduced ability to generate IFNγ and IL-2, and their numbers were positively associated with CMV viral load (Sester *et al*., 2008). Inhibition of T cell activity during CMV viraemia would reduce the immune response to infection with other viruses, providing a mechanism for disease pathology in immunosuppressed individuals. Other methods of CMV-mediated immunosuppression include the expression of viral proteins that inhibit the surface expression of MHC-peptide complexes on infected cells. However, cells that abnormally downregulate their MHC-expression are in danger of recognition and killing by NK cells. CMV-infected cells do escape NK-mediated lysis, though their mechanism of evasion is controversial, and there are genetic differences between cultured laboratory CMV strains and clinical isolates, rendering some research of lab strains inconclusive.

Wills and colleagues identified a cell-surface viral protein encoded by *UL142* that conferred resistance against NK killing to autologous fibroblasts engineered to express the protein. *UL142* is predicted to encode a highly glycosylated transmembrane protein containing an MHC class I-like antigen recognition domain, and is a CMV late gene. A CMV strain lacking *UL142* was not as efficient at preventing NK-lysis of infected cells, in comparison to clinical and lab strains expressing *UL142*, and knockdown of *UL142* in infected cells increased the sensitivity of the cells to NK killing, but did not completely abrogate CMV-mediated protection (Wills *et al*., 2005). Taken together, these data suggest that CMV infection induces immunosuppression by a variety of mechanisms, presumably to take into account the myriad T and NK cell specificities and HLA-restrictions of each

individual. The variety of immunosuppressive viral proteins expressed by the large (>230 Kb) CMV genome (Dunn *et al*., 2003), suggests that other undefined genes may also encode proteins that modify the host's immune response.

The CMV genome can be subdivided into a unique short (US) region and a unique long (UL) region, and as mentioned previously, the genomes of the laboratory strains all differ slightly. Three CMV genes, present in the UL region, *UL119*, *UL120* and *UL121* were isolated and cloned (Dr. Richard Stanton and Prof. Gavin Wilkinson, University of Cardiff) for examination in our model system. There are no published data on the CMV *UL119* gene (NCBI database, Gene ID3077514); however, *UL119* is believed to encode a putative type 1 membrane protein, with IgG Fc-binding properties, and some similarity to CD200. An adjacent gene in the CMV genome, *UL120* has also been sequenced (NCBI, Gene ID3077520); it is believed to encode a type 1 transmembrane protein, but its functional activities have also not been elucidated. The CMV *UL121* (NCBI Gene ID3077529) also encodes a transmembrane protein. Dunn and colleagues created deletion mutants of the fully sequenced Towne strain of CMV, incorporated into a BAC (Dunn *et al*., 2003). They discovered that neither *UL119* nor *UL121* were required for *in vitro* replication of the virus in human foreskin fibroblasts (Dunn *et al*., 2003). However, though the genes may not be essential for virus replication, they appear to be conserved across species. A distinct strain of CMV infects the rhesus macaque (rhCMV); Barry *et al*. demonstrated that the region encoding *UL119*, *UL120* and *UL121* in human CMV is conserved in rhCMV. The translated gene products showed between 52.1% (for *UL121*) and 66.3% (*UL120*) similarity with human CMV (Barry *et al*., 1996). The conservation of these genes, and the observed similarity of the *UL119* sequence to *CD200*, indicates that they may play an important functional role in the host upon CMV infection. The alignment of KSHV vOX2, human

CD200 and CMV 119, 120 and 121 proteins (**Figure 8.9**) confirms that CMV 119 and CD200 share some protein identity.

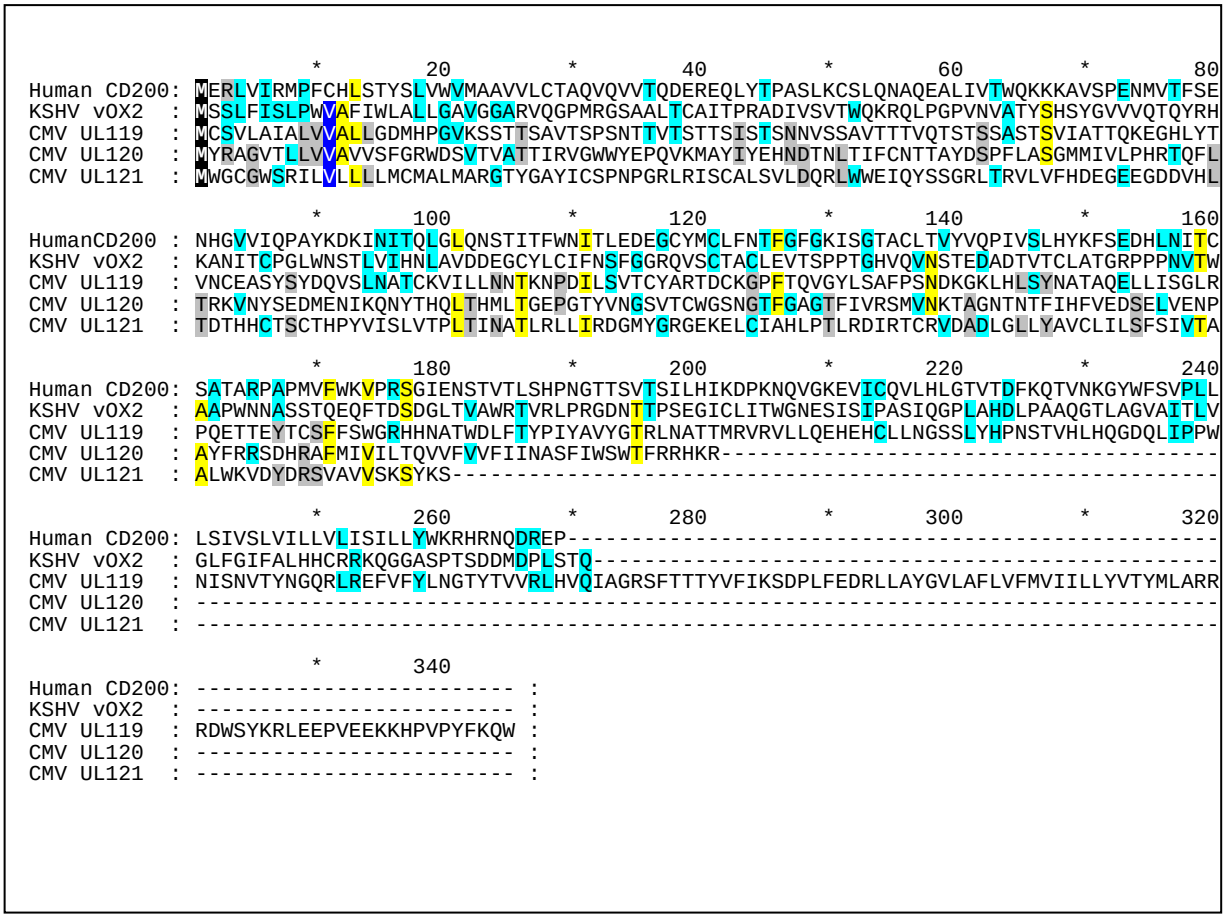

Figure 8.9 Conserved protein identity between human CD200, KSHV vOX2 and three CMV proteins. The translated regions of Human *CD200*, KSHV *K14* (vOX2) and CMV *UL119*, *UL120* and *UL121* were aligned (GeneDoc Version 2.7) to identify conserved residues. Amino acid residues conserved between two proteins are highlighted in yellow or turquoise. Residues conserved across three proteins are highlighted in yellow, and those conserved between KSHV vOX2 and the CMV proteins are highlighted in blue. Residues conserved across all five proteins are shaded in black.

UL119, *UL120* and *UL121* were cloned, fused in-frame with GFP, and inserted into the retroviral expression vector, pQCXIP, by a member of G. Wilkinson's research group in Cardiff (Stanton, R.). These vectors were sent to our lab in Birmingham where BJAB cells were then transduced with the infectious retrovirus, and expanded by antibiotic selection,

creating CMV 119-GFP-BJAB, 120-GFP-BJAB and 121-GFP-BJAB. Once stable cell lines had been established, the expression of each GFP-tagged protein was determined by flow cytometry (**Figure 8.10**). We do not have access to antibodies directed against CMV proteins 119, 120 or 121, so GFP expression served as a measure of protein expression. The three CMV proteins were expressed to variable levels by the BJAB cells, with CMV 121-GFP expressed (or at least fluorescing) better than 120-GFP and 119-GFP. In all cases, the GFP fluorescence of each BJAB cell line engineered to express a CMV vOX2 homologue was higher than the Empty-BJAB cells, indicating that the CMV proteins were expressed.

Next, cell-surface HLA-ABC expression was determined by flow cytometric analysis with a fluorophore-conjugated monoclonal antibody. The raw data were normalised to the isotype control value, and then to the median fluorescent value for Empty-BJAB control. Data from three independent experiments were pooled, and the error bars represent the SEM between experiments. Similarly to RRV vOX2-EGFP, the CMV vOX2-GFP proteins all appeared to amplify the expression of HLA-ABC (**Figure 8.11**), though none of the differences reached statistical significance by one-way ANOVA. CMV 119-GFP-BJAB cells expressed 115.03% ± 9.23 SEM of the HLA-ABC expressed by the Empty-BJAB control, though the deviation between experiments largely negated this increase. Again, CMV 120-GFP-BJAB cells expressed higher HLA-ABC (124.67% ± 33.38 SEM) than control cells, but the deviation was so large that this increase may be artefactual. The increase in HLA-ABC expression on CMV 121-GFP-expressing cells is noticeable, with the engineered cells expressing 136.37% ± 19.14 SEM of the Empty-BJAB control, but does not reach statistical significance by one-way ANOVA.

The total HLA-ABC protein expression in the cells was determined by lysing the engineered BJAB cells, and analysing either the whole cell lysates, or the cytosolic fractions (**Figure 8.12**) by SDS-PAGE and immunoblotting (Chapter 2.3). Interestingly, cytosolic

fractionation of the cells revealed a slight increase in HLA-ABC expression in CMV 119-GFP-BJAB and CMV 120-GFP-BJAB cells (103.74% and 115.31% of control, respectively), but a reduction in the HLA-ABC levels of cells expressing CMV 121-GFP, to 78.61% of control (**Figure 8.12**, **a**), though the difference did not reach statistical significance by one-way ANOVA. In contrast, whole cell lysates of all three engineered BJAB cell lines contained less HLA-ABC than the Empty-BJAB control cells (**Figure 8.12**, **b**). Cumulatively, neither CMV 119-GFP nor 120-GFP proteins altered the expression of HLA-ABC. However, CMV 121-GFP-BJAB cells, which showed enhanced surface HLA-ABC levels by flow cytometric analysis, consistently and surprisingly contained less total cellular protein (**Figure 8.12**, **c**). HLA-ABC protein expression was reduced to 74.59% ± 4.01 SEM of the Empty-BJAB control in CMV 121-GFP-BJAB cells.

The physiological activities of the putative CMV CD200 homologues were analysed in our T cell clone model system. The experiments were carried out as before, using vOX2-BJAB and CD200-BJAB cells as positive internal controls to ensure that suppression of the T cell clones was possible. Three replicate experiments were carried out, though not every clone was analysed in each experiment (see Fig. legend for the number of replicates), and the data presented are representative of the replicates. KSHV vOX2 was consistently able to inhibit the secretion of IFNγ by the T cell clones, in contrast to CD200 which was variable, but suppression by one or both proteins was evident for each clone (**Figure 8.13**). In contrast to vOX2 and CD200, but in a similar manner to RRV vOX2-EGFP, the three CMV proteins were unable to suppress T cell activity, and in fact consistently amplified IFNγ-secretion in comparison to Empty-BJAB control cells.

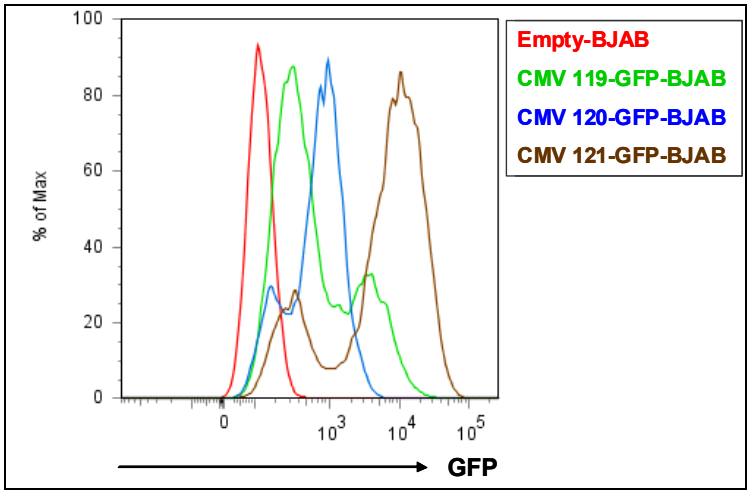

Figure 8.10 BJAB cells engineered to express three putative CMV homologues of vOX2, fused in-frame with GFP. BJAB cells were transduced with a retrovirus containing one of three CMV open reading frames (*UL119*, *UL120* and *UL121*) fused in-frame with *GFP*. Following selection with puromycin, protein expression could be visualised by flow cytometric analysis of GFP.

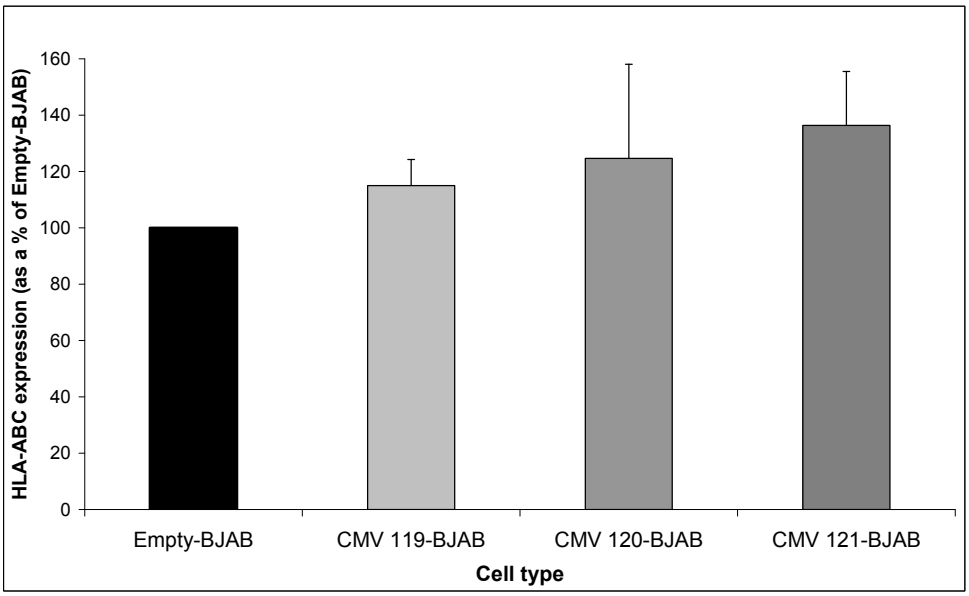

Figure 8.11 Expression of putative CMV homologues of vOX2 does not alter HLA-ABC expression on the engineered cell. BJAB cells were engineered to express one of three putative CMV CD200 homologues (*UL119*, *UL120* and *UL121*) fused in-frame with *GFP*. Extracellular HLA-ABC was quantified by flow cytometry, using specific monoclonal antibodies conjugated to a fluorophore. Three independent experiments were carried out, and the value of the isotype control median fluorescence subtracted from the sample before normalising to the fluorescence value obtained for the Empty-BJAB control. The differences in HLA-ABC expression between CMV-expressing BJAB cells and Empty-BJAB did not reach statistical significance by one-way ANOVA (SPSS software).

(a) Cytosolic fractionation (densitometric data) **(immunoblot)**

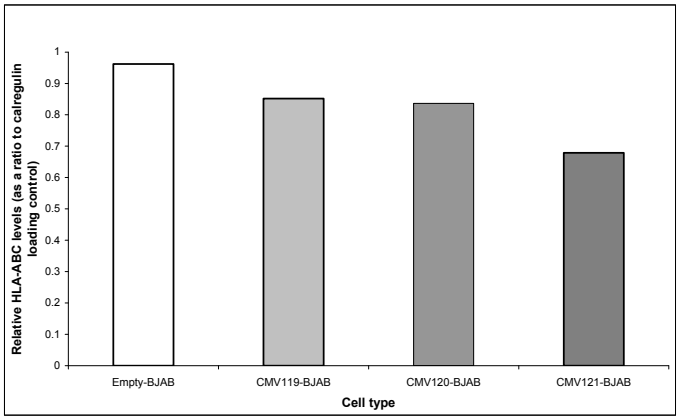

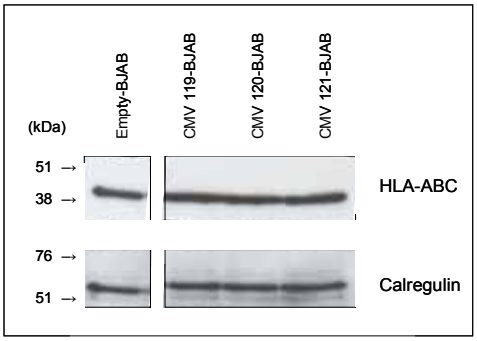

(b) Whole cell lysate (densitometric data) **(immunoblot)**

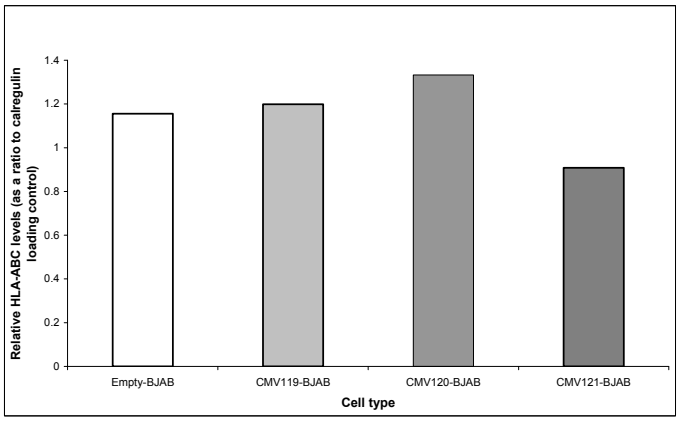

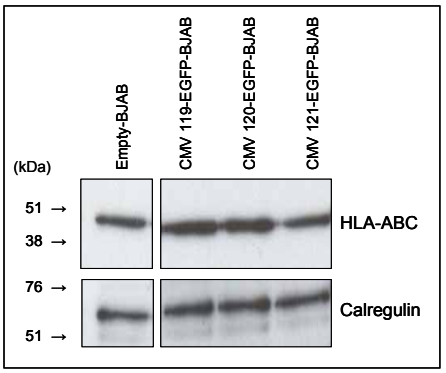

(c) Cumulative data

	Empty-BJAB	CMV119-GFP-BJAB	CMV120-GFP-BJAB	CMV121-GFP-BJAB
Mean	100	96.13	101.14	74.59
SEM		± 7.60	± 14.17	± 4.01

Figure 8.12 HLA-ABC protein levels are similar in CMV 119/120/121-GFP-BJAB cells to Empty-BJAB control cells. Protein extracts of engineered BJAB cells were prepared by two methods, isolating either **(a)** cytosolic fractions or **(b)** whole cell lysates. The proteins were separated by SDS-PAGE and Western Blotting, and immunoblotted with an anti-HLA-ABC antibody. Densitometry was carried out on each immunoblot and the data normalised by calculating the ratio of HLA-ABC to a calregulin loading control for each sample. **(c)** The densitometric data were pooled and presented as a % of the Empty-BJAB control. Differences in HLA-ABC expression did not reach statistical significance when the data were analysed by one-way univariate ANOVA (SPSS software).

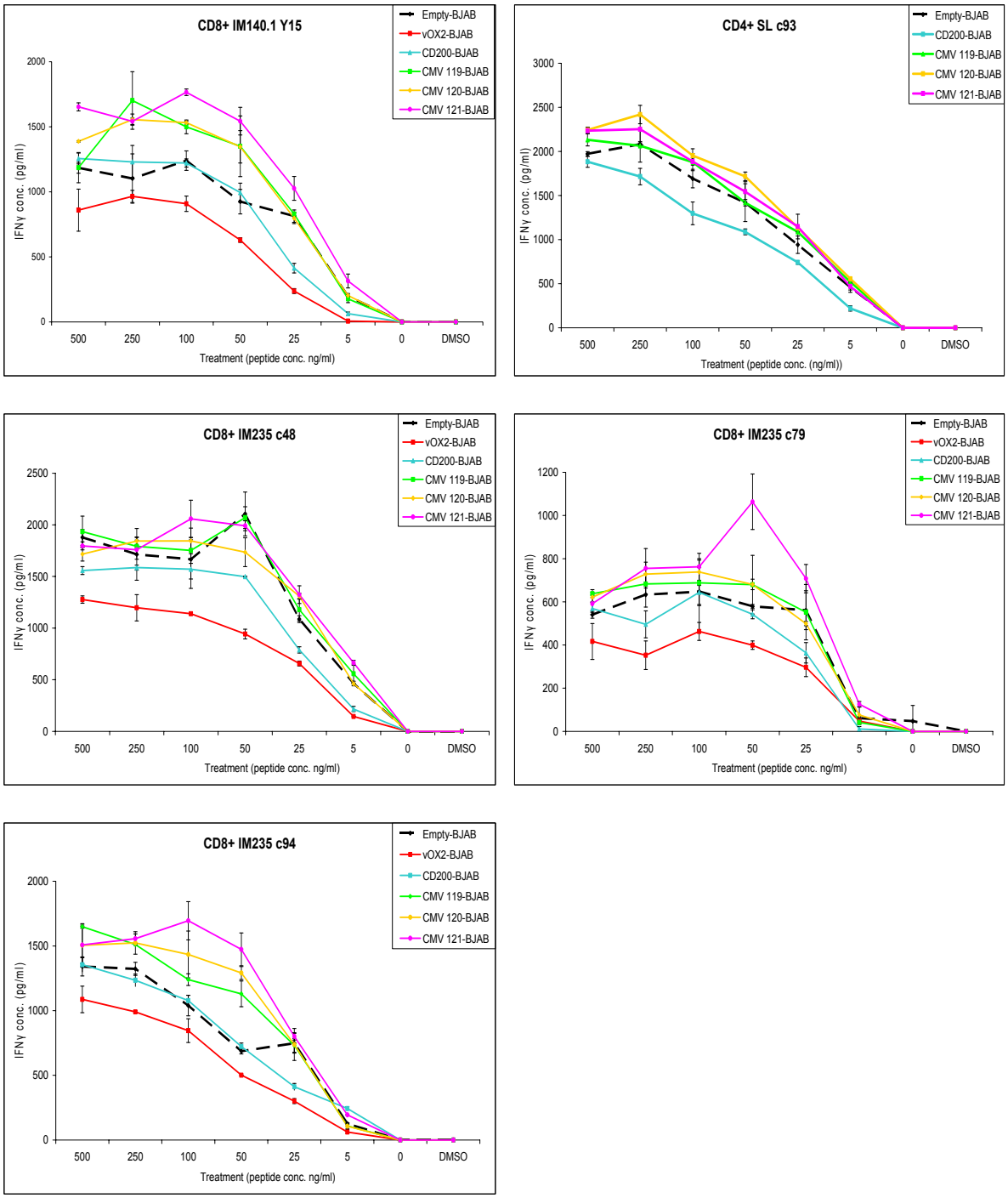

Figure 8.13 CMV proteins UL119, UL120 and UL121 do not suppress the activity of CD4$^+$ or CD8$^+$ T cell clones. BJAB cells engineered to express an empty vector, native vOX2, native CD200 or one of three putative CMV homologues of CD200, were pulsed with either YVLDHLIVV (a BRLF1 peptide, IM235 and IM140.1 clones) or PRSTVFYNIPPMPLPPSQL (an EBNA2 peptide, SL c93 clone) for one hour, washed, and then co-cultured with the T cell clone for 16 hours (each treatment was carried out in duplicate). IFNγ-release was quantified by ELISA. All values represented as 0pg/ml IFNγ were beyond the limit of detection of this ELISA (<31.25pg/ml). The data are representative of replicate experiments in which suppression of T cell clone activity by vOX2 or CD200 was evident (IM140.1, n=2; SL c93, n=1; IM235 c48, n=2; c79, n=2; c94, n=3).

8.3. Discussion

Previous observations that a homologue of CD200 encoded by RRV (RRV vOX2:Fc) could suppress cytokine production by THP-1 cells and primary macrophages (Langlais *et al*., 2006), implied that the full-length transmembrane protein may be able to suppress the activity of T cell clones in our model system. However, RRV vOX2-EGFP-BJAB cells were unable to suppress the secretion of IFNγ by T cell clones, and in fact appeared to exacerbate the production of this cytokine (**Figure 8.8**). An immunogenic protein, R1 has been identified in RRV, with homology to the KSHV protein K1. Damania *et al*. demonstrated that the intracellular domain of chimaeric R1 activated BJAB cells. Stimulation of the R1 cytoplasmic tail induced calcium mobilisation, tyrosine phosphorylation and activated NFAT in BJAB cells (Damania *et al*., 2000). So the presence of lymphocyte-activating RRV proteins is not unusual, though obviously further analysis of the RRV vOX2 protein is necessary in order to verify its physiological activity.

Interestingly, the lack of RRV vOX2-mediated suppression correlated with increased cell-surface HLA-ABC expression on RRV vOX2-EGFP-BJAB cells (**Figure 8.7**), in contrast with the consistent downregulation of HLA-ABC on the T cell-suppressive vOX2-BJAB cells (Chapter 6, **Figure 6.24**). It had been previously noted that both the surface and total expression of HLA-ABC by vOX2-EGFP-BJAB and CD200-EGFP-BJAB cells were unaltered (Chapter 6, **Figure 6.24/5**). The difference in HLA-ABC expression by vOX2/vOX2-EGFP expressing BJAB cells suggests that tagging vOX2 with EGFP may alter its biological properties. However, only untagged vOX2 was investigated in our T cell model system. It would be interesting to note the activities of untagged RRV vOX2 in our model system. However, the absence of a specific antibody renders its detection impossible.

The putative CD200 homologues encoded by CMV *UL119*, *UL120* and *UL121*, have unknown activity *in vivo*, and are not essential for virus replication *in vitro* (Dunn *et al*.,

2003). Again, due to the lack of an antibody for detection, the genes were fused in-frame with *GFP* (Stanton, R., Cardiff) before expressing on the surface of BJAB cells. Cell surface expression of HLA-ABC was not altered on CMV 119-GFP-BJAB or CMV 120-GFP-BJAB cells, though was enhanced on CMV 121-GFP-BJAB cells (**Figure 8.11**). In contrast to this, total HLA-ABC levels were reduced in CMV 121-GFP-BJAB cells (**Figure 8.12**). CMV 121-EGFP-BJAB cells appeared to be more immunogenic than either CMV 119 or 120 in the T cell activity experiments (**Figure 8.13**). Enhanced IFNγ-secretion by T cells stimulated by CMV 121-GFP-BJAB cells seems to correlate with enhanced surface HLA-ABC expression, suggesting that the SDS-PAGE data may be inaccurate.

As mentioned briefly in this chapter and in Chapter 1, CMV encodes several proteins capable of suppressing the immune response, primarily by inhibiting the expression of MHCI by infected cells, thus suppressing T cell activity. Deleting the primary downregulators of MHCI (US2, US3, US6 and US11) from a CMV strain, increased the number of identifiable CMV-specific $CD8^+$ T cells in CMV-seropositive donors, indicating that there is a complex response to many CMV antigens, but that the T cell responses to these proteins are partly suppressed by the downregulation of MHCI in infected cells (Manley *et al*., 2004). CMV infection also induces a population of $CD4^+CD27^-CD28^-$ Tregs that inhibit the proliferation of PBMCs in response to CMV antigen (Tovar-Salazar *et al*., 2009). The suppression of T cell responses by CMV is an important factor enabling CMV maintenance *in vivo*, and may explain the pathology in CMV-seropositive immunocompromised individuals, by suppressing the T cell response to other pathogens. The proteins encoded by CMV *UL119*, *UL120* and *UL121* did not suppress the secretion of IFNγ by CTLs in our model system, though like RRV vOX2, these proteins are tagged with a fluorescent protein to enable detection. Analysis of the untagged proteins in this system may produce different results.

Chapter 9. Conclusions

9.1 Conclusions

The purpose of this study was to investigate the roles of a cellular protein, CD200, with known immunoregulatory properties, and a KSHV protein with homology to CD200, in modulating human leukocyte function *in vitro* and *ex vivo*. Initially, soluble recombinant vOX2 and CD200 proteins, fused in-frame with human IgG1 (Fc) were utilised to determine the effects of these proteins on granulocyte activity. Rezaee *et al*. had previously demonstrated a suppressive effect of vOX2:Fc on granulocyte oxidative burst in whole blood (Rezaee *et al*., 2005), but had not investigated the function of CD200:Fc, nor examined their activities on isolated neutrophils. As discussed previously, Fc-fusion proteins are commonly used for researching the activities of transmembrane proteins because they can be produced in large quantities, and can be used *in vivo* at low concentrations (Kamei *et al*., 2005). However, though vOX2:Fc and CD200:Fc moderately suppressed granulocytic oxidative activity in whole blood (**Figure 4.6**), they did not alter the response of primary isolated neutrophils to stimulation (**Figures 4.4-4.8**). Contamination with bacterial endotoxin was an issue requiring constant monitoring, and the biological activity and specificity of the recombinant proteins could not be readily analysed. Therefore, the direction of the research altered slightly, and existing B lymphoblastoid cells engineered to express native vOX2 and CD200 on their cell surface were used for all later experiments. This method is more physiologically relevant, as vOX2 is expressed by KSHV-infected reactivated B cells (**Figure 5.4**) and CD200 is expressed on the surface of B cells, T cells, endothelia and neurons (Wright *et al*., 2001).

Initially, cells expressing full-length vOX2 and CD200 were used to determine a mechanism for the modest suppression of granulocyte oxidative activity by vOX2:Fc and

CD200:Fc. Native vOX2 and CD200 moderately suppressed the release of IL-8, a potent neutrophil chemoattractant, from a monocytic cell line. However, these data are questionable because though IL-8 production by CD200R-negative THP-1 cells (**Figure 4.9**, **b**) was suppressed by vOX2 and CD200 (**Figure 4.9**, **a**), neither CD200R-positive U937 cells (**Figure 4.9**, **b**) nor CD200R-expressing primary human monocytes (**Figure 4.1**) were affected by vOX2 or CD200 (**Figures 4.9-10**).

Observations had been made in our laboratory that native vOX2 and CD200 suppressed the secretion of IFNγ by antigen-specific T cell clones (Colman and Blackbourn, unpublished). Thus, the focus of this project moved to investigating the putative suppression of viral antigen-specific T cell responses by vOX2 and CD200. A model system was established and the assays optimised to increase sensitivity and reproducibility (data not shown). Fortunately we had access to a library of EBV peptide antigen-specific T cell clones and EBV-positive donors from whom further clones could be derived, with thanks to A.R. Rickinson and his research group. Six further $CD8^+$ T cell clones, HLA-matched to the engineered vOX2-BJAB, CD200-BJAB and Empty-BJAB cells, were derived from an IM patient ($CD8^+$ IM235 c48, c79, c94, c108 and c132). Initially, the suppressive activities of vOX2 and CD200 on IFNγ production by the T cell clones were measured over time post-restimulation of the T cells (Chapter 5). The attenuation of T cell responses by vOX2 and CD200 was variable but reproducible over time, in the six new clones and in two previously isolated clones, $CD8^+$ IM140.1 Y15 and $CD4^+$ SL c93 (**Figures 5.-14**). The latter clones became the 'workhorses' and were used extensively in later experiments.

The obvious drawback of quantifying IFNγ secretion by ELISA is that a threshold concentration must be reached before the cytokine can be detected. Thus, the cells must be stimulated and cultured for at least 16hrs for the cytokine to accumulate in the culture supernatant. In order to reduce the length of time of stimulation, a new assay was optimised

to quantify the accumulation of IFNγ and IL-2 intracellularly by flow cytometry. The new technique was more sensitive and allowed the co-culture of the stimulating peptide-loaded BJAB cells with the T cell clones for only 3hrs before assaying cytokine production (**Figures 5.15-5.19**). By this method, vOX2 and CD200 were found to suppress IFNγ production more consistently, though the suppression of IL-2 was more variable. CD200 was more efficacious than vOX2, though the expression of vOX2 by engineered BJAB cells was harder to maintain (data not shown) and may have been lower than that of CD200, indicating that vOX2 may be somewhat toxic to the cell.

Thus, a suppressive action of vOX2 and CD200 on the activity of stimulated antigen-specific T cell clones had been demonstrated. The next step was to determine the mechanism underlying this inhibition. Zhang *et al*. had elucidated the downstream signalling partners of mCD200R1, activated upon ligation with mCD200:Fc, that led to the suppression of mast cell activity (Zhang *et al*., 2004). Some of the components identified by these researchers that are also involved in the TCR signalling cascade following peptide presentation, and for which phospho-specific antibodies for flow cytometry are available, were investigated. Thus, a flow cytometric assay was developed and optimised to quantify the phosphorylation of three upstream mediators of TCR signalling, Zap70, LAT and SLP-76, and three downstream kinases, ERK1/2, p38 and Akt that activate transcription factors and thus influence cytokine production. The two 'workhorse' clones, $CD8^+$ IM140.1 Y15 and $CD4^+$ SL c93 were investigated, along with one of the new clones, $CD8^+$ IM235 c48. Though vOX2 and CD200 expression did not alter the phosphorylation of upstream adaptor molecules, the phosphorylation of ERK1/2 and Akt was significantly inhibited in all three clones, and there was a trend towards suppression of p38 phosphorylation (**Table 6.1**).

Therefore, the next question to answer was whether the level of suppression of ERK1/2 phosphorylation by vOX2 and CD200 correlated with the level of suppression of

IFNγ production. The concentration of a pharmacological inhibitor of ERK1/2, PD98059 (that inhibits the activation of upstream MEK1/2), at which it suppressed phospho-ERK1/2 in the flow cytometric assay to the same degree as vOX2 and CD200 was elucidated (**Figure 6.18**). This concentration of PD98059 was then administered to the BJAB-T cell cocultures and extracellular IFNγ production quantified by ELISA. PD98059 inhibited IFNγ production by the workhorse clones in a similar fashion to vOX2 and CD200, but to a greater degree (**Table 6.2**). These results suggest that the inhibitory activity of vOX2 and CD200 may reduce over time, as indicated by greater inhibition in the shorter flow cytometric assay, whereas PD98059 remains active throughout the culture period.

In order to elucidate whether the suppressive effects of vOX2 and CD200 were due to ligation of the CD200R on the T cell clones, or due to an unrelated factor such as downregulation of ligands on the engineered BJAB cells, surface expression of proteins by the BJABs were quantified. CD80, a ligand of CD28 and CTLA-4, was significantly reduced on vOX2- and CD200-BJAB cells, but conversely, the expression of their alternate ligand CD86 was slightly increased (though the difference was not statistically significant) (**Figure 6.22**, **b**, **c**). CD80 has a slightly higher affinity for CTLA-4 and CD28 than CD86 (reviewed in Sansom and Walker, 2006), though the alteration in expression levels was so low that the physiological significance is probably slight. The expression of HLA-DR was slightly reduced on vOX2-BJAB cells, though the difference was not statistically significant, and it was unaltered in CD200-BJAB (**Figure 6.22**, **a**). The EBNA2 PRS peptide is restricted through HLA-DR-7, 52a, 52b or 52c, and it is this peptide that the workhorse clone $CD4^+$ SL c93 is directed against. In contrast, the expression of HLA-ABC was reduced by approximately 30% on the surface of vOX2 and CD200-expressing BJAB cells (**Figure 6.23**, **a**), and was not due to increased internalisation of the protein (**Figure 6.24**) but to a reduction in the total cellular HLA-ABC (**Figure 6.25**). Interestingly, BJAB cells engineered

to express vOX2 and CD200 tagged with EGFP showed no alteration of their surface or total HLA-ABC levels (**Figures 6.23/5**). These data suggest that the EGFP tag may modify the activity of vOX2 and CD200, though these proteins were not used in the T cell function assays and so conclusions cannot be drawn. The $CD8^+$ clones are directed against the BRLF1 peptide YVL, restricted through HLA-A2.01. However, the level of suppression of the HLA-ABC-restricted $CD8^+$ clones was not increased above that of the HLA-DR-restricted $CD4^+$ clone overall. Thus, the alteration in the number of MHC molecules on the surface of vOX2 or CD200-expressing APCs is unlikely to account for their suppressive activities.

An illustration of the major findings relating to the roles of vOX2 and CD200 in modulating antigen-specific T cell function (**Figure 9.1**) summarises the putative mechanism of action of these proteins. Suppression of ERK1/2 phosphorylation correlated with reduced IFNγ production, and therefore indicates that gene transcription downstream of this kinase was altered. The suppression of phospho-Akt may have an additive effect upon the suppression of T cell activity observed in cells in which ERK1/2 phosphorylation is inhibited. A trend towards suppression of p38 was also observed, but JNK could not be investigated due to a lack of suitable phospho-specific antibodies. Downregulation of JNK following the recruitment of inhibitory adaptor molecules to the signalling residues of the mCD200R1 has been reported previously (Zhang *et al*., 2004). Unfortunately, due to the dual cell population, the separation of the BJAB and T cells and subsequent analysis of signalling molecules associated with the CD200R was impossible. Therefore, the inhibitory pathways identified by Zhang *et al*. and the associated proteins are also illustrated, though the link between CD200R signalling and suppression of protein phosphorylation is as yet unknown.

The lack of inhibition of upstream adaptor molecules Zap70 and SLP-76 may be due to the CD200R signalling pathway intercepting the TCR signalling cascade further downstream. However, the modulation of some of these upstream proteins is less certain as

they are more difficult to detect than the amplified molecules downstream, evidenced by the inability of this assay to detect phospho-LAT in the $CD8^+$ IM140.1 Y15 clone (Appendix D).

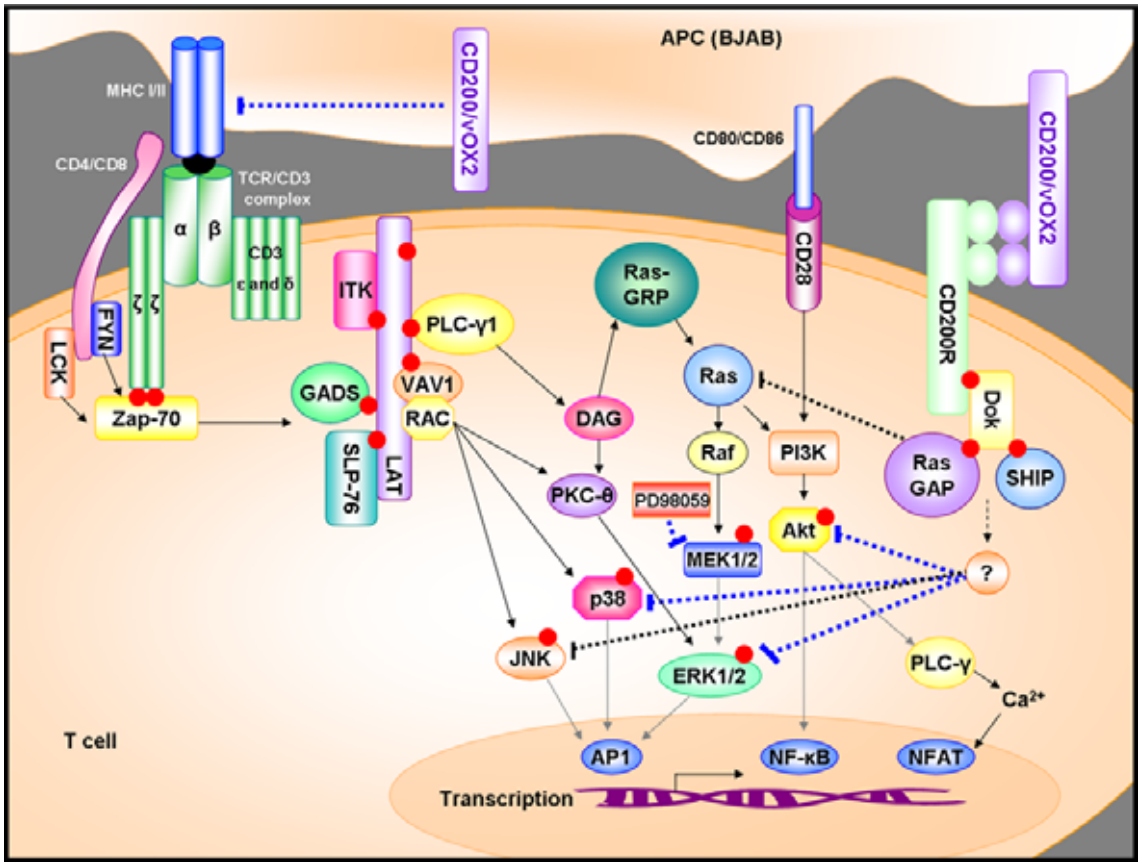

Figure 9.1 Proposed inhibition of the T cell receptor (TCR) signalling pathway by vOX2 and CD200. Upon TCR ligation to a MHC-peptide complex, a signalling cascade is initiated, ultimately resulting in gene transcription (e.g. IL-2 production). The phosphorylation of ERK1/2, p38 and Akt molecules (indicated by red dots) was reduced in T cell clones stimulated by vOX2 or CD200-expressing BJAB cells (blue dashed lines) in the present study, though levels of phospho-LAT, Zap-70 and SLP-76 were not altered. The pharmacological inhibitor of ERK1/2, PD98059, inhibits the phosphorylation of MEK1/2. HLA-ABC (MHC I) cell-surface expression was downregulated by BJAB cells engineered to express vOX2 or CD200, though total HLA-ABC levels were suppressed in only vOX2-BJAB, in comparison to control cells. Earlier evidence for the inhibition of the MAP kinase pathway by ligation of the mCD200R was identified in murine mast cells (Zhang *et al*., 2004). The inhibition of Ras and JNK by mCD200R1 ligation, which was not repeated in this study, is illustrated by black dashed lines. Amended from Schwartzberg *et al*. (2005), Alegre *et al*. (2001), Abraham and Weiss (2004) and Zhang *et al*. (2004).

Proteins that may contribute to the vOX2- and CD200-mediated suppression of T cell activity are CD200R and two other receptors, specifically the stimulatory CD28, and the inhibitory CTLA-4. Native expression of CD200R by antigen specific $CD8^+$ T cells *ex vivo* was confirmed (**Figures 7.1-7**). CD200R was also detected on the surface of the T cell clones, along with barely detectable levels of CTLA-4, consistent with the literature, and CD28 (**Figure 7.8**). In order to discover any modification of CD200R, CD28 or CTLA-4 expression by vOX2 or CD200, the culture conditions of the extracellular IFNγ assay were simulated. After 16hrs of incubation, the T cell clones were analysed for CD200R, CD28 and CTLA-4 expression by flow cytometry. Interestingly, the two inhibitory receptors, CD200R and CTLA-4, were significantly reduced in the presence of vOX2 and CD200, and this downregulation was enhanced when the cells were stimulated with cognate peptide antigen (**Figures 7.11-12**). In contrast, the expression of CD28, a receptor that amplifies the TCR signalling cascade, was unaltered. CTLA-4 is naturally upregulated on activated T cells, but dowregulated on resting T cells (Jago *et al*., 2004), likewise the CD200R (Masocha, 2009). The similarity between the expression patterns of CD200R and CTLA-4 suggests that both receptors may be regulated by similar mechanisms, and that both may be withdrawn from the cell surface upon inhibition of the cellular response to peptide stimulation by vOX2 and CD200. Both CD200R and CTLA-4 therefore appear to deliver complementary negative regulatory signals to T cells. However, the downregulation of CD200R and CLTA-4 must first be confirmed to ensure that the flow cytometric data are not a result of an occlusion of Ab-binding sites following ligand-receptor ligation. This could be achieved by testing several Abs that bind to different epitopes of the proteins, and by investigating whether the internalisation of the proteins is altered.

Having identified a role for both KSHV vOX2 and CD200 in reducing the T cell response to antigen, another viral homologue of CD200, RRV vOX2, was studied in a

similar fashion. In order to replicate previous studies, the full-length RRV vOX2 protein was expressed on the surface of BJAB cells, but was tagged with EGFP to enable detection of the protein. RRV vOX2 did not suppress the activity of human T cell clones (**Figure 8.8**), but in fact modestly increased their secretion of IFNγ. Expressing RRV vOX2-EGFP on the surface of BJAB cells also increased the expression of HLA-ABC by these cells (**Figure 8.7**), perhaps providing a mechanism for the observed increase in T cell response to peptide. Three CMV proteins with unknown physiological properties were also analysed. Similarly to RRV vOX2, CMV proteins UL119, UL120 and UL121 (tagged with GFP) did not suppress T cell activity, but moderately enhanced it (**Figure 8.13**). Surface expression of HLA-ABC was not altered on the CMV protein-expressing BJAB cells (**Figure 8.11**), but overall, the whole cell load of HLA-ABC was reduced in cells expressing UL121 (**Figure 8.12**). However, again these proteins were tagged with GFP which may have altered their stability and activity, and the immunoblotting data were inconclusive.

There were a number of limitations in the present study that must be addressed. Initially, the use of soluble Fc-fusion proteins was deemed to be ineffective and plagued with problems so the methodology was altered in favour of cells expressing native vOX2 and CD200 proteins. However, though this method is more physiologically relevant, experiments involving dual cell populations are limited and are restricted to assays such as flow cytometry which allow the distinction of each cell type by antigen labelling. The flow cytometric assays used in this study were optimised and showed high specificity and reproducibility, but the number of intracellular signalling molecules investigated was limited by the availability of antibodies.

Taken together, these data suggest a role for vOX2 in modulating the immune response to KSHV infection, specifically the T cell response to viral antigens presented by KSHV-infected cells. Importantly, the suppressive role of vOX2 does not appear to be

restricted by HLA allelic variation, nor was it restricted to either $CD8^+$ or $CD4^+$ T cells. vOX2 would be expressed by only a small subset of KSHV-infected cells *in vivo*, because KSHV exists mainly in the latent phase of infection. However, the small percentage of cells infected with lytically replicating KSHV are important for maintenance of infection by propagation and dissemination of the virus. The inflammatory infiltrate characteristic of KS lesions promotes the survival of KSHV-infected spindle cells (Grossmann *et al*., 2006). Thus, the primary role of vOX2 is probably not to reduce inflammation, but rather to prevent direct killing of KSHV-infected cells by antigen-specific cytotoxic T cells either during lytic replication, since vOX2 is a lytic cycle protein, or even during latency or soon after *de novo* infection when *in vivo* data suggest KSHV lytic gene expression occurs without demonstrable virion production (Butler, Nash and Blackbourn, personal communication). The demarcation between genes expressed during latency and lytic replication may be blurred (see Rezaee *et al*, 2006 review). In addition, these data suggest a mechanism for the reported CD200-mediated suppression of inflammation (Hoek et al., 2000; Snelgrove et al., 2008; Broderick et al., 2002; Gorczynski et al., 2001). These data are the first to demonstrate inhibition of antigen-specific T cell activity by either vOX2 or CD200.

9.2 Recommendations for future research

Future research in this area should aim to confirm the binding of vOX2 and CD200 to CD200R expressed by T cell clones, and to prove specificity of binding by blocking their interaction. One method by which this could be achieved would be to examine the level of vOX2- and CD200-mediated suppression of T cell clones that have downregulated their expression of the CD200R following initial culture with vOX2 or CD200. Another means would be to attempt to inhibit the expression of CD200R by retroviral transduction of the T cell clones with a vector encoding a small hairpin RNA in order to silence *CD200R* gene expression.

Downregulation of CD200R and CTLA4 proteins on the T cell clones in the presence of vOX2 and CD200 should be confirmed to ensure the data are not artefactual, e.g. due to occlusion of the Ab-binding sites. The experiments should also be repeated on resting T cells *ex vivo* as their receptor expression levels will differ from cultured T cell clones. The observed downregulation of HLA-ABC on the surface of BJAB cells engineered to express vOX2 and CD200 should be further examined. Does the reduction in HLA expression correlate with reduced vOX2/CD200 expression? Is the HLA targeted for degradation by these proteins or is it sequestered within the cell?

The studies outlined in this thesis should be reproduced in T cell clones with other specificities and HLA-restrictions. Replication of these methods in a KSHV antigen-specific T cell clone model system would be ideal. Cytotoxicity of the T cells should be analysed in conjunction with cytokine production, by labelling perforin in the intracellular granules of the T cell clones.

In addition, the signalling molecules associated with human CD200R should be elucidated. This could be achieved by incubating vOX2-BJAB and CD200-BJAB cells with $CD200R^+$ human T cell clones in order to stimulate the CD200R. Alternatively, stimulatory anti-CD200R Abs can be used if available. CD200R and its associated proteins could be isolated by co-immunoprecipitation of cellular lysates, and putative CD200R-signalling proteins subsequently identified by mass spectrometry.

Finally, the activities of the RRV vOX2 protein should be investigated in a relevant model system utilising rhesus macaque T cell clones and APCs.

Appendix A. Primers and Plasmids

Table I. Primers

Identifying number	Description	Sequence
1F	CD200:Fc (sense)	5’ GCTCTAGATGGAGAGGCTGGTGATCA 3’ (*XbaI*)
1R	CD200:Fc (anti-sense)	5’ TATGCGGCCGCGCCTTTGTTGACGGTTTGC 3’ (*NotI*)
2F	RRV vOX2 translated region (sense)	5’ TTAACGCTGCTGCTGGCG 3’
2R	RRV vOX2 translated region (anti-sense)	5’ ATGCCTAAAACGGCGGCC 3’
3F	Rhesus macaque β-actin (sense)	5’ TACGTGGCCATCCAGGCTG 3’
3R	Rhesus macaque β-actin (anti-sense)	5’ GATGACCTGGCCATCGGG 3’
4F	Full-length RRV vOX2 (sense): for ligation into pCR®-Blunt II-TOPO to act as template for vOX2-EGFP	5’ CGTGTCGGTGGCAACCTTTTTG 3’
4R	Full-length RRV vOX2 (anti-sense): for ligation into pCR®-Blunt II-TOPO to act as template for vOX2-EGFP	5’ ACCACCCTAAAAAGCCAGCCTC 3’

Identifying number	Description	Sequence
5F	RRV vOX2 (sense): to amplify extracellular region before ligation into EGFP-N1 vector	5’ TTTTTGAAAAAGCTTTATTGCCGCCGG 3’ (*HindIII*)
5R	RRV vOX2 (anti-sense): to amplify extracellular region before ligation into EGFP-N1 vector	5’ GGACACGCGCTGCAGCATAGACCTATA 3’ (*PstI*)
6F	RRV vOX2-EGFP (sense): to amplify vOX2 and EGFP before ligation into pQCXIP	5’ CCGGGTGTTAATTAACAACACCGACCG 3’ (*PacI*)
6R	RRV vOX2-EGFP (anti-sense): to amplify vOX2 and EGFP before ligation into pQCXIP	5’ GATTATGATGAATTCTCGCGGCCGCT 3’ (*EcoRI*)

Table II. Plasmids

Plasmid name	Description
pCR®-Blunt II-TOPO® (Invitrogen)	Upon ligation of blunt-ended PCR fragments into pCR®-Blunt II-TOPO®, the lethal *lacZα-ccd*B gene is disrupted, allowing growth of bacteria containing the recombinant vector on kanamycin (or zeocin)-LB agar. There is an *EcoRI* site on either side of the ligated blunt PCR product, along with 3 sequencing primer-binding sites to enable analysis of recombinants.
pTorsten	pTorsten vector has a multiple cloning site upstream of the gene encoding for the Fc region of human IgG_1. Ligating a PCR product into this region results in the translation of the protein of interest fused in-frame with the IgG_1 Fc. Once expressed in eukaryotic cells, the soluble Fc-fusion protein will be secreted into the growth medium. It incorporates both ampicillin and hygromycin B resistance genes.
EGFP-N1 (Clontech)	The EGFP-N1 plasmid contains the gene encoding a variant of GFP, mutated to enhance its fluorescence and level of expression. Genes can be inserted into the plasmid upstream of EGFP, and downstream of the immediate early CMV promoter, via several restriction sites. A neomycin/kanamycin resistance cassette is integrated into the plasmid. Cells engineered to express the plasmid express the protein of interest fused C-terminally to EGFP.
pQCXIP (Clontech)	Genes inserted into the pQCXIP plasmid are driven by the immediate early CMV promoter ($P_{CMV\ IE}$). An internal ribosomal entry site (IRES) downstream of the gene of interest, results in dual transcription of a puromycin resistance gene in cells- both under control of the $P_{CMV\ IE}$.

Appendix B. Antibodies

Table I. Primary antibodies

Antigen	Conjugate	Target Species	Host	Application	Supplier	Catalogue Number
p-Akt (pS473)	Alexa Fluor 647	Human	Mouse	FC	BD Biosciences	560343
β-actin	n/a	Human	Mouse	WB	Sigma	A5441
CD200	n/a	Human	Goat	WB	R&D Systems	AF2724
CD200	n/a	Human	Mouse	FC	BD Pharmingen	552023
CD200	PE	Mouse	Rat	FC	Abcam	ab33739
CD200R	n/a	Human	Mouse	FC	Abcam	ab24104
CD200R1	n/a	Mouse	Goat	FC	R&D Systems	AF2554
CD200R	PE	Mouse	Rat	FC	Abcam	ab35327
CD28	APC	Mouse	Human	FC	BD Biosciences	559770
CD4	VioBlue	Human	Mouse	FC	Miltenyi Biotec	130-094-153
CD4	PE	Human	Mouse	FC	DAKO	R0805
CD4	FITC	Human	Mouse	FC	Immunotools	21270043
CD4	PE/Cy5	Human	Mouse	FC	Caltag	MHCD0406
CD8	PE	Human	Mouse	FC	DAKO	R0806
CD8	PE	Human	Mouse	FC	Miltenyi Biotec	130-091-084
CD8	VioBlue	Human	Mouse	FC	Miltenyi Biotec	130-094-152
CD80	n/a	Human	Mouse	FC	Invitrogen	MHCD8000
CD86	n/a	Human	Mouse	FC	Invitrogen	MHCD8600
CTLA-4	PE	Human	Mouse	FC	BD Biosciences	555853
p-ERK1/2 (T202/&204)	Alexa Fluor 647	Human	Mouse	FC	BD Biosciences	612593

Antigen	Conjugate	Target Species	Host	Application	Supplier	Catalogue Number
p-ERK1/2 (T202/&204)	PE	Human	Mouse	FC	BD Biosciences	612566
HLA-ABC	n/a	Human	Mouse	FC	n/a	n/a
HLA-ABC (HC10)	n/a	Human	Mouse	WB	n/a	n/a
HLA-ABC	Alexa Fluor 647	Human	Mouse	FC	BioLegend	311416
HLA-ABC	PE	Human	Mouse	FC	Serotec	MCA81PE
HLA-DR	n/a	Human	Mouse	FC	R&D Systems	mAB4869
IgG (Fc-specific)	Biotin	Human	Mouse	Microbeads	Calbiochem	411543
IgG (Fc-specific)	HRP	Human	Goat	WB	Sigma	A0170
IFNγ	n/a	Human	Mouse	ELISA	Thermo Scientific	M700A
IFNγ	Biotin	Human	Mouse	ELISA	Thermo Scientific	M701B
IFNγ	APC	Human	Mouse	FC	eBiosciences	17-7319
IL-2	PE	Human	Mouse	FC	eBiosciences	12-7029
LANA 25	n/a	(Viral)	Mouse	IFA	n/a	n/a
p-LAT (pY226)	PE	Human	Mouse	FC	BD Biosciences	558433
p-p38 (pT180/pY182)	Alexa Fluor 647	Human	Mouse	FC	BD Biosciences	612595
p-SLP-76 (pY128)	PE	Human	Mouse	FC	BD Biosciences	558437
vOX2 1172	n/a	(Viral)	Rabbit	WB, IFA	n/a	n/a
vOX2	n/a	(Viral)	Mouse	WB, IFA	n/a	n/a
p-Zap70 (pY292)	Alexa Fluor 647	Human	Mouse	FC	BD Biosciences	558515

Table II. Secondary antibodies

Target Species	Conjugate	Supplier	Host	Application	Catalogue Number
Mouse	HRP	DakoCytomation	Goat	WB	P0447
Mouse IgG1	Alexa Fluor 594	Invitrogen	Goat	IFA	A21125
Mouse IgG	FITC	Sigma	Sheep	FC	F6257
Mouse IgG	R-PE	Invitrogen	Goat	FC	P852
Mouse IgG	FITC	DAKO	Goat	FC	F0479
Goat	HRP	Abcam	Rabbit	WB	ab6741
Rabbit	HRP	DakoCytomation	Goat	WB	P0448
Rabbit IgG	Alexa Fluor 594	Invitrogen	Goat	IFA	A11037
Rabbit	R-PE	Invitrogen	Goat	FC	P2771MP

Table III. Isotype control antibodies

Antibody	Conjugate	Supplier	Species	Application	Catalogue Number
IgG1	--	Sigma	Mouse	FC	M5284
IgG1	APC	BD Biosciences	Mouse	FC	555751
IgG1	PE/Cy5	Serotec	Mouse	FC	MCA1209C
IgG2a	FITC	BD Biosciences	Mouse	FC	349051
IgG2a	PE/CY5	Immunotools	Mouse	FC	21335025
IgG2a	PE	EBioscience	Rat	FC	12-4321
IgG2a κ	PE	BD Biosciences	Mouse	FC	555574
IgG2b	PE	Ancell	Mouse	FC	284-050

Appendix C. Reagents and solutions

Table I. Reagents and consumables

Reagents/consumables	Supplier	Catalogue Number
16% formaldehyde (methanol-free)	TAAB	F017
1700cm^2 expanded cell culture roller bottles	Corning	430852
3,3'-dihexyloxacarbocyanine iodide (DiOC6)	Sigma	318426
3,3'5,5'-Tetramethyl-benzidine (TMB)	Sigma	T8665
3,3'5,5'-Tetramethyl-benzidine (TMB) ELISA peroxidase substrate	Rockland	TMBE-1000
5ml polystyrene round bottom tubes	BD (Falcon)	352054
96-well, tissue culture-treated luminometer plates	Greiner	655083
96-well maxi-sorp immunoplates for ELISA	Nunc	442404
96-well v-bottomed plates	Nunc	249946
Bovine serum albumin (endotoxin-free)	Sigma	A9430
Brefeldin A (in DMSO)	Sigma	B5936
Bursttest (Phagoburst®)	Orpegen	10-0200
Cell dissociation solution (non-enzymatic)	Sigma	C5789
Centricon Ultracell YM-50 centrifugal filter device	Millipore	4224
Chloroquine	Sigma	C6228
Chromium-51	Perkin Elmer	NEZ147010MC
DAPI (4′,6-Diamidino-2-phenylindole dihydrochloride)	Sigma	D9542
Defined foetal bovine serum	Hyclone	SH30070.02
Deoxycytidine 5'-triphosphate [α-^{32}P]	PerkinElmer	NEG513H250UC
DePex	Sigma	317616
Dextran 500	Amersham Biosciences	17-0320-01
DMEM	Invitrogen	41966-025
(PfU) DNA polymerase	Promega	M744
DuoSet ELISA Development kit (Human CXCL8/IL-8)	R&D Systems	DY208
Endo-free plasmid maxi kit	Qiagen	12362
Ethylenediaminetetraacetic acid disodium salt solution (0.5M)	Sigma	E7889
ExtrAvidin-peroxidase	Sigma	E2886
Foetal bovine serum (FBS)	PAA	A15-043

Reagents/consumables	Supplier	Catalogue Number
Granulocyte-macrophage colony-stimulating factor (GM-CSF)	Sigma	G5035
Hanks' balanced salt solution (HBSS)	Sigma	H8264
Hexadimethrine bromide (polybrene)	Sigma	H9268
HiTrap Protein A HP column	Amersham Biosciences	17-0403-01
Hybond-N nylon membrane for nucleic acid transfer	Amersham Biosciences	RPN303N
Hygromycin B	Invitrogen	10687-010
Hyperfilm MP	Amersham Biosciences	28906846
Immobilon-P transfer membrane (PVDF)	Millipore	IPVH07850
LB broth	Acros Organics	AC612725000
L-Glutamine 200mM	Invitrogen	25030
Limulus Amebocyte Lysate (LAL) QCL-1000	Lonza	50-647U
Lipofectamine reagent	Invitrogen	18324
Lipofectamine 2000	Invitrogen	11668
Lymphoprep™	Axis-Shield Poc	LYS 3772
M-MLV reverse transcriptase	Invitrogen	28025
Mouse serum	Sigma	M5905
N,N'-dimethyl-9,9-biacridinium dinitrate (lucigenin)	Sigma	M8010
N-Formyl-L-methionyl-L-leucyl-L-phenylalanine (fMLP)	Sigma	F3506
Penicillin-Streptomycin (PenStrep)	Invitrogen	15070-063
Percoll	Sigma	P1644
Phosphate buffered saline sterile powder (PBS)	Sigma	D5773
Phytohaemagglutinin (PHA)	Sigma	L1668
ProLong® Gold anti-fade reagent	Invitrogen	P36934
ProSieve® colour protein marker	Lonza	50550
Protease inhibitor cocktail tablets	Roche	11 836 153 001
PureYield™ Plasmid Midiprep system	Promega	A2493
Puromycin dihydrochloride	Sigma	P9620
QIAprep® Spin Miniprep kit	Qiagen	27106
QIAquick® Gel Extraction kit	Qiagen	28704
QIAquick® Nucleotide Removal kit	Qiagen	28304
Random primers	Promega	C1181
Random primers DNA labelling system	Invitrogen	18187-013
Recombinant human interferon-γ	R&D Systems	285-IF

Reagents/consumables	Supplier	Catalogue Number
RNAse OUT	Invitrogen	10777-019
RNeasy Mini Kit	Qiagen	74104
RPMI 1640	Invitrogen	15070-063
Stericup vacuum filter system (0.22µm membrane)	Millipore	SCGPU10RE
Sterile water	Aguettant	0459
T cell expansion kit (microbeads)	Miltenyi Biotec	130-091-441
TOPO TA cloning kit for sequencing	Invitrogen	K4575
Trypsin-EDTA	Invitrogen	25300
Tumour necrosis factor-α (TNFα)	Serotec	PHP051A
Western Lightning™ Chemiluminescence Reagent Plus	PerkinElmer	NEL103

Table II. Common solutions

Name/Purpose	Composition
Buffer E for cell lysis	100mM TrisHCl pH 8, 2mM EDTA, 2mM EGTA, 1% NP40, 0.5% Na deoxycholate, 0.5mM PMSF
Colloidal coomassie stain for SDS-PAGE	0.08% coomassie brilliant blue G250, 1.6% orthophosphoric acid, 8% ammonium sulphate, 20% methanol
Denaturation buffer (southern blotting)	1.5M NaCl, 500mM NaOH
Complete medium	RPMI 1640, 10% FBS, 1% PenStrep
Complete BJAB medium	RPMI 1640, 10% FBS, 1% PenStrep, 1µg/ml puromycin
Complete CHO medium	RPMI 1640, 10% FBS, 1% PenStrep, 400µg/ml Hygromycin B
Complete GP2-293 medium	DMEM, 10% FBS, 1% PenStrep, 1% L-Glutamine
Complete neutrophil medium	RPMI 1640, 10% FBS, 1% L-Glutamine, 1% PenStrep
Complete RFB medium	DMEM, 1x non-essential amino acids, 10% defined FBS, 1% L-Glutamine

Name/Purpose	Composition
Complete T cell cloning medium	RPMI 1640, 30% MLA supernatant (from the IL-2-producing gibbon leukaemia MLA 144 line), 10% FBS, 1% human serum, 1% Pen-Strep, 50U/ml IL-2
ELISA coating buffer	0.1M Na_2HPO_4, pH9
ELISA blocking buffer	1% BSA, 0.05% Tween 20, PBS
ELISA stop solution	1M HCl
ELISA wash buffer	1x PBS, 0.05% Tween 20
Enhanced chemiluminescence solutions	Solution 1: 2.5mM luminol, 396μM coumaric acid, 100mM TrisHCl pH 8.5; Solution 2: 0.019% H_2O_2, 100mM TrisHCl pH 8.5
MOPS buffer (10x)	197mM 3-(N-morpholino)propanesuphonic acid, 80mM sodium acetate 3-hydrate, 12.7mM EDTA sodium salt, pH 7
MOPS/formaldehyde gel	0.7M formaldehyde, 1x MOPS buffer, 1.2% agarose
Neutralisation buffer (southern blotting)	1.5M NaCl, 500mM Tris base, pH 7.5
Nobles agar (virus plaque assay)	1.4% Nobles agar, 2x DMEM, 2.5% 1M $MgCl_2$, 1.15% Na bicarbonate, 2% L-glutamine, 4% FBS, 2% Pen-Strep
NP-40 buffer (SDS-PAGE)	20mM Tris HCl (pH 8), 137mM NaCl, 10% glycerol, 1% NP-40, 2mM EDTA
Nucleic acid transfer buffer (20x SSC)	300mM tri-sodium citrate, 3M NaCl, pH 7-8
Pre-transfection medium	RPMI 1640, 10% FBS
Post-transfection medium	RPMI 1640, 20% FBS
PVDF membrane stripping buffer	100mM 2-mercaptoethanol, 2% SDS, 62.5mM TrisHCl pH 6.7
Sample loading buffer (2x)	0.125M TrisHCl pH 6.8, 4% SDS, 18.4M glycerol, 286mM 2-mercaptoethanol, 0.004% bromophenol blue
SDS-PAGE running buffer (10x)	250mM Tris base, 1.92M glycine, 0.01% SDS, pH 8.6
SDS-PAGE transfer buffer (10x)	250mM Tris base, 1.92M glycine

Name/Purpose	Composition
SDS-PAGE resolving gel (12%)	12% bis-acrylamide, 375mM TrisHCl pH 8.8, 0.1% SDS, 0.08% ammonium persulphate, 151mM N,N,N,N'-tetramethylethylenediamine
SDS-PAGE stacking gel	5% bis-acrylamide, 126mM TrisHCl pH 6.8, 0.1% SDS, 0.12% ammonium persulphate, 116mM N,N,N,N'-tetramethylethylenediamine
TAE (50x)	2M Tris base, 2M EDTA sodium salt, 50mM glacial acetic acid
TBS (10x)	1.54M NaCl, 2M Tris base

Appendix D. Raw data

Table I. Neutrophil Phagoburst assay (raw median fluorescence data)

(8µg recombinant protein)

	Median fluorescence								
Donor number	**T07.116**	**T07.117**	**T07.118**	**T07.102**	**T07.212**	**T07.213**	**T07.214**	**T07.255**	**T07.256**
E. coli	2.37	2.36	6.75	5.54	6.19	4.83	7.34	5.94	5.76
E. coli	3.28	4.14	6.35		4.86	5.61	9.13	5.95	8.36
E. coli + vOX2:Fc	2.18	3.29	7.04	2.14				5.53	6.46
E. coli + vOX2:Fc	3.12	2.13	3.99						
E. coli + CD200:Fc					5.59	6.29	6.29	5.19	6.03
E. coli + CD200:Fc					5.25	3.49	6.13	3.01	3.6
E. coli + KCPmut:Fc	2.34	2.66	6.79	4.68	4.25	6.02	7.81	6.72	5.73
E. coli + KCPmut:Fc	2.09	2.93	7.37		5.75	7.03	7.13		

(24µg recombinant protein)

	Median fluorescence		
Donor number	**T07.240**	**T07.255**	**T07.256**
E. coli	9.1	5.94	5.76
E. coli	6.73	5.95	8.36
E. coli + vOX2:Fc		4.65	6.44
E. coli + vOX2:Fc		4.43	4.72
E. coli + CD200:Fc	5.04	3.54	5.76
E. coli + CD200:Fc	5.33	5.89	5.84
E. coli + KCPmut:Fc	8.12	3.86	5.34
E. coli + KCPmut:Fc	9.66	4.92	5.58

Table II. Flow cytometric analysis of intracellular cytokines in the $CD4^+$ SL c93 T cell clone (raw median fluorescence data)

IL-2 (FL2 Median fluorescence)

1hr post-Brefeldin A treatment

	28-Apr-09	08-May-09
Empty vector		
No peptide	596.27	268.83
Peptide (50ng/ml)	1106.51	445.16
vOX2		
No peptide	533.29	238.33
Peptide (50ng/ml)	837.47	380.89
CD200		
No peptide	542.16	229.71
Peptide (50ng/ml)	754.3	322.99

2hr post-Brefeldin A treatment

	28-Apr-09	08-May-09	01-May-09	05-May-09
Empty vector				
No peptide	508.11	252.42	447.7	608.99
Peptide (50ng/ml)	1131.41	472.45	775.42	1003.14
vOX2				
No peptide	475.82	252.67	396.26	512.82
Peptide (50ng/ml)	878.94	405.21	578.47	1126.46
CD200				
No peptide	427.95	228.72	399.01	523.42
Peptide (50ng/ml)	825.85	326.93	541.49	858.41

4hr post-Brefeldin A treatment

	28-Apr-09	08-May-09
Empty vector		
No peptide	514.05	235.94
Peptide (50ng/ml)	1210.93	440.3
vOX2		
No peptide	503.84	238.5
Peptide (50ng/ml)	810.14	446.72
CD200		
No peptide	504.42	228.98
Peptide (50ng/ml)	748.12	337.67

IFNγ (FL4 Median fluorescence)

	28-Apr-09	08-May-09
Empty vector		
No peptide	212.12	136.12
Peptide (50ng/ml)	5385.31	5465
vOX2		
No peptide	186.3	119.53
Peptide (50ng/ml)	2904.27	3963.21
CD200		
No peptide	185.42	111.36
Peptide (50ng/ml)	2273.84	2867.57

	28-Apr-09	08-May-09	01-May-09	05-May-09
Empty vector				
No peptide	167.63	128.7	166.25	206.15
Peptide (50ng/ml)	11706.58	7262.72	9212.23	29120.67
vOX2				
No peptide	157.12	123.64	152	174.51
Peptide (50ng/ml)	6070.05	5817.27	5827.09	20787.29
CD200				
No peptide	141.69	105.85	159.06	172.93
Peptide (50ng/ml)	3619.63	2988	4015.58	10243.85

	28-Apr-09	08-May-09
Empty vector		
No peptide	158.69	114.46
Peptide (50ng/ml)	10531.76	8088.01
vOX2		
No peptide	162.63	114.85
Peptide (50ng/ml)	3855.47	8028.52
CD200		
No peptide	162.66	110.4
Peptide (50ng/ml)	4555.95	5222.93

Table III. Flow cytometric analysis of intracellular cytokines in the CD8$^+$ IM140.1 and IM235 T cell clones (raw median fluorescence data)

	IL-2 (FL2 Median fluorescence)			IFNγ (FL4 Median fluorescence)		
IM140.1 Y15	**15-Jul-09**	**17-Jul-09**	**13-Jul-09**	**15-Jul-09**	**17-Jul-09**	**24-Jul-09**
Empty vector						
No peptide	184.54	68.98	69.87	242.03	498.4	635.84
PRS (500ng/ml)	402.22	199.37	247.04	7731.71	2740.11	20003.12
vOX2						
No peptide	174.42	85.99	75.72	238.46	455.18	681.01
PRS (500ng/ml)	378.5	140.78	142.06	5948.53	2115.09	6781.01
CD200						
No peptide	183.17	83.62	73.17	245.13	483.83	676.84
PRS (500ng/ml)	413.1	140	162.92	4595.03	1305.75	2836.2
IM235 c48						
Empty vector						
No peptide	160.4	69.2		201.83	346.66	
PRS (500ng/ml)	486.17	341.04		8790.51	18381.05	
vOX2						
No peptide	161.75	70.11		212.99	469.57	
PRS (500ng/ml)	424.87	346.66		5156.5	2349.15	
CD200						
No peptide	161.58	78.88		203.18	494.97	
PRS (500ng/ml)	508.38	365.57		4404.21	903.39	
IM235 c79						
Empty vector						
No peptide	182.66	114.11	87.28	217.54	495.11	645.82
PRS (500ng/ml)	456.94	369.07	363.08	9245.53	575.78	1210.58
vOX2						
No peptide	193.55	101.46	86.8	237.6	524.35	638.85
PRS (500ng/ml)	403.88	356.47	344.77	7055.24	563.88	1695.17
CD200						
No peptide	194.9	89.36	91.13	227	368.99	659.74
PRS (500ng/ml)	479.51	400.58	399.81	2420.3	426.03	976.11
IM235 c94						
Empty vector						
No peptide	135.86	57.67		171.61	351.41	
PRS (500ng/ml)	179.07	68.09		9859.22	22501.32	
vOX2						
No peptide	140.78	72.36		173.62	362.34	
PRS (500ng/ml)	165.69	94.03		7078.59	20116.25	
CD200						
No peptide	147.03	76.95		183.69	441	
PRS (500ng/ml)	158.93	89.79		7649.53	12283.51	

Table IV. Flow cytometric analysis of intracellular signalling molecules in the $CD4^+$ SL c93 T cell clone (raw median fluorescence data)

ERK1/2	Empty-BJAB	26/01/2009	02/02/2009	13/02/2009	17/03/2009	23/03/2009	05/05/2009	03/04/2009
	No peptide	190.31	223.71	177.7	179.32	185.31	202.66	179.46
	Peptide (500ng/ml)	304.33	338.04	500.18	540.73	441.97	580.09	478.72
	Peptide (50ng/ml)				535.44			
	vOX2-BJAB							
	No peptide	177.34	207.79	178.8	223.9	159.8	234.41	
	Peptide (500ng/ml)	212.11	273.5	445.09	276.08	406.37	345.53	
	Peptide (50ng/ml)				382.8			
	CD200-BJAB							
	No peptide	178.45	205.77	159.02	193.58	177.19	203.06	166.01
	Peptide (500ng/ml)	188.72	338.35	313.85	516.47	296.06	391.38	304.51
	Peptide (50ng/ml)				372.6			

p38	Empty-BJAB	23/01/2009	26/01/2009	02/02/2009	13/02/2009	17/03/2009	23/03/2009	05/05/2009	03/04/2009
	No peptide	138.24	129.68	175.52	113.63	112.14	117.96	26.13	119.28
	Peptide (500ng/ml)	204.46	329.95	257.1	506.55	303.22	346.01	110.79	282.49
	Peptide (50ng/ml)	247.48				287.56			
	vOX2								
	No peptide	129.51	118.06	160.2	118.91	111.64	112.54	23.39	
	Peptide (500ng/ml)	179.81	201.4	209.07	419.28	263.32	292.59	115.15	
	Peptide (50ng/ml)	128.18				246.83			
	CD200								
	No peptide	127.63	113.6	151	111.99	112.11	118.93	24.47	111.89
	Peptide (500ng/ml)	192.01	206.1	237.42	390.61	309.07	248.03	102.87	225.22
	Peptide (50ng/ml)	130.41				255.3			

SLP-76	Empty-BJAB	02/02/2009	03/02/2009	13/02/2009	05/05/2009	21/07/2009
	No peptide	153.08	117.2	156.81	119.82	78.95
	Peptide (500ng/ml)	171.9	129.86	224.85	213.44	117.9
	vOX2					
	No peptide	135.94	114.33	222.21	135.06	83.3
	Peptide (500ng/ml)	171.2	119.18	247.93	191.87	152.64
	CD200					
	No peptide	148.55	110.56	175.61	155.27	86.13
	Peptide (500ng/ml)	186.29	120.59	279.43	266	130.41

Akt	Empty-BJAB	02/02/2009	03/02/2009	13/02/2009	05/05/2009	29/05/2009
	No peptide	403.56	344.24	241.46	64.45	210.56
	Peptide (500ng/ml)	680.65	435.5	634.85	178.41	608.7
	vOX2					
	No peptide	367.91	310.41	228.96	59.68	211.22
	Peptide (500ng/ml)	471.99	370.09	514.37	141.64	525.83
	CD200					
	No peptide	330.82	296.83	211.65	59.11	212.12
	Peptide (500ng/ml)	531.44	368.95	518.36	150.25	532.81

LAT	Empty-BJAB	02/02/2009	13/02/2009	17/07/2009	29/05/2009
	No peptide	127.67	82.91	78.97	88.67
	Peptide (500ng/ml)	139.97	93.86	95.67	110.8
	vOX2				
	No peptide	124.11	84.65	76.06	89.9
	Peptide (500ng/ml)	133.05	98.66	100.02	113.19
	CD200				
	No peptide	118.42	82.86	67.71	92.35
	Peptide (500ng/ml)	125.42	92.51	96.4	115.64

Zap70	Empty-BJAB	17/07/2009	21/07/2009	22/07/2009	15/07/2009
	No peptide	166.35	122.29	125.95	170.69
	Peptide (500ng/ml)	315.21	179.16	170.12	253.44
	vOX2				
	No peptide	177.7	126.52	116.9	168.74
	Peptide (500ng/ml)	298.26	218.58	197.63	224.18
	CD200				
	No peptide	164.56	131.48	119.19	173.71
	Peptide (500ng/ml)	305.19	193.02	192.61	263.32

Table V. Flow cytometric analysis of intracellular signalling molecules in the CD8$^+$ IM140.1 Y15 T cell clone (raw median fluorescence data)

ERK1/2	Empty-BJAB	17/03/2009	23/03/2009	24/11/2008	22/05/2009	
	No peptide	115.57	142.17	244.07	171.08	
	Peptide (50ng/ml)	357.72	776.62	593.91	327.77	
	vOX2-BJAB					
	No peptide	102.11	135.72	221.1	171.36	
	Peptide (50ng/ml)	212.46	210.69	344.15	346.96	
	CD200-BJAB					
	No peptide	114.49	155.67	227.83	144.69	
	Peptide (50ng/ml)	267.55	227.09	346.69	273.89	

p38	Empty-BJAB	17/03/2009	23/03/2009	02/12/2008	22/05/2009	03/04/2009
	No peptide	82.12	84.65	121.49	116.68	87.81
	Peptide (50ng/ml)	255.12	414.6	184.48	407.66	252.62
	vOX2-BJAB					
	No peptide	80.42	83.19	119.38	124.82	
	Peptide (50ng/ml)	237.24	190.23	159.57	480.33	
	CD200-BJAB					
	No peptide	77.64	85.68	120.85	114.19	76.46
	Peptide (50ng/ml)	265.67	177.66	192.59	405.95	174.54

SLP-76	Empty-BJAB	23/03/2009	22/05/2009	09/07/2009	15/07/2009
	No peptide	86.14	113.36	136.1	169.53
	Peptide (50ng/ml)	175.87	180.51	509.74	355.38
	vOX2-BJAB				
	No peptide	122.7	105.56	140.76	162.27
	Peptide (50ng/ml)	112.04	265.92	463.71	332.97
	CD200-BJAB				
	No peptide	96.45	136.11	148.06	145.87
	Peptide (50ng/ml)	174.69	191.2	425.81	318.18

Akt	Empty-BJAB	17/03/2009	23/03/2009	22/05/2009	09/07/2009	17/07/2009
	No peptide	229.76	203.03	302.68	249.92	168.18
	Peptide (50ng/ml)		891.17	640.96	1045.78	712.21
	vOX2-BJAB	469.18				
	No peptide					
	Peptide (50ng/ml)	214.8	204.75	303.69	258.73	167.71
	CD200-BJAB		364.82	644.8	967.53	568.79
	No peptide	282.02				
	Peptide (50ng/ml)					
	No peptide	202.78	179.1	320.73	236.59	154.47
	Peptide (50ng/ml)		503.68	522.06	839.5	582.54
	Peptide (5ng/ml)	319.9				

LAT	Empty-BJAB	09/07/2009	15/07/2009	17/07/2009	24/07/2009	
	No peptide	55.48	66.45	68.4	62.65	
	Peptide (50ng/ml)	90.15	84.95	62	58.74	No detectable response
	vOX2-BJAB					
	No peptide	57.54	65.39	58.92	50.17	
	Peptide (50ng/ml)	78.46	87.12	78.72	55.11	
	CD200-BJAB					
	No peptide	57.74	67.2	71.19	47.32	
	Peptide (50ng/ml)	84.83	82.36	80.98	52.47	

Zap70	Empty-BJAB	18/11/2008	22/05/2009	09/07/2009	15/07/2009
	No peptide	354.01	202.04	276.85	170.69
	Peptide (50ng/ml)	421.84	232.69	559.67	253.44
	vOX2-BJAB				
	No peptide	322.99	209.51	277.37	168.74
	Peptide (50ng/ml)	315.34	233.34	637.37	224.18
	CD200-BJAB				
	No peptide	289.59	202.56	268.99	173.71
	Peptide (50ng/ml)	329.95	228.01	584.18	263.32

Table VI. Flow cytometric analysis of intracellular signalling molecules in the $CD8^+$ IM235 c48 T cell clone (raw median fluorescence data)

ERK1/2

Empty-BJAB	15/07/2009	17/07/2009	21/07/2009	22/07/2009
No peptide	168.58	118.17	67.31	69.73
Peptide (50ng/ml)	690.53	512.61	234.44	354.71
vOX2-BJAB				
No peptide	154.36	116.49	68.96	71.19
Peptide (50ng/ml)	445.4	559.8	129.22	282.88
CD200-BJAB				
No peptide	154.33	114.79	66.89	72.27
Peptide (50ng/ml)	338.16	409.38	175.42	265.17

p38

Empty-BJAB				
No peptide	74.61	74.75	59.25	43.59
Peptide (50ng/ml)	465.89	353.72	157.43	288.91
vOX2-BJAB				
No peptide	72.68	71.09	64.85	42.2
Peptide (50ng/ml)	471.16	454.89	133.28	324.2
CD200-BJAB				
No peptide	67.32	76.24	65.18	44.59
Peptide (50ng/ml)	387.01	356.96	172.01	268.55

Table VII. Flow cytometric analysis of proteins expressed on the surface of the engineered BJAB cells (raw median fluorescence data)

	Median fluorescence					
	03/03/2009	10/03/2009	19/03/2009	26/03/2009	02/04/2009	07/05/2009
HLA-ABC isotype						
Empty-BJAB		0.34	0.33	0.28	0.33	0.26
vOX2-BJAB			0.29		0.3	0.33
CD200-BJAB		0.29	0.31	0.26	0.32	0.25
HLA-ABC						
Empty-BJAB		46.22	40.63	29.55	53.33	43.6
vOX2-BJAB			28.68		33.33	30.09
CD200-BJAB		35.35	30.58	21.55	34.19	29.47
IgG1 isotype						
Empty-BJAB	0.3	0.3	0.32	0.29	0.32	0.34
vOX2-BJAB	0.3		0.31		0.24	0.31
CD200-BJAB	0.21	0.25	0.24	0.25	0.22	0.3
HLA-DR						
Empty-BJAB			250.35	134.25	177.43	189.88
vOX2-BJAB			144.83		136.15	188.83
CD200-BJAB			192.25	118.66	216.81	166.53
CD80						
Empty-BJAB	3.81	4.48	3.57	2.67	2.55	
vOX2-BJAB	3.23		2.66		2.16	
CD200-BJAB	2.95	3.22	2.74	2.68	2.02	
CD86						
Empty-BJAB	22.81	21.18	26.5	19.14	24.67	
vOX2-BJAB	29.29		23.58		35.41	
CD200-BJAB		23.69	31.37	20.63	33.23	

	02/06/2009	08/07/2009	25/05/2009	25/06/2009
HLA-ABC isotype				
Empty-BJAB	82.61	77.94	60.97	72.27
vOX2EGFP-BJAB	82.48	63.22	58.75	72.57
CD200EGFP-BJAB	86.66	71.63	66.7	69.81
HLA-ABC				
Empty-BJAB	62385.86	85183.55	57719.1	69141.57
vOX2EGFP-BJAB	41852.82	85823.06	46375.98	67386.52
CD200EGFP-BJAB	45287.92	86332.8	53489.45	63898.68

	08/07/2009
HLA-ABC isotype	
Empty	77.94
CMV 119-BJAB	82
CMV 120-BJAB	76.46
CMV 121-BJAB	69.99
HLA-ABC	
Empty-BJAB	85183.55
CMV 119-BJAB	91134.48
CMV 120-BJAB	87680.77
CMV 121-BJAB	89960.83

Table VIII. Flow cytometric analysis of CD200R, CTLA-4 and CD28 on the surface of the $CD8^+$ IM140.1 Y15 T cell clone cocultured with APCs engineered to express either vOX2 or CD200 (raw median fluorescence data)

$CD8^+$ IM140.1 Y15 T cell clone				
CD200R	**Median fluorescence**			
	13/08/2009	11/08/2009	29/08/2009	30/08/2009
Empty-BJAB no peptide	527.87	792.12	1271.75	1463.25
Empty-BJAB + peptide	497.03	864.87	1631.47	1715.28
vOX2-BJAB no peptide			583.81	695.59
vOX2-BJAB + peptide			464.76	507.09
CD200-BJAB no peptide	242.06	393.61	515.02	
CD200-BJAB + peptide	128.48	255.15	458.2	
CTLA-4				
	13/08/2009	11/08/2009	29/08/2009	30/08/2009
Empty-BJAB no peptide	271.11	292.6	382.88	441.45
Empty-BJAB + peptide	327.85	427.06	566.63	617.06
vOX2-BJAB no peptide			238.81	275.29
vOX2-BJAB + peptide			329.27	278.32
CD200-BJAB no peptide	165.03	207.64	218.8	
CD200-BJAB + peptide	171.09	275.4	344.07	
CD28				
	13/08/2009	11/08/2009	29/08/2009	30/08/2009
Empty-BJAB no peptide	229.12	231.43	263.86	343.26
Empty-BJAB + peptide	282.32	354.05	324.31	423.01
vOX2-BJAB no peptide			237.81	325.63
vOX2-BJAB + peptide			314.32	300.13
CD200-BJAB no peptide	222.73	235.25	238.15	
CD200-BJAB + peptide	223.95	376.39	341.27	

Table IX. Flow cytometric analysis of CD200R, CTLA-4 and CD28 on the surface of the CD4$^+$ SL c93 T cell clone cocultured with APCs engineered to express either vOX2 or CD200 (raw median fluorescence data)

CD4$^+$ SL c93 T cell clone					
CD200R	**Median fluorescence**				
	13/08/2009	11/08/2009	29/08/2009	30/08/2009	31/08/2009
Empty-BJAB no peptide	867.03	1360.49	1933.84	2426.5	1652.71
Empty-BJAB + peptide	689.82	1198.5	2063.49	2003.35	1530.3
vOX2-BJAB no peptide			860.78	1282.72	782.94
vOX2-BJAB + peptide			687.05	637.53	559.58
CD200-BJAB no peptide	422.7	560.04	859.24		
CD200-BJAB + peptide	184.38	340.67	723.88		
CTLA-4					
	13/08/2009	11/08/2009	29/08/2009	30/08/2009	31/08/2009
Empty-BJAB no peptide	430.29	476.65	605.02	723.64	691.21
Empty-BJAB + peptide	467.76	574.89	879.36	877.69	797.7
vOX2-BJAB no peptide			396.02	479.06	417.68
vOX2-BJAB + peptide			623.49	530.56	553.39
CD200-BJAB no peptide	263.16	275.57	394.87		
CD200-BJAB + peptide	260.61	377.02	697.42		
CD28					
	13/08/2009	11/08/2009	29/08/2009	30/08/2009	31/08/2009
Empty-BJAB no peptide	2438.43	1474.64	2695.88	2259.86	2577.51
Empty-BJAB + peptide	1939.8	1548.86	2030.14	1840.96	2510.96
vOX2-BJAB no peptide			2484.79	2082.87	2449.37
vOX2-BJAB + peptide			1902.55	1761.83	2356.16
CD200-BJAB no peptide	2436.25	1443.07	2664.92		
CD200-BJAB + peptide	2243.1	1671.6	2064.8		

References

Abraham, R. T. & Weiss, A. (2004). Jurkat T cells and development of the T-cell receptor signalling paradigm. *Nat Rev Immunol* **4**, 301-8.

Afanas'ev, I. B., Ostrakhovitch, E. A., Mikhal'chik, E. V. & Korkina, L. G. (2001). Direct enzymatic reduction of lucigenin decreases lucigenin-amplified chemiluminescence produced by superoxide ion. *Luminescence* **16**, 305-7.

Ahn, K., Gruhler, A., Galocha, B., Jones, T. R., Wiertz, E. J., Ploegh, H. L., Peterson, P. A., Yang, Y. & Fruh, K. (1997). The ER-luminal domain of the HCMV glycoprotein US6 inhibits peptide translocation by TAP. *Immunity* **6**, 613-21.

Akkaya, M. & Barclay, A. N. (2009). Heterogeneity in the CD200R paired receptor family. *Immunogenetics*.

Alberola-Ila, J. & Hernandez-Hoyos, G. (2003). The Ras/MAPK cascade and the control of positive selection. *Immunol Rev* **191**, 79-96.

Alegre, M. L., Frauwirth, K. A. & Thompson, C. B. (2001). T-cell regulation by CD28 and CTLA-4. *Nat Rev Immunol* **1**, 220-8.

Alegre, M. L., Noel, P. J., Eisfelder, B. J., Chuang, E., Clark, M. R., Reiner, S. L. & Thompson, C. B. (1996). Regulation of surface and intracellular expression of CTLA4 on mouse T cells. *J Immunol* **157**, 4762-70.

Alessi, D. R., Cuenda, A., Cohen, P., Dudley, D. T. & Saltiel, A. R. (1995). PD 098059 is a specific inhibitor of the activation of mitogen-activated protein kinase kinase in vitro and in vivo. *J Biol Chem* **270**, 27489-94.

Alkharsah, K. R., Dedicoat, M., Blasczyk, R., Newton, R. & Schulz, T. F. (2007). Influence of HLA alleles on shedding of Kaposi sarcoma-associated herpesvirus in saliva in an African population. *J Infect Dis* **195**, 809-16.

Ambroziak, J. A., Blackbourn, D. J., Herndier, B. G., Glogau, R. G., Gullett, J. H., McDonald, A. R., Lennette, E. T. & Levy, J. A. (1995). Herpes-like sequences in HIV-infected and uninfected Kaposi's sarcoma patients. *Science* **268**, 582-3.

Andreasen, A. S., Krabbe, K. S., Krogh-Madsen, R., Taudorf, S., Pedersen, B. K. & Moller, K. (2008). Human endotoxemia as a model of systemic inflammation. *Curr Med Chem* **15**, 1697-705.

Aoki, Y., Jaffe, E. S., Chang, Y., Jones, K., Teruya-Feldstein, J., Moore, P. S. & Tosato, G. (1999). Angiogenesis and hematopoiesis induced by Kaposi's sarcoma-associated herpesvirus-encoded interleukin-6. *Blood* **93**, 4034-43.

Areste, C. & Blackbourn, D. J. (2009). Modulation of the immune system by Kaposi's sarcoma-associated herpesvirus. *Trends Microbiol* **17**, 119-29.

Areste, C., Mutocheluh, M. & Blackbourn, D. J. (2009). Identification of caspase-mediated decay of interferon regulatory factor-3, exploited by a Kaposi sarcoma-associated herpesvirus immunoregulatory protein. *J Biol Chem* **284**, 23272-85.

Au-Yeung, B. B., Deindl, S., Hsu, L. Y., Palacios, E. H., Levin, S. E., Kuriyan, J. & Weiss, A. (2009). The structure, regulation, and function of ZAP-70. *Immunol Rev* **228**, 41-57.

Baine, I., Abe, B. T. & Macian, F. (2009). Regulation of T-cell tolerance by calcium/NFAT signaling. *Immunol Rev* **231**, 225-40.

Bais, C., Santomasso, B., Coso, O., Arvanitakis, L., Raaka, E. G., Gutkind, J. S., Asch, A. S., Cesarman, E., Gershengorn, M. C. & Mesri, E. A. (1998). G-protein-coupled receptor of Kaposi's sarcoma-associated herpesvirus is a viral oncogene and angiogenesis activator. *Nature* **391**, 86-9.

Barclay, A. N. (1981). Different reticular elements in rat lymphoid tissue identified by localization of Ia, Thy-1 and MRC OX 2 antigens. *Immunology* **44**, 727-36.

Barry, M. & Bleackley, R. C. (2002). Cytotoxic T lymphocytes: all roads lead to death. *Nat Rev Immunol* **2**, 401-9.

Barry, P. A., Alcendor, D. J., Power, M. D., Kerr, H. & Luciw, P. A. (1996). Nucleotide sequence and molecular analysis of the rhesus cytomegalovirus immediate-early gene and the UL121-117 open reading frames. *Virology* **215**, 61-72.

Ben Yebdri, F., Kukulski, F., Tremblay, A. & Sevigny, J. (2009). Concomitant activation of P2Y(2) and P2Y(6) receptors on monocytes is required for TLR1/2-induced neutrophil migration by regulating IL-8 secretion. *Eur J Immunol* **39**, 2885-94.

Beral, V. & Newton, R. (1998). Overview of the epidemiology of immunodeficiency-associated cancers. *J Natl Cancer Inst Monogr*, 1-6.

Beral, v., Peterman, T., Berkelman, R. & Jaffe, H. (1990). Kaposi's sarcoma among persons with AIDS: a sexually transmitted infection? *The Lancet* **335**, 123-128.

Bhatia, S., Edidin, M., Almo, S. C. & Nathenson, S. G. (2006). B7-1 and B7-2: similar costimulatory ligands with different biochemical, oligomeric and signaling properties. *Immunol Lett* **104**, 70-5.

Blackbourn, D. J., Lennette, E. T., Ambroziak, J., Mourich, D. V. & Levy, J. A. (1998). Human herpesvirus 8 detection in nasal secretions and saliva. *J Infect Dis* **177**, 213-6.

Blackbourn, D. J. & Levy, J. A. (1997). Human herpesvirus 8 in semen and prostate. *Aids* **11**, 249-50.

Blackbourn, D. J., Osmond, D., Levy, J. A. & Lennette, E. T. (1999). Increased human herpesvirus 8 seroprevalence in young homosexual men who have multiple sex contacts with different partners. *J Infect Dis* **179**, 237-9.

Blandino, P., Jr., Barnum, C. J., Solomon, L. G., Larish, Y., Lankow, B. S. & Deak, T. (2009). Gene expression changes in the hypothalamus provide evidence for regionally-selective changes in IL-1 and microglial markers after acute stress. *Brain Behav Immun* **23**, 958-68.

Borriello, F., Lederer, J., Scott, S. & Sharpe, A. H. (1997). MRC OX-2 defines a novel T cell costimulatory pathway. *J Immunol* **158**, 4548-54.

Bouvard, V., Baan, R., Straif, K., Grosse, Y., Secretan, B., El Ghissassi, F., Benbrahim-Tallaa, L., Guha, N., Freeman, C., Galichet, L. & Cogliano, V. (2009). A review of human carcinogens--Part B: biological agents. *Lancet Oncol* **10**, 321-2.

Brayfield, B. P., Kankasa, C., West, J. T., Muyanga, J., Bhat, G., Klaskala, W., Mitchell, C. D. & Wood, C. (2004). Distribution of Kaposi sarcoma-associated herpesvirus/human herpesvirus 8 in maternal saliva and breast milk in Zambia: implications for transmission. *J Infect Dis* **189**, 2260-70.

Brimo, F., Michel, R. P., Khetani, K. & Auger, M. (2007). Primary effusion lymphoma: a series of 4 cases and review of the literature with emphasis on cytomorphologic and immunocytochemical differential diagnosis. *Cancer* **111**, 224-33.

Broderick, C., Hoek, R. M., Forrester, J. V., Liversidge, J., Sedgwick, J. D. & Dick, A. D. (2002). Constitutive retinal CD200 expression regulates resident microglia and activation state of inflammatory cells during experimental autoimmune uveoretinitis. *Am J Pathol* **161**, 1669-77.

Brown, E. E., Fallin, D., Ruczinski, I., Hutchinson, A., Staats, B., Vitale, F., Lauria, C., Serraino, D., Rezza, G., Mbisa, G., Whitby, D., Messina, A., Goedert, J. J. & Chanock, S. J. (2006a). Associations of classic Kaposi sarcoma with common variants in genes that modulate host immunity. *Cancer Epidemiol Biomarkers Prev* **15**, 926-34.

Brown, E. E., Whitby, D., Vitale, F., Marshall, V., Mbisa, G., Gamache, C., Lauria, C., Alberg, A. J., Serraino, D., Cordiali-Fei, P., Messina, A. & Goedert, J. J. (2006b). Virologic, hematologic, and immunologic risk factors for classic Kaposi sarcoma. *Cancer* **107**, 2282-90.

Bubeck Wardenburg, J., Fu, C., Jackman, J. K., Flotow, H., Wilkinson, S. E., Williams, D. H., Johnson, R., Kong, G., Chan, A. C. & Findell, P. R. (1996). Phosphorylation of SLP-76 by the ZAP-70 protein-tyrosine kinase is required for T-cell receptor function. *J Biol Chem* **271**, 19641-4.

Cameron, C. M., Barrett, J. W., Liu, L., Lucas, A. R. & McFadden, G. (2005). Myxoma virus M141R expresses a viral CD200 (vOX-2) that is responsible for down-regulation of macrophage and T-cell activation in vivo. *J Virol* **79**, 6052-67.

Cannon, M. J., Laney, A. S. & Pellett, P. E. (2003). Human herpesvirus 8: current issues. *Clin Infect Dis* **37**, 82-7.

Carbone, A. & Gloghini, A. (2008). KSHV/HHV8-associated lymphomas. *Br J Haematol* **140**, 13-24.

Cesarman, E., Nador, R. G., Aozasa, K., Delsol, G., Said, J. W. & Knowles, D. M. (1996). Kaposi's sarcoma-associated herpesvirus in non-AIDS related lymphomas occurring in body cavities. *Am J Pathol* **149**, 53-7.

Chadburn, A., Hyjek, E. M., Tam, W., Liu, Y., Rengifo, T., Cesarman, E. & Knowles, D. M. (2008). Immunophenotypic analysis of the Kaposi sarcoma herpesvirus (KSHV; HHV-8)-infected B cells in HIV+ multicentric Castleman disease (MCD). *Histopathology* **53**, 513-24.

Chang, Y., Cesarman, E., Pessin, M. S., Lee, F., Culpepper, J., Knowles, D. M. & Moore, P. S. (1994). Identification of herpesvirus-like DNA sequences in AIDS-associated Kaposi's sarcoma. *Science* **266**, 1865-9.

Chen, L., Glover, J. N., Hogan, P. G., Rao, A. & Harrison, S. C. (1998). Structure of the DNA-binding domains from NFAT, Fos and Jun bound specifically to DNA. *Nature* **392**, 42-8.

Chen, Z., Marsden, P. A. & Gorczynski, R. M. (2009). Role of a distal enhancer in the transcriptional responsiveness of the human CD200 gene to interferon-gamma and tumor necrosis factor-alpha. *Mol Immunol* **46**, 1951-63.

Chen, Z., Zeng, H. & Gorczynski, R. M. (1997). Cloning and characterization of the murine homologue of the rat/human MRC OX-2 gene. *Biochim Biophys Acta* **1362**, 6-10.

Cheng, F., Weidner-Glunde, M., Varjosalo, M., Rainio, E. M., Lehtonen, A., Schulz, T. F., Koskinen, P. J., Taipale, J. & Ojala, P. M. (2009). KSHV reactivation from latency requires Pim-1 and Pim-3 kinases to inactivate the latency-associated nuclear antigen LANA. *PLoS Pathog* **5**, e1000324.

Cherwinski, H. M., Murphy, C. A., Joyce, B. L., Bigler, M. E., Song, Y. S., Zurawski, S. M., Moshrefi, M. M., Gorman, D. M., Miller, K. L., Zhang, S. L., Sedgwick, J. D. & Phillips, J. H. (2005). The CD200 receptor is a novel and potent regulator of murine and human mast cell function. *Journal of Immunology* **174**, 1348-1356.

Chidrawar, S., Khan, N., Wei, W., McLarnon, A., Smith, N., Nayak, L. & Moss, P. (2009). Cytomegalovirus-seropositivity has a profound influence on the magnitude of major lymphoid subsets within healthy individuals. *Clin Exp Immunol* **155**, 423-32.

Chung, Y. H., Means, R. E., Choi, J. K., Lee, B. S. & Jung, J. U. (2002). Kaposi's sarcoma-associated herpesvirus OX2 glycoprotein activates myeloid-lineage cells to induce inflammatory cytokine production. *J Virol* **76**, 4688-98.

Clark, D. A., Wong, K., Banwatt, D., Chen, Z., Liu, J., Lee, L., Gorczynski, R. M. & Blajchman, M. A. (2008). CD200-dependent and nonCD200-dependent pathways of NK cell suppression by human IVIG. *J Assist Reprod Genet* **25**, 67-72.

Coluzzi, M., Calabro, M. L., Manno, D., Chieco-Bianchi, L., Schulz, T. F. & Ascoli, V. (2003). Reduced seroprevalence of Kaposi's sarcoma-associated herpesvirus (KSHV), human herpesvirus 8 (HHV8), related to suppression of Anopheles density in Italy. *Med Vet Entomol* **17**, 461-4.

Coscoy, L. & Ganem, D. (2000). Kaposi's sarcoma-associated herpesvirus encodes two proteins that block cell surface display of MHC class I chains by enhancing their endocytosis. *Proc Natl Acad Sci U S A* **97**, 8051-6.

Coscoy, L., Sanchez, D. J. & Ganem, D. (2001). A novel class of herpesvirus-encoded membrane-bound E3 ubiquitin ligases regulates endocytosis of proteins involved in immune recognition. *J Cell Biol* **155**, 1265-73.

Dahlgren, C. & Karlsson, A. (1999). Respiratory burst in human neutrophils. *J Immunol Methods* **232**, 3-14.

Damania, B., DeMaria, M., Jung, J. U. & Desrosiers, R. C. (2000). Activation of lymphocyte signaling by the R1 protein of rhesus monkey rhadinovirus. *J Virol* **74**, 2721-30.

Damania, B. & Desrosiers, R. C. (2001). Simian homologues of human herpesvirus 8. *Philos Trans R Soc Lond B Biol Sci* **356**, 535-43.

Dang, P. M., Elbim, C., Marie, J. C., Chiandotto, M., Gougerot-Pocidalo, M. A. & El-Benna, J. (2006). Anti-inflammatory effect of interleukin-10 on human neutrophil respiratory burst involves inhibition of GM-CSF-induced p47PHOX phosphorylation through a decrease in ERK1/2 activity. *Faseb J* **20**, 1504-6.

Davison, A. J., Eberle, R., Ehlers, B., Hayward, G. S., McGeoch, D. J., Minson, A. C., Pellett, P. E., Roizman, B., Studdert, M. J. & Thiry, E. (2009). The order Herpesvirales. *Arch Virol* **154**, 171-7.

Demmler-Harrison, G. J. (2009). Congenital cytomegalovirus: Public health action towards awareness, prevention, and treatment. *J Clin Virol* **46 Suppl 4**, S1-5.

Desrosiers, R. C., Sasseville, V. G., Czajak, S. C., Zhang, X., Mansfield, K. G., Kaur, A., Johnson, R. P., Lackner, A. A. & Jung, J. U. (1997). A herpesvirus of rhesus monkeys related to the human Kaposi's sarcoma-associated herpesvirus. *J Virol* **71**, 9764-9.

Dick, A. D., Broderick, C., Forrester, J. V. & Wright, G. J. (2001). Distribution of OX2 antigen and OX2 receptor within retina. *Invest Ophthalmol Vis Sci* **42**, 170-6.

Dong, S., Corre, B., Foulon, E., Dufour, E., Veillette, A., Acuto, O. & Michel, F. (2006). T cell receptor for antigen induces linker for activation of T cell-dependent activation of a negative signaling complex involving Dok-2, SHIP-1, and Grb-2. *J Exp Med* **203**, 2509-18.

Dukers, N. H. & Rezza, G. (2003). Human herpesvirus 8 epidemiology: what we do and do not know. *Aids* **17**, 1717-30.

Dunbar, P. R., Ogg, G. S., Chen, J., Rust, N., van der Bruggen, P. & Cerundolo, V. (1998). Direct isolation, phenotyping and cloning of low-frequency antigen-specific cytotoxic T lymphocytes from peripheral blood. *Curr Biol* **8**, 413-6.

Dunn, W., Chou, C., Li, H., Hai, R., Patterson, D., Stolc, V., Zhu, H. & Liu, F. (2003). Functional profiling of a human cytomegalovirus genome. *Proc Natl Acad Sci U S A* **100**, 14223-8.

Ellis, M., Gupta, S., Galant, S., Hakim, S., VandeVen, C., Toy, C. & Cairo, M. S. (1988). Impaired neutrophil function in patients with AIDS or AIDS-related complex: a comprehensive evaluation. *J Infect Dis* **158**, 1268-76.

Faurschou, M. & Borregaard, N. (2003). Neutrophil granules and secretory vesicles in inflammation. *Microbes Infect* **5**, 1317-27.

Fisher, M. S. & Kripke, M. L. (1982). Suppressor T lymphocytes control the development of primary skin cancers in ultraviolet-irradiated mice. *Science* **216**, 1133-4.

Flores-Borja, F., Jury, E. C., Mauri, C. & Ehrenstein, M. R. (2008). Defects in CTLA-4 are associated with abnormal regulatory T cell function in rheumatoid arthritis. *Proc Natl Acad Sci U S A* **105**, 19396-401.

Foster-Cuevas, M., Wright, G. J., Puklavec, M. J., Brown, M. H. & Barclay, A. N. (2004). Human herpesvirus 8 K14 protein mimics CD200 in down-regulating macrophage activation through CD200 receptor. *J Virol* **78**, 7667-76.

Foster, C. B., Lehrnbecher, T., Samuels, S., Stein, S., Mol, F., Metcalf, J. A., Wyvill, K., Steinberg, S. M., Kovacs, J., Blauvelt, A., Yarchoan, R. & Chanock, S. J. (2000). An IL6 promoter polymorphism is associated with a lifetime risk of development of Kaposi sarcoma in men infected with human immunodeficiency virus. *Blood* **96**, 2562-7.

Fowell, D. J., Shinkai, K., Liao, X. C., Beebe, A. M., Coffman, R. L., Littman, D. R. & Locksley, R. M. (1999). Impaired NFATc translocation and failure of Th2 development in Itk-deficient CD4+ T cells. *Immunity* **11**, 399-409.

Freeman, R. B., Jr. (2009). The 'indirect' effects of cytomegalovirus infection. *Am J Transplant* **9**, 2453-8.

Glaunsinger, B. & Ganem, D. (2004). Lytic KSHV infection inhibits host gene expression by accelerating global mRNA turnover. *Mol Cell* **13**, 713-23.

Gorczynski, R., Chen, Z., Kai, Y., Lee, L., Wong, S. & Marsden, P. A. (2004a). CD200 is a ligand for all members of the CD200R family of immunoregulatory molecules. *J Immunol* **172**, 7744-9.

Gorczynski, R. M., Cattral, M. S., Chen, Z., Hu, J., Lei, J., Min, W. P., Yu, G. & Ni, J. (1999). An immunoadhesin incorporating the molecule OX-2 is a potent immunosuppressant that prolongs allo- and xenograft survival. *J Immunol* **163**, 1654-60.

Gorczynski, R. M., Chen, Z., Clark, D. A., Kai, Y., Lee, L., Nachman, J., Wong, S. & Marsden, P. (2004b). Structural and functional heterogeneity in the CD200R family of immunoregulatory molecules and their expression at the feto-maternal interface. *Am J Reprod Immunol* **52**, 147-63.

Gorczynski, R. M., Chen, Z., Kai, Y., Wong, S. & Lee, L. (2004b). Induction of tolerance-inducing antigen-presenting cells in bone marrow cultures in vitro using monoclonal antibodies to CD200R. *Transplantation* **77**, 1138-44.

Gorczynski, R. M., Chen, Z., Lee, L., Yu, K. & Hu, J. (2002a). Anti-CD200R ameliorates collagen-induced arthritis in mice. *Clin Immunol* **104**, 256-64.

Gorczynski, R. M., Chen, Z., Yu, K. & Hu, J. (2001). CD200 immunoadhesin suppresses collagen-induced arthritis in mice. *Clin Immunol* **101**, 328-34.

Gorczynski, R. M., Hu, J., Chen, Z., Kai, Y. & Lei, J. (2002b). A CD200FC immunoadhesin prolongs rat islet xenograft survival in mice. *Transplantation* **73**, 1948-53.

Gorczynski, R., Khatri, I., Lee, L. & Boudakov, I. (2008). An interaction between CD200 and monoclonal antibody agonists to CD200R2 in development of dendritic cells that preferentially induce populations of CD4+CD25+ T regulatory cells. *J Immunol* **180**, 5946-55.

Gorczynski, R. M., Lee, L. & Boudakov, I. (2005). Augmented Induction of CD4+CD25+ Treg using monoclonal antibodies to CD200R. *Transplantation* **79**, 1180-3.

Greensill, J., Sheldon, J. A., Renwick, N. M., Beer, B. E., Norley, S., Goudsmit, J. & Schulz, T. F. (2000). Two distinct gamma-2 herpesviruses in African green monkeys: a second gamma-2 herpesvirus lineage among old world primates? *J Virol* **74**, 1572-7.

Grossmann, C., Podgrabinska, S., Skobe, M. & Ganem, D. (2006). Activation of NF-kappaB by the latent vFLIP gene of Kaposi's sarcoma-associated herpesvirus is required for the spindle shape of virus-infected endothelial cells and contributes to their proinflammatory phenotype. *J Virol* **80**, 7179-85.

Grundhoff, A. & Ganem, D. (2004). Inefficient establishment of KSHV latency suggests an additional role for continued lytic replication in Kaposi sarcoma pathogenesis. *J Clin Invest* **113**, 124-36.

Haas, A., Weckbecker, G. & Welzenbach, K. (2008). Intracellular Phospho-Flow cytometry reveals novel insights into TCR proximal signaling events. A comparison with Western blot. *Cytometry A* **73**, 799-807.

Hansen, T. H. & Bouvier, M. (2009). MHC class I antigen presentation: learning from viral evasion strategies. *Nat Rev Immunol* **9**, 503-13.

Harris, C. L., Williams, A. S., Linton, S. M. & Morgan, B. P. (2002). Coupling complement regulators to immunoglobulin domains generates effective anti-complement reagents with extended half-life in vivo. *Clin Exp Immunol* **129**, 198-207.

Hatherley, D., Cherwinski, H. M., Moshref, M. & Barclay, A. N. (2005). Recombinant CD200 protein does not bind activating proteins closely related to CD200 receptor. *J Immunol* **175**, 2469-74.

Hislop, A. D., Taylor, G. S., Sauce, D. & Rickinson, A. B. (2007). Cellular responses to viral infection in humans: lessons from Epstein-Barr virus. *Annu Rev Immunol* **25**, 587-617.

Hoek, R. M., Ruuls, S. R., Murphy, C. A., Wright, G. J., Goddard, R., Zurawski, S. M., Blom, B., Homola, M. E., Streit, W. J., Brown, M. H., Barclay, A. N. & Sedgwick, J. D. (2000). Down-regulation of the macrophage lineage through interaction with OX2 (CD200). *Science* **290**, 1768-71.

Hong, Y. K., Foreman, K., Shin, J. W., Hirakawa, S., Curry, C. L., Sage, D. R., Libermann, T., Dezube, B. J., Fingeroth, J. D. & Detmar, M. (2004). Lymphatic reprogramming of blood vascular endothelium by Kaposi sarcoma-associated herpesvirus. *Nat Genet* **36**, 683-5.

Horenstein, M. G., Moontasri, N. J. & Cesarman, E. (2008). The pathobiology of Kaposi's sarcoma: advances since the onset of the AIDS epidemic. *J Cutan Pathol* **35 Suppl 2**, 40-4.

Howard, M. R., Whitby, D., Bahadur, G., Suggett, F., Boshoff, C., Tenant-Flowers, M., Schulz, T. F., Kirk, S., Matthews, S., Weller, I. V., Tedder, R. S. & Weiss, R. A. (1997). Detection of human herpesvirus 8 DNA in semen from HIV-infected individuals but not healthy semen donors. *Aids* **11**, F15-9.

Huang, Y. Q., Li, J. J., Kaplan, M. H., Poiesz, B., Katabira, E., Zhang, W. C., Feiner, D. & Friedman-Kien, A. E. (1995). Human herpesvirus-like nucleic acid in various forms of Kaposi's sarcoma. *Lancet* **345**, 759-61.

Jago, C. B., Yates, J., Camara, N. O., Lechler, R. I. & Lombardi, G. (2004). Differential expression of CTLA-4 among T cell subsets. *Clin Exp Immunol* **136**, 463-71.

Jarviluoma, A. & Ojala, P. M. (2006). Cell signaling pathways engaged by KSHV. *Biochim Biophys Acta* **1766**, 140-58.

Jenmalm, M. C., Cherwinski, H., Bowman, E. P., Phillips, J. H. & Sedgwick, J. D. (2006). Regulation of myeloid cell function through the CD200 receptor. *J Immunol* **176**, 191-9.

Johnson, G. M. & Gomez-Cambronero, J. (1995). Priming of tyrosine phosphorylation in GM-CSF-stimulated adherent neutrophils. *J Leukoc Biol* **57**, 692-8.

Jordan, M. S., Sadler, J., Austin, J. E., Finkelstein, L. D., Singer, A. L., Schwartzberg, P. L. & Koretzky, G. A. (2006). Functional hierarchy of the N-terminal tyrosines of SLP-76. *J Immunol* **176**, 2430-8.

Kalli, K., Huntoon, C., Bell, M. & McKean, D. J. (1998). Mechanism responsible for T-cell antigen receptor- and CD28- or interleukin 1 (IL-1) receptor-initiated regulation of IL-2 gene expression by NF-kappaB. *Mol Cell Biol* **18**, 3140-8.

Kamei, D. T., Lao, B. J., Ricci, M. S., Deshpande, R., Xu, H., Tidor, B. & Lauffenburger, D. A. (2005). Quantitative methods for developing Fc mutants with extended half-lives. *Biotechnol Bioeng* **92**, 748-60.

Kane, L. P., Andres, P. G., Howland, K. C., Abbas, A. K. & Weiss, A. (2001). Akt provides the CD28 costimulatory signal for up-regulation of IL-2 and IFN-gamma but not TH2 cytokines. *Nat Immunol* **2**, 37-44.

Kang, T., Ye, F. C., Gao, S. J. & Wang, L. D. (2008). Angiogenesis, Kaposi's Sarcoma and Kaposi's Sarcoma-Associated Herpesvirus. *Virol Sin* **23**, 449-458.

Karlsson, A., Markfjall, M., Stromberg, N. & Dahlgren, C. (1995). Escherichia coli-induced activation of neutrophil NADPH-oxidase: lipopolysaccharide and formylated peptides act synergistically to induce release of reactive oxygen metabolites. *Infect Immun* **63**, 4606-12.

Kedes, D. H. & Ganem, D. (1997). Sensitivity of Kaposi's sarcoma-associated herpesvirus replication to antiviral drugs. Implications for potential therapy. *J Clin Invest* **99**, 2082-6.

Kedes, D. H., Lagunoff, M., Renne, R. & Ganem, D. (1997). Identification of the gene encoding the major latency-associated nuclear antigen of the Kaposi's sarcoma-associated herpesvirus. *J Clin Invest* **100**, 2606-10.

Kedes, D. H., Operskalski, E., Busch, M., Kohn, R., Flood, J. & Ganem, D. (1996). The seroepidemiology of human herpesvirus 8 (Kaposi's sarcoma-associated herpesvirus): distribution of infection in KS risk groups and evidence for sexual transmission. *Nat Med* **2**, 918-24.

Khan, N. (2007). The immunological burden of human cytomegalovirus infection. *Arch Immunol Ther Exp (Warsz)* **55**, 299-308.

Ko, Y. C., Chien, H. F., Jiang-Shieh, Y. F., Chang, C. Y., Pai, M. H., Huang, J. P., Chen, H. M. & Wu, C. H. (2009). Endothelial CD200 is heterogeneously distributed, regulated and involved in immune cell-endothelium interactions. *J Anat* **214**, 183-95.

Kojima, T., Obata, K., Mukai, K., Sato, S., Takai, T., Minegishi, Y. & Karasuyama, H. (2007). Mast cells and basophils are selectively activated in vitro and in vivo through CD200R3 in an IgE-independent manner. *J Immunol* **179**, 7093-100.

Koning, N., Swaab, D. F., Hoek, R. M. & Huitinga, I. (2009). Distribution of the immune inhibitory molecules CD200 and CD200R in the normal central nervous system and multiple sclerosis lesions suggests neuron-glia and glia-glia interactions. *J Neuropathol Exp Neurol* **68**, 159-67.

Langlais, C. L., Jones, J. M., Estep, R. D. & Wong, S. W. (2006). Rhesus rhadinovirus R15 encodes a functional homologue of human CD200. *J Virol* **80**, 3098-103.

Lee, K. M., Chuang, E., Griffin, M., Khattri, R., Hong, D. K., Zhang, W., Straus, D., Samelson, L. E., Thompson, C. B. & Bluestone, J. A. (1998). Molecular basis of T cell inactivation by CTLA-4. *Science* **282**, 2263-6.

Lennette, E. T., Blackbourn, D. J. & Levy, J. A. (1996). Antibodies to human herpesvirus type 8 in the general population and in Kaposi's sarcoma patients. *Lancet* **348**, 858-61.

Levitskaya, J., Coram, M., Levitsky, V., Imreh, S., Steigerwald-Mullen, P. M., Klein, G., Kurilla, M. G. & Masucci, M. G. (1995). Inhibition of antigen processing by the internal repeat region of the Epstein-Barr virus nuclear antigen-1. *Nature* **375**, 685-8.

Li, Q., Zhou, F., Ye, F. & Gao, S. J. (2008). Genetic disruption of KSHV major latent nuclear antigen LANA enhances viral lytic transcriptional program. *Virology* **379**, 234-44.

Li-Weber, M., Treiber, M. K., Giaisi, M., Palfi, K., Stephan, N., Parg, S. & Krammer, P. H. (2005). Ultraviolet irradiation suppresses T cell activation via blocking TCR-mediated ERK and NF-kappa B signaling pathways. *J Immunol* **175**, 2132-43.

Lin, J. C., Lin, S. C., Mar, E. C., Pellett, P. E., Stamey, F. R., Stewart, J. A. & Spira, T. J. (1995). Is Kaposi's-sarcoma-associated herpesvirus detectable in semen of HIV-infected homosexual men? *Lancet* **346**, 1601-2.

Liu, D., Ren, D., Huang, H., Dankberg, J., Rosenfeld, R., Cocco, M. J., Li, L., Brems, D. N. & Remmele, R. L., Jr. (2008). Structure and stability changes of human IgG1 Fc as a consequence of methionine oxidation. *Biochemistry* **47**, 5088-100.

Liu, J., Martin, H. J., Liao, G. & Hayward, S. D. (2007). The Kaposi's sarcoma-associated herpesvirus LANA protein stabilizes and activates c-Myc. *J Virol* **81**, 10451-9.

Lu, J., Verma, S. C., Murakami, M., Cai, Q., Kumar, P., Xiao, B. & Robertson, E. S. (2009). Latency-associated nuclear antigen of Kaposi's sarcoma-associated herpesvirus (KSHV) upregulates survivin expression in KSHV-Associated B-lymphoma cells and contributes to their proliferation. *J Virol* **83**, 7129-41.

Lyons, A., McQuillan, K., Deighan, B. F., O'Reilly, J. A., Downer, E. J., Murphy, A. C., Watson, M., Piazza, A., O'Connell, F., Griffin, R., Mills, K. H. & Lynch, M. A. (2009). Decreased neuronal CD200 expression in IL-4-deficient mice results in increased neuroinflammation in response to lipopolysaccharide. *Brain Behav Immun* **23**, 1020-7.

Manley, T. J., Luy, L., Jones, T., Boeckh, M., Mutimer, H. & Riddell, S. R. (2004). Immune evasion proteins of human cytomegalovirus do not prevent a diverse CD8+ cytotoxic T-cell response in natural infection. *Blood* **104**, 1075-82.

Mansouri, M., Douglas, J., Rose, P. P., Gouveia, K., Thomas, G., Means, R. E., Moses, A. V. & Fruh, K. (2006). Kaposi sarcoma herpesvirus K5 removes CD31/PECAM from endothelial cells. *Blood* **108**, 1932-40.

Marcelin, A. G., Motol, J., Guihot, A., Caumes, E., Viard, J. P., Dussaix, E., Cadranel, J., Frances, C., Carcelain, G., Calvez, V. & Dupin, N. (2007). Relationship between the quantity of Kaposi sarcoma-associated herpesvirus (KSHV) in peripheral blood and effusion fluid samples and KSHV-associated disease. *J Infect Dis* **196**, 1163-6.

Mark, L., Lee, W. H., Spiller, O. B., Proctor, D., Blackbourn, D. J., Villoutreix, B. O. & Blom, A. M. (2004). The Kaposi's sarcoma-associated herpesvirus complement control protein mimics human molecular mechanisms for inhibition of the complement system. *J Biol Chem* **279**, 45093-101.

Mark, L., Spiller, O. B., Okroj, M., Chanas, S., Aitken, J. A., Wong, S. W., Damania, B., Blom, A. M. & Blackbourn, D. J. (2007). Molecular characterization of the rhesus rhadinovirus (RRV) ORF4 gene and the RRV complement control protein it encodes. *J Virol* **81**, 4166-76.

Mark, L., Spiller, O. B., Villoutreix, B. O. & Blom, A. M. (2007). Kaposi's sarcoma-associated herpes virus complement control protein: KCP--complement inhibition and more. *Mol Immunol* **44**, 11-22.

Markert, M. L., Boeck, A., Hale, L. P., Kloster, A. L., McLaughlin, T. M., Batchvarova, M. N., Douek, D. C., Koup, R. A., Kostyu, D. D., Ward, F. E., Rice, H. E., Mahaffey, S. M., Schiff, S. E., Buckley, R. H. & Haynes, B. F. (1999). Transplantation of thymus tissue in complete DiGeorge syndrome. *N Engl J Med* **341**, 1180-9.

Martin, J. N., Amad, Z., Cossen, C., Lam, P. K., Kedes, D. H., Page-Shafer, K. A., Osmond, D. H. & Forghani, B. (2000). Use of epidemiologically well-defined subjects and existing immunofluorescence assays to calibrate a new enzyme immunoassay for human herpesvirus 8 antibodies. *J Clin Microbiol* **38**, 696-701.

Masocha, W. (2009). Systemic lipopolysaccharide (LPS)-induced microglial activation results in different temporal reduction of CD200 and CD200 receptor gene expression in the brain. *J Neuroimmunol*.

Masood, R., Cai, J., Tulpule, A., Zheng, T., Hamilton, A., Sharma, S., Espina, B. M., Smith, D. L. & Gill, P. S. (2001). Interleukin 8 is an autocrine growth factor and a surrogate marker for Kaposi's sarcoma. *Clin Cancer Res* **7**, 2693-702.

Matsumoto, H., Kumon, Y., Watanabe, H., Ohnishi, T., Takahashi, H., Imai, Y. & Tanaka, J. (2007). Expression of CD200 by macrophage-like cells in ischemic core of rat brain after transient middle cerebral artery occlusion. *Neurosci Lett* **418**, 44-8.

Mbulaiteye, S., Marshall, V., Bagni, R. K., Wang, C. D., Mbisa, G., Bakaki, P. M., Owor, A. M., Ndugwa, C. M., Engels, E. A., Katongole-Mbidde, E., Biggar, R. J. & Whitby, D. (2006). Molecular evidence for mother-to-child transmission of Kaposi sarcoma-associated herpesvirus in Uganda and K1 gene evolution within the host. *J Infect Dis* **193**, 1250-7.

Mbulaiteye, S. M. & Goedert, J. J. (2008). Transmission of Kaposi sarcoma-associated herpesvirus in sub-Saharan Africa. *Aids* **22**, 535-7.

Menegazzi, R., Zabucchi, G., Knowles, A., Cramer, R. & Patriarca, P. (1992). A new, one-step assay on whole cell suspensions for peroxidase secretion by human neutrophils and eosinophils. *J Leukoc Biol* **52**, 619-24.

Mettenleiter, T. C., Klupp, B. G. & Granzow, H. (2006). Herpesvirus assembly: a tale of two membranes. *Curr Opin Microbiol* **9**, 423-9.

Meuth, S. G., Simon, O. J., Grimm, A., Melzer, N., Herrmann, A. M., Spitzer, P., Landgraf, P. & Wiendl, H. (2008). CNS inflammation and neuronal degeneration is aggravated by impaired CD200-CD200R-mediated macrophage silencing. *J Neuroimmunol* **194**, 62-9.

Miller, J. F. (1961). Immunological function of the thymus. *Lancet* **2**, 748-9.

Miller, R. E., Fayen, J. D., Mohammad, S. F., Stein, K., Kadereit, S., Woods, K. D., Sramkoski, R. M., Jacobberger, J. W., Templeton, D., Shurin, S. B. & Laughlin, M. J. (2002). Reduced CTLA-4 protein and messenger RNA expression in umbilical cord blood T lymphocytes. *Exp Hematol* **30**, 738-44.

Mihrshahi, R., Barclay, A. N. & Brown, M. H. (2009). Essential roles for Dok2 and RasGAP in CD200 receptor-mediated regulation of human myeloid cells. *J Immunol* **183**, 4879-86.

Monini, P., Colombini, S., Sturzl, M., Goletti, D., Cafaro, A., Sgadari, C., Butto, S., Franco, M., Leone, P., Fais, S., Leone, P., Melucci-Vigo, G., Chiozzini, C., Carlini, F., Ascherl, G., Cornali, E., Zietz, C., Ramazzotti, E., Ensoli, F., Andreoni, M., Pezzotti, P., Rezza, G., Yarchoan, R., Gallo, R. C. & Ensoli, B. (1999). Reactivation and persistence of human herpesvirus-8 infection in B cells and monocytes by Th-1 cytokines increased in Kaposi's sarcoma. *Blood* **93**, 4044-58.

Monini, P., de Lellis, L., Fabris, M., Rigolin, F. & Cassai, E. (1996). Kaposi's sarcoma-associated herpesvirus DNA sequences in prostate tissue and human semen. *N Engl J Med* **334**, 1168-72.

Montaner, S., Sodhi, A., Servitja, J. M., Ramsdell, A. K., Barac, A., Sawai, E. T. & Gutkind, J. S. (2004). The small GTPase Rac1 links the Kaposi sarcoma-associated herpesvirus vGPCR to cytokine secretion and paracrine neoplasia. *Blood* **104**, 2903-11.

Moore, P. S., Gao, S. J., Dominguez, G., Cesarman, E., Lungu, O., Knowles, D. M., Garber, R., Pellett, P. E., McGeoch, D. J. & Chang, Y. (1996). Primary characterization of a herpesvirus agent associated with Kaposi's sarcomae. *J Virol* **70**, 549-58.

Mukaida, N. (2003). Pathophysiological roles of interleukin-8/CXCL8 in pulmonary diseases. *Am J Physiol Lung Cell Mol Physiol* **284**, L566-77.

Murphy, K., Travers P., Walport M. (2008). Janeway's Immunobiology, 7th edn: Garland Science.

Nascimento, M. C., de Souza, V. A., Sumita, L. M., Freire, W., Munoz, F., Kim, J., Pannuti, C. S. & Mayaud, P. (2007). Comparative study of Kaposi's sarcoma-associated herpesvirus serological assays using clinically and serologically defined reference standards and latent class analysis. *J Clin Microbiol* **45**, 715-20.

Nick, J. A., Avdi, N. J., Gerwins, P., Johnson, G. L. & Worthen, G. S. (1996). Activation of a p38 mitogen-activated protein kinase in human neutrophils by lipopolysaccharide. *J Immunol* **156**, 4867-75.

Nimmerjahn, F. & Ravetch, J. V. (2006). Fcgamma receptors: old friends and new family members. *Immunity* **24**, 19-28.

Oksenhendler, E., Cazals-Hatem, D., Schulz, T. F., Barateau, V., Grollet, L., Sheldon, J., Clauvel, J. P., Sigaux, F. & Agbalika, F. (1998). Transient angiolymphoid hyperplasia and Kaposi's sarcoma after primary infection with human herpesvirus 8 in a patient with human immunodeficiency virus infection. *N Engl J Med* **338**, 1585-90.

Pallasch, C. P., Ulbrich, S., Brinker, R., Hallek, M., Uger, R. A. & Wendtner, C. M. (2009). Disruption of T cell suppression in chronic lymphocytic leukemia by CD200 blockade. *Leuk Res* **33**, 460-4.

Palmeri, D., Spadavecchia, S., Carroll, K. D. & Lukac, D. M. (2007). Promoter- and cell-specific transcriptional transactivation by the Kaposi's sarcoma-associated herpesvirus ORF57/Mta protein. *J Virol* **81**, 13299-314.

Parkin, D. M. (2006). The global health burden of infection-associated cancers in the year 2002. *Int J Cancer* **118**, 3030-44.

Parkin, D. M., Nambooze, S., Wabwire-Mangen, F. & Wabinga, H. R. (2010). Changing cancer incidence in Kampala, Uganda, 1991-2006. *Int J Cancer* **126**, 1187-95.

Pauk, J., Huang, M. L., Brodie, S. J., Wald, A., Koelle, D. M., Schacker, T., Celum, C., Selke, S. & Corey, L. (2000). Mucosal shedding of human herpesvirus 8 in men. *N Engl J Med* **343**, 1369-77.

Paz, P. E., Wang, S., Clarke, H., Lu, X., Stokoe, D. & Abo, A. (2001). Mapping the Zap-70 phosphorylation sites on LAT (linker for activation of T cells) required for recruitment and activation of signalling proteins in T cells. *Biochem J* **356**, 461-71.

Pellett, P. E., Spira, T. J., Bagasra, O., Boshoff, C., Corey, L., de Lellis, L., Huang, M. L., Lin, J. C., Matthews, S., Monini, P., Rimessi, P., Sosa, C., Wood, C. & Stewart, J. A. (1999). Multicenter comparison of PCR assays for detection of human herpesvirus 8 DNA in semen. *J Clin Microbiol* **37**, 1298-301.

Plancoulaine, S., Gessain, A., van Beveren, M., Tortevoye, P. & Abel, L. (2003). Evidence for a recessive major gene predisposing to human herpesvirus 8 (HHV-8) infection in a population in which HHV-8 is endemic. *J Infect Dis* **187**, 1944-50.

Pratt, C. L., Estep, R. D. & Wong, S. W. (2005). Splicing of rhesus rhadinovirus R15 and ORF74 bicistronic transcripts during lytic infection and analysis of effects on production of vCD200 and vGPCR. *J Virol* **79**, 3878-82.

Preston, S., Wright, G. J., Starr, K., Barclay, A. N. & Brown, M. H. (1997). The leukocyte/neuron cell surface antigen OX2 binds to a ligand on macrophages. *Eur J Immunol* **27**, 1911-8.

Renne, R., Lagunoff, M., Zhong, W. & Ganem, D. (1996a). The size and conformation of Kaposi's sarcoma-associated herpesvirus (human herpesvirus 8) DNA in infected cells and virions. *J Virol* **70**, 8151-4.

Renne, R., Zhong, W., Herndier, B., McGrath, M., Abbey, N., Kedes, D. & Ganem, D. (1996b). Lytic growth of Kaposi's sarcoma-associated herpesvirus (human herpesvirus 8) in culture. *Nat Med* **2**, 342-6.

Reth, M. (1995). Immunodeficiency. Trapping the nude mouse gene. *Curr Biol* **5**, 18-20.

Rettig, M. B., Ma, H. J., Vescio, R. A., Pold, M., Schiller, G., Belson, D., Savage, A., Nishikubo, C., Wu, C., Fraser, J., Said, J. W. & Berenson, J. R. (1997). Kaposi's sarcoma-associated herpesvirus infection of bone marrow dendritic cells from multiple myeloma patients. *Science* **276**, 1851-4.

Rezaee, S. A., Cunningham, C., Davison, A. J. & Blackbourn, D. J. (2006). Kaposi's sarcoma-associated herpesvirus immune modulation: an overview. *J Gen Virol* **87**, 1781-804.

Rezaee, S. A., Gracie, J. A., McInnes, I. B. & Blackbourn, D. J. (2005). Inhibition of neutrophil function by the Kaposi's sarcoma-associated herpesvirus vOX2 protein. *Aids* **19**, 1907-10.

Rijkers, E. S., de Ruiter, T., Buitenhuis, M., Veninga, H., Hoek, R. M. & Meyaard, L. (2007). Ligation of CD200R by CD200 is not required for normal murine myelopoiesis. *Eur J Haematol* **79**, 410-6.

Rochman, Y., Spolski, R. & Leonard, W. J. (2009). New insights into the regulation of T cells by gamma(c) family cytokines. *Nat Rev Immunol* **9**, 480-90.

Rose, T. M. (2005). CODEHOP-mediated PCR - a powerful technique for the identification and characterization of viral genomes. *Virol J* **2**, 20.

Rudd, C. E., Taylor, A. & Schneider, H. (2009). CD28 and CTLA-4 coreceptor expression and signal transduction. *Immunol Rev* **229**, 12-26.

Russo, J. J., Bohenzky, R. A., Chien, M. C., Chen, J., Yan, M., Maddalena, D., Parry, J. P., Peruzzi, D., Edelman, I. S., Chang, Y. & Moore, P. S. (1996). Nucleotide sequence of the Kaposi sarcoma-associated herpesvirus (HHV8). *Proc Natl Acad Sci U S A* **93**, 14862-7.

Rygiel, T. P., Rijkers, E. S., de Ruiter, T., Stolte, E. H., van der Valk, M., Rimmelzwaan, G. F., Boon, L., van Loon, A. M., Coenjaerts, F. E., Hoek, R. M., Tesselaar, K. & Meyaard, L. (2009). Lack of CD200 enhances pathological T cell responses during influenza infection. *J Immunol* **183**, 1990-6.

Sadagopan, S., Sharma-Walia, N., Veettil, M. V., Bottero, V., Levine, R., Vart, R. J. & Chandran, B. (2009). Kaposi's sarcoma-associated herpesvirus upregulates angiogenin during infection of human dermal microvascular endothelial cells, which induces 45S rRNA synthesis, antiapoptosis, cell proliferation, migration, and angiogenesis. *J Virol* **83**, 3342-64.

Salata, C., Curtarello, M., Calistri, A., Sartori, E., Sette, P., de Bernard, M., Parolin, C. & Palu, G. (2009). vOX2 glycoprotein of human herpesvirus 8 modulates human primary macrophages activity. *J Cell Physiol* **219**, 698-706.

Sanchez-Velasco, P., Ocejo-Vinyals, J. G., Flores, R., Gomez-Roman, J. J., Lozano, M. J. & Leyva-Cobian, F. (2001). Simultaneous multiorgan presence of human herpesvirus 8 and restricted lymphotropism of Epstein-Barr virus DNA sequences in a human immunodeficiency virus-negative immunodeficient infant. *J Infect Dis* **183**, 338-342.

Sansom, D. M. & Walker, L. S. (2006). The role of CD28 and cytotoxic T-lymphocyte antigen-4 (CTLA-4) in regulatory T-cell biology. *Immunol Rev* **212**, 131-48.

Santos, L. L., Dacumos, A., Yamana, J., Sharma, L. & Morand, E. F. (2008). Reduced arthritis in MIF deficient mice is associated with reduced T cell activation: down-regulation of ERK MAP kinase phosphorylation. *Clin Exp Immunol* **152**, 372-80.

Sato, K., Eizumi, K., Fukaya, T., Fujita, S., Sato, Y., Takagi, H., Yamamoto, M., Yamashita, N., Hijikata, A., Kitamura, H., Ohara, O., Yamasaki, S., Saito, T. & Sato, K. (2009). Naturally occurring regulatory dendritic cells regulate murine cutaneous chronic graft-versus-host disease. *Blood* **113**, 4780-9.

Schroder, K., Hertzog, P. J., Ravasi, T. & Hume, D. A. (2004). Interferon-gamma: an overview of signals, mechanisms and functions. *J Leukoc Biol* **75**, 163-89.

Schwartzberg, P. L., Finkelstein, L. D. & Readinger, J. A. (2005). TEC-family kinases: regulators of T-helper-cell differentiation. *Nat Rev Immunol* **5**, 284-95.

Searles, R. P., Bergquam, E. P., Axthelm, M. K. & Wong, S. W. (1999). Sequence and genomic analysis of a Rhesus macaque rhadinovirus with similarity to Kaposi's sarcoma-associated herpesvirus/human herpesvirus 8. *J Virol* **73**, 3040-53.

Sester, U., Presser, D., Dirks, J., Gartner, B. C., Kohler, H. & Sester, M. (2008). PD-1 expression and IL-2 loss of cytomegalovirus- specific T cells correlates with viremia and reversible functional anergy. *Am J Transplant* **8**, 1486-97.

Shiratori, I., Yamaguchi, M., Suzukawa, M., Yamamoto, K., Lanier, L. L., Saito, T. & Arase, H. (2005). Down-regulation of basophil function by human CD200 and human herpesvirus-8 CD200. *J Immunol* **175**, 4441-9.

Simelyte, E., Criado, G., Essex, D., Uger, R. A., Feldmann, M. & Williams, R. O. (2008). CD200-Fc, a novel antiarthritic biologic agent that targets proinflammatory cytokine expression in the joints of mice with collagen-induced arthritis. *Arthritis Rheum* **58**, 1038-43.

Simpson, G. R., Schulz, T. F., Whitby, D., Cook, P. M., Boshoff, C., Rainbow, L., Howard, M. R., Gao, S. J., Bohenzky, R. A., Simmonds, P., Lee, C., de Ruiter, A., Hatzakis, A., Tedder, R. S., Weller, I. V., Weiss, R. A. & Moore, P. S. (1996). Prevalence of Kaposi's sarcoma associated herpesvirus infection measured by antibodies to recombinant capsid protein and latent immunofluorescence antigen. *Lancet* **348**, 1133-8.

Siva, A., Xin, H., Qin, F., Oltean, D., Bowdish, K. S. & Kretz-Rommel, A. (2008). Immune modulation by melanoma and ovarian tumor cells through expression of the immunosuppressive molecule CD200. *Cancer Immunol Immunother* **57**, 987-96.

Snelgrove, R. J., Goulding, J., Didierlaurent, A. M., Lyonga, D., Vekaria, S., Edwards, L., Gwyer, E., Sedgwick, J. D., Barclay, A. N. & Hussell, T. (2008). A critical function for CD200 in lung immune homeostasis and the severity of influenza infection. *Nat Immunol* **9**, 1074-83.

Spiller, O. B., Blackbourn, D. J., Mark, L., Proctor, D. G. & Blom, A. M. (2003). Functional activity of the complement regulator encoded by Kaposi's sarcoma-associated herpesvirus. *J Biol Chem* **278**, 9283-9.

Spits, H. (2002). Development of alphabeta T cells in the human thymus. *Nat Rev Immunol* **2**, 760-72.

Staskus, K. A., Zhong, W., Gebhard, K., Herndier, B., Wang, H., Renne, R., Beneke, J., Pudney, J., Anderson, D. J., Ganem, D. & Haase, A. T. (1997). Kaposi's sarcoma-associated herpesvirus gene expression in endothelial (spindle) tumor cells. *J Virol* **71**, 715-9.

Steven, N. M., Annels, N. E., Kumar, A., Leese, A. M., Kurilla, M. G. & Rickinson, A. B. (1997). Immediate early and early lytic cycle proteins are frequent targets of the Epstein-Barr virus-induced cytotoxic T cell response. *J Exp Med* **185**, 1605-17.

Stumpfova, M., Ratner, D., Desciak, E. B., Eliezri, Y. D. & Owens, D. M. (2010). The Immunosuppressive Surface Ligand CD200 Augments the Metastatic Capacity of Squamous Cell Carcinoma. *Cancer Res*.

Subramanian, R., Sehgal, I., D'Auvergne, O. & Kousoulas, K. G. (2010). Kaposi's sarcoma-associated herpesvirus glycoproteins B and K8.1 regulate virion egress and synthesis of vascular endothelial growth factor and viral interleukin-6 in BCBL-1 cells. *J Virol* **84**, 1704-14.

Sun, R., Lin, S. F., Staskus, K., Gradoville, L., Grogan, E., Haase, A. & Miller, G. (1999). Kinetics of Kaposi's sarcoma-associated herpesvirus gene expression. *J Virol* **73**, 2232-42.

Thirunarayanan, N., Cifire, F., Fichtner, I., Posner, S., Benga, J., Reiterer, P., Kremmer, E., Kolble, K. & Lipp, M. (2007). Enhanced tumorigenicity of fibroblasts transformed with human herpesvirus 8 chemokine receptor vGPCR by successive passage in nude and immunocompetent mice. *Oncogene* **26**, 5702-12.

Thomas, M., Boname, J. M., Field, S., Nejentsev, S., Salio, M., Cerundolo, V., Wills, M. & Lehner, P. J. (2008). Down-regulation of NKG2D and NKp80 ligands by Kaposi's sarcoma-associated herpesvirus K5 protects against NK cell cytotoxicity. *Proc Natl Acad Sci U S A* **105**, 1656-61.

Tomescu, C., Law, W. K. & Kedes, D. H. (2003). Surface downregulation of major histocompatibility complex class I, PE-CAM, and ICAM-1 following de novo infection of endothelial cells with Kaposi's sarcoma-associated herpesvirus. *J Virol* **77**, 9669-84.

Torrero, M. N., Larson, D., Hubner, M. P. & Mitre, E. (2009). CD200R surface expression as a marker of murine basophil activation. *Clin Exp Allergy* **39**, 361-9.

Tovar-Salazar, A., Patterson-Bartlett, J., Jesser, R. & Weinberg, A. (2009). Regulatory function of cytomegalovirus-specific CD4(+)CD27(-)CD28(-) T cells. *Virology*.

Trus, B. L., Heymann, J. B., Nealon, K., Cheng, N., Newcomb, W. W., Brown, J. C., Kedes, D. H. & Steven, A. C. (2001). Capsid structure of Kaposi's sarcoma-associated herpesvirus, a gammaherpesvirus, compared to those of an alphaherpesvirus, herpes simplex virus type 1, and a betaherpesvirus, cytomegalovirus. *J Virol* **75**, 2879-90.

Valk, E., Leung, R., Kang, H., Kaneko, K., Rudd, C. E. & Schneider, H. (2006). T cell receptor-interacting molecule acts as a chaperone to modulate surface expression of the CTLA-4 coreceptor. *Immunity* **25**, 807-21.

Valk, E., Rudd, C. E. & Schneider, H. (2008). CTLA-4 trafficking and surface expression. *Trends Immunol* **29**, 272-9.Vieira, J., Huang, M. L., Koelle, D. M. & Corey, L. (1997). Transmissible Kaposi's sarcoma-associated herpesvirus (human herpesvirus 8) in saliva of men with a history of Kaposi's sarcoma. *J Virol* **71**, 7083-7.

Vieites, J. M., de la Torre, R., Ortega, M. A., Montero, T., Peco, J. M., Sanchez-Pozo, A., Gil, A. & Suarez, A. (2003). Characterization of human cd200 glycoprotein receptor gene located on chromosome 3q12-13. *Gene* **311**, 99-104.

Voehringer, D., Rosen, D. B., Lanier, L. L. & Locksley, R. M. (2004). CD200 receptor family members represent novel DAP12-associated activating receptors on basophils and mast cells. *J Biol Chem* **279**, 54117-23.

Voigt, S., Sandford, G. R., Hayward, G. S. & Burns, W. H. (2005). The English strain of rat cytomegalovirus (CMV) contains a novel captured CD200 (vOX2) gene and a spliced CC chemokine upstream from the major immediate-early region: further evidence for a separate evolutionary lineage from that of rat CMV Maastricht. *J Gen Virol* **86**, 263-74.

Walker, D. G., Dalsing-Hernandez, J. E., Campbell, N. A. & Lue, L. F. (2009). Decreased expression of CD200 and CD200 receptor in Alzheimer's disease: a potential mechanism leading to chronic inflammation. *Exp Neurol* **215**, 5-19.

Wallace, L. E., Rowe, M., Gaston, J. S., Rickinson, A. B. & Epstein, M. A. (1982). Cytotoxic T cell recognition of Epstein-Barr virus-infected B cells. III. Establishment of HLA-restricted cytotoxic T cell lines using interleukin 2. *Eur J Immunol* **12**, 1012-8.

Walsh, G. & Jefferis, R. (2006). Post-translational modifications in the context of therapeutic proteins. *Nat Biotechnol* **24**, 1241-52.

Walter, J. B., Garboczi, D. N., Fan, Q. R., Zhou, X., Walker, B. D. & Eisen, H. N. (1998). A mutant human beta2-microglobulin can be used to generate diverse multimeric class I peptide complexes as specific probes for T cell receptors. *J Immunol Methods* **214**, 41-50.

Wang, H. W., Trotter, M. W., Lagos, D., Bourboulia, D., Henderson, S., Makinen, T., Elliman, S., Flanagan, A. M., Alitalo, K. & Boshoff, C. (2004). Kaposi sarcoma herpesvirus-induced cellular reprogramming contributes to the lymphatic endothelial gene expression in Kaposi sarcoma. *Nat Genet* **36**, 687-93.

Ward, R. A., Nakamura, M. & McLeish, K. R. (2000). Priming of the neutrophil respiratory burst involves p38 mitogen-activated protein kinase-dependent exocytosis of flavocytochrome b558-containing granules. *J Biol Chem* **275**, 36713-9.

Wells, A. D. (2009). New insights into the molecular basis of T cell anergy: anergy factors, avoidance sensors, and epigenetic imprinting. *J Immunol* **182**, 7331-41.

Wen, K. W. & Damania, B. (2009). Kaposi sarcoma-associated herpesvirus (KSHV): Molecular biology and oncogenesis. *Cancer Lett*.

Whitby, D., Marshall, V. A., Bagni, R. K., Miley, W. J., McCloud, T. G., Hines-Boykin, R., Goedert, J. J., B, A. C., Nagashima, K., Mikovits, J., Dittmer, D. P. & Newman, D. J. (2007). Reactivation of Kaposi's sarcoma-associated herpesvirus by natural products from Kaposi's sarcoma endemic regions. *Int J Cancer* **120**, 321-8.

Wills, M. R., Ashiru, O., Reeves, M. B., Okecha, G., Trowsdale, J., Tomasec, P., Wilkinson, G. W., Sinclair, J. & Sissons, J. G. (2005). Human cytomegalovirus encodes an MHC class I-like molecule (UL142) that functions to inhibit NK cell lysis. *J Immunol* **175**, 7457-65.

Wong, S. W., Bergquam, E. P., Swanson, R. M., Lee, F. W., Shiigi, S. M., Avery, N. A., Fanton, J. W. & Axthelm, M. K. (1999). Induction of B cell hyperplasia in simian immunodeficiency virus-infected rhesus macaques with the simian homologue of Kaposi's sarcoma-associated herpesvirus. *J Exp Med* **190**, 827-40.

Wright, G. J., Cherwinski, H., Foster-Cuevas, M., Brooke, G., Puklavec, M. J., Bigler, M., Song, Y., Jenmalm, M., Gorman, D., McClanahan, T., Liu, M. R., Brown, M. H., Sedgwick, J. D., Phillips, J. H. & Barclay, A. N. (2003). Characterization of the CD200 receptor family in mice and humans and their interactions with CD200. *J Immunol* **171**, 3034-46.

Wright, G. J., Jones, M., Puklavec, M. J., Brown, M. H. & Barclay, A. N. (2001). The unusual distribution of the neuronal/lymphoid cell surface CD200 (OX2) glycoprotein is conserved in humans. *Immunology* **102**, 173-9.

Wright, G. J., Puklavec, M. J., Willis, A. C., Hoek, R. M., Sedgwick, J. D., Brown, M. H. & Barclay, A. N. (2000). Lymphoid/neuronal cell surface OX2 glycoprotein recognizes a novel receptor on macrophages implicated in the control of their function. *Immunity* **13**, 233-42.

Xie, J., Ajibade, A. O., Ye, F., Kuhne, K. & Gao, S. J. (2008). Reactivation of Kaposi's sarcoma-associated herpesvirus from latency requires MEK/ERK, JNK and p38 multiple mitogen-activated protein kinase pathways. *Virology* **371**, 139-54.

Young, N. S., Levin, J. & Prendergast, R. A. (1972). An invertebrate coagulation system activated by endotoxin: evidence for enzymatic mediation. *J Clin Invest* **51**, 1790-7.

Young, L. S. & Rickinson, A. B. (2004). Epstein-Barr virus: 40 years on. *Nat Rev Cancer* **4**, 757-68.

Zhang, J., Wang, J. Z., Wood, C., Xu, D. S. & Zhang, L. W. (2005). Kaposi's sarcoma-associated herpesvirus/human herpesvirus 8 replication and transcription activator regulates viral and cellular genes via interferon-stimulated response elements. *Journal of Virology* **79**, 5640-5652.

Zhang, L., Stanford, M., Liu, J., Barrett, C., Jiang, L., Barclay, A. N. & McFadden, G. (2009). Inhibition of macrophage activation by the myxoma virus M141 protein (vCD200). *J Virol* **83**, 9602-7.

Zhang, S., Cherwinski, H., Sedgwick, J. D. & Phillips, J. H. (2004). Molecular mechanisms of CD200 inhibition of mast cell activation. *J Immunol* **173**, 6786-93.

Zhang, S. & Phillips, J. H. (2006). Identification of tyrosine residues crucial for CD200R-mediated inhibition of mast cell activation. *J Leukoc Biol* **79**, 363-8.

Zhou, L., Chong, M. M. & Littman, D. R. (2009). Plasticity of CD4+ T cell lineage differentiation. *Immunity* **30**, 646-55.

Ziegler, J., Newton, R., Bourboulia, D., Casabonne, D., Beral, V., Mbidde, E., Carpenter, L., Reeves, G., Parkin, D. M., Wabinga, H., Mbulaiteye, S., Jaffe, H., Weiss, R. & Boshoff, C. (2003). Risk factors for Kaposi's sarcoma: a case-control study of HIV-seronegative people in Uganda. *Int J Cancer* **103**, 233-40.

Zong, J. C., Arav-Boger, R., Alcendor, D. J. & Hayward, G. S. (2007). Reflections on the interpretation of heterogeneity and strain differences based on very limited PCR sequence data from Kaposi's sarcoma-associated herpesvirus genomes. *J Clin Virol* **40**, 1-8.